A Linear Free-Energy Approach to the Study of Substituted Phenoxazines as a Potent Family of Radical Trapping Antioxidants

By

Luke Farmer

A thesis submitted to the Department of Chemistry and Biomolecular Sciences in partial fulfillment of the requirements for the degree of:

Master of Science in Chemistry

University of Ottawa
Ottawa, Ontario, Canada
May 2018

Abstract

Radical mediated autoxidation is a pervasive phenomenon in commercial (i.e. rubbers, fuels, lubricants, etc.) and biological contexts (i.e. lipid peroxidation associated with neurodegeneration, cancer, and aging), which can be strategically managed with radical-trapping antioxidants (RTAs). While various phenol and polyphenol RTAs have enjoyed much academic fanfare, particularly in biochemical circles, there are other RTA scaffolds that tend to be overlooked despite possessing rather promising activity. Among these seldom studied RTA scaffolds is that of the tricyclic aromatic amine phenoxazine.

The inherent reactivity of phenoxazines as RTAs was explored using a quantitative linear free energy approach. A library of phenoxazines was synthesized and Hammett correlations developed between BDE/(log k_{inh}^{PhCl})/E^o and the electrophilicity substituent parameters ($\sum \sigma_p^+$) served to unambiguously demonstrate that phenoxazine RTAs collectively represent the most reactive family of RTAs yet reported. The high inherent reactivity of phenoxazine RTAs towards peroxyl radicals necessitated the co-development of an approach to enable the accurate prediction of k_{inh}^{PhCl} based on the inhibition rate constants measured in hydrogen-bond accepting solvent mixtures containing chlorobenzene, 1,4-dioxane, and/or dimethylsulfoxide.

The catalytic antioxidant activity of phenoxazines was established in hexadecane autoxidations at elevated temperatures, where they demonstrated superior activity to industry standard alkylated diphenylamine (ADPA), but also an inferiority to phenothiazine. These results combined with amine/nitroxide monitoring experiments

serve to re-emphasize some current design considerations for high-temperature RTAs while challenging others.

Lastly the activity of these as inhibitors of lipid peroxidation was assessed in liposomes and mammalian cell culture. The kinetics of peroxyl radical-trapping of the various phenoxazines in phosphatidylcholine liposomes enabled the quantitation of H-bonding interactions to the phosphate head groups of the phospholipids on RTA activity – which diminish the kinetics by up to two orders of magnitude relative to non-H-bonding hydrocarbons. The potency of these phenoxazines to subvert ferroptosis corresponds well with their inhibition activity in liposomes which further affirms the role that non-enzymatic autoxidation plays in this form of cell death.

Acknowledgements

There are many people to thank for the completion of this work, which would have been lessened in their absence. It would not have been possible at all without the opportunity afforded to me by my supervisor Dr. Derek Pratt. Beyond material support, he has been an indispensable source of knowledge and advice, and any graduate student would be fortunate to work under the supervision of such a knowledgeable and experienced professor.

I am also grateful to have worked with so many helpful colleagues, who have been a constant comfort in these past years. The comradery of Jean-Phillipe Chauvin, Zosia Zielinski, Ron Shah, Omkar Zilka, Kareem Harrison, Emily Schaefer, Anas Abou-Zaid, Katie Shirley, Dr. Evan Haidasz, Dr. Markus Griesser, Dr. Jia-Fei Poon, Dr. Demar Pitter, Melodie Mallais, Derek Meng, Neill Penner, Mark Slodki, Dr. Manuel Petroselli, and Dr. Pierre Faudot dit Bel made my time in The Pratt Group not only educational but immensely enjoyable.

The support from my family and friends, both in past and continuing, has been of such an epic proportion that it is difficult to fully articulate. In particular, I wish to thank my parents, Pam and Brian Farmer, for their unwavering spiritual and emotional support throughout my academic endeavors. Last, but certainly *not* least, I wish to dedicate this work to my wife Carly Farmer whose love, patience, and support have been of inestimable value.

Statement of Originality

I hereby declare that the research in this document is the original work of the author, Luke Farmer, expect for contributions from fellow researchers (both published and unpublished) which are explicitly identified in the form of statements in a chapter's "Preface" or citations to published work found in the "References" section.

Luke Farmer

Publications Resulting From This Work

The following publications included/made use of the inhibited autoxidation protocols for dioxane/chlorobenzene and dioxane/DMSO/chlorobenzene as well as the associated β_2^H parameters necessary for determining k_{inh}^0 which were developed/determined by the present author:

1. Haidasz, E. A.; Pratt, D. A. *Org. Lett.* **2017**, *19*, 1854-1857.
2. Chauvin, J-P. R.; Griesser, M.; Pratt, D. A. *J. Am. Chem. Soc.* **2017**, *139*, 6484-6493.

The following publication entirely comprised the contents of Chapter 2 of the present document:

3. Farmer, L. A.; Haidasz, E. A.; Griesser, M.; Pratt, D. A. *J. Org. Chem.* **2017**, *82*, 10523-10536.

The following publication made use of the novel preparation/isolation of phenoxazine-N-oxyl (**3.20**) which facilitated a major point of discussion in the paper:

4. Griesser, M.; Shah, R.; Van Kessel, A. T.; Zilka, O.; Haidasz, E. A.; Pratt, D. A. *J. Am. Chem. Soc.* **2018**, *140*, 3798-3808.

Table of Contents

List of Schemes/Charts

List of Figures

List of Tables

List of Abbreviations

α-Toc/ α-TOH	α-tocopherol
ADPA	alkylated-diphenylamine
AIBN	azobisisobutyronitrile
BDE	bond dissociation enthalply
CV	cyclic volatmmetry
DPA	diphenylamine
DPPH	2,2-diphenyl-1-picryhydrazyl
DMSO	dimethylsulfoxide
EDG	electron donating group
Egg PC	egg phosphatidylcholine
EPR	electron paramagnetic resonance
HAT	hydrogen-atom transfer
HBA	hydrogen-bond acceptor
HBD	hydrogen-bond donnor
HOMO	highest occupied molecular orbital
HPLC	high-pressure liquid chromatography
IP	ionization potential
KSE	kinetic solvent effect
LUMO	lowest unoccupied molecular orbital

NHE	normal hydrogen electrode
PCET	proton coupled electron transfer
PDA	photo diode array
PMC	2,2,5,7,8-pentamethyl-6-chromanol
PNX	phenoxazine
PTZ	phenothiazine
RTA	radical trapping antioxidant
SOMO	singly occupied molecular orbital
TEMPO	(2,2,6,6-tetramethylpiperidin-1-yl)oxyl
THN	tertahydronaphthyridinol

Chapter 1: Background and Significance of Autoxidation and Radical-Trapping Antioxidants

1.1 Hydrocarbon Autoxidation

The revolutions in production, transportation, and quality of life of the past 150 years have been enabled, in part, by the discovery and utilization of massive petroleum reservoirs. The service/shelf life of products derived from these hydrocarbons (plastics, rubbers, fuels, lubricants) are dictated in part by their reactivity to oxygen to produce peroxidic species in process referred to as 'autoxidation'. The key fundamental concepts associated with autoxidation were largely established by researchers at the Natural Rubber Producers' Research Association in the 1940s, with notable contributions from L. Bateman[1] and J. L. Bolland.[2] Hydrocarbon autoxidation can be characterized by the following general statements:

i) Autoxidation is a radical chain process with a distinct set of rate determining initiation, propagation, and termination reactions.

ii) The rate of autoxidation under a given set of conditions (temperature, oxygen concentration, initiator concentration) begins with an induction period where the rate of peroxide production is constant.

iii) The induction can be followed by an autocatalytic period where the rate of autoxidation accelerates if the accumulating peroxidic hydrocarbons behave as initiators.[3]

The peroxidic hydrocarbons produced, ie hydroperoxides (ROOH) and peroxides (ROOR) can decompose to produce corresponding alcohols, aldehydes, ketones, and carboxylic acids which, in summary, changes the properties of the original substrate.[4] Beyond

petroleum, the lipids that comprise the membranes of living cells are also susceptible to autoxidation,[5,6] the excess of which is implicated in several disease states.[7–10] In this segment, some foundations of hydrocarbon autoxidation will be discussed.

1.1.1 Initiation

While the hydrocarbon substrate can act as an 'initiator' via thermolysis of a C-C bond (BDE ~ 84 kcal/mol), under the typical service conditions this occurs at a relatively low rate. A certain amount of hydroperoxide ($BDE_{MeO\text{-}OH}$ = 44.6 kcal/mol)[11] and/or peroxide ($BDE_{MeO\text{-}OMe}$ = 37.8 kcal/mol)[11] is usually present in the substrate which typically acts as the principle initiator due to the much weaker nature of O-O bonds. The pair of alkoxyl ($RO^{\bullet}$) and hydroxyl radicals ($HO^{\bullet}$) produced through the homolysis of the peroxidic species do not react with O_2 directly; however, they are highly reactive towards hydrocarbons via hydrogen atom transfer (HAT):[12]

$$\text{(Initiation)} \qquad \text{ROOR} \xrightarrow{k_1} 2\,\text{RO}^{\bullet} \qquad \text{Eq. 1.1}$$

$$\text{RO}^{\bullet} + \text{RH} \xrightarrow[\text{(very fast)}]{k_2} \text{ROH} + \text{R}^{\bullet} \qquad \text{Eq. 1.2}$$

The rate of HAT (Eq. 1.2) is much greater than the peroxide homolysis (Eq. 1), therefore the rate of initiation (R_i) can be expressed as such:

$$R_i = 2ek_1[\text{ROOR}] \qquad \text{Eq. 1.3}$$

Where 'e' is the efficiency coefficient, a factor that accounts for the proportion of alkoxyl pairs produced that escape the solvent cage in lieu of undergoing either recombination or disproportionation to produce non-radical products. A higher rate of initiation enables efficient autoxidation due to the higher steady-state concentration of

highly reactive alkyl radicals. The k_1 is acutely affected by the temperature of the system due to the high activation energy (E_a,tBuO-OtBu = 36.7 kcal/mol)[13] and Arrhenius pre-exponential factor (log A ~ 15.6) of the peroxide initiator, therefore precise temperature control is an important consideration when studying autoxidation kinetics. Azo initiators such as AIBN are often used to initiate radical reactions at ambient temperatures due to their much lower activation energies (E_a,AIBN = 32 kcal/mol)[13] which renders two alkyl radicals and a single N_2.

1.1.2 Propagation

Carbon centered radicals produced from the substrate are highly reactive intermediates. These radicals can add to vinyl substrates (styrene, ethylene, methacrylate, etc.), which is an important transformation for the highly lucrative polymer industry as the unpaired electron is 'passed' to the end of the growing polymer chain which can further grow by adding to another vinylic monomer.

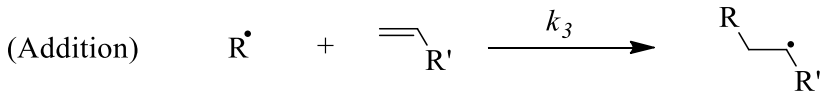

Eq. 1.4

Such transformations are often in steep competition with the diffusion limited reaction between a carbon centred radical and oxygen ($k_4 \sim 3 \times 10^9$ M^{-1} s^{-1}):[14]

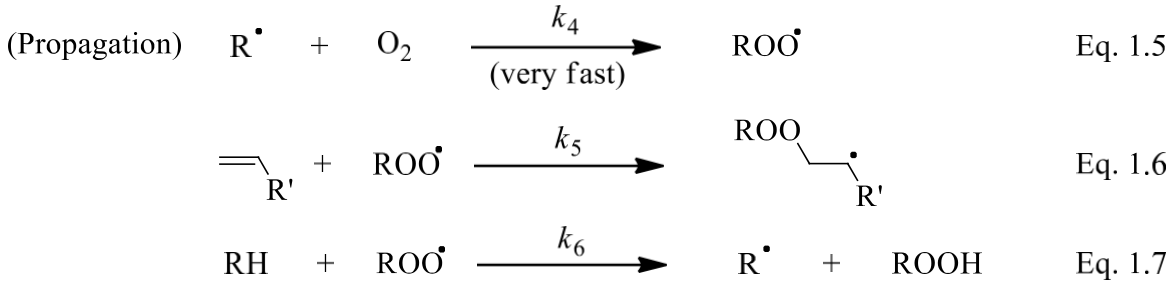

The rate at which peroxyl radicals ($ROO^{\bullet}$) react with hydrocarbons, through addition reactions (Eq. 1.6) and/or HAT (Eq. 1.7), determines the rate of propagation as these reactions are much slower than addition of oxygen to a carbon centered radical (Eq. 1.5). Whether a peroxide is formed via addition or a hydroperoxide via HAT, is dependent on whether the reaction site of the hydrocarbon is vinylic or saturated. A substantial catalogue of these propagation rate constants have been painstakingly measured for a wide assortment of oxidizable substrates, to better understand the how the hydrocarbon structure affects their reactivity with peroxyl radicals.

The rate constant for propagation ($k_5 + k_6 = k_p$), varies substantially between substrates, but generally the k_p increases with increasing thermodynamic stability of the carbon centred radicals rendered. The k_p for HAT tends to increase in reactivity in the order of the site being primary < secondary < tertiary due to increased stabilization of the alkyl radical via hyperconjugation. When the hydrogen atom is abstracted from an sp^3 carbon, the carbon adopts an sp^2 hybridization with the unpaired electron occupying a 2p atomic orbital which can be stabilized by conjugation with adjacent π systems. The general trend in k_p follows that unconjugated < acyclic conjugated with a single π system < cyclic conjugated with a single π system < acyclic conjugated with two π systems < cyclic conjugated with two π systems.[17]

Table 1.1. Representative rate constants (k_5, k_6, and k_t) of some oxidizable substrates.

	Structure	$k_p/(2k_t)^{1/2}$ ($M^{-1/2}$ $s^{-1/2}$)	k_5 (M^{-1} s^{-1})	k_6 (M^{-1} s^{-1})	k_t (M^{-1} s^{-1})
Hexadecane[15,16]	$C_{16}H_{34}$	2.0×10^{-6}	-	0.01	1.3×10^{7}
Toluene[17]	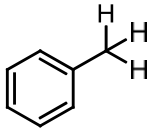	1.4×10^{-5}	-	0.24	1.5×10^{8}
Ethylbenzene[17]	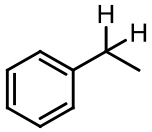	2.1×10^{-4}	-	1.3	2.0×10^{7}
Cumene[17]	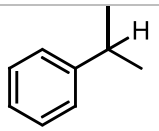	1.5×10^{-3}	-	0.18	7.5×10^{3}
Styrene[17]	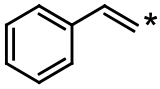	8.9×10^{-3}	41	-	2.1×10^{7}
Indene[17]	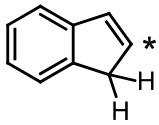	2.8×10^{-2}	128	14	2.5×10^{7}
1,4-Dioxane[18]	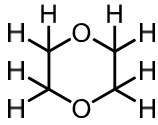	6.9×10^{-5}	-	0.50	2.5×10^{7}

The hydrogen atoms which are abstracted by peroxyl are explicitly drawn. The sites where peroxyl addition occurs are marked with an asterisk (*).

The third column of Table 1 provides what is termed the 'oxidizability' of the hydrocarbon can numerically be cast as (Eq. 1.8), a ratio between k_p and the rate constant of peroxyl self termination (k_t):

$$\frac{k_p}{\sqrt{2k_t}} \qquad \text{Eq.1.8}$$

$$\frac{d[ROOH]}{dt} + \frac{d[ROOR]}{dt} = \frac{-d[O_2]}{dt} \qquad \text{Eq. 1.9}$$

$$\frac{-d[O_2]}{dt} = \frac{k_p[RH]\sqrt{R_i}}{\sqrt{2k_t}} \qquad \text{Eq. 1.10}$$

For some allylic/vinylic substrates addition and HAT reactions are competitive (e.g. indene),[17] but the sum of peroxide formation can conveniently be monitored by oxygen consumption in a closed system. Where [RH] is the concentration of the oxidizable substrate, a higher k_p relative to k_t will result in a proportionally higher rate of propagation and longer chain length due to a lower instance chain termination.

1.1.3 Termination

Due to the intervention of multiple initiating and propagating species in an autoxidation there are many possible terminating radical-radical reactions:

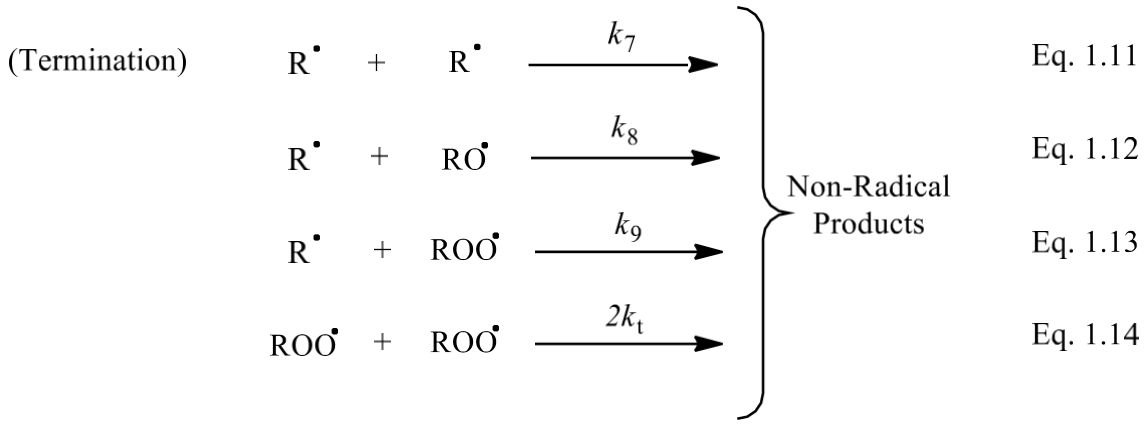

Due to the high reactivity of alkyl radicals towards molecular oxygen and alkoxyl radicals towards most hydrocarbons, and considering the relatively high concentration of O_2 and

substrate relative to these radicals, the observed rate of termination is reflected by the radical-radical termination of the relatively concentrated peroxyl radicals. Unlike the rapid and effectively irreversible reactions depicted in (Eq. 1.11), Eq. 1.12), and (Eq. 1.13), peroxyl-peroxyl termination initially forms a rather unstable tetroxide with an extremely weak central O-O bond. Product analysis of the self-reactions of ethylbenzene-derived peroxyls conducted by Russell provides strong evidence for the stoichiometric formation of acetophenone, which was rationalized to form along with 1-phenylethanol via the six membered cyclic transition state:[19]

Scheme 1.1 Russell's proposed mechanism for the termination of two peroxyl radicals derived from ethylbenzene.

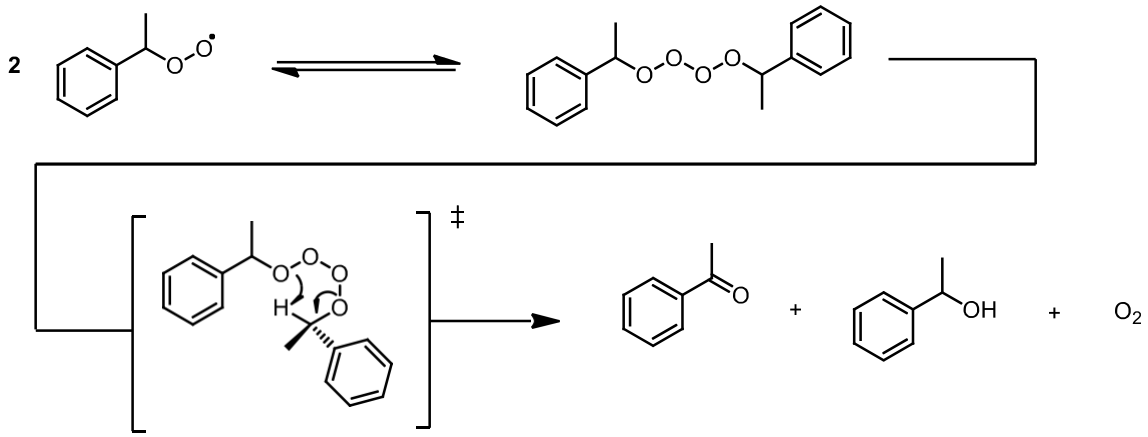

This peroxyl-peroxyl reaction, generally referred to as 'Russell Termination', was thought to be the dominant termination reaction with primary and secondary peroxyl radicals which renders an alcohol, an aldehyde/ketone, and one equivalent of O_2. For a substrate where the peroxyl forms at a tertiary position, such as cumene ($k_t = 7.5 \times 10^3$ M^{-1} s^{-1}),[17] the k_t is markedly lower than otherwise comparable secondary and primary substrates such as ethylbenzene ($k_t = 2.5 \times 10^7$ M^{-1} s^{-1}) and toluene ($k_t = 1.5 \times 10^8$ M^{-1} s^{-1}). Since there is no α hydrogen to transfer when two tertiary peroxyls combine, it was reasoned that an

alternative forward reaction of homolysis of the 1st and 2nd oxygen bond as well as the 3rd and 4th would render two alkoxyl radicals and one equivalent of oxygen. The alkoxyl radicals either combine to form a peroxide, resulting in the successful termination of two radical chains, or they react with the substrate which continues to propagate. All of these assertions were more than reasonable based on the experimental evidence available to Russell at the time, though some later observations regarding the behaviour of secondary peroxyl-peroxyl termination caused some doubt in the veracity of the concerted mechanism proposed by Russell. For example, some secondary peroxyl termination products observed by Lindsay *et al.* in 1973 indicated the formation of alkoxyl radicals and peroxides,[20] while Howard and Bennet observed that the Arrhenius parameters of the self-termination reactions of cyclopentylperoxyl, cyclopentenylperoxyl, s-butylperoxyl, *and* t-butylperoxyl converged around log $A \sim 7.8\text{-}10$.[21] The latter observation is rather inconsistent with the notion of a concerted cyclic transition state for secondary peroxyl termination, as one would expect the log A to be significantly lower. Recently the Coote Group in collaboration with K. U. Ingold suggested that primary, secondary, and tertiary peroxyl termination reactions proceed through the same aforementioned homolysis rendering two alkoxyl radicals and molecular O_2 (depicted in Scheme 1.2).[22] They demonstrated with high accuracy DFT calculations that a hydrogen bond between the alpha hydrogen and the evolving oxygen stabilizes the transition state which they used to explain the improved kinetics observed for primary and secondary peroxyl termination reactions.

Scheme 1.2. The proposed reactions and products of cumene peroxyl termination.

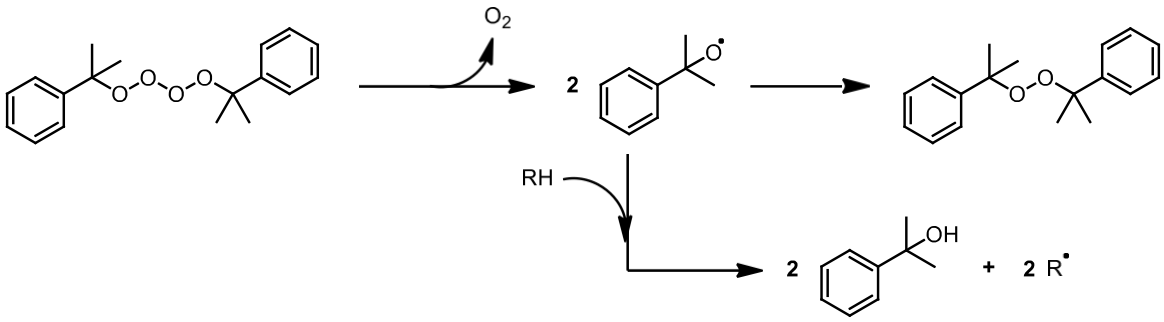

When directly observing autoxidation by oxygen consumption it is, in fact, difficult to separate terms of k_p and k_t due to the simultaneous and consistently proportional nature of these chemical reactions, though determining these terms independently is possible. The challenge of disaggregating k_p from k_t can be met through the use of a rotating sector where an opaque rotating disc with a slit is placed between a sample containing the oxidizable substrate and a photoinitiator and the incident initiating beam of light. Without the rotating sector, the photoinitiation would be constant, but instead the autoxidation is only initiated intermittently. The oxidation rates are measured at different rotation speeds which can enable the derivation of the radical chain length, from which the k_p and k_t can be calculated.[23] Generally, if the chain length is greater than 5 these rate constants can be accurately resolved.

1.2 Radical Trapping Antioxidants

While there is a degree of self moderation of substrate autoxidation via peroxyl termination, the longevity of hydrocarbon-based materials depends on the addition of other chemicals to promote chain-termination and extend the induction period as long as possible. Broadly these additives are referred to as radical trapping antioxidants (RTA).[24,25] A feature that makes RTAs far more effective at terminating chains than the peroxyls

generated in-situ is that RTAs are not reactive with the substrate but are highly reactive with the peroxyl radicals, which means that a relatively high concentration of RTA can be added for the sole purpose of terminating radical chains.

$$AH + ROO^{\bullet} \xrightarrow{k_{inh}} A^{\bullet} + ROOH \qquad \text{Eq. 1.15}$$

$$A^{\bullet} + ROO^{\bullet} \xrightarrow[\text{(very fast)}]{k_{10}} \text{Non-Radical Products} \qquad \text{Eq. 1.16}$$

The rate of radical-trapping depends on the amount of RTA added as well as the inherent reactivity of the inhibitor to peroxyls. Using phenols and aromatic amines as the typical examples of RTAs, the measured rate constant of inhibition (k_{inh}) is predicated on the hydrogen-transfer reaction to the chain carrying peroxyl. For effective RTAs, the inhibitor derived radical ($A^{\bullet}$) is unreactive towards the substrate and can often trap another peroxyl radical. This follow up reaction, a radical-radical reaction, is much faster than the initial hydrogen transfer reaction.[26]

It should be noted that the hydrogen-transfer reaction for phenols and diarylamines tends to proceed through a proton coupled electron transfer (PCET) which is distinct from the HAT mechanism by which the hydrocarbon transfers their hydrogen atoms to peroxyl radicals.[25] Unlike HAT, where the proton and electron of the H-atom move together between a single pair of orbitals (the SOMO formed from departure of the H-atom from the donor and the SOMO of the acceptor), PCET involves the transfer of the proton and electron between two different pairs of orbitals. In the case of a phenol/aromatic amine reacting with a peroxyl, the proton is transferred between lone pairs on the phenolic/aminic oxygen/nitrogen and peroxyl radical while the electron is transferred

from the π HOMO of the aryl ring of the phenol/aromatic amine to the overlapping π*-SOMO of the peroxyl. The transition state of the PCET reaction is generally lower in energy than for the HAT (for similar thermodynamic driving forces), enabled by the formation of a H-bonded pre- reaction complex, explaining why even though the C-H BDE of toluene and the O-H BDE of phenol are similar the rate constant of hydrogen transfer from phenol ($k_{inh} = 3 \times 10^3$ M^{-1} s^{-1}) is over 4 orders of magnitude greater than that of toluene ($k_6 = 0.24$ M^{-1} s^{-1}).[25] It is this difference in reactivity that makes stabilizing oxidizable hydrocarbon stocks feasible with comparatively miniscule quantities of inhibitor.

When an effective RTA is added to an autoxidation system, the rate of chain termination sharply increases so the rate of termination is no longer dictated by the rate of peroxyl-peroxyl termination but is instead dictated by RTA-peroxyl termination. The rate of an inhibited autoxidation can be expressed as (Eq. 1.17):

$$\frac{-d[O_2]}{dt} = \frac{k_p[RH]R_i}{nk_{inh}[AH]} \qquad \text{Eq. 1.17}$$

$$n = \frac{t_{inh}R_i}{[AH]} \qquad \text{Eq. 1.18}$$

Where [AH] is the concentration of RTA and '*n*', the stochiometric factor, is the number of radical chains trapped per equivalent of RTA and 't_{inh}' is the time of inhibition. The "ideal" RTA has a high k_{inh} and *n*, such that propagation is inhibited for as long as possible. If the PCET reaction of a phenol or aromatic amine is particularly facile, k_{inh} will be high and only a low concentration the RTA will be required to completely supress chain propagation. Having a high stochiometric factor will ensure that the RTA inhibits for a

long period of time, relative to the amount that is added, before being completely consumed. The stochiometric factor of a given RTA can be determined simply by measuring the t_{inh} of an inhibited autoxidation at a given [AH] and R_i.

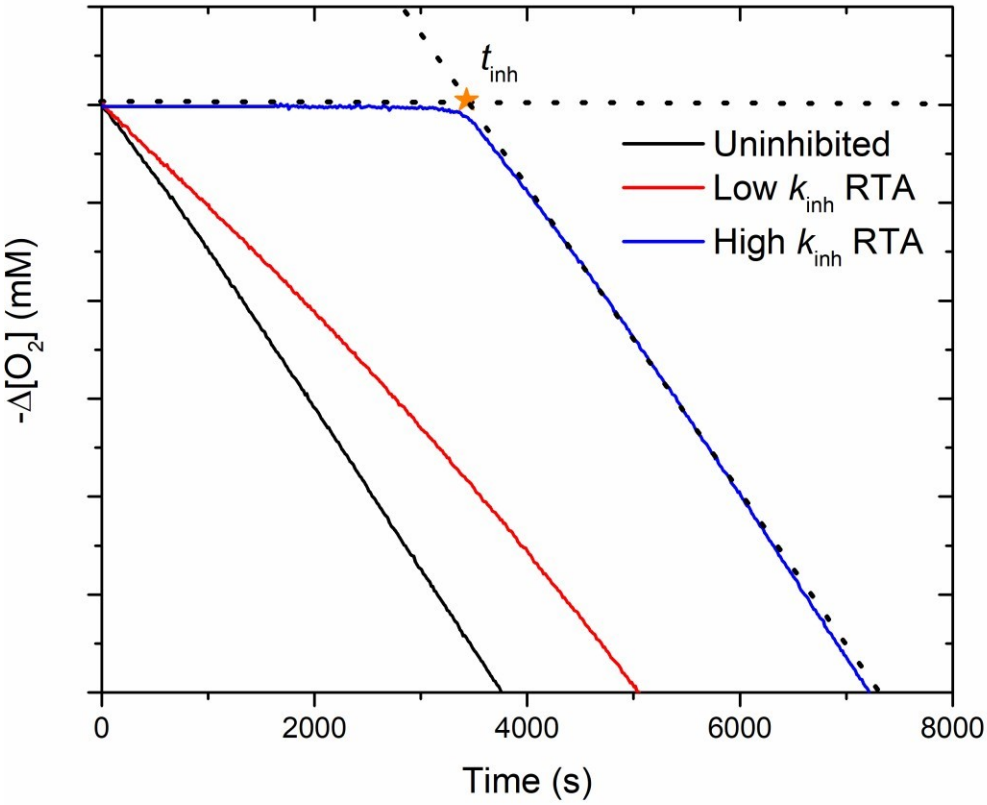

Figure 1.1. Mock-up oxygen consumption traces from systems that are uninhibited (**black**), inhibited by a poor RTA (**red**), and inhibited by a good RTA (**blue**). The t_{inh} for the 'good' RTA is defined by the inflection between the inhibited and uninhibited periods.

1.2.1 Electronic Effects on The Reactivity of Phenol and Diarylamine RTAs

Given the general usefulness of RTAs in stabilizing hydrocarbons, understanding their reactivity trends has been a topic of considerable interest from both an academic and

industrial/commercial perspective, as it will enable the design of more efficient inhibitors. The substituent effects on the k_{inh} of phenols has been well studied as well as for diarylamines, though to a lesser extent, since these RTA families are of high commercial importance. Howard and Ingold were the first to report on the substituent effects on phenolic RTAs in 1963.[27] They observed that the inhibited autoxidation of styrene with para and meta substituted phenols followed a trend that coincided with a ρ = -1.58 when they plotted the log k_{inh}/k_{PhOH} (where k_{PhOH} is the inhibition rate constant for phenol) against the σ^+ electrophilic substituent constants developed by Brown and Okamoto.[28]

$$\log (k_{inh}/k_{PhOH}) = 0.002 - 1.58\sigma^+ \qquad \text{Eq. 1.19}$$

They observed that with an EDG ($\sigma^+ > 0$), such as an alkyl or alkoxy substituent, the log k_{inh} was higher compared to phenol but with an EWG ($\sigma^+ < 0$), such as a chloro or cyano substituent, the log k_{inh} was lower. Later Mahoney and DaRooge[29] reported that the electronic substituent effects of such substituted phenols were accompanied by large differences in BDE, lowered with EDGs and increased with EWGs. The linear relationship observed between the log k_{inh} and BDE values conform to the Evans-Polanyi principle where the phenol to peroxyl hydrogen-transfer reactions of the substituted phenols are mechanistically the same between the substituted phenols (i.e. same log A and position of transition state along a reaction coordinate), but increasingly exothermic reactions (lower BDE) have correspondingly lower $\Delta H^{\ddagger}$. This Evans-Polanyi relationship has also been observed by a number of authors that followed.[30–32] The same correlations between log k_{inh}, BDE, and σ^+ also apply to substituted diarylamines, aspects of which have been demonstrated by Brownlie and Ingold, Lucarini et. al., and Pratt et. al.[33–35]

Table 1.2. Hammett inspired σ_p^+ and σ_p^- parameters for some common substituents.[36]

Substituent	σ_p^+**Parameters**	σ_p^+**Parameters**
-H	0	0
$-CH_3$	-0.31	-0.17
$-C(CH_3)_3$	-0.26	-0.13
$-OCH_3$	-0.78	-0.26
$-N(CH_3)_2$	-1.70	-0.12
$-CF_3$	+0.61	+0.65
$-SO_2N(CH_3)_2$	+0.86	+0.99
-CN	+0.66	+1.00
$-NO_2$	+0.79	+1.27

One should be mindful that Hammett-type parameters are essentially a sum of resonance and inductive/field effects. While oxygen is rather inductively withdrawing, the alkoxy substituent bears a p-type lone-pair which stabilizes the electron-deficient phenoxyl via resonance donation. Therefore, the steric environment of the EDG can have a rather dramatic influence on the orbital alignment between the lone pair and the aryl ring resulting in an equally dramatic change in resonance stabilization. This is nicely illustrated in the series of compounds shown in Scheme 1.3.

Scheme 1.3. The k_{inh} and θ' of 4-methoxy-2,3,5,6-tertamethylphenol, 4-methoxy-2,3,6-trimethylphenol, PMC, and 2,3-dihydro-5-hydroxy-2,2,4,6,7-pentamethylbenzofuran. Where θ' is the dihedral angle between CH_2R moiety of the alkoxy substituent and the aryl ring.

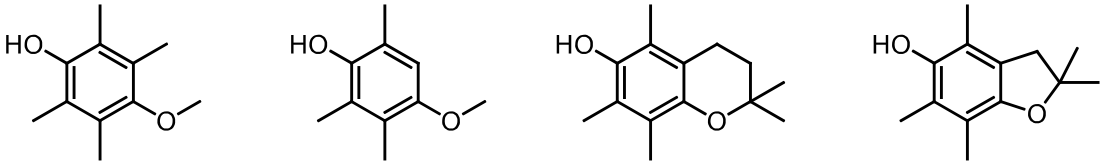

k_{inh}	$3.9 \times 10^5\ M^{-1}\ s^{-1}$	$1.3 \times 10^6\ M^{-1}\ s^{-1}$	$3.8 \times 10^6\ M^{-1}\ s^{-1}$	$5.7 \times 10^6\ M^{-1}\ s^{-1}$
θ'	89°	8°	17°	6°

Ingold and Burton observed that while 4-methoxy-2,3,6-trimethylphenol was about 3-fold slower compared to PMC, a truncated analogue of Vitamin E α-tocopherol, 4-methoxy-2,3,5,6-tertamethylphenol was found to be 10-fold slower by comparison.[37] They attributed this profound difference in reactivity to a stereoelectronic effect which corresponded to θ' where at 90° there would be minimal overlap between the oxygen lone-pair and p-orbitals of the aryl ring and maximum overlap, and therefore stabilization, at 0°. The insight into this stereoelectronic effect inspired Burton et. al to synthesize 2,3-dihydro-5-hydroxy-2,2,4,6,7-pentamethylbenzofuran which, corresponding to its smaller θ', had a k_{inh} that was 50% greater compared to PMC.

Scheme 1.4. Depiction of the difference in methoxy lone pair alignment with aromatic p oribitals which explains the stereoelectronic difference between 4-methoxy-2,3,5,6-tertamethylphenol (left) and 4-methoxy-2,3,6-trimethylphenol (right.)

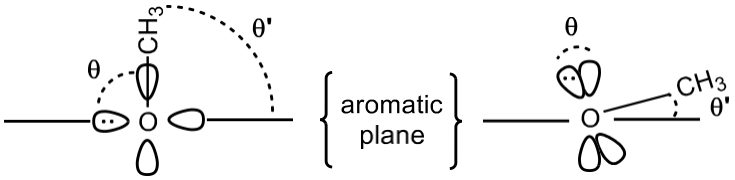

While one could improve the reactivity of a phenol/diarylamine towards peroxyl radicals simply by further stabilizing the electron-deficient phenoxyl/aminyl radical with even 'stronger' EDGs, this does not necessitate that the compound will be effective as an inhibitor. In the same manner that phenoxyl/aminyl radicals are stabilized by EDGs, they also stabilize their corresponding radical cation – an interaction that results in a lowered oxidation potential. If the oxidation potential is sufficiently low, reduction of molecular oxygen to form superoxide via electron-transfer (essentially autoxidation of the antioxidant) will become the prevailing reaction pathway and shown in Scheme 1.5.

Scheme 1.5. The competing peroxyl trapping and hydroperoxyl generating reaction pathways proposed for excessively electron-rich phenols.

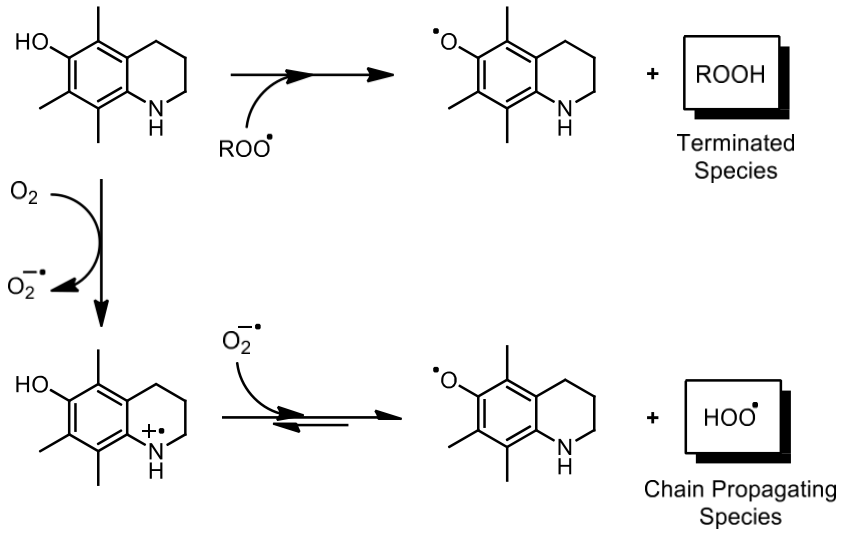

The example shown in Scheme 1.5 was an attempt to mimic the 6-chromanol motif found in PMC with a tetrahydroquinoline moiety such that the phenolic hydroxyl is now para to the more ED nitrogen atom in lieu of the oxygen atom in PMC. Comparing the electrophilic substituent parameters of a dialkylamino substituent (σ^+ = -1.70) against a methoxy substituent (σ^+ = -0.79), one would anticipate a much higher rate of peroxyl

trapping compared to PMC, but this was not observed. Not only was it apparently less reactive than PMC, but Burton et. al observed that even as a crystalline solid, 1,2,3,4-tetrahydro-6-hydroxy-5,7,8-trimethylquinoline was unstable in the presence of air over a period of a few days.[38] It is not merely an issue of consumption of the parent phenol/diarylamine that makes this process problematic for 'would be' RTAs, a radical-chain is initiated through the hydroperoxyl generated. Depending on how prevalent this side reaction is, the compound in question might be better characterized as a 'pro-oxidant' as opposed to an antioxidant. Therefore, when designing an RTA it is prudent to strike a balance in design where the BDE is as low as it can be without compromising the oxidative stability of the compound.

The structure-activity relationships established with phenols later precipitated new research efforts to systematically seek out RTAs using the aforementioned 'balance' to guide the design. Among the first fruits of this approach, Pratt et. al published their initial results regarding novel RTAs based on substituted 3-pyridinols and 5-pyrimidinols.[39] The key innovation over the use of simple phenols is that the nitrogen heteroatoms, according to DFT calculations, affects the stability of the phenoxyl radical and the radical cation disproportionately. While the BDE of 5-pyrimidinol only increases slightly compared to phenol (89.6 kcal mol^{-1} *vs* 87.1 kcal mol^{-1}), the ionization potential (IP) increases far more dramatically (219.7 kcal mol^{-1} *vs* 195.4 kcal mol^{-1}). The net result in terms of design is that more potent electron rich substituents can be positioned para with respect to the hydroxyl group without decreasing the oxidation potential to untenable levels, meanwhile the electron deficient heteroatoms do not completely counteract the effect of the EDG on the BDE. Among these new RTAs are simple pyrimidinols that surpass the k_{inh} of PMC in

solution, as well as pyridinols inspired by 6-chromanol and 2,3-dihydro-5-hydroxybenzofuran which surpass PMC by nearly 20-fold and 70-fold respectively.[40,41]

Scheme 1.6. Some representative examples of some highly reactive pyridinol/pyrimidinol based RTAs.

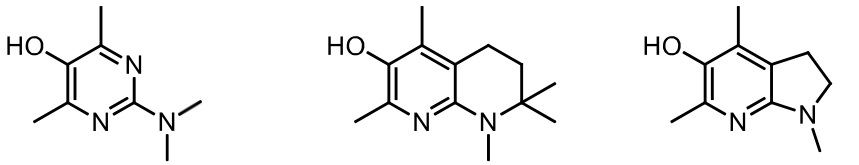

k_{inh} $8.6 \times 10^6\ M^{-1}\ s^{-1}$ $7.8 \times 10^7\ M^{-1}\ s^{-1}$ $2.8 \times 10^8\ M^{-1}\ s^{-1}$

Similar research was conducted with heterocyclic diarylamines where DFT calculations revealed a similar structure electronic relationship between the relative stability of the aminyl radical and radical cation. This approach made it feasible to synthesize and study diarylamine inhibitors that were orders of magnitude more reactive than 4,4'-dioctyldiphenylamine, the industrial standard, even achieving enthalpically-barrierless reactions for this class of RTA (log $k_{inh} \sim 7.5 \sim \log A$).[42]

Scheme 1.7. The k_{inh} of a standard ADPA compared to highly reactive heterocyclic diarylamine RTAs.

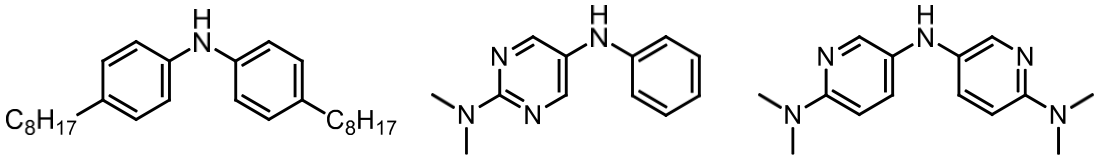

k_{inh} $1.8 \times 10^5\ M^{-1}\ s^{-1}$ $3.0 \times 10^6\ M^{-1}\ s^{-1}$ $3.4 \times 10^7\ M^{-1}\ s^{-1}$

1.2.2 Solvent Effects on Inhibition Rate Constants

Prior to the turn of the century, there was no quantitative way to predict the effect of solvent on H-atom transfer reactions. While it had been observed that the solution C-H

BDEs of hydrocarbons such as 1,4-cyclohexadiene did not significantly differ from the gas phase BDE regardless of the solvent, the same could not be said of the O-H BDE of phenol. For example, while the O-H BDE of phenol in an apolar solvent such as isooctane was measured at 88.2 kcal mol^{-1}, compared to 87 kcal mol^{-1} in the gas phase, the observed O-H BDE in acetonitrile was 95.0 kcal mol^{-1}.[43] Furthermore, the rate of H-atom abstraction from cyclohexane by cumyloxyl radicals was not influenced by the solvent,[12] while the same reaction with phenol and with t-butyl-hydroperoxide was.[44] While it was clear that solvation of phenols could have a dramatic effect on the thermodynamics/kinetics of H-atom transfer, predicting the degree of the effect for different phenol/solvent pairs had not been devised.

Ingold and co-workers sought to develop a framework that would adequately predict the kinetics of essentially any hydrogen abstraction reaction in any solvent, as opposed to the tedious tabulation of rate constants for each reaction pair (radical and H-atom donor) in each solvent system of interest. To that end, based on their observations of the H-atom abstraction from phenol and from t-butyl-hydroperoxide, they proposed the following assumptions:

i) Each H-atom donor (i.e. phenol) can act as a hydrogen-bond donor (HBD) to a single hydrogen-bond acceptor (HBA) solvent molecule forming a corresponding 1:1 complex.

ii) The magnitude of the hydrogen-bond solvation constant (K^S) is independent of the surrounding medium.

iii) A hydrogen atom donor that is engaged in a 1:1 hydrogen-bonded complex is unreactive to H-atom transfer, due to steric reasons.

The rate constant for k_{inh}, or any other H-atom transfer rate constant, assuming the above predissociation model is accurate, can then be expressed as follows:

Scheme 1.8. Proposed model for KSE observed for hydrogen abstraction from HBD species in a HBA solvent.

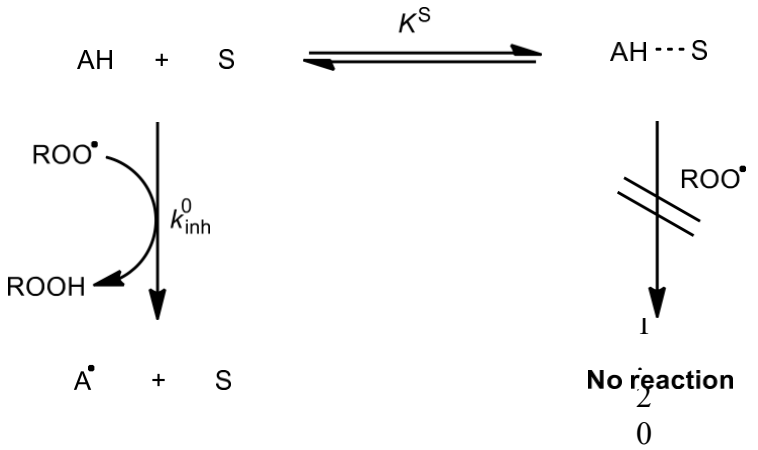

$$k_{inh}^{S} = \frac{k_{inh}^{0}}{1 + K^{S}[\boldsymbol{S}]} \qquad \text{Eq. 1.20}$$

Where k_{inh}^{0} is the inhibition rate constant that would be observed in the absence of predissociation and k_{inh}^{S} is the inhibition rate constant observed in solvent 'S'. While the model seemed to generally describe the KSE observed for the majority of phenol/solvent pairs with different types of radicals (alkoxyl, DPPH, peroxyl), Ingold and co-workers recognized that for this to be a useful predictive model, simple prediction of K^S would be necessary.[45]

A scale for inherent hydrogen-bond basicity for HBA species was initially developed by Taft and co-workers though this was further refined and expanded by Abraham and co-workers in the 1980s to include a complimentary scale for hydrogen-bond acidity of HBD species.[46,47]

$$\log K_f = 7.354\alpha_2^H\beta_2^H - 1.094 \quad \text{Eq. 1.21}$$

Where K_f is the 1:1 complex formation constant (ie $K_f \equiv K^S$), α_2^H is the parameter for hydrogen-bond acidity, and β_2^H is the parameter for hydrogen-bond basicity. Both scales range from 0 to 1, where 0 represents species that do not donate/accept hydrogen-bonds, like alkanes, and approaching 1 are the strongest hydrogen-bond acids ($\alpha_{2\,\mathrm{TFA}}^H = 0.95$) and bases ($\beta_{2\,\mathrm{HMPA}}^H = 1.00$). Through determination of hydrogen abstraction rate constants of 8 different phenols ($0.26 \leq \alpha_2^H \leq 0.73$) in up to 12 different solvents ($0 \leq \beta_2^H \leq 0.49$), the following empirically derived relationship was determined:

$$\log k_{inh}^S = \log k_{inh}^0 - 8.3\alpha_2^H\beta_2^H \quad \text{Eq. 1.22}$$

In principle, if the α_2^H of an RTA is known, and its k_{inh} is determined in a solvent with a known β_2^H, the k_{inh} that will be observed in any other solvent with a known β_2^H can be accurately predicted. α_2^H and β_2^H values have been measured for hundreds of compounds making Eq. 1.22 an especially useful expression. It was noted, however that the proposed model does not account for the polarization of the activated complex which can accelerate hydrogen abstraction in a polar medium. However, this is, as the authors point out, only significant when the α_2^H of the hydrogen atom donor is particularly low such as in the case glutathione (α_2^H = 0.00) reacting with an alkyl radical, where an increase in rate constant is observed with increasing solvent polarity. Apart from such fringe cases, the magnitude of K^S dominates the behaviour of the observed hydrogen abstraction kinetics.

1.2.3 The Catalytic Trapping Ability of Diarylamines at Elevated Temperatures

While diarylamine antioxidants may have a smaller academic mindshare than phenolic ones, this is not a reflection of their effectiveness as RTAs or practical utility, particularly at elevated temperatures. A typical phenol will trap 2 radical chains before expiring ($n = 2$)[49] as does diphenylamine (DPA) – at least at 65 °C in styrene.[50] At elevated temperatures (≥ 100 °C) diarylamine RTAs are characterized by unusually protracted inhibition times, an observation that was first explicitly demonstrated by Bolsman et. al who calculated a stoichiometry of n = 52 for 4,4'-di-tert-butyldiphenylamine in the inhibited autoxidation of paraffin oil at 130 °C.[51] It was clear that the first radical chain must be quenched by the transfer of the H-atom from the amine to a peroxyl, and that a second peroxyl likely adds to the aminyl forming an adduct which quickly decomposes into the respective alkoxyl and nitroxide radicals, but the fate of the nitroxide and its potential role in radical trapping catalysis was ambiguous. At lower temperatures, it was proposed that the nitroxide trapped another peroxyl radical or possibly an alkyl radical to terminate the second chain (Scheme 1.9 A).

Scheme 1.9. (A) The proposed non-catalytic fates of nitroxides derived from diphenylamine. **(B)** The proposed cycle of regeneration for catalytic diarylamine RTAs (Korcek Cycle).

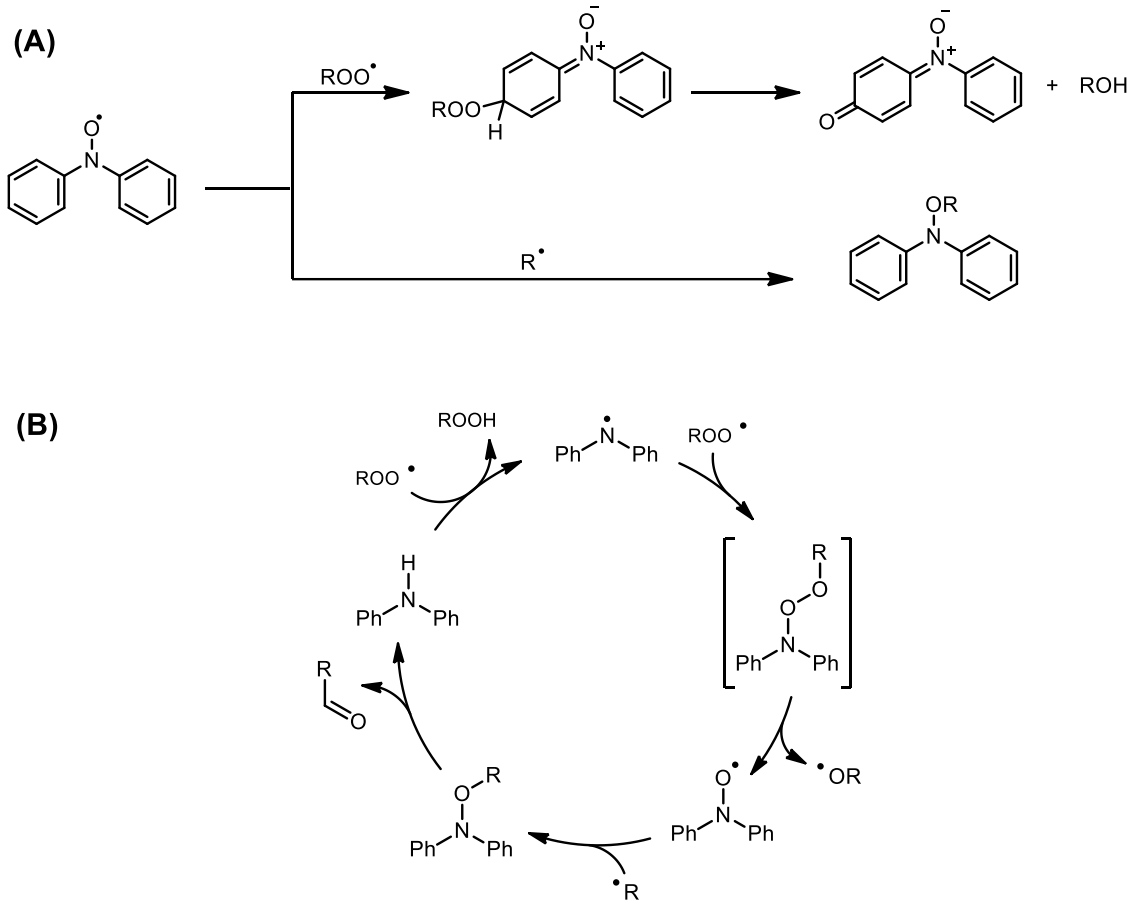

The most coherent mechanistic proposal provided for the fascinating catalytic activity was put forth by Korcek and co-workers in 1995 (Scheme 1.9 B).[52] They proposed that the diarylamine could be regenerated from the corresponding alkoxyamine via N-O homolysis followed by in-cage disproportionation to render the diarylamine and a ketone/aldehyde. The "Korcek Cycle" is supported by several experimental observations:

i) An inhibited autoxidation of pre-oxidized hexadecane, ($[ROOH]_0$ = 11 mM, T = 160 °C, 100% O_2) with 4,4'-di-octyl-diphenylamine ($[Ar_2NH]_0$ = 0.38 mM) showed a linear decrease in amine concentration which was completely

depleted by 4500 seconds. A small amount of the nitroxide was detectable by EPR, peaking at ~1000 seconds ($[Ar_2NO]_{1000}$ ~ 25 μM).

ii) If the nitroxide was added initially ($[Ar_2NO]_0$ = 0.41 mM) instead of the amine, the nitroxide was depleted in ~1200 seconds and the amine accumulated, peaking at ~1100 seconds ($[Ar_2NH]_{1100}$ ~ 0.20 mM) and being consumed entirely by 4500 seconds.

iii) When the atmosphere was exchanged for 10% oxygen, the nitroxide was depleted by ~900 seconds, with the amine peaking at ~1000 seconds ($[Ar_2NH]_{1000}$ ~ 0.31 mM).

If the proposed mechanism is correct, these observations suggest that the initial reaction of the amine must be rate limiting. Particularly experiments ii) and iii) demonstrate that the concentration of oxygen has a dramatic effect on the rate at which nitroxide is converted to amine. This supports the proposal that the amine is regenerated via the alkoxyamine, as the reduced concentration of oxygen enables the combination of nitroxide and alkyl radicals. In addition to these observations, the authors explicitly demonstrate that the corresponding alkoxyamines are stable at 90 ºC, but decompose rapidly at 120 ºC rendering approximately a 64% conversion to the amine.

The original mechanistic proposal for regeneration of the amine from the alkoxyamine, i.e. by homolysis and in-cage disproportionation, was re-evaluated by Haidasz et al. in 2014.[53] Experimental evidence and computational predictions supported the homolysis disproportionation mechanism as being feasible and indeed favoured with the non-allylic alkoxy-diphenylamine. However, a concerted 6-electron pericyclic mechanism, described as a retro-carbonyl-ene reaction, prevailed for allylic alkoxy-

diphenylamine and non-allylic alkoxy-N-phenyl-β-naphthylamine. The experimental evidence for the divergent mechanisms was rather overwhelming, with rate constants of decomposition and Arrhenius parameters that were highly consistent with a less entropically demanding homolysis reaction (log A ~ 15.1) and a concerted pericyclic transition state (log A ~ 13.2). Even more compelling was when the alkoxyamine hydrocarbon was deuterated, for the non-allylic alkoxy-diphenylamine there was no incorporation of deuterium upon decomposition, while the allylic alkoxy-diphenylamine had a 49% incorporation at the 1 position of the diarylamine when decomposed at 90 ºC. Based on the experimental evidence they concluded that the mechanism of alkoxyamine decomposition was very important in regards to the efficiency of regeneration, noting that the alkoxyamine which favoured the homolysis pathway had a distinctly lower time of inhibition compared to an equivalent amount of diphenylamine in the inhibited autoxidation of hexadecane at 160 ºC, while the alkoxyamine which followed the retro-carbonyl-ene mechanism inhibited for the same amount of time as the diphenylamine. While N-phenyl-β-naphthylamine was found to be a worse inhibitor in general compared to diphenylamine, the alkoxyamines derived from it strongly favoured the retro-carbonyl-ene mechanism which demonstrated that structure of the amine could be tuned to favour this more sustainable reaction pathway.

Scheme 1.10. (A) The activation energies and Arrhenius parameters for the decomposition of diphenylamine and N-phenyl-β-naphthylamine derived alkoxyamines. **(B)** The retro-carbonyl-ene reaction pathway.

A

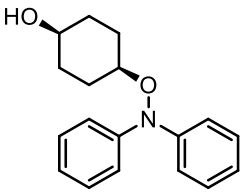

$k_d^{120C} = 4.1 \times 10^{-5}\ s^{-1}$
$E_a = 35.1 \pm 0.7$ kcal mol^{-1}
log A = 15.1 ± 0.4

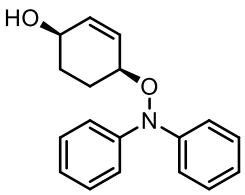

$k_d^{120C} = 2.4 \times 10^{-4}\ s^{-1}$
$E_a = 30.2 \pm 0.7$ kcal mol^{-1}
log A = 13.2 ± 0.4

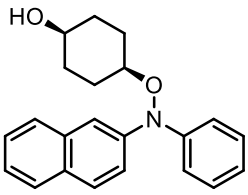

$k_d^{120C} = 6.4 \times 10^{-4}\ s^{-1}$
$E_a = 29.0 \pm 0.4$ kcal mol^{-1}
log A = 12.9 ± 0.2

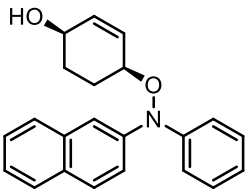

$k_d^{120C} = 2.1 \times 10^{-5}\ s^{-1}$
$E_a = 28.2 \pm 0.4$ kcal mol^{-1}
log A = 13.0 ± 0.3

B

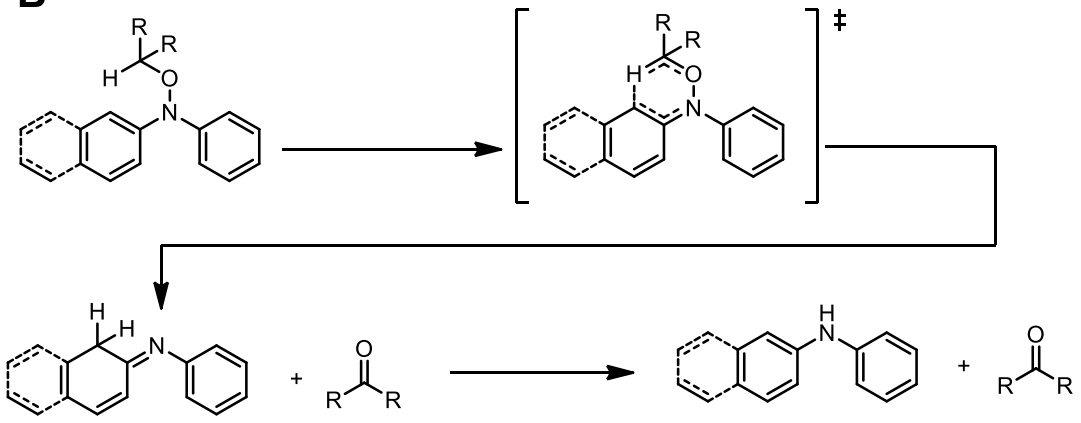

The Korcek Cycle framework has been rather useful in furthering the study of catalytic diarylamines. Under the working hypothesis that alkylated diphenylamine (ADPA) RTAs, like those used in high performance lubricants, are rate-limited by the formation of the aminyl radical, the Pratt Research Group began to conduct high temperature experiments with diarylamines with higher k_{inh}. Specifically, the aforementioned heterocyclic diarylamines seemed to be the logical candidates for investigation as many of them showed significant improvement in their k_{inh} relative to ADPA, while not being excessively susceptible to single electron oxidation.[42] Initially, the results were rather disappointing as the authors discovered that in hexadecane at 160 °C that none of the tested heterocyclic diarylamines performed significantly better than ADPA.

Scheme 1.11. ADPA compared to various heterocyclic diarylamines at 160 °C in hexadecane with 1 mM TTBP.

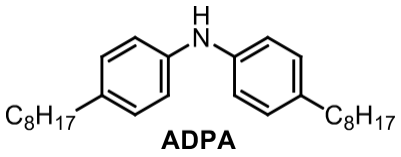

ADPA

k_{inh} = 1.8 x 10^5 M^{-1} s^{-1}
E_{pa} = 1.02 V
$\Delta t_{2\%}$ = 534 s

1.1

k_{inh} = 3.0 x 10^4 M^{-1} s^{-1}
E_{pa} = 1.55 V
$\Delta t_{2\%}$ ~ 0 s

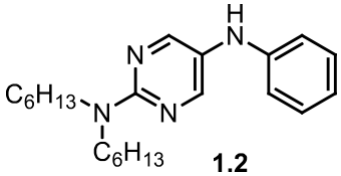

1.2

k_{inh} = 3.0 x 10^6 M^{-1} s^{-1}
E^0 = 0.81 V
$\Delta t_{2\%}$ = 6651 s

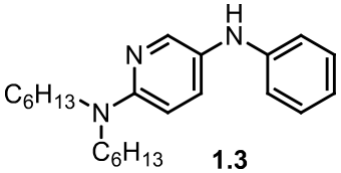

1.3

k_{inh} = 1.1 x 10^7 M^{-1} s^{-1}
E^0 = 0.60 V
$\Delta t_{2\%}$ = 2161 s

With further experimentation, it was discovered that carboxylic acids formed as a product of the autoxidation interfered with the functionality of the heterocyclic diarylamines due to the formation of their corresponding conjugate acids. It was proposed that the pyridinium/pyrimidinium containing diarylamines are entirely inactive as RTAs due to an anticipated sharp increase in BDE. Addition of 1 mM of 2,4,6-tri-tert-butylpyridine (TTBP) as a base additive to the hexadecane buffered the system against acid formation increasing the inhibition time drastically.[54] Representative results from the hexadecane autoxidations inhibited by 40 μM of diarylamine are given in Scheme 1.11.

Where E_{pa} is the anodic peak potential relative to NHE (used in lieu of E^0 for non-reversible oxidations), E^0 is the half-wave potential relative to NHE, and $\Delta t_{2\%}$ is the delay between [ROOH] = 10 mM (the initial amount of tetralin hydroperoxide initiator) and the accumulation of hydroperoxide to achieve [ROOH] = 68 mM (=2%) relative to an uninhibited autoxidation. Pratt and co-workers noted some rather interesting relationships between oxidation potential, k_{inh}, and inhibition time. The slowest of these compounds (**1.1**) has a k_{inh} which is ~6-fold lower with respect to ADPA and showed essentially no inhibition under these experimental conditions. The best performer (**1.2**) is ~17-fold greater than ADPA in terms of k_{inh} and inhibited >12-fold greater than ADPA in terms of $\Delta t_{2\%}$. The fastest of these compounds (**1.3**) has a k_{inh} which is ~60-fold greater than ADPA, however it regresses in performance relative to (**1.2**) having only 1/3 the inhibition time. Compound **1.1** highlights the importance of k_{inh} in terms of having an effective catalyst, and **1.3** demonstrates the issues associated with low oxidation potentials. The authors demonstrated that at 160 ^{o}C in hexadecane continuously purged with O_2 and in the absence of initiator

that **1.3** had a half-life of ~22 minutes while ADPA, **1.1**, and **1.2** did not decompose significantly.

In short, **1.2** showed substantially improved performance compared to the current commercial standard which generated renewed research interest in diarylamine inhibitors. Having examined the diarylamines of both extremes, very electron-rich (**1.3**) and very electron-poor (**1.1**) as well as many compounds in between, it appeared that the key to further improvement in performance was to design an aromatic amine RTA having an $E^0 \geq 0.8$ V that was even faster than **1.2**, as it was assumed that such compounds would recycle even faster and would better suppress the accumulation of hydroperoxide.

1.2.4 Tricyclic Aromatic Amines

The pursuit of a superior catalytic diarylamine prompted us to expand our investigation of diarylamines to include other related scaffolds. A rather interesting report by Lucarini et al. on the topic of tricyclic aromatic amines was published in 1999.[34] Specifically, they reported on the N-H BDE and rate constants for reactions with alkyl and peroxyl radicals for a number of aromatic amines including diphenylamine, phenoxazine, phenoselenazine, iminostilbene, and some substituted phenothiazines which are given in Table 1.3. The authors cite the numerous instances where tricyclic aromatic amines can be applied as effective RTAs in both industrial[55,56] and biological[57] contexts, but also note that:

"*Despite the great potential and practical interest for this class of molecules not much is known about their homolytic reactivity and data available in the literature are often contradictory.*"

Table 1.3. The N-H BDEs, k_H R˙, and k_{inh} for diphenylamine and the tricyclic aromatic amines measured by Lucarini *et al*.[34]

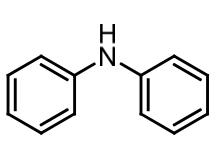

1.4

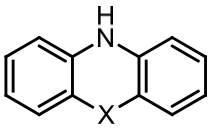

1.5 X = O
1.6 X = S
1.7 X = Se

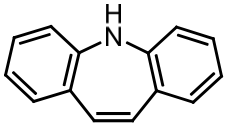

1.8

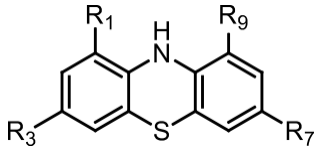

1.9 $R_3 = R_7$ = OMe **1.12** $R_3 = R_7$ = Cl
1.10 $R_3 = R_7$ = t-Bu **1.13** $R_3 = R_7 = NO_2$
1.11 $R_1 = R_9$ = Me

Compound	N-H BDE (kcal mol^{-1})	k_H (M^{-1} s^{-1}) R˙	k_{inh} (M^{-1} s^{-1})
1.4	84.7	_	1.5×10^4
1.5	76.1	4.8×10^5	2.9×10^7
1.6	78.2	6.0×10^4	8.8×10^6
1.7	79.3	2.2×10^4	3.2×10^6
1.8	81.3	_	3.7×10^4
1.9	75.1	2.7×10^6	5.0×10^7
1.10	77.0	8.0×10^4	1.2×10^7
1.11	76.6	2.1×10^4	1.4×10^5
1.12	78.7	3.6×10^4	5.1×10^6
1.13	79.9	_	_

During the massive expansion of the industrial antioxidant sector in the 1950's and 60's, phenothiazine (**1.6**) was an additive of great interest due to the long periods of inhibition observed relative to its weight (i.e. high stoichiometry),[58] though it developed a reputation for producing sludgy deposits particularly at temperatures above 150 °C,[59–61] making it untenable for high temperature applications. Phenothiazine has been successfully deployed in some lower temperature applications to great effect, which is

consistent with what Lucarini et al. observed which is that phenothiazine is very reactive with peroxyl radicals (k_{inh} = 8.8 × 10^6 M^{-1} s^{-1}). Examining phenothiazine against the heterocyclic diarylamine **1.2** makes for an interesting comparison as phenothiazine is ~3-fold greater in terms of k_{inh} however the E^0 of phenothiazine (E^0 = 0.82 V) is almost identical to that of **1.2** (E^0 = 0.81 V). A similar comparison between 3,7-dimethoxyphenothaizne (**1.9**) and heterocyclic diarylamine **1.3** shows a ~4.5-fold greater inhibition rate constant for the phenothiazine (k_{inh} = 5.0 × 10^7 M^{-1} s^{-1}) but again they have identical half-wave potentials (E^0 = 0.60 V). Perhaps the most intriguing compound among the tricyclic aromatic amines characterized by Lucarini et al. was phenoxazine. The k_{inh} of phenoxazine was nearly *10-fold* greater than that **1.2** and again, as determined by Kowert *et al.*,[62] has a similar half-wave potential (E^0 = 0.83 V). Moreover, phenoxazine was characterized by an abnormally high stoichiometry in the inhibited autoxidation of styrene (n = 5) particularly considering that the experiment was conducted at only 50 ºC and normally diarylamines are reported to have a n = 2 in that temperature range. Moreover, an explanation regarding the high ratio between k_{inh} and E^o seen in phenoxazine and phenothiazine when compared to similarly reactive diarylamines is lacking.

1.3 Research Objectives

The exciting catalytic activity of the heterocyclic diarylamines[54] suggested that other amine scaffolds that possess high k_{inh}, while not being excessively oxidizable, could be similarly impressive as catalytic RTAs. The limited, but compelling, results for phenoxazine suggested that this scaffold would be an ideal candidate to study, especially considering the apparent superiority of phenoxazine in the metrics that were considered central to the design strategy (high k_{inh} and high E^o). Additionally, it was observed that the most electron-rich diarylamines demonstrated log k_{inh} values no greater than ~7.5, and Arrhenius plots of a handful of diarylamines indicated a log A between 6.9 and 7.1.[42] This data suggested that a hard entropic limit for diarylamine was hit at log $A \leq 7.5$, and we hypothesized that using a tricyclic scaffold like phenothiazine or phenoxazine would allow us to surpass this entropic limit. Very little was known outside of the values published by Lucarini et al. making it a line of inquiry that could serve to fill this 'gap' in the literature. One challenge recognized early on was the fact that the unsubstituted phenoxazine was too efficient of an inhibitor for an accurate measurement of k_{inh} with our in-house tools,[63] let alone being able to measure more electron-rich members of the family. Specifically we aimed to do the following:

i) Develop a convenient strategy for the accurate measurement of the peroxyl radical-trapping kinetics (*i.e.* k_{inh}) of phenoxazines and other highly reactive RTAs (*i.e.* log k_{inh} >7).

ii) Investigate the factors responsible for the increasing ratio of k_{inh} and E^0 when comparing similarly-substituted diarylamines, phenothiazines and phenoxazines.

iii) Determine the extent to which the restricted rotational freedom of the phenyl moieties in the tricyclic aromatic amines affect their fundamental reactivity.

iv) Based on the previous comparisons between ADPA and **1.2** at elevated temperatures, we predicted that a phenoxazine derived RTA would be an ideal candidate for a superior catalytic RTA as phenoxazine was much more reactive towards peroxyl radicals compared to **1.2** but maintained a similar resistance to single-electron oxidation. We wanted to explore an electronically diverse set of substituted phenoxazines in this regard.

v) Determine the reactivity of substituted phenoxazines at high temperatures to further assess the influence of k_{inh} and E^{o} on catalytic turnover.

vi) In light of the association of lipid autoxidation (peroxidation) with disease and aging, and the preventive role of RTAs such as α-tocopherol, we sought to assess the general efficacy of phenoxazine RTAs to inhibit lipid peroxidation and associated cell death.

1.4 References

(1) Bateman, L. *Q. Rev. Chem. Soc.* **1954**, *8*, 147.

(2) Bolland, J. L. *Q. Rev. Chem. Soc.* **1948**, *3*, 1.

(3) Jensen, R. K.; Korcek, S.; Zinbo, M.; Johnson, M. D. *Int. J. Chem. Kinet.* **1990**, *22*, 1095.

(4) Jensen, R. K.; Korcek, S.; Mahoney, L. R.; Zinbo, M. *J. Am. Chem. Soc.* **1979**, *101*, 7574.

(5) Pryor, W. A.; Porter, N. A. *Free Radic. Biol. Med.* **1990**, *8*, 541.

(6) Yin, H.; Xu, L.; Porter, N. A. *Chem. Rev.* **2011**, *111*, 5944.

(7) Finkel, T.; Holbrook, N. J. *Nature* **2000**, No. 408, 239.

(8) Di Paolo, G.; Kim, T.-W. *Nat. Rev. Neurosci.* **2011**, *12*, 284.

(9) Barnham, K. J.; Masters, C. L.; Bush, A. I. *Nat. Rev. Drug Discov.* **2004**, *3*, 205.

(10) Hussain, S. P.; Hofseth, L. J.; Harris, C. C. *Nat. Rev. Cancer* **2003**, *3*, 276.

(11) Baker, J. R.; Benson, S. W.; Golden, D. M. *Int. J. Chem. Kinet.* **1977**, *9*, 31.

(12) Avila, D. V.; Brown, C. E.; Ingold, K. U.; Lusztyk, J. *J. Am. Chem. Soc.* **1993**, *115*, 466.

(13) Sasaki, H.; Nagayama, M. *J. Appl. Polym. Sci.* **1967**, *11*, 2097-2108.

(14) Maillard, B.; Ingold, K. U.; Scaiano, J. C. *J. Am. Chem. Soc.* **1983**, *105*, 5095.

(15) Korcek, S.; Chenier, J. H. B.; Howard, J. A.; Ingold, K. U. *Can. J. Chem.* **1972**, *50*, 2285.

(16) Jensen, R. K.; Korcek, S.; Zinbo, M. *Int. J. Chem. Kinet.* **1994**, *26*, 673.

(17) Howard, J. A.; Ingold, K. U. *Can. J. Chem.* **1967**, *45*, 793.

(18) Howard, J. A.; Ingold, K. U. *Can. J. Chem.* **1969**, *47*, 3809.

(19) Russell, G. A. *J. Am. Chem. Soc.* **1957**, *79*, 3871.

(20) Lindsay, D.; Howard, J. A.; Horswill, E. C.; Iton, L.; Ingold, K. U.; Cobbley, T.; Ll, A. *Can. J. Chem.* **1973**, *51*, 870.

(21) Howard, J. A.; Bennett, J. E. *Can. J. Chem.* **1972**, *50*, 2374.

(22) Lee, R.; Gryn'ova, G.; Ingold, K. U.; Coote, M. L. *Phys. Chem. Chem. Phys.* **2016**, *18*, 23673.

(23) Howard, J. A.; Ingold, K. U. *Can. J. Chem.* **1965**, *43*, 2729.

(24) Ingold, K. U. *Chem. Rev.* **1961**, *61*, 563.

(25) Ingold, K. U.; Pratt, D. A. *Chem. Rev.* **2014**, *114*, 9022.

(26) Erben-Russ, M.; Bors, W.; Saran, M. *Int. J. Radiat. Biol.* **1987**, *52*, 393.

(27) Howard, J. A.; Ingold, K. U. *Can. J. Chem.* **1963**, *41*, 1744.

(28) Brown, H. C.; Okamoto, Y. *J. Am. Chem. Soc.* **1958**, *80*, 4979.

(29) Mahoney, L. R.; DaRooge, M. A. *J. Am. Chem. Soc.* **1970**, *92*, 890.

(30) Mulder, P.; Saastad, O. W.; Griller, D. *J. Am. Chem. Soc.* **1988**, *110*, 4090.

(31) Bordwell, F. G.; Cheng, J. *J. Am. Chem. Soc.* **1991**, *113*, 1736.

(32) Wayner, D. D. M.; Lusztyk, E.; Ingold, K. U.; Mulder, P. *J. Org. Chem.* **1996**, *61*, 6430.

(33) Brownlie, I. T.; Ingold, K. U. *Can. J. Chem.* **1967**, *45*, 2419.

(34) Lucarini, M.; Pedrielli, P.; Pedulli, G. F.; Valgimigli, L.; Gigmes, D.; Tordo, P. *J. Am. Chem. Soc.* **1999**, *121*, 11546.

(35) Pratt, D. A.; Dilabio, G. A.; Valgimigli, L.; Pedulli, G. F.; Ingold, K. U. *J. Am. Chem. Soc.* **2002**, *124*, 11085.

(36) Hansch, C.; Leo, A.; Taft, R. W. *Chem. Rev.* **1991**, *91*, 165.

(37) Burton, G. W.; Ingold, K. U. *Acc. Chem. Res.* **1986**, *19*, 194.

(38) Burton, G. W.; Doba, T.; Gabe, E.; Hughes, L.; Lee, F. L.; Prasad, L.; Ingold, K. U. *J. Am. Chem. Soc.* **1985**, *107* (24), 7053.

(39) Pratt, D. A.; DiLabio, G. A.; Brigati, G.; Pedulli, G. F.; Valgimigli, L. *J. Am. Chem. Soc.* **2001**, *123*, 4625.

(40) Valgimigli, L.; Bartolomei, D.; Amorati, R.; Haidasz, E.; Hanthorn, J. J.; Nara, S. J.; Brinkhorst, J.; Pratt, D. A. *Beilstein J. Org. Chem.* **2013**, *9*, 2781.

(41) Wijtmans, M.; Pratt, D. A.; Valgimigli, L.; DiLabio, G. A.; Pedulli, G. F.; Porter, N. A. *Angew. Chemie Int. Ed.* **2003**, *42*, 4370.

(42) Hanthorn, J. J.; Amorati, R.; Valgimigli, L.; Pratt, D. A. *J. Org. Chem.* **2012**, *77*, 6895.

(43) Wayner, D. D. M.; Lusztyk, E.; Page, D.; Ingold, K. U.; Mulder, P.; Laarhoven, L. J. J.; Aldrich, H. S. *J. Am. Chem. Soc.* **1995**, *117*, 8737.

(44) Avila, D. V.; Ingold, K. U.; Lusztyk, J.; Green, W. H.; Procopio, D. R. *J. Am. Chem. Soc.* **1995**, *117*, 2929.

(45) Snelgrove, D. W.; Lusztyk, J.; Banks, J. T.; Mulder, P.; Ingold, K. U. *J. Am. Chem. Soc.* **2001**, *123*, 469.

(46) Abraham, M. H.; Grellier, P. L.; Prior, D. V.; Morris, J. J.; Taylor, P. J. *J. Chem. Soc. Perkin Trans. 2* **1990**, 521.

(47) Abraham, M. H.; Grellier, P. L.; Prior, D. V.; Duce, P. P.; Morris, J. J.; Taylor, P. J. *J. Chem. Soc. Perkin Trans. 2* **1989**, 699.

(48) Abraham, M. H. *J. Phys. Org. Chem.* **1993**, *6*, 660.

(49) Boozer, C. E.; Hammond, G. S.; Hamilton, C. E.; Sen, T. N. *J. Am. Chem. Soc.* **1955**, *77*, 3233.

(50) Brownlie, I. T.; Ingold, K. U. *Can. J. Chem.* **1965**, *44*, 861.

(51) Bolsman, T. A. B. M.; Blok, A. P.; Frijns, J. H. G. *Recl. des Trav. Chim. des Pays-Bas* **1978**, *97*, 313.

(52) Jensen, R. K.; Korcek, S.; Zinbo, M.; Gerlock, J. L. *J. Org. Chem.* **1995**, *60*, 5396.

(53) Haidasz, E. A.; Shah, R.; Pratt, D. A. *J. Am. Chem. Soc.* **2014**, *136*, 16643.

(54) Shah, R.; Haidasz, E. A.; Valgimigli, L.; Pratt, D. A. *J. Am. Chem. Soc.* **2015**, *137*, 2440.

(55) Fukuzumi, K.; Ikeda, N.; Egawa, M. *J. Am. Oil Chem. Soc.* **1976**, *53*, 623.

(56) Yamamura, T.; Suzuki, K.; Yamaguchi, T.; Nishiyama, T. *Bull. Chem. Soc. Jpn.* **1997**, *70*, 413.

(57) Cini, M.; Fariello, R. G.; Bianchetti, A.; Moretti, A. *Neurochem. Res.* **1993**, *19*, 283.

(58) Murphy, C. M.; Ravner, H.; Smith, N. L. *Ind. Eng. Chem.* **1950**, *42*, 2479.

(59) Adams, H. W. In *ASLE Meeting*; Cincinnati, Ohio, 1960; p 60AM 3B-3.

(60) Elliot, J. S.; Edwards, E. D. *Inst. Pet.* **1961**, *47*, 39.

(61) Strange, H. O.; McGrath, J. J.; Pellegrini, J. P. *Ind. Eng. Chem. Prod. Res. Dev.* **1967**, *6*, 33.

(62) Kowert, B. A.; Marcoux, L.; Bard, A. J. *J. Am. Chem. Soc.* **1972**, *94*, 5538.

(63) Haidasz, E. A.; Van Kessel, A. T. M.; Pratt, D. A. *J. Org. Chem.* **2016**, *81*, 737.

CHAPTER 2: Phenoxazine: A Privileged Scaffold for Radical-Trapping Antioxidants

2.1 Preface

Diphenylamines are widely used to protect petroleum-derived products from autoxidation. Their efficacy as radical-trapping antioxidants (RTAs) relies on a balance of fast H-atom transfer kinetics and stability to one electron oxidation by peroxidic species. Both H-atom transfer and one-electron oxidation are enhanced by substitution with electron-donating substituents, such as the S-atom in phenothiazines, another important class of RTA. Herein we report the results of our investigations of the RTA activity of the structurally-related, but essentially ignored, phenoxazines. We find that the H-atom transfer reactivity of substituted phenoxazines follows an excellent Evans-Polanyi correlation spanning $k_{inh}^{37℃}$ = 4.5×10^6 M^{-1} s^{-1} and N-H BDE = 77.4 kcal mol^{-1} for 3-CN,7-NO_2-phenoxazine to $k_{inh}^{37℃}$ = 6.6×10^8 M^{-1} s^{-1} and N-H BDE = 71.8 kcal mol^{-1} for 3,7-$(OMe)_2$-phenoxazine. The reactivity of the latter compound is the greatest of any RTA ever reported, and is likely to represent a reaction without enthalpic barrier since log *A* for this reaction is likely ~8.5. The very high reactivity of most of the phenoxazines studied required the determination of their kinetic parameters by inhibited autoxidations in the presence of a very strong H-bonding co-solvent (DMSO), which slowed the observed rates by up to two orders of magnitude by dynamically reducing the equilibrium concentration of (free) phenoxazine as an H-atom donor. Despite their remarkably high reactivity toward peroxyl radicals, the phenoxazines were found to be comparatively stable to one-electron oxidation relative to diphenylamines and phenothiazines ($E°$ ranging from 0.59 V to 1.38 V *vs.* NHE). Thus, phenoxazines with comparable oxidative stability to commonly used diphenylamine and

phenothiazine RTAs had significantly greater reactivity (by up to 2 orders of magnitude). Computations suggest that this remarkable balance in H-atom transfer kinetics and stability to one electron oxidation results from the ability of the bridging oxygen atom in phenoxazine to serve as both a π-electron donor to stabilize the aminyl radical and σ-electron acceptor to destabilize the aminyl radical cation. Perhaps most excitingly, phenoxazines have "non-classical" RTA activity – where they trap >2 peroxyl radicals each – *at ambient temperatures*. This chapter comprises the manuscript of the same title published in the Journal of Organic Chemistry (Farmer, L. A.; Haidasz, E. A.; Griesser, M.; Pratt, D. A. J. Org. Chem. 2017, 82, 10523-10536.) The computations and concept regarding the dualistic role of the heteroatom bridge on the relative stabilities of the aminyl radical and the radical cation were contributed by former Ph.D. student Evan Haidasz and calculations of the BDE and IP were contributed by Dr. Markus Griesser.

2.2 Introduction

Autoxidation, the radical-mediated chain reaction responsible for the spontaneous oxidation of hydrocarbons, is a ubiquitous process limiting the longevity of all living things and petroleum-derived materials. Radical trapping antioxidants (RTAs) compete with propagation of the autoxidation chain reaction by H-atom transfer to a chain-carrying peroxyl radical (Eq. 2.1).[1,2] Subsequent reaction of the RTA-derived radical with another chain-carrying peroxyl radical can inhibit a second chain reaction (Eq. 2.2). The efficacy of RTAs is largely governed by two metrics: the rate constant of the initial H-atom transfer reaction (the inhibition rate constant, k_{inh}) and the number of chains that are broken (the inhibition reaction stoichiometry, n).

$$\text{A-H} + \text{ROO}^{\bullet} \rightarrow \text{A}^{\bullet} + \text{ROOH} \qquad \text{Eq. 2.1}$$

$$\text{A}^{\bullet} + \text{ROO}^{\bullet} \rightarrow \text{non-radical products} \qquad \text{Eq. 2.2}$$

Among the most widely-used RTAs are substituted phenols (e.g. butylated hydroxytoluene, BHT) and diphenylamines (e.g. alkylated diphenylamines, ADPAs). The reactivity of both classes of RTA obey good Evans-Polanyi relationships, where decreases in the phenolic O-H and aminic N-H bond dissociation enthalpies (BDEs) brought about by substitution of the aryl ring(s) with electron-donating groups (EDGs) give rise to larger k_{inh}.[3,4] The drop in BDE associated with the introduction of EDGs is accompanied by a drop in E° and concomitant stability to one electron oxidation (by product hydroperoxides or O_2), which can lead to production of radical species rather than their trapping. Thus, achieving a balance of reactivity to H-atom transfer and stability to one-electron oxidation must be at the center of any RTA development strategy.

Although the structure-reactivity relationships in phenolic RTAs have been extensively studied, diphenylamines have been comparatively less well-investigated.[2,5–8] Of the existing work in this area, the careful thermochemical and kinetic studies of the reactivity of phenothiazines – diphenylamines (**2.1**) fused together by a central thiazine ring (**2.2**) – by Lucarini *et al* is particularly noteworthy.[6] They showed that phenothiazine has an N-H bond that is 6.5 kcal/mol weaker than in diphenylamine (78.2 *vs.* 84.7 kcal mol^{-1})[9] and a ~600-fold greater reactivity toward peroxyl radicals (k_{inh} = 8.8 × 10^6 *vs.* 1.5 × 10^4 M^{-1} s^{-1} at 50 °C). Introduction of electron-donating methoxy substituents *para* relative to the aminic N-H further decreased the N-H BDE by 3.1 kcal mol^{-1} and further increased k_{inh} by ~6-fold to 5.0 × 10^7 M^{-1} s^{-1} – the largest k_{inh} ever reported for a diarylamine.[10]

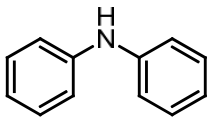

2.1

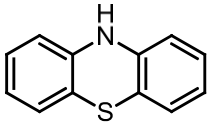

2.2

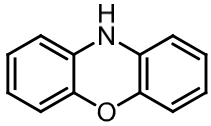

2.3

In the same manuscript, Lucarini et al. presented corresponding data for phenoxazine (**2.3**), revealing that it possessed an even weaker N-H bond than phenothiazine (76.1 *vs.* 78.2 kcal mol^{-1})[9] and a correspondingly greater k_{inh} of 2.9 × 10^7 M^{-1} s^{-1}. No substituted phenoxazines were investigated. Perhaps most interestingly, while phenothiazine and the substituted phenothiazines that were investigated trapped ~2 peroxyl radicals each in inhibited autoxidations (i.e. $n \sim 2$), phenoxazine apparently trapped five. This was not explained. Moreover, although not pointed out at the time, despite its greater reactivity and stoichiometry, phenoxazine is (marginally) more stable to one-electron oxidation than phenothiazine (*vide infra*).[11] Hence, it would appear that phenoxazine is a privileged scaffold for RTA design and development. Herein we describe

our efforts to characterize the structure-reactivity relationships in phenoxazines as RTAs, from which it is revealed that they are privileged structures with compelling prospects for real-world applications.

2.3 Results

2.3.1 Exploiting Kinetic Solvent Effects to Clock the Fastest RTAs

The very high reactivity of phenoxazine to peroxyl radicals makes precise quantitation of the kinetics of the reaction challenging. Determination of inhibition rate constants of this magnitude (mid-10^7 $M^{-1}s^{-1}$) requires pushing the venerable inhibited autoxidation approach,[12,13] by which reaction progress is generally monitored by O_2 consumption, to its limit. Our own variation of the inhibited autoxidation approach,[14] in which a small amount of a highly absorbing co-substrate (PBD-BODIPY, Figure 1A) is added to the reaction mixture as a signal carrier, has an even lower limit ($k_{inh} \leq 10^7$ M^{-1} s^{-1}) due to the inherent reactivity of the co-substrate to peroxyl radicals (i.e. k_{BODIPY}= 2720 M^{-1} s^{-1} in styrene/chlorobenzene) and the maximum PBD-BODIPY concentration that can be achieved without saturating the photomultipliers in a conventional spectrophotometer (10 μM). Indeed, phenoxazine completely inhibits PBD-BODIPY consumption in styrene autoxidations in chlorobenzene under standard conditions (black trace, Figure 1B), precluding determination of k_{inh} from the initial rate (Eq. 3) as in Figure 1C.[14]

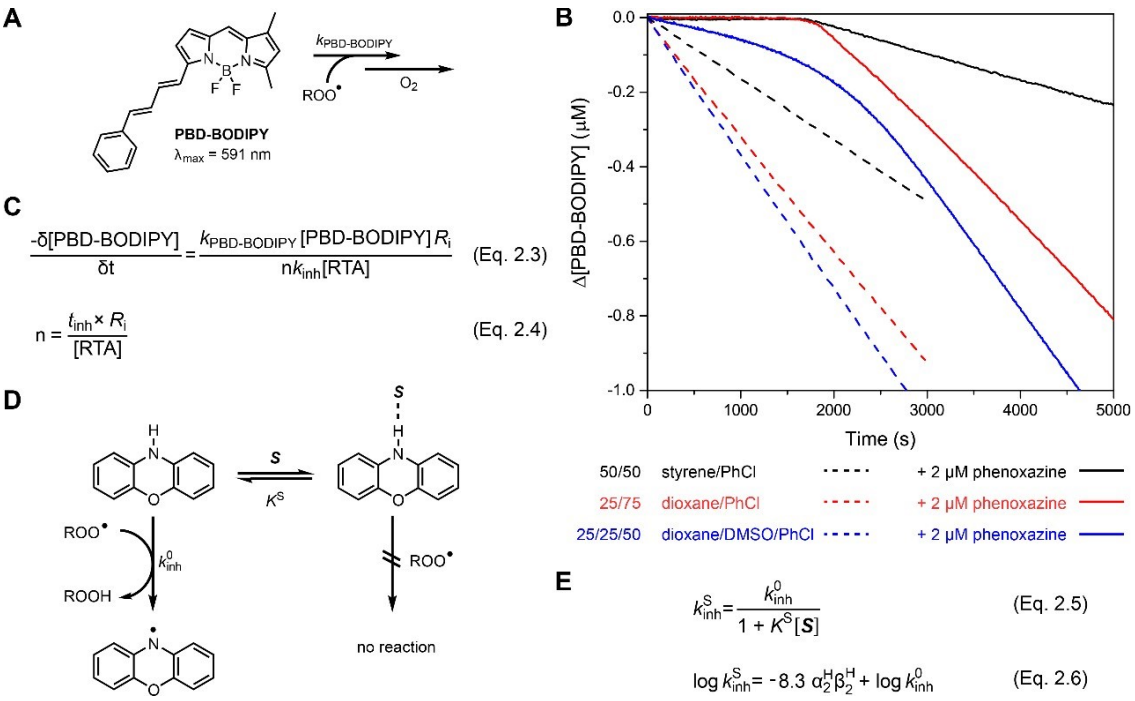

Figure 2.1. (**A**) PBD-BODIPY is used as a signal carrier in the autoxidation of styrene or 1,4-dioxane. (**B**) Co-autoxidation of styrene (4.3 M) and PBD-BODIPY (10 μM) in PhCl (black), 1,4-dioxane (2.9 M) in PhCl, and 1,4-dioxane (2.9 M) in 2:1 PhCl:DMSO initiated with 6 mM AIBN at 37 °C. Reaction progress was monitored at 591 nm (ε = 139 000 M^{-1} cm^{-1}), 587 nm (ε = 123 000 M^{-1} cm^{-1}), and 587 nm (ε = 118 200 M^{-1} cm^{-1}), respectively. (**C**) Rate constants (k_{inh}) and stoichiometries (n) for the reactions of inhibitors (RTAs) with chain-carrying peroxyl radicals can be determined from the initial rates and the duration of the inhibited periods as in Eqs. 2.3 and 2.4, respectively. (**D**/**E**) The equilibrium between 'free' RTA (illustrated by phenoxazine) and RTA participating in a 1:1 hydrogen-bond complex with arbitrary solvent *S*. Assuming the 1:1 complex does not react with peroxyl radicals, the kinetics of radical-trapping can be described as in Eq. 2.5 or Eq. 2.6.

In an attempt to circumvent this limitation, we exchanged styrene for an oxidizable substrate that would make H-bonds with phenoxazine (Figure 2.1D). This would lower the (free) concentration of phenoxazine in solution, thereby increasing the rate of the inhibited autoxidation such that it could be reliably measured. Ingold has shown that the kinetics of H-atom transfer reactions are retarded in a wholly predictable fashion in H-bond accepting

media, wherein the kinetics obey a pre-dissociation model as in Eq. 5 in Figure 1E.[15,16] Thus, if the equilibrium constant for H-bond formation between phenoxazine and the substrate (K_{HB}) is known, the rate constant for its reaction in the absence of strong H-bonding interactions (k_{inh}^{0}) can be derived from the observed rate constant (k_{inh}^{S}). This expression can be recast using Abraham's H-bond acidity (α_2^H)[17] and H-bond basicity (β_2^H)[18] parameters – which generally range from 0 to 1 – as in Eq. 2.6, a relationship that has been shown to hold for a variety of H-atom transfer reactions under a variety of conditions.

Thus, styrene was exchanged for dioxane as the oxidizable substrate. Dioxane is relatively easily oxidized (k_p = 0.5 M^{-1} s^{-1})[19] – ensuring that a free radical chain reaction is maintained in the autoxidation – and is also a good H-bond acceptor (β_2^H = 0.41).[18] However, using dioxane as the substrate was insufficient to decrease the rate of the phenoxazine-inhibited autoxidation to a measurable level (Figure 1D). Hence, an even stronger H-bond acceptor was added as a co-solvent: DMSO (β_2^H = 0.78).[18] Upon doing so, the inhibited autoxidation clearly proceeded with a non-zero slope. Derivation of k_{inh} from the initial rate required determination of k_{BODIPY} in this solvent system (5900 M^{-1} s^{-1}, see Supporting Information), from which k_{inh}^{DMSO}= (5.3 ± 0.5) × 10^5 M^{-1} s^{-1} could be derived using Eq. 2.3.

To correct for the H-bonding interaction of phenoxazine with DMSO, thereby enabling derivation of the inherent reactivity of phenoxazine to peroxyl radicals, required that we determine α_2^H of phenoxazine and β_2^H of the solvent system. While exhaustive compilations of β_2^H parameters exist for a wide array of HBAs, our systems of interest consist of an amalgam of 2 or 3 potential HBDs. A direct approach to β_2^H determination of

a HBA would be to determine K_{HB} using quantitative IR spectroscopy in CCl_4.[20,21] We, however, opted for the ^{19}F NMR method devised by Taft et. al.,[22] where differences in the chemical shift of 4-fluorophenol and 4-fluoroanisole are related directly to K_{HB} (see the Supporting Information for further details). Using this method, an effective β_2^H of 0.35 was determined in 25% v/v dioxane in PhCl and β_2^H of 0.60 in 25% v/v dioxane with 25% v/v DMSO in PhCl.[23]

Similarly, the α_2^H of phenoxazine was determined by ^1H NMR. Abraham and co-workers have established that the chemical shift difference of the acidic proton of an HBD in $CDCl_3$ and *d*$_6$-DMSO obeys an excellent linear relationship with α_2^H (R^2 = 0.938 for 54 different species with a total of 72 different protic functionalities).[24] Unfortunately, we found that phenoxazines are generally characterized by poorly resolved ^1H NMR spectra in $CDCl_3$. However, ^1H NMR spectra in benzene-*d*$_6$ are very well resolved and further, the chemical shift difference of the acidic protons of a variety of HBDs in this solvent relative to *d*$_6$-DMSO were also found to correlate very nicely to α_2^H according to the expression in Eq. 7 (R^2 = 0.972 for 11 different species ranging from α_2^H = 0.08 to 0.82, see ESI for the correlation).

$$\alpha_2^H = 0.134\,\Delta\delta_{DMSO-PhH} - 0.1087 \qquad \text{Eq. 2.7}$$

The determination of $\Delta\delta_{DMSO-PhH}$ for phenoxazine affords α_2^H = 0.44 from this correlation. Using this value of α_2^H, β_2^H = 0.60 for the autoxidation solvent system and k_{inh} = (5.3 ± 0.5) × 10^5 M^{-1} s^{-1} determined from the inhibited autoxidation enables the derivation of k_{inh} = (3.9 ± 0.4) × 10^7 M^{-1} s^{-1} in chlorobenzene (β_2^H = 0.09),[18,25] which is in excellent agreement with the value obtained by Lucarini et al. in that solvent (2.9 × 10^7 M^{-1} s^{-1}).[6]

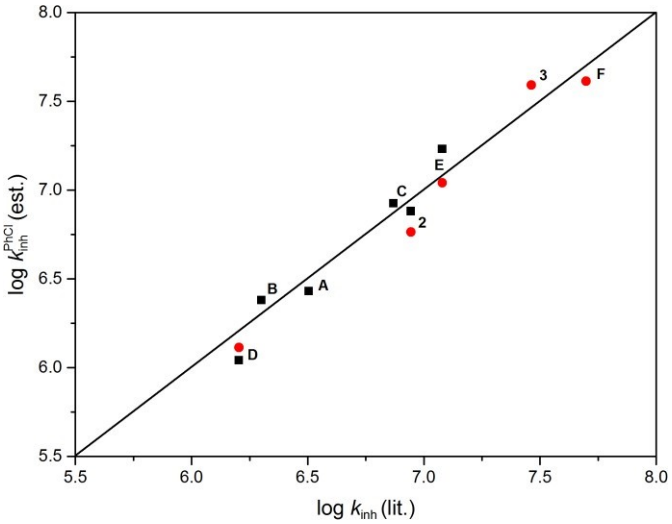

Figure 2.2. Inhibition rate constants derived from dioxane autoxidations in PhCl (black squares) or PhCl/DMSO (red circles) correlate very well with inhibition rate constants directly determined from styrene or 1-hexadecene autoxidations in PhCl. Representative inhibitors: PMC (**A**), 5-hydroxy-2-dimethylaminopyrimidine (**B**), 5-hydroxy-4,6-dimethyl-2-dimethylaminopyrimidine (**C**), 2-methylundecan-2-persulfide (**D**), phenothiazine (**2.2**), 3,7-di-tert-butylphenothiazine (**E**), 3,7-dimethoxyphenothiazine (**F**), phenoxazine (**2.3**). See ESI for full details.

In order to further validate the use of kinetic solvent effects to enable the determination of rate constants for very fast reactions of RTAs with peroxyl radicals, we carried out additional autoxidations inhibited by phenothiazine, 3,7-dimethoxyphenothiazine and 3,7-di-*tert*-butylphenothiazine, as studied by Lucarini et al. by O_2 consumption in the inhibited autoxidation of styrene.[6] Moreover, since these compounds have largely similar HBD ability (α_2^H = 0.34-0.38), we also studied a few examples that were either excellent H-bond donors (two substituted pyrimidinols, α_2^H = 0.56/0.65)[26] or very poor ones (a hydropersulfide, α_2^H = 0.09).[27] The data is shown in Figure 2, along with the data for 2,2,5,7,8-pentamethylchroman-6-ol (PMC), a truncated form of α-tocopherol – Nature's premier RTA and an important benchmark compound in

any RTA study.[28] Overall, the agreement with literature values determined directly in a non-H-bonding solvent (chlorobenzene) is excellent.

2.3.2 Structure-Activity Relationships in Phenoxazines as RTAs

With a methodology established to enable quantitative studies of very fast RTAs, the synthesis of a small library of substituted phenoxazines was carried out in order to evaluate the substituent effects on the parent structure's reactivity. 2-Trifluoromethylphenoxazine **2.4**, 3-trifluoromethylphenoxazine **2.5**, 2-*tert*-butylphenoxazine **2.6**, 3-*tert*-butylphenoxazine **2.7** and 3,7-di-*tert*-butylphenoxazine **2.8**, were each synthesized via intramolecular Cu-catalyzed Ullman-type couplings of the acetamido and bromo/iodo functionalities of corresponding diaryl ethers as in Scheme 2.1A.

2,4,6,8-Tetra-*tert*-butylphenoxazine **2.9** was synthesized by reduction of 2,4-di-*tert*-butyl-6-nitrophenol followed by self-condensation in acetic acid with zinc dust in a manner previously described.[29] 2,8-Di-*tert*-butylphenoxazine **2.10** was synthesized by the same method (Scheme 2.1B).

N,N-Diethyl-3-sulfonamidephenoxazine **2.11**, 3-cyanophenoxazine **2.12**, and 3-methoxy-7-nitrophenoxazine **2.13** were obtained by S_NAr of the appropriate o-aminophenol on a o-haloaryl/2-nitro-haloaryl (Scheme 2.1C). The formation of the diaryl ether followed by a Smiles rearrangement brokers an exclusive formation of the phenoxazine derivative wherein the substituent is located para to the reactive N-H.[30,31]

3- Nitrophenoxazine **2.14** and 3-cyano-7-nitrophenoxazine **2.15** were obtained by electrophilic nitration of 10-acetylphenoxazine[32] (with subsequent hydrolysis) and 3-cyanophenoxazine, respectively (Scheme 2.1D). 3-Methoxyphenoxazine **2.16** and 3,7-dimethoxyphenoxazine **2.17** were obtained by alkylation and then hydrolysis of hydroxy-*N*-acetylphenoxazines derived from the reduction and acylation of phenoxazin-3-one and 7-hydroxy-phenoxazin-3-one, respectively (Scheme 2.1E).

Inhibited autoxidations of dioxane in DMSO/PhCl were carried out as described above, with the choice of conditions dictated largely by the α_2^H values determined by NMR. The data are assembled in Table 2.1. As expected, phenoxazines with electron-withdrawing groups (EWGs) had substantially higher α_2^H parameters than phenoxazine, such that their k_{inh}^{PhCl} could be determined directly from inhibited autoxidations of dioxane sans DMSO whereas the phenoxazines substituted with electron-donating groups (EDGs) had marginally lower α_2^H – and were substantially more reactive than phenoxazine – so DMSO was added to the inhibited autoxidations. The quality of the α_2^H determinations for the substituted phenoxazines is reflected in the excellent correlation of these values with the corresponding σ_p^- substituent constants[33] (Figure 2.3A); this is expected since they are essentially partially dissociated Brønsted acids in the H-bonded complexes.

Scheme 2.1. Preparation of Substituted Phenoxazines.

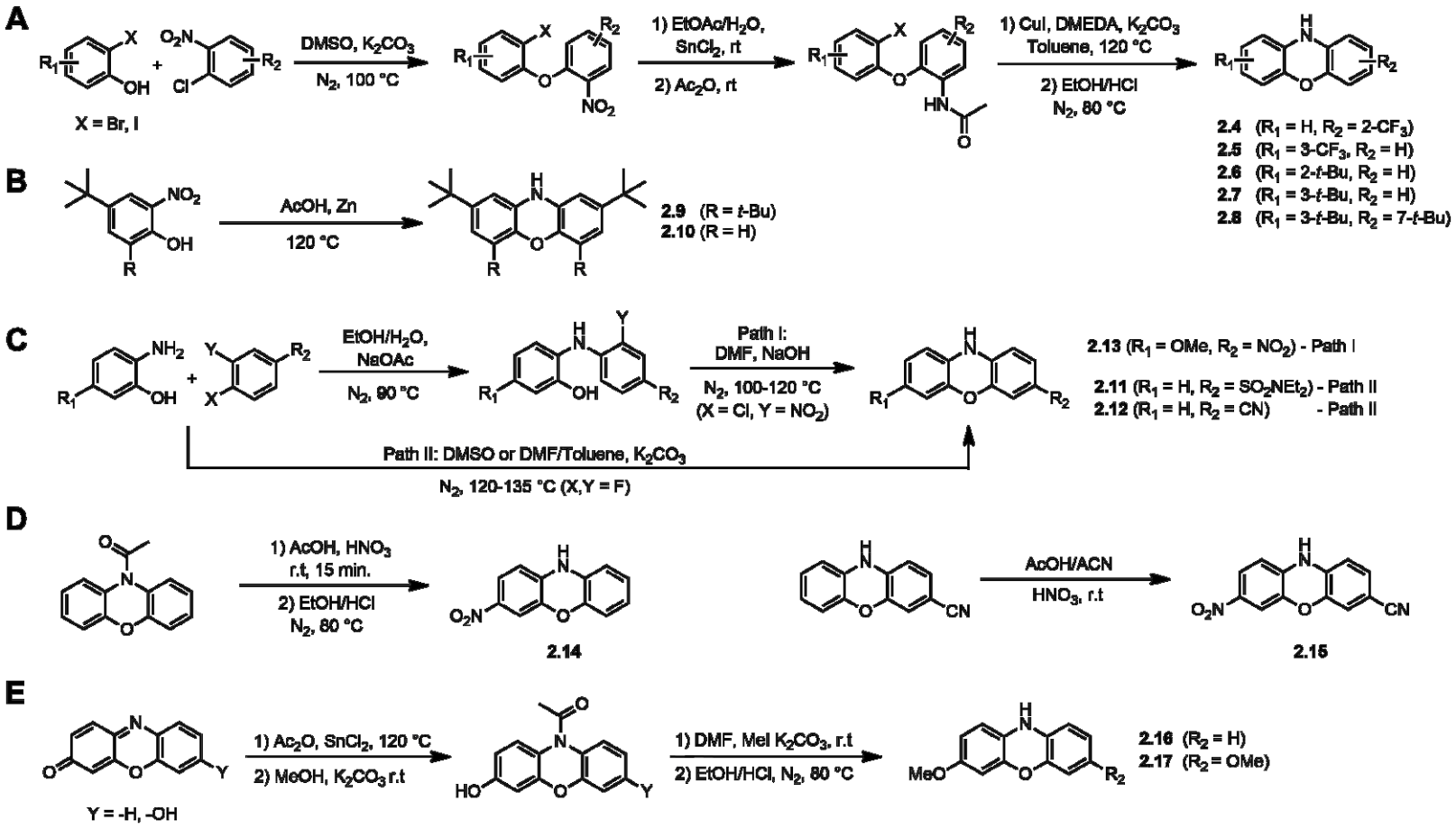

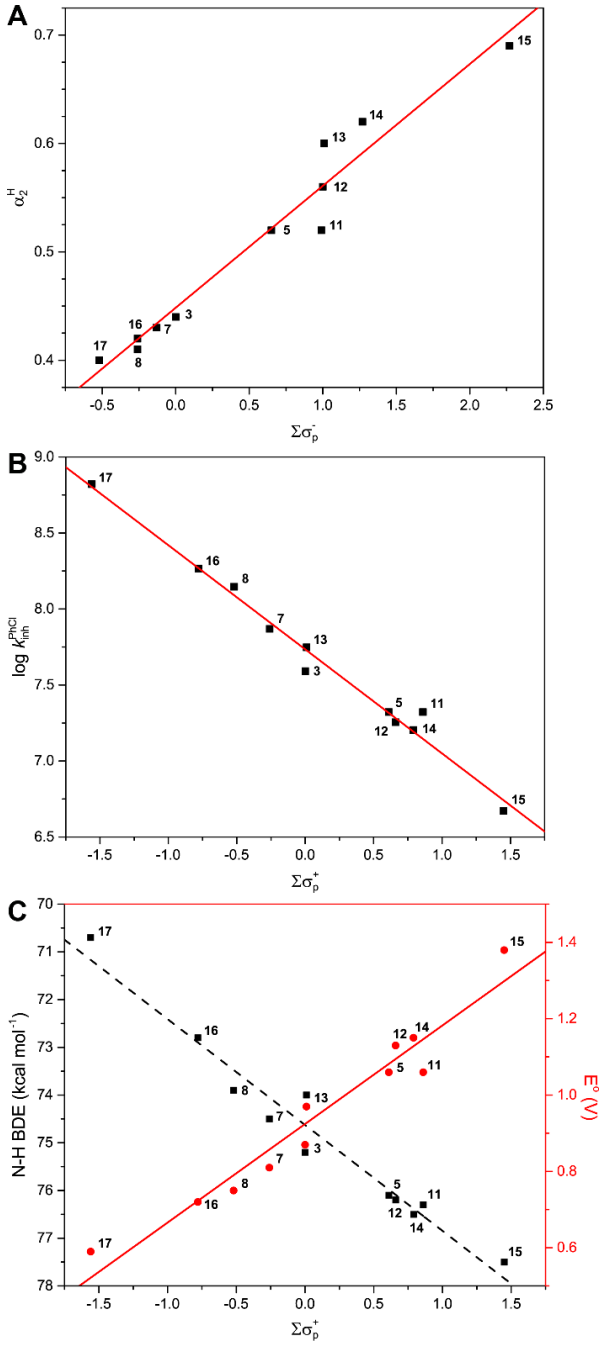

Figure 2.3. (**A**) Linear free energy relationship of $\Sigma\sigma_p^-$ and α_2^H for 3-substituted, or 3,7-disubstituted phenoxazines (R^2 = 0.955) (**B**) Linear free energy relationship of $\Sigma\sigma_p^+$ and $\log k_{inh}^{PhCl}$ for 3-substituted and 3,7-disubstituted phenoxazines (ρ^+ = -0.68, R^2 = 0.982) (**C**) Linear free energy relationship of $\Sigma\sigma_p^+$ and N-H BDE (black squares, R^2 = 0.959) and $\Sigma\sigma_p^+$ and E^o (red circles, R^2 = 0.944) for 3-substituted and 3,7-disubstituted phenoxazines.

The rate constants derived from the inhibited autoxidations span more than two orders of magnitude; the lowest determined for 3-CN,7-NO_2-phenoxazine ($4.5 \pm 0.1 \times 10^6$ M^{-1} s^{-1}) and the highest determined for 3,7-$(OMe)_2$-phenoxazine ($6.6 \pm 1.1 \times 10^8$ M^{-1} s^{-1}). In general, and as expected based on the kinetics of the reactions of other diarylamines with peroxyl radicals,[5,6,8] substitution with EDGs increase the rate and EWGs decrease the rate. In fact, the values of k_{inh} for the substituted phenoxazines correlate very well with the corresponding σ_p^+ substituent constants[33] – or sum of the substituent constants in the case of multiple substitutions – as is evident in Figure 2.3B. Also given in Table 1 are N-H BDEs that were calculated by the high-accuracy CBS-QB3 complete basis set methodology[34] and the standard potentials determined by cyclic voltammetry. As expected, both properties correlate well with $\Sigma\sigma_p^+$ (Figure 2.3C).[35]

2.3.3 Understanding the Superiority of Phenoxazine as an RTA

The CBS-QB3 calculations used to predict the N-H BDEs given in Table 1 were expanded to provide a view of the transition state structure for H-atom transfer from phenoxazine to peroxyl radicals (Figure 2.4A). The structure greatly resembles that of the reaction between diphenylamine and a peroxyl radical (Figure 2.4B) in that the proton is transferred roughly in the plane of the molecular framework, while the electron is delocalized in approximately perpendicular orbitals (i.e. the π-HOMO of phenoxazine and π*-SOMO of the peroxyl radical).[8] Thus, the reaction can be described as a proton-coupled electron transfer, where the proton and electron are exchanged between different pairs of orbitals.[7,8,27,36–39] The greater reactivity of phenoxazine is based on both enthalpic and entropic factors: the N-H bond is weaker, decreasing $\Delta H^{\ddagger}$ (0.8 vs. 5.1 kcal mol^{-1}), and the aryl rings are already fixed in optimal positions to maximize delocalization of the unpaired

electron in the aminyl radical, minimizing the entropic cost ($\Delta S^{\ddagger}$ = -36.4 vs. -37.7 cal mol^{-1} for phenoxazine and diarylamine respectively).

In carrying out these calculations we also sought some insight into the origin of the relatively high $E°$ of phenoxazine (0.87 V *vs.* NHE) despite its low N-H BDE (76.1 kcal mol^{-1}) and corresponding high reactivity ($k_{inh} = 3 \times 10^7$ M^{-1} s^{-1}). To put this into context, diarylamines of similar or lower reactivity are generally characterized by $E°$ values which are ∼0.4 V lower.[8] Of course, a fundamental difference between phenoxazine and diphenylamine is the planar structure of the latter – in both the starting material and the incipient radical and radical cation – which should improve spin delocalization. Indeed, the N-H BDE and IP in 9,10-dihydroacridine are predicted to be 2.4 and 4.3 kcal mol^{-1} lower, respectively, than in diphenylamine. However, when the CH_2 bridge is replaced with an O-atom the predicted N-H BDE decreases by 11.2 kcal mol^{-1}, but this is accompanied by a decrease of only 8.7 kcal mol^{-1} in IP. The decrease in BDE upon inclusion of a heteroatom bridge in lieu of a methylene unit was anticipated, given that electron-donation from the heteroatom can better stabilize the electron poor aminyl radical by resonance. However, an even greater effect was expected on the ionization potential, given that the radical cation is inherently more electron poor than the amine. In order to eliminate the resonance contribution of the oxygen atom on the stability of the aminyl radical and/or cation, and focus only its inductive/field effect, we also calculated the N-H BDEs and IPs in piperidine and morpholine. Although the N-H BDEs are essentially identical, the oxygen atom clearly raises the IP of the amine. The inductive/field effect is even more obvious when the conformation of the piperidine and morpholine rings are constrained to be planar (as

Table 2.1. Inhibition Rate Constants, α_2^H H-Bond Donor Parameters, Inhibition Stoichiometries, N-H Bond Dissociation Enthalpies and Oxidation Potentials for Substituted Phenoxazines.

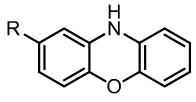

2.4 (R = CF_3)
2.6 (R = t-Bu)

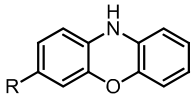

2.5 (R = CF_3)
2.7 (R = t-Bu)
2.11 (R = SO_2NEt_2)
2.12 (R = CN)
2.14 (R = NO_2)
2.16 (R = MeO)

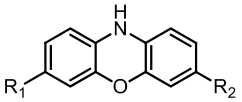

2.8 (R_1 = R_2 = t-Bu)
2.13 (R_1 = MeO, R_2 = NO_2)
2.15 (R_1 = NO_2, R_2 = CN)
2.17 (R_1 = R_2 = MeO)

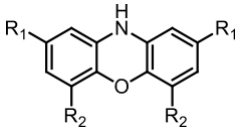

2.9 (R_1 = R_2 = t-Bu)
2.10 (R_1 = t-Bu, R_2 = H)

RTA	k_{inh}^{S} (M^{-1} s^{-1}) [a]	*n*	α_2^{H} [b]	k_{inh}^{PhCl} (M^{-1} s^{-1})	BDE (kcal mol^{-1}) [c]	E^{o} [d]
2.15[e]	$1.5 \pm 0.1 \times 10^5$	2.4 ± 0.1	0.69	$4.5 \pm 0.1 \times 10^6$	77.5	1.38
2.14[e]	$7.3 \pm 0.2 \times 10^5$	2.5 ± 0.1	0.62	$1.6 \pm 0.1 \times 10^7$	76.5	1.15
2.12[e]	$1.1 \pm 0.1 \times 10^6$	2.2 ± 0.2	0.56	$1.8 \pm 0.1 \times 10^7$	76.2	1.13
2.5[e]	$1.5 \pm 0.2 \times 10^6$	2.3 ± 0.1	0.53	$2.0 \pm 0.3 \times 10^7$	76.1	1.06
2.11[e]	$1.5 \pm 0.1 \times 10^6$	2.2 ± 0.1	0.53	$2.1 \pm 0.2 \times 10^7$	76.3	1.06
2.4[e]	$2.0 \pm 0.1 \times 10^6$	2.3 ± 0.1	0.51	$2.5 \pm 0.2 \times 10^7$	76.2	1.05
2.13[e]	$2.8 \pm 0.2 \times 10^6$	1.5 ± 0.1	0.60	$5.6 \pm 0.5 \times 10^7$	74.0	0.97
2.3[f]	$5.3 \pm 0.5 \times 10^5$	2.2 ± 0.1	0.44	$3.9 \pm 0.4 \times 10^7$	75.2	0.87
2.6[f]	$9.0 \pm 0.3 \times 10^5$	2.0 ± 0.1	0.43	$6.0 \pm 0.2 \times 10^7$	74.6	0.83
2.7[f]	$1.1 \pm 0.1 \times 10^6$	2.1 ± 0.1	0.43	$7.4 \pm 0.6 \times 10^7$	74.5	0.81
2.10[f]	$1.5 \pm 0.1 \times 10^6$	1.8 ± 0.1	0.43	$1.0 \pm 0.1 \times 10^8$	74.0	0.78
2.8[f]	$2.6 \pm 0.2 \times 10^6$	1.9 ± 0.1	0.41	$1.4 \pm 0.1 \times 10^8$	73.9	0.75
2.16[f]	$3.1 \pm 0.2 \times 10^6$	1.8 ± 0.1	0.42	$1.8 \pm 0.1 \times 10^8$	72.8	0.72
2.9[f]	$4.7 \pm 0.8 \times 10^6$	1.7 ± 0.1	0.39	$2.1 \pm 0.4 \times 10^8$	-	0.67
2.17[f]	$(1.3 \pm 0.2 \times 10^7)$[g]	1.4± 0.1	0.40	$(6.6 \pm 1.1 \times 10^8)$	70.7	0.59

[a]Rates of inhibition determined for 2 μM of inhibitor a minimum of three times. [b]Calculated from $\Delta\delta_{DMSO\text{-}PhH}$ of the relevant proton in the ^{1}H NMR spectrum in conjunction with Eq. 7. Spectra can be found in the ESI. [c]Calculated by CBS-QB3. [d]Values in V *vs.* NHE determined by cyclic voltammetry in acetonitrile. [e]k_{inh}^{PhCl} was calculated from k_{inh}^{Diox}. [f]k_{inh}^{PhCl} was calculated from k_{inh}^{DMSO}. [g]$k_{inh}^{DMSO}$was determined via kinetic modeling as described previously, see ref. 14.

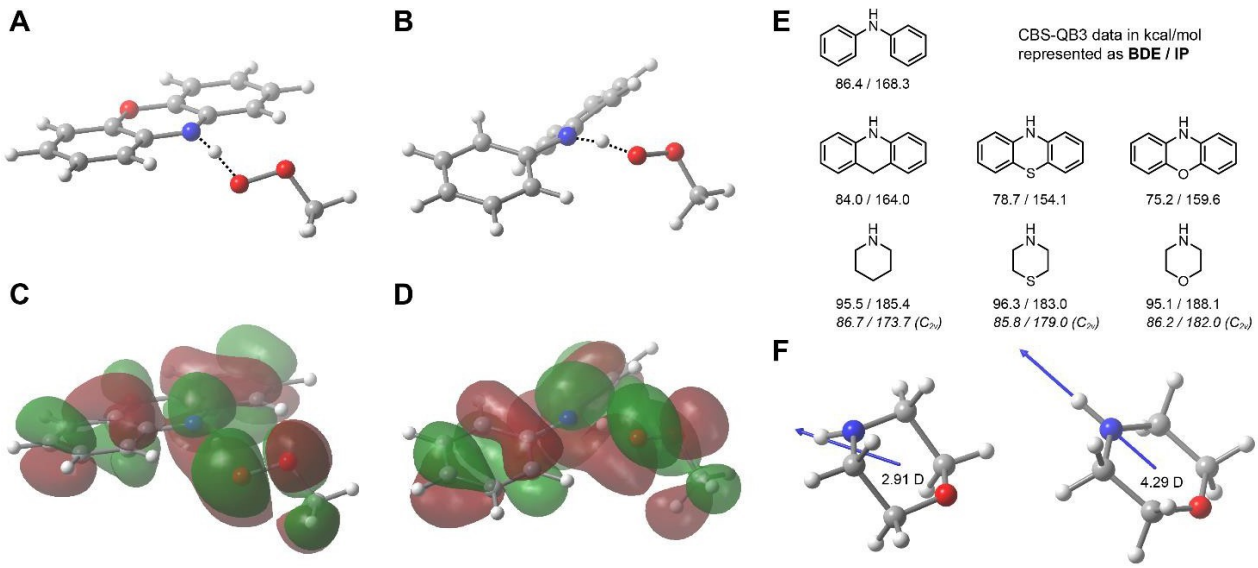

Figure 2.4. (A/B) Calculated TS structures of the reaction between a peroxyl radical (exemplified by methylperoxyl) and phenoxazine and diphenylamine. **(C/D)** Calculated singly occupied molecular orbitals of the TS. **(E)** CBS-QB3 calculated N-H BDEs and IPs of diphenylamine (top), 9,10-dihydroacridine, phenothiazine and phenoxazine (middle) and piperidine, thiomorpholine and morpholine (bottom). For piperidine, thiomorpholine and morpholine, data are presented for both the minimum energy conformation, as well as a planarized (C_{2v}) structure. **(F)** Calculated minimum energy and planarized structures of morpholine radical cation and molecular dipole moment vector.

opposed to the minimum energy chair conformer); the IPs now differ by 8.3 kcal mol^{-1}, while the N-H BDEs remain essentially the same. A similar, but attenuated, trend exists in the corresponding sulfur compounds. These data are summarized in Figure 2.4E.

2.4 Discussion

Phenothiazines, which are synthesized simply by treating diphenylamines with elemental sulfur in the presence of a catalytic oxidant (e.g. I_2), have been used as antioxidants since the 1950s.[40] Phenoxazines, despite being known to possess a weaker N-H bond and greater reactivity toward peroxyl radicals,[6] are not widely used – if at all. One consideration may be that they are not as conveniently prepared on industrial scale.[41] Another consideration may be that early reports suggested that phenoxazines were no more

reactive than phenothiazines – at least at elevated temperatures – discouraging further investigation.[42] The more recent results of Lucarini et al.[6] strongly suggested to us that phenoxazines merit further investigation as RTAs; in particular, since they possess greater reactivity toward peroxyl radicals *and* greater stability to one-electron oxidation compared to phenothiazines.

The application of the spectrophotometric inhibited co-autoxidation approach[14] to the determination of the peroxyl radical-trapping kinetics of phenoxazines required slowing the inhibition reaction sufficiently to obtain a measurable rate for the inhibited part of the autoxidation. This was accomplished by the addition of a very strong H-bond accepting co-solvent (DMSO) to the reaction medium, precluding H-atom transfer from all but the tiny amount of non-H-bonded phenoxazine present at equilibrium. Although there are many examples of the utilization of the empirical equation derived by Ingold to estimate H-atom transfer rate constants in solvents of differing H-bond accepting ability (to which we refer as the Ingold-Abraham relationship, see Eq. 6),[21,43,44] we believe this to be the most extreme, given that DMSO is such an excellent H-bond acceptor (β_2^H = 0.78) and the very high inherent reactivity of some of the H-atom donors (i.e. in the absence of H-bonding interactions) are the fastest ever observed (k_{inh} up to mid 10^8 M^{-1} s^{-1}). As such, prior to our investigations of substituted phenoxazines, we first vetted the use of DMSO in combination with the Ingold-Abraham relationship by deriving the inhibition rate constants for other highly reactive RTAs whose kinetics had already been determined by oxygen consumption. The excellent agreement instilled confidence that data derived from PBD-BODIPY/dioxane co-autoxidations in DMSO are reliable.

The reactivity of the substituted phenoxazines was, as expected, impressive. At the low end, substitution at the 3- and 7- positions with cyano and nitro groups yields $k_{inh} = 4.5 \times 10^6$ M^{-1} s^{-1}; roughly one order of magnitude lower than phenoxazine. At the high end, substitution at the 3- and 7-positions with methoxy groups yields $k_{inh} = 6.6 \pm 1.1 \times 10^8$ M^{-1} s^{-1}; roughly one order of magnitude greater than phenoxazine. Phenoxazines substituted with single substituents were characterized by intermediate reactivity which correlated very well with the σ^+ Hammett-type electrophilic substituent constant to yield a strong linear free energy relationship (Figure 2.3B) whose negative reaction constant ($\rho^+ = -0.68$) is consistent with increasing electron-poorness of the aryl rings upon H-atom transfer from the phenoxazines to peroxyl radicals.

As far as we are aware, 3,7-dimethoxyphenoxazine is the most reactive radical-trapping antioxidant ever reported. In fact, it would appear that this reactivity is essentially the limit for these types of reactions. Previous work from our group had suggested that log A ~7.5 for the reactions of diarylamines with peroxyl radicals,[45] but the fact that the two aryl rings are fixed in phenoxazines reduces the entropy requirement to achieve the transition state (wherein optimal delocalization of the unpaired electron in the incipient aminyl radical can occur). To a first approximation, these two bond rotations may contribute at most (since they are coupled) ½ log unit each to log A, suggesting that a value of ~8.5 is reasonable for phenoxazines. The only similarly reactive RTA reported to date is the 5-hydroxy-7-aza-2,3-dihydroindole shown in Chart 2.1, which was also believed to react with peroxyl radicals with essentially no enthalpic barrier (i.e. $E_a \sim 0$).[46]

Chart 2.1. Radical-trapping antioxidants with log k_{inh} ~ log A ~ 8.5.

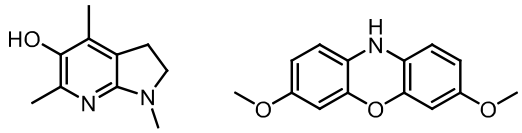

$k_{inh, PhCl}$ ($M^{-1}s^{-1}$)	(2.8 ± 1.8) × 10^8	(6.6 ± 1.1) × 10^8

Although they react more slowly, phenoxazines substituted with electron-withdrawing groups are arguably of greater practical interest. For example, the slowest phenoxazine we studied (3-CN, 7-NO_2) is ~300 fold more reactive than diphenylamine (compare k_{inh}^{PhCl} = 4.5 × 10^6 and 1.5 × 10^4 M^{-1} s^{-1}, respectively)[6] yet possesses greater stability to one-electron oxidation (compare $E°$ = 1.38 and 1.24 V *vs*. NHE, respectively).[47] Moreover, phenoxazines substituted with a single strong electron-withdrawing group (CN, NO_2, CF_3, SO_2NEt_2) were roughly 100-fold more reactive than the ADPAs used commercially (compare k_{inh}^{PhCl} ~2×10^7 versus 1.8 × 10^5 M^{-1} s^{-1},[8] respectively) while also being at least as stable to one electron oxidation ($E°$ >1 V *vs*. NHE). A particularly interesting compound is 3-methoxy-7-nitrophenoxazine. Since methoxy and nitro groups have the same magnitude of σ^+ constants, but of opposite sign (-0.78 and 0.79, respectively),[33] we expected their effects on the reactivity of phenoxazine to negate one another. However, this compound reacted 50% more quickly with peroxyl radicals than phenoxazine – and was characterized by a $E°$ value that was 100 mV greater – hence, the best of each substituent is contributed to these two key RTA parameters. The greater reactivity is consistent with the lower calculated N-H BDE in this compound compared to phenoxazine (74.4 vs. 75.2 kcal mol^{-1}), perhaps suggesting the role of captodative stabilization of the aminyl due to polarization across the two rings.

The unique combination of increased oxidative stability and increased H-atom transfer reactivity of phenoxazines relative to phenothiazines and diphenylamines is most clearly illustrated in Figure 2.5, where log k_{inh} is plotted versus $E°$ for the three types of arylamines. The three essentially parallel correlations reflect the fact that in compounds with a similar reactivity toward peroxyl radicals, the phenoxazine is considerably more stable to one-electron oxidation than phenothiazine, which is then more stable than the diphenylamine. Likewise, for compounds of the same oxidative stability, the phenoxazine is 5 to 10-fold more reactive than the phenothiazine, and even more so than the

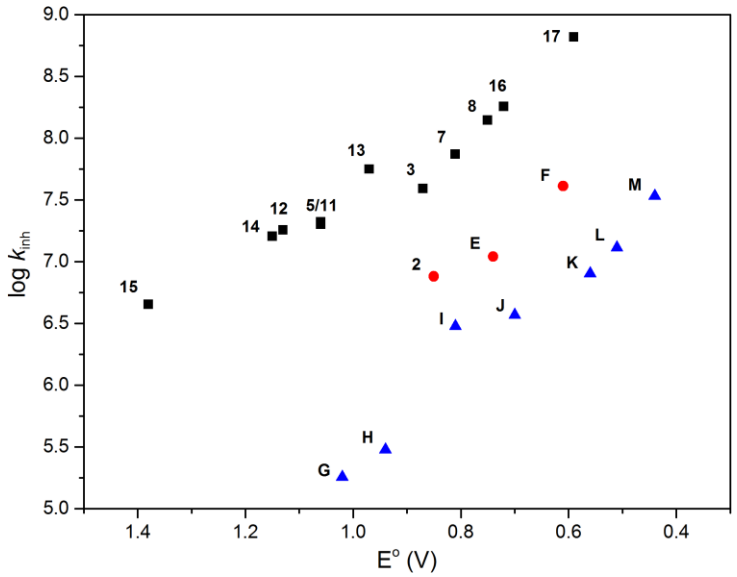

Figure 2.5. Inhibition rate constants of substituted phenoxazines (black), phenothiazines (red), and diarylamines (blue) plotted as a function of their oxidation potentials (E°). Representative inhibitors: 4,4'-dioctyldiphenylamine (**G**), 4-methoxydiphenylamine (**H**), N^2,N^2-dimethyl-N^5-phenylpyrimidine-2,5-diamine (**I**), 4,4'-dimethoxydiphenylamine (**J**), N^1,N^1-dibutyl-N^4-(pyrimidin-5-yl)benzene-1,4-diamine(**K**), 4-dimethylaminodiphenylamine (**L**), N^5-(6-(dimethylamino)pyridin-3-yl)-N^2,N^2-dimethylpyridine-2,5-diamine (**M**).[8] See ESI for structures.

diphenylamine. The calculations described above provide good rationale for this; the π-donor ability of the oxygen atom in phenoxazine is responsible for the weaker N-H bond and larger k_{inh} compared to diphenylamine, but its σ-acceptor ability (electronegativity) minimizes the drop in $E°$. Although the sulfur atom in phenothiazine is also a good π-donor, such that it also possesses a weak N-H bond and large k_{inh}, since sulfur is less electronegative than oxygen it has a smaller effect on $E°$.

One of the most interesting observations made by Lucarini et al. in their original work[6] was that styrene autoxidations inhibited by phenoxazine had inhibited periods that corresponded to the trapping of five (5!) peroxyl radicals. The foregoing dioxane/PBD-BODIPY co-autoxidations were characterized by inhibited periods that correspond to $n \sim 2$, similar to phenols and other aminic antioxidants. However, when phenoxazine-inhibited co-autoxidations were carried out in styrene, a dramatic increase in the stoichiometric factor was observed (Figure 2.6A). Interestingly, the kinetic traces featured two distinct inhibited periods: an initial fully inhibited period ($t_{inh}^{(1)} \sim 1700$ s) corresponding to $n \sim 2$ and a secondary inhibited period ($t_{inh}^{(2)} \sim 6700$ s) corresponding to an additional $n \sim 8$, for a total of $n \sim 10$. Moreover, the rate of the autoxidation beyond the second inhibited period remained retarded relative to the uninhibited rate. As far as we are aware, this level of radical-trapping capacity at ambient temperatures is unprecedented. It is noteworthy that two distinct inhibited phases (and subsequent retarded phase) in the phenoxazine-inhibited autoxidation of styrene were not reported by Lucarini et al.[6] This may be due to the significantly greater rate of initiation that they used to produce a non-zero inhibited autoxidation rate (necessary for them to derive k_{inh}), which would lead to a much less

pronounced inflection point at $t_{inh}^{(1)}$. Furthermore, the discontinuous nature of their approach to monitor reaction progress (where O_2 uptake was determined every few minutes by the change in linewidth of the EPR spectra of an added nitroxide) would make it more difficult to see the changes in the inhibited rate between the three different intervals.

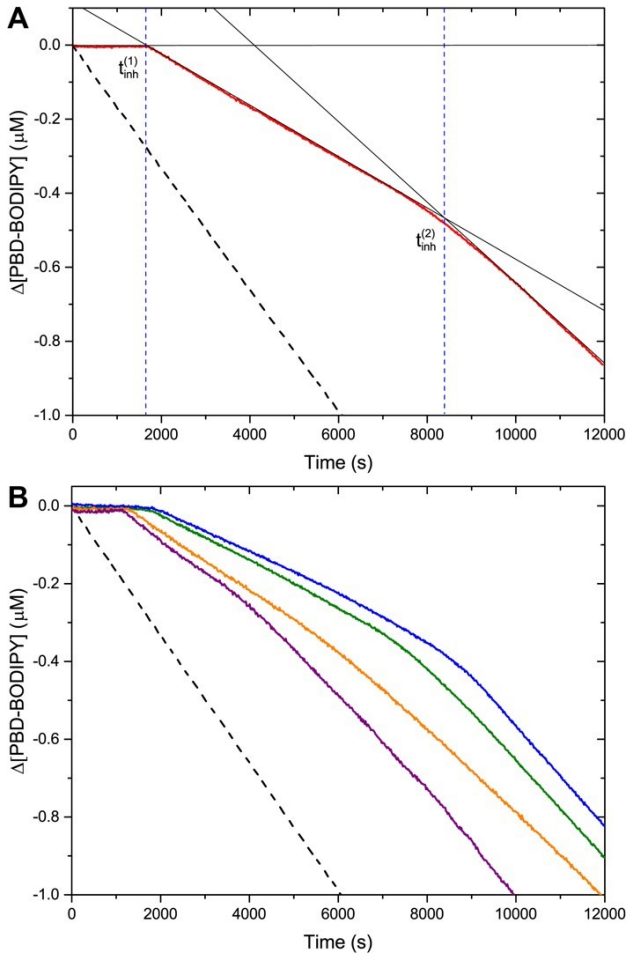

Figure 2.6. (**A**) Co-autoxidation of styrene (4.3 M) and PBD-BODIPY (10 uM) initiated by AIBN (6 mM) in PhCl at 37 °C (black) and inhibited by 2 μM phenoxazine **2.3** (red, $n^{(1)} = 2.2 \pm 0.1$, $n^{(2)} = 8.0 \pm 1.9$). (**B**) Corresponding autoxidations inhibited by 2 μM of 3-cyanophenoxazine **2.12** (blue, $n^{(1)} = 2.4 \pm 0.1$, $n^{(2)} = 9.4 \pm 0.5$), 3-(N,N-diethylsulfonamide)-phenoxazine **2.11** (green, $n^{(1)} = 2.3 \pm 0.1$, $n^{(2)} = 8.1 \pm 0.6$), 3-tert-butylphenoxazine **7** (orange, $n^{(1)} = 1.9 \pm 0.3$, $n^{(2)} = 6.7 \pm 1.4$) and 3-methoxyphenoxazine **2.16** (violet, $n^{(1)} = 1.8 \pm 0.3$, $n^{(2)} = 3.9 \pm 0.5$).

In addition to the striking substrate-dependence of this "non-classical" RTA behaviour, we also found that the rate of the secondary inhibited period is largely independent of the structure of the phenoxazine. Representative examples are shown in Figure 2.6B, which features data for styrene autoxidations inhibited by both electron-rich (methoxy- or *tert*-butyl-substituted) and electron-poor (sulfonamide- or cyano-substituted) phenoxazines. The major difference between these data sets is the difference in the lengths of both the primary and secondary inhibited periods, with the more electron-rich phenoxazines giving rise to noticeably shorter overall inhibited periods, such that the overall n decreases upon increasing electron-richness: 11.6 (3-CN), 10.4 (3-Et_2NSO_2), 10.2 (3-H), 8.6 (3-*t*-Bu), 5.7 (3-OMe). This is presumably due to the increased oxidative lability of the phenoxazines along this series, which depletes the RTA and generates radicals rather than traps them.

Non-classical (n > 2) RTA activity of diarylamines is well known, but only at elevated temperatures (i.e. >100 °C)[2] – such as those experienced by engine oil lubricants, rubbers and plastics to which ADPAs are added. The need for elevated temperatures is easily understood upon consideration of the accepted mechanism for the catalytic activity of ADPAs, shown in Scheme 2.2.[48] Following the initial H-atom transfer to a peroxyl radical, the diphenylaminyl radical reacts with a second peroxyl radical to form a nitroxide. The nitroxide then combines with an alkyl radical to form an alkoxyamine, that can undergo rate-limiting fragmentation to reform the ADPA. The fragmentation requires cleavage of the N-O bond either by homolysis/disproportionation or a concerted retro-carbonyl-ene pericyclic process,[49] both of which do not operate on the timescale of the inhibited autoxidations shown in Fig. 6 at 37 °C ($k \sim 3 \times 10^{-9}$ s^{-1}).[49] Of course, the rate may

increase if the aminyl radical formed upon N-O homolysis is significantly more stable, as is the aminyl derived from phenoxazine. However, the difference in the aminyl radical stabilities – which can be estimated from the difference in the N-H BDEs between ADPAs (~82 kcal mol^{-1}) and phenoxazine (~76 kcal mol^{-1}) – is too little to increase the rate of fragmentation of the putative alkoxyamine sufficiently to account for the secondary inhibition observed in the styrene autoxidations (Figure 2.6).[50] Moreover, the rates during the secondary inhibited periods to which the "non-classical" RTA activity is attributed are almost independent of the structure of the phenoxazine – inconsistent with N-O homolysis to yield aminyl radicals of significantly different stability being rate-determining (i.e. the difference in N-H BDEs of the cyano and methoxy substituted phenoxazines is 3.2 kcal/mol). Clearly, another mechanism must operate – and must do so in styrene, but not dioxane. Efforts to elucidate this mechanism continue in our laboratories.

Scheme 2.2. Mechanism of Diarylamine RTAs at Elevated Temperatures.

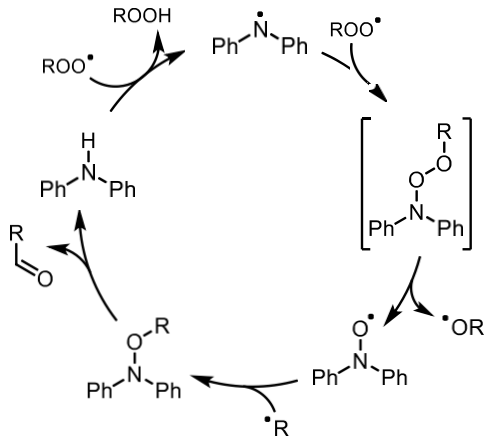

Given the higher reactivity, radical-trapping capacity and oxidative stability of phenoxazines compared to other aminic RTAs, it will be interesting to see how they compare in industrially-relevant contexts. Moreover, given that even the least reactive phenoxazine studied here is still more reactive than α-TOH, the most biologically-active

form of Vitamin and Nature's premier RTA (k_{inh} = 3.2 × 10^6 M^{-1} s^{-1}),[28] it would be interesting to see if these compounds have any biological activity. Again, this is particularly interesting given that α-TOH is comparatively easy to oxidize ($E°$ = 0.93 V).[51] Indeed, we recently found that phenoxazine is the most potent inhibitor of lipid autoxidation driven cell death (also called ferroptosis) ever reported,[52] corroborating an earlier study that suggested that phenoxazine was a potent neuroprotectant.[53] Thus, some of the compounds described here may provide leads toward potential preventive and/or therapeutic agents for degenerative conditions wherein lipid autoxidation has been implicated.

2.5 Conclusions

Application of the kinetic solvent effect model of Ingold has enabled quantitation of the kinetics of the reactions of substituted phenoxazines with peroxyl radicals (k_{inh}). The addition of DMSO as a co-solvent to dioxane autoxidations suppressed the reactivity of phenoxazines by up to two orders of magnitude, thereby enabling derivation of their inhibition rate constants under more relevant (i.e. non-H-bonding) conditions via the Ingold-Abraham relationship. The reliability of this approach can be appreciated explicitly by the accuracy of the derived rate constants with respect to previously characterized RTAs, as well as implicitly based on the strong linear correlation between σ_p^+ and log k_{inh}^{PhCl} for the newly studied substituted phenoxazines.

The reactivity of the phenoxazines spanned 4.5 × 10^6 M^{-1} s^{-1} for 3-CN,7-NO_2-phenoxazine to 6.6 × 10^8 M^{-1} s^{-1} for 3,7-$(OMe)_2$-phenoxazine. The reactivity of the latter compound is the greatest of any RTA ever reported, and is likely to represent a reaction without enthalpic barrier since log A for this reaction is likely ~8.5. Linear free energy

relationships observed between the inhibition rate constants, standard potentials and N-H bond strengths of phenoxazines parallel those of substituted diarylamines and phenothiazines. However, with respect to the other classes of aminic RTAs, the substituted phenoxazines are decisively privileged since compounds of similar oxidative stability (quantified by E^{o}) are orders of magnitude more reactive to peroxyl radicals. The results of computations account for this, by indicating that the heteroatom bridge in phenoxazines (and to a lesser extent, phenothiazines) stabilizes the aminyl radical by electron donation resonance while destabilizing the aminyl radical cation by electron withdrawal by induction. Perhaps most interestingly, we confirm the once-reported non-classical RTA behavior of phenoxazine at ambient temperatures, and show that 1) it is dependent on the rate of initiation of autoxidation, 2) is only weakly dependent on the electronic characteristics of the phenoxazine, and 3) is dependent on the substrate undergoing autoxidation. The precise mechanism of this non-classical RTA behavior remains unknown.

2.6 Experimental

General Methods All chemicals and solvents were purchased from commercial suppliers unless otherwise indicated. ^{1}H, ^{13}C, and ^{19}F NMR spectra were recorded on either a 300 or 400 MHz instrument. UV-visible spectra and associated kinetics were measured with a spectrophotometer equipped with a temperature controller unit and a thermostated 6 × 6 multicell holder. Styrene was washed thrice with 1 M NaOH, once with water and then dried with $MgSO_4$ prior to distillation under reduced pressure at 50 °C. Thereafter, it was passed through a column of silica and stored at -20 °C for up to 4 days. Immediately prior

to use, it was passed through a column filled with 2/3 basic alumina (bottom) and 1/3 silica (top). 3-Cyanophenoxazine,[30] 10-acetylphenoxazine,[54] 3,7-dihydroxy-10-acetylphenoxazine,[55] phenoxazone,[56] *N*-[2-(4-(*tert*-butyl)-2-iodophenoxy)phenyl]acetamide,[57] 5-hydroxy-2-dimethylaminopyrimidine,[58] 5-hydroxy-4,6-dimethyl-2-dimethylaminopyrimidine,[58] 2-methylundecan-2-persulfide,[27] 3,7-di-*tert*-butylphenothiazine,[59] and 3,7-dimethoxy-phenothiazine[60] were prepared according to previously reported procedures.

2-Iodo-5-*tert*-butylphenol (2.18). 3-*tert*-Butylphenol (2.6 g, 17 mmol), potassium iodide (2.8 g, 17 mmol), and NaOH (0.68 g, 17 mmol) were dissolved in MeOH (46 mL) under stirring, cooled with an ice bath. Approximately 22 mL of 6% sodium hypochlorite solution (bleach) was added drop wise over an hour until the potassium iodide was consumed. On completion, the reaction mixture was poured into water, the aqueous mixture extracted thrice with EtOAc. The organic phase washed twice with water, dried over $MgSO_4$, filtered and the solvent removed under reduced pressure. The residue was purified by column chromatography (9:1, hexanes:EtOAc) to render the product as a clear oil, which quickly changed to a reddish color and under cooling in a freezer, formed prismatic crystals (3.3 g, 69%). ^{1}H NMR (400 MHz; $CDCl_3$): δ 7.56 (d, J = 8.3 Hz, 1H), 7.05 (d, J = 2.3 Hz, 1H), 6.74 (dd, J = 2.3, 8.3 Hz, 1H), 5.20 (br, 1H), 1.30 (s, 9H). Spectra were consistent with previous reports.[61]

4-(*tert*-Butyl)-2-chloronitrobenzene (2.19). 5-(*tert*-Butyl)-2-nitroaniline (0.98 g, 5.0 mmol) was dissolved in 20 mL concentrated HCl at room temperature under vigorous stirring, to which sodium nitrite (0.42 g, 6.1 mmol) in a minimum of water was added slowly. The suspension was allowed to stir for 1 hour at room temperature. Copper(I) chloride (0.05 g, 0.5 mmol)

dissolved in a small amount of HCl was added slowly and the mixture heated to 100 °C for 1 hour. The reaction mixture was poured into water and the aqueous mixture extracted thrice with Et_2O. The organic phase was washed twice with water, dried over $MgSO_4$, filtered and the solvent removed under reduced pressure. The orange residue (0.33 g) was largely the desired product based on crude spectra (*see ESI*), though attempts to completely isolate the product from the side products by column chromatography were unsuccessful, so the crude product was used without further purification.

4-(*tert*-Butyl)-1-iodo-2-(2-nitrophenoxy)benzene (2.20). 2-Iodo-5-*tert*-butylphenol (2.8 g, 10 mmol) and 2-chloronitrobenzene (1.6 g, 10 mmol) were dissolved in DMSO (15 mL) to which K_2CO_3 was added (2.8 g, 20 mmol) and the reaction mixture was placed under a N_2 atmosphere. With vigorous stirring, the reaction was heated to 100 °C overnight. The reaction mixture was poured into water and extracted thrice with EtOAc. The organic phase was washed twice with water, dried over $MgSO_4$, filtered and the solvent removed under reduced pressure. The product was purified by column chromatography (9:1, pet. ether:Et_2O) to render a colourless oil (2.9 g, 73%). ^{1}H NMR (300 MHz; $CDCl_3$): δ 8.01 (dd, *J* = 1.7, 8.0 Hz, 1H), 7.79 (d, *J* = 8.3 Hz, 1H), 7.51-7.45 (m, 1H), 7.21-7.16 (m, 1H), 7.09 (d, *J* = 2.2 Hz, 1H), 7.03 (dd, *J* = 2.2, 8.3 Hz, 1H), 6.78 (dd, *J* = 1.1, 8.3 Hz, 1H), 1.28 (s, 9H). ^{13}C NMR (75 MHz; $CDCl_3$): δ 154.4, 154.2, 150.7, 139.6, 134.1, 125.9, 124.5, 122.6, 118.6, 118.2, 85.4, 34.8, 31.1. HRMS (EI, magnetic sector): calcd for $C_{16}H_{16}INO_3$ 397.01749, found 397.01553.

1-(2-Bromophenoxy)-2-nitro-4-(trifluoromethyl)benzene (2.21). Same general procedure where 2-bromophenol (1.8 g, 10 mmol) and 4-chloro-3-nitrobenzotrifluoride (2.3 g, 10 mmol) were heated in DMSO with K_2CO_3. The resulting oil (3.5 g; 97%) was used

in the subsequent reaction without further purification. ^{1}H NMR (400 MHz; $CDCl_3$): δ 8.28 (d, 2.3 Hz, 1H), 7.72-7.69 (m, 2H), 7.45-7.40 (m, 1H), 7.24-7.18 (m, 2H), 6.87 (d, 8.8Hz, 1H). ^{13}C NMR (101 MHz; $CDCl_3$): δ 153.0, 150.7, 139.6, 134.5, 130.9 (q, J_{C-F} = 3.3Hz), 129.4, 127.7, 125.1 (q, J_{C-F} = 34.9 Hz), 123.7 (q, J_{C-F} = 4.0 Hz), 122.8 (q, J_{C-F} = 272.2 Hz), 122.6, 118.2, 115.8. ^{19}F NMR (376 MHz, $CDCl_3$): δ -63.40. HRMS (EI, magnetic sector): calcd for $C_{13}H_7BrF_3NO_3$ 360.95614, found 360.95252.

1-Iodo-2-(2-nitrophenoxy)-4-(trifluoromethyl)benzene (2.22). Same general procedure where 2-iodo-5-trifluoromethylphenol (1.6 g, 5.6 mmol) and 2-chloronitrobenzene (0.66 g, 4.2 mmol) were heated in DMSO with K_2CO_3. Attempts to completely isolate the product from the side products by column chromatography were unsuccessful, so the crude product was used without further purification. See ESI for crude ^{1}H and ^{13}C NMR spectra. HRMS (EI, magnetic sector): calcd for $C_{13}H_7IF_3NO_3$ 408.94227, found 408.94262.

4-(*tert*-Butyl)-2-(5-(tert-butyl)-2-iodophenoxy)-1-nitrobenzene (2.23). Same general procedure where 2-iodo-5-tert-butylphenol (0.42 g, 1.5 mmol) and 4-(*tert*-butyl)-2-chloronitrobenzene (0.32 g, 1.5 mmol) were heated in DMSO with K_2CO_3. The product was purified by column chromatography (9:1, pet. ether:Et_2O) to afford a white solid (0.34 g, 50%). ^{1}H NMR (400 MHz; $CDCl_3$): δ 7.98 (d, J = 8.6 Hz, 1H), 7.79 (dd, J = 0.6, 7.9 Hz, 1H), 7.22 (dd, J = 2.0, 8.6 Hz, 1H), 7.00-6.97 (m, 2H), 6.86 (d, J = 2.0 Hz, 1H), 1.26 (s, 9H), 1.24 (s, 9H). ^{13}C NMR (101 MHz; $CDCl_3$): δ 159.0, 154.7, 154.1, 150.0, 139.6, 138.1, 125.9, 123.6, 120.2, 117.1, 116.5, 84.6, 35.4, 34.8, 31.0, 30.8. HRMS (EI, magnetic sector): calcd for $C_{20}H_{24}INO_3$ 453.08009, found 453.08007.

N-(2-(5-(tert-butyl)-2-iodophenoxy)phenyl)acetamide (2.24). 4-(*tert*-Butyl)-1-iodo-2-(2- nitrophenoxy)benzene (2.9 g, 7.2 mmol) and 5 equivalents of $SnCl_2$ (6.8 g, 36 mmol) were dissolved in EtOAc along with 10 equivalents of H_2O (1.3 mL). The reaction stirred at room temperature overnight, then was poured into water and extracted thrice with EtOAc. The organic phase was washed twice with water, dried over $MgSO_4$, filtered and the solvent removed under reduced pressure. The residue was dissolved in neat acetic anhydride (3.4 mL) and allowed to stir overnight. The reaction was quenched with saturated Na_2CO_3 solution and extracted thrice with EtOAc. The organic phase was washed once with water, dried over $MgSO_4$, filtered and the solvent removed under reduced pressure. The resulting product (2.7 g, 90%) was further purified by column chromatography (4:1, pet. ether:Et_2O) to afford a colorless oil. ^{1}H NMR (300 MHz; $CDCl_3$): δ 8.45 (dd, J = 1.3, 8.1 Hz, 1H), 7.84 (br, 1H), 7.79 (d, J = 8.3 Hz, 1H), 7.15-7.09 (m, 1H), 7.03-6.96 (m, 3H), 6.69 (dd, J = 1.4, 8.1 Hz, 1H), 2.23 (s, 3H), 1.27 (s, 9H). ^{13}C NMR (75 MHz; $CDCl_3$): δ 168.3, 154.7, 154.3, 145.3, 139.3, 129.0, 123.7, 123.7, 121.0, 117.5, 115.9, 104.5, 85.0, 34.8, 31.1, 25.0. HRMS (EI, magnetic sector): calcd for $C_{18}H_{20}INO_2$ 409.05387, found 409.05556.

N-(2-(2-bromophenoxy)-5-(trifluoromethyl)phenyl)acetamide (2.25). Same general procedure where 1-(2-bromophenoxy)-2-nitro-4-(trifluoromethyl)benzene (3.5 g, 9.6 mmol) is reduced with $SnCl_2$, then acetylated in neat acetic anhydride. The resulting solid (3.2 g, 90%) was used in the subsequent reaction without further purification. ^{1}H NMR (400 MHz; $CDCl_3$): δ 8.82 (br, 1H), 7.94 (br, 1H), 7.70 (dd, J = 1.6, 8.0 Hz, 1H), 7.39 (ddd, J = 1.6, 8.0, 8.0 Hz, 1H), 7.24-7.21 (m, 1H), 7.19-7.15 (m, 1H), 7.12 (dd, J = 1.5, 8.1 Hz, 1H), 6.68 (d, J = 8.5 Hz, 1H), 2.27 (s, 3H). ^{13}C NMR (101 MHz; $CDCl_3$): δ 168.5, 151.4, 147.7, 134.3, 129.2, 129.0, 126.9, 125.8 (q, $J_{C\text{-}F}$ = 33.0 Hz), 123.9 (q, 272.2 Hz), 122.1,

120.7 (q, $J_{C\text{-}F}$ = 3.7 Hz), 117.9 (q, $J_{C\text{-}F}$ = 3.7 Hz), 115.5, 114.9, 24.9. ^{19}F NMR (376 MHz, $CDCl_3$): δ -63.11. HRMS (EI, magnetic sector): calcd for $C_{15}H_{11}BrF_3NO_2$ 372.99253, found 372.98824.

N-(2-(2-iodo-5-(trifluoromethyl)phenoxy)phenyl)acetamide (2.26). Same general procedure where 1-iodo-2-(2-nitrophenoxy)-4-(trifluoromethyl)benzene (0.41 g, 1.0 mmol) is reduced with $SnCl_2$, then acetylated in neat acetic anhydride. The isolated crude solid was recrystallized from hexanes to afford pure white needles (0.21 g, 50%); mp 114-115 °C; ^{1}H NMR (400 MHz; $CDCl_3$): δ 8.48 (d, J = 8.4 Hz, 1H), 8.03 (d, J = 8.2 Hz, 1H), 7.69 (b, 1H), 7.23-7.08 (m, 4H), 6.80 (dd, J = 1.0, 8.2 Hz, 1H), 2.22 (s, 3H). ^{13}C NMR (101 MHz; $CDCl_3$): δ 168.3, 155.9, 144.3, 140.7, 132.6 (q, $J_{C\text{-}F}$ = 33.4 Hz), 129.5, 125.2, 124.1, 123.2 (q, $J_{C\text{-}F}$ = 272.5 Hz), 122.3 (q, $J_{C\text{-}F}$ = 3.7 Hz), 121.5, 117.3, 115.3 (q, $J_{C\text{-}F}$ = 3.7 Hz), 92.8, 24.9. ^{19}F NMR (376 MHz, $CDCl_3$): δ -64.09. HRMS (EI, magnetic sector): calcd for $C_{15}H_{11}F_3INO_2$ 420.97866, found 420.97881.

N-(4-(*tert*-butyl)-2-(5-(tert-butyl)-2-iodophenoxy)phenyl)acetamide (2.27). 4-(*tert*-Butyl)-2- (5-(*tert*-butyl)-2-iodophenoxy)-1-nitrobenzene (0.71 g, 1.6 mmol) and 5 equivalents of $SnCl_2$ dihydrate (1.5 g, 8.0 mmol) were dissolved in EtOAc. The reaction was stirred at room temperature overnight, then poured into water and extracted thrice with Et_2O. The organic phase was washed twice with water, dried over $MgSO_4$, filtered and the solvent removed under reduced pressure. The residue was dissolved in THF (10 mL) to which were added triethylamine (0.30 mL, 2.1 mmol) and acetyl chloride (0.13 mL, 1.8 mmol). The mixture was stirred overnight, then poured into water and extracted twice with Et_2O. The organic phase was washed twice with water, dried over $MgSO_4$, filtered and the solvent removed under reduced pressure. The resulting product (0.68 g,

91%) was further purified by column chromatography (9:1 hexanes:EtOAc) to afford a colourless oil. ^{1}H NMR (300 MHz; $CDCl_3$): δ 8.32 (d, *J* = 8.6 Hz, 1H), 7.78 (d, *J* = 8.6 Hz, 1H), 7.72 (br, 1H), 7.16 (dd, *J* = 2.2, 8.6 Hz, 1H), 6.97-6.93 (m, 2H), 6.86 (d, *J* = 2.2 Hz, 1H), 2.19 (s, 3H), 1.24 (s, 18H). ^{13}C NMR (75 MHz; $CDCl_3$): δ 168.2, 155.0, 154.0, 147.3, 144.4, 139.2, 126.8, 122.9, 120.9, 120.8, 115.7, 114.6, 84.0, 34.8, 34.5, 31.2, 31.0, 24.8. HRMS (EI, magnetic sector): calcd for $C_{22}H_{28}INO_2$ 465.11647, found 465.11865.

2-*tert*-Butyl-10-acetylphenoxazine (2.28). Into a N_2 flushed sealed tube were added N-(2-(4- (*tert*-butyl)-2-iodophenoxy)phenyl)acetamide (3.4 g, 8.3 mmol), K_2CO_3 (2.3 g, 17 mmol), copper(I) iodide (0.09 g, 0.05 eq.), N,N'-dimethylethylenediamine (0.09 mL, 0.1 eq.), and toluene (35 mL). The reaction mixture was heated to 120 °C for at least 10 hours under vigorous stirring, After completion, the reaction mixture was diluted with dichloromethane and passed through a plug of silica, after which the solvent was removed under reduced pressure. The crude product was purified by column chromatography (3:1, hexanes:EtOAc) to render 2-*tert*-butyl-10-acetylphenoxazine as an off-white solid (1.65 g, 71%). ^{1}H NMR (400 MHz; $CDCl_3$): δ 7.53 (d, *J* = 7.9 Hz, 1H), 7.47 (d, *J* = 2.2 Hz, 1H), 7.23 (dd, *J* = 2.4, 8.6 Hz, 1H), 7.21-7.10 (m, 3H), 7.06 (d, *J* = 8.5 Hz, 1H), 2.34 (s, 3H), 1.34 (s, 9H). Spectra were consistent with previous reports.[57]

3-*tert*-Butyl-10-acetylphenoxazine (2.29). Same general procedure using N-(2-(5-(*tert*-butyl)-2- iodophenoxy)phenyl)acetamide (2.6 g, 6.4 mmol) for the CuI catalyzed intramolecular Ullmann coupling. The product (1.3 g, 70%) was recrystallized from hexanes to render 3- *tert*-butyl-10-acetylphenoxazine as white needles; mp 139-140 °C; ^{1}H NMR (400 MHz; $CDCl_3$): δ 7.50-7.47 (m, 1H), 7.42-7.39 (m, 1H), 7.22-7.11 (m, 5H). ^{13}C NMR (101 MHz; $CDCl_3$): δ 169.3, 151.1, 150.7, 150.6, 129.6, 126.8, 125.1, 124.4,

123.2, 120.3, 116.9, 114.0, 34.7, 31.2, 23.0. HRMS (EI, magnetic sector): calcd for $C_{18}H_{19}NO_2$ 281.14158, found 281.14291.

2-Trifluoromethyl-10-acetylphenoxazine (2.30). Same general procedure using N-(2-(2- bromophenoxy)-5-(trifluoromethyl)phenyl)acetamide (3.2 g, 8.5 mmol) for the CuI catalyzed intramolecular Ullmann coupling. The crude product was purified by column chromatography (3:1, hexanes:EtOAc) to render 2-trifluoromethyl-10-acetylphenoxazine as an off-white solid (2.1 g, 85%). ^{1}H NMR (400 MHz; $CDCl_3$): δ 7.87 (d, *J* = 1.8 Hz, 1H), 7.48-7.46 (m, 1H), 7.42-7.39 (s, 1H), 7.26-7.15 (m, 4H), 2.35 (s, 3H). Spectra were consistent with previous reports.[57]

O-acetyl-3-hydroxy-10-acetylphenoxazine (2.31). Phenoxazone (0.80 g, 4.1 mmol) and anhydrous $SnCl_2$ (2.4 g, 13 mmol) were suspended in acetic anhydride (10 mL) with triethylamine (0.11 mL, 0.20 eq.). The reaction was heated to 120 °C under vigorous stirring and reaction progress monitored by TLC. After completion, the reaction was quenched in saturated Na_2CO_3 and the aqueous mixture extracted thrice with EtOAc. The organic phase was washed twice with water, dried over $MgSO_4$, filtered and the solvent removed under reduced pressure. This afforded the crude product as a light yellow solid (0.64 g, 56%) which was further purified by column chromatography (9:1, hexanes:EtOAc). ^{1}H NMR (400 MHz; benzene-d_6): δ 7.26-7.21 (m, 2H), 6.93 (d, *J* = 2.6 Hz, 1H), 6.89-6.87 (m, 1H), 6.79-6.72 (m, 2H), 6.69 (dd, *J* = 2.6, 8.7 Hz, 1H), 1.75 (s, 3H), 1.68 (s, 3H). ^{13}C NMR (101 MHz; benzene-d_6): δ 169.6, 168.5, 152.0, 151.4, 149.7 130.4, 128.0, 127.1, 126.1, 125.9, 124.0, 117.3, 117.0, 111.2, 22.8, 20.7. HRMS (EI, magnetic sector): calcd for $C_{16}H_{13}NO_4$ 283.08446, found 283.08662.

3-Methoxy-10-acetylphenoxazine (2.32). O-acetyl-3-hydroxy-10-acetylphenoxazine (0.59 g, 2.1 mmol) was dissolved in methanol (20 mL) under a N_2 atmosphere. Stirring at room temperature, 4 mL of aqueous 10% K_2CO_3 solution was added. The reaction was monitored by TLC, with the starting material (1:1 Hexane:EtOAc, Rf = 0.50) giving way to the hydrolyzed intermediate (Rf = 0.40). The reaction mixture was quenched with 1 M HCl and extracted thrice with EtOAc. The organic phase was dried over $MgSO_4$, filtered and the solvent removed under reduced pressure. The green residue was immediately dissolved into DMF (15 mL) to which K_2CO_3 was added (0.75 g, 5.4 mmol) and the mixture was placed under a N_2 atmosphere. Under vigorous stirring, methyl iodide was added (0.17 mL 2.7 mmol) and the reaction left to stir overnight. On completion, the reaction mixture was poured into water, and the aqueous mixture extracted thrice with EtOAc. The organic phase was washed twice with water, dried over $MgSO_4$, filtered and the solvent removed under reduced pressure. The residue was purified by column chromatography (3:1, hexanes:EtOAc) to render 3-methoxy-10-acetylphenoxazine as an amber coloured transparent residue (0.38 g, 71%). ^{1}H NMR (400 MHz; benzene-d_6): δ 7.37 (br, 1H), 7.20 (br, 1H), 6.98-6.96 (m, 1H), 6.83-6.76 (m, 2H), 6.63 (d, J = 2.7 Hz, 1H), 6.44 (dd, J = 2.8, 8.8 Hz, 1H), 3.16 (s, 1H), 1.83 (s, 1H). ^{13}C NMR (101 MHz; benzene-d_6): δ 168.8, 159.1, 152.6, 151.6, 130.9, 127.0, 126.3, 126.0, 123.8, 123.5, 117.2, 109.7, 102.9, 55.4, 22.8. HRMS (EI, magnetic sector): calcd for $C_{15}H_{13}NO_3$ 255.08954, found 255.09214.

3,7-Dimethoxy-10-acetylphenoxazine (2.33). 3,7-Dihydroxy-10-acetylphenoxazine (0.69 g, 2.7 mmol) and methyl iodide (0.34 mL, 5.5 mmol) were dissolved in DMF (15 mL) to which K_2CO_3 was added (0.79 g, 5.7 mmol). The mixture was stirred overnight at

room temperature, then poured into water and the aqueous mixture extracted thrice with EtOAc. The organic phase was washed twice with water, dried over $MgSO_4$, filtered and the solvent removed under reduced pressure. An orange residue was afforded which solidified overnight on standing in a freezer. The solid was recyrstallized twice from ethanol to afford orange needles (0.42 g, 55%); mp 118-120 °C; ^{1}H NMR (400 MHz; $CDCl_3$): δ 7.38-7.36 (m, 2H), 6.70-6.67 (m, 4H), 3.81 (s, 6H), 2.29 (s, 3H). ^{13}C NMR (101 MHz; $CDCl_3$): δ 169.6, 158.3, 151.7, 125.5, 122.6, 109.0, 102.5, 55.7, 22.8. HRMS (EI, magnetic sector): calcd for $C_{16}H_{15}NO_4$ 285.10011, found 285.09708.

3-Nitro-10-acetylphenoxazine (2.34). In glacial acetic acid (12 mL) was suspended 10-acetylphenoxazine (1.1 g, 5.0 mmol) and solution of HNO_3 diluted in acetic acid (3:4, HNO_3:AcOH, 1.4 mL) was added with swirling for ~3 minutes where the suspension dissolves to give a single red phase. The reaction mixture is allowed to stand (without stirring) for ~15 minutes after which the reaction was poured into 50 mL of water. The resulting precipitate was filtered and recrystallized from ethanol to afford the 3-nitro-10-acetylphenoxazine as orange needles (1.1 g, 82%); mp 136-138 °C; ^{1}H NMR (400 MHz; DMSO-d_6): δ 8.08 (dd, J = 2.7, 8.9 Hz, 1H), 8.00 (d, J = 2.6 Hz, 1H), 7.89 (d, J = 8.9 Hz, 1H), 7.65 (dd, J = 1.9, 7.9 Hz, 1H), 7.36-7.23 (m, 3H), 2.32 (s, 3H). ^{13}C NMR (101 MHz; DMSO-d_6): δ 168.9, 150.2, 149.4, 145.3, 135.2, 128.3, 127.6, 125.9, 125.2, 124.4, 119.0, 116.8, 111.9, 22.9. HRMS (EI, magnetic sector): calcd for $C_{14}H_{10}N_2O_4$ 270.06406, found 270.06128.

2-(2,4-Dinitrophenyl)amino-5-methoxyphenol (2.35). 2-Amino-5-methoxyphenol (0.32 g, 2.3 mmol) and 1-chloro-2,4-dinitrobenzene (0.47 g, 2.3 mmol) were dissolved in a

mixture of ethanol (25 mL) and water (5 mL) to which sodium acetate (0.76 g, 9.3 mmol) was added. The solution was heated to reflux, under vigorous stirring for 4 hours, then allowed to cool. The reddish precipitate was filtered and purified by column chromatography (3:1, hexanes:EtOAc) to afford the product as red needles (0.59 g, 84% yield); mp 168-170 °C; ^{1}H NMR (400 MHz; DMSO-d_6): δ 9.96 (br, 1H), 9.81 (br, 1H), 8.89 (d, *J* = 2.7 Hz, 1H), 8.21 (dd, *J* = 2.7, 9.6 Hz, 1H), 7.17 (d, *J* = 8.6 Hz, 1H), 6.78 (d, *J* = 9.6 Hz, 1H), 6.57 (d, *J* = 2.7 Hz, 1H) 6.52 (dd, *J* = 2.7, 8.6 Hz, 1H), 3.75 (s, 3H). ^{13}C NMR (101 MHz; DMSO-d_6): δ 159.5, 153.5, 147.7, 135.7, 130.4, 129.6, 128.7, 123.3, 117.1, 117.0, 105.3, 102.2, 55.2. HRMS (EI, magnetic sector): calcd for $C_{13}H_{11}N_3O_6$ 305.06479, found 305.06249.

3-Methoxy-7-nitrophenoxazine (2.13). 2-(2,4-Dinitrophenyl)amino-5-methoxyphenol (0.2 g, 0.7 mmol) was dissolved in dry DMF (4 mL) and heated to 100 °C with stirring under a N_2 atmosphere. At 100 °C, crushed NaOH was added (0.07 g, 2 mmol) and the mixture was heated to 120 °C for 2 hours. The reaction mixture was poured into water and extracted 3 times with Et_2O. The organic solution was washed twice with water, dried over $MgSO_4$, filtered and the solvent removed under reduced pressure. The product was purified by column chromatography (3:1, hexanes:EtOAc) to afford a deep red solid (0.10 g, 55%) ^{1}H NMR (400 MHz; DMSO-d_6): δ 9.27 (br, 1H), 7.69 (dd, *J* = 2.6, 8.8 Hz, 1H), 7.31 (d, *J* = 2.6 Hz), 6.48 (d, *J* = 8.5 Hz, 1H), 6.47 (d, *J* = 8.8 Hz, 1H), 6.40 (dd, *J* = 2.7, 8.5 Hz, 1H), 6.36 (d, *J* = 2.7 Hz, 1H), 3.65 (s, 3H). ^{13}C NMR (75 MHz; DMSO-d_6): δ 155.3, 142.8, 141.4, 139.9, 138.8, 122.5, 122.2, 114.6, 111.6, 110.0, 108.7, 102.5, 55.4. HRMS (EI, magnetic sector): calcd for $C_{13}H_{10}N_2O_4$ 258.06406, found 258.06296.

N,N-Diethyl-3-sulfonamidephenoxazine (2.11). 3,4-Difluorobenzenesulfonyl chloride

(0.81 g, 3.8 mmol) was dissolved into dry DCM (4.3 mL) cooled to 0 °C. Under vigorous stirring, diethylamine was added (1.4 mL, 3 eq.). Once the difluorobenzenesulfonyl chloride was consumed, the mixture was poured into water and extracted twice with EtOAc. The organic solution was dried over $MgSO_4$, filtered and the solvent removed under reduced pressure. The resulting solid was dissolved in DMSO (20 mL) and placed in a sealed tube along with 2-aminophenol (0.42 g, 3.8 mmol) to which K_2CO_3 was added (1.3 g, 9.6 mmol). The reaction was heated to 135 °C for 14 hours with vigorous stirring after which the reaction was cooled, quenched with water and the aqueous mixture extracted thrice with EtOAc. The organic phase was washed twice with water, dried over $MgSO_4$, filtered and the solvent removed under reduced pressure. The crude solid was purified by column chromatography (3:1, hexanes:EtOAc) to render the product as off-white solid (0.85 g, 70%) and subsequently recrystallized from Et_2O to afford off-white needles; mp 154-156 °C; ^{1}H NMR (400 MHz; DMSO-d_6): δ 8.81 (b, 1H), 7.14 (dd, J = 2.1, 8.2 Hz, 1H), 6.84 (d, J = 2.1 Hz, 1H), 6.77-6.74 (m, 1H), 6.66-6.61 (m, 2H), 6.52 (d, J = 8.2 Hz, 1H), 6.49-6.47 (m, 1H), 3.10 (q, J = 7.2 Hz, 4H), 1.04 (t, J = 7.2 Hz, 6H). ^{13}C NMR (101 MHz; DMSO-d_6): δ 142.6, 142.4, 136.6, 130.7, 130.2, 124.4, 123.9, 121.5, 115.2, 113.2, 113.1, 112.7, 41.7, 14.1. HRMS (EI, magnetic sector): calcd for $C_{16}H_{18}N_2O_3S$ 318.10381, found 318.10173.

2,4,6,8-Tetra-*tert*-butylphenoxazine (2.9). To a solution of 2,4-di-*tert*-butyl-6-nitrophenol (5.5 g, 22 mmol) in glacial acetic acid (88 mL) was added zinc dust (5.0 g, 77 mmol) in portions with vigorous stirring while heating to 90 °C. The slurry was held at 90 °C for 45 minutes and refluxed for 15 minutes. After cooling the mixture was poured into water and extracted thrice with Et_2O. The organic phase was washed with water, dried

over $MgSO_4$, filtered and the solvent removed under reduced pressure. The residue was purified by column chromatography (95:5, pet. ether:Et_2O) to render a light purple solid which was recyrstallized from hexanes to afford 2,4,6,8-tetra-*tert*-butylphenoxazine (0.76 g, 17%); mp 191-193 °C; ^{1}H NMR (400 MHz; DMSO-d_6): δ 7.83 (br, 1H), 6.53 (s, 2H), 6.29 (s, 2H), 1.38 (s, 18H), 1.18 (s, 18H). ^{13}C NMR (101 MHz; DMSO-d_6): δ 144.8, 139.3, 135.1, 132.0, 114.4, 108.8, 34.2, 33.8, 31.0, 30.5. HRMS (EI, magnetic sector): calcd for $C_{28}H_{41}NO$ 407.31881, found 407.32343.

2,8-Di-*tert*-butylphenoxazine (2.10). To a solution of 2,4-di-*tert*-butyl-6-nitrophenol (5.5 g, 22 mmol) in glacial acetic acid (88 mL) was added zinc dust (5.0 g, 77 mmol) by portion with vigorous stirring while heating to 90 °C. The slurry was held at 90 °C for 45 minutes and refluxed for 30 minutes. After cooling the mixture was poured into water and extracted thrice with EtOAc. The organic phase was washed with water, dried over $MgSO_4$, filtered and the solvent removed under reduced pressure. The residue was purified by column chromatography (95:5,hexane:EtOAc) to render a dark violet oil. It was dissolved in glacial acetic acid and zinc was added until the solution was colorless, which was then quenched with Na_2CO_3 solution and extracted with EtOAc. After removal of the solvent, a violet solid was afforded which was recrystallized from hexanes to afford the 2,8-di-*tert*-butylphenoxazine (0.24 g, 7%) as purple needles; mp 161-162 °C; ^{1}H NMR (400 MHz; benzene-d_6): δ 6.71 (d, J = 8.3 Hz, 2H), 6.54 (dd, J = 2.3, 8.3 Hz, 2H), 6.11 (d, J = 2.3 Hz, 2H), 4.07 (b, 1H), 1.24 (s, 18H). ^{13}C NMR (101 MHz; DMSO-d_6): δ 146.1, 140.7, 131.8, 116.6, 114.4, 110.4, 33.8, 31.1. HRMS (EI, magnetic sector): calcd for $C_{20}H_{25}NO$ 295.19361, found 295.19103.

3-Nitro-7-cyanophenoxazine (2.15). 3-Cyanophenoxazine (0.50 g, 2.4 mmol) was

suspended in glacial acetic acid (25 mL) and acetonitrile was added until the solute dissolved (6 mL). With stirring, 1.1 eq. of 70% HNO_3 was added, immediately the product crashed out as an orange amorphous precipitate (0.39 g, 65%) which was filtered and rinsed with Et_2O. The product was further purified by column chromatography (1:1, hexanes:EtOAc) and recrystallized from ethanol to afford fine red needles; 215-220 °C (decomposes); ^{1}H NMR (400 MHz; DMSO-d_6): δ 9.83 (s, 1H), 7.71 (dd, *J* = 2.6, 8.7 Hz, 1H), 7.34 (d, *J* = 2.5 Hz, 1H), 7.24 (dd, *J* = 1.8, 8.1 Hz, 1H), 7.07 (d, *J* = 1.7 Hz, 1H), 6.58 (d, *J* = 8.1 Hz, 1H), 6.56 (d, *J* = 8.7 Hz, 1H). ^{13}C NMR (101 MHz; DMSO-d_6): δ 142.3, 142.1, 140.7, 137.8, 134.8, 130.1, 121.9, 118.6, 118.1, 114.4, 113.0, 110.2, 103.4, HRMS (EI, magnetic sector): calcd for $C_{13}H_7N_3O_3$ 253.04874, found 253.04391.

3-Trifluoromethylphenoxazine (2.5). In sealed tube flushed with N_2 were added 1-iodo-2-(2-nitrophenoxy)-4-(trifluoromethyl)benzene (0.97 g, 2.3 mmol), K_2CO_3 (0.64 g, 4.6 mmol), copper(I) iodide (0.02 g, 0.05 eq.), N,N'-dimethylethylenediamine (0.03 mL, 0.1 eq.), and toluene (10 mL). The reaction was heated to 130 °C under vigorous stirring for at least 10 hours. After completion, the reaction mixture was diluted with dichloromethane and passed through a plug of silica, after which the solvent was removed under reduced pressure. The residue was dissolved in EtOH (20 mL) with stirring and was placed under N_2 and heated to 75 °C to which 33% aqueous HCl was added (5 mL). The reaction was monitored by TLC, and after 2 hours the mixture was cooled then quenched with Na_2CO_3 solution. The aqueous mixture was extracted 3 times with EtOAc. The organic solution was washed twice with water, dried over $MgSO_4$, filtered and the solvent removed under reduced pressure. The crude product was recrystallized from hexanes to afford beige plates (0.36 g, 61%); mp 145-146 °C; ^{1}H NMR (400 MHz; DMSO-d_6): δ 8.70 (br, 1H), 7.07-7.04 (m, 1H), 6.85 (d, *J* = 2.0 Hz, 1H), 6.79-6.73 (m, 1H), 6.65-6.61 (m, 2H) 6.54 (dd, 0.7, 8.2

Hz, 1H), 6.49-6.47 (m, 1H). ^{13}C NMR (101 MHz; DMSO-d_6): δ 142.8, 142.4, 136.3, 131.0, 124.4, 124.1 (q, $J_{C\text{-}F}$ = 270.7 Hz), 121.5 (q, $J_{C\text{-}F}$ = 4.4 Hz), 121.4, 120.2 (q, $J_{C\text{-}F}$ = 32.6 Hz), 115.2, 113.7, 112.9, 111.7 (q, $J_{C\text{-}F}$ = 3.7 Hz). ^{19}F NMR (376 MHz, $CDCl_3$): δ -63.41. HRMS (EI, magnetic sector): calcd for $C_{15}H_{11}F_3NO$ 251.05580, found 251.05612.

3,7-Di-*tert*-butylphenoxazine (2.8). Same general procedure using N-(4-(*tert*-butyl)-2-(5-(*tert*-butyl)-2-iodophenoxy)phenyl)acetamide (0.68 g, 1.5 mmol) for the CuI catalyzed intramolecular Ullmann coupling followed by subsequent amide hydrolysis in EtOH. The product was recrystallized from hexanes to afford white needles (0.18 g, 41%); mp 185-187 °C; ^{1}H NMR (400 MHz; DMSO-d_6): δ 7.96 (br, 1H), 6.72 (dd, *J* = 2.2, 8.1 Hz, 2H), 6.61 (d, *J* = 2.1 Hz, 2H), 6.36 (d, *J* = 8.1 Hz, 2H), 1.18 (s, 18H). ^{13}C NMR (101 MHz; DMSO-d_6): δ 142.9, 142.3, 130.0, 119.9, 112.6, 112.3, 33.7, 31.1. HRMS (EI, magnetic sector): calcd for $C_{20}H_{25}NO$ 295.19361, found 295.19103.

2-*tert*-Butylphenoxazine (2.6). 10-Acetyl-2-*tert*-butylphenoxazine (0.24 g, 0.84 mmol) was dissolved in EtOH (5 mL) with stirring and was placed under N_2 and heated to 75 °C to which 33% aqueous HCl was added (1 mL). The reaction was monitored by TLC, and after 2 hours the mixture was cooled then quenched with Na_2CO_3 solution. The aqueous mixture was extracted 3 times with EtOAc. The organic phase was washed twice with water, dried over $MgSO_4$, filtered and the solvent removed under reduced pressure. The crude product was recrystallized from hexanes to afford silver plates (0.13 g, 65%); mp 125-127 °C; ^{1}H NMR (400 MHz; DMSO-d_6): δ 8.10 (br, 1H), 6.70 (ddd, *J* = 1.8, 7.6, 7.6 Hz, 1H), 6.59-6.51 (m, 4H), 6.47 (d, *J* = 2.2 Hz, 1H), 6.43 (dd, *J* = 1.4, 7.6 Hz, 1H), 1.19 (s, 9H). ^{13}C NMR (101 MHz; DMSO-d_6): δ 146.3, 142.8, 140.5, 132.5, 131.7, 123.7, 120.1,

116.8, 115.0, 114.4, 113.2, 110.5, 33.8, 31.1. HRMS (EI, magnetic sector): calcd for $C_{16}H_{17}NO$ 239.13101, found 239.12987.

3-*tert*-Butylphenoxazine (2.7). Same general amide hydrolysis with 10-acetyl-3-tert-butylphenoxazine (0.16 g, 0.55 mmol). The product was recrystallized from hexanes to afford fine white needles (0.09 g, 70%); mp 132-135 °C; ^{1}H NMR (400 MHz; DMSO-d_6): δ 8.06 (br, 1H), 6.73-6.68 (m, 2H), 6.62 (d, J = 2.1 Hz, 1H), 6.59-6.52 (m, 2H), 6.43 (dd, J = 1.5, 7.7 Hz, 1H), 6.37 (d, J = 8.1 Hz, 1H), 1.18 (s, 9H). ^{13}C NMR (101 MHz; DMSO-d_6): δ 143.2, 142.7, 142.3, 132.6, 129.7, 123.8, 120.0(2), 120.0(0), 115.0, 113.2, 112.7, 112.3, 33.7, 31.1. HRMS (EI, magnetic sector): calcd for $C_{16}H_{17}NO$ 239.13101, found 239.12987.

2-Trifluoromethylphenoxazine (2.4). Same general amide hydrolysis with 10-acetyl-2-trifluoromethylphenoxazine (2.2 g, 7.4 mmol). The product was resolved as white prismatic crystals (1.5 g, 80%); mp 153-154 °C; ^{1}H NMR (400 MHz; DMSO-d_6): δ 8.51 (br, 1H), 6.90-6.87 (m, 1H), 6.79-6.73 (m, 2H), 6.66-6.59 (m, 3H), 6.46 (dd, J = 1.4, 7.6 Hz, 1H). ^{13}C NMR (101 MHz; DMSO-d_6): δ 145.8, 142.2, 133.3, 131.2, 124.5(5), 124.6(0) (q, J_{C-F} = 32.3 Hz), 124.0 (q, J_{C-F} = 271.4 Hz), 121.1, 117.5 (q, J_{C-F} = 4.4 Hz), 115.4, 115.3, 113.6, 109.2 (q, J_{C-F} = 3.7 Hz) ^{19}F NMR (376 MHz, $CDCl_3$): δ -63.78. HRMS (EI, magnetic sector): calcd for $C_{15}H_{11}F_3NO$ 251.05580, found 251.07123.

***3*-Nitrophenoxazine (2.14).** Same general amide hydrolysis with 10-acetyl-3-nitrophenoxazine (0.30 g, 1.1 mmol). After quenching with Na_2CO_3 solution the product precipitated out and was then filtered and washed with a minimum of methanol followed by petroleum ether to afford fine olive coloured needles (0.23 g, 91%); mp 185-188 °C; ^{1}H NMR (400 MHz; DMSO-d_6): δ 9.34 (br, 1H), 7.67 (dd, J = 2.4, 8.7 Hz, 1H), 7.31 (d, J

= 2.4 Hz, 1H), 6.81-6.77 (m, 1H), 6.71-6.64 (m, 2H), 6.53-6.48 (m, 2H). ^{13}C NMR (101 MHz; DMSO-d_6): δ 142.2(0), 142.1(8), 139.7, 139.5, 129.5, 124.5, 122.6, 121.9, 115.3, 114.3, 111.9, 110.00. HRMS (EI, magnetic sector): calcd for $C_{12}H_8N_2O_3$ 228.05349, found 228.05201.

3-Methoxyphenoxazine (2.16). Same general amide hydrolysis with 10-acetyl-3-methoxyphenoxazine (0.38 mg, 1.5 mmol). The charcoal coloured solid afforded required no further purification. ^{1}H NMR (400 MHz; DMSO-d_6): δ 7.93 (br, 1H), 6.72 (ddd, *J* = 1.6, 7.6, 7.6 Hz, 1H), 6.60-6.51 (m, 2H), 6.43 (dd, *J* = 1.5, 7.7 Hz, 1H), 6.40-6.29 (m, 3H), 3.63 (s, 3H). ^{13}C NMR (101 MHz; DMSO-d_6): δ 153.7, 143.2, 142.1, 132.8, 125.6, 124.0, 119.7, 115.0, 113.4, 113.1, 108.1, 102.4, 55.3. HRMS (EI, magnetic sector): calcd for $C_{13}H_{11}NO_2$ 213.07898, found 213.07801.

3,7-Dimethoxyphenoxazine (2.17). Same general amide hydrolysis with 10-acetyl-3,7-dimethoxyphenoxazine (0.40 g, 1.4 mmol). After quenching with Na_2CO_3 solution the product began to precipitate as needles. The flask was placed in the freezer overnight and the product was filtered the following day to afford the maroon coloured product (0.26 g, 75%). ^{1}H NMR (400 MHz; DMSO-d_6): δ 7.68 (br, 1H), 6.39-6.30 (m, 6H), 3.63 (s, 6H). ^{13}C NMR (101 MHz; DMSO-d_6): δ 155.3, 142.5, 126.1, 113.4, 108.3, 102.4, 55.3. HRMS (EI, magnetic sector): calcd for $C_{14}H_{13}NO_3$ 243.08954, found 243.09118.

Inhibited Co-autoxidation of PBD-BODIPY and Styrene. To a 3 mL cuvette was added 1.25 mL of purified styrene and 1.18 mL of PhCl. The cuvette was placed in the sample holder of a UV-visible spectrophotometer and equilibrated to 37 °C. PBD-BODIPY (12.5 μL of a 2.0 mM solution in 1,2,4-trichlorobenzene) was added, succeeded by 50 μL of 0.3 M AIBN in PhCl, and the contents of cuvette briefly agitated to

thoroughly mix the contents. The absorbance at 591 nm was monitored for 15 minutes to ensure linear reaction progress, after which 10 μL of a 0.5 mM solution of inhibitor was added followed by thorough mixing for a final antioxidant concentration of 2 μM (unless noted otherwise). The rate of initiation ($R_i = 2.7 \times 10^{-9}$ M s^{-1}) was determined using PMC as a standard, which has an established stoichiometry of n = 2.[62]

Inhibited Co-autoxidation of PBD-BODIPY and Dioxane. To a 3 mL cuvette was added 620 μL of certified ACS 1,4-dioxane and either 1.80 mL of PhCl or 1.18 mL of PhCl with 620 μL of DMSO. The following steps are identical to the protocol described immediately above) though the absorbance was monitored at 587 nm (ε = 123 000 M^{-1} cm^{-1} in PhCl, ε = 118 200 M^{-1} cm^{-1} in 2:1 PhCl:DMSO). The rate of initiation in PhCl ($R_i = 2.4 \times 10^{-9}$ M s^{-1}) and in 2:1 PhCl:DMSO ($R_i = 2.1 \times 10^{-9}$ M s^{-1}) required to determine stoichiometric data were standardized by PMC and tetrahydronaphthyridinol (C_{10}-THN, structure in ESI)[63] respectively maintaining that n = 2. The rate constant for propagation by PBD-BODIPY in the aforementioned solvent systems ($k_{\text{PBD-BODIPY}}$ = 5310 M^{-1} s^{-1} and $k_{\text{PBD-BODIPY}}$ = 5900 M^{-1} s^{-1}) were determined from the uninhibited rate of PBD-BODIPY consumption under the conditions of the experiment assuming that k_t is equal to that of the peroxyl derived from 1,4-dioxane ($k_t = 2.5 \times 10^7$ M^{-1} s^{-1})[19] and calculated from the previously derived Eq. 2.8:[14]

$$\frac{-\delta[\text{PBD}-\text{BODIPY}]}{\delta t} = \frac{k_{\text{PBD}-\text{BODIPY}}}{\sqrt{2k_t}}\sqrt{R_i}[\text{PBD} - \text{BODIPY}] \qquad \text{Eq. 2.8}$$

R_i and $k_{\text{PBD-BODIPY}}$ provide the means to calculate k_{inh}^{Diox} and k_{inh}^{DMSO} with Eq. 2.3 in Figure 2.1C.

Determination of Solvent Mixture β_2^H by ^{19}F NMR. The H-bond accepting solvent mixture of interest was diluted into CCl_4 to render four dilute solutions of varying concentrations (see ESI) and one 1.2 M solution. To these were added 4-fluorophenol and 4-fluoroanisole to a final concentration of 0.01 M of each. The solutions were transferred into NMR tubes containing sealed capillaries of benzene-d_6 with α,α,α-trifluorotoluene, after which their ^{19}F NMR spectra were obtained at multiple temperatures using a thermostatted 300 MHz NMR instrument. At a given temperature, the K_f of the 4-fluorophenol and the H-bond acceptor(s) is described by Eq. 2.9:[22]

$$K_f = \frac{(\delta/\Delta)A_0}{\{A_0[1-(\delta/\Delta)]\}[B_0-(\delta/\Delta)A_0]} \qquad \text{Eq. 2.9}$$

where A_0 is the concentration of 4-fluorophenol, B_0 is the concentration of H-bond acceptor(s), Δ is the chemical shift difference between 4-fluorophenol and 4-fluoroanisole at B_0 = 1.20 M and δ is the chemical shift difference between 4-fluorophenol and 4-fluoroanisole at the dilute concentrations of H-bond acceptor(s). The effective β_2^H can be calculated from this K_f via Eq. 2.10 and Eq. 2.11:

$$\log K_f = L_A \, log \, K_B^H + D_A \qquad \text{Eq. 2.10}$$

$$\beta_2^H = (\log K_B^H + 1.1)/\, 4.636 \qquad \text{Eq. 2.11}$$

where L_A = 1 and D_A = 0 when the reference H-bond donor is 4-fluorophenol.[18]

Determination of Phenoxazine α_2^H by ^{1}H NMR. Two ~3 mg portions of the H-bond donor species of interest were dissolved into 700 μL of each of DMSO-d_6 and benzene-d_6. The ^{1}H NMR spectra of each were obtained and the chemical shifts were referenced to the residual solvent peaks of the solvents (2.50 ppm and 7.16 ppm for DMSO and benzene, respectively.) The α_2^H value was then determined from the difference in the chemical shift of the proton of interest between the two spectra ($\Delta\delta_{DMSO\text{-}Ben}$) as in Eq. 2.7:

$$\alpha_2^H = 0.134\Delta\delta_{DMSO-Ben} - 0.1087 \qquad \text{Eq. 2.7}$$

The correlation of α_2^H and $\Delta\delta_{DMSO\text{-}Ben}$ was constructed by obtaining ^{1}H NMR spectra in both DMSO-d_6 and benzene-d_6 for 11 different H-bond donors whose α_2^H values (ranging from 0.08 to 0.82) were independently determined and plotting the chemical shift differences ($\Delta\delta_{DMSO\text{-}Ben}$) vs. α_2^H. See ESI for further elaboration.

Electrochemistry. Standard potentials were measured by cyclic voltammetry at 25 °C in dry acetonitrile containing $Bu_4N{\cdot}PF_6$ (0.1 M) as electrolyte. Experiments were carried out with a potentiostat equipped with a glassy-carbon working electrode, a platinum auxiliary electrode, and a $Ag/AgNO_3$ (0.005 M) reference electrode. The given E^o were determined relative to the ferrocene/ferrocenium couple under the same conditions (Fc/Fc^+ vs NHE +0.64 V).[64]

Computations. Quantum chemical calculations were carried out using the CBS-QB3 complete basis set method[65] as it is implemented in the Gaussian 09 suite of programs.[66] Molecular orbitals were rendered at an isovalue of 0.015 using the B3LYP/CBSB7 wavefunctions.

2.7 References

(1) Ingold, K. U. *Chem. Rev.* **1961**, *61*, 563–589.

(2) Ingold, K. U.; Pratt, D. A. *Chem. Rev.* **2014**, *114*, 9022–9046.

(3) Pratt, D. A.; DiLabio, G. A.; Mulder, P.; Ingold, K. U. *Acc. Chem. Res.* **2004**, *37*, 334–340.

(4) Valgimigli, L.; Pratt, D. A. In *Encyclopedia of Radicals in Chemistry, Biology and Materials*; John Wiley & Sons, Ltd: Chichester, UK, 2012; pp 1623–1677.

(5) (a) Brownlie, I. T.; Ingold, K. U. *Can. J. Chem.* **1967**, *45*, 2419–2425; (b) Hansch, C.; Gao, H. *Chem. Rev.*, **1997**, *97*, 2995-3059.

(6) Lucarini, M.; Pedrielli, P.; Pedulli, G. F.; Valgimigli, L.; Gigmes, D.; Tordo, P. *J. Am. Chem. Soc.* **1999**, *121*, 11546–11553.

(7) Pratt, D. A.; Dilabio, G. A.; Valgimigli, L.; Pedulli, G. F.; Ingold, K. U. *J. Am. Chem. Soc.* **2002**, *124*, 11085–11092.

(8) (a) Hanthorn, J. J.; Valgimigli, L.; Pratt, D. A. *J. Am. Chem. Soc.* **2012**, *134*, 8306–8309; (b) Hanthorn, J. J.; Valgimigli, L.; Pratt, D. A. *J. Org. Chem.* **2012**, *77*, 6895-6907.

(9) The value reported in reference 6 should be reduced by 1.1 kcal mol^{-1} to account for the revised O−H BDE of 2,4,6-tri-*tert*-butylphenol used as the reference in the radical equilibration EPR measurements. See: Mulder, P.; Korth, H.-G.; Pratt, D. A.; Dilabio, G. A.; Valgimigli, L.; Pedulli, G. F.; Ingold, K. U. *J. Phys. Chem. A* **2005**, *109*, 2647–2655.

(10) In previous work we have shown that some substituted heteroaryl (i.e. pyridyl and pyrimidyl) analogues of diphenylamines are similarly reactive, with k_{inh} values up to $\sim 4 \times 10^7$ M^{-1} s^{-1}. See references 8a and 8b.

(11) The half-wave potentials of phenothiazine (0.82 V [6] and 0.83 V,[a] $E^{1/2}$ vs. NHE) and

phenoxazine (0.83 V,[b] $E^{1/2}$ vs. NHE) have been reported (measured in acetonitrile with a saturated calomel electrode). Using an identical potentiostat, condition and internal standard (see Experimental VII) we consistently measured E^o ($E^{1/2}$ vs. NHE) of 0.85 and 0.87 V for phenothiazine and phenoxazine, respectively. See: (a) Billon, J.-P. *Ann. Chim.*, **1962**, *7*, 183. (b) Kowert, B. A.; Marcoux, L.; Bard, A. J. *J. Am. Chem. Soc.*, **1972**, *94*, 5538–5550.

(12) Howard, J. A.; Ingold, K. U. *Can. J. Chem.* **1962**, *40*, 1851–1864.

(13) Burton, G. W.; Ingold, K. U. *J. Am. Chem. Soc.* **1981**, *103*, 6472–6477.

(14) Haidasz, E. A.; Van Kessel, A. T. M.; Pratt, D. A. *J. Org. Chem.* **2016**, *81*, 737–744.

(15) Snelgrove, D. W.; Lusztyk, J.; Banks, J. T.; Mulder, P.; Ingold, K. U. *J. Am. Chem. Soc.* **2001**, *123*, 469–477.

(16) Litwinienko, G.; Ingold, K. U. *Acc. Chem. Res.* **2007**, *40*, 222–230.

(17) Abraham, M. H.; Grellier, P. L.; Prior, D. V.; Duce, P. P.; Morris, J. J.; Taylor, P. J. *J. Chem. Soc. Perkin Trans. 2* **1989**, 699–711.

(18) Abraham, M. H.; Grellier, P. L.; Prior, D. V.; Morris, J. J.; Taylor, P. J. *J. Chem. Soc. Perkin Trans. 2* **1990**, 521–529.

(19) Howard, J. A.; Ingold, K. U. *Can. J. Chem.* **1969**, *47*, 3809–3815.

(20) Arnett, E. M.; Joris, L.; Mitchell, E.; Murty, T. S. S. R.; Gorrie, T. M.; Schleyer, P. von R. *J. Am. Chem. Soc.* **1970**, *92*, 2365–2377.

(21) Foti, M. C.; Barclay, L. R. C.; Ingold, K. U. *J. Am. Chem. Soc.* **2002**, *124*, 12881–12888.

(22) Taft, R. W.; Gurka, D.; Joris, L.; von Schleyer, R.; Rakshys, J. W. *J. Am. Chem. Soc.* **1969**, *91*, 4794–4801.

(23) The log K_f for complex formation between 4-fluorophenol and the HBA was determined for the temperature at which the inhibited autoxidations were carried out (37 °C). See ESI for further elaboration.

(24) Abraham, M. H.; Abraham, R. J.; Byrne, J.; Griffiths, L. *J. Org. Chem.* **2006**, *71*, 3389–3394.

(25) Chlorobenzene is the most commonly used solvent for inhibited autoxidation experiments, dating back over 50 years. Hence, we have used this as the reference medium in order to enable comparisons to previously reported data.

(26) The synthesis of 5-hydroxy-4,6-dimethyl-2-dimethylaminopyrimidine **C**[a] and 5-hydroxy-2-dimethylaminopyrimidine **B**[b] and the α_2^H of PMC **A** (0.38)[c] and compound **C** (0.53)[c] were previously reported. See: (a) Pratt, D. A.; DiLabio, G. A.; Brigati, G.; Pedulli G. F.; Valgimigli, L. *J. Am. Chem. Soc.*, **2001**, *123*,4625–4626. (b) Nara, S. J.; Jha, M.; Brinkhorst, J.; Zemanek, T. J.; Pratt, D. A. *J. Org. Chem.*, **2008**, *73*, 9326–9333. (c) Valgimigli, L.; Bartolomei, D.; Amorati, R.; Haidasz, E.; Hanthorn, J. J.; Nara, S. J.; Brinkhorst, J.; Pratt, D. A. *Beilstein J. Org. Chem.*, **2013**, *9*, 2781–2792.

(27) Chauvin, J.-P. R.; Griesser, M.; Pratt, D. A. *J. Am. Chem. Soc.* **2017**, *139*, 6484–6493.

(28) Burton, G. W.; Ingold, K. U. *Acc. Chem. Res.* **1986**, *19*, 194–201.

(29) Rickert, H. B.; Geiger, W. M. 2,4,6,8-Tetra-Tertiarybutylphenoxazine. US 2945856, 1960.

(30) Eastmond, G. C.; Gilchrist, T. L.; Paprotny, J.; Steiner, A. *New J. Chem.* **2001**, *25*, 385–390.

(31) Kolchina, E. F.; Kargapolova, I. Y.; Gerasimova, T. N. *Bull. Acad. Sci. USSR Div. Chem. Sci.* **1986**, *35*, 1685–1689.

(32) Moore, L. O. Reactions of phenoxazine and some of its derivatives. Ph. D. Dissertation, Iowa State College, 1957.

(33) Hansch, C.; Leo, A.; Taft, R. W. *Chem. Rev.* **1991**, *91*, 165–195.

(34) These calculations exhibit strong spin contamination presumably due to the the heavily delocalized π-system of the phenoxazine aminyl radical. Calculations

carried out within the restricted open shell formalism (ROCBS-QB3) were also performed for a few representative cases. Interestingly, these calculations further underestimated the BDEs (e.g. the BDE of phenoxazine was calculated to be 73.0 and 75.2 kcal mol^{-1} by ROCBS-QB3 and CBS-QB3, respectively, which can be compared to the experimental value of 76.1 kcal mol^{-1}).

(35) It has previously been observed that the N-H BDEs in di-substituted diphenylamines and phenothiazines also correlate very well with the sum of the σ_p^+ substituent constants. See ref. 7.

(36) DiLabio, G. A.; Johnson, E. R. *J. Am. Chem. Soc.* **2007**, *129*, 6199–6203.

(37) Vaidya, V.; Ingold, K. U.; Pratt, D. A. *Angew. Chemie Int. Ed.* **2009**, *48*, 157–160.

(38) Amorati, R.; Pedulli, G. F.; Pratt, D. A.; Valgimigli, L. *Chem. Commun.* **2010**, *46*, 5139–5141.

(39) Zielinski, Z.; Presseau, N.; Amorati, R.; Valgimigli, L.; Pratt, D. A. *J. Am. Chem. Soc.* **2014**, *136*, 1570–1578.

(40) Massie, S. P. *Chem. Rev.* **1954**, *54*, 797–833.

(41) The synthesis of phenoxazine has historically been accomplished by high temperature melts of catechol and o-aminophenol or o-aminophenol along with its corresponding hydrochloride salt. However, isolation and purification of the product from these routes can be arduous. Judging by more recent attempts to improve the process, it would seem a highly efficient and cost effective synthetic route has yet to be identified. See: (a) Bernthsen, A. *Chem. Ber.* **1887**, *20*, 943. (b) Kehrmann, F.; Neil, A. A. *Chem. Ber.***1914**, *47*, 3102. (c) Gaddam, O. R.; Mamillapali, R. S.; Batchu, C.; Chebiyyam, P. An Improved Process for the Preparation of 10H-Phenoxazine. WO2002034732, 2000.

(42) Murphy, C. M.; Ravner, H.; Smith, N. L. *Ind. Eng. Chem.* **1950**, *42*, 2479–2489.

(43) Warren, J. J.; Mayer, J. M. *Proc. Natl. Acad. Sci.* **2010**, *107*, 5282–5287.

(44) Bietti, M.; Salamone, M.; DiLabio, G. A.; Jockusch, S.; Turro, N. J. *J. Org. Chem.*

2012, *77*, 1267–1272.

(45) Previously Arrhenius plots spanning 310-368 K for H-atom transfer to peroxyl radicals by diarylamines indicated log A ~ 6.9-7.1. However, examples of highly reactive diarylamines converge at log k ~ 7.5, suggesting that log A ~ 7.5 is probable – see ref. 8.

(46) Wijtmans, M.; Pratt, D. A.; Valgimigli, L.; DiLabio, G. A.; Pedulli, G. F.; Porter, N. A. *Angew. Chemie Int. Ed.* **2003**, *42*, 4370–4373.

(47) Jonsson, M.; Wayner, D. D. M.; Lusztyk, J. *J. Phys. Chem.* **1996**, *100*, 17539–17543.

(48) Jensen, R. K.; Korcek, S.; Zinbo, M.; Gerlock, J. L. *J. Org. Chem.* **1995**, *60*, 5396–5400.

(49) Haidasz, E. A.; Shah, R.; Pratt, D. A. *J. Am. Chem. Soc.* **2014**, *136*, 16643–16650.

(50) The activation energy required to regenerate the diarylamine via homolysis and in-cage disproportionation is intrinsically related to the N-O BDE. Assuming that the difference in N-H BDEs of ADPAs and phenoxazine (6.1 kcal mol^{-1}) manifests itself fully in the difference in the strength of the weaker N-O bond, E_a for a phenoxazine-derived alkoxyamine can be estimated to be 27.4 kcal mol^{-1} (compared to ADPA where E_a = 33.5 kcal mol^{-1}),[49] which corresponds to a unimolecular rate constant on the order of 10^{-5} s^{-1} at 37°C – 10 orders of magnitude lower than that required to produce the observed secondary inhibited period (~ 10^5 M^{-1} s^{-1}).

(51) Calculated from the half wave potential from the cyclic voltammogram of α-tocopherol and adjusted to a NHE reference (Fc/Fc^+ *vs.* NHE = +0.64 V). See: Williams, L. L.; Webster, R. D. *J. Am. Chem. Soc.*, **2004**, *126*, 12441–12450.

(52) Shah, R.; Margison, K. D.; Pratt, D. A. *Submitted*.

(53) Moosmann, B.; Skutella, T.; Beyer, K.; Behl, C. *Biol. Chem.* **2001**, *382*, 1601–1612.

(54) Kehrmann, F.; Boubis, A. *Berichte der Dtsch. Chem. Gesellschaft* **1917**, *50*, 1662–1667.

(55) Du, C.; Zheng, C.; Fifth, Z. Hepatitis b surface antigen and antibody detection method. CN 101334407 A, 2008.

(56) Granick, S.; Michaelis, L.; Schubert, M. P. *J. Am. Chem. Soc.* **1940**, *62*, 1802–1810.

(57) Thomé, I.; Bolm, C. *Org. Lett.* **2012**, *14*, 1892–1895.

(58) Nara, S. J.; Jha, M.; Brinkhorst, J.; Zemanek, T. J.; Pratt, D. A. *J. Org. Chem.* **2008**, *73*, 9326–9333.

(59) Kormos, A.; Móczár, I.; Sveiczer, A.; Baranyai, P.; Párkányi, L.; Tóth, K.; Huszthy, P. *Tetrahedron* **2012**, *68*, 7063–7069.

(60) Delor, M.; Keane, T.; Scattergood, P. A.; Sazanovich, I. V.; Greetham, G. M.; Towrie, M.; Meijer, A. J. H. M.; Weinstein, J. A. *Nat. Chem.* **2015**, *7*, 689–695.

(61) Doad, G. J. S.; Barltrop, J. A.; Petty, C. M.; Owen, T. C. *Tetrahedron Lett.* **1989**, *30*, 1597–1598.

(62) Burton, G. W.; Doba, T.; Gabe, E.; Hughes, L.; Lee, F. L.; Prasad, L.; Ingold, K.U. *J. Am. Chem. Soc.* **1985**, *107*, 7053–7065.

(63) Zilka, O.; Shah, R.; Li, B.; Friedmann Angeli, J. P.; Griesser, M.; Conrad, M.; Pratt, D. A. *ACS Cent. Sci.* **2017**, *3*, 232–243.

(64) Pegis, M. L.; Roberts, J. A. S.; Wasylenko, D. J.; Mader, E. A.; Appel, A. M.; Mayer, J. M. *Inorg. Chem.* **2015**, *54*, 11883–11888.

(65) Montgomery, J. A.; Frisch, M. L.; Ochterski, J. W.; Petersson, G. A. *J. Chem. Phys.* **1999**, 110, 2822–2827.

(66) Frisch, M. J.; Trucks, G. W.; Schlegel, H. B.; Scuseria, G. E.; Robb, M. A.; Cheeseman, J. R.; Scalmani, G.; Barone, V.; Mennucci, B.; Petersson, G. A.; Nakatsuji, H.; Caricato, M.; Li, X.; Hratchian, H. P.; Izmaylov, A. F.; Bloino, J.; Zheng, G.; Sonnenberg, J. L.; Hada, M.; Ehara, M.; Toyota, K.; Fukuda, R.; Hasegawa, J.; Ishida, M.; Nakajima, T.; Honda, Y.; Kitao, O.; Nakai, H.; Vreven, T.; Montgomery, J. A., Jr.; Peralta, J. E.; Ogliaro, F.; Bearpark, M. J.; Heyd, J.; Brothers, E. N.; Kudin, K. N.; Staroverov, V. N.; Kobayashi, R.; Normand, J.;

Raghavachari, K.; Rendell, A. P.; Burant, J. C.; Iyengar, S. S.; Tomasi, J.; Cossi, M.; Rega, N.; Millam, N. J.; Klene, M.; Knox, J. E.; Cross, J. B.; Bakken, V.; Adamo, C.; Jaramillo, J.; Gomperts, R.; Stratmann, R. E.; Yazyev, O.; Austin, A. J.; Cammi, R.; Pomelli, C.; Ochterski, J. W.; Martin, R. L.; Morokuma, K.; Zakrzewski, V. G.; Voth, G. A.; Salvador, P.; Dannenberg, J. J.; Dapprich, S.; Daniels, A. D.; Farkas, Ö.; Foresman, J. B.; Ortiz, J. V.; Cioslowski, J.; Fox, D. J. Gaussian 09, Revision E.01; Gaussian, Inc.: Wallingford, CT, 2009.

2.8 Supporting Information

2.8.1 Standardization of Co-Autoxidations

The rate of decomposition of PBD-BODIPY via co-autoxidation for both, the uninhibited and inhibited region is described by equations I and II respectively:

$$\frac{-\delta[\text{PBD-BODIPY}]}{\delta t} = \frac{k_{\text{PBD-BODIPY}}}{\sqrt{2k_t}}\sqrt{R_i}[\text{PBD-BODIPY}] \quad \text{(I)}$$

$$\frac{-\delta[\text{PBD-BODIPY}]}{\delta t} = \frac{k_{\text{PBD-BODIPY}}[\text{PBD-BODIPY}]R_i}{nk_{inh}[AH]} \quad \text{(II)}$$

The rate of initiation (R_i) is standardized using a phenolic inhibitor where the stoichiometric factor (n) will be 2, and is derived from equation III:

$$R_i = \frac{n[AH]}{t_{inh}} \quad \text{(III)}$$

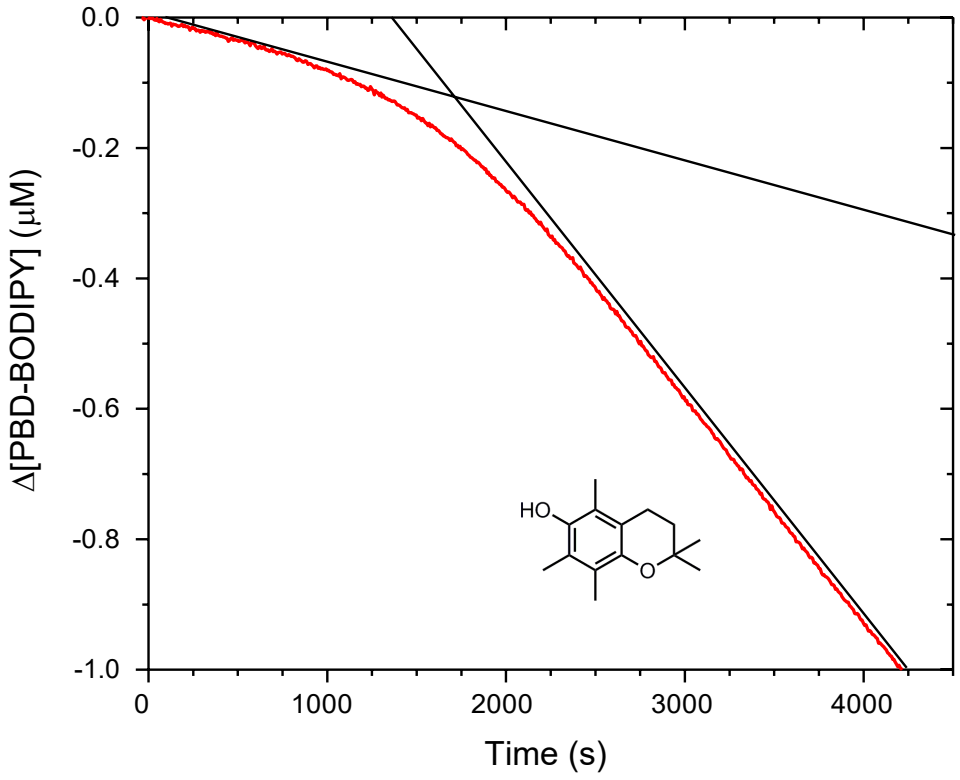

Figure S2.1. Tangential intercept between inhibited and uninhibited phases of the co-autoxidation of 10 μM PBD-BODIPY with 2.9 M 1,4-dioxane in chlorobenzene at 37 °C inhibited by 2 μM PMC (average $R_i = 2.4 \times 10^{-9}$ M s^{-1}).

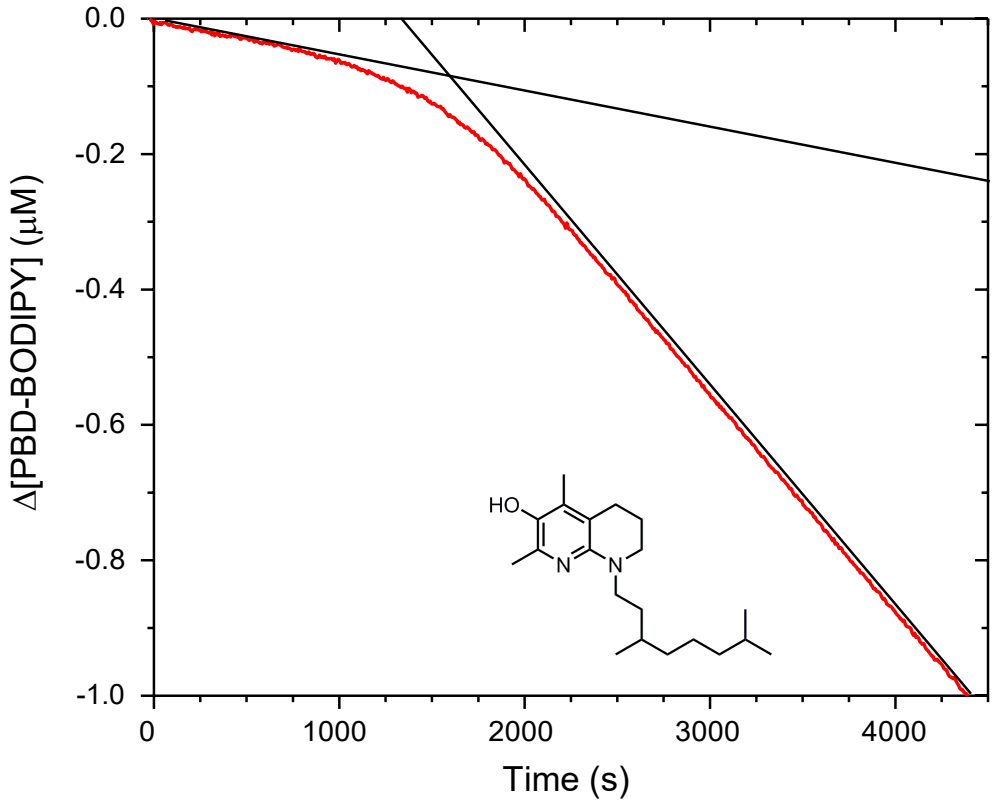

Figure S2.2. Tangential intercept between inhibited and uninhibited phases of the co-autoxidation of 10 μM PBD-BODIPY with 2.9 M 1,4-dioxane in 2:1 chlorobenzene:DMSO at 37 °C inhibited by 2 μM C10-THN (average $R_i = 2.1 \times 10^{-9}$ M s^{-1}).

Where [AH] is the concentration of reference phenol (2×10^{-6} M) and t_{inh} is the time of inhibition determined by the intercept between the tangents of the inhibited period and the uninhibited period. Reported R_i is an average of three replicate experiments. $k_{PBD\text{-}BODIPY}$, which is substrate/solvent/temperature dependent, was determined by measuring the rate of PBD-BODIPY oxidation in uninhibited co-autoxidations at 6 concentrations and calculating $k_{PBD\text{-}BODIPY}$ using Eq. I assuming k_t is equivalent to k_t of 1,4-dioxane ($k_t = 2.5 \times 10^7$ M^{-1} s^{-1}). Reported $k_{PBD\text{-}BODIPY}$ is an average of three replicate experiments. When $k_{PBD\text{-}BODIPY}$, R_i, [PBD-BODIPY], inhibitor concentration ([AH]), and 'n' are known for Eq. II (it is assumed that n = 2 when measuring initial rates of inhibition for phenolic and aminic AOs) and when $\frac{-\delta[\text{PBD-BODIPY}]}{\delta t}$ is measured, then k_{inh} for the inhibitor can be solved.

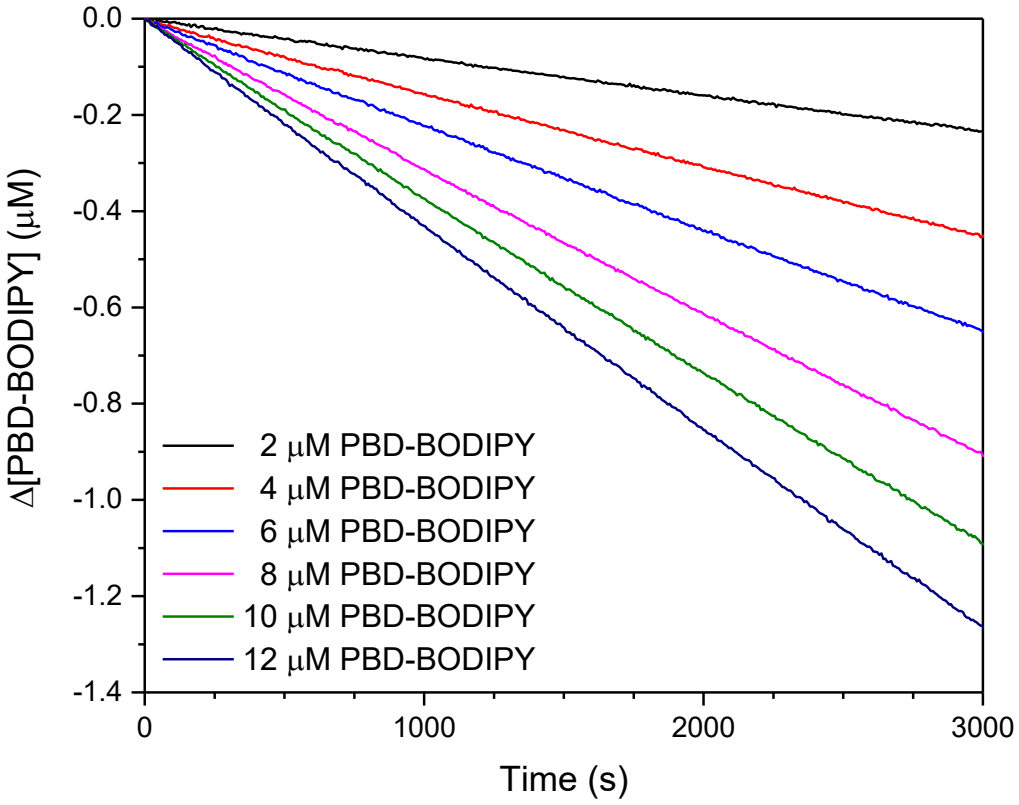

Figure S2.3. Uninhibited co-autoxidation of 2-12 μM of PBD-BODIPY with 2.9 M 1,4-dioxane in chlorobenzene at 37 °C, determined $\boldsymbol{k_{PBD\text{-}BODIPY}}$ = 5310 M^{-1} s^{-1}.

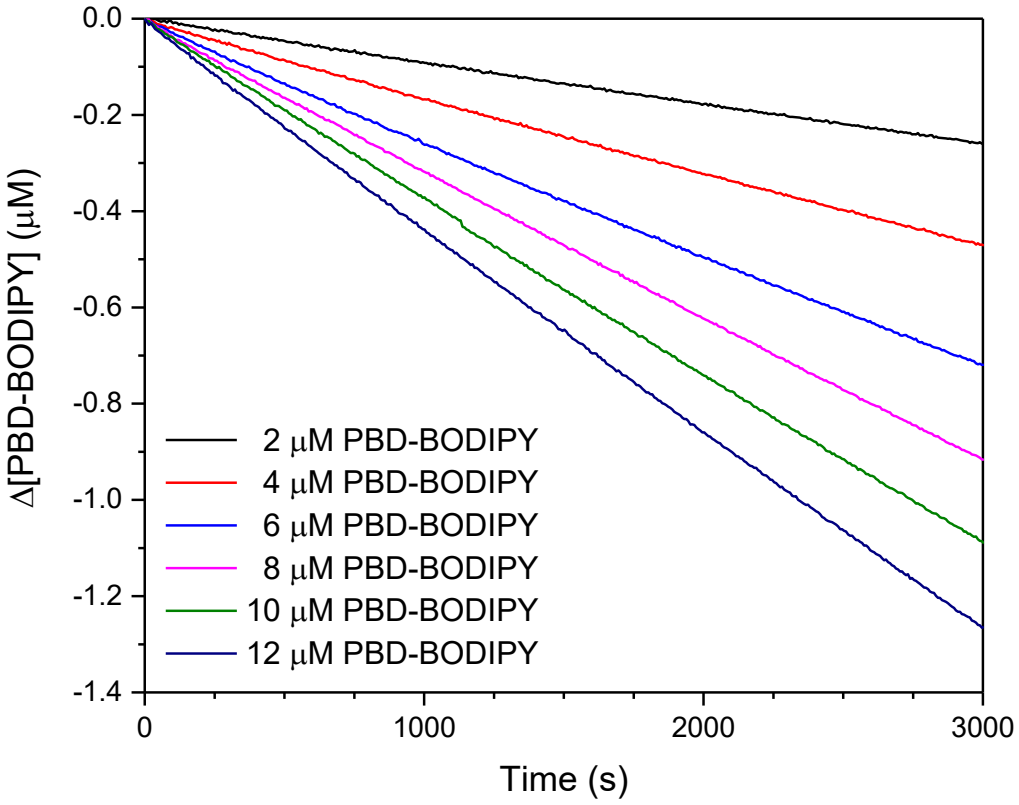

Figure S2.4. Uninhibited co-autoxidation of 2-12 μM of PBD-BODIPY with 2.9 M 1,4-dioxane in 2:1 chlorobenzene:DMSO at 37 °C, determined $\boldsymbol{k_{PBD\text{-}BODIPY}}$ = 5900 M^{-1} s^{-1}.

2.8.2 β_2^H Parameter Determination

The H-bond accepting solvent mixture of interest was diluted in CCl_4 to render four dilute solutions of differing concentrations and one 1.20 M solution. To these were added 4-fluorophenol and 4-fluoroanisole for a final concentration of 0.01 M of each. The solutions were transferred into NMR tubes containing sealed capillaries of benzene-d_6 with α,α,α-trifluorotoluene, after which their ^{19}F spectra were obtained a multiple temperatures using a Bruker Avance II 300 equipped with a thermostat. At a given temperature, the K_f of 4-fluorophenol and the H-bond acceptor(s) is described:

$$K_f = \frac{(\delta/\Delta)A_0}{\{A_0[1-(\delta/\Delta)]\}[B_0-(\delta/\Delta)A_0]}$$

Where A_0 is the concentration of 4-fluorophenol, B_0 is the concentration of H-bond acceptor(s), Δ is the difference in chemical shift seen between 4-fluorophenol and 4-fluoroanisole at B_0 = 1.20 M and δ is the difference in chemical shift seen between 4-fluorophenol and 4-fluoroanisole at the dilute concentrations of H-bond acceptor(s). The empirical relationship between K_f and $\Delta\delta_{Phen\text{-}Anis}$ (the delta between the 4-fluorophenol singlet and 4-fluoroanisole singlet at a given concentration of HBA) rests on the assumption that log $K_f \propto \Delta E_p°$ (electronic potential energy change.) Taft et. al. further elaborated that since log $K_f \propto T^{-1}$, one should also observe a linear shielding free energy relationship between $\Delta E_p°$ and T^{-1} that would correspond to the proportional change in log K_f.[1] We observe a linear decrease in $\Delta\delta_{Phen\text{-}Anis}$ as we increased the temperature of our ^{19}F NMR experiments which we used to construct a Van 't Hoff type plot for the formation 1:1 complex between 4-fluorophenol and our hydrogen-bond acceptors (Figure S5.) We assume that in terms of applying the Ingold-Abraham relationship that the entirety of the temperature dependence of log $K_f^{(T)}$ can be accounted for by the effective $\beta_2^{H(T)}$ parameter and that the α_2^H term can be treated as being independent of temperature.

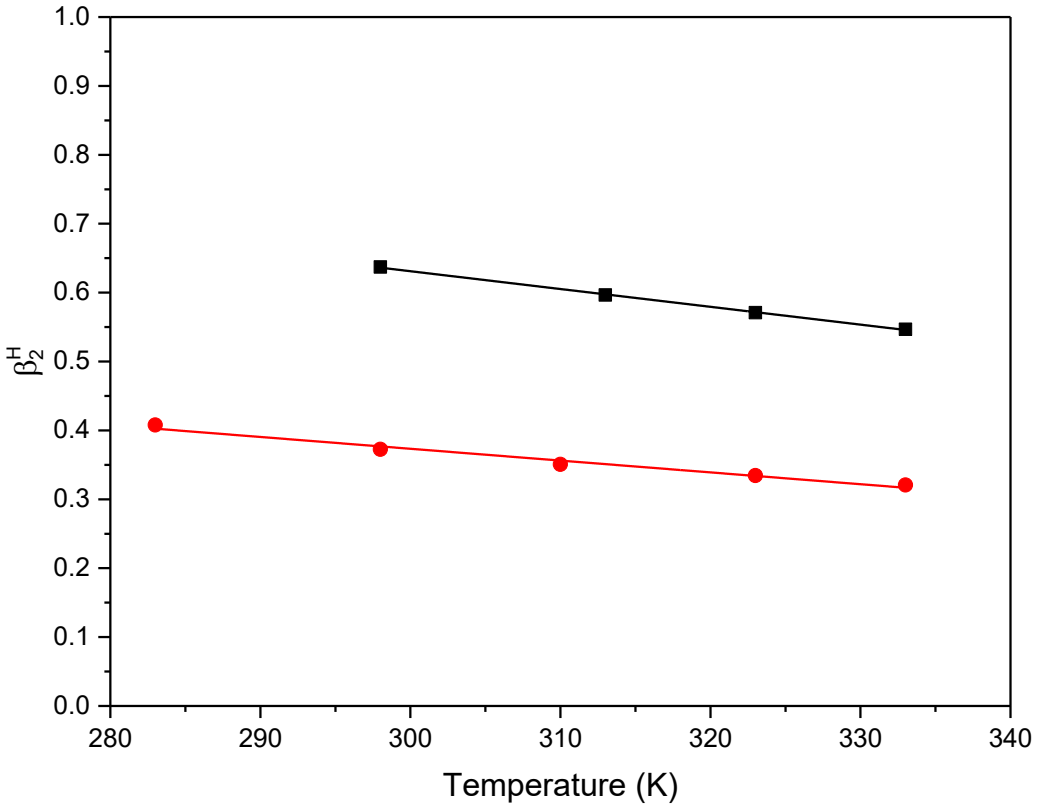

Figure S2.5. Effective $\boldsymbol{\beta_2^H}$ over a range in temperatures for 1:1:2 1,4-Dioxane:DMSO:PhCl (black squares, y = -0.00258 x + 1.4063, R^2 = 0.999) and 1:3 1,4-Dioxane:PhCl (red circles, y = -0.00171 x + 0.8877, R^2 = 0.980)

Table S2.1. Chemical shifts of 0.01 M 4-fluorophenol and 0.01 M 4-fluoroanisole by ^{19}F NMR in CCl_4 at various concentrations of HBA (1:1:2 1,4-Dioxane:DMSO:PhCl) at multiple temperatures and the realized K_f between HBA and 4-fluorophenol and effective $\boldsymbol{\beta_2^H}$ of the HBA.

Temperature	B_O (M)	Chemical Shift 4-Fluoroanisole (ppm)	Chemical Shift 4-Fluorophenol (ppm)	Normalized δ (ppm)	K_f	$\boldsymbol{\beta_2^H}$
298 K	0.03	123.20	124.74	1.54	58	0.64
	0.06	123.18	125.27	2.09	73	
	0.09	123.19	125.46	2.27	75	
	0.12	123.20	125.57	2.37	79	
	1.20	123.47	126.11	2.64 (Δ)	-	
313 K	0.03	123.27	124.61	1.34	41	0.60
	0.06	123.25	125.15	1.90	47	
	0.09	123.26	125.38	2.12	48	
	0.12	123.27	125.52	2.25	49	
	1.20	123.53	126.19	2.66 (Δ)	-	
323 K	0.03	123.32	124.51	1.19	32	0.57
	0.06	123.30	125.06	1.76	36	
	0.09	123.31	125.31	2.00	37	
	0.12	123.32	125.47	2.15	37	
	1.20	123.57	126.24	2.67 (Δ)	-	
333 K	0.03	123.37	124.43	1.06	25	0.55
	0.06	123.35	124.95	1.60	28	
	0.09	123.36	125.22	1.86	28	
	0.12	123.37	125.40	2.03	28	
	1.20	123.61	126.28	2.67 (Δ)	-	

Table S2.2. Chemical shifts of 0.01 M 4-fluorophenol and 0.01 M 4-fluoroanisole by ^{19}F NMR in CCl_4 at various concentrations of HBA (1:3 1,4-Dioxane:PhCl) at multiple temperatures and the realized K_f between HBA and 4-fluorophenol and effective $\boldsymbol{\beta_2^H}$ of the HBA.

Temperature	B_O (M)	Chemical Shift 4-Fluoroanisole (ppm)	Chemical Shift 4-Fluorophenol (ppm)	Normalized δ (ppm)	K_f	$\boldsymbol{\beta_2^H}$
283 K	0.06	123.10	123.38	0.28	5.9	0.41
	0.12	123.11	123.56	0.45	6.0	
	0.18	123.11	123.69	0.58	6.4	
	0.24	123.14	123.80	0.66	6.4	
	1.20	123.29	124.39	1.10 (Δ)	-	
298 K	0.06	123.19	123.38	0.19	3.9	0.37
	0.12	123.20	123.53	0.33	4.1	
	0.18	123.20	123.64	0.44	4.3	
	0.24	123.22	123.75	0.53	4.6	
	1.20	123.36	124.38	1.02 (Δ)	-	
310 K	0.06	123.25	123.39	0.14	3.0	0.35
	0.12	123.26	123.52	0.26	3.3	
	0.18	123.26	123.61	0.35	3.4	
	0.24	123.28	123.71	0.43	3.7	
	1.20	123.41	124.34	0.93 (Δ)	-	
323 K	0.06	123.31	123.42	0.11	2.6	0.33
	0.12	123.32	123.52	0.20	2.7	
	0.18	123.33	123.61	0.28	2.9	
	0.24	123.34	123.69	0.35	3.1	
	1.20	123.69	124.30	0.83 (Δ)	-	
333 K	0.06	123.36	123.45	0.09	2.3	0.32
	0.12	123.37	123.53	0.16	2.2	
	0.18	123.38	123.62	0.24	2.6	
	0.24	123.38	123.68	0.30	2.7	
	1.20	123.50	124.27	0.77	-	

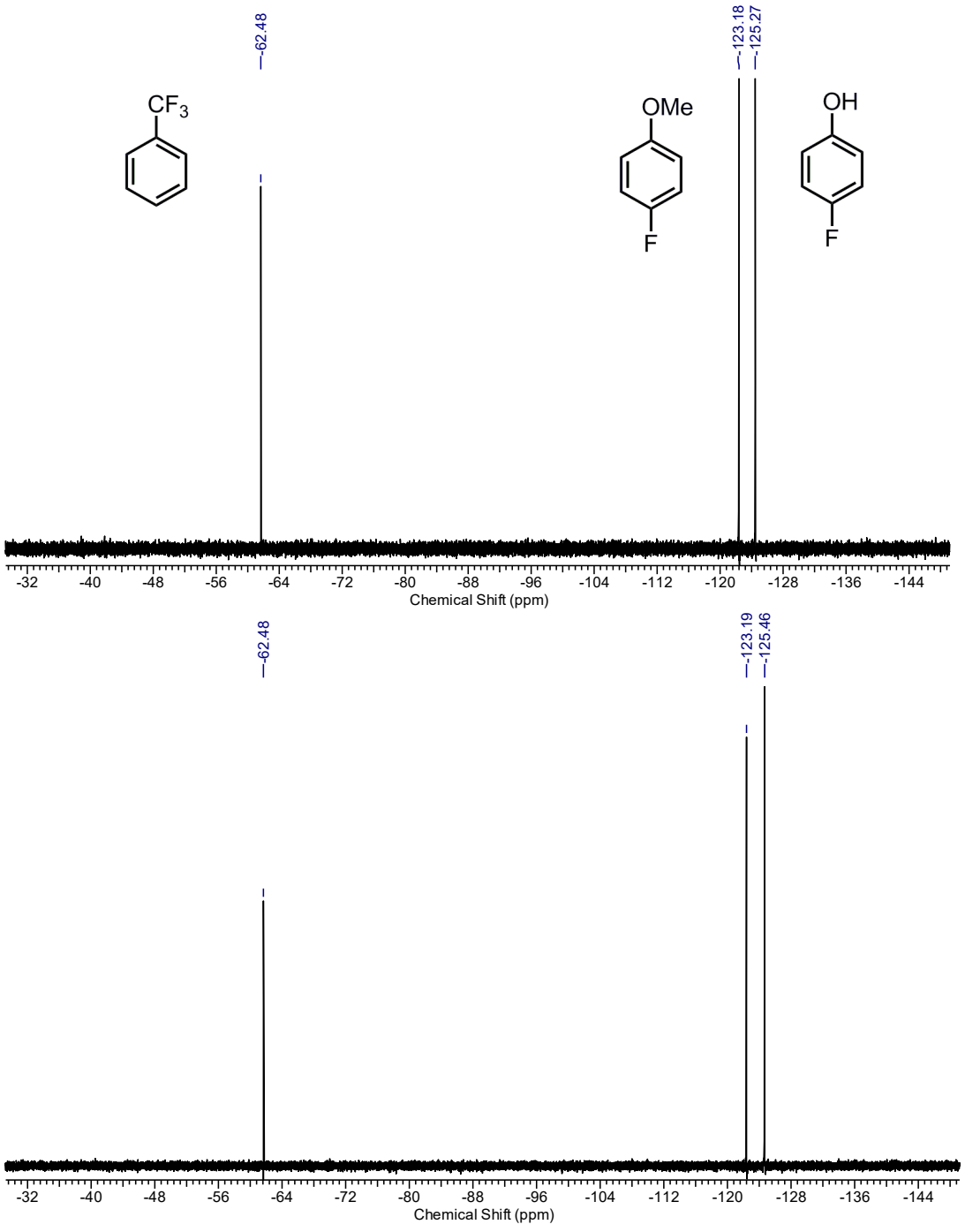

Figure S2.6. Examples of ^{19}F NMR in CCl_4 with 0.01 M 4-fluorophenol and 0.01 M 4-fluoroanisole as internal reference. Trifluorotoluene in benzene-d_6 in a glass capillary used as external reference. 0.06 M 1:1:2 1,4-Dioxane:DMSO:PhCl (top), 0.09 M 1:1:2 1,4-Dioxane:DMSO:PhCl (bottom).

2.8.3 α_2^H Parameter Determination

The correlation between $\boldsymbol{\alpha_2^H}$ and $\Delta\delta_{DMSO\text{-}Ben}$ was constructed by obtaining ^{1}H NMR spectra in both DMSO-d_6 and benzene-d_6 for 11 different H-bond donors which have had their $\boldsymbol{\alpha_2^H}$ independently determined (ranging from $\boldsymbol{\alpha_2^H}$ = 0.08 to 0.82) and plotted their $\Delta\delta_{DMSO\text{-}Ben}$ vs. reference $\boldsymbol{\alpha_2^H}$ values.

Table S2.3. Chemical shifts of acidic protons in select H-bond donors in DMSO-d_6 and benzene-d_6, their $\Delta\delta_{DMSO\text{-}Ben}$, and reference $\boldsymbol{\alpha_2^H}$ values.

Reference H-bond Donor	**Chemical Shift of X-H (X = O, N, C) in DMSO-d_6 (ppm)**	**Chemical Shift of X-H (X = O, N, C) in benzene-d_6 (ppm)**	**$\Delta\delta_{DMSO\text{-}Ben}$**	**Reference α_2^H** [2]
Diethylamine	1.29 [3]	0.33	0.96	0.08
Dichloromethane	5.79 [3]	4.30	1.49	0.10
Aniline	4.94 [3]	2.77	2.17	0.13
Chloroform	8.32 [3]	6.14	2.18	0.15
Diphenylamine	8.13	4.98	3.15	0.30
Methanol	4.05 [3]	0.53	3.52	0.43
Resorcinol	9.14	3.82	5.32	0.55
Phenol	9.29 [3]	3.81	5.48	0.60
4-Fluorophenol	9.31 [4]	3.61	5.70	0.63 [5]
4-Cyanophenol	10.58 [4]	4.38	6.20	0.79
4-Nitrophenol	11.00 [4]	4.30	6.70	0.82

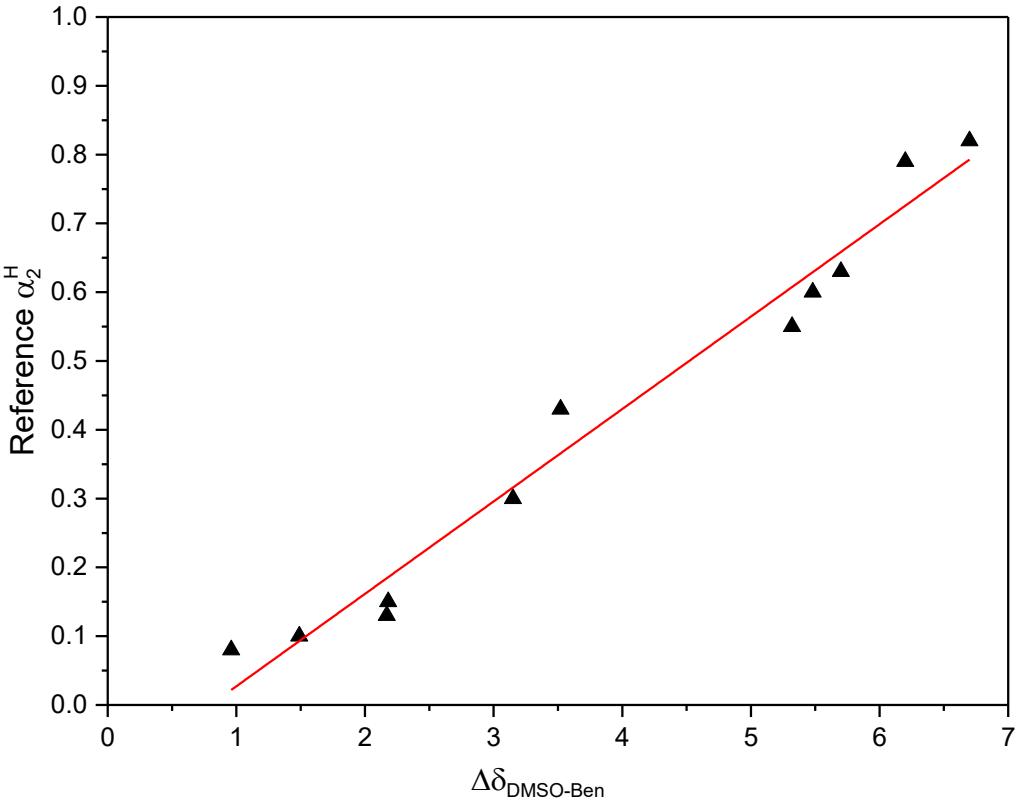

Figure S2.7. Correlation between $\boldsymbol{\alpha_2^H}$ and $\Delta\delta_{DMSO-Ben}$ from the reference $\boldsymbol{\alpha_2^H}$ values of compounds described in Table S2.3. ($y = 0.1343\ x\ -0.1072$, $R^2 = 0.972$).

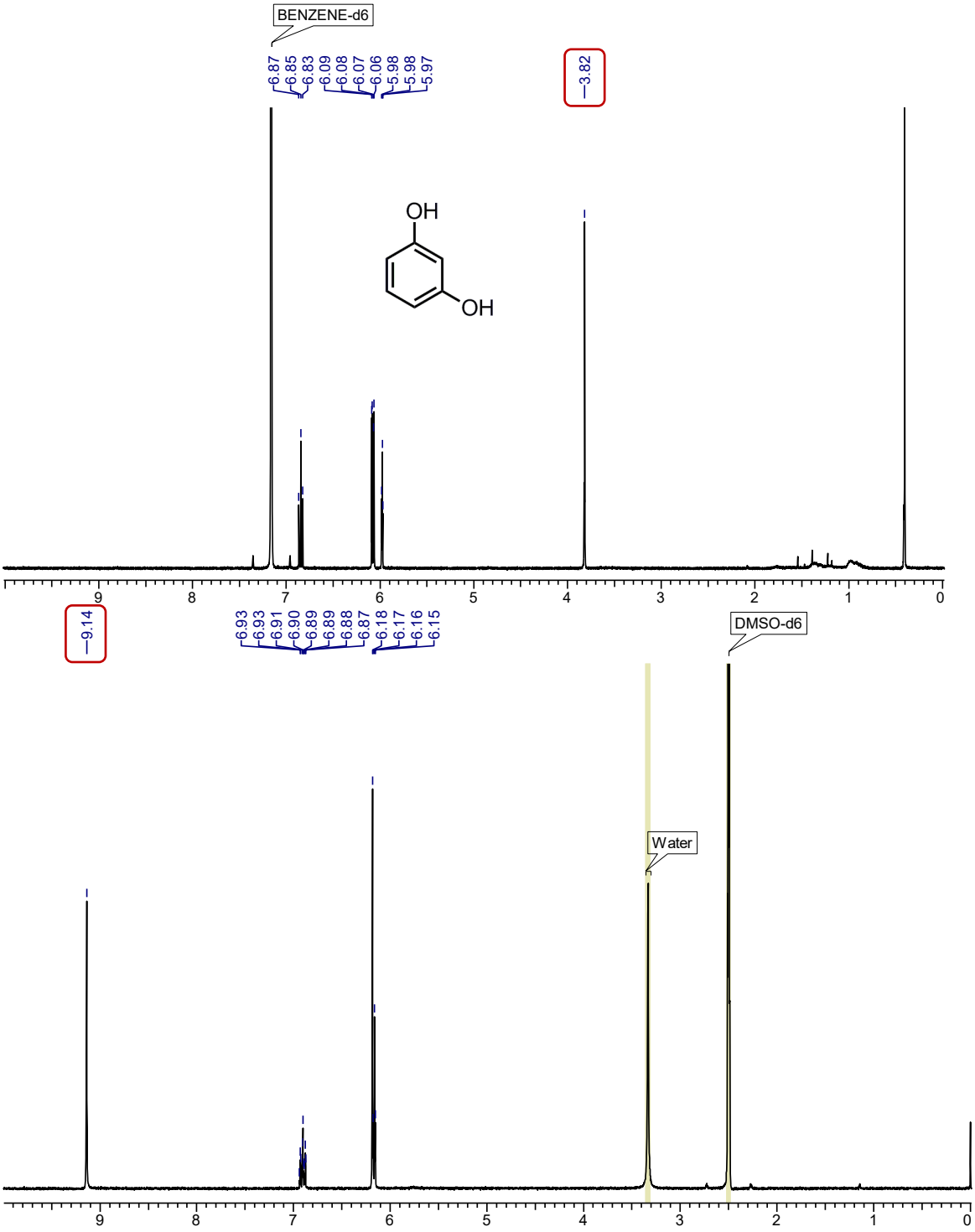

Figure S2.8. Examples of ^{1}H NMR of resorcinol in benzene-d_6 (top) and DMSO-d_6 (bottom) with the O-H peak labeled at 3.82 and 9.14 ppm respectively.

2.8.4 Kinetics of Reference RTAs in Dioxane/PhCl and Dioxane/PhCl+DMSO Co-autoxidation.

Inhibited co-autoxidation of 1,4-dioxane (2.9 M) and PBD-BODIPY (10 uM) were initiated by AIBN (6 mM) in either PhCl or a 2:1 PhCl:DMSO mixture at 37 °C and inhibited by RTAs with known rate constants which were used as a point of reference to assess the accuracy by which calculated k_{inh}^{PhCl} values reflect the k_{inh} determined directly in styrene/PhCl or hexadecene/PhCl substrate systems.

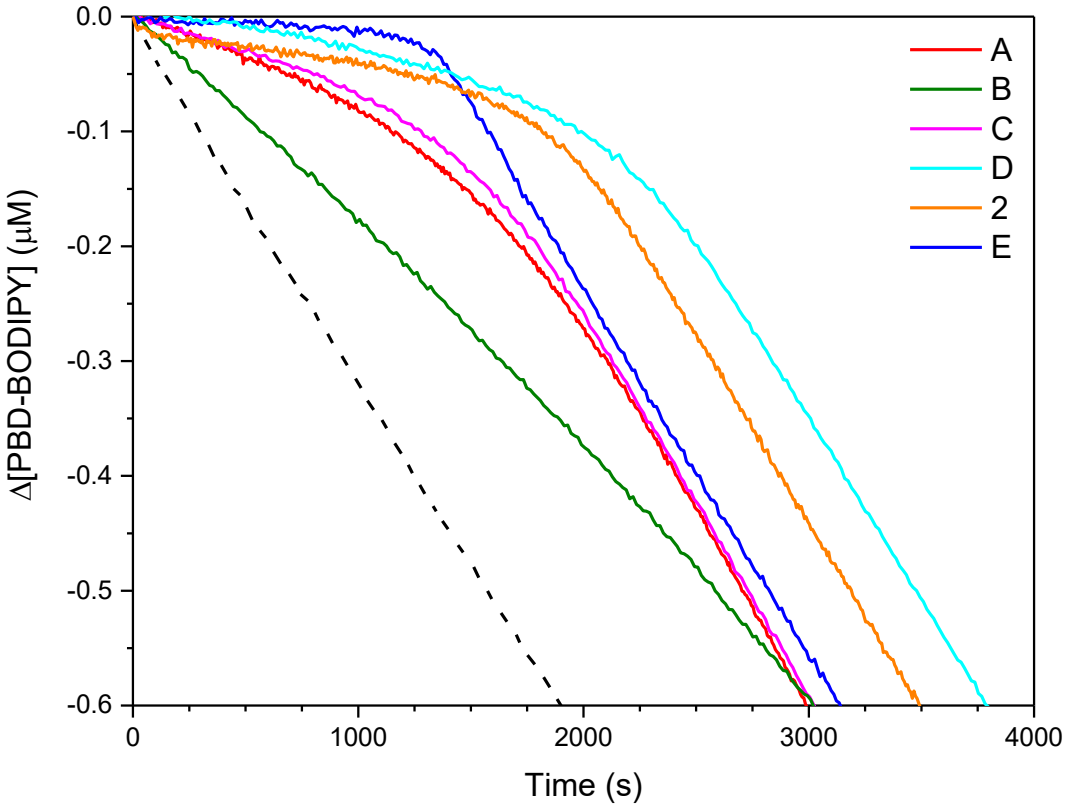

Figure S2.9. Co-autoxidation of 1,4-dioxane (2.9 M) and PBD-BODIPY (10 μM) initiated by AIBN (6 mM) in PhCl at 37 °C (black) and inhibited by 2 μM PMC (**A**, red), 4 μM 2-(N,N-dimethylamino)-5-pyrimidinol (**B**, green), 2 μM 2-(N,N-dimethylamino)-4,6-dimethyl-5-pyrimidinol (**C**, magenta), 5 μM *tert*-dodecyl-hydropersulfide (**D**, cyan), 2 μM phenothiazine (**2.2**, yellow), and 2 μM 3,7-di-*tert*-butylphenothiazine (**E**, blue). Reaction progress was monitored by absorbance at 587 nm (ε = 123 000 M^{-1} cm^{-1}).

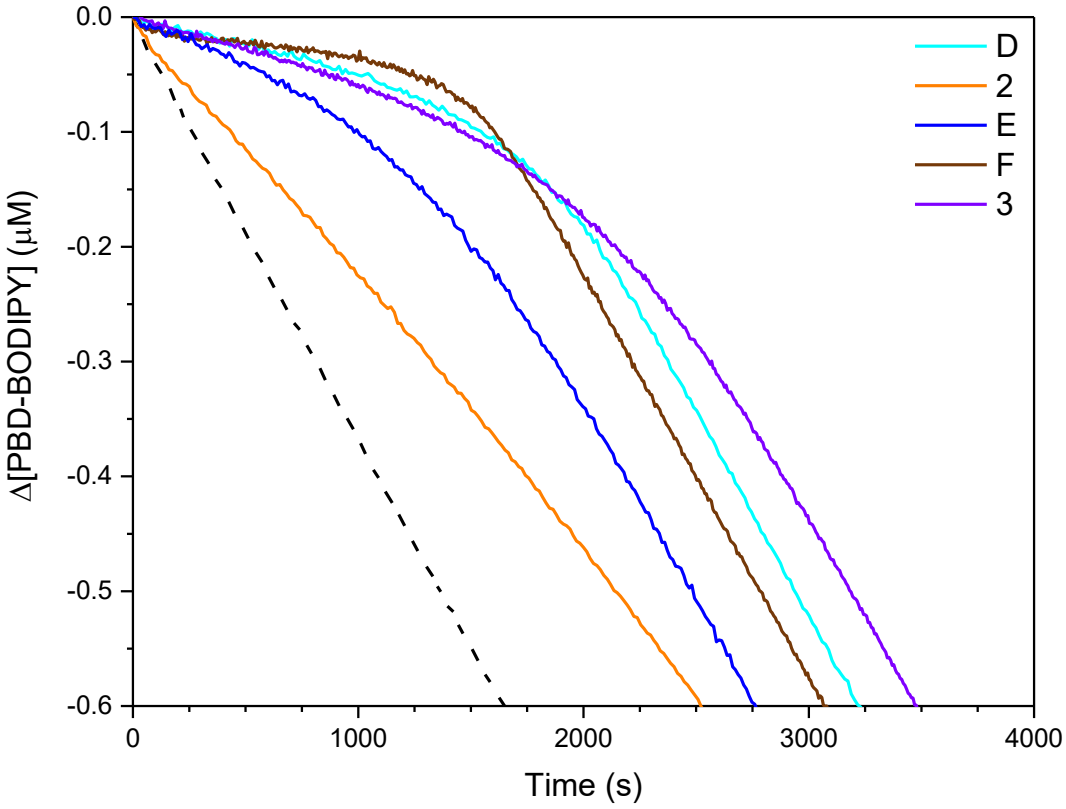

Figure S2.10. Co-autoxidation of 1,4-dioxane (2.9 M) and PBD-BODIPY (10 μM) initiated by AIBN (6 mM) in 2:1 PhCl and DMSO at 37 °C (black) and inhibited by 5 μM *tert*-dodecyl-hydropersulfide (**D**, cyan), 2 μM phenothiazine (**2.2**, yellow), 2 μM 3,7-di-*tert*-butylphenothiazine (**E**, blue), 2 μM 3,7-dimethoxyphenothiazine (**F**, brown), and 2 μM phenoxazine (**2.3**, purple). Reaction progress was monitored by absorbance at 587 nm (ε = 118 200 M^{-1} cm^{-1})

Table S2.4. Inhibition Rate Constants and Stoichiometries for Selected RTAs as Measured in the Dioxane and Dioxane/DMSO Co-autoxidation Substrate Systems and their Estimated Inhibition Rate Constants in Styrene/PhCl.

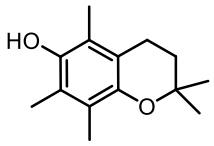

A

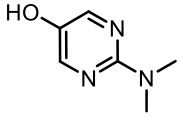

B

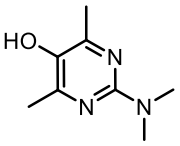

C

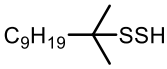

D

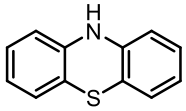

2

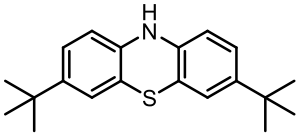

E

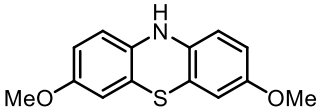

F

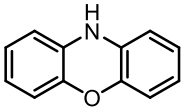

3

RTA	n^{Diox} (n^{DMSO})	α_2^{H} [a]	k_{inh}^{Diox} ($\mathrm{M^{-1}\ s^{-1}}$) [b] ($\beta_2^{H(37)} = 0.35$)	k_{inh}^{DMSO} ($\mathrm{M^{-1}\ s^{-1}}$) [b] ($\beta_2^{H(37)} = 0.60$)	k_{inh}^{PhCl} ($\mathrm{M^{-1}\ s^{-1}}$) ($\beta_2^{H} = 0.09$)	lit. k_{inh} ($\mathrm{M^{-1}\ s^{-1}}$)
A	2 (too slow)	0.38 (ref. 0.38)[6]	$4.1 \pm 0.2 \times 10^5$	too slow	$2.7 \pm 0.1 \times 10^6$	3.2×10^6 (30 °C)[6]
B	1.7 ± 0.1 (too slow)	0.65	$9.5 \pm 0.1 \times 10^4$	too slow	$2.4 \pm 0.1 \times 10^6$	2.0×10^6 (30 °C)[6]
C	1.8 ± 0.1 (too slow)	0.56 (ref. 0.53)[6]	$5.2 \pm 0.1 \times 10^5$	too slow	$8.4 \pm 0.2 \times 10^6$	7.4×10^6 (30 °C)[6]
D [d]	0.9 ± 0.1 (0.6 ± 0.2)	(ref. 0.09)[7]	$7.1 \pm 0.9 \times 10^5$	$5.3 \pm 0.8 \times 10^5$	$1.1 \pm 0.1 \times 10^6$ [e] $1.3 \pm 0.2 \times 10^6$ [f]	1.6×10^6 (37 °C)[7]
2	2.1 ± 0.1 (1.9 ± 0.1)	0.38	$1.2 \pm 0.1 \times 10^6$	$1.4 \pm 0.1 \times 10^5$	$7.6 \pm 0.3 \times 10^6$ [e] $5.8 \pm 0.2 \times 10^6$ [f]	8.8×10^6 (50 °C)[8]
E	1.6 ± 0.1 (1.6 ± 0.1)	0.35	$3.0 \pm 0.8 \times 10^6$	$3.6 \pm 0.2 \times 10^5$	$1.7 \pm 0.5 \times 10^7$ [e] $1.1 \pm 0.1 \times 10^7$ [f]	1.2×10^7 (50 °C)[8]
F	1.6 ± 0.1 (1.6 ± 0.1)	0.34	too fast	$1.5 \pm 0.1 \times 10^6$	$4.1 \pm 0.4 \times 10^7$	5.0×10^7 (50 °C)[8]
3	2.3 ± 0.1 (2.2 ± 0.1)	0.44	too fast	$5.3 \pm 0.5 \times 10^5$	$3.9 \pm 0.4 \times 10^7$	2.9×10^7 (50 °C)[8]

[a]Calculated by $\Delta\delta_{\mathrm{DMSO\text{-}Ben}}$ of the pertinent acid proton determined by ^{1}H NMR in conjunction with the Eq. 15. (y = 0.1343 x -0.1072) [b]Rates of inhibition measured at 2 uM of inhibitor at a minimum of three times, unless otherwise indicated. [d]$k_{\mathrm{inh}}^{\mathrm{Diox}}$ and $k_{\mathrm{inh}}^{\mathrm{DMSO}}$ determined as an average of triplicate co-autoxidations with 5 μM and 10 μM 2-methylundecan-2-persulfide. [e]$k_{\mathrm{inh}}^{\mathrm{PhCl}}$ is calculated from the determined $k_{\mathrm{inh}}^{\mathrm{Diox}}$. [f]$k_{\mathrm{inh}}^{\mathrm{PhCl}}$ is calculated from the determined $k_{\mathrm{inh}}^{\mathrm{DMSO}}$.

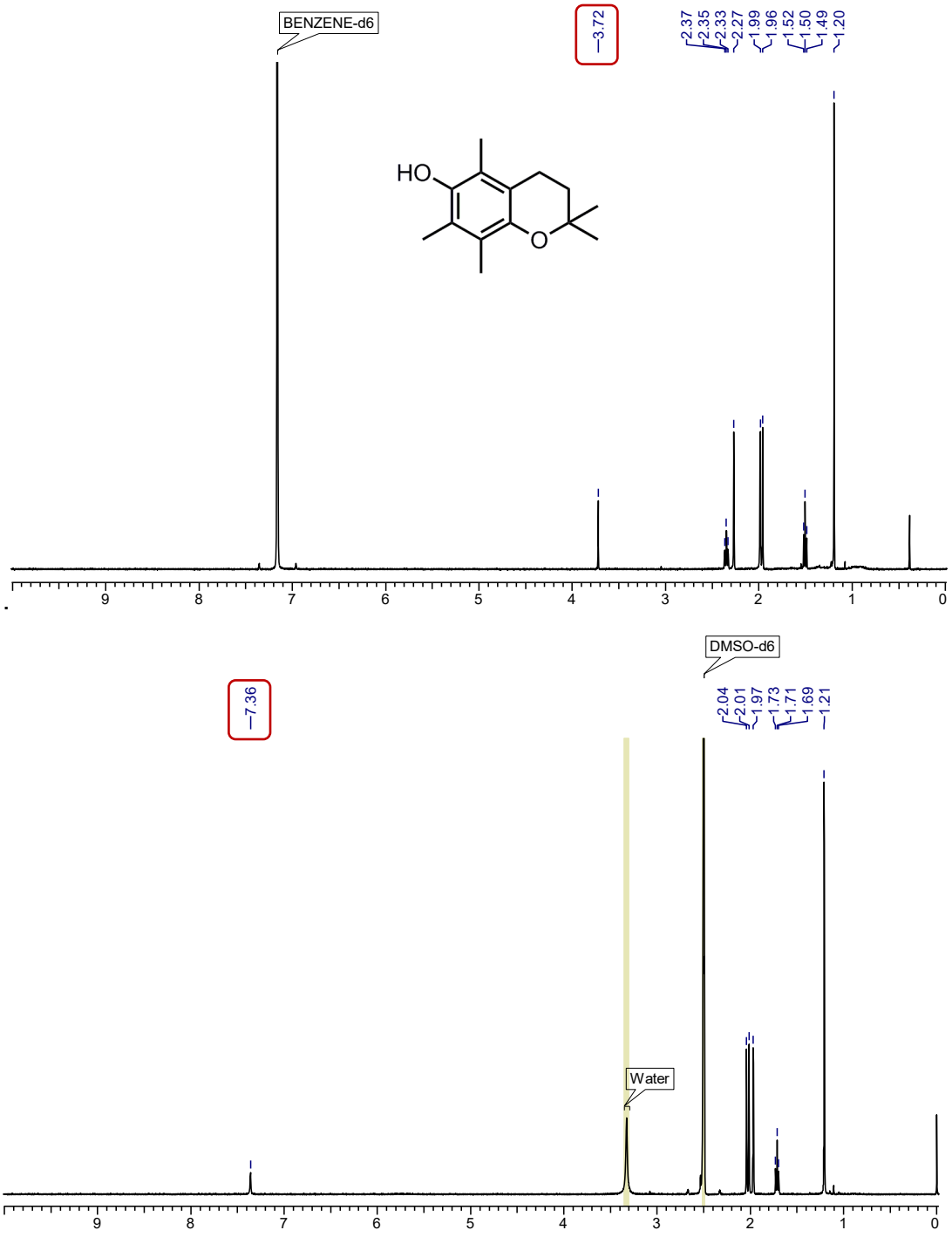

Figure S2.11. ^{1}H NMR of PMC in benzene-d_6 (top) and DMSO-d_6 (bottom) used to determine $\boldsymbol{\alpha_2^H}$ with the O-H peak labeled.

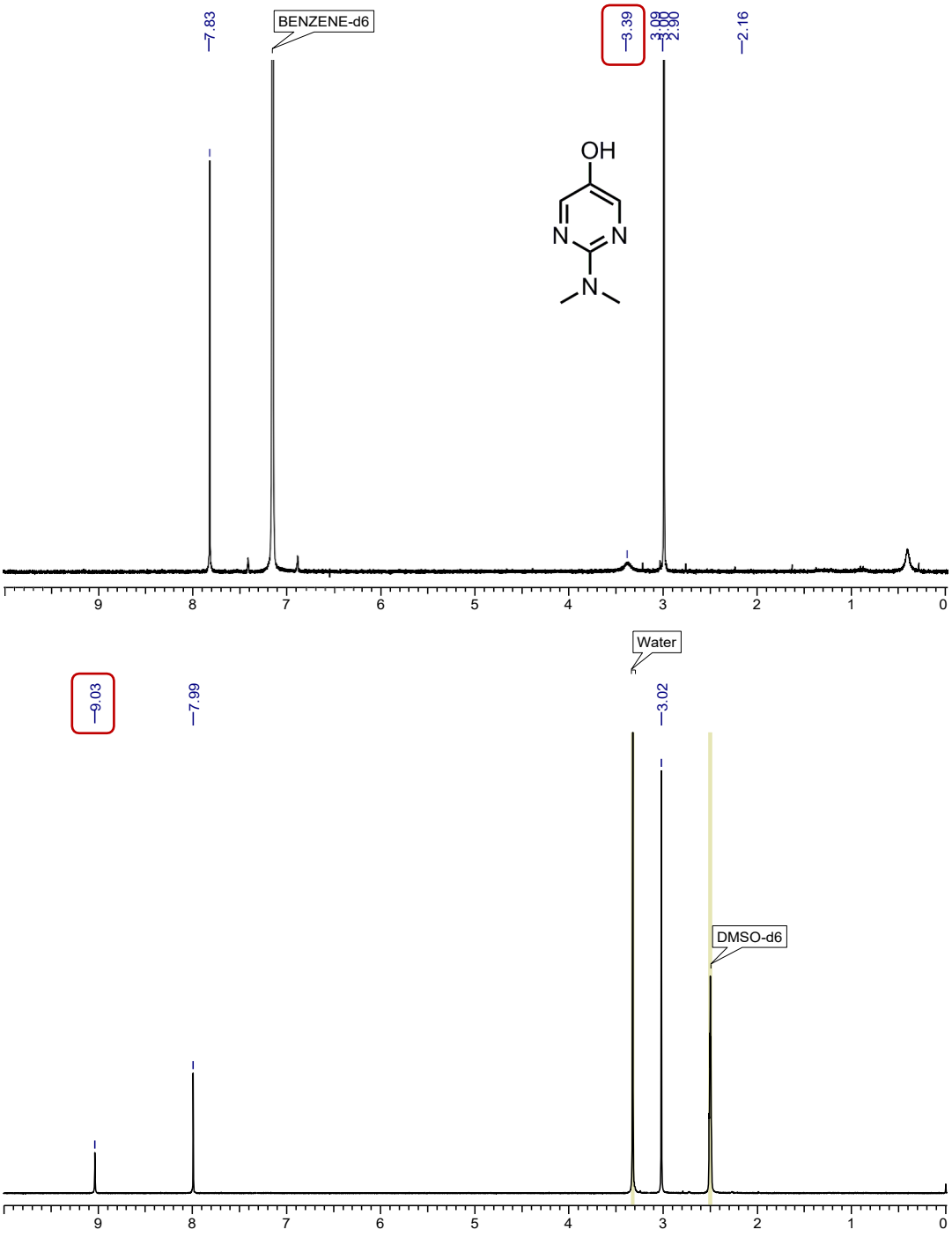

Figure S2.12. ^{1}H NMR of 2-(N,N-dimethylamino)-5-pyrimidinol in benzene-d_6 (top) and DMSO-d_6 (bottom) used to determine $\boldsymbol{\alpha_2^H}$ with the O-H peak labeled.

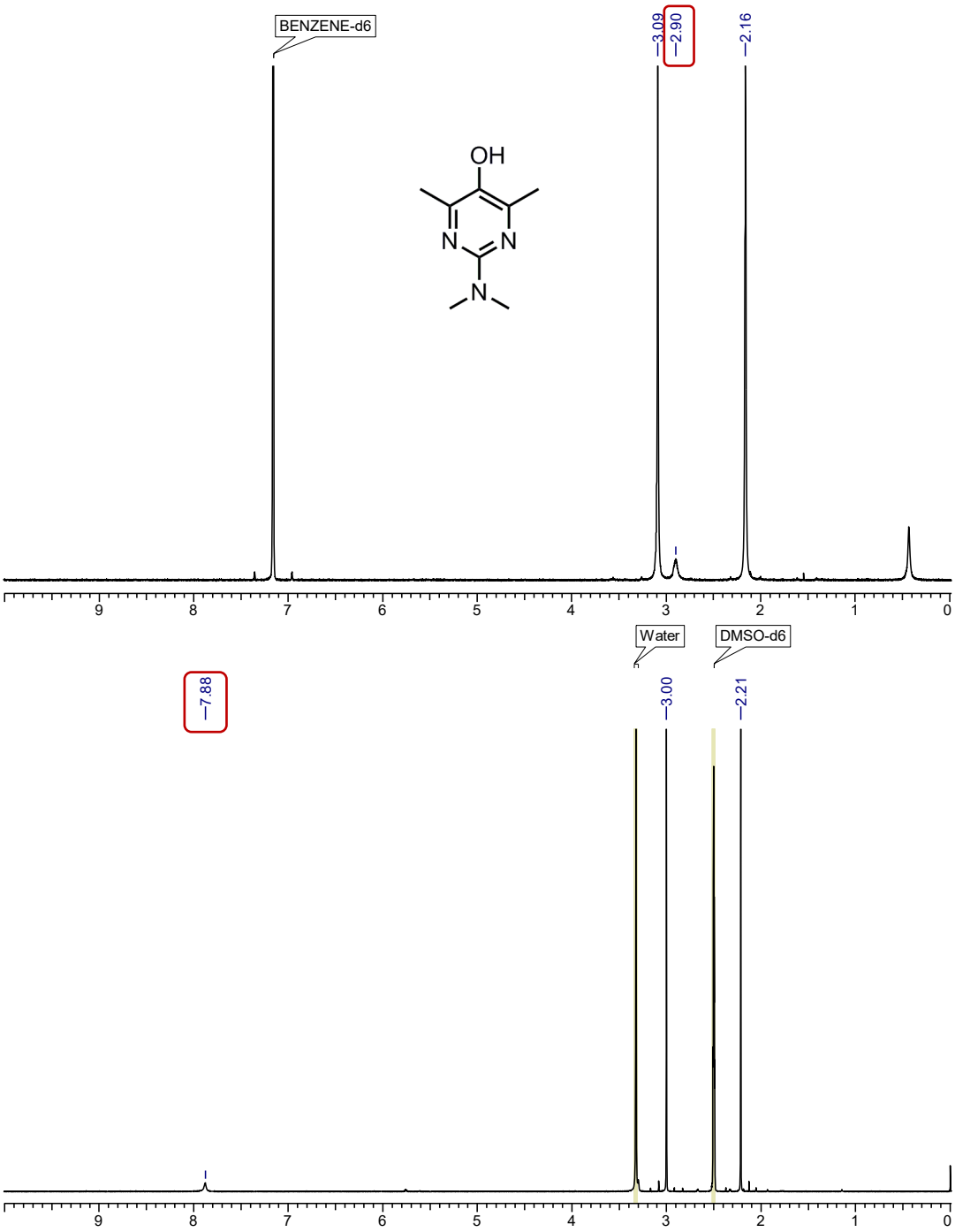

Figure S2.13. ^{1}H NMR of 2-(N,N-dimethylamino)-4,6-dimethyl-5-pyrimidinol in benzene-d_6 (top) and DMSO-d_6 (bottom) used to determine $\boldsymbol{\alpha_2^H}$ with the O-H peak labeled.

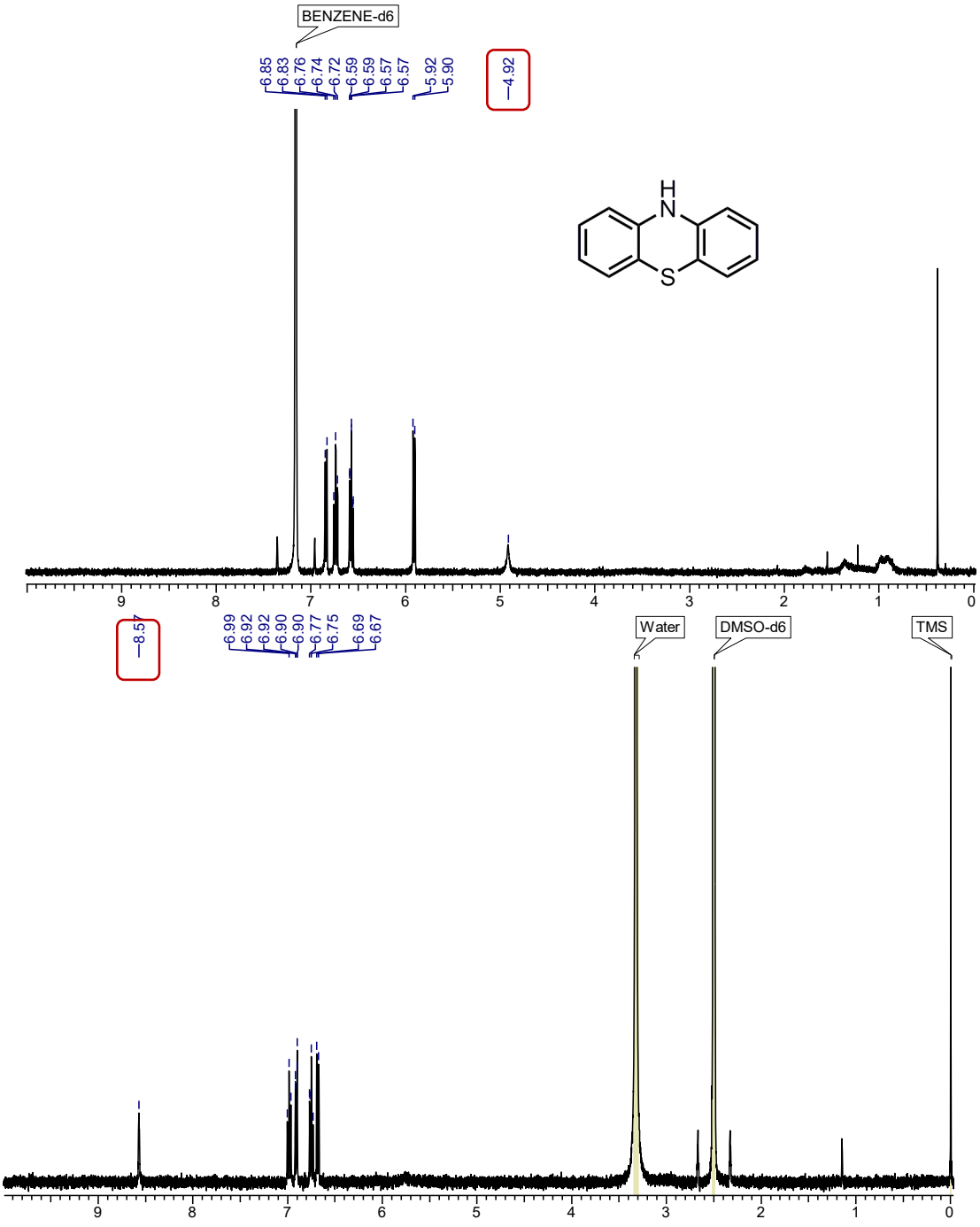

Figure S2.14. ^{1}H NMR of phenothiazine in benzene-d_6 (top) and DMSO-d_6 (bottom) used to determine $\boldsymbol{\alpha_2^H}$ with the N-H peak labeled.

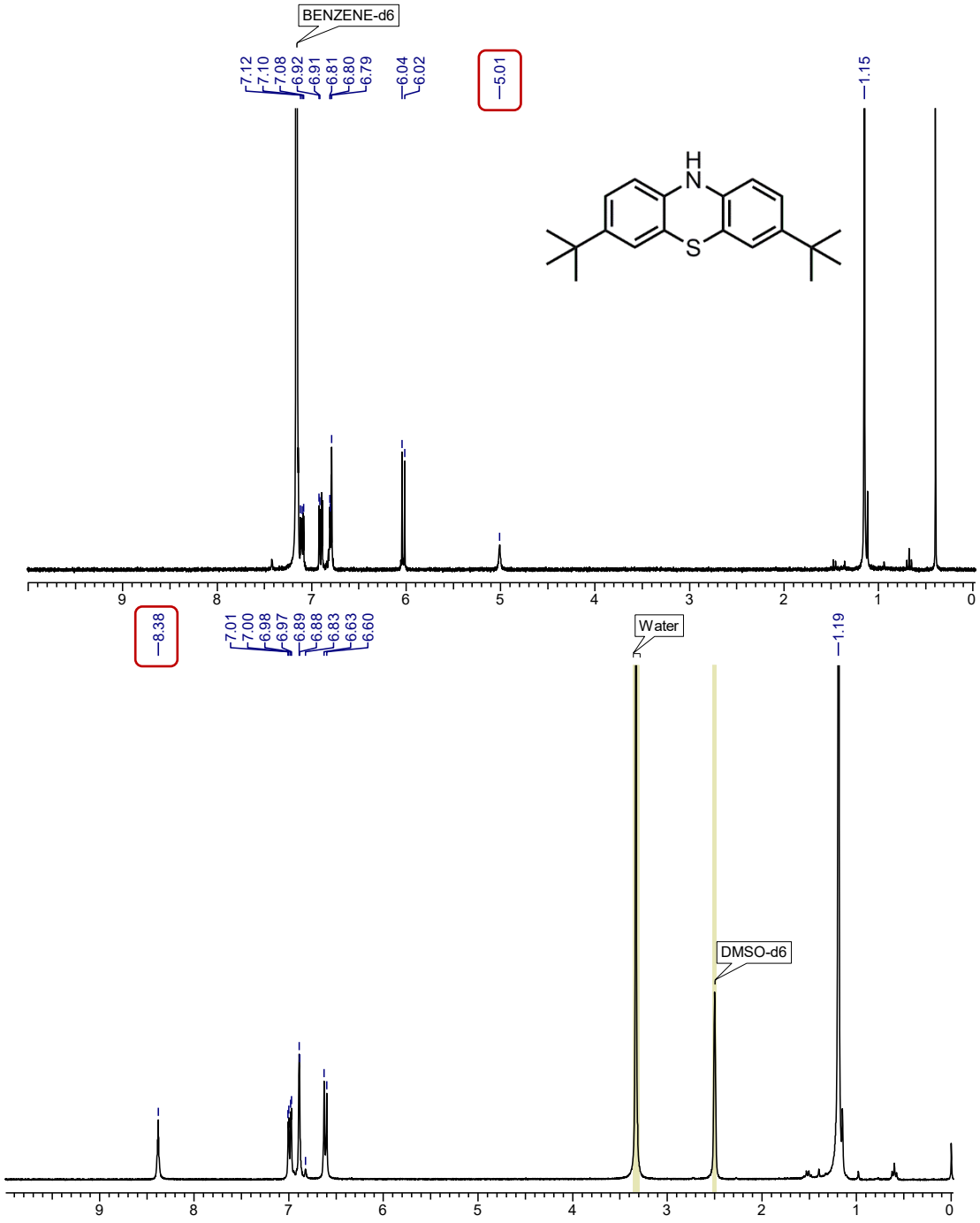

Figure S2.15. ^{1}H NMR of 3,7-di-tert-butylphenothiazine in benzene-d_6 (top) and DMSO-d_6 (bottom) used to determine $\boldsymbol{\alpha_2^H}$ with the N-H peak labeled.

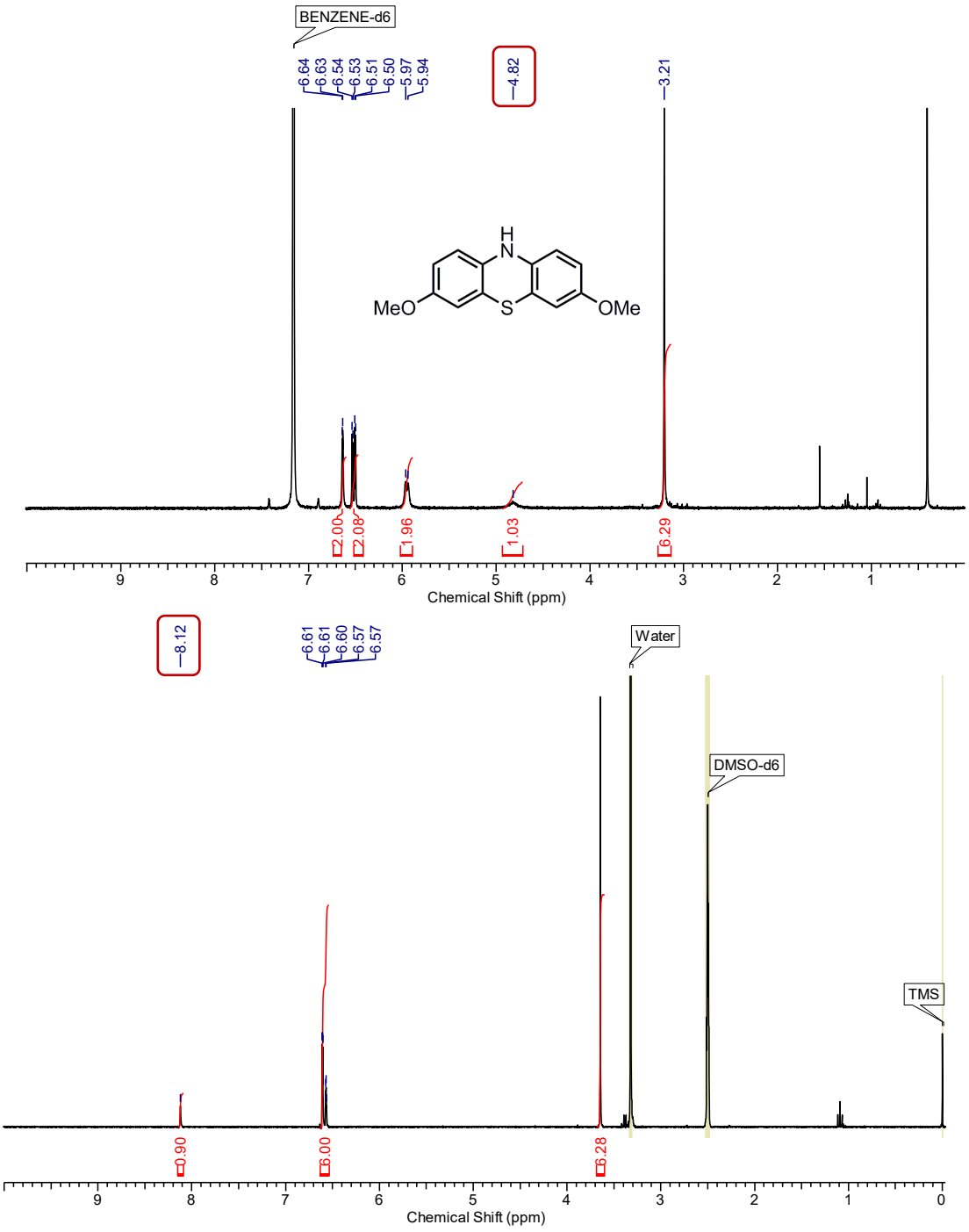

Figure S2.16. ^{1}H NMR of 3,7-di-methoxyphenothiazine in benzene-d_6 (top) and DMSO-d_6 (bottom) used to determine $\boldsymbol{\alpha_2^H}$ with the N-H peak labeled.

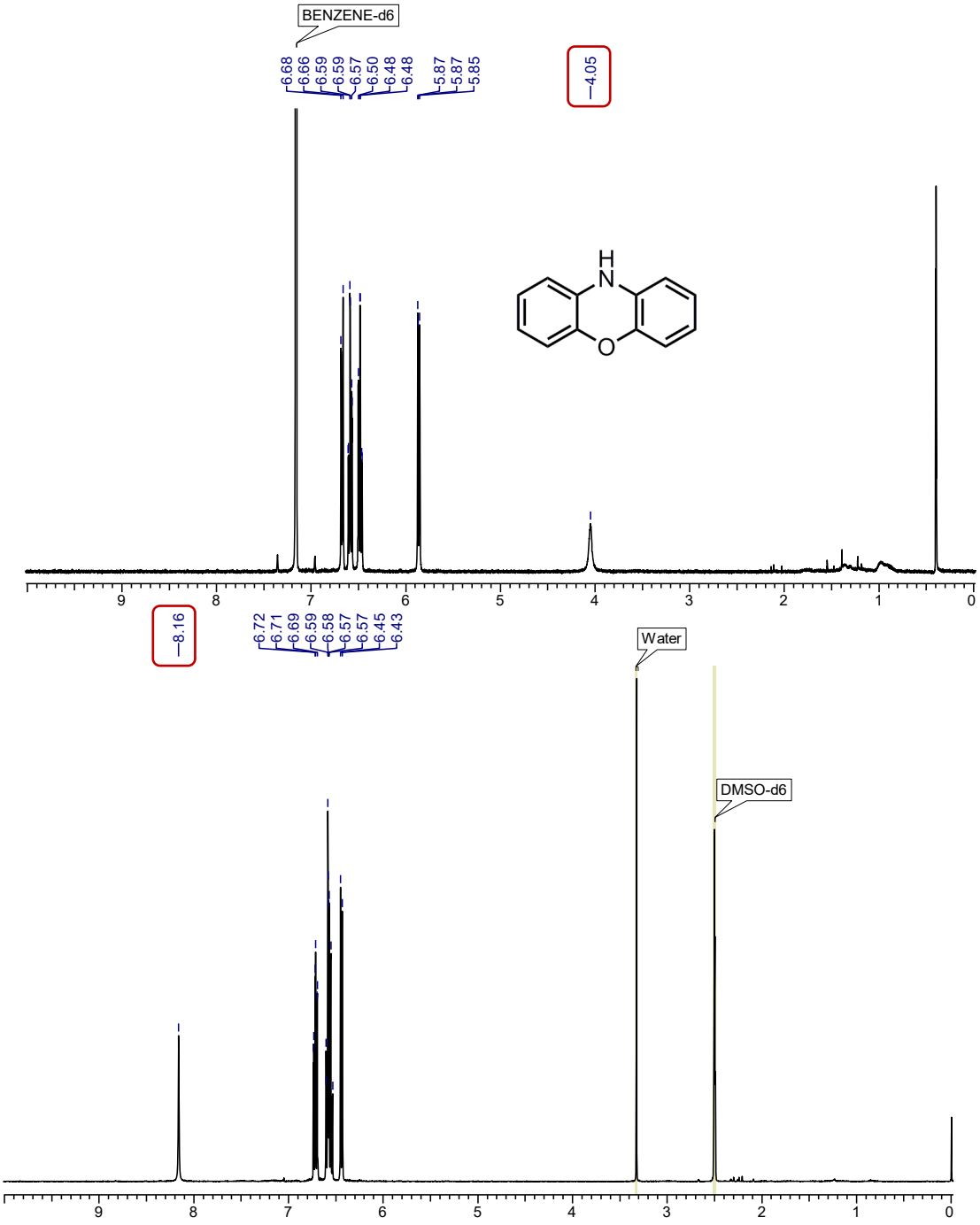

Figure S2.17. ^{1}H NMR of phenoxazine in benzene-d_6 (top) and DMSO-d_6 (bottom) used to determine $\boldsymbol{\alpha_2^H}$ with the N-H peak labeled.

2.8.5 Phenoxazine Inhibited Autoxidation Data

Inhibited co-autoxidation of 1,4-dioxane (2.9 M) and PBD-BODIPY (10 μM) were initiated by AIBN (6 mM) in either PhCl or a 2:1 PhCl:DMSO mixture at 37 °C and inhibited by phenoxazine derived RTAs **4-17** to determine their stoichiometry and k_{inh}^{S} to calculate theirk_{inh}^{PhCl} values. Stoichiometry was determined based on the observed t_{inh} and its relationship between R_i, [AH], and n described in Eq. 9 in the manuscript. $k_{inh}^{S}$was determined either mathematically based on the initial slope of inhibition (Eq. II) or by fitting and parameter determination with COPASI, which has been previously described.[9] See *NMR Spectra* for ^{1}H spectra used to determine $\boldsymbol{\alpha_2^H}$**.**

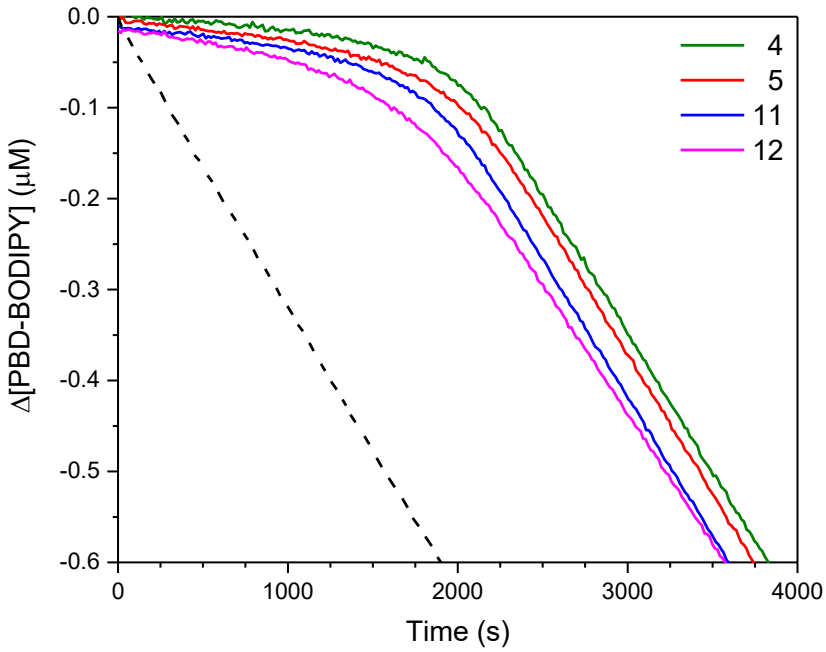

Figure S2.18. Co-autoxidation of 1,4-dioxane (2.9 M) and PBD-BODIPY (10 uM) initiated by AIBN (6 mM) in PhCl at 37 °C (black) and inhibited by 2 μM 2-trifluoromethylphenoxazine (4, green), 2 μM 3-trifluoromethylphenoxazine (5, red), 2 μM N,N-diethyl-3-sulfonamidephenoxazine (11, blue), and 2 μM 3-cyanophenoxazine (12, magenta). Reaction progress was monitored by absorbance at 587 nm (ε = 123 000 M^{-1} cm^{-1}).

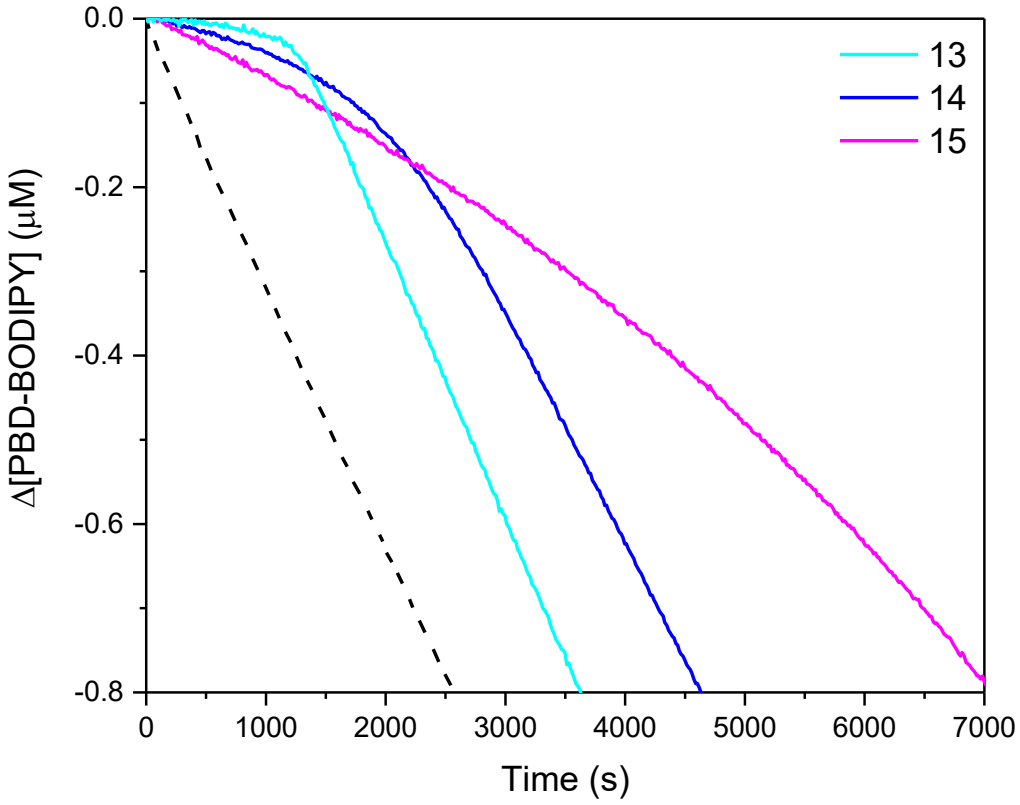

Figure S2.19. Co-autoxidation of 1,4-dioxane (2.9 M) and PBD-BODIPY (10 μM) initiated by AIBN (6 mM) in PhCl at 37 °C (black) and inhibited by 2 μM 3-methoxy-7-nitrophenoxazine (13, cyan), 2 μM 3-nitrophenoxazine (14, blue), and 6 μM 3-nitro-7-cyanophenoxazine (15, magenta). Reaction progress was monitored by absorbance at 587 nm (ε = 123 000 M^{-1} cm^{-1}).

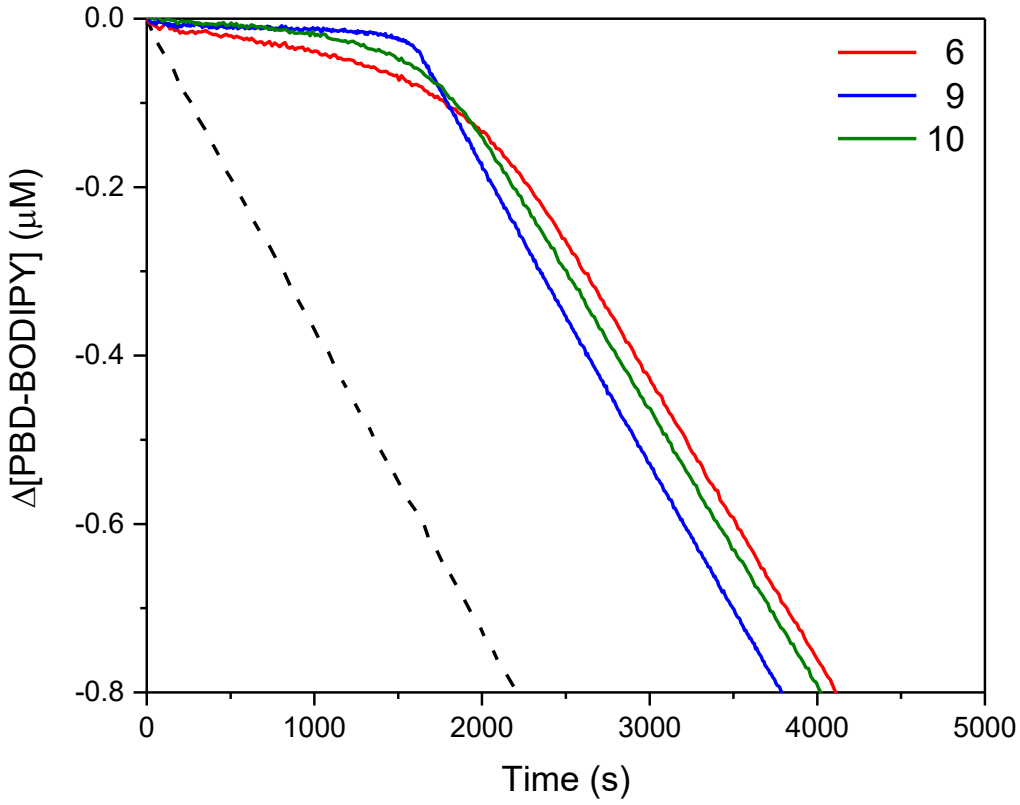

Figure S2.20. Co-autoxidation of 1,4-dioxane (2.9 M) and PBD-BODIPY (10 μM) initiated by AIBN (6 mM) in 2:1 PhCl and DMSO at 37 °C (black) and inhibited by 2 μM 2-tert-butylphenoxazine (6. red), 2 μM 2,4,6,8-tetra-tert-butylphenoxazine (9. blue), and 2 μM 2,8-di-tert-butylphenoxazine (10. green). Reaction progress was monitored by absorbance at 587 nm (ε = 118 200 M^{-1} cm^{-1}).

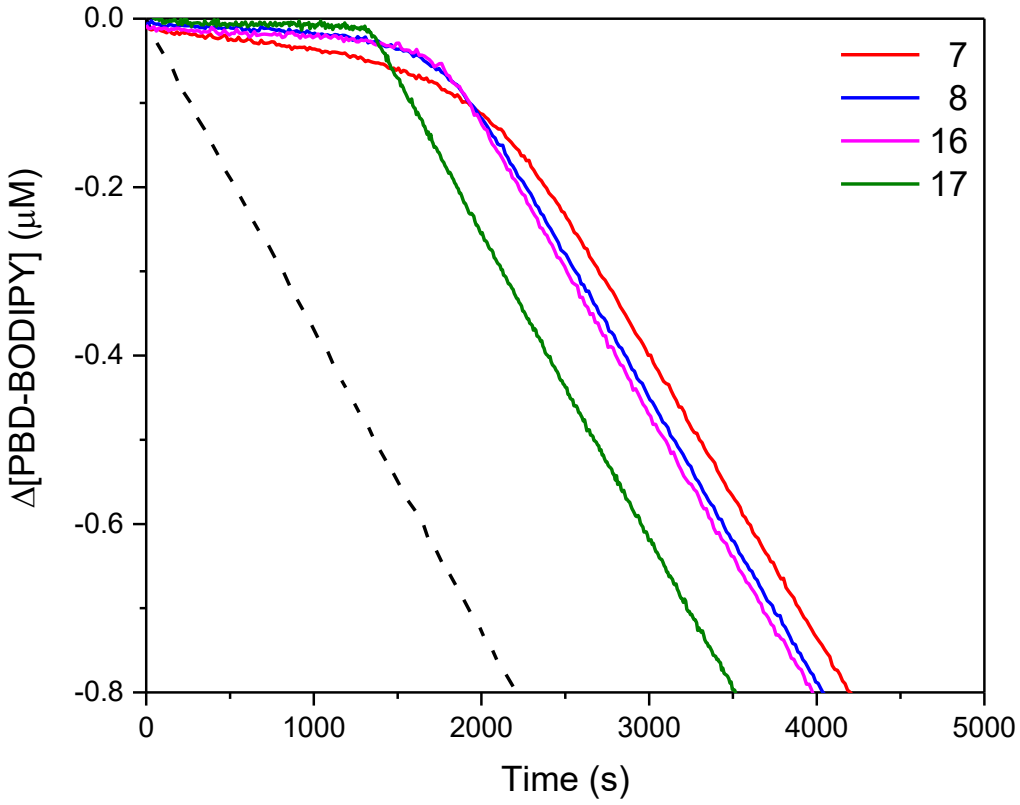

Figure S2.21. Co-autoxidation of 1,4-dioxane (2.9 M) and PBD-BODIPY (10 μM) initiated by AIBN (6 mM) in 2:1 PhCl and DMSO at 37 °C (black) and inhibited by 2 μM 3-tert-butylphenoxazine (7, red), 2 μM 3,7-tetra-tert-butylphenoxazine (8, blue), 2 μM 3-methoxyphenoxazine (16, magenta), and 2 μM 3,7-dimethoxyphenoxazine (17, green). Reaction progress was monitored by absorbance at 587 nm (ε = 118 200 M^{-1} cm^{-1}).

.

2.8.6 Cyclic Voltammograms (CV)

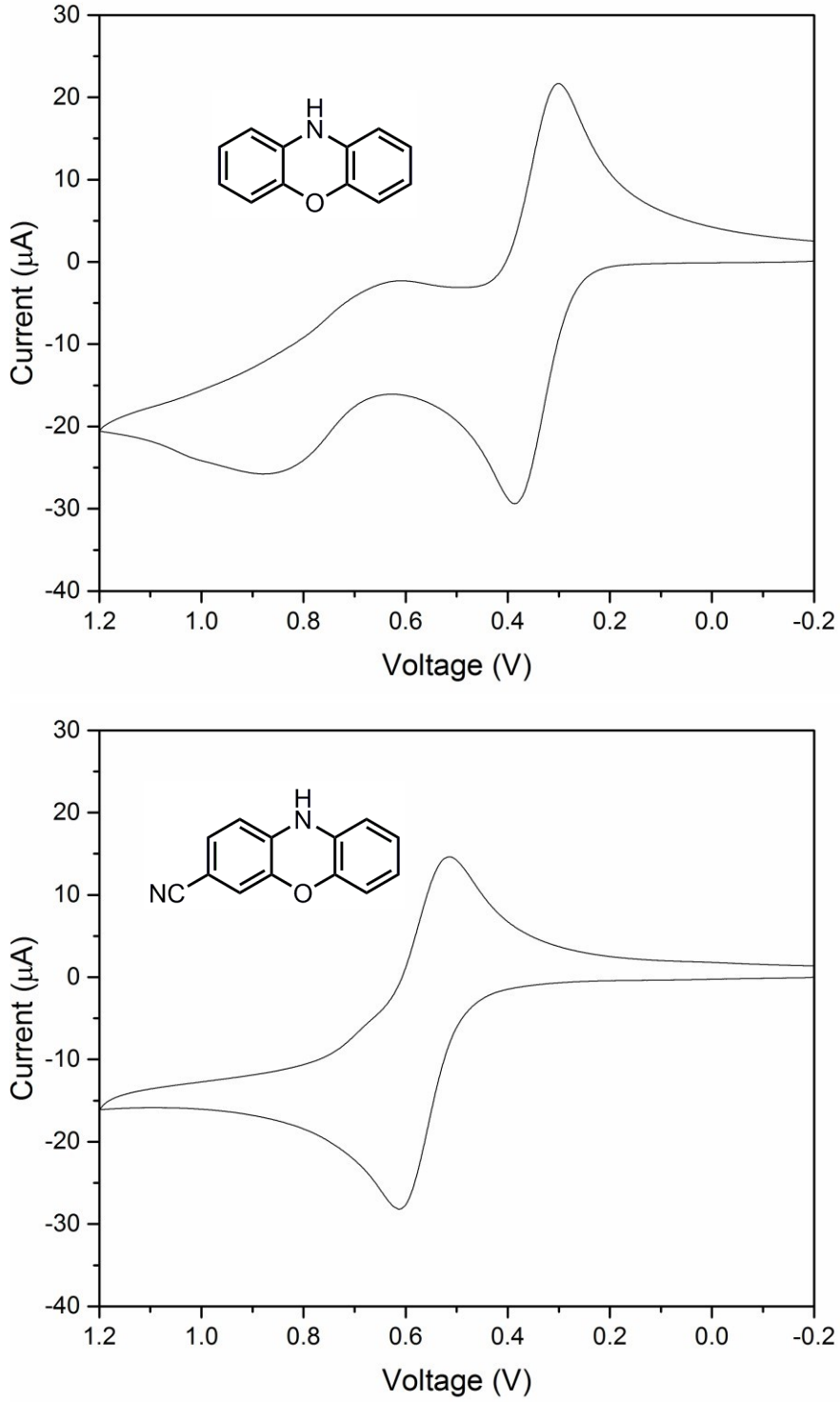

Figure S2.22. CV of phenoxazine (**2.3**) vs. Ag/Ag^+. $E°$ = 0.87 V vs. NHE (top). CV of 3-cyanophenoxazine (**2.12**) vs. Ag/Ag^+. $E°$ = 1.13 V vs. NHE (bottom).

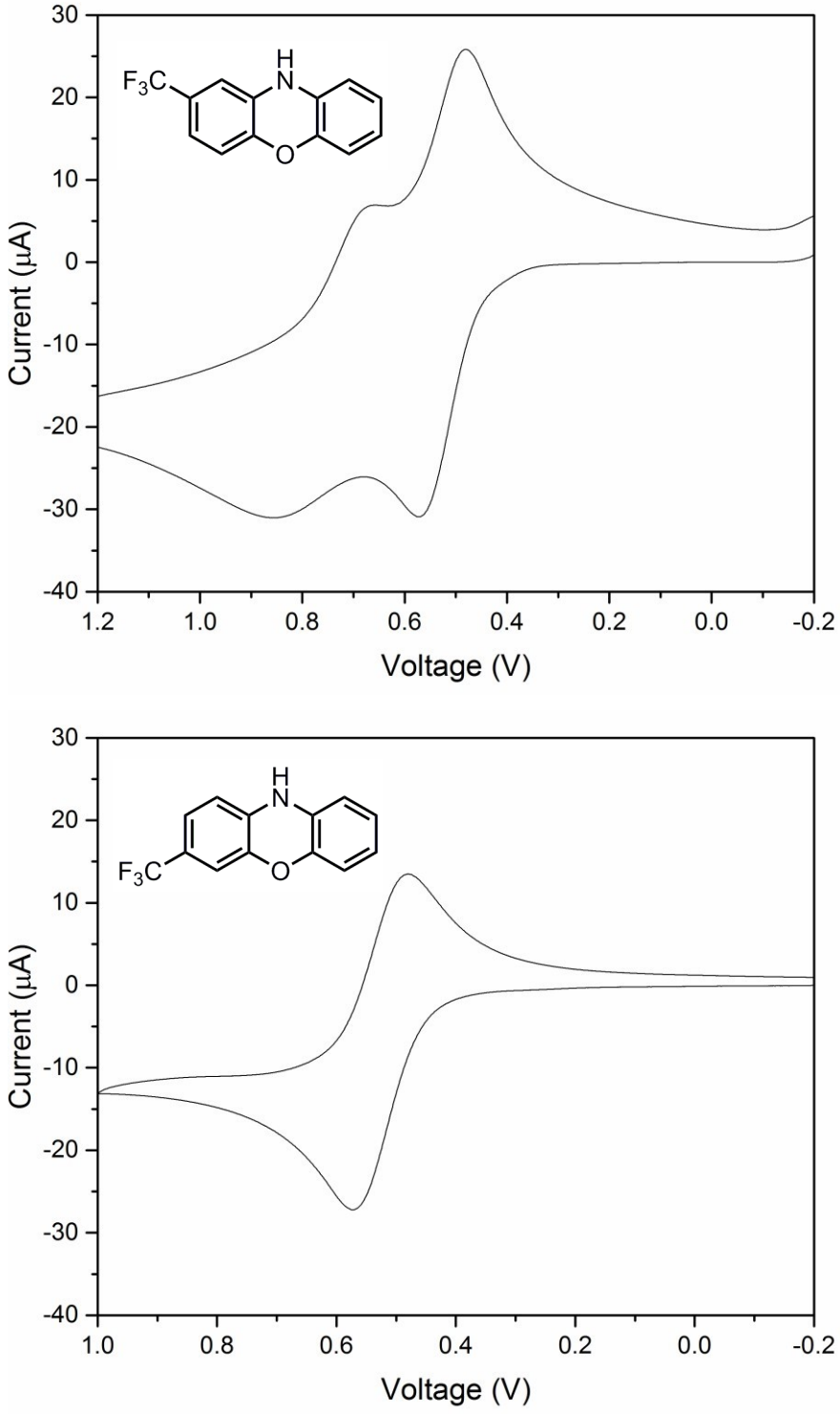

Figure S2.23. CV of 2-trifluoromethylphenoxazine (**2.4**) vs. Ag/Ag^{+}. $E°$ = 1.05 V vs. NHE (top). CV of 3-trifluoromethylphenoxazine (**2.5**) vs. Ag/Ag^{+}. $E°$ = 1.06 V vs. NHE (bottom).

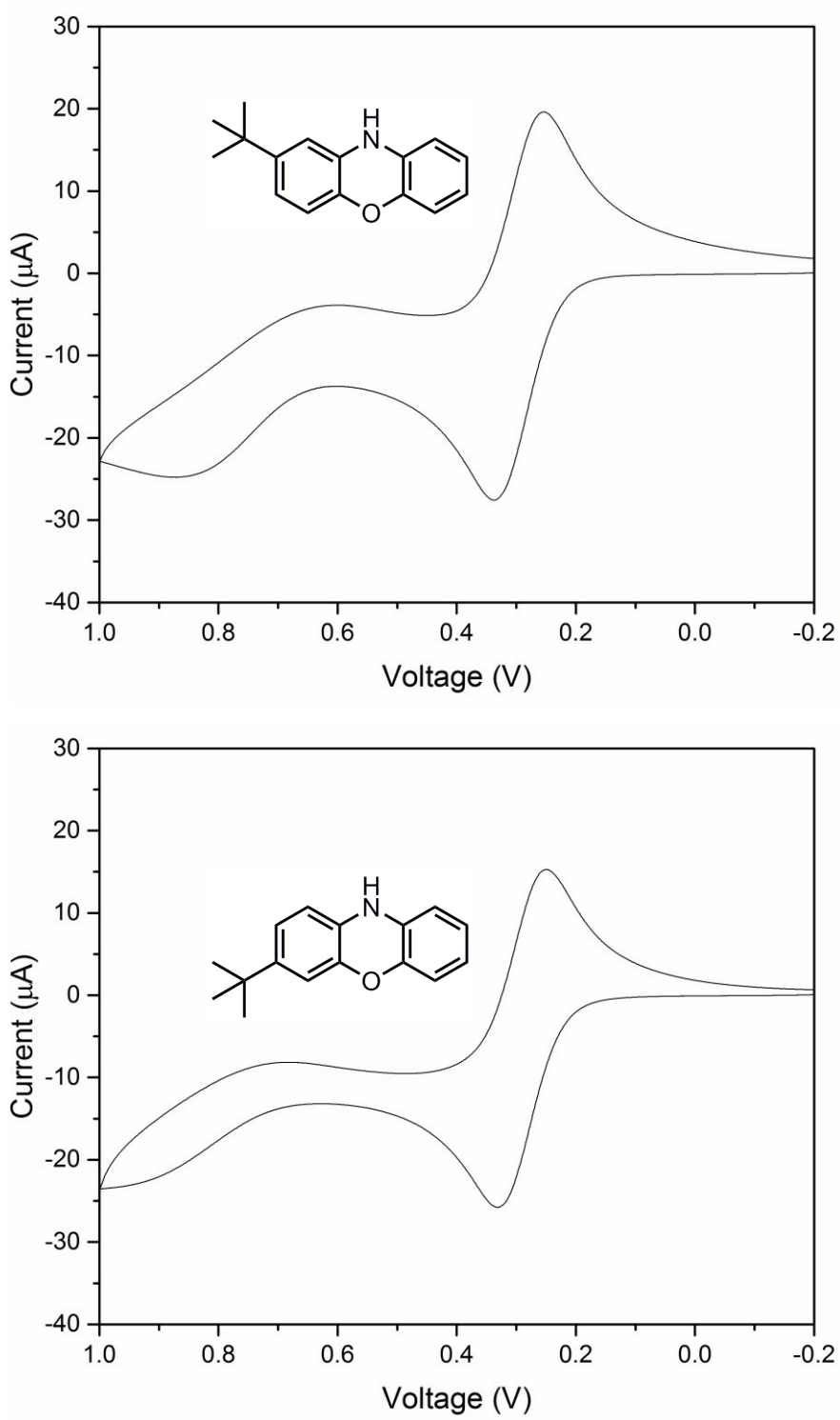

Figure S2.24. CV of 2-tert-butylphenoxazine (**2.6**) vs. Ag/Ag^{+}. $E°$ = 0.83 V vs. NHE (top). CV of 3-tert-butylphenoxazine (**2.7**) vs. Ag/Ag^{+}. $E°$ = 0.81 V vs. NHE (bottom).

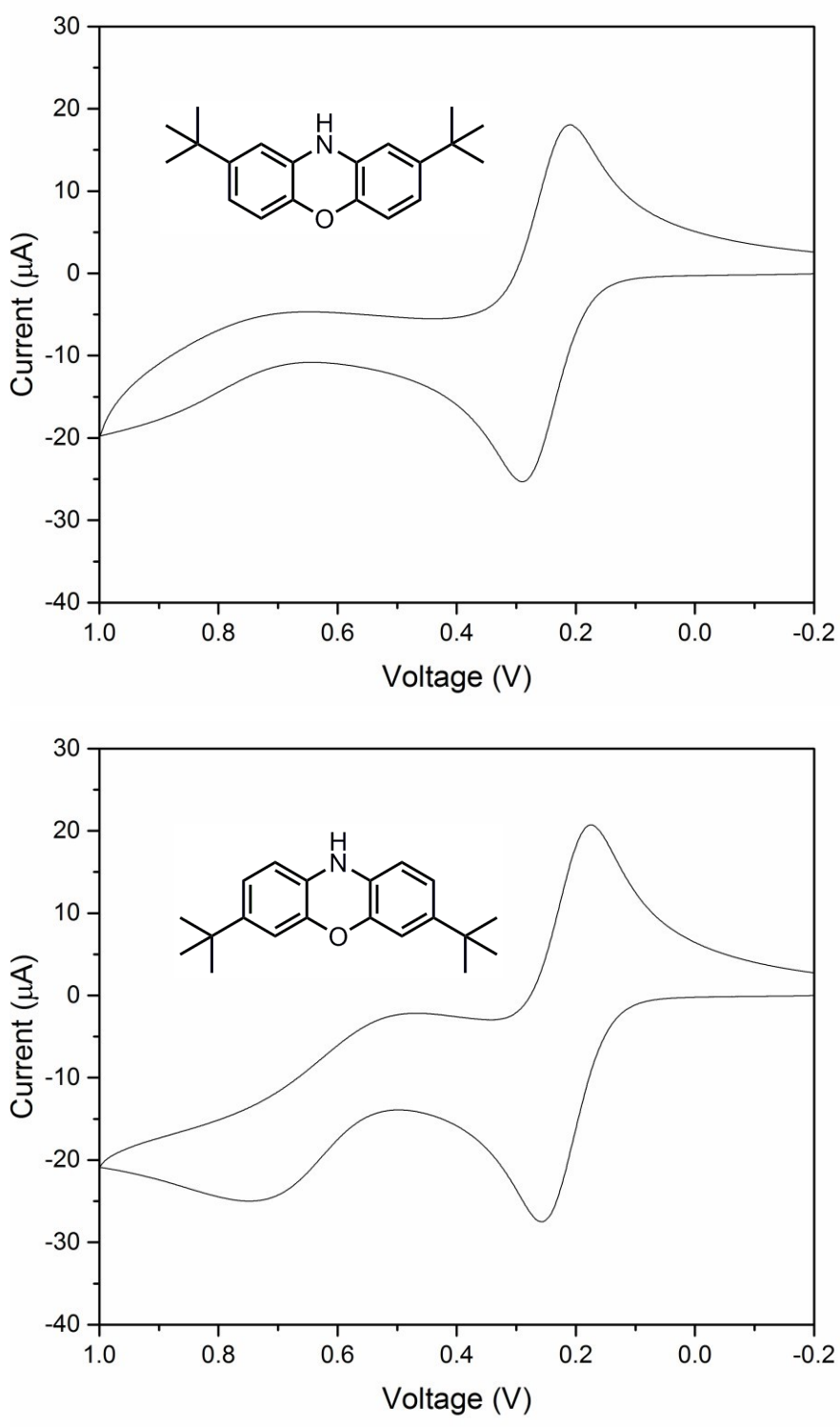

Figure S2.25. CV of 2,8-di-tert-butylphenoxazine (**2.10**) vs. Ag/Ag^{+}. $E°$ = 0.78 V vs. NHE (top). CV of 3,7-di-tert-butylphenoxazine (**2.8**) vs. Ag/Ag^{+}. $E°$ = 0.75 V vs. NHE (bottom).

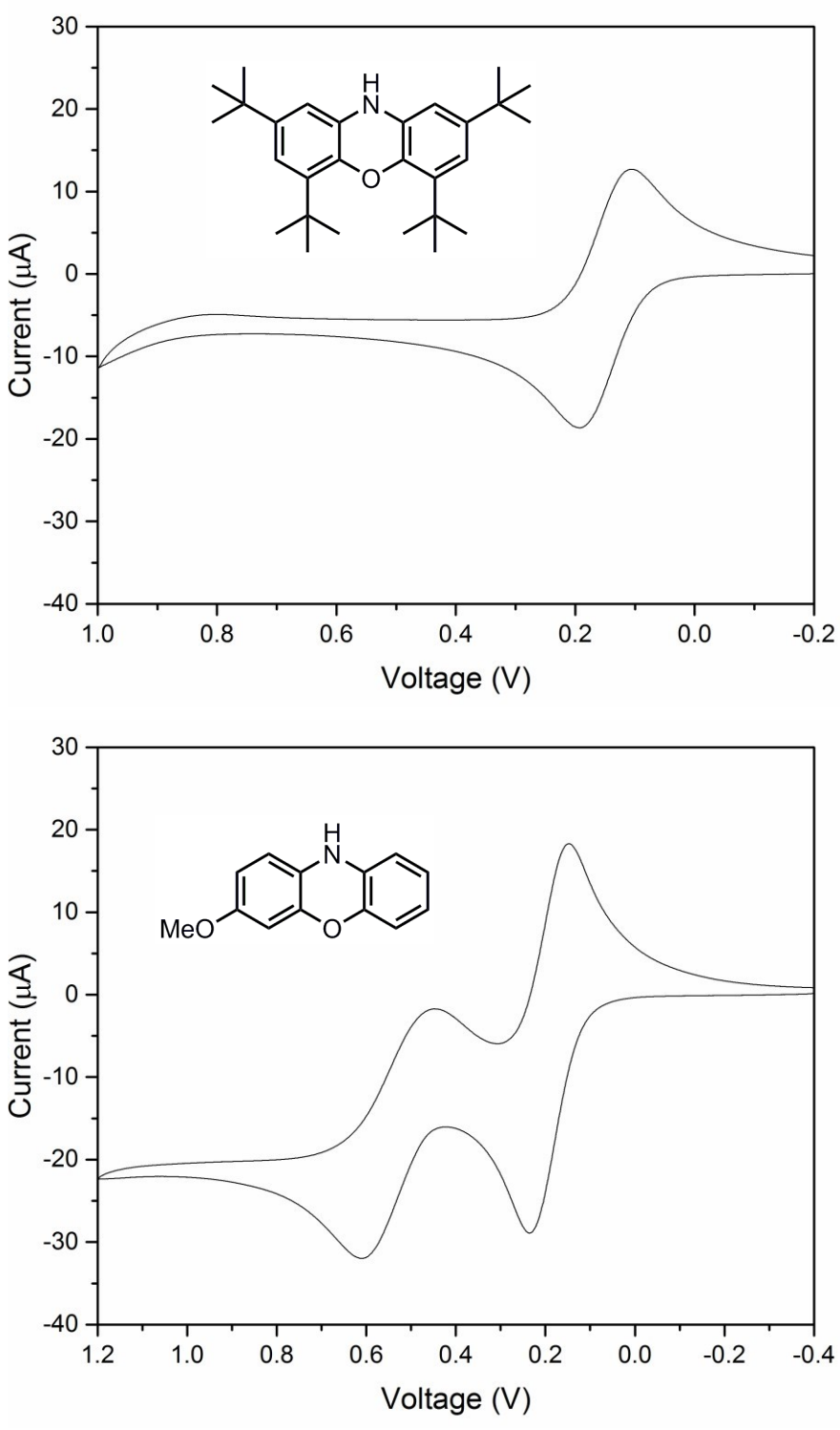

Figure S2.26. CV of 2,4,6,8-tetra-tert-butylphenoxazine (**2.9**) vs. Ag/Ag^+. $E°$ = 0.67 V vs. NHE (top). CV of 3-methoxyphenoxazine (**2.16**) vs. Ag/Ag^+. $E°$ = 0.72 V vs. NHE (bottom).

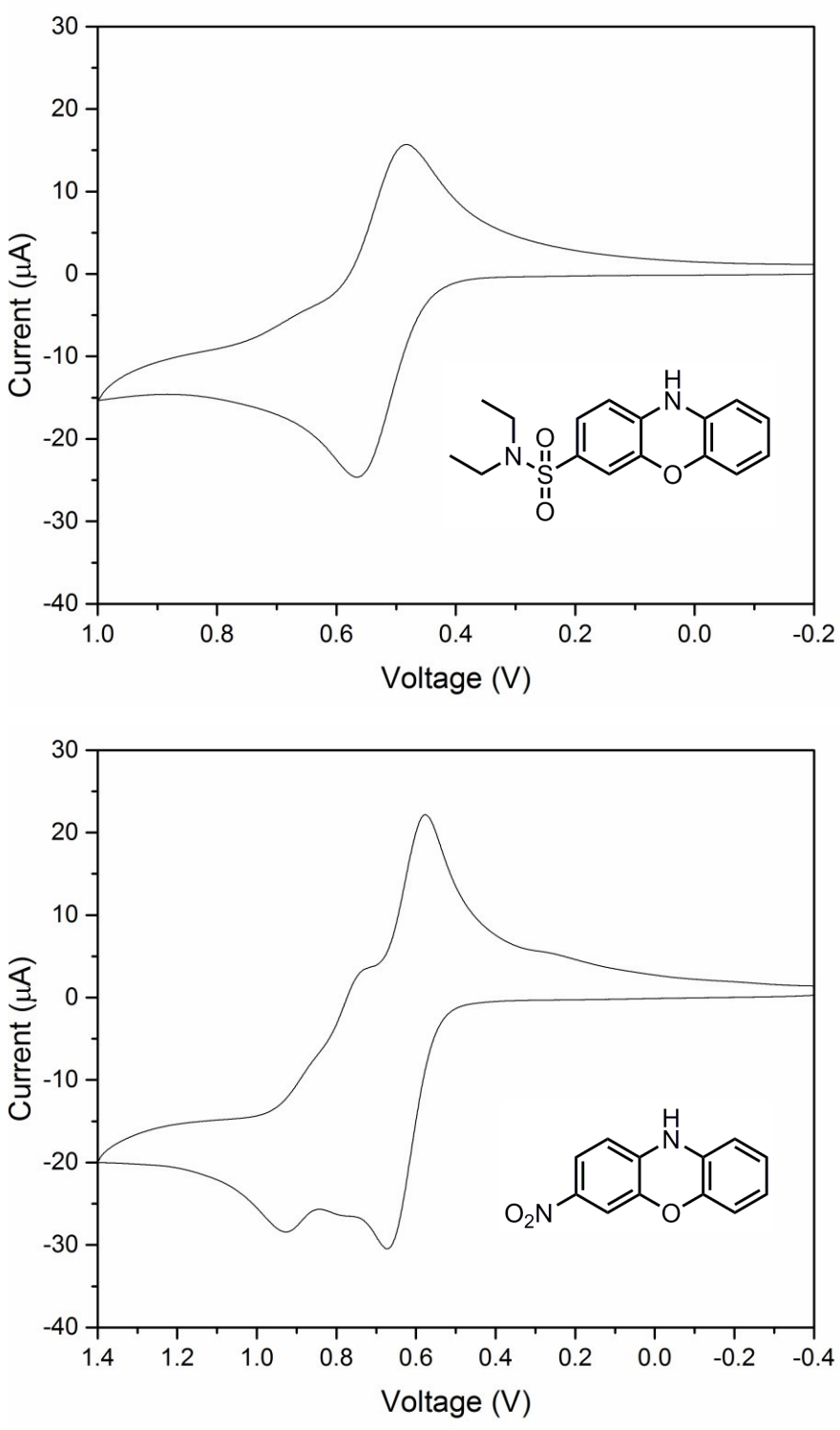

Figure S2.27. CV of N,N-di-ethyl-3-sulfonamidephenoxazine (**2.11**) vs. Ag/Ag^{+}. $E°$ = 1.06 V vs. NHE (top). CV of 3-nitrophenoxazine (**2.14**) vs. Ag/Ag^{+}. $E°$ = 1.15 V vs. NHE (bottom).

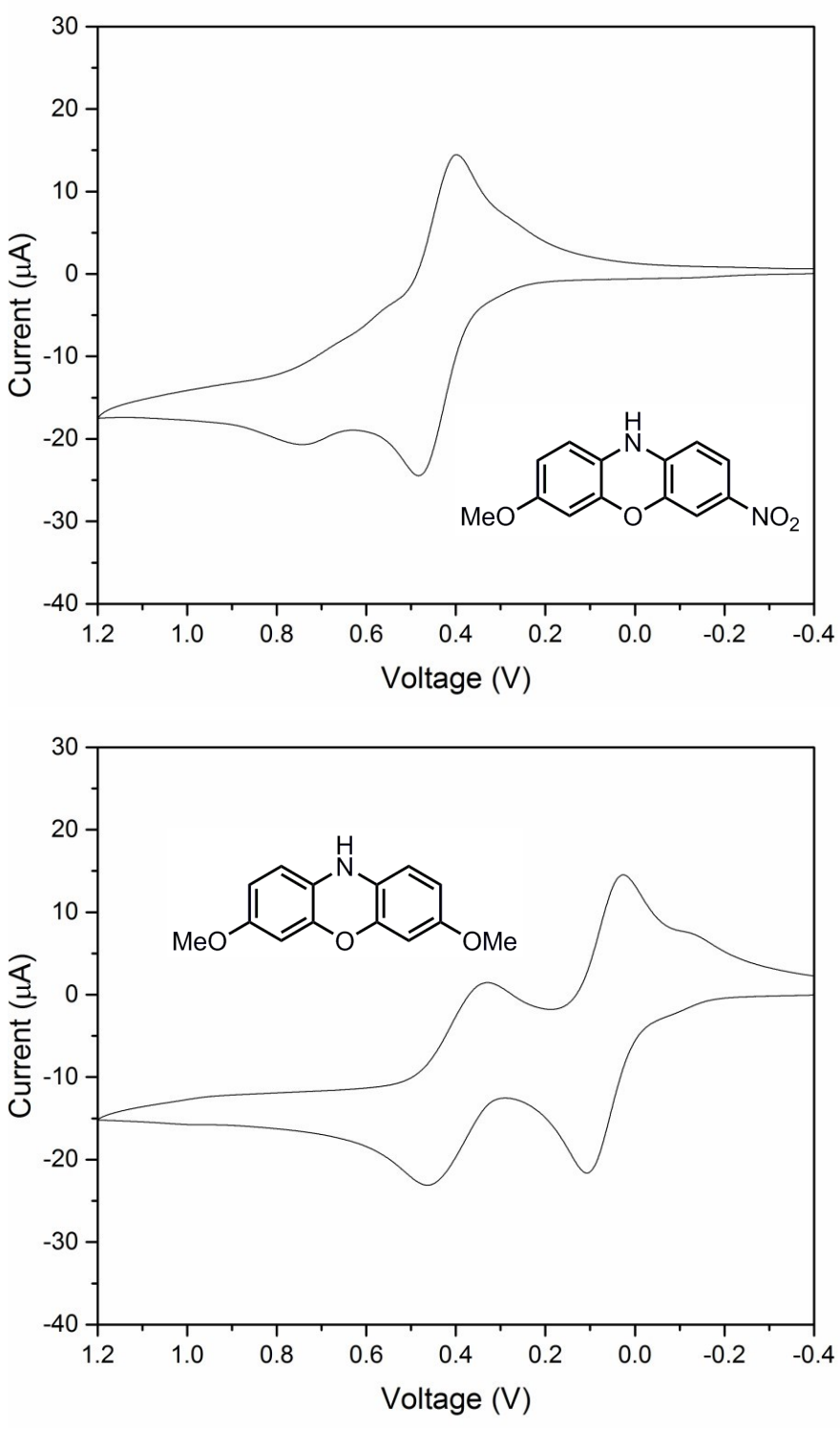

Figure S2.28. CV of 3-methoxy-7-nitrophenoxazine (**2.13**) vs. Ag/Ag^+. $E°$ = 0.97 V vs. NHE (top). CV of 3,7-dimethoxyphenoxazine (**2.17**) vs. Ag/Ag^+. $E°$ = 0.59 V vs. NHE (bottom).

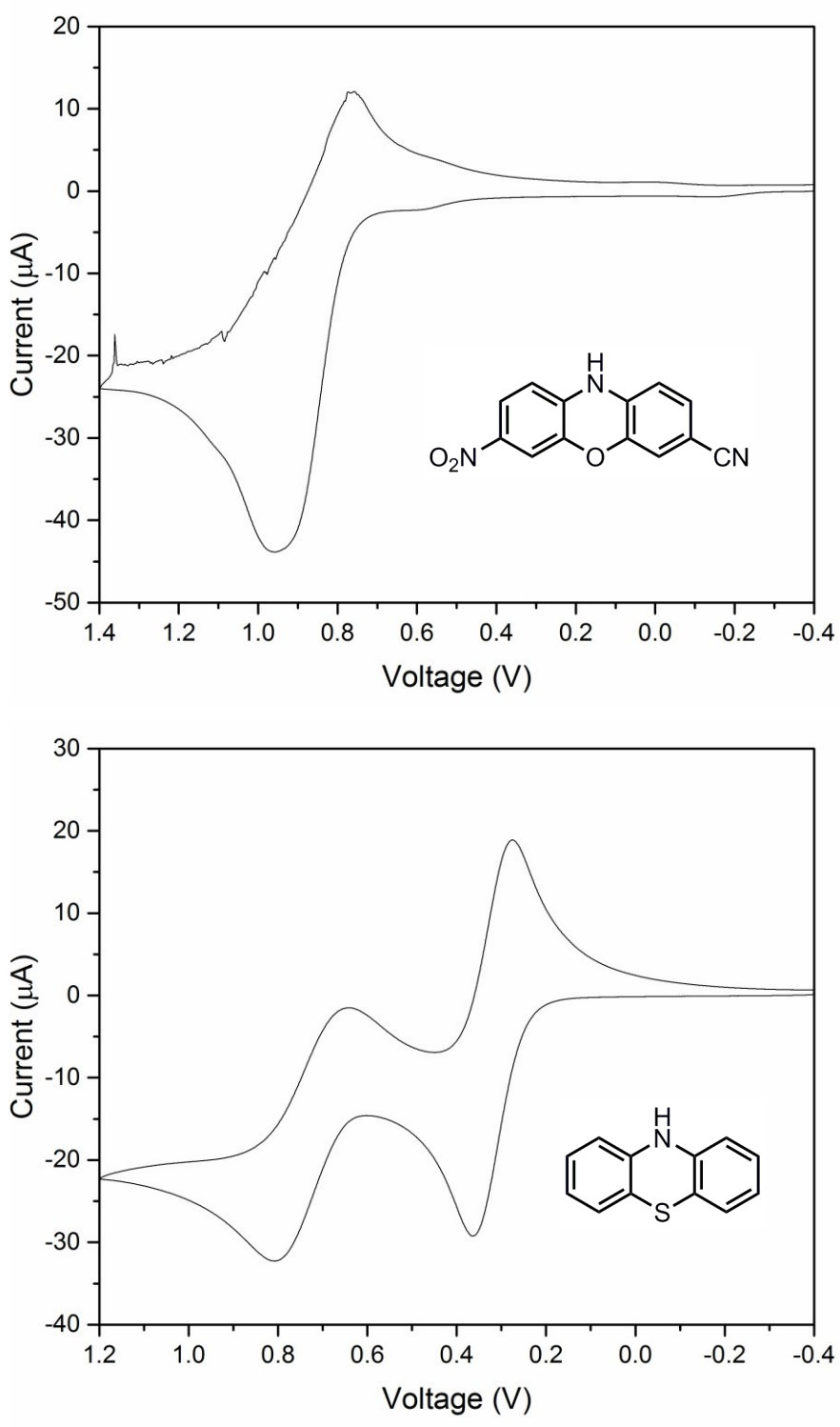

Figure S2.29. CV of 3-nitro-7-cyanophenoxazine (**2.15**) vs. Ag/Ag^+. $E°$ = 0.97 V vs. NHE (top). CV of phenothiazine (**2.2**) vs. Ag/Ag^+. $E°$ = 0.85 V vs. NHE (bottom).

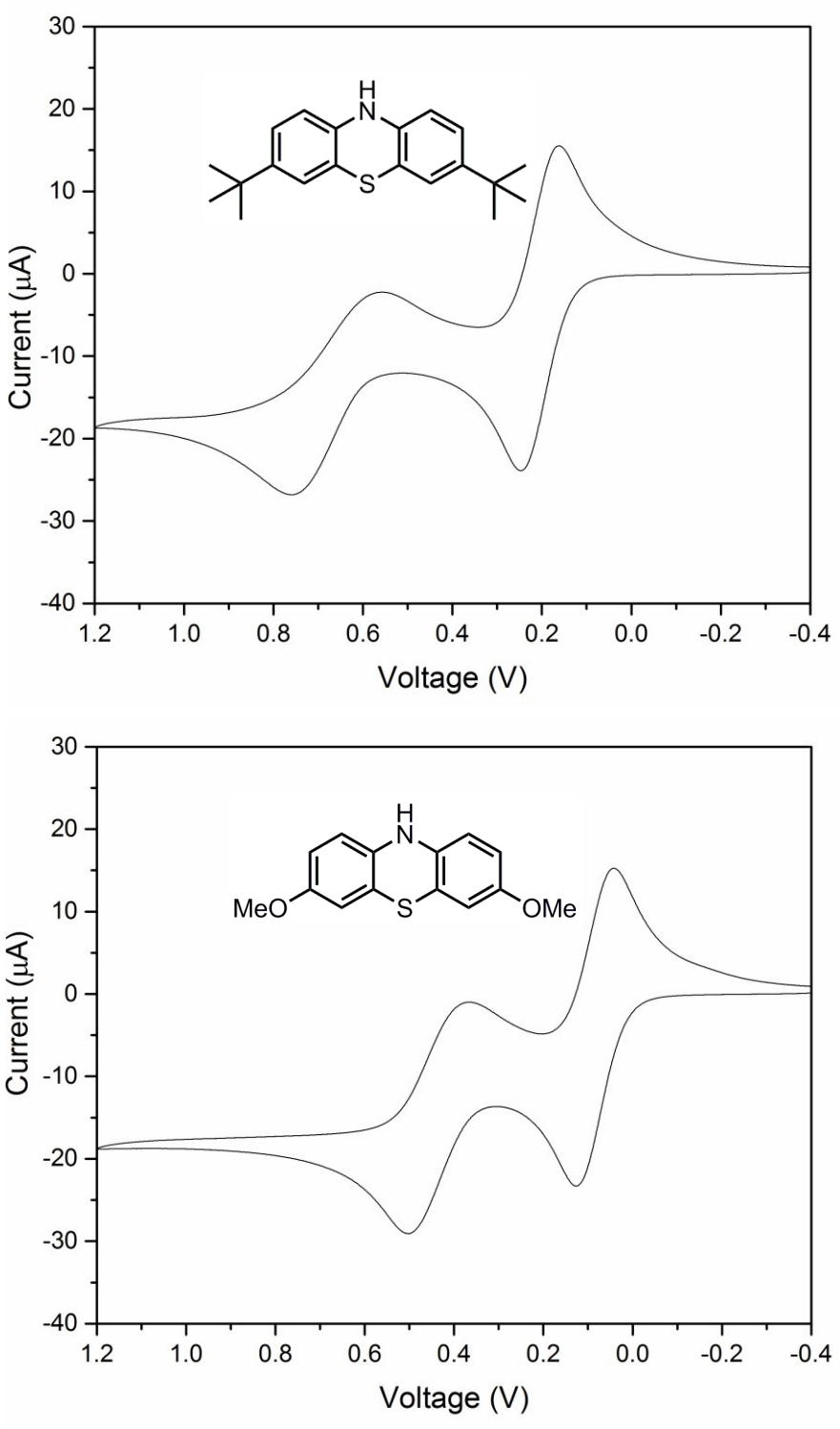

Figure S2.30. CV of 3,7-di-tert-butylphenothiazine (**E**) vs. Ag/Ag^{+}. $E°$ = 0.75 V vs. NHE (top). CV of 3,7-dimethoxyphenothiazine (**F**) vs. Ag/Ag^{+}. $E°$ = 0.61 V vs. NHE (bottom).

2.8.7 Diarylamine Structures

The standard/anodic potentials and rate constants of peroxyl trapping of the diarylamines cited in Figure 2.5 in the manuscript can be found in our previous published work on heterocyclic diarylamine RTAs.[10]

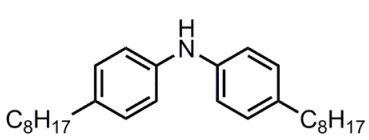

G

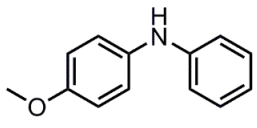

H

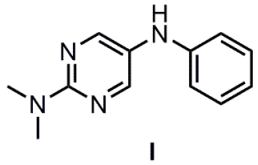

I

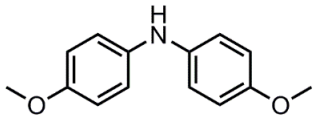

J

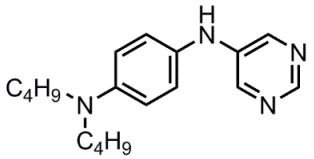

K

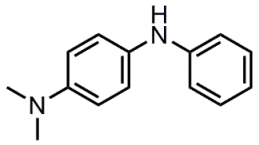

L

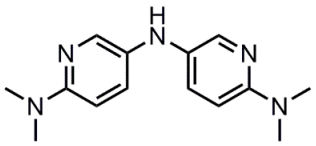

M

2.8.8 Computational Data

Table S2.5. Calculated BDE and IP (CBS-QB3) as well as experimental standard potential ($E°$) for substituted phenoxazines.

	BDE (kcal mol^{-1})	**IP (kcal mol^{-1})**	***E*° (V)**
2.15	77.5	181.7	1.38
2.14	76.5	171.7	1.15
2.12	76.2	169.7	1.13
2.5	76.1	166.9	1.06
2.11	76.3	166.0	1.06
2.4	76.2	166.8	1.05
2.13	74.0	163.5	0.97
2.3	75.2	159.6	0.87
2.6	74.6	155.1	0.83
2.7	74.5	154.8	0.81
2.10	74.0	151.3	0.78
2.8	73.9	151.1	0.75
2.16	72.8	152.1	0.72
2.17	70.7	146.2	0.59

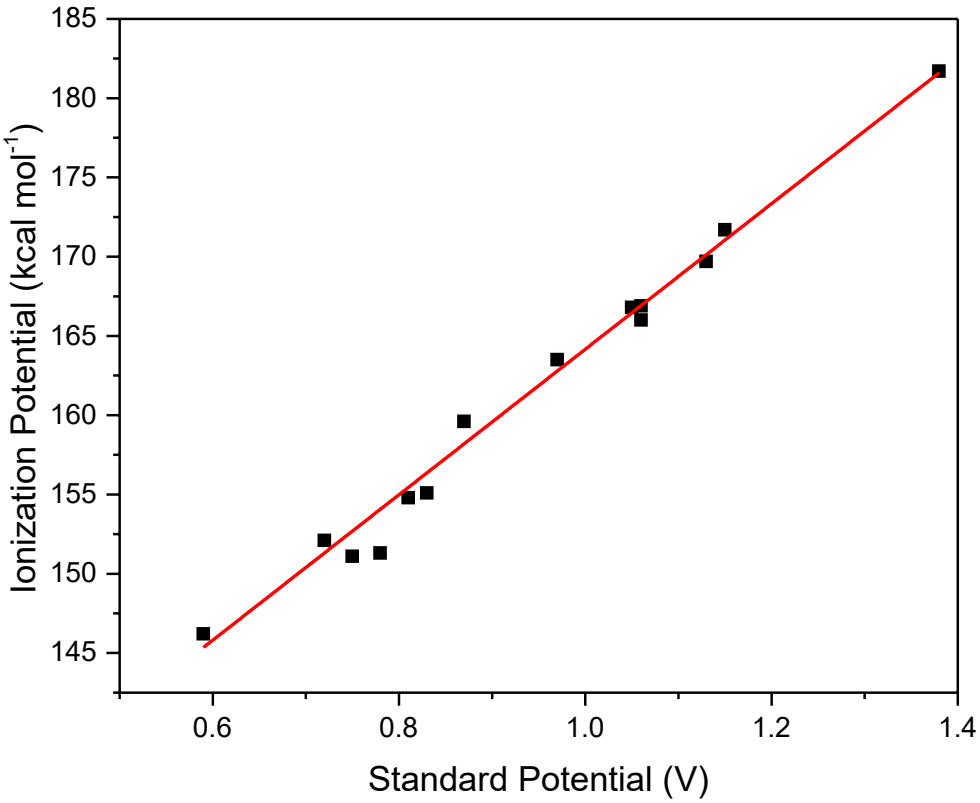

Figure S2.31. Calculated adiabatic ionization potential (CBS-QB3) vs. experimental standard potential ($E°$).

2.8.9 References (SI)

1 R. W. Taft, D. Gurka and J. W. Rakshys, *J. Am. Chem. Soc.*, 1969, **91**, 4801–4808.

2 M. H. Abraham, R. J. Abraham, J. Byrne and L. Griffiths, *J. Org. Chem.*, 2006, **71**, 3389–3394.

3 R. J. Abraham, J. J. Byrne, L. Griffiths and M. Perez, *Magn. Reson. Chem.*, 2006, **44**, 491–509.

4 R. J. Abraham and M. Mobli, *Magn. Reson. Chem.*, 2007, **45**, 865–877.

5 M. H. Abraham, P. L. Grellier, D. V. Prior, P. P. Duce, J. J. Morris and P. J. Taylor, *J. Chem. Soc. Perkin Trans. 2*, 1989, 699–711.

6 L. Valgimigli, D. Bartolomei, R. Amorati, E. Haidasz, J. J. Hanthorn, S. J. Nara, J. Brinkhorst and D. A. Pratt, *Beilstein J. Org. Chem.*, 2013, **9**, 2781–2792.

7 J.-P. R. Chauvin, M. Griesser and D. A. Pratt, *J. Am. Chem. Soc.*, 2017, **139**, 6484–6493.

8 M. Lucarini, P. Pedrielli, G. F. Pedulli, L. Valgimigli, D. Gigmes and P. Tordo, *J. Am. Chem. Soc.*, 1999, **121**, 11546–11553.

9 E. A. Haidasz, A. T. M. Van Kessel and D. A. Pratt, *J. Org. Chem.*, 2016, **81**, 737–744.

10 J. J. Hanthorn, R. Amorati, L. Valgimigli and D. A. Pratt, *J. Org. Chem.*, 2012, **77**, 6895–6907.

Chapter 3: Substituted Phenoxazine RTAs in High-Temperature Autoxidation of Hexadecane & the Mechanism of Catalyst Depletion

3.1 Preface

The impressive activity of phenoxazine RTAs in styrene and 1,4-dioxane at 37 °C can be ascribed to their relatively weak N-H BDEs and inherently high reactivity to peroxyl radicals. Oxidizable monomers/substrates in storage for extended periods of time can be interchangeably stabilized with inexpensive commercial phenols, catechols, and diphenylamines which are likely to be more cost effective than phenoxazines. However, new RTA technology based on phenoxazines could be commercially viable if their vast superiority at ambient temperatures extends to elevated temperatures (i.e. under usage conditions) where diarylamines are catalytic.

Formulation of oxidation resistant lubricants, greases, and service fluids geared towards high temperature operation is continuously in demand, even if most take it for granted. From transportation to manufacturing equipment, these products are necessary and need to be replaced on a regular basis. Indeed, in light of continuously stricter emission requirements, manufacturers will compensate by increasing the operating temperatures of their engines to improve combustion efficiency, which of course requires the lubricants to operate under increasingly punitive circumstances. Owners and operators have a strong incentive to purchase longer lasting lubricants and greases to reduce operating costs, which incentivises businesses who deal in such wares to provide more sustainable products. ADPA is a staple of the high temperature lubricant business due their catalytic radical trapping activity, making up 0.1-1% of the weight of some formulations. At elevated

temperatures we previously have observed major improvements in inhibition times by using more reactive heterocyclic diarylamines.[1] Given this apparent correlation between the time of inhibition and the increased inhibition rate constant, we anticipated that inherently more reactive phenoxazines would be a boon for inhibited high temperature autoxidations. For example, even the very electron poor 3-cyano-7-nitrophenoxazine we synthesized is >20 times faster than 4,4'-di-octyl-diphenylamine and ~1.5 times faster than our best performing heterocyclic diarylamine.[2]

Herein we present the results of our preliminary investigations of the phenoxazine-based RTAs introduced in Chapter 2 as RTAs at the elevated temperatures where we expect them to be catalytic. Specifically, we present the results of inhibited autoxidations of hexadecane at 160 ºC and compare their performance to that of ADPA, N^2,N^2-dimethyl-N^5-phenylpyrimidine-2,5-diamine, and phenothiazine. In selected experiments, the loss of phenoxazine and the corresponding phenoxazine-N-oxyl were monitored throughout the autoxidation experiment by HPLC and EPR, respectively, in order to monitor the speciation of the RTA and its key intermediate over the course of the experiment to better understand the trends in efficiency.

I would like to express my gratitude to fellow co-worker Dr. Jia-Fei Poon for sharing the data he collected for the inhibited autoxidation of phenothiazine and to co-worker Dr. Markus Griesser for his assistance with recording the EPR spectra.

3.2 Introduction

As previously introduced in section **1.2.3** of this thesis, the interest in diarylamine type antioxidants is based on their ability to be regenerated at elevated temperatures.

Scheme 3.1. The Korcek Cycle of diarylamine regeneration. (i) Diarylamine trapping peroxyl radical. (ii) Nitroxide trapping an alkyl radical. (iii) Alkoxyamine decomposing to form diarylamine.

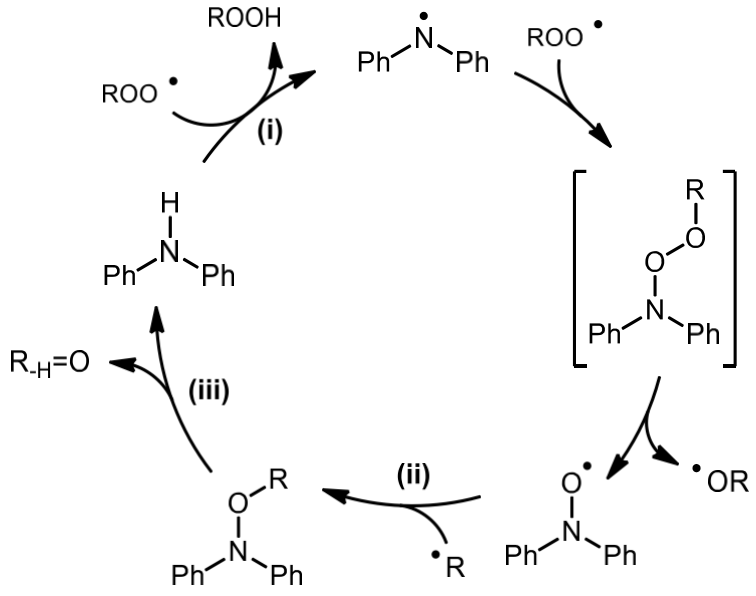

To briefly reiterate the salient content of **1.2.3**, there are three potential rate limiting processes in the proposed Korcek Cycle.[3] The first is the rate of the initial peroxyl trapping step (i) which will mainly be predicated on the concentration of the amine and its rate constant of inhibition (k_{inh}). The second is the rate of trapping of an alkyl radical by the nitroxide (ii) which will likely be limited by the steady state concentration of alkyl radicals. The steady state concentration of alkyl radicals is rather low as they are converted into peroxyl radicals as essentially fast as they are generated since its reaction with oxygen

is effectively diffusion controlled ($k_4 \sim 10^9$ M^{-1} s^{-1}).[4] While the cross reaction between nitroxide and R• has a comparable rate constant (e.g. the addition of TEMPO to a t-butyl radical has a $k_{11} = 7.6 \times 10^8$ M^{-1} s^{-1}),[5] but to actually form alkoxyamine, the nitroxide has to compete with oxygen which is continuously supplied to the system.

Scheme 3.2. (Top) Formation of alkoxyamine from nitroxide and alkyl radical. (Bottom) Rate expression for consumption of alkyl radicals (Eq. 3.1).

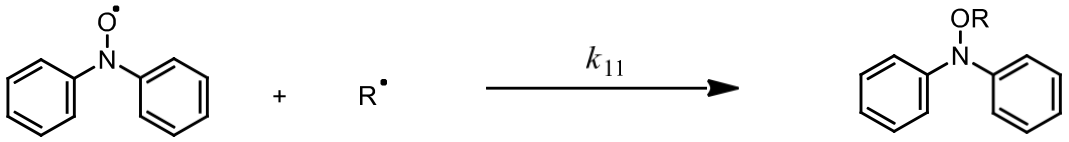

$$-\frac{d[R^{\cdot}]}{dt} = [R^{\cdot}][O_2]k_4 + [R^{\cdot}][Ar_2NO^{\cdot}]k_{11} - 2[Int]k_1 \qquad \textbf{Eq. 3.1}$$

The other potential rate limiting process is the regeneration of the diarylamine (iii) from the corresponding alkoxyamine via either homolysis and disproportionation or the retro-carbonyl-ene reaction.[6] It seems reasonable to assume that the rate constant for this unimolecular reaction should be proportional to the k_{inh} of the parent amine at least for homolysis and disproportionation, since both processes involve the formation of the same diarylaminyl radical. In the seminal work by Korcek and co-workers, the presence of alkoxyamine was never observed in their sampling of the inhibited autoxidation of hexadecane at 160 ºC, implying that this unimolecular process is not rate determining under those conditions. Indeed, when alkoxyamines were prepared in the absence of O_2, they were found to be stable at 95 ºC but rapidly decomposed at 120 ºC which suggests that this reaction will likely only be rate determining at lower temperatures.[3]

Scheme 3.3. Inhibition rate constants and redox potentials of **3.1**-**3.5**

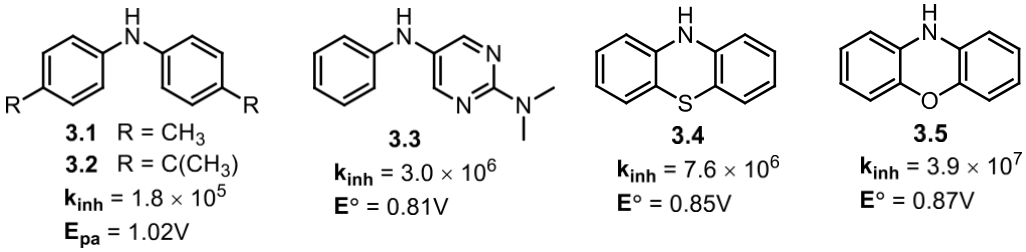

Based on previous work on the catalytic activity of heterocyclic diarylamines, promoting (i) by using more reactive diarylamines seemed to result in a substantial and proportionate improvement in the duration of the inhibited period at 160 °C.[1] We wanted to perform a similar set of experiments with the substituted phenoxazines in light of their high inherent reactivity to peroxyl radicals and apparent robustness to single electron oxidation. These results could then be compared to those obtained with ADPA (**3.1**/**3.2**), N^2,N^2-dimethyl-N^5-phenylpyrimidine-2,5-diamine (**3.3**), and phenothiazine (**3.4**). In addition, we wanted to perform a parallel diagnostic on the speciation of the phenoxazine (**3.5**) in an analogous fashion to the experimental work by Korcek[3] and co-workers on ADPA in order to better understand reactivity trends of phenoxazine.

.

3.3 Results/Discussion

3.3.1 Experimental Design

The design of the stirred-flow reactor we have used previously to carry out autoxidations at elevated temperatures (i.e. 160 ºC)[1,7,8] limits us to the study of a single RTA under a single set of conditions. Thus, the evaluation of a sizable library of RTAs would be a rather time-consuming undertaking. I therefore elected instead to utilize the more efficient parallel single heated block reactor (PSHBR) that was recently designed and calibrated in our lab to conduct the evaluation of the 15 substituted phenoxazines alongside a handful of reference RTAs.

Scheme 3.4. A) Collection of hexadecane samples from the parallel single heated block reactor. **B)** Measured 5 μL portions of hexadecane samples are loaded into a 96-well plate reader.

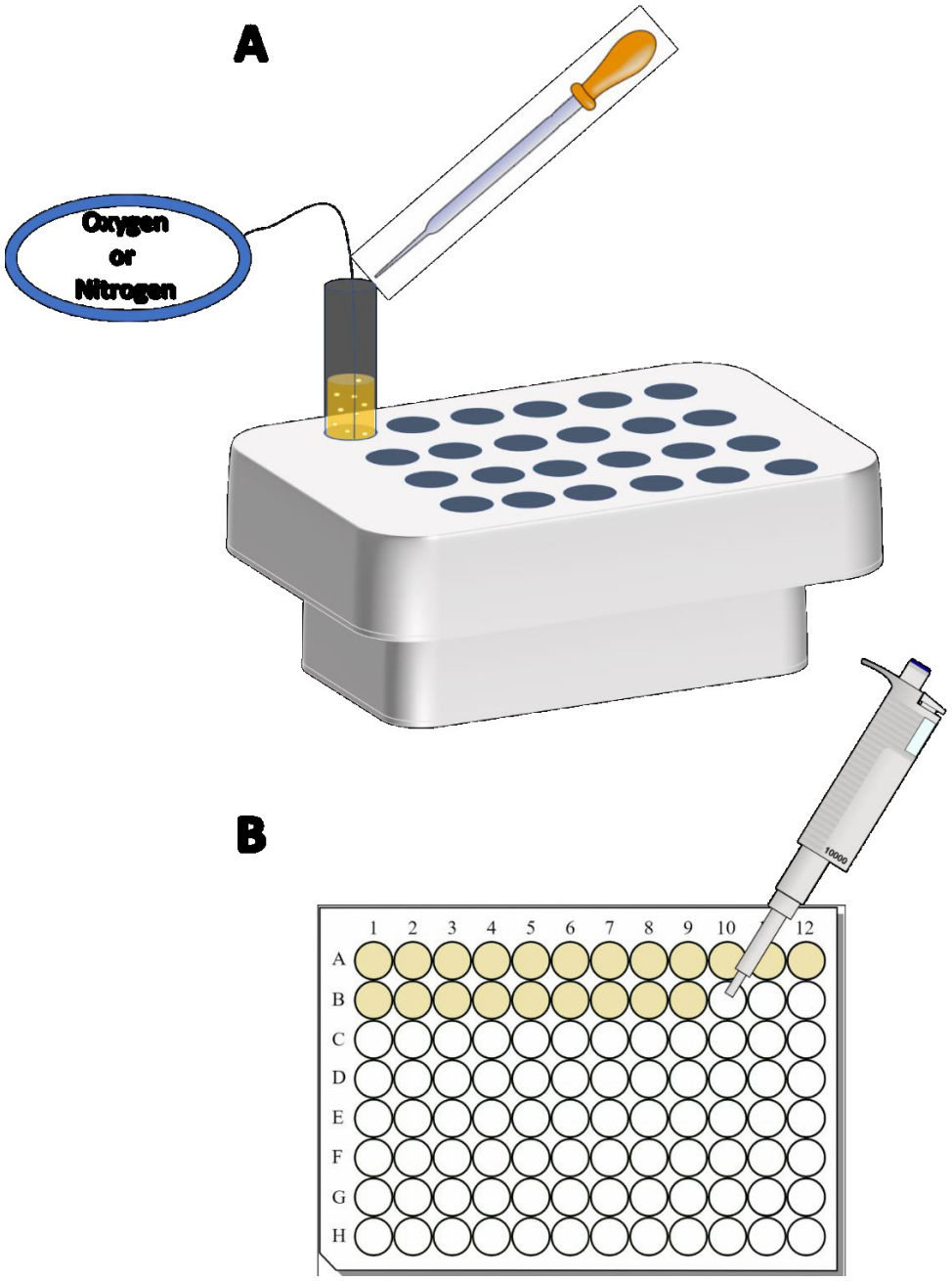

The key advantage to this approach, of course, is that it enables up to 24 concurrent autoxidation experiments, conducted inside 20 mL test tubes (as depicted in Scheme 3.4A.) Where the flow reactor used ~100 mL of hexadecane per experiment, approximately only 10 mL is used per test tube in this setup. This higher throughput approach is well complemented by the use of a profluorescent coumarin-conjugated phosphine probe developed in the lab for quantitation of the hydroperoxide present in the sample.[7,9] This technique effectively supplants the more time consuming iodometric titration method of determining [ROOH] used in the past.[10,11] The method is coupled with a BODIPY-based acid probe,[9] as acid production/accumulation is another indicator of autoxidation progress, though the time lapsed increase in [H^+] can be entirely superimposed with the [ROOH] data we collected for all of the RTAs we examined.

Scheme 3.5. Phosphine probe for detecting [ROOH] (top), and probe for measuring [H^+] (bottom).

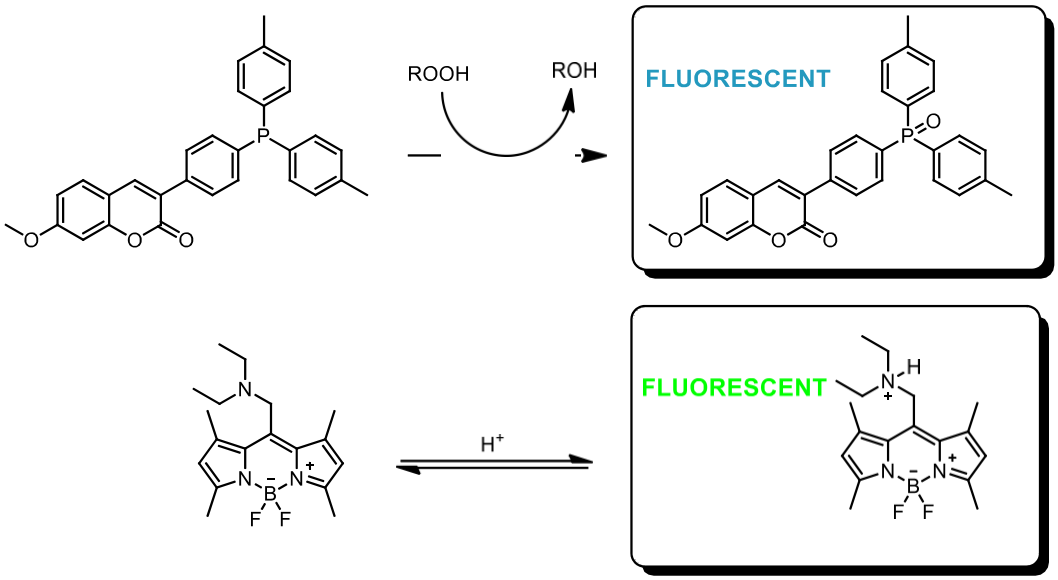

There are a couple of drawbacks to the PSHBR, the first being a lack of direct temperature control in each individual reaction vessel. With the stir flow reactor, a single vessel had a dedicated heat source and a thermometer inside the actual substrate so the temperature of the experiment could be directly monitored and adjusted as necessary. On the other hand, in the PSHBR all the reaction vessels must share a single heat source. Relatively small temperature differences will result in some variation of the R_i, and thus variations in t_{inh}. While we have observed some minor variation in temperature between some wells we believe that we have taken the necessary precautions to mitigate its effect on the observed trends by randomizing tube placement for replicate inhibition experiments. The second drawback is the smaller amount of substrate in the vessel which requires the operator to be more considerate of how frequently aliquots are taken lest they remove too much substrate prior to the end of the experiment.

Another change in the experimental setup that is noteworthy is a change of substrate from 99% to a 95% hexadecane which required a small amount of tweaking in the experimental setup. Previously, 11 mM of tetralin hydroperoxide was used to initiate the autoxidation; however, we found that even after removing the hydroperoxide from the hexadecane in the usual manner (see the Experimental), there was still a substantial amount of chain initiation even in the absence of added initiator as evidenced by the rapid consumption of TEMPO at 160 ºC under N_2 (Figure 3.1).

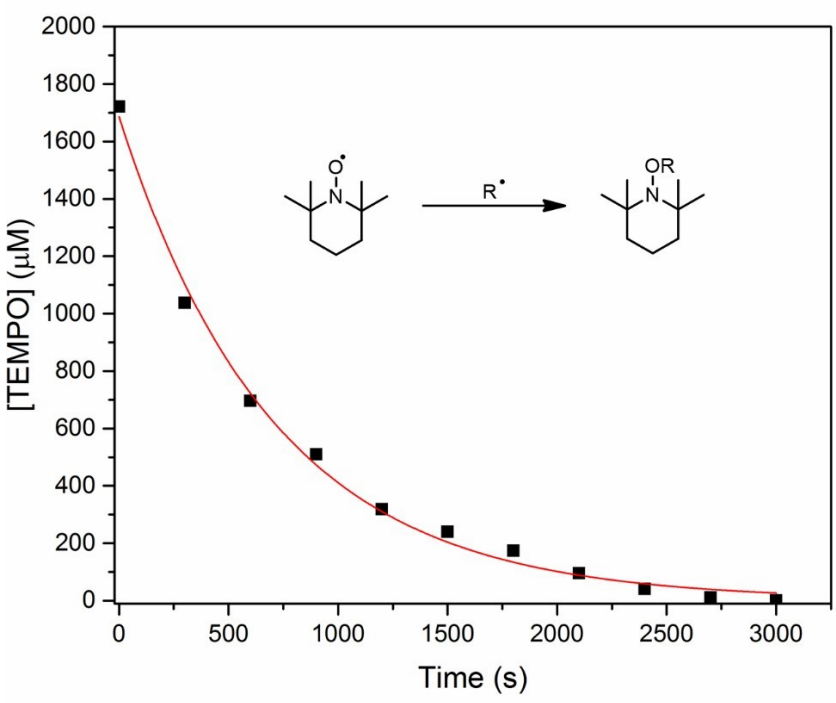

Figure 3.1. TEMPO (2 mM) consumption over time at 160 °C in n-hexadecane under N_2.

The autoxidation is most likely being initiated by peroxide (ROOR) which would not be detected by the phosphine probe (the probe is unreactive to ROOR under the standard assay conditions) and conceivably it would not be removed by percolating the substrate through silica and basic alumina due to the lack of O-H functionality. Finding that the R_i was sufficiently high as it was, we used this substrate and did not add additional hydroperoxide initiator.

3.3.2 Structure-Reactivity Relationships in Phenoxazines.

In order to establish a baseline for comparison, we first conducted inhibited autoxidations of phenoxazine (**3.5**), ditolylamine (**3.1**), and our best heterocyclic diarylamine (**3.3**). As expected, in the absence of inhibitor the [ROOH] reached ~2% of the molarity of hexadecane ([ROOH]/[$C_{16}H_{34}$] = 0.07/3.41 = 0.02) in only ~ 440 s. Meanwhile, **3.1** extended this induction period by approximately 1 hr, while **3.3** and **3.5** managed to extend it to 3 hrs.

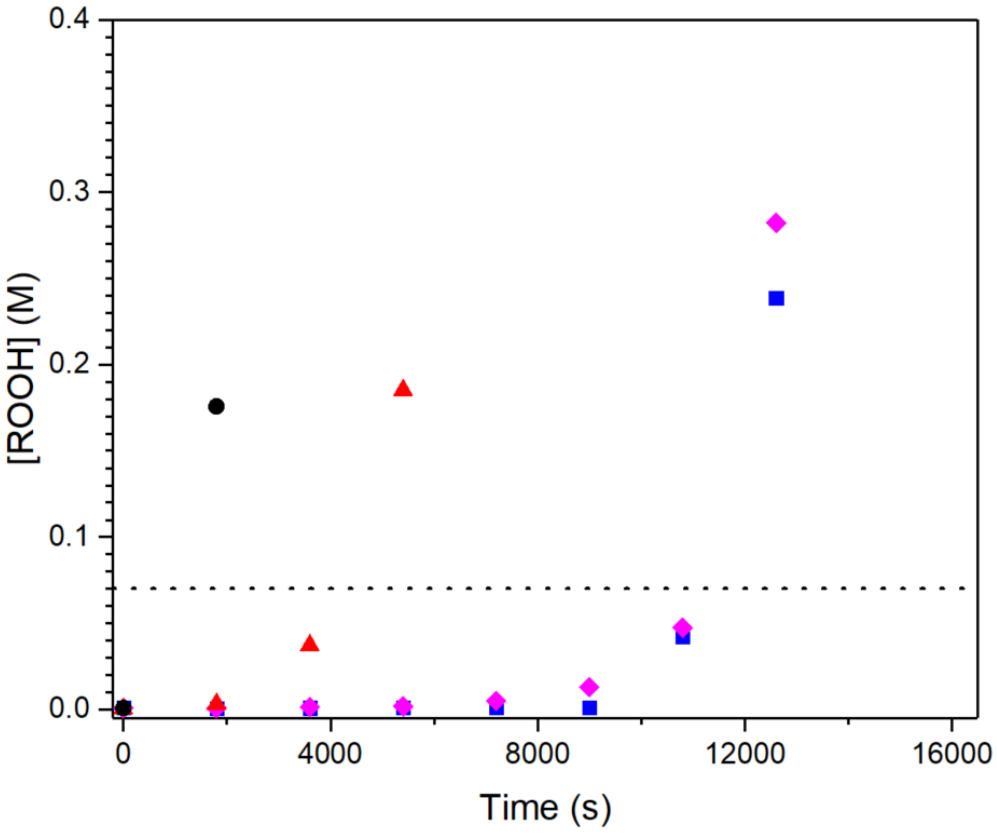

Figure 3.2. Inhibited n-hexadecane autoxidation (160 °C) with 2 mM primary amine base: uninhibited (**black circle**); 300 μM ditolylamine **3.1** (**red triangle**), $\Delta t_{2\%}$ = 3560 s; 300 μM N^2,N^2-dimethyl-N^5-phenylpyrimidine-2,5-diamine **3.3** (**magenta diamond**), $\Delta t_{2\%}$ = 10610 s; 300 μM phenoxazine **3.5** (**blue square**), $\Delta t_{2\%}$ = 10610 s.

It should be noted that the difference in inhibition time between **3.1** and **3.3** is only about a factor of 3 ($\Delta t_{2\%}$ = 3560 and 10610 seconds respectively), a significantly smaller margin than the 12-fold difference reported previously for analogous diarylamines.[1] This difference may be accounted for by the amount of amine present in the autoxidation; the earlier experiments utilized 40 μM, whereas the current experiments utilize 300 μM. Given that the k_{inh} for ADPA is about an order of magnitude lower than **3.3**, it is reasonable to suggest that the chain-length of propagation is significantly higher for the autoxidation inhibited by ADPA, thus faster accumulation of ROOH leads to an earlier autocatalytic curve. This may be more pronounced at lower concentrations. In real-world applications, where the concentration of RTA would be orders of magnitude greater than either of the assayed values, the actual *rate* of inhibition would increase to a point where the chain-length of either ADPA or **3.3** inhibited autoxidations would be more similar for the majority of the experiment.

Comparing **3.5** and **3.3**, they have identical inhibition times despite **3.5** possessing a 10-fold advantage in terms of k_{inh}. We suspected that there must be one or multiple key off-cycle reaction(s) consuming the phenoxazine which was lowering its turnover. We proceeded to conduct inhibited autoxidations with our electronically diverse catalogue of phenoxazines to see how their time of inhibitions would differ from **3.5**, alongside phenothiazine (**3.4**). The results are presented in Table 3.1.

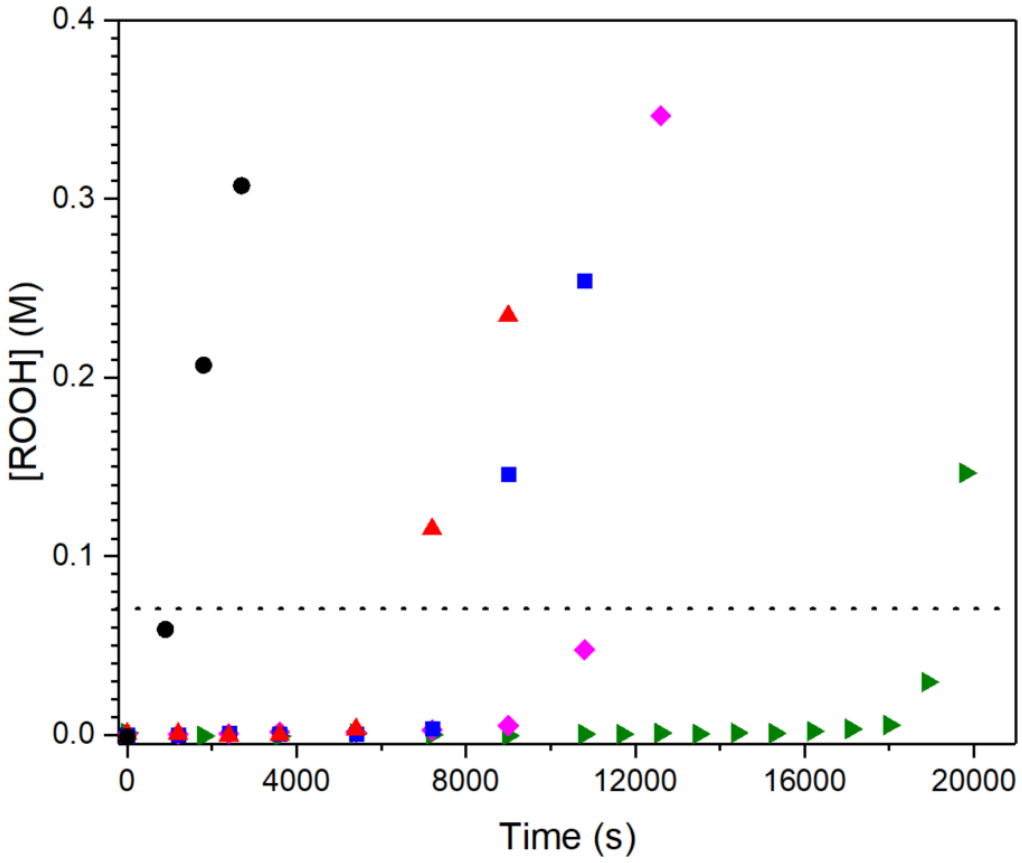

Figure 3.3. Inhibited n-hexadecane autoxidation (160 ºC) with 2mM primary amine base: uninhibited (**black circle**); 200 µM 3,7-dimethoxyphenoxazine **3.19** (**red triangle**), $\Delta t_{2\%}$ = 5760 ± 300 s; 200 µM phenoxazine **3.5** (**blue square**), $\Delta t_{2\%}$ = 7830 ± 1020 s; 200 µM 3-cyano-7-nitrophenoxaizne **3.6** (**magenta diamond**), $\Delta t_{2\%}$ = 10260 ± 1250 s; 200 µM phenothiazine **3.4** (**green triangle**), $\Delta t_{2\%}$ = 19090 ± 1050 s.

Table 3.1. The $\Delta t_{2\%}$ of the substituted phenoxazines (**3.5-3.19**) and phenothiazine (**3.4**) in the inhibited autoxidation of n-hexadecane at 160 °C with 200 μM of inhibitor. Accompanying k_{inh}^{PhCl}

RTA	Substituents	$\Delta t_{2\%}$ (s)	$\Delta t_{RTA}/\Delta t_{PNX}$	k_{inh}^{PhCl} ($M^{-1}s^{-1}$)	E^o (V)
3.6	3-CN-7-NO_2	10260 ± 1250	1.31	$(4.5 \pm 0.1) \times 10^6$	1.38
3.7	3-NO_2	9400 ± 290	1.20	$(1.6 \pm 0.1) \times 10^7$	1.15
3.8	3-CN	9690 ± 1150	1.24	$(1.8 \pm 0.1) \times 10^7$	1.13
3.9	3-SO_2NEt_2	10250 ± 850	1.31	$(2.1 \pm 0.2) \times 10^7$	1.06
3.10	3-CF_3	9530 ± 680	1.22	$(2.0 \pm 0.3) \times 10^7$	1.06
3.11	2-CF_3	9880 ± 760	1.26	$(2.5 \pm 0.2) \times 10^7$	1.05
3.5	H	7830 ± 1020	1	$(3.9 \pm 0.4) \times 10^7$	0.87
3.4	_	19090 ± 1050	2.44	$(7.6 \pm 0.3) \times 10^6$	0.85
3.12	3-MeO-7-NO_2	6430 ± 810	0.82	$(5.6 \pm 0.5) \times 10^7$	0.97
3.13	2-tBu	8260 ± 1090	1.05	$(6.0 \pm 0.2) \times 10^7$	0.83
3.14	3-tBu	7640 ± 1120	0.98	$(7.4 \pm 0.6) \times 10^7$	0.81
3.15	2,8-tBu	8270 ± 670	1.06	$(1.0 \pm 0.1) \times 10^8$	0.78
3.16	3,7-tBu	6810 ± 1150	0.87	$(1.4 \pm 0.1) \times 10^8$	0.75
3.17	3-MeO	6260 ± 850	0.80	$(1.8 \pm 0.1) \times 10^8$	0.72
3.18	2,4,6,8-tBu	6210 ± 210	0.79	$(2.1 \pm 0.4) \times 10^8$	0.67
3.19	3-7-MeO	5760 ± 300	0.74	$(6.6 \pm 1.1) \times 10^8$	0.59

The periods of inhibition for phenoxazines **3.5-3.19** ranged from ~1.6 to 2.9 h while phenothiazine **3.4** consistently inhibited for ~5.3 h. Interestingly the more electron-poor compounds with lower k_{inh}^{PhCl} and higher E^O (**3.6-3.11**) have consistently longer inhibition times compared to **3.1** by about 20-30% (~25-40 min), while the more electron-

rich compounds having substantially higher k_{inh}^{PhCl} and progressively lower E^o values (**3.16-3.19**) are anywhere from ~15-25% lower than **3.1** in terms of $\Delta t_{2\%}$ (~20-33 min) on average. Based on the previously observed regression in performance with electron-rich heterocyclic diarylamines (E^o ~ 0.50-0.65 V),[1] we had anticipated a similar regression for the more electron-rich phenoxazines. Given the sharp drop in $\Delta t_{2\%}$ between the otherwise comparable **3.15** and **3.16**, it would appear that threshold where counterproductive single-electron oxidation overwhelms the inherent RTA activity might lie between their two redox potentials (0.78 and 0.75 V respectively). If such a threshold exists and above that there is no additional benefit to having ever higher E^o values, there is a question as to why the $\Delta t_{2\%}$ is higher for **3.6-3.11** bearing in mind that these also have markedly lower k_{inh}^{PhCl} values compared to **3.1**. Another interesting result is that of 3-methoxy-7-nitrophenoxazine (**3.12**) which has E^o of 0.97 V, but has a $\Delta t_{2\%}$ comparable to 3-methoxyphenoxazine (**3.17**) and 3,7-dimethoxyphenoxazine (**3.19**). Maybe there is an additional off-cycle reaction where either the corresponding phenoxazinyl or phenoxazine-N-oxyl radical decomposes by cleaving the C-O bond of the alkoxy group to render an alkyl radical and the corresponding phenoxazone or the p-quinone-nitrone respectively, though this is just speculation.

Scheme 3.6. A proposed decomposition of 3-MeO containing phenoxazines.

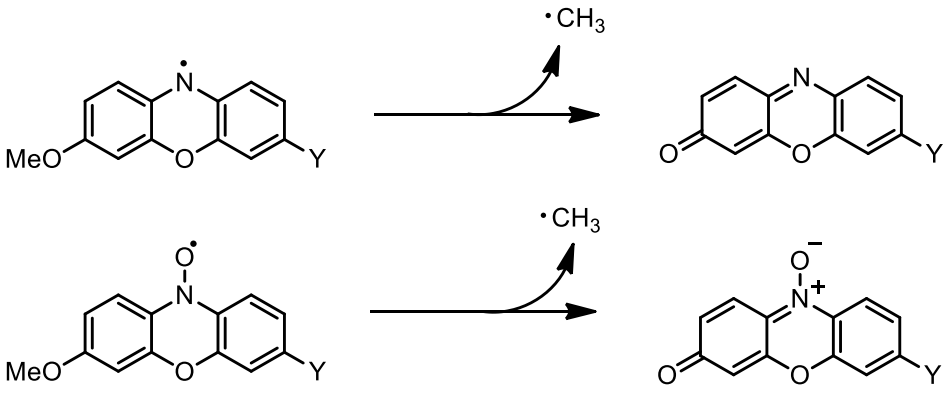

Contrasting the somewhat incremental differences between the electronically diverse substituted phenoxazines, **3.4** outperforms **3.5** by about 145% despite the fact that in most respects these compounds seem very similar expect that **3.5** is more reactive towards peroxyl radicals by a factor of 5. The superiority of phenothiazine in terms of inhibition time is consistent with what Murphy et al. observed for the inhibition of diester oils back in 1950.[12] Neither electron-rich nor the electron-poor phenoxazine RTAs improve the $\Delta t_{2\%}$ to a level comparable to what is observed with **3.4**, suggesting that the difference is fundamental to the scaffold itself as opposed to minor differences in the BDE or IP. As of yet, there is no proposal to explain the dramatic differences in $\Delta t_{2\%}$ that have been observed between the phenoxazine and phenothiazine scaffold.

3.3.3. The Fates of Phenoxazine and Radical Intermediates

Based on these results, it became clear that the differences in $\Delta t_{2\%}$ between different diarylamine-type scaffolds was more nuanced than a simple correlation with the k_{inh}^{PhCl} above the proposed 0.8V 'threshold'. If we wanted to make any headway with understanding the structural factors which influenced the catalytic turnover for the various aromatic amines, we would need to better understand the fate(s) of these RTAs. Towards this general aim we decided that a logical place to begin would be to firstly establish if phenoxazine behaved as expected within the framework of the Korcek Cycle. Korcek and co-workers had used HPLC and EPR to track the concentration of 4,4'-dioctyldiphenylamine and its corresponding nitroxide at different time points during the inhibited autoxidation of hexadecane.[3]

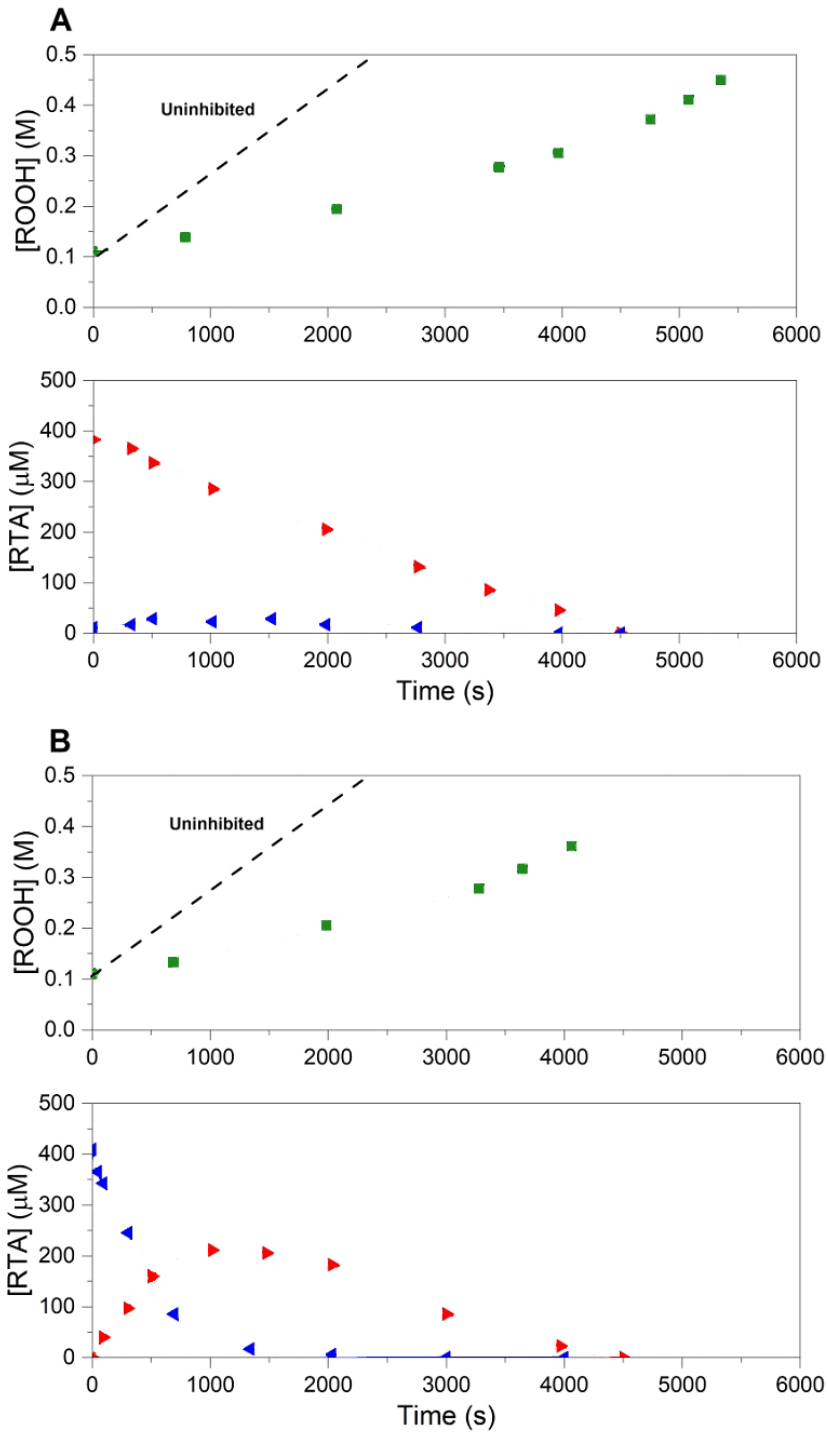

Figure 3.4. Re-plotted of data of the autoxidation of n-hexadecane at 160 °C (100% O_2) from Korcek and co-worker's seminal paper.[3] (**A**) Concentration of ADPA (**red triangle**) and nitroxide (**blue triangle**) and [ROOH] (**green square**) starting with 0.38 mM 4,4'-di-octyl-diphenylamine. (**B**) Starting with 0.41 mM 4,4'-di-octyl-diphenylamine-N- oxyl.

In autoxidations inhibited by either 0.38 mM diphenylamine or 0.41 mM nitroxide, they analyzed the speciation of the RTA over the course of the autoxidation. Interestingly, when starting with diphenylamine less than 30 μM of nitroxide was detected at any time, but when they started with the nitroxide, it was consumed within the first 1000 seconds and a substantial accumulation of the diphenylamine occurred (up to ~0.20 mM). The behaviour clearly demonstrated that the trapping of peroxyl with the amine (i) (Scheme 3.1) was the rate determining step as opposed the formation of alkoxyamine (ii). We hypothesized that (i) would no longer be rate determining for **3.5** and sought to demonstrate this using the same experiment.

In order to conduct this experiment from both starting points, we needed to synthesize the nitroxide of phenoxazine. There has been no prior report for the isolation of the nitroxide of **3.5**, though it has previously been observed by EPR.[13–15] Gratifyingly, we were able to identify a set of conditions which lead to the precipitation of phenoxazine-N-oxyl (**3.20**) as black crystalline needles, upon oxidation of the amine with MCPBA. The product had a HRMS that matched the theoretical mass, lacked any signal in the attempt to record a ^{1}H NMR spectra, had an EPR spectra that is consistent with what is found in the literature, and the spin counting indicated that the sample was >98% pure.

Scheme 3.7. Synthesis of phenoxazine-N-oxyl (**3.20**).

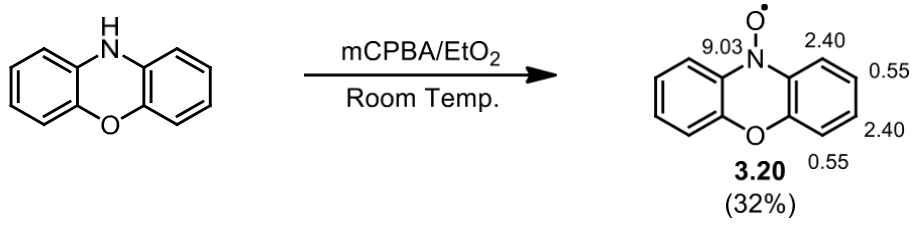

We attempted to use **3.20** as an intermediate in the synthesis of some alkoxyamines based on phenoxazine so that we could experimentally determine whether these would decompose via the homolysis-disproportionation or the retro-carbonyl-ene mechanism. Being advised of the difficulties faced with preparing and isolating the alkoxyamines derived from ADPA, due to their instability on silica, I attempted to synthesize the alkoxyamine in a manner which would cleanly afford a crystalline product. Reducing the nitroxide to the hydroxylamine with hydrazine followed by nucleophilic substitution with an alkyl halide was found to be effective for synthesizing

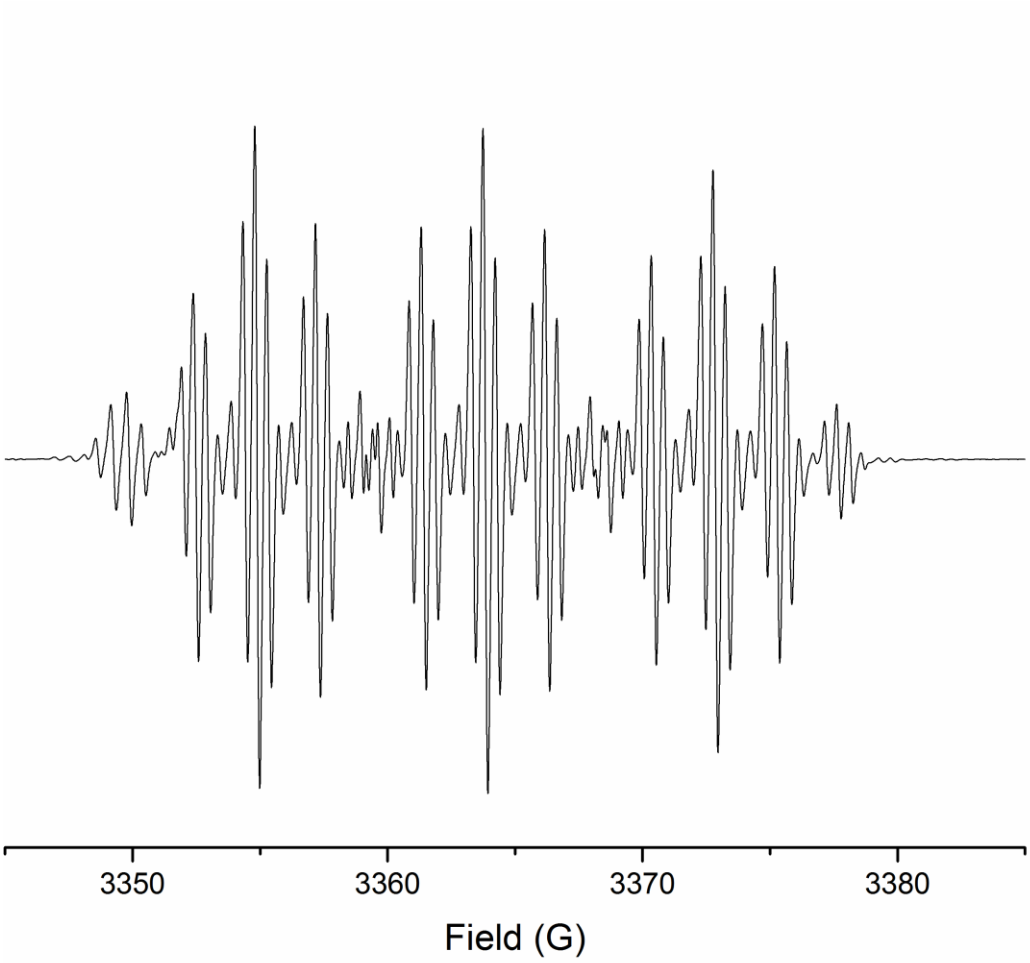

Figure 3.5. EPR spectra of **3.20** recorded in degassed benzene at room temperature.

alkoxyamines derived from the nitroxides of 4,4'-di-tert-butyldiphenylamine and 4,4'-di-methoxy-diphenylamine.[16] Unfortunately, phenoxazine-N-oxyl does not form the hydroxylamine but instead cleanly affords **3.5**. Interestingly, when the reduction was attempted with 1 equivalent of ascorbate, **3.5** was obtained in addition to more polar fluorescent products whose ^{1}H NMR spectra appear to be consistent with dimers and even *trimers* of phenoxazine (such as the ones proposed in Scheme 3.8) as they contain 16 and 23 protons respectively with one of their protons having a shift equivalent to the N-H proton found in the spectrum of **3.5**. The fact that trimers are observed indicates that there are phenoxazine dimers which are reducing nitroxides, thus generating dimeric aminyl radicals which proceed to react with the monomeric radicals. I also observed that co-spotting **3.5** and **3.20** on a silica TLC plate resulted in a reaction where the nitroxide was consumed, which is evident based on its absence when compared to the track with just nitroxide.

Scheme 3.8. The attempted reduction of **3.20** to N-hydroxyphenoxazine.

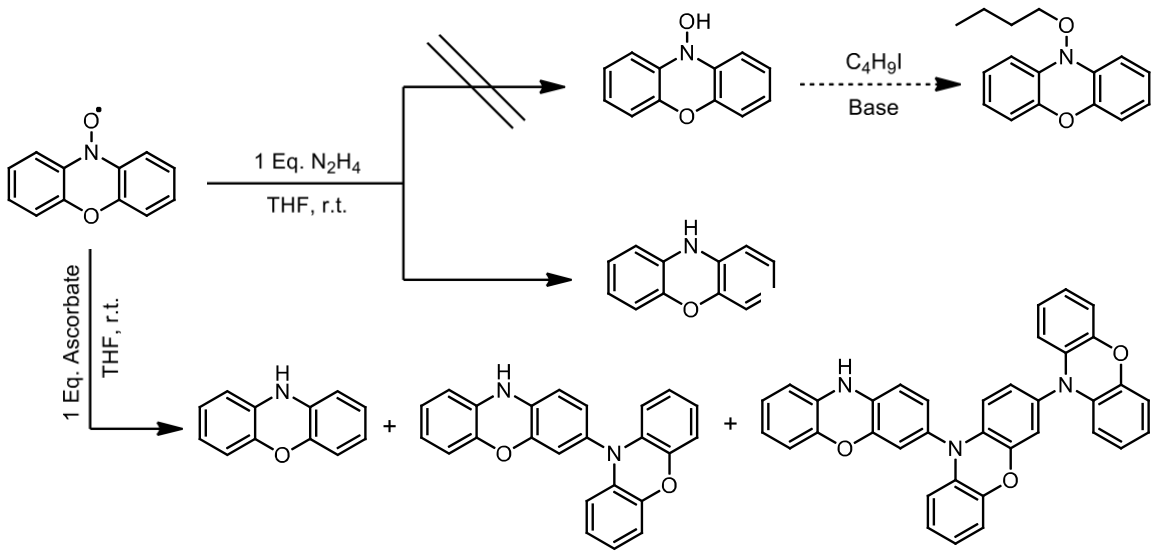

The hydroxylamine seems to be quite transient, and synthesizing an alkoxyamine by this route may not be tenable. Korcek and co-workers prepared their alkoxyamine derivatives by radical addition under an argon atmosphere and did not isolate the products but instead performed the decomposition study on a mixture of isomers, which may be a more feasible approach.[3] This of course assumes that an alkoxyamine of phenoxazine is appreciably more stable than the hydroxylamine.

We carried out autoxidations of hexadecane inhibited with 0.3 mM of **3.5**, **3.20,** and **3.2** and monitored the nitroxide concentration by EPR and the amine concentration by HPLC. The first thing to note is how much lower the $\Delta t_{2\%}$ is when inhibiting the autoxidation with an equivalent amount of **3.20** versus **3.5**. The drop is rather dramatic, providing approximately 1/3 the inhibition time (1 h vs 3 h), a behaviour that contrasts what Korcek and co-workers observed where the amine and the nitroxide of 4,4'-di-octyl-diphenylamine resulted in equivalent inhibition times (Figure 3.4). The actual concentration of phenoxazine and phenoxazine-N-oxyl throughout the autoxidations depicted in Figures 3.6B and 3.7A is a mirror of what is seen in Figure 3.4. When starting with 0.3 mM of **3.5** there is a sharp decrease in phenoxazine concentration and a rather substantial accumulation of phenoxazine-N-oxyl (up to ~0.1 mM.) Comparing this to Figure 3.4B, the concentration of the nitroxide decreases rapidly with a substantial accumulation of the diarylamine. On the other hand, when starting with 0.3 mM of **3.20**, it is consumed with only a trace amount of phenoxazine present at any time (<15 μM) which is reciprocal to Figure 3.4A where the diarylamine steadily decreases with only trace amounts of nitroxide detected.

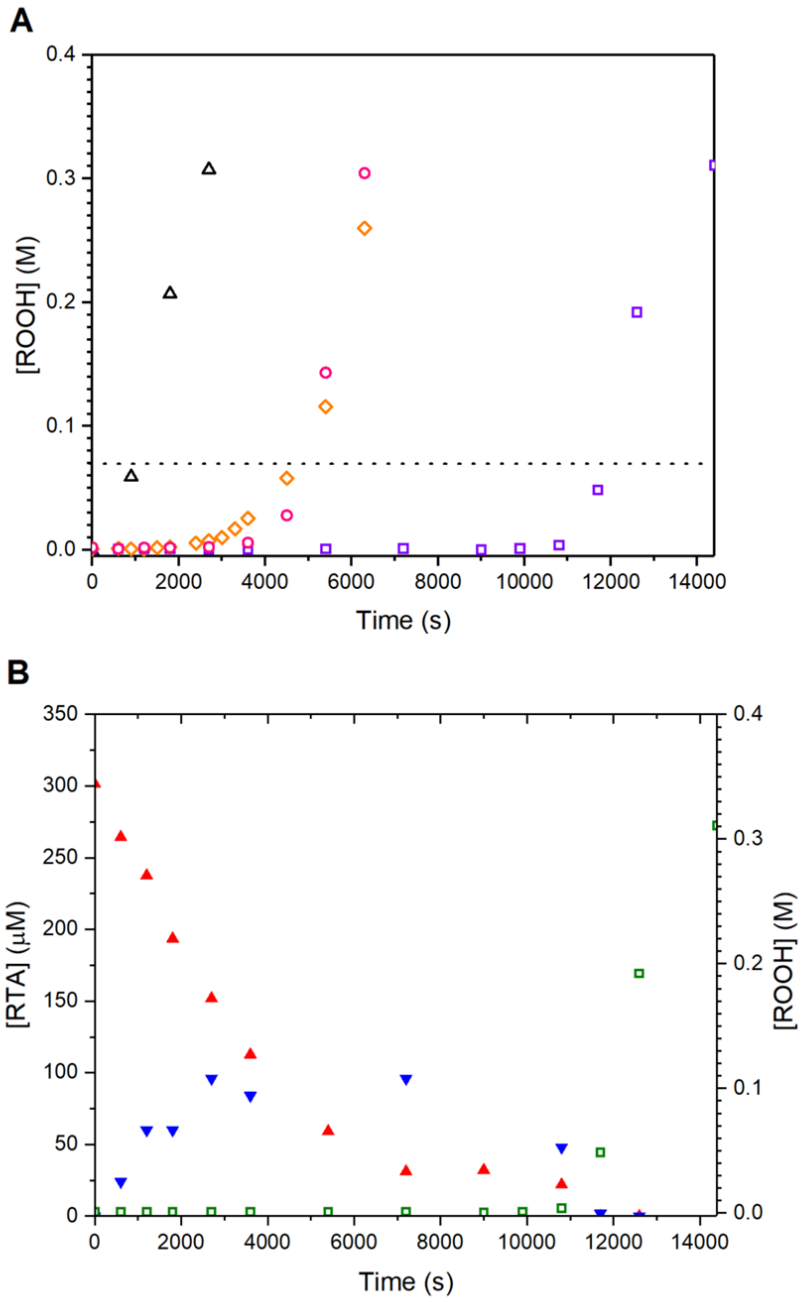

Figure 3.6. (**A**) Inhibited n-hexadecane autoxidation (160 °C) with 2 mM primary amine base: uninhibited (**black triangle**); 300 μM 4,4'-di-tert-butyldiphenylamine **3.2** (**orange diamond**) $\Delta t_{2\%}$ = 3860 s; 300 μM phenoxazine-N-oxyl **3.20** (**pink circle**) $\Delta t_{2\%}$ = 4070 s; 300 μM phenoxazine **3.5** (**purple square**) $\Delta t_{2\%}$ = 10995 s. (**B**) [RTA] and [ROOH] monitored over time starting with 300 μM **3.5**: phenoxazine (**red triangle**); phenoxazine-N-oxyl (**blue inverted-triangle**); [ROOH] (**green square**).

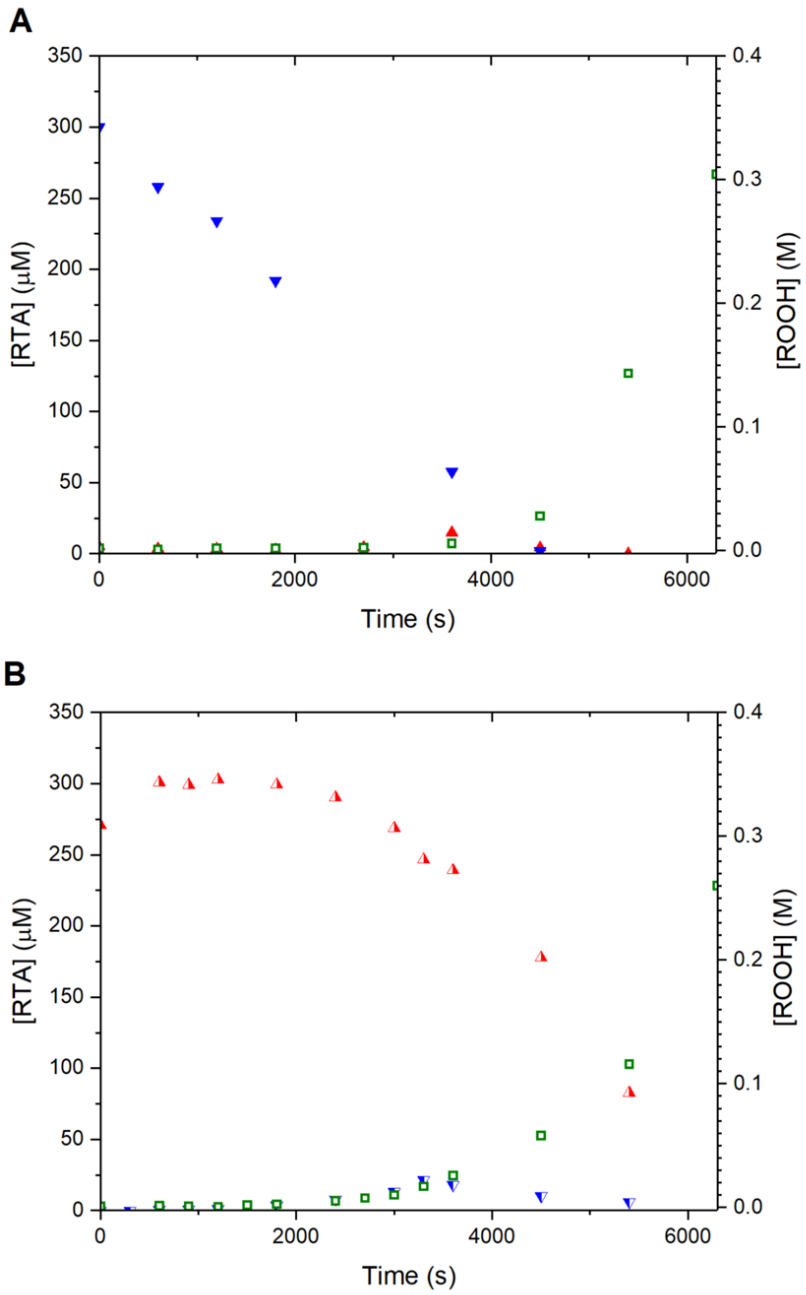

Figure 3.7. (**A**) Inhibited n-hexadecane autoxidation (160 °C) with 2 mM primary amine base. [RTA] and [ROOH] monitored over time starting with 300 μM **3.20**: phenoxazine (**red triangle**); phenoxazine-N-oxyl (**blue inverted-triangle**); [ROOH] (**green square**). (**B**) [RTA] and [ROOH] monitored over time starting with 300 μM **3.2**: 4,4'-di-tert-butyldiphenylamine (**red triangle**); 4,4'-di-tert- butyldiphenylamine-N-oxyl (**blue inverted-triangle**); [ROOH] (**green square**).

Where with 4,4'-di-octyl-diphenylamine the evidence indicates that the rate determining process is the hydrogen atom transfer from the amine a peroxyl radical (i), for phenoxazine the formation of alkoxyamine (ii) is the rate determining step. The autoxidation with 0.3 mM of **3.2** (Figure 3.7 B) is consistent with the fact that ADPA is rate limited by (i), as there is nearly no accumulation of nitroxide (≤ 20 μM). It is interesting that for the first 2400 seconds there is actually quite a high conservation of the RTA, but as the [ROOH] increases and the autoxidation becomes autocatalytic, the concentration of 4,4'- di-tert-butyl-diphenylamine noticeably decreases from 3000 seconds on, suggesting that the deleterious side reactions are less competitive at lower rates of initiation with respect to the turnover. It is worth noting that the accumulation of [ROOH] is essentially negligible for **3.5** and **3.20** until essentially all of the RTA is consumed, and the resulting curves are visually similar to the uninhibited curve. For **3.2**, the hydroperoxide accumulates while most of the RTA is still present as the amine is too slow to compete with propagation. The conservation of **3.2** for those first 40 minutes suggests that the ADPA is actually quite robust, but is undermined by its low k_{inh}; however, this deficiency would be less pronounced at the much higher concentrations used in 'real life' applications. The shift of the rate limiting process with phenoxazine is not unexpected as the k_{inh} of phenoxazine ~200-fold greater than ADPA, meanwhile the reaction between $R^{\bullet}$ and the nitroxides derived from these two aromatic amines should have similar rate constants that approach the rate of diffusion, therefore in essence the rate of (i) has been independently increased. If (ii) were rate limiting, there would be no additional benefit to using phenoxazine RTAs with higher k_{inh} than **3.5** which is consistent with our observations. Instead it is the formation of alkoxyamine that dictates the rate of regeneration and the

rate of reaction between nitroxide and alkyl radical should be entirely dependent on the relative concentrations of nitroxide, $R^{\bullet}$, and O_2. If (ii) is the rate limiting process, then it stands to reason that decreasing the concentration of O_2 would increase the rate of alkoxyamine formation. This is relevant when you consider that while these accelerated autoxidations are carried out in an atmosphere of O_2, the conditions under which these diarylamine RTAs are typically used may have lower partial pressures of O_2. It would be interesting to study how the relative inhibition efficiency changes for RTAs which are rate limited by (i) versus those rate limited by (ii) when the concentration of O_2 is lowered.

The significant decrease in nitroxide longevity when starting with **3.20** provides a lead to at least one of the major off-cycle pathways. While all of the nitroxide is completely consumed at ~4500 seconds in Figure 3.7A, intersecting with the end of the induction period, when starting with the same amount of **3.5** there is still about 90 μM of both amine and nitroxide at ~4500 seconds with a total concentration of ~180 μM of combined RTA (just under 2/3 of the initial 300 μM) which is less than halfway through the induction period. Looking at Figure 3.6B, for the first 1200 seconds the total molar balance of phenoxazine and phenoxazine-N-oxyl appears to remain close to 300 μM, but as the concentration of phenoxazine continues to steadily decrease, the increase in nitroxide concentration plateaus at about 100 μM, resulting in a net decline in RTA molarity. It seems accumulation of the nitroxide is detrimental to conservation of RTA and that this intermediate is more vulnerable to unproductive off-cycle reactions.

Scheme 3.9. Addition of methylperoxyl to diphenylaminyl: competition between the formation of nitroxide and the 2 or 4 phenoxyl diphenylamine.

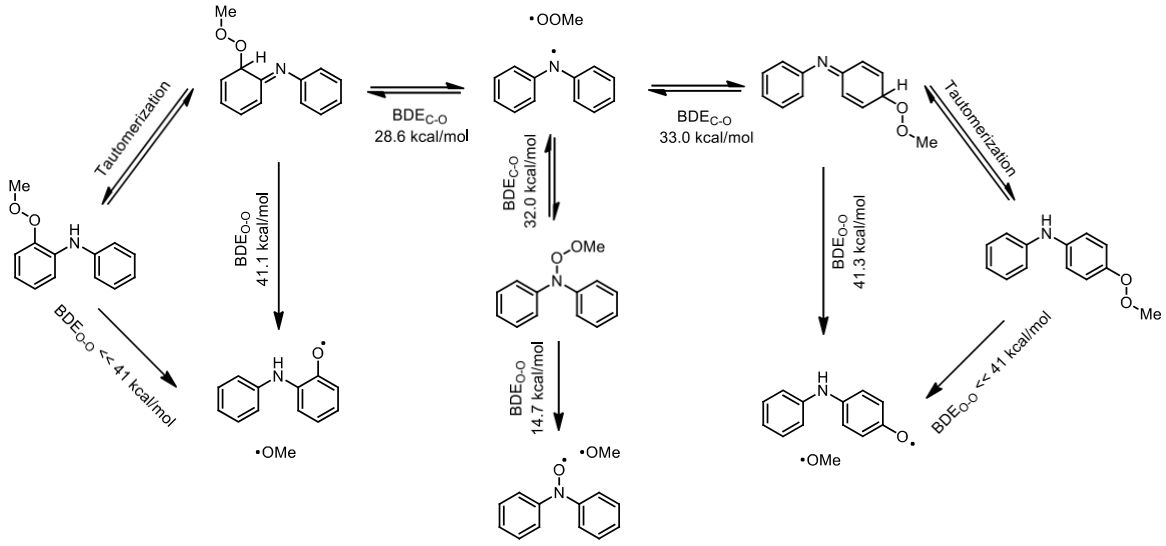

The proposal of the nitroxide and aminyl radical intermediates being the reactive partners of the off-cycle reactions is not a new propsal.[17] Along with the proposal of the retro-carbonyl-ene mechanism, Haidasz et al. provided high level CBS-QB3 calculations to demonstrate how favourable peroxyl addition at the ortho and para positions of the aminyl of diphenylamine.[6] In summary, while peroxyl addition will occur competitively at the nitrogen, ortho, and para positions of the aminyl radical, these addition reactions are all reversible. The following O-O bond cleavage, which determines whether the compound remains on cycle or not, is much more favourable for the N-O adduct which leads to nitroxide production. While the C-O bond for the ortho and para adducts is much weaker than their O-O bonds, if these were to tautomerize into the 2-peroxy or 4-peroxy-diphenylamine, the O-O bond would almost certainly break, producing their corresponding phenoxyl radicals. The ultimate products of these reactions would be the quinones of the amine. Analogous 2-peroxy and 4-peroxy hydroxylamines can also in principle be produced from the nitroxide of diphenylamine. Bolsman et. al. inferred that the formation

of nitrobenzene and paraquinone, by the oxidation of diphenylamine with tert-butylperoxyl radicals, were the result of late stage products derived from peroxyl addition to the 4-position of diphenylamine-N-oxyl.[17]

With the experimental evidence suggesting that phenoxazine-N-oxyl is an acutely vulnerable intermediate, there are two questions that need to be answered: what side reactions are responsible for its decomposition and how can the reactions be mitigated? The two reaction manifolds considered hereim are the aforementioned addition reactions, and an electron transfer reaction producing an electrophilic oxoammonium species which may subsequently react with present nucleophiles:

Scheme 3.10. Proposed off-cycle reactions for phenoxazine-N-oxyl in autoxidation.

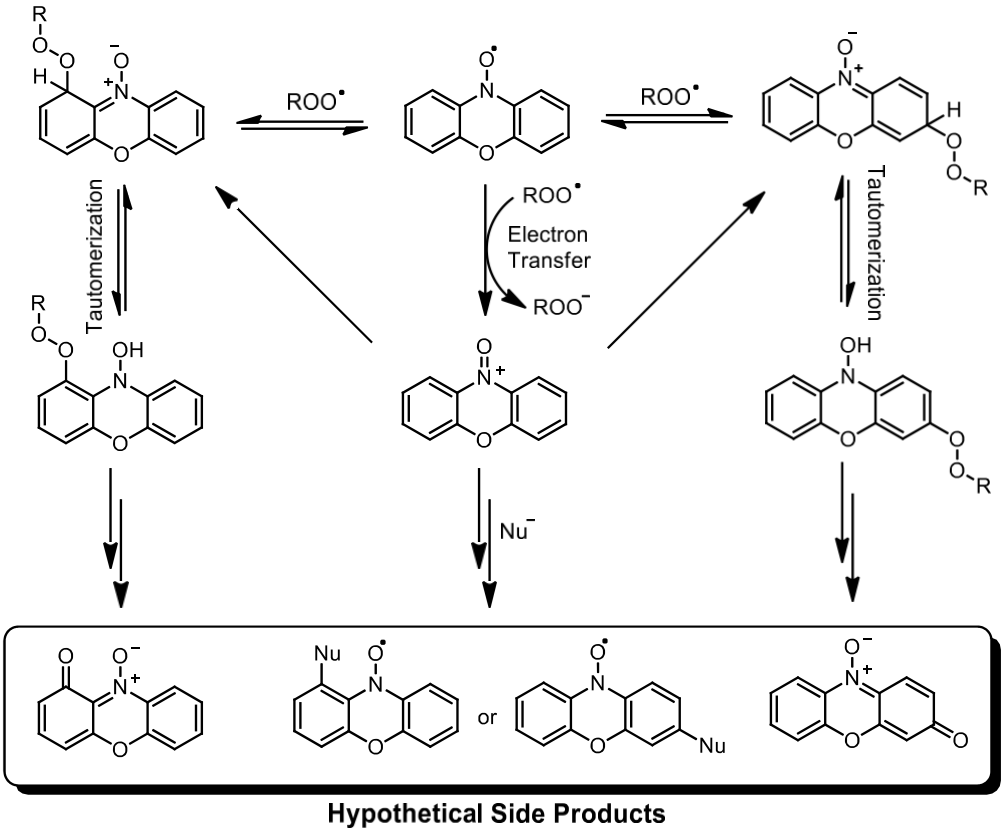

We measured the half-wave potential of phenoxazine-N-oxyl to assess how oxidatively labile it was compared to the parent phenoxazine. The phenoxazine-N-oxyl had an E^o of 0.78V, about 90mV lower than phenoxazine (E^o = 0.87V). Based on the peak height of both the formation and reduction of oxoammonium, there was no loss of oxoammonium. Assuming that a similar difference in oxidation potential exists for the various substituted phenoxazines and their respective nitroxides, the nitroxide for the electron-poor phenoxazines would be more robust ($E^o \geq 0.94$V) and this could account for the slight improvement in $\Delta t_{2\%}$. Even if this is the reason for the observed improvement seen with the electron-poor phenoxazines', given the minor difference compared to phenoxazine it would have to also be a minor contribution to the loss of nitroxide.

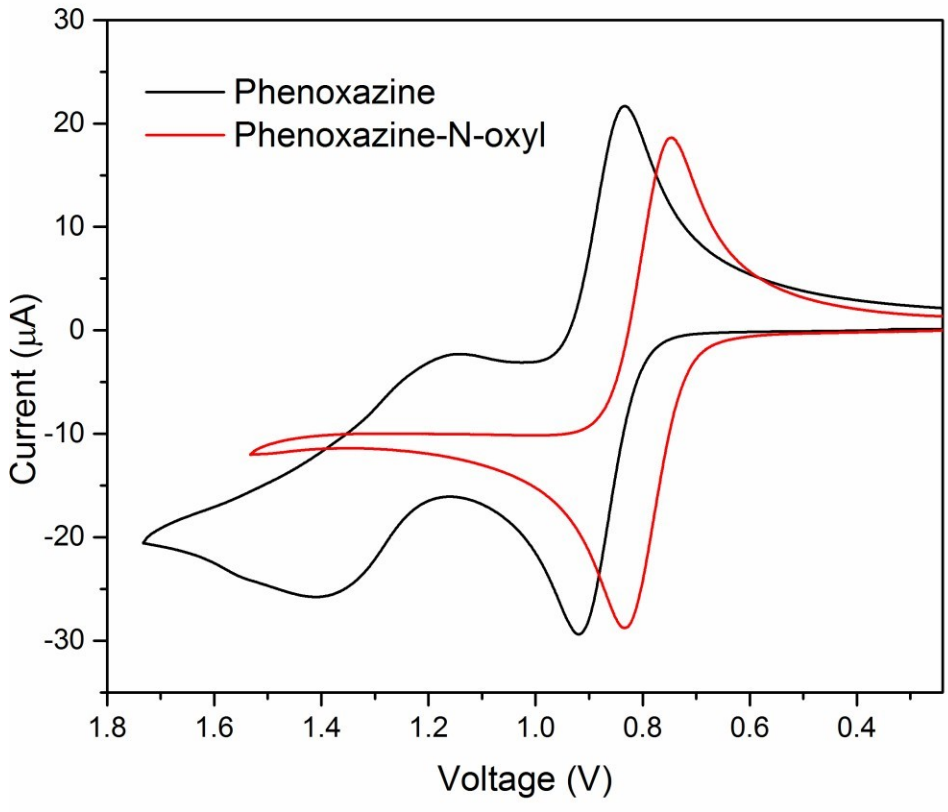

Figure 3.8. Cyclic voltammogram of phenoxazine **3.5** (E^0 = 0.87 V) and phenoxazine-N-oxyl **3.20** (E^0 = 0.78 V) vs NHE.

Conceptually peroxyl addition at the ortho and para positions of the ring should be highly reversible due to the anticipated stability of the nitroxide on account of a highly conjugated planar structure and its low E^o and reversible electrochemistry. Such a side reaction would not likely prevail for the aminyl radical of phenoxazine, but there is a key difference when comparing the aminyl radical and the nitroxide. The reason why the aminyl radical is so transient is because the nitrogen centred radical is highly reactive towards relatively abundant peroxyl radicals. The competing reactions, depicted in Scheme 3.9, between aminyl and peroxyl radicals are all competing for the same type of radical. On the other hand, in order for phenoxazine to be regenerated from its nitroxide, the nitroxide must trap a much less abundant alkyl radical. If the steady-state concentration of $[R^{\bullet}] << [ROO^{\bullet}]$, then despite the potentially unfavourable equilibrium between phenoxazine-N-oxyl and its peroxyl addition adducts, the formation of the adduct could be feasible due to the sheer concentration advantage afforded to $[ROO^{\bullet}]$ which could lead to formation of the ortho and para quinones of nitrone. When examining the phenoxazines with both 3 and 7 positions occupied by substituents other than hydrogen, which should sterically hinder peroxyl addition and render tautomerization of the para adducts impossible, there seemed to be no strong indication of a statistically significant increase in $\Delta t_{2\%}$ when measured against compounds with comparable E^o values. While the apparent lack of effect seems to discredit this hypothesis, there has been no attempt to characterize the catalytic activity of such compounds which contain substituents in the 1 and 9 positions. It is worth bearing in mind that spin distribution between the 1 and the 3 positions are identical, so one would not anticipate addition strongly favouring the ortho

positions, but perhaps tautomerization of the ortho adduct is more facile which better facilitates the formation of 2-peroxy-phenoxazine.

Scheme 3.11. The assignment of hyperfine splitting (G) for ^{17}O labelled phenoxazine-N-oxyl and phenothiazine-N-oxyl.[15]

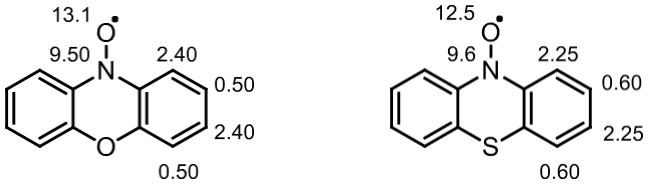

Sterically crowding the amine with ortho substituents will certainly have an impact on the k_{inh}, though it may not necessarily cripple it as an RTA as 1,9-dimethylphenothiazine has a serviceable of k_{inh} of 1.4×10^5 M^{-1} s^{-1},[18] and presumably 1,9-dimethylphenoxazine would be significantly more reactive. The implications go beyond the reactivity towards peroxyls though, the reactivity of the alkoxyamine would be different as the retro-carbonyl-ene reaction would not be possible and in-cage disproportionation may be less efficient. Normalizing the differences in nitroxide decomposition between the isomers of 1,9-dimethylphenoxazine, 2,8-dimethylphenoxazine, and 3,7-dimethylphenoxazine could be very difficult on account of these steric considerations, though it could be a worthwhile line of inquiry. The steric environment of the 1,9, and 10 positions of the ring is a point of differentiation between phenoxazine and phenothiazine due to the larger sulfur heteroatom. It would be presumptuous to suggest that the steric crowding of the 1 and 9 positions accounts for the 2.4-fold increase in $\Delta t_{2\%}$ compared to phenoxazine; however, I believe that determining the significance of the proposed peroxyl addition pathways for phenoxazine may help explain trends seen with other aromatic amines.

3.4 Conclusions

It has been demonstrated that the inherent reactivity of phenoxazine **3.5** toward peroxyl radicals translates to a greater efficacy as an inhibitor of hexadecane autoxidation at an elevated temperature compared to industry-standard alkylated diphenylamines. The 3-fold difference in inhibition time observed for phenoxazine compared to ADPA **3.1**, is equivalent to our best heterocyclic diarylamine **3.3**, but 2.4-fold shorter than phenothiazine **3.4**. The electronically diverse substituted phenoxazines showed activity very similar to phenoxazine with the electron-poor compounds being 1.2 to 1.3-fold greater in terms of $\Delta t_{2\%}$ and the most electron-rich compounds being 15-25% worse in this regard. The observation of these compounds with $\log k_{inh} > 7$ and $E^o \geq 0.8$V all having rather consistent performance, but under performing relative to phenothiazine, raises some questions about the importance of these metrics on catalytic turnover beyond a certain point.

The first synthesis, isolation and purification of phenoxazine-N-oxyl **3.20** is reported. The ability to monitor phenoxazine and phenoxazine-N-oxyl consumption/formation over the course of an inhibited autoxidation provided evidence that the rate determining process of the Korcek Cycle for phenoxazine is the reaction between nitroxide and $R^\bullet$ and not amine and $ROO^\bullet$. Furthermore, the 3-fold difference in inhibition time between phenoxazine and phenoxazine-N-oxyl indicates that the nitroxide is a uniquely vulnerable intermediate. The deleterious formation of oxoammonium by electron-transfer might account for some loss of activity, and there is insufficient information at this time to know if peroxyl addition to the nitroxide contributes significantly. In general, monitoring amine and nitroxide concentration offers a more detailed diagnostic of the

catalytic cycle and should prove to be an effective tool to better understanding important structure-activity relationships which govern catalytic turnover.

3.5 Experimental

General Commercial reagents were used as provided except where otherwise indicated. Reagent quality phenoxazine (Ark Pharm, 98%) was purified for analytical analysis by vacuum sublimation followed by recrystallization out of ethanol under N_2. n-Hexadecane (Alfa Aesar, 95%) was percolated through a column (450 mm × 40 mm) filled with 2/3 silica and 1/3 basic alumina to remove polar impurities prior to being used. Primene^{TM} 81-R is mixture of branched primary aliphatic amines with a mixture of C12-C14 chain lengths which is used as a base. NMR spectra were recorded on a high-field 400 MHz instrument. EPR spectra were recorded with a Bruker ELEXSYS-II system. The Alliance Waters 2695 Separation Module equipped with an Atlantis dC_{18} column (5 $_{uM}$, 4.6 × 150 mm) was used to perform the reverse-phase HPLC experiments. The analytes were monitored using a Waters 2996 PDA.

Autoxidation of Hexadecane at 160 ºC To each 20 mL test tube was added 10 mL of n-hexadecane along with 50 μL of Primene^{TM} stock solution (0.4 M in dioxane). While continuously purging with N_2, the block with the tubes was heated to a target temperature of 170 ^{o}C over a period of 20 minutes. The RTA stock solutions (dioxane) were added before heating, except in the case of the monitored autoxidation of **3.2**, **3.5**, and **3.20** where the RTA was added when the block reached its target temperature. The first samples are taken as the 0 min time point, after which the N_2 is switched to a continuous flow of O_2, and ~150-200 μL samples are collected at the desired time interval.

Procedure for Determination of Hydroperoxide Into a 96-well microplate, the automated reagent dispenser of the microplate reader was used to dilute each sample with 20% isopropyl alcohol in methanol (280 μL) and the plate was stirred for 15 seconds. Afterward 20 μL of a acetonitrile solution containing a fluorogenic phosphine dye and a fluorogenic amine (a mixture containing 250 μM of the former and 630 μM of the latter as described by Shah and Pratt)[9] was added. The plate was stirred for 8 seconds, and the fluorescence of each well was measured every 5 seconds for 60 seconds. The excitation wavelength of the phosphine probe was 340 nm and the emission wavelength was 425 nm. The concentration of hydroperoxide was determined from the rate of phosphine oxidation in 20% isopropyl alcohol in methanol ($k = 5.1\ M^{-1}\ s^{-1}$) assuming pseudo-first-order kinetics.

Monitoring Amine/Nitroxide Concentration Samples were analyzed two of the following ways. To monitor nitroxide (phenoxazine-N-oxyl and 4,4'-di-tert-butyldiphenylamine-N-oxyl), 100 μL of hexadecane sample was dissolved into 500 μL of hexanes, which was transferred into an EPR tube. The concentration of nitroxide was assessed by integration of the first derivative of the EPR absorption spectra. Amine content (phenoxazine and 4,4'-di-tert-butyldiphenylamine) was assessed by reverse-phase HPLC with a PDA. The analytes were extracted out of 300 μL n-hexadecane samples by vortexing them 3 times with a single 150 μL portion of methanol, which was directly injected onto the HPLC instrument. The extraction efficiency was estimated at ~84% and ~39% for phenoxazine and 4,4'-di-tert-butyldiphenylamine respectively. The peak corresponding with phenoxazine (MeCN:MeOH:H_2O/30:60:10, 0.5 ml/min) eluted at 6.28 minutes and was monitored at 238 nm (39690 area/μM). The peak corresponding with 4,4'-di-tert-

butyldiphenylamine (MeCN:MeOH:H_2O/50:35:5, 0.5 ml/min) eluted at 10.29 minutes and was monitored at 285 nm (25330 area/μM).

Phenoxazine-N-oxyl. Phenoxazine 1.8 g (10 mmol) and 30 mL of diethyl ether were placed in a 150 mL Erlenmeyer flask, which was swirled till phenoxazine was dissolved. In a separate 50 mL Erlenmeyer, 3.5 g of 77% mCPBA was dissolved in 14 mL of solution, after which the mCPBA was gradually pipetted into the phenoxazine solution (with only very mild swirling). After ~2 minutes or so, the solution turned from colourless to yellow/black, and it was found that scratching the glass with a pipette promoted crystallization. Black crystalline needles rapidly formed on the flask, after which the flask was placed aside undisturbed for ~1 hour. The solvent was decanted, and the crystals were rinsed three times with cold diethyl ether then three times with petroleum ether which afforded 0.64 g (3.2 mmol) of the phenoxazine-N-oxyl; mp ~127 ^oC (sublimation/decomp); EPR (benzene at room temp.): a^N (9.03 G), $a^H_{1,3,7,9}$ (2.40 G), $a^H_{2,4,6,8}$ (0.55 G). HRMS (EI, magnetic sector): calcd for $C_{12}H_8NO_2$ 198.05550, found 198.05705.

N-Hydroxyphenoxazine (attempt #1). In a 25 mL round bottom flask was dissolved 0.2 g of phenoxazine-N-oxyl (1 mmol) into 7 mL of THF. The system was purged with N_2, after which 0.07 mL of hydrazine hydrate (50-60% N_2H_2) was added via syringe, causing the solution to change from yellow/black to colourless. After removing the solvent under vacuum, a ^1H NMR spectra was recorded which was found to be identical to that of phenoxazine.[19]

N-Hydroxyphenoxazine (attempt #2). Similar to attempt #1, except that the relative amount of hydrazine hydrate was reduced to 25% to conform to a single reducing equivalent of hydrazine. This rendered a mixture of phenoxazine and phenoxazine-N-oxyl, but no N-hydroxyphenoxazine.

N-Hydroxyphenoxazine (attempt #3). In a 5 mL round bottom flask was dissolved 50 mg of phenoxazine-N-oxyl (0.25 mmol) into 1.25 mL of THF, after which 43 mg of ascorbate (0.25 mmol) was added. With some swirling, the colour of the solution lightened, and after ~5 minutes or so, the composition was tested by TLC (9:1 hexanes/ethyl acetate). Phenoxazine-N-oxyl (RF ~ 0.48) was not present, but phenoxazine was present (RF ~ 0.43) as well as 3 fluorescent blue spots which were designated as A (RF ~ 0.25), B (RF ~ 0.15), and C (RF ~ 0.10). Using a preparation TLC plate (20 cm × 20 cm), spots A and C were separated and rendered ^{1}H spectra that were consistent with a dimer of phenoxazine (16 protons) and a trimer (23 protons) respectively (see support information). Spot B was a mixture of oligomers and not a single product. No N-hydroxyphenoxazine was isolated.

3.6 References

(1) Shah, R.; Haidasz, E. A.; Valgimigli, L.; Pratt, D. A. *J. Am. Chem. Soc.* **2015**, *137*, 2440.

(2) Hanthorn, J. J.; Amorati, R.; Valgimigli, L.; Pratt, D. A. *J. Org. Chem.* **2012**, *77*, 6895.

(3) Jensen, R. K.; Korcek, S.; Zinbo, M.; Gerlock, J. L. *J. Org. Chem.* **1995**, *60*, 5396.

(4) Maillard, B.; Ingold, K. U.; Scaiano, J. C. *J. Am. Chem. Soc.* **1983**, *105*, 5095.

(5) Chateauneuf, J.; Lusztyk, J.; Ingold, K. U. *J. Org. Chem.* **1988**, *53*, 1629.

(6) Haidasz, E. A.; Shah, R.; Pratt, D. A. *J. Am. Chem. Soc.* **2014**, *136*, 16643.

(7) Hanthorn, J. J.; Haidasz, E. A.; Gebhardt, P.; Pratt, D. A. *Chem. Commun.* **2012**, *48*, 10141.

(8) Haidasz, E. A.; Meng, D.; Amorati, R.; Baschieri, A.; Ingold, K. U.; Valgimigli, L.; Pratt, D. A. *J. Am. Chem. Soc.* **2016**, *138*, 5290.

(9) Shah, R.; Pratt, D. A. *J. Org. Chem.* **2016**, *81*, 6649.

(10) Li, B.; Pratt, D. A. *Free Radic. Biol. Med.* **2015**, *82*, 187.

(11) Amorati, R.; Valgimigli, L. *Free Radic. Res.* **2015**, *49*, 633.

(12) Murphy, C. M.; Ravner, H.; Smith, N. L. *Ind. Eng. Chem.* **1950**, *42*, 2479.

(13) Scheffler, K.; Stegmann, H. B. *Tetrahedron Lett.* **1968**, *9*, 3619.

(14) Terabe, S.; Kuruma, K.; Konaka, R. *Chem. Lett.* **1972**, *1*, 115.

(15) Aurich, H. G.; Hahn, K.; Stork, K.; Weiss, W. *Tetrahedron* **1977**, *33*, 969.

(16) Haidasz, E. A. PhD. Dissertation, University of Ottawa, 2017.

(17) Bolsman, T. A. B. M.; Blok, A. P.; Frijns, J. H. G. *Recl. des Trav. Chim. des Pays-Bas* **1978**, *97*, 313.

(18) Lucarini, M.; Pedrielli, P.; Pedulli, G. F.; Valgimigli, L.; Gigmes, D.; Tordo, P. *J. Am. Chem. Soc.* **1999**, *121*, 11546.

(19) See Figure S2.16 for phenoxazine's ^{1}H spectrum.

3.7. Supporting Information

3.7.1. HPLC Calibration Curves

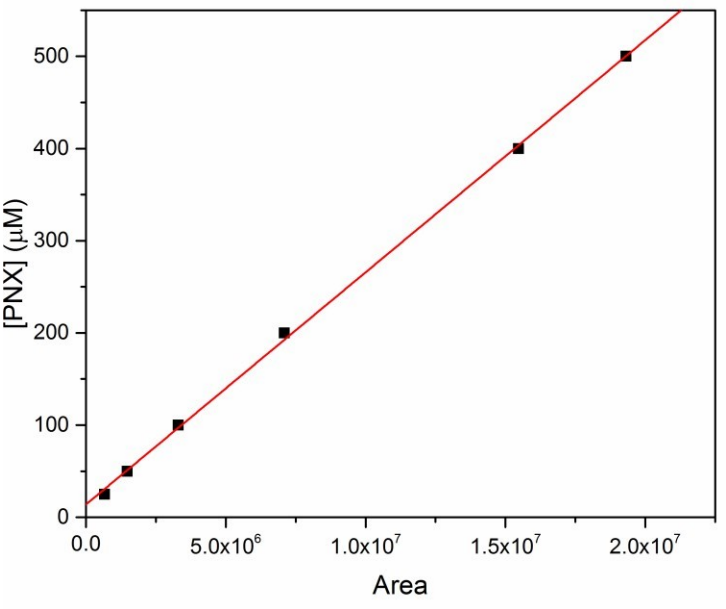

Figure S3.1. Calibration curve of phenoxazine **3.5** (MeCN:MeOH:H_2O/30:60:10, 0.5 ml/min) monitored at 238 nm (39690 area/μM, $R^2 = 0.999$).

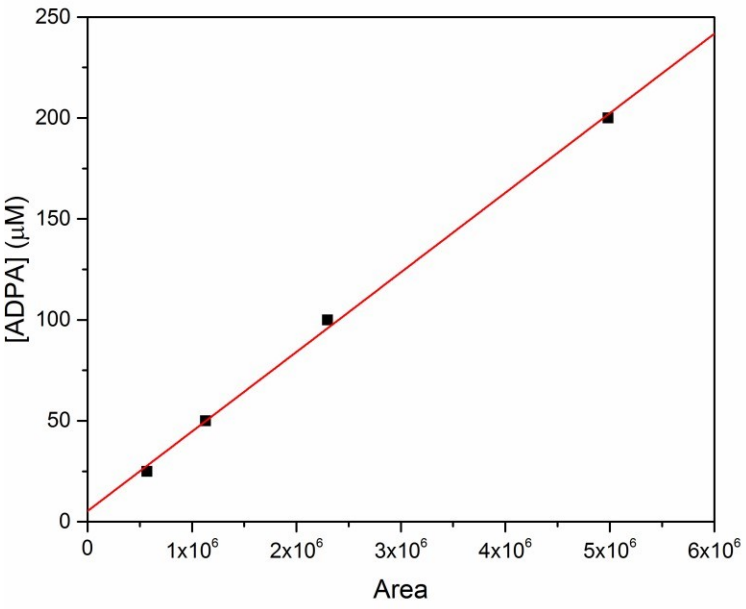

Figure S3.2. Calibration curve of phenoxazine **3.5** (MeCN:MeOH:H_2O/30:60:10, 0.5 ml/min) monitored at 238 nm (25330 area/μM, $R^2 = 0.999$)

3.7.2. Inhibited Hexadecane Autoxidation Traces

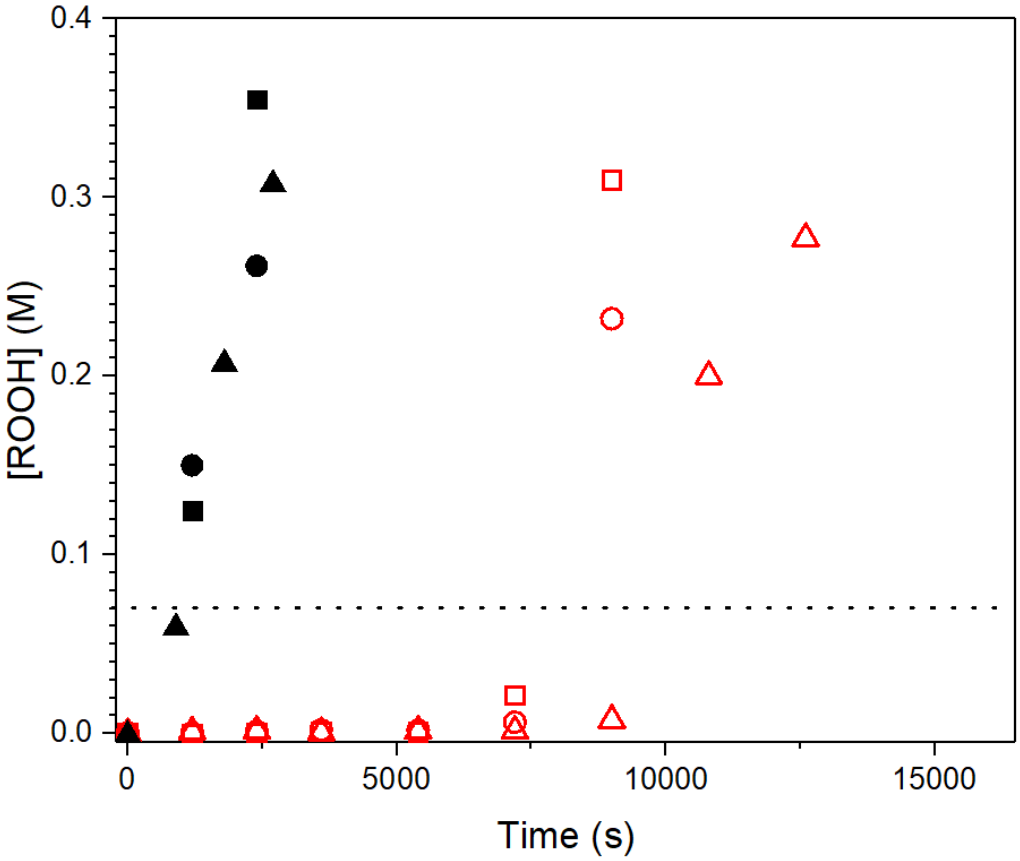

Figure S3.3. Autoxidation of hexadecane at 160 °C: Uninhibited (**black**); 200 μM 3-tBu-phenoxazine **3.14** (**red**). Replicate 1 (square), 2 (circle), and 3 (triangle) shown.

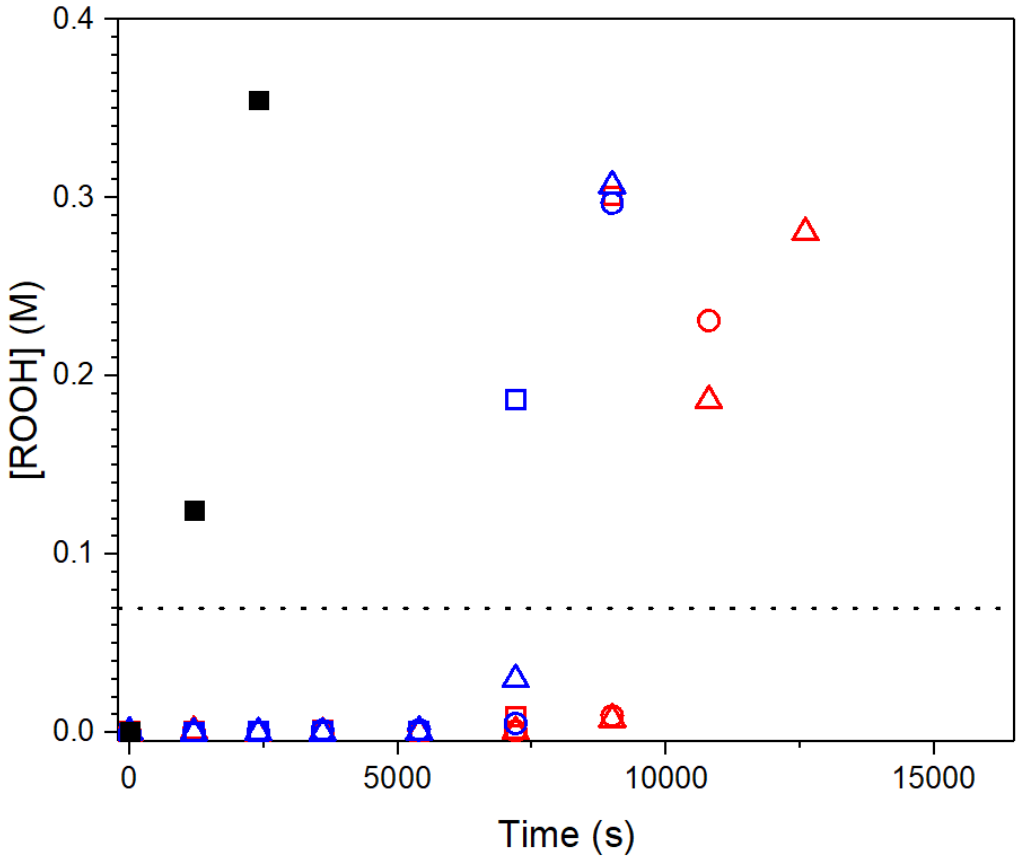

Figure S3.4. Autoxidation of hexadecane at 160 °C: 200 μM 3-MeO-7-NO_2-Phenoxazine **3.12** (**blue**); 200 μM 2-tBu-Phenoxazine **3.13** (**red**). Replicate 1 (square), 2 (circle), and 3 (triangle) shown.

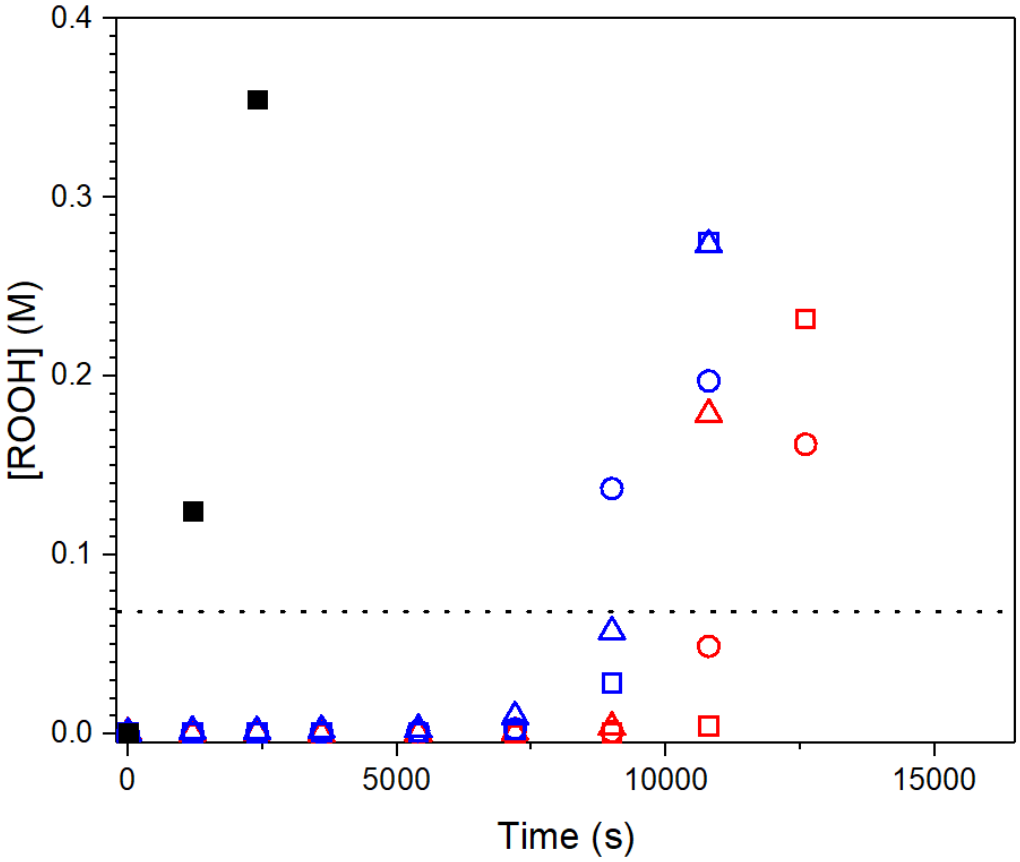

Figure S3.5. Autoxidation of hexadecane at 160 ºC: 200 µM 2,8-tBu-Phenoxazine **3.15** (**blue**); 200 µM 3-SO_2NEt_2-Phenoxazine **3.9** (**red**). Replicate 1 (square), 2 (circle), and 3 (triangle) shown.

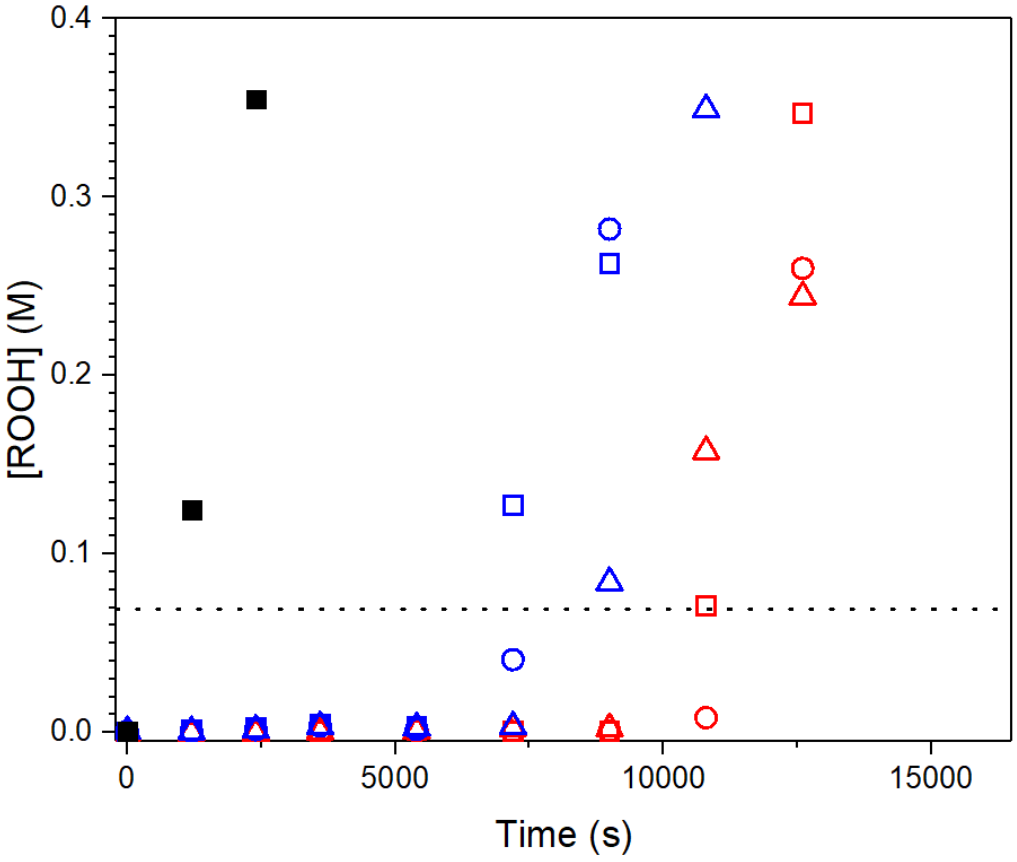

Figure S3.6. Autoxidation of hexadecane at 160 °C: 200 μM 3,7-tBu-Phenoxazine **3.16** (**blue**); 200 μM 2-CF_3-Phenoxazine **3.11** (**red**). Replicate 1 (square), 2 (circle), and 3 (triangle) shown.

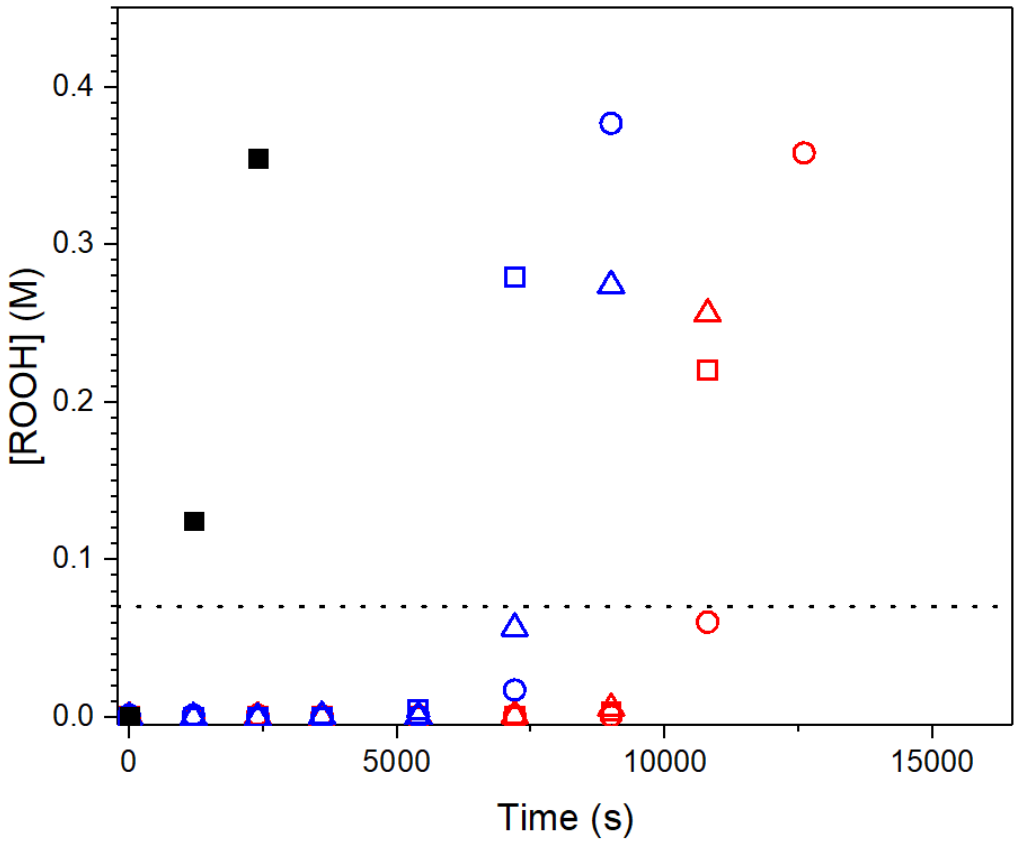

Figure S3.7. Autoxidation of hexadecane at 160 °C: 200 μM 3-MeO-Phenoxazine **3.17** (**blue**); 200 μM 3-CF_3-Phenoxazine **3.10** (**red**). Replicate 1 (square), 2 (circle), and 3 (triangle) shown.

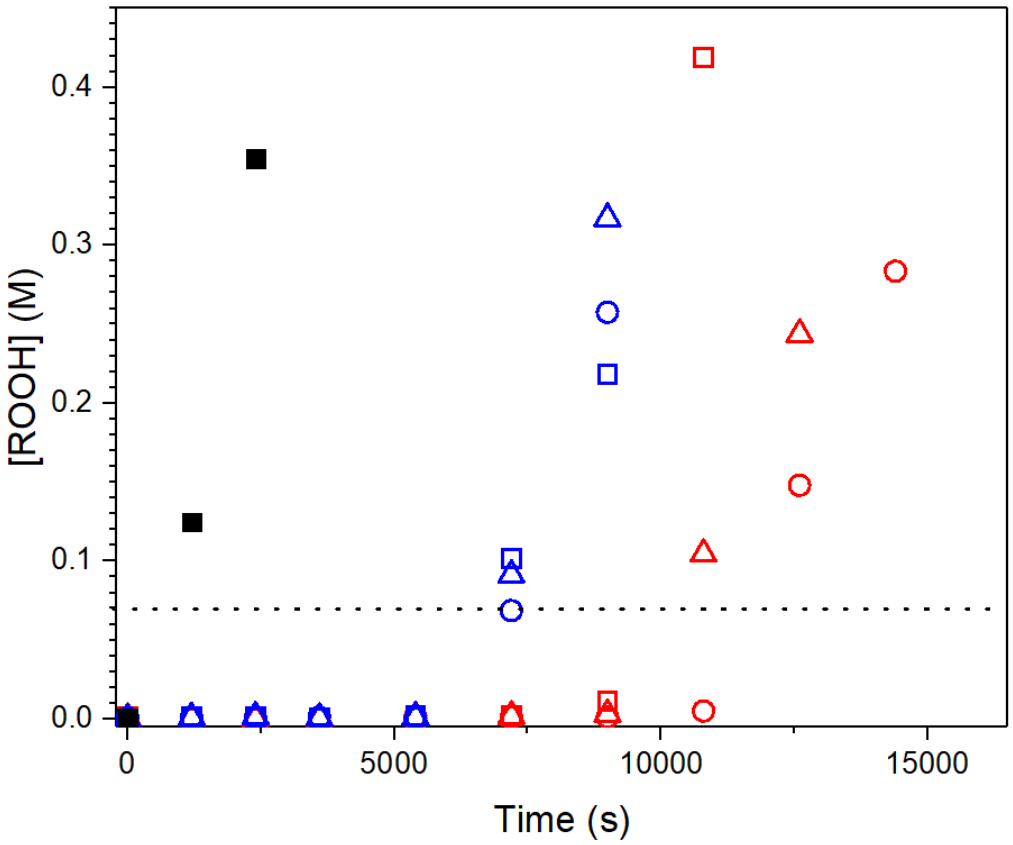

Figure S3.8. Autoxidation of hexadecane at 160 °C: 200 μM 2,4,6,8-tBu-Phenoxazine **3.18** (**blue**); 200 μM 3-CN-Phenoxazine **3.8** (**red**). Replicate 1 (square), 2 (circle), and 3 (triangle) shown.

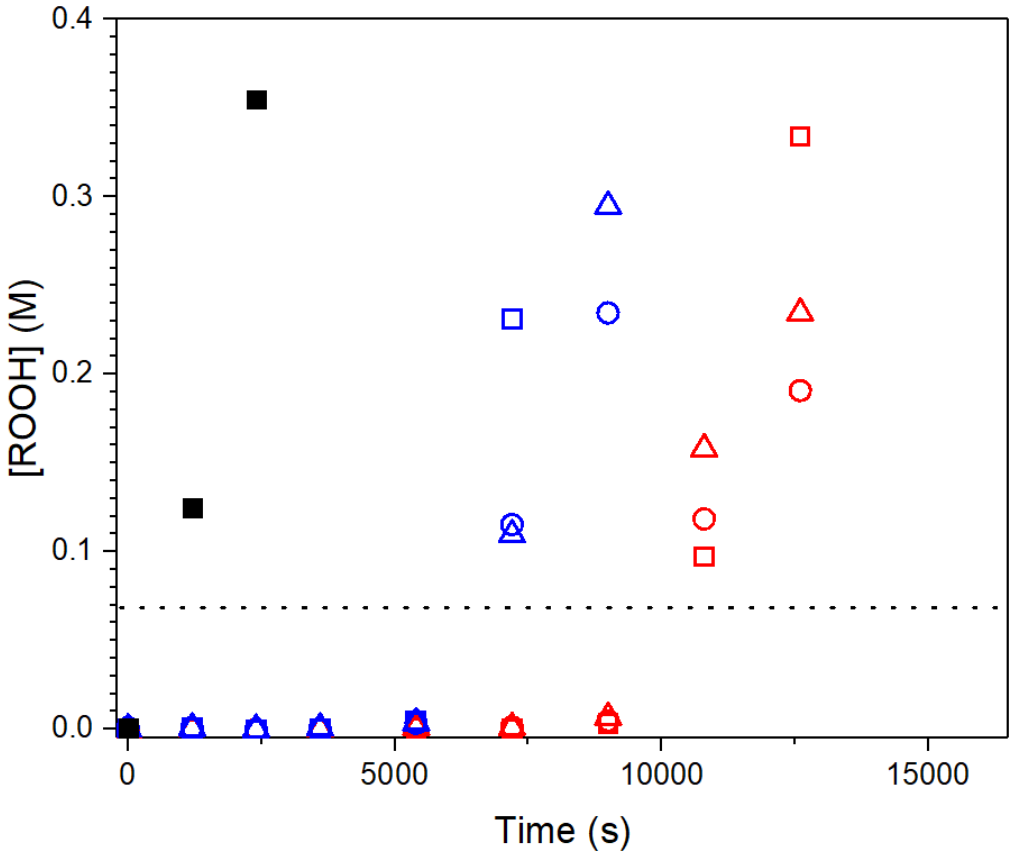

Figure S3.9. Autoxidation of hexadecane at 160 °C: 200 μM 3,7-MeO-Phenoxazine **3.19** (**blue**); 200 μM 3-NO_2-Phenoxazine **3.7** (**red**). Replicate 1 (square), 2 (circle), and 3 (triangle) shown.

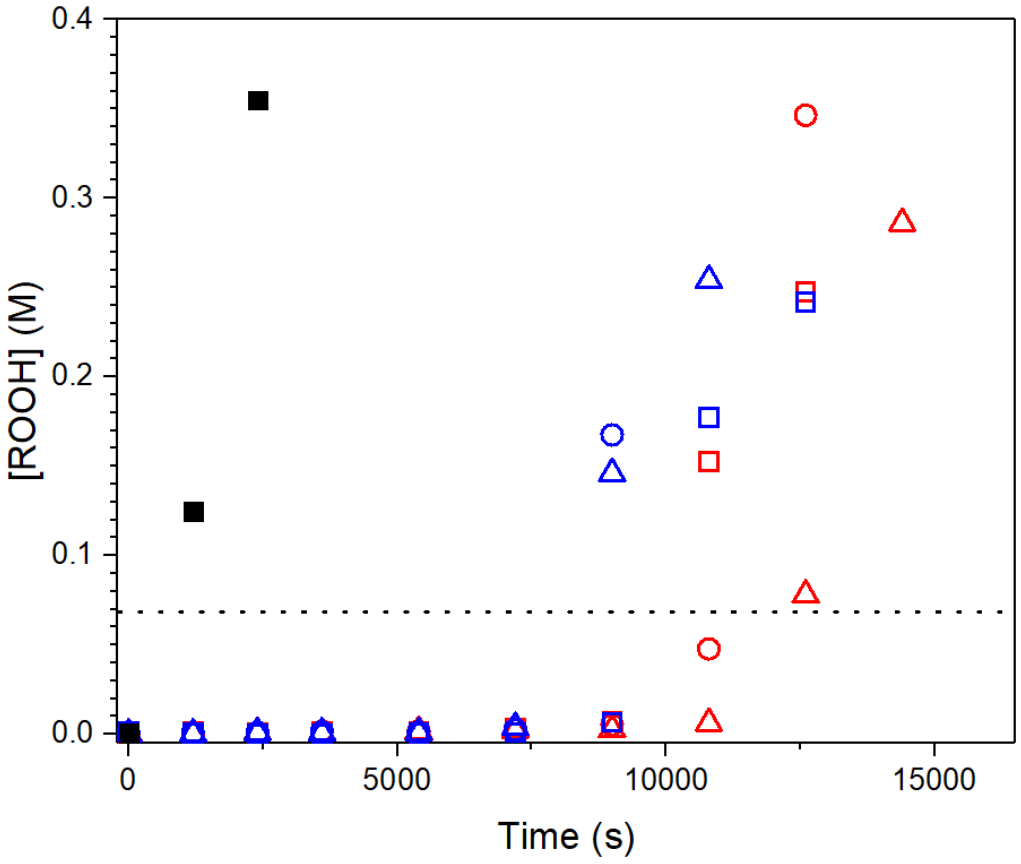

Figure S3.10. Autoxidation of hexadecane at 160 °C: 200 μM Phenoxazine **3.5** (**blue**); 200 μM 3-CN-7-NO_2-Phenoxazine **3.6** (**red**). Replicate 1 (square), 2 (circle), and 3 (triangle) shown.

3.7.3. ^{1}H NMR Spectra

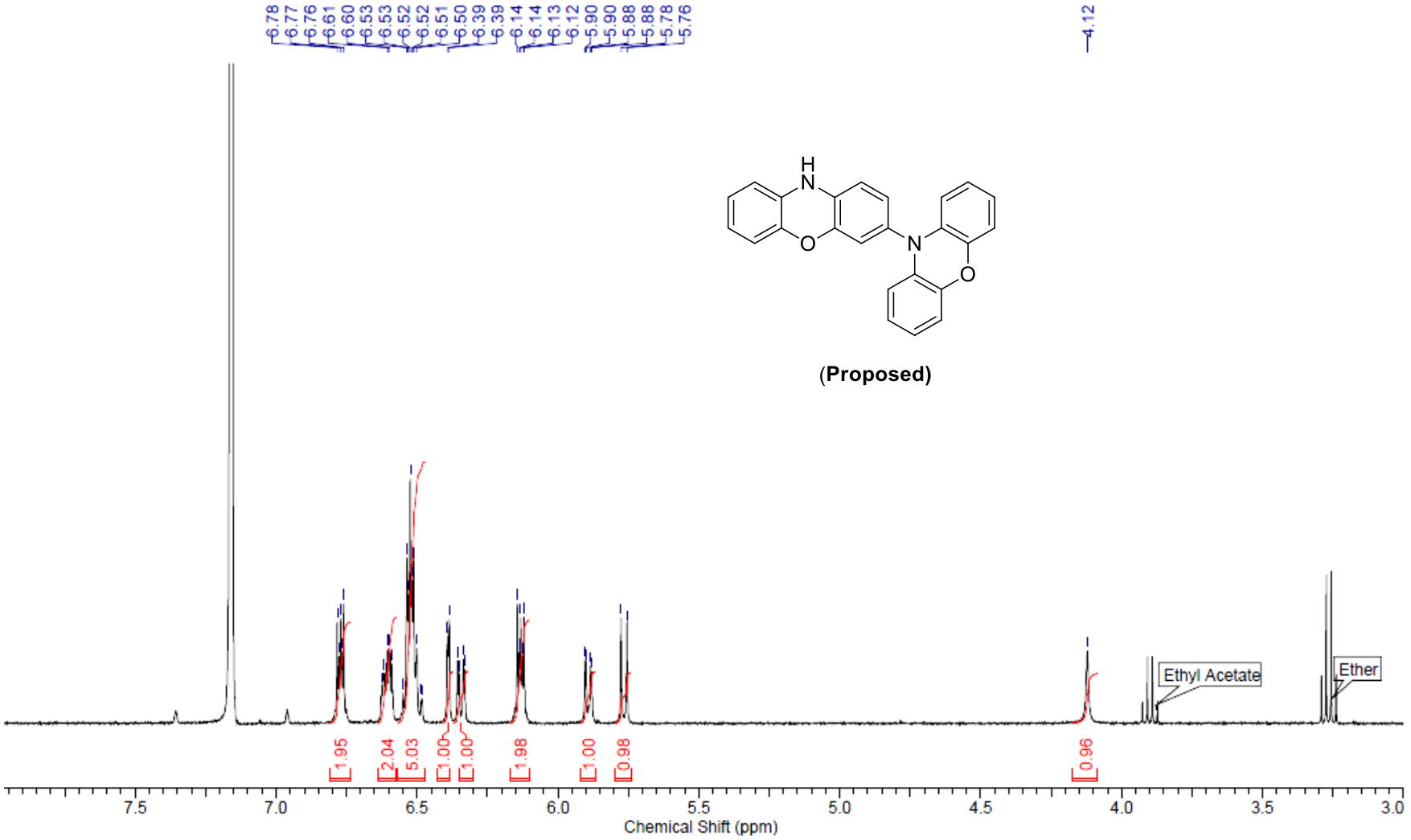

(**Proposed**)

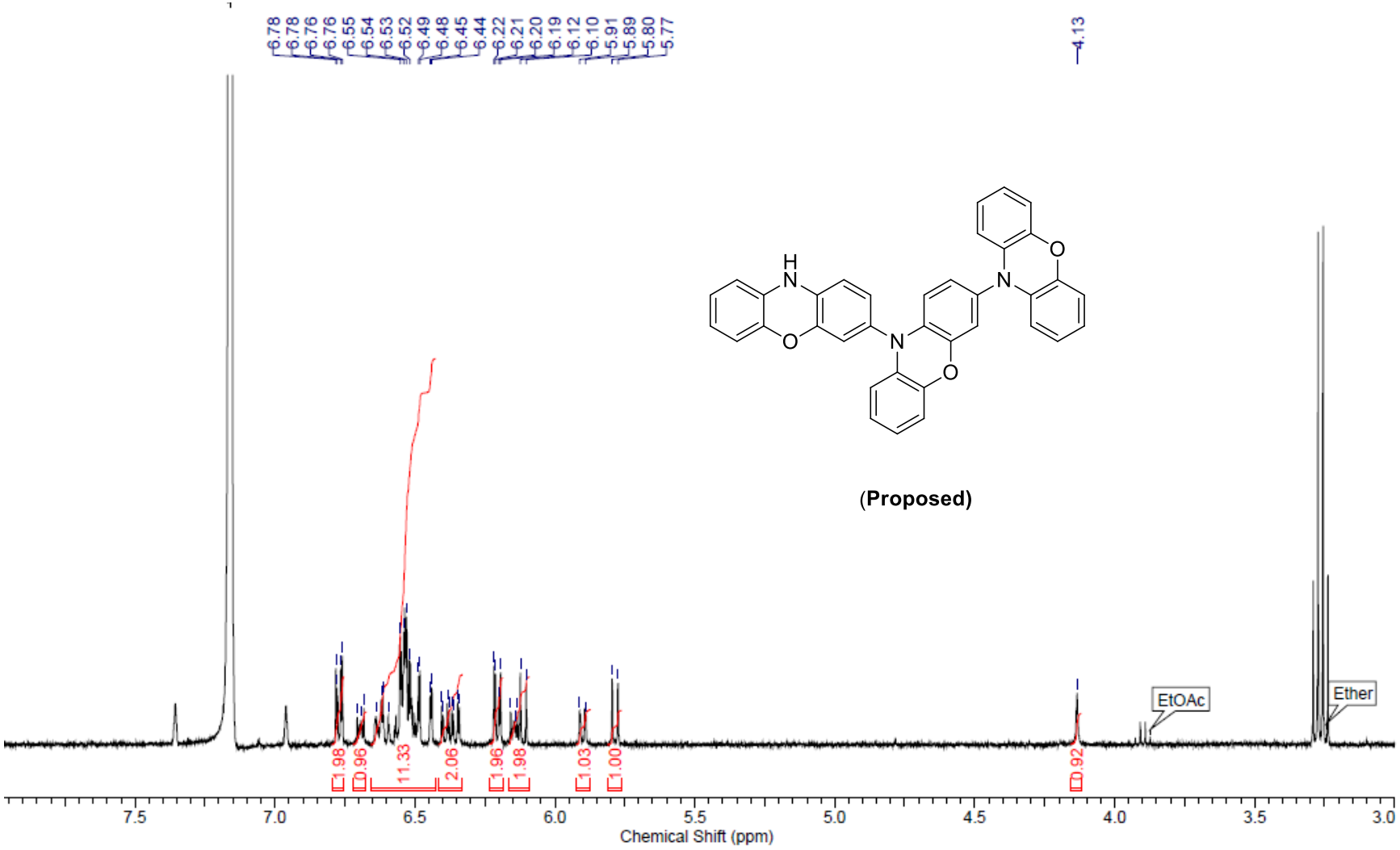
6.78
6.78
6.76
6.76
6.55
6.54
6.53
6.52
6.49
6.48
6.45
6.44
6.22
6.21
6.20
6.19
6.12
6.10
5.91
5.89
5.80
5.77
4.13
H
N
O
N
O
N
O
(Proposed)
1.98
0.96
11.33
2.06
1.96
1.98
1.03
1.00
0.92
EtOAc
Ether
7.5
7.0
6.5
6.0
5.5
5.0
4.5
4.0
3.5
3.0
Chemical Shift (ppm)

Chapter 4: Preliminary Studies of Phenoxazines as Inhibitors of Lipid Peroxidation and the Correlation of this Activity with Their Potency to Subvert Ferroptosis

4.1 Preface

Since lipid peroxidation is associated with a litany of ailments including Alzheimer's disease,[1,2] cancer,[3,4] and even ageing itself,[5] the subject is a topic of perennial interest. Lipid peroxidation is the autoxidation of lipids, leading to accumulation of lipid hydroperoxides – toxic molecules associated with a specific cell death pathway that has recently been coined ferroptosis. Part of the routine defense against lipid peroxidation are naturally occurring RTAs, the most potent being the lipophilic phenols that comprise Vitamin E.[6] Considering the impressive k_{inh} observed for phenoxazine in solution, we anticipated that phenoxazine RTAs could be useful as cytoprotective compounds. To assess the cytoprotective potential, k_{inh} was first determined for the catalogue of substituted phenoxazines in inhibited autoxidations of the unsaturated lipids of egg phosphatidylcholine liposomes. These results were normalized to the α_2^H of the phenoxazines to reveal a very strong and semi-predictable KSE that arises due to their interaction with the phosphate headgroups of the phospholipids. On the basis of their high reactivity in lipid liposomes, several of the phenoxazines were assessed for their efficacy in rescuing cells from ferroptosis, demonstrating a moderate correspondence between RTA activity in lipid bilayers and cytoprotective potency.[7,8]

Note: All experimental work pertaining to the treatment of RLS3 induced fibroblasts with substituted phenoxazine RTAs was conducted by fellow graduate researcher Ron Shah.

4.2 Introduction: Ferroptosis and Lipid Peroxidation

Excessive lipid peroxidation is implicated in several disease states.[1–5] Cells control lipid peroxidation by two primary mechanisms: a non-enzymatic approach where autoxidation chain-carrying peroxyls are trapped with RTAs (Scheme 4.1B) such as α-tocopherol which inhibit the formation of lipid hydroperoxides,[9] and an enzymatic system that reduces the hydroperoxides to their corresponding alcohols (Scheme 4.1C). The first mechanism is considered a "primary antioxidant" mechanism, since it intervenes directly to break the autoxidation chain reaction. The second mechanism is considered a "preventative antioxidant" mechanism since it does not intervene in the propagation of the chain reaction, but slows the rate of initiation. Glutathione peroxidase 4 (GPX4) is a selenocysteine-containing enzyme that catalyzes the reduction of lipid hydroperoxides through the oxidation of its selenol residue into selenic acid. Active GPX4 is regenerated by the step-wise reduction of selenenic acid by two equivalents of glutathione.[10] Disruption of GPX4 activity, either directly by inhibition of GPX4 with inhibitor RSL3,[8] or indirectly by preventing cystine uptake via inhibition of the cystine/glutamate antiporter (system x_c^-)[7] will increase the iron-dependent accumulation of lipid hydroperoxide. High levels of lipid hydroperoxide in a cell can trigger a novel form of nonapoptotic cell death known as 'ferroptosis' a term coined by Stockwell and co-workers.[7] Ferroptosis is mechanistically unique from the other currently identified forms of regulated cell death, possessing unique triggers and inhibitors.

Scheme 4.1. A) The ferrous catalyzed initiation (i.e. Fenton reaction) forms highly reactive alkoxyl radicals. **B)** Formation of peroxide facilitated enzymatically by LOX (bottom) or non-enzymatically through radical mediated autoxidation (top). **C)** GPX4 catalyzed reduction of hydroperoxides prevents accumulation of toxic peroxidic lipids. GPX4 can be inhibited by RSL3 which will eventually trigger ferroptosis. **D)** Glutamate/cysteine antiporter (system x_c^-)[7] brings cysteine into the cell (which is needed for glutathione synthesis). Inhibition of cysteine transport will trigger ferroptosis.

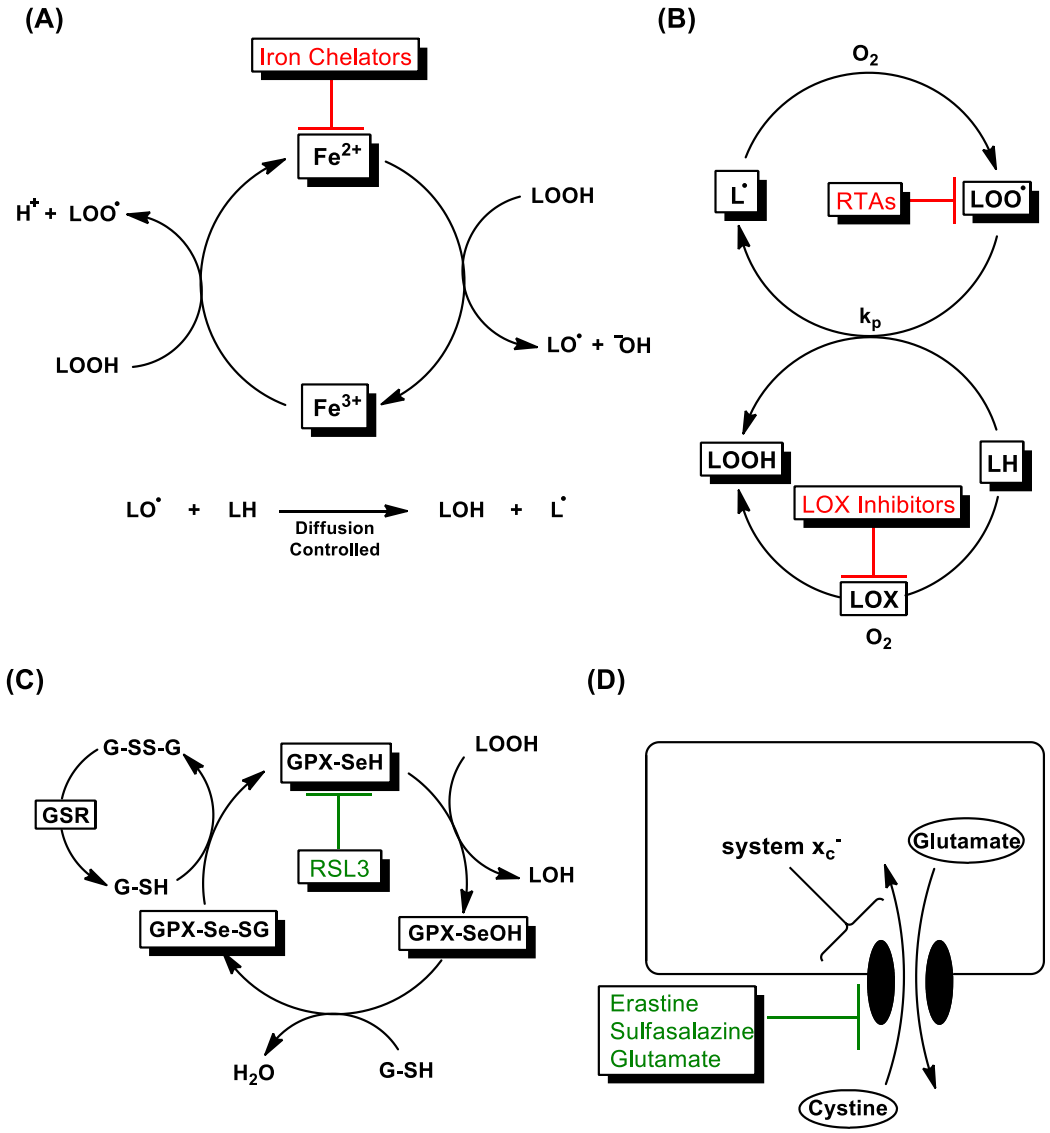

Scheme 4.1 provides a basic depiction of the proposed systems involved in regulating ferroptotic cell death. The ferroptosis moniker was inspired by the observation that this nonapoptotic form of cell death was iron dependent. Indeed, production of intracellular ROS in cells in which GPX4 was pharmacologically inhibited, or the gene encoding it deleted, was found to be suppressed by the addition of iron chelators or by genetic inhibition of iron uptake.[11,12] The precise role of iron in the process has not been unambiguously determined, but there are two theories to explain its dependence.

The first is a non-enzymatic role where free ferrous iron catalyzes the initiation phase of autoxidation by reducing a lipid hydroperoxide to an alkoxyl radical and hydroxide ion via a Fenton-type reaction (Scheme 4.1A).[13,14] If the free ferrous were chelated to a bidentate ligand such as 2,2'-bipyridyl,[7] it would unable to catalyze the formation of alkoxyl which would be consistent with a supressed rate of peroxidation and suppression of ferroptosis. The second proposed role of intracellular iron is that of nonheme iron which is a component of lipoxygenase enzymes (LOX) which catalyzes the formation of lipid hydroperoxides (Scheme 4.1B), thus the iron is required for the biosynthesis of LOX.[15,16] It should noted that while this seems reasonable where cells have been genetically modified to restrict iron uptake into the cell, the acute suppression of ferroptosis observed by treatment with iron chelators seems less consistent with this explanation as there would still be functional LOX enzymes present in the cells.

Understanding the key drivers for lipid peroxidation and ferroptosis is essential as it may inform rational drug design to prevent and/or treat conditions in which lipid peroxidation and/or ferroptosis have been implicated. Glutamate induced disruption of system x_c^- is associated with neurodegeneration and peroxidation,[17,18] so inhibitors of

ferroptosis should suppress neurotoxicity induced by cystine dysregulation. In the past few years, two high profile inhibitors of ferroptosis with nanomolar potency have been discovered: Ferrostatin-1 (Fer-1) and Liproxstatin-1 (Lip-1).

Scheme 4.2. The structures of Ferrostatin-1 and Liproxstatin-1.

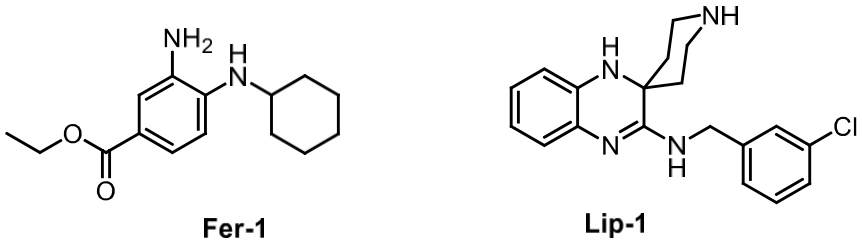

Fer-1 **Lip-1**

These compounds were identified through high throughput screening (9,517 compounds tested to find Fer-1[7] and more than 40,000 small molecules tested to find Lip-1[8]). Stockwell recognized a correlation between the inhibition of ferroptosis and the antioxidant activity of Fer-1 derivatives, which was deduced using a DPPH assay. However, he concludes with a rather vague allusion to a "unique profile of radical reactivity" which he uses to explain the 2 to 2.5 order of magnitude increase in potency over Trolox and BHT. Lip-1 was discovered a few years later which was found to be similar to Fer-1 in terms of potency, though again a definitive mechanism of action was not proposed.[8]

Scheme 4.3. Structures of PMC, α-Tocopherol, and C_{15}-THH.

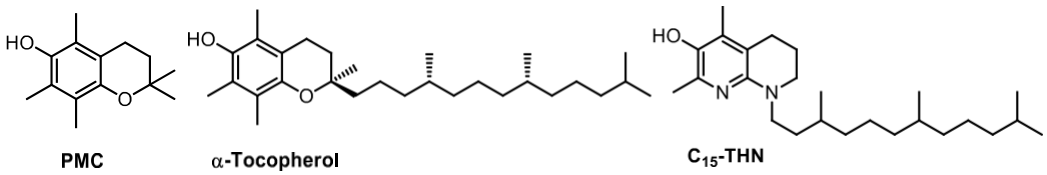

PMC **α-Tocopherol** **C_{15}-THN**

Our group recently provided a less ambiguous explanation for the strong anti-ferroptotic activity of Fer-1 and Lip-1.[19] Using the STY/PBD-BODIPY co-autoxidation method, the k_{inh} and n were determined for Fer-1 and Lip-1 in both styrene/PhCl and in egg lecithin phosphatidylcholine liposomes suspended in buffer. For comparison α-tocopherol, PMC and C_{15}-THN – an aza analog of α-tocopherol developed in the Pratt group – were also measured in these systems. The k_{inh} for Fer-1 and Lip-1 in styrene/PhCl ($3.5 \pm 0.1 \times 10^5$ and $2.4 \pm 0.2 \times 10^5$ respectively) was an order of magnitude lower than that of PMC and α-tocopherol ($3.1 \pm 0.2 \times 10^6$ and $3.6 \pm 0.2 \times 10^6$ respectively), interestingly the relative k_{inh} in liposome/buffer decreases for all the compounds, but far more dramatically for the phenols. The k_{inh} for Fer-1 and Lip-1 in liposome/buffer ($4.6 \pm 0.8 \times 10^4$ and $1.2 \pm 0.1 \times 10^4$ respectively) only decreased by about an order of magnitude relative to the k_{inh} in styrene/PhCl while PMC decreased by 2 orders of magnitude ($3.7 \pm 0.2 \times 10^4$) and α-tocopherol by nearly *3 orders of magnitude* ($4.7 \pm 0.4 \times 10^3$). The difference between PMC and α-tocopherol has long been explained by differences in their dynamics; PMC has been shown to have greater mobility within the lipid domain of the liposome.[20,21] The difference between PMC versus Fer-1 and Lip-1 comes down to the relatively strong hydrogen-bond acidity of PMC ($\alpha_2^H = 0.37$) compared to the apparently low α_2^H of Fer-1 and Lip-1 (estimated ~0.17). The anti-ferroptotic potency of Fer-1 (EC_{50} = 45 ± 5nM), Lip-1 (EC_{50} = 38 ± 3nM), PMC (EC_{50} = 59 ± 3nM), and α-tocopherol (EC_{50} = 1.8 ± 0.3μM) in RSL3 induced fibroblasts generally seemed to correlate well with rate constants derived from the liposome co-autoxidations. Encouraged by these results, similar sets of experiments were conducted on other RTAs to establish a relationship between the inherent peroxyl

radical-trapping reactivity of the compounds in liposomes and their potency as inhibitors of ferroptotic cell death (Fig. 4.1B).[22]

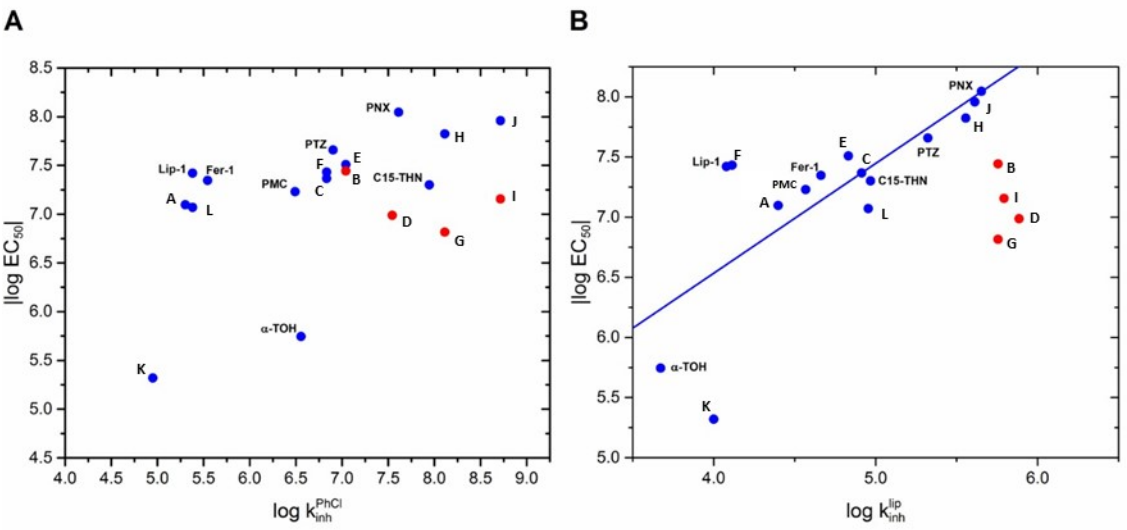

Figure 4.1. A) Replotted log k_{inh}^{PhCl} vs |log EC_{50}| anti-ferroptosis activity data from Shah et. al. **B)** Replotted log k_{inh}^{Lip} vs |log EC_{50}| data.[22] **Linear fit**: $y = 0.690x + 3.846$ ($R^2 = 0.573$). See Chart S4.1 in supporting information for structures associated with labels.

In Figure 4.1A, the | log EC_{50}| of Fer-1/Lip-1, PMC, and C15-THN are quite similar despite having log k_{inh}^{PhCl} values that differ by up to 2 orders of magnitude. There is no obvious reactivity/potency relationship between these parameters as a least squares linear analysis revealed an $R^2 = 0.327$. When a similar analysis was conducted between |log EC_{50}| and log k_{inh}^{Lip} (Figure 4.1B) a comparatively better correlation ($R^2 = 0.569$) is rendered. In both instances, the poorly lipophilic heterocyclic diarylamines (marked in red) are excluded, as the authors proposed that their anti-ferroptotic activity is diminished due to inefficient uptake into the cells as a result of partitioning. Phenoxazine (**4.1**) is the most reactive RTA in liposomes ($4.5 \pm 0.5 \times 10^5$) and the most potent inhibitor of ferroptosis ($EC_{50} = 9 \pm 2$ nM). The aza-phenoxazine (**4.2**) far surpassed phenoxazine in RTA activity in organic solution but fell slightly behind in liposomes and in the cell assay.

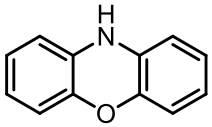

4.1

$k^{PhCl} = 3.9 \pm 0.4 \times 10^7\ M^{-1}\ s^{-1}$
$k^{Lip} = 4.5 \pm 0.5 \times 10^5\ M^{-1}\ s^{-1}$
EC_{50} = 9 ± 2nM
α_H^2 = 0.44

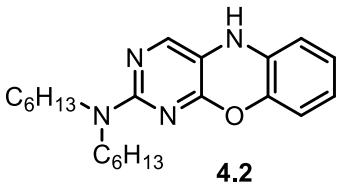

4.2

$k^{PhCl} = 5.2 \pm 0.1 \times 10^8\ M^{-1}\ s^{-1}$
$k^{Lip} = 4.1 \pm 0.1 \times 10^5\ M^{-1}\ s^{-1}$
EC_{50} = 11 ± 2nM
α_H^2 = 0.50

The di-hexyl-amino moiety is principally responsible for the prodigious $\log k_{inh}^{PhCl}$ of **4.2**, though it would seem that the nitrogen heteroatoms at the 2 and 4 positions contribute to increasing the H-bond acidity of the compound. From a design standpoint this represents an interesting dilemma as the electron-deficient heteroatoms were incorporated to stabilize the phenoxazine from electron-transfer to O_2, but they subvert the RTA activity in a strongly hydrogen bonding environment. We were curious to see how dramatic the differences in $\log k_{inh}^{Lip}$ and $|EC_{50}|$ would be for the EWG containing phenoxazines compared to phenoxazine itself, even though many of them are within a factor of 2 in terms of $\log k_{inh}^{PhCl}$. Additionally, we were interested to see how the phenoxazines containing EDGs would perform as they, unlike **4.2**, have both higher $\log k_{inh}^{PhCl}$ values *and* lower α_2^H parameters.

4.3 Results and Discussion

Phosphatidylcholine liposomes supplemented with STY-BODIPY and suspended in buffer were used to determine the reactivity of the substituted phenoxazines as previously described.[19,22] In short, apparent inhibition rate constants (k_{inh}^{lip}) were determined for phenoxazines **4.3**-**4.16** as well as their reaction stoichiometry (n) with the exception of 3-cyano-7-nitrophenoxazine (**4.3**). Some representative results are included

in Figure 4.2 (for the complete set see **4.7 Supporting Information**) and the data summarized in Table 4.1.

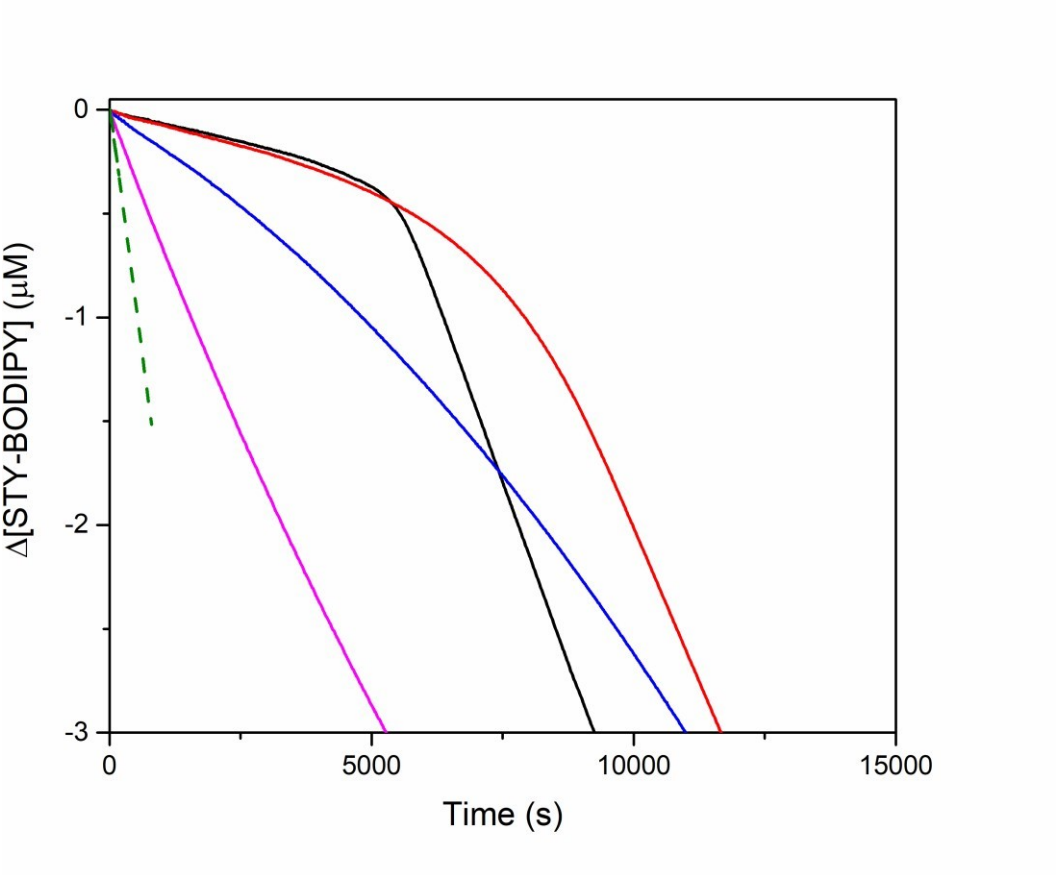

Figure 4.2. Inhibited autoxidation of STY-BODIPY (10 μM) in EGG-PC (1 mM) initiated with MeOAMVN (0.2 mM) monitored at 565 nm (121200 M^{-1} cm^{-1}): 6 μM 3-MeO-7-NO_2-Phenoxazine **4.8** (**black**); 6 μM 3-CN-Phenoxazine **4.5** (**red**); 6 μM 3-NO_2-Phenoxazine **4.4** (**blue**); 10 μM 3-CN-7-NO_2-Phenoxaizne **4.3** (**magenta**); Uninhibited (**green**).

Table 4.1. Rate constants of inhibition in Egg-PC liposomes

RTA	Substituents	k_{inh}^{Lip} (M^{-1} s^{-1}) [a]	$n_{(Lip)}$	α_2^H	k_{inh}^0 (M^{-1} s^{-1})[b]
4.3	3-CN-7-NO_2	$3.8 \pm 0.1 \times 10^3$	(too slow)	0.69	$1.5 \pm 0.1 \times 10^7$
4.4	3-NO_2	$2.1 \pm 0.1 \times 10^4$	2.7 ± 0.1	0.62	$4.7 \pm 0.1 \times 10^7$
4.5	3-CN	$6.1 \pm 0.5 \times 10^4$	3.0 ± 0.1	0.56	$4.7 \pm 0.1 \times 10^7$
4.6	3-SO_2NEt_2	$6.1 \pm 0.2 \times 10^4$	2.8 ± 0.1	0.53	$5.2 \pm 0.3 \times 10^7$
4.7	3-CF_3	$6.4 \pm 0.1 \times 10^4$	2.8 ± 0.1	0.53	$5.0 \pm 0.2 \times 10^7$
4.8	3-MeO-7-NO_2	$7.0 \pm 0.4 \times 10^4$	2.4 ± 0.2	0.60	$1.5 \pm 0.5 \times 10^8$
4.9	2-CF_3	$1.2 \pm 0.1 \times 10^5$	2.8 ± 0.1	0.51	$6.0 \pm 0.2 \times 10^7$
4.1	H	$4.7 \pm 0.5 \times 10^5$	2.0 ± 0.1	0.44	$8.3 \pm 0.4 \times 10^7$
4.10	2-tBu	$4.6 \pm 0.4 \times 10^5$	2.0 ± 0.1	0.43	$1.3 \pm 0.2 \times 10^8$
4.11	3-tBu	$6.1 \pm 0.9 \times 10^5$	1.9 ± 0.1	0.43	$1.6 \pm 0.6 \times 10^8$
4.12	2,8-tBu	$4.7 \pm 0.2 \times 10^5$	1.7 ± 0.1	0.43	$2.1 \pm 0.1 \times 10^8$
4.13	3,7-tBu	$7.3 \pm 0.9 \times 10^5$	1.8 ± 0.1	0.41	$2.8 \pm 0.1 \times 10^8$
4.14	3-MeO	$7.6 \pm 1.4 \times 10^5$	2.3 ± 0.1	0.42	$3.7 \pm 0.1 \times 10^8$
4.15	2,4,6,8-tBu	$2.2 \pm 0.6 \times 10^5$	1.0 ± 0.1	0.39	$4.1 \pm 0.4 \times 10^8$
4.16	3-7-MeO	$2.2 \pm 0.9 \times 10^6$	1.6 ± 0.1	0.40	$(1.3 \pm 0.6 \times 10^9)$

[a]Rates of inhibition determined for either 2, 6, or 10 μM of inhibitor a minimum of three times. [b]The k_{inh}^0 values were calculated from the k_{inh}^{Diox} or k_{inh}^{DMSO} described in Chapter 2.

Also included in Table 4.1 are the H-bond acidity values of the phenoxazines (which were presented in Chapter 2), as it is has been reported that H-bonding interactions are one of two key factors in the dramatic difference between inhibition rate constants measured in homogeneous solution and those measured in lipid bilayers – the other being limited diffusion.[23,24] Indeed, consideration of the kinetic data in Table 4.1 reveals differences between the RTAs which roughly correspond with HBD ability of the compounds. For example, **4.4** and **4.5** have the same calculated k_{inh}^0 but the k_{inh}^{Lip} of **4.4** is 3-fold lower than **4.5**, situation which seems to correspond to the higher α_2^H of **4.5**. Comparing **4.5** to **4.8**, their calculated k_{inh}^0 differ by a factor of 3, but the k_{inh}^{Lip} of **4.8** is

only ~15% greater, which again seems to follow the change in α_2^H. Since most of the compounds investigated are expected to have similar dynamics within the lipid bilayer, this kinetic data combined with that determined in dioxane (which were presented in Chapter 2) was used to determine an effective β_2^H for the liposome suspension. Since the convention has been to assume $n = 1$ for the calculation of k_{inh}^{Lip} and $n = 2$ for the $k_{inh}^{Diox}/k_{inh}^{DMSO}$ from which k_{inh}^0 is derived, the relationship in Eq. 4.1 was employed wherein the Ingold-Abraham relationship was recast to set the β_2^H as the y-intercept.

$$\frac{\log(k_{inh}^0)}{(8.3\alpha_2^H)} = \frac{\log(k_{inh}^{lip}/2)}{(8.3\alpha_2^H)} + \beta_2^H \qquad \textbf{Eq. 4.1}$$

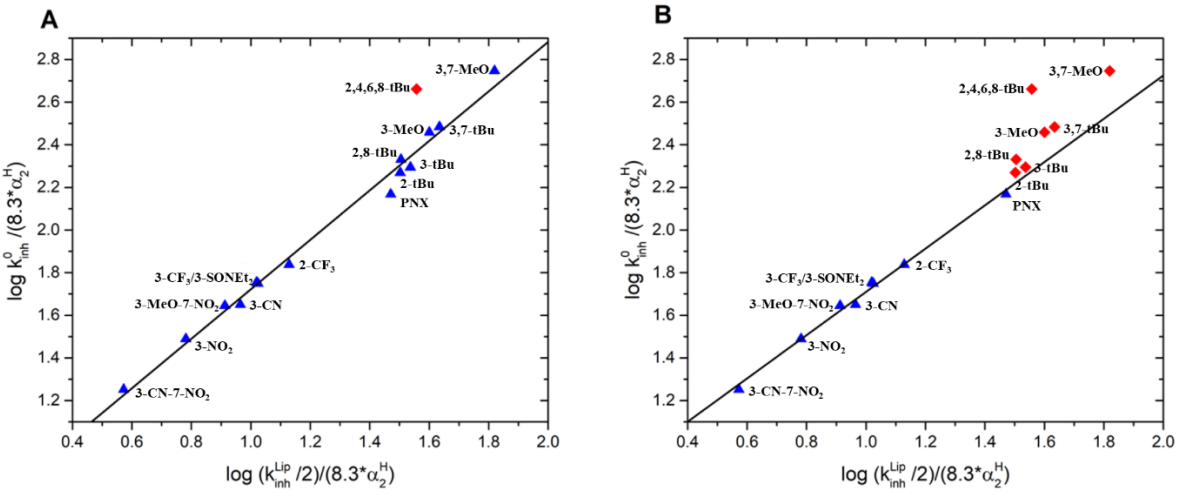

Figure 4.3. A) Eq. 4.1 plotted and fit for substituted phenoxazines 4.1, 4.3-4.14, and 4.16. (R^2 =0.990, β_2^H = 0.561). **B)** Eq. 4.1 plotted and fit for substituted phenoxazines 4.1 and 4.3-4.10 (R^2 = 0.994, β_2^H = 0.694).

The linear fit in Figure 4.3A is based on the 13 phenoxazine compounds, **4.1**, **4.3**-**4.14**, and **4.16**, and on casual inspection it appears that generally the data points do not significantly deviate from the trendline (R^2 = 0.990). The 2,4,6,8-tetra-*tert*-butylphenoxazine (**4.15**) is excluded from the fit due to its anomalously low log k_{inh}^{Lip} and n values (more on this later). The intercept of the line is 0.56. In order to ascertain the predictive nature of this value as the 'effective' β_2^H value of the liposome system, we used it to predict the k_{inh}^{Lip} for other RTAs with known α_2^H and log k_{inh}^0 values using the Ingold-Abraham relationship. Doing so for phenothiazine and PMC yielded k_{inh}^{Lip} values of 5.1 and 1.8 × 10^5 M^{-1} s^{-1}, respectively, roughly 2.5- and 5-fold greater than their reported k_{inh}^{Lip} values of (2.1 ± 0.3)×10^5 and (3.7 ± 0.2)×10^4 $M^{-1}s^{-1}$, respectively.[19,22] When the data for only an 8-member subset of these phenoxazines (**4.1** and **4.3-4.10**) were fit to Eq. 4.1 (Figure 4.3B), the correlation coefficient increased marginally (R^2 = 0.994) along with the y-intercept (β_2^H = 0.69), resulting in predicted k_{inh}^{Lip} of 2.0 × 10^5 and 6.9 × 10^4 $M^{-1}s^{-1}$ for phenothiazine and PMC, respectively – in much better agreement with the values determined directly. Thus, we recommend that the latter value of β_2^H = 0.69 be used to estimate H-bonding interactions in egg PC liposomes. It should be noted that the effective β_2^H values determined from either Figure 4.1A or 4.1B are substantially greater than that of H_2O (β_2^H = 0.39), and are reasonably close to that reported for trimethylphosphate (0.77).[25] Such a massive KSE provides some quantitative support for the long noted observation that inhibition rate constants derived from inhibited autoxidations of phosphatidylcholine liposomes are significantly smaller than those measured in homogenous organic solution such as benzene or chlorobenzene.[26]

Furthermore, it suggests that there is a strong H-bond interaction between the phenoxazine and the head group of the phospholipid which would make RTAs with high α_2^H values significantly worse off even if they have comparable k_{inh}^0.

Scheme 4.4. Structure of 1-linoleoyl-2-palmitoyl-phosphatidylcholine and β_2^H of trialkylphosphate.

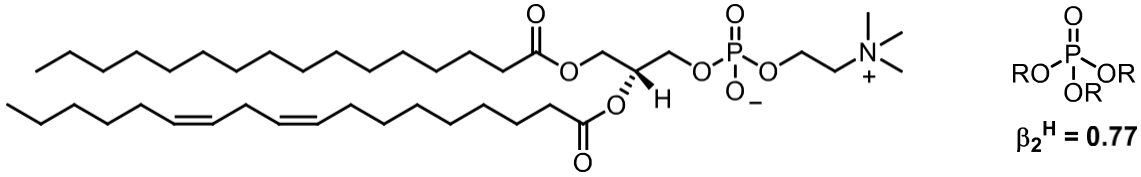

Of course, H-bonding interactions are only one of at least two factors that must contribute to k_{inh}^{Lip}. The other is illustrated upon consideration of the fact that α-tocopherol and PMC differ by an order of magnitude in k_{inh}^{Lip} despite having indistinguishable k_{inh}^0 and α_2^H. Another example is the difference between the highly lipophilic **4.15** against 3,7-dimethoxyphenoxazine (**4.16**), which are similar in terms of k_{inh}^{PhCl} and α_2^H, but are again separated by an order of magnitude in reactivity in liposomes. While these are extreme examples, there are also some more subtle differences one could not anticipate such as the ~30% increase in k_{inh}^{Lip} for **4.11** over **4.10** or the ~50% increase of **4.13** over **4.12** despite those sets having nearly identical k_{inh}^{PhCl} and α_2^H values. It would be naïve to assume that differences in the partition coefficients of the 13 phenoxazines or perhaps subtle differences in how they interact with the liposome interface do not affect the observed k_{inh}^{Lip} to varying degrees, let alone if we try extending the comparison to other scaffolds.

Suffice it to say, to make a reliable and general empirical relationship to predict k_{inh}^{Lip}, a two-parameter equation is obviously insufficient. A logical place to start would be to incorporate log *P* to account for the partition between the aqueous and lipid phase, which one could test by keeping k_{inh}^{0} and α_2^H the same while varying the lipophilicity with varying lengths of alkyl side chains (which could be easily done for **4.6** or **4.14** as an example).

To further clarify the relationship between k_{inh}^{Lip} and the inhibition of ferroptosis, the ability of the phenoxazines to subvert RSL3-induced ferroptosis in mouse embryonic fibroblasts was determined. Compounds **4.3-4.5**, **4.8**, and **4.12-4.18** were selected to represent a diverse range of $\log k_{inh}^{Lip}$ values with more emphasis on the electron-rich compounds which we felt had the best potential to surpass **4.1** which is the most potent anti-ferroptotic agent reported to date.[22]

Table 4.2. Rate constants of inhibition (k_{inh}^{Lip}), $n_{(Lip)}$, and EC_{50} values for substituted phenoxazines added to RLS3 induced Pfa-1 cells.

RTA	Substituents	k_{inh}^{lip} ($M^{-1}s^{-1}$) [a]	$n_{(lip)}$	EC_{50} (nM)
4.3	3-CN-7-NO_2	$3.8 \pm 0.1 \times 10^3$	n.d	602 ± 76
4.4	3-NO_2	$2.1 \pm 0.1 \times 10^4$	2.7 ± 0.1	227 ± 50
4.5	3-CN	$6.1 \pm 0.5 \times 10^4$	3.0 ± 0.1	129 ± 11
4.8	3-MeO-7-NO_2	$7.0 \pm 0.4 \times 10^4$	2.4 ± 0.2	39 ± 3
4.1	H	$4.7 \pm 0.5 \times 10^5$	2.0 ± 0.1	9 ± 2
4.12	2,8-tBu	$4.7 \pm 0.2 \times 10^5$	1.7 ± 0.1	42 ± 7
4.13	3,7-tBu	$7.3 \pm 0.9 \times 10^5$	1.8 ± 0.1	12 ± 2
4.14	3-MeO	$7.6 \pm 1.4 \times 10^5$	2.3 ± 0.1	30 ± 3
4.15	2,4,6,8-tBu	$2.2 \pm 0.6 \times 10^5$	1.0 ± 0.1	>500
4.16	3-7-MeO	$2.2 \pm 0.9 \times 10^6$	1.6 ± 0.1	15 ± 3

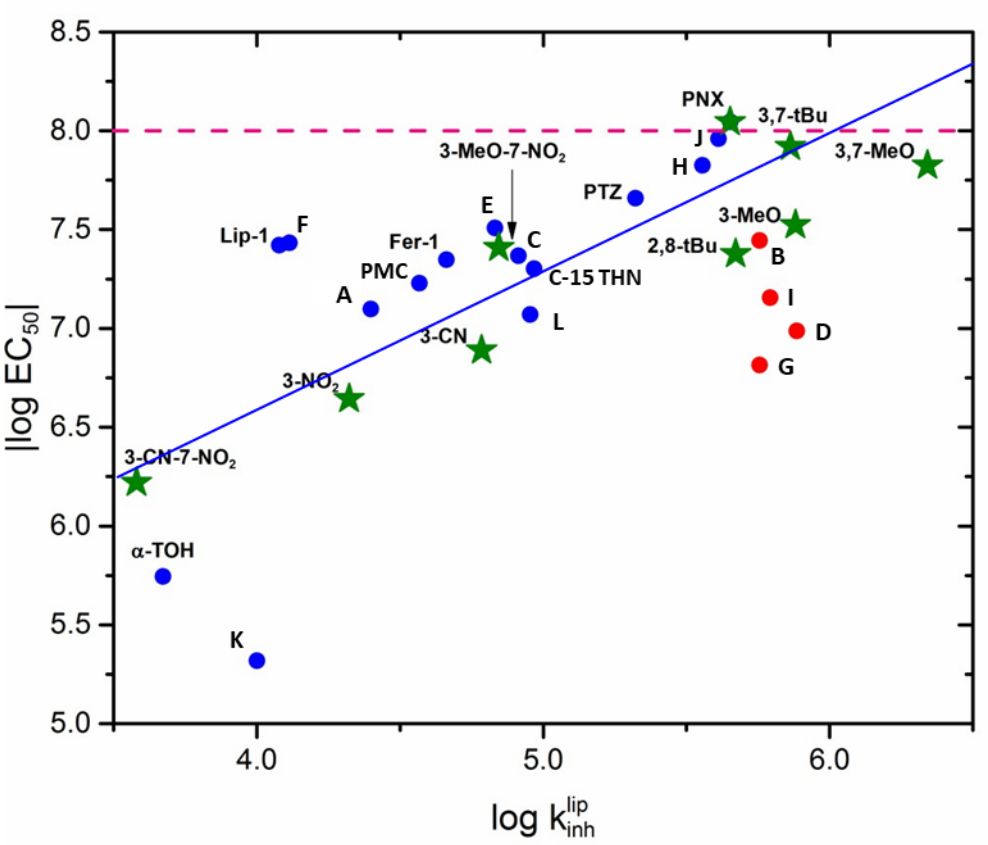

Figure 4.4. The log k_{inh}^{Lip} vs |log EC_{50}| of phenoxazine-based RTAs superimposed over the data in Figure 4.1B. **Linear fit**: $y = 0.690x + 3.846$ ($R^2 = 0.573$).

The data was overlaid on the existing | log EC_{50}| *vs* log k_{inh}^{Lip} correlation recently published by Shah et al.[22] (Figure 4.4) and a least squares analysis maintains the linear correlation previously seen with Figure 4.1B (R^2 = 0.573 vs 0.569) compared to what would be a slight decrease in R^2 if the data were overlaid onto a | log EC_{50}| *vs* log k_{inh}^{PhCl} analogous to Figure 4.1A (R^2 = 0.315 vs 0.327). This continues to demonstrate that the inhibition rate constant rendered in a biphasic system (k_{inh}^{Lip}) serves as a more meaningful parameter when relating RTA activity to anti-ferropotic efficacy when compared to those obtained in homogenous organic solution. Starting with the most electron-deficient phenoxazine, **4.3**, we observe a relatively modest EC_{50} of ~600 nM which is approximately 3 times more potent than α-tocopherol even though their log k_{inh}^{Lip} values are similar (3.8×10^3 M^{-1} s^{-1} vs 4.7×10^3 M^{-1}

s^{-1} respectively). This data suggests that physical characteristics (i.e. cell permeability and/or diffusibility within the cell and/or lipid bilayers) can be even more impactful than inherent chemical reactivity (the sum of intrinsic log k_{inh}^{0} and HBD ability) in cells than in liposomes. Progressively, **4.4** (3-NO_2) and **4.5** (3-CN) are more potent than **4.3** (3-CN-7-NO_2), but interestingly **4.8** (3-MeO-7-NO_2) is much more potent than **4.5** despite their very similar k_{inh}^{Lip} values. Compound **4.13** (3,7-tBu) is very similar in potency to **4.1** (PNX), but **4.12** (2,8-tBu) is notably less potent suggesting that placing the alkyl substituents in the meta-positions with respect to the amine is detrimental to its activity. Interestingly **4.13** and **4.14** (3-MeO) behave in a similar fashion in liposomes though **4.13** again is more potent. Finally, although **4.16** (3,7-MeO) is the fastest RTA we have ever measured in the liposome/STY-BODIPY co-autoxidation experiment, and exhibits an excellent EC_{50} = (15 ± 3) nM, it fails to best phenoxazine.

Essentially all of these compounds are relatively potent inhibitors of ferroptosis, with the exception of **4.15** which failed to rescue the cells to any significant degree in its tested concentration range. The failure of **4.15** is a useful result as it suggests that a highly lipophilic phenoxazine, which likely resides entirely inside the lipid-bilayer, does not effectively prevent lipid peroxidation. The efficacy of lipid permeable RTAs such as α-tocopherol are greatly enhanced by being regenerated by co-reductants which are outside the lipid bilayer such as ubiquinol or ascorbate.[27,28] Phenoxazine likely benefits from the same type of synergism, so mobility between the two phases would be requisite for the high potencies observed, all of which would put such a lipophilic/hydrophobic compound such as **4.15** at a disadvantage.

We were surprised that neither **4.13** nor **4.16** were any more potent than **4.1**. While the simple explanation would be to propose that they are more oxidatively labile and show some pro-oxidant activity, counteracting their inherently superior peroxyl trapping chemistry, the differences in their stoichiometry in liposomes are not that significant. The most active RTAs, **4.1**, **4.2**, **4.13**, and **4.16** all seem to converge around $|\log EC_{50}| = 8$, which prompts the question: is it possible to design an inhibitor with a lower EC_{50}, and if not, why not? Perhaps regardless of k_{inh}, diffusion in and out of the bilayer required for trapping/regeneration becomes rate limiting, or perhaps at a certain concentration it simply is too dilute to protect the comparatively massive amount of lipid substrate.

In summary, while there may be some individual idiosyncrasies that may be difficult to completely explain at this time, typically the anti-ferroptosis activity of the phenoxazines correlate well with the rate of reactivitytowards peroxyl radicals in strongly hydrogen-bonding liposomal environment. The dilemma between increasing E^o or keeping the α_2^H down comes down to the point that phenoxazine **4.1** already has an inherently high E^o relative to its k_{inh}, so unless there is evidence suggesting that it is too oxidatively unstable for the target system there is little incentive to specifically increase E^o by introducing EWGs as it will also have a significant influence on its α_2^H. That being said, *in vivo*, major metabolites derived from phenothiazine are the 3-hydroxy and 3,7-dihydroxyphenothiazines,[29] so there could an argument for modifying phenoxazine to resist similar transformations. To punctuate this discussion, beyond the demonstrated *in vitro* potency, the efficacy of such tricyclic aminic antioxidants could prove to be credible *in vivo* as well. Behl and co-workers have published a number of papers regarding the potency of phenoxazine and phenothiazine in inhibiting oxidative neurotoxicity, and they

point out that these compounds have a profile that indicates strong candidacy for effective blood brain barrier permeability as they are small, uncharged, and they are lipophilic (phenoxazine log P = 1.98, phenothiazine log P = 3.34) without the inclusion of a long alkyl chain which can disrupt passive permeability.[30,31]

4.4 Conclusion

In conclusion, the k_{inh}^{Lip} determined here for 15 different phenoxazines are linearly related to the k_{inh}^{0} and α_2^H that we had previously determined for the same compounds. The resultant correlation between and has enabled the determination of an apparent β_2^H = 0.56 for phosphatidylcholine liposomes. An 8-compound subset (everything with a k^{Lip} equal or lower than **4.1**, without **4.15**) yields an apparent β_2^H = 0.69, which we recommend based on its success in predicting the k_{inh}^{Lip} for other RTAs. Both β_2^H values are substantially higher than that of H_2O (0.39) which strongly implies that there is a strong hydrogen-bonding interaction with the phosphate headgroup at the membrane interface.

All but one of the phenoxazines were able to rescue cells in which ferroptosis had been initiated with RSL3, and did so with EC_{50} values ranging from ~600 nM to 12 nM. In many cases, the potencies of the phenoxazines matched or surpassed the top archetype ferroptosis inhibitors Fer-1 and Lip-1. The activity of these substituted phenoxazines *in vitro* generally conformed with our expectations based on the kinetics of their reactivity to peroxyl radicals in liposomes, and further demonstrated a rational correlation between RTA activity and anti-ferroptosis activity.

4.5 Experimental

Inhibited Co-Autoxidation of STY-BODIPY in Egg-PC Liposomes. Into a 3 mL quartz cuvette were added 2.34 mL of 10 mM PBS (pH 7.4) and 125 μL of a 20 mM solution of unilamellar Egg-PC liposomes (in PBS at pH 7.4). After equilibrating at 37°C in the carrier block for ~5 minutes, a 12.5 μL portion of STY-BODIPY solution (2 mM in DMSO) was added. Following this 10 μL of MeOAMVN solution was added (0.05 M in acetonitrile), and the solution was mixed thoroughly. The oxidation of STY-BODIPY was monitored at a wavelength of 565 nm for ~5 minutes, after which monitoring was paused and 10 μL of the RTA solution (of appropriate concentration) was added, mixed, and monitoring was resumed. The inhibition rate constants (k_{inh}^{Lip}) and stoichiometries (n) were calculated based on the previously published propagation rate constant (k_p = 894 M^{-1} s^{-1}) for STY-BODIPY and the rate of initiation ($R_i = 2.55 \times 10^{-9}$ s^{-1}) for the described experimental conditions.[19,22]

Inhibition of Ferroptosis of RSL3 Induced Cells. Pfa-1 cells (~3000 in 100 μL) were seeded in 96-well plates and incubated overnight. The media was removed the following day. Cells were washed twice with PBS, and suspended in new media and treated with the RTA compounds of interest for 30 minutes before the addition of (1S,3R)-RSL3 (100 nM) to a final volume of 100 μL. Cell viability was determined 6 hours later using the AquaBluer assay (MultiTarget Pharmaceuticals, LLC) as per the manufacturer's instructions. Cell viability was calculated by normalizing the data with untreated controls. Each experiment was carried out in six analytical replicates per concentration of RTA.

4.6 References

(1) Di Paolo, G.; Kim, T.-W. *Nat. Rev. Neurosci.* **2011**, *12*, 284.

(2) Barnham, K. J.; Masters, C. L.; Bush, A. I. *Nat. Rev. Drug Discov.* **2004**, *3*, 205.

(3) Hussain, S. P.; Hofseth, L. J.; Harris, C. C. *Nat. Rev. Cancer* **2003**, *3*, 276.

(4) Benz, C. C.; Yau, C. *Nat. Rev. Cancer* **2008**, *8*, 875.

(5) Finkel, T.; Holbrook, N. J. *Nature* **2000**, No. 408, 239.

(6) Burton, G. W.; Ingold, K. U. *J. Am. Chem. Soc.* **1981**, *103*, 6472.

(7) Dixon, S. J.; Lemberg, K. M.; Lamprecht, M. R.; Skouta, R.; Zaitsev, E. M.; Gleason, C. E.; Patel, D. N.; Bauer, A. J.; Cantley, A. M.; Yang, W. S.; Morrison, B.; Stockwell, B. R. *Cell* **2012**, *149*, 1060.

(8) Friedmann Angeli, J. P.; Schneider, M.; Proneth, B.; Tyurina, Y. Y.; Tyurin, V. A.; Hammond, V. J.; Herbach, N.; Aichler, M.; Walch, A.; Eggenhofer, E.; Basavarajappa, D.; Radmark, O.; Kobayashi, S.; Seibt, T.; Beck, H.; Neff, F.; Esposito, I.; Wanke, R.; Forster, H.; Yefremova, O.; Heinrichmeyer, M.; Bornkamm, G. W.; Geissler, E. K.; Thomas, S. B.; Stockwell, B. R.; O'Donnell, V. B.; Kagan, V. E.; Schick, J. A.; Conrad, M. *Nat. Cell Biol.* **2014**, *16*, 1180.

(9) Niki, E. *Chem. Phys. Lipids* **1987**, *44*, 227.

(10) Banjac, A.; Perisic, T.; Sato, H.; Seiler, A.; Bannai, S.; Weiss, N.; Kolle, P.; Tschoep, K.; Issels, R. D.; Daniel, P. T.; Conrad, M.; Bornkamm, G. W. *Oncogene* **2008**, *27*, 1618.

(11) Yagoda, N.; von Rachenberg, M.; Zaganjor, E.; Bauer, A. J.; Yang, W. S.; Fridman, D. J.; Wolpaw, A. J.; Smukste, I.; Peltier, J. M.; Boniface, J. J.; Smith, R.; Lessnick, S. L.; Sahasrabudhe, S.; Stockwell, B. R. *Nature* **2007**, *447*, 864.

(12) Yang, W. S.; Stockwell, B. R. *Chem. Biol.* **2008**, *15*, 234.

(13) Yin, H.; Xu, L.; Porter, N. A. *Chem. Rev.* **2011**, *111*, 5944.

(14) Pryor, W. A.; Porter, N. A. *Free Radic. Biol. Med.* **1990**, *8*, 541.

(15) Girotti, A. W. *J. Lipid Res.* **1998**, *39*, 1529.

(16) Haeggstrom, J. Z.; Funk, C. D. *Lipoxygenase Leukot. Pathways Biochem. Biol. Roles Dis.* **2011**, *111*, 5866.

(17) Morison, B.; Pringle, A. K.; McManus, T.; Ellard, J.; Bradley, M.; Signorelli, F.; Iannotti, F.; Sundstrom, L. E. *Br. J. Pharmacol.* **2002**, *137*, 1255.

(18) Sundstrom, L. E.; Morrison, B.; Bradley, M.; Pringle, A. K. *Drug Discov. Today* **2005**, *10*, 993.

(19) Zilka, O.; Shah, R.; Li, B.; Friedmann Angeli, J. P.; Griesser, M.; Conrad, M.; Pratt, D. A. *ACS Cent. Sci.* **2017**, *3* (3), 232.

(20) Takahashi, M.; Tsuchiya, J.; Niki, E. *J. Am. Chem. Soc.* **1988**, *111*, 6350.

(21) Gotoh, N.; Noguchi, N.; Tsuchiya, J.; Morita, K.; Sakai, H.; Shimasaki, H.; Niki, E. *Free Radic. Res.* **1996**, *24*, 123.

(22) Shah, R.; Margison, K. D.; Pratt, D. A. *ACS Chem. Biol.* **2017**, *12*, 2538.

(23) Valgimigli, L.; Banks, J. T.; Lusztyk, J.; Ingold, K. U. *J. Org. Chem.* **1999**, *64*, 3381.

(24) Niki, E.; Noguchi, N. *Acc. Chem. Res.* **2004**, *37*, 45.

(25) Abraham, M. H.; Grellier, P. L.; Prior, D. V.; Morris, J. J.; Taylor, P. J. *J. Chem. Soc. Perkin Trans. 2* **1990**, 521.

(26) Barclay, L. R. C.; Ingold, K. U. *J. Am. Chem. Soc.* **1981**, *103*, 6478.

(27) Shi, H.; Noguchi, N.; Niki, E. *Free Radic. Biol. Med.* **1999**, *27*, 334.

(28) Sato, K.; Niki, E.; Shimasaki, H. *Arch. Biochem. Biophys.* **1990**, *279*, 402.

(29) Mitchell, S. C. *Curr. Drug Targets* **2006**, *7* (9), 1181.

(30) Moosmann, B.; Skutella, T.; Beyer, K.; Behl, C. *Biol. Chem.* **2001**, *382*, 1601.

(31) Hajieva, P.; Mocko, J. B.; Moosmann, B.; C., B. *J. Neurochem.* **2009**, *110*, 118.

4.7 Supporting Information

4.7.1 Inhibited Egg-PC Co-Autoxidation Traces

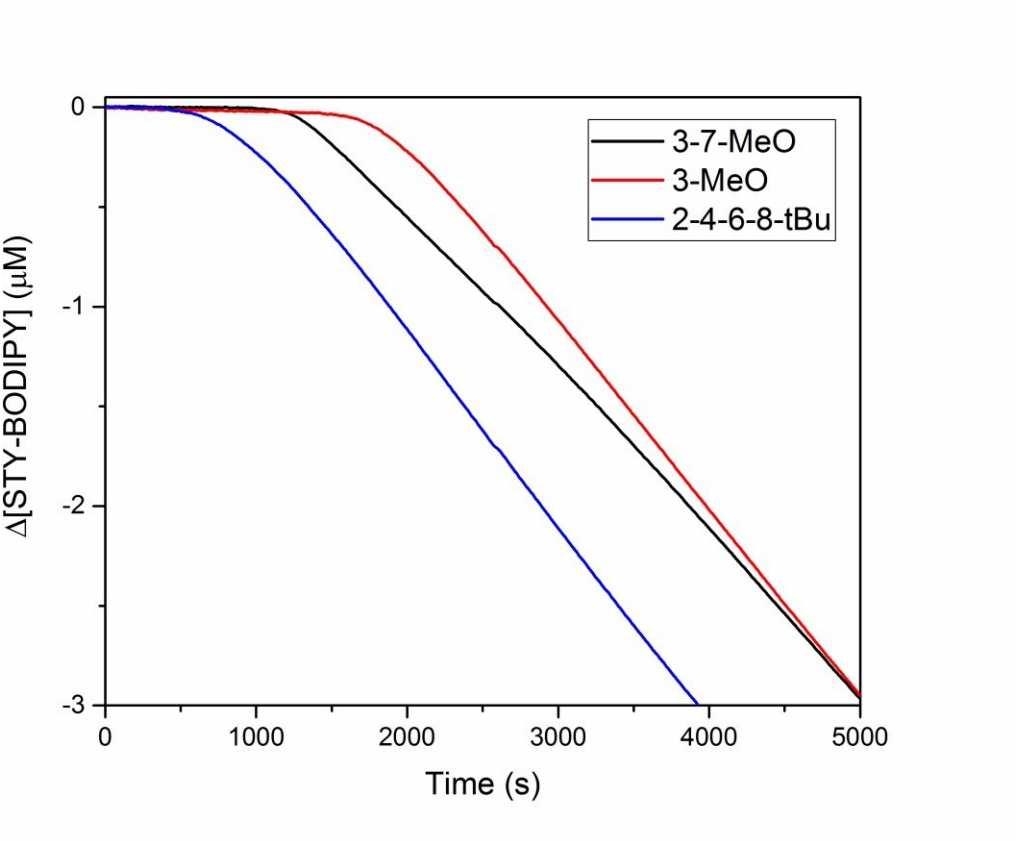

Figure S4.1. Inhibited autoxidation of STY-BODIPY (10 μM) in EGG-PC (1 mM) initiated with MeOAMVN (0.2 mM) monitored at 565 nm (121200 M^{-1} cm^{-1}): 2 μM 3-7-MeO-Phenoxazine **4.16** (**black**); 2 μM 3-MeO-Phenoxazine **4.14** (**red**); 2 μM 2,4,6,8-tBu-Phenoxazine **4.15** (**blue**).

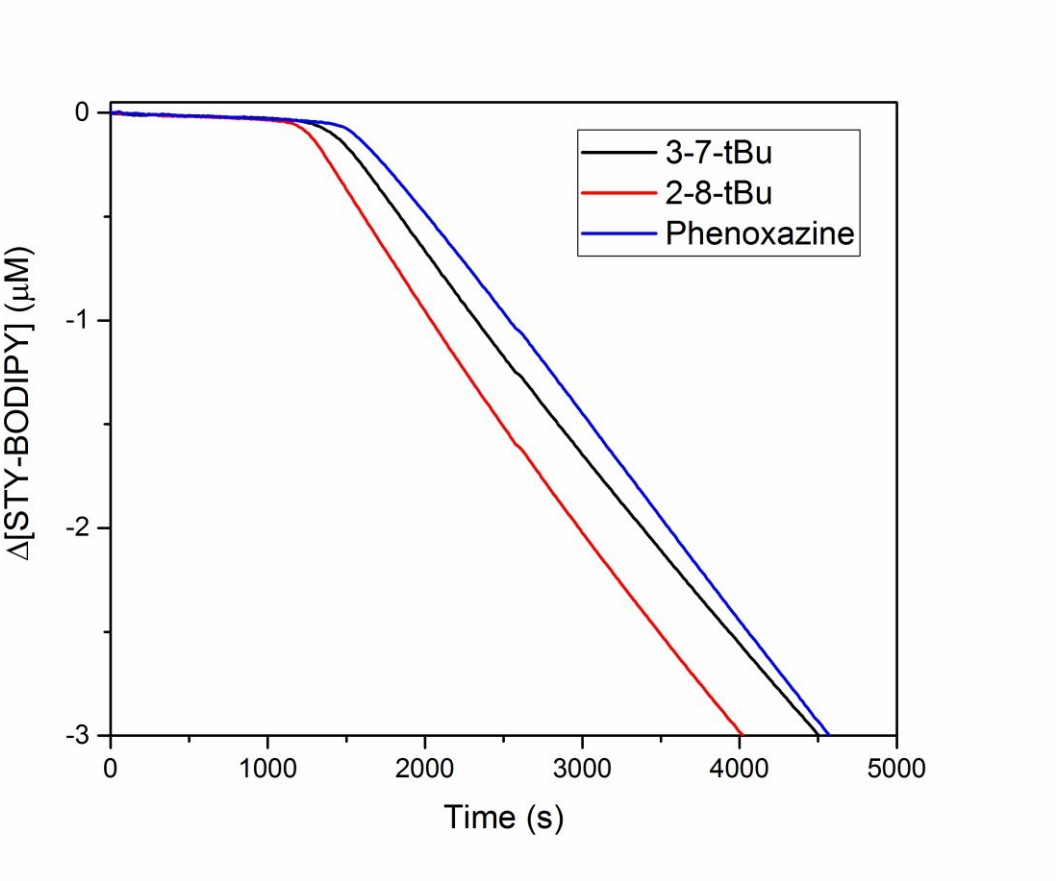

Figure S4.2. Inhibited autoxidation of STY-BODIPY (10 μM) in EGG-PC (1 mM) initiated with MeOAMVN (0.2 mM) monitored at 565 nm (121200 M^{-1} cm^{-1}): 2 μM 3,7-tBu-Phenoxazine **4.13** (**black**); 2 μM 2,8-tBu-Phenoxazine **4.12** (**red**); 2 μM Phenoxazine **4.1** (**blue**).

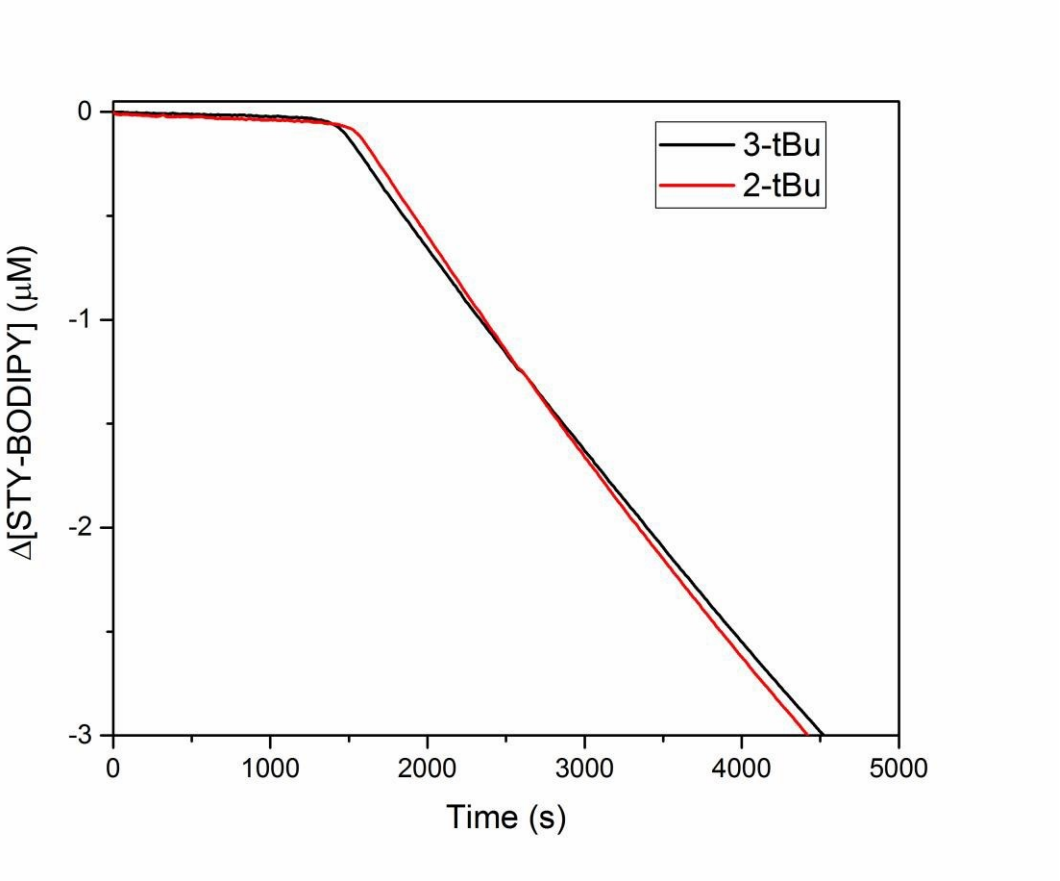

Figure S4.3. Inhibited autoxidation of STY-BODIPY (10 μM) in EGG-PC (1 mM) initiated with MeOAMVN (0.2 mM) monitored at 565 nm (121200 M^{-1} cm^{-1}): 2 μM 3-tBu-Phenoxazine **4.11** (**black**); 2 μM 2-tBu-Phenoxazine **4.10** (**red**).

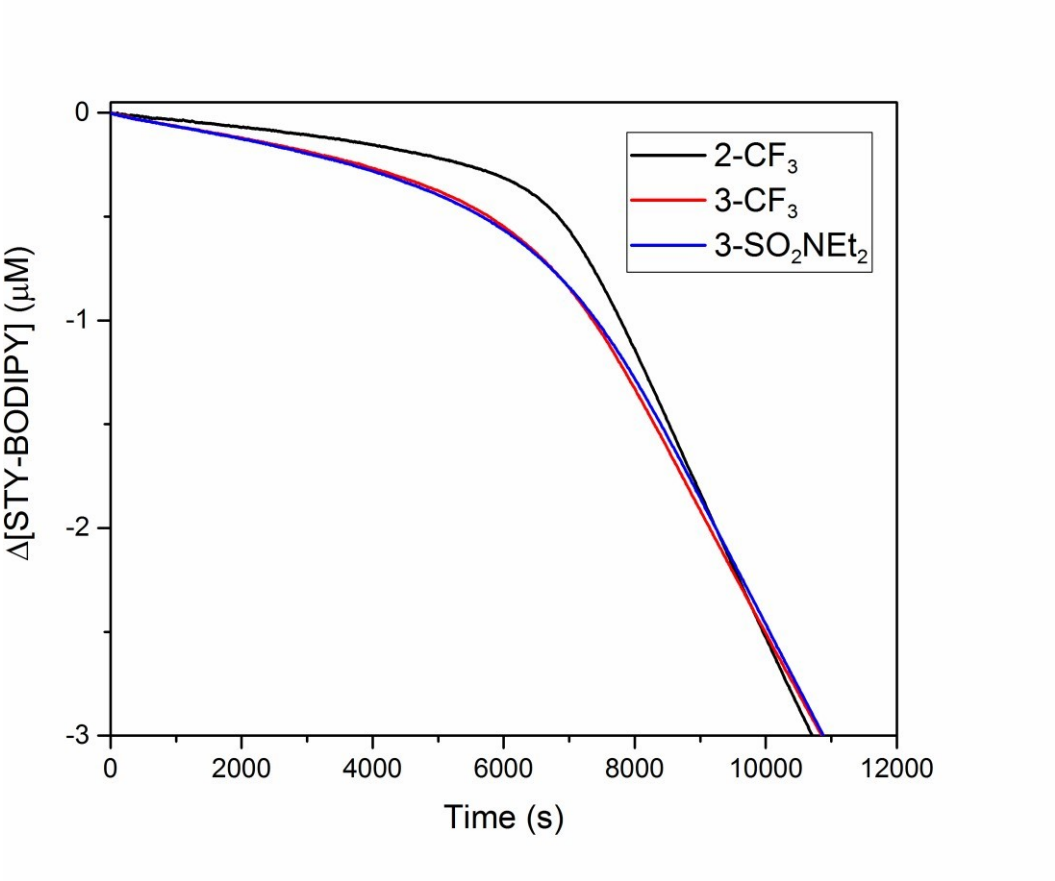

Figure S4.4. Inhibited autoxidation of STY-BODIPY (10 μM) in EGG-PC (1 mM) initiated with MeOAMVN (0.2 mM) monitored at 565 nm (121200 M^{-1} cm^{-1}): 6 μM 2-CF_3-Phenoxazine **4.9** (**black**); 6 μM 3-CF_3-Phenoxazine **4.7** (**red**); 6 μM 3-SO_2NEt_2-Phenoxazine **4.6** (**blue**).

4.7.2 Cell Viability Curves

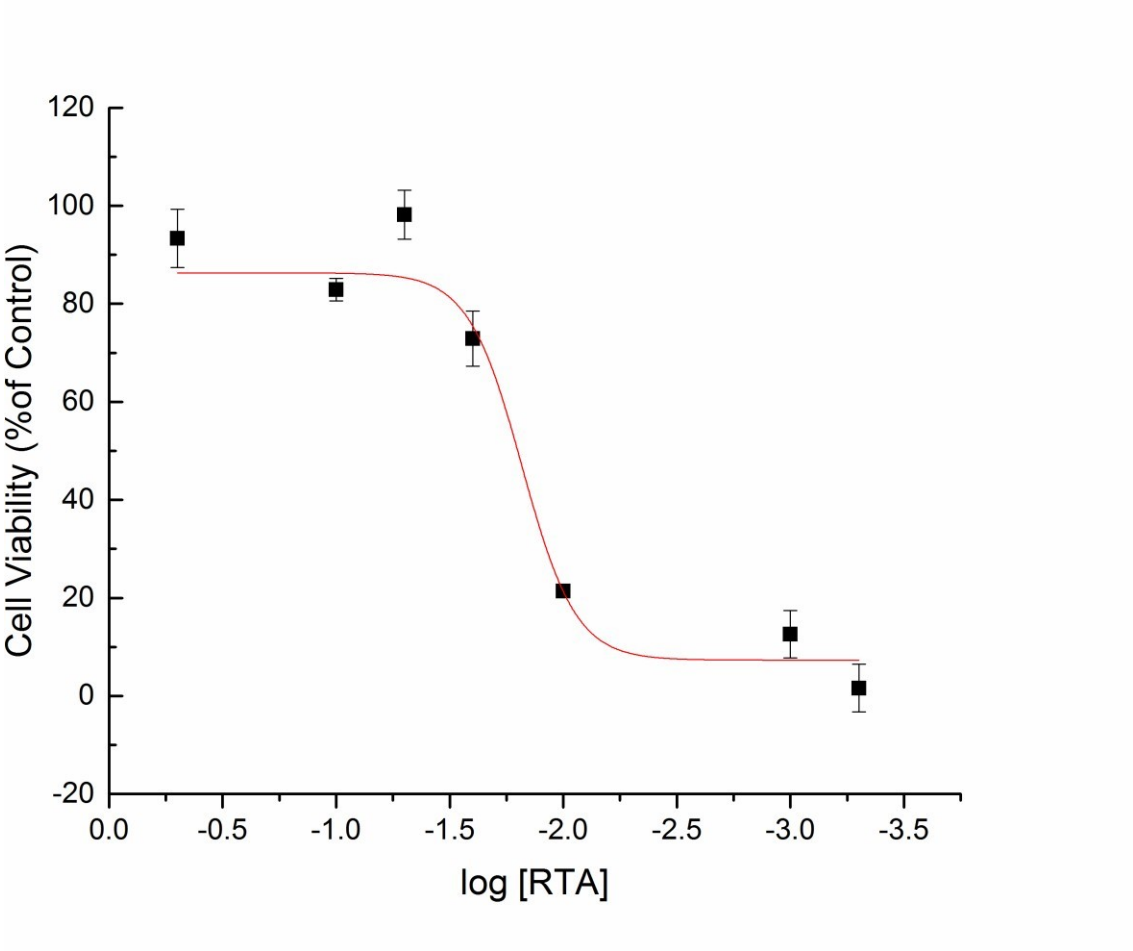

Figure S4.5. Normalized response curve for cell viability of RSL-3 induced Pfa-1 cells treated with 3,7-MeO-Phenoxazine **4.16**.

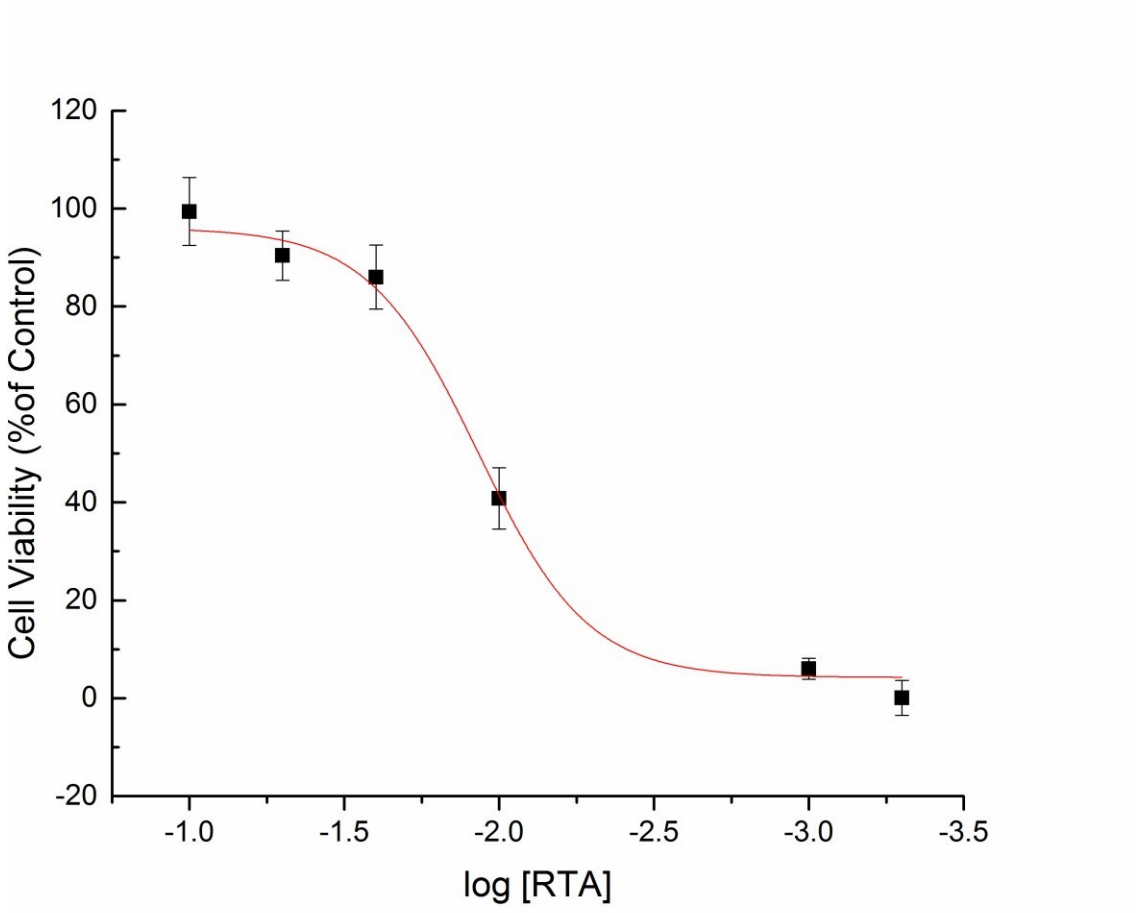

Figure S4.6. Normalized response curve for cell viability of RSL-3 induced Pfa-1 cells treated with 3,7-tBu-Phenoxazine **4.13**.

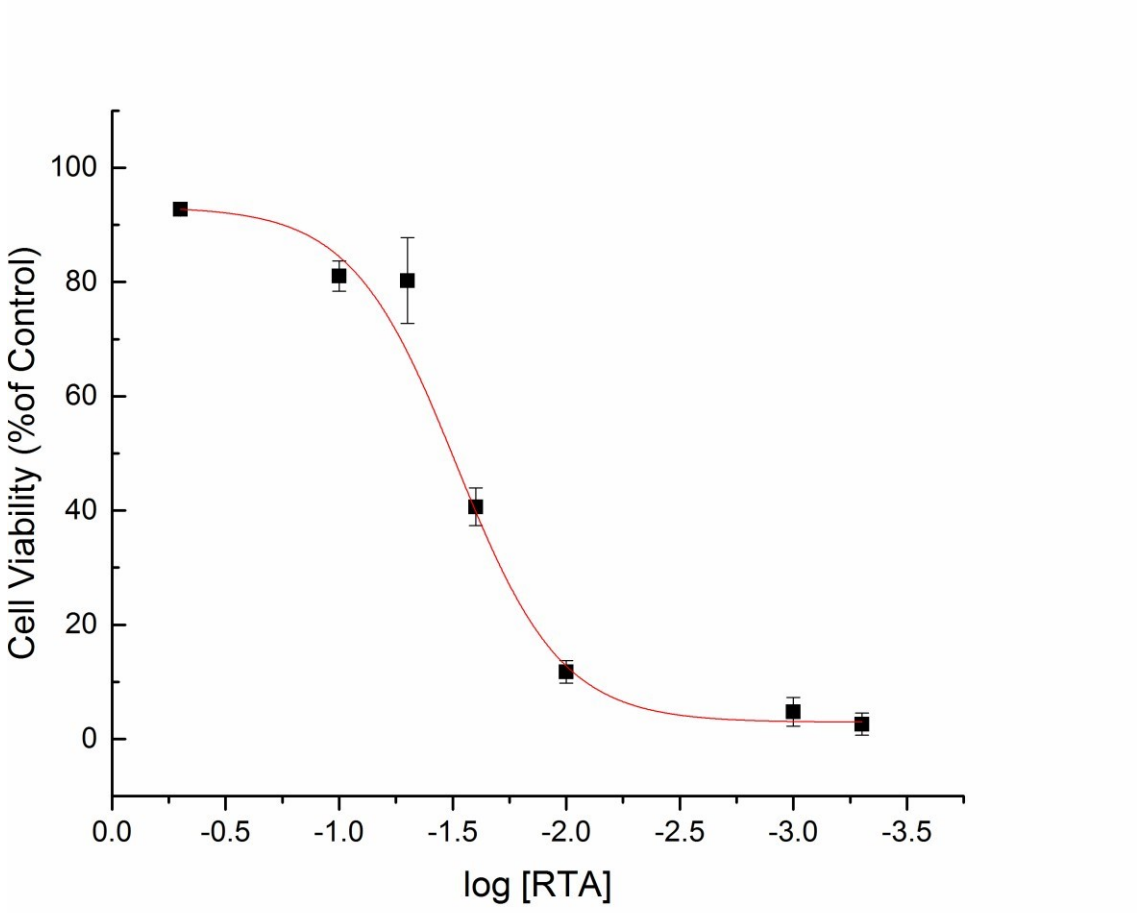

Figure S4.7. Normalized response curve for cell viability of RSL-3 induced Pfa-1 cells treated with 3-MeO-Phenoxazine **4.14**.

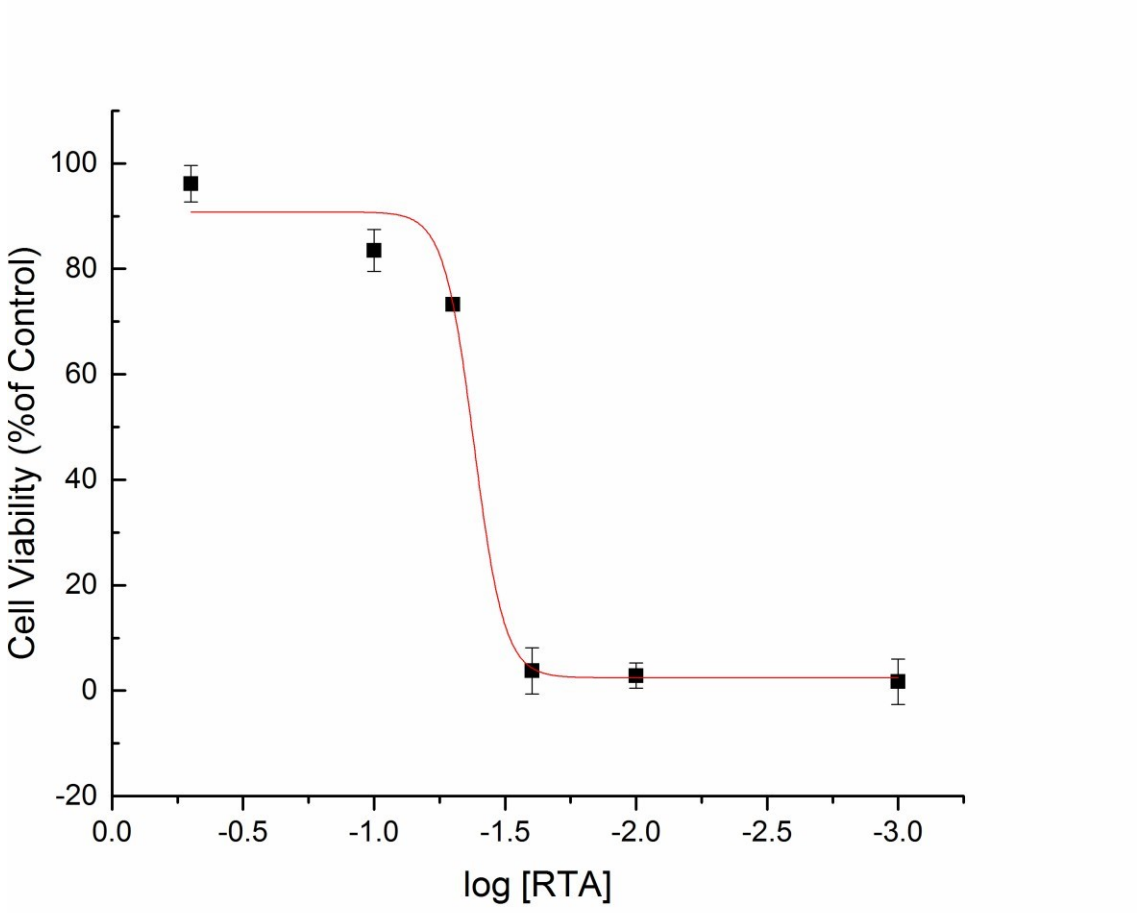

Figure S4.8. Normalized response curve for cell viability of RSL-3 induced Pfa-1 cells treated with 2,8-tBu-Phenoxazine **4.12**.

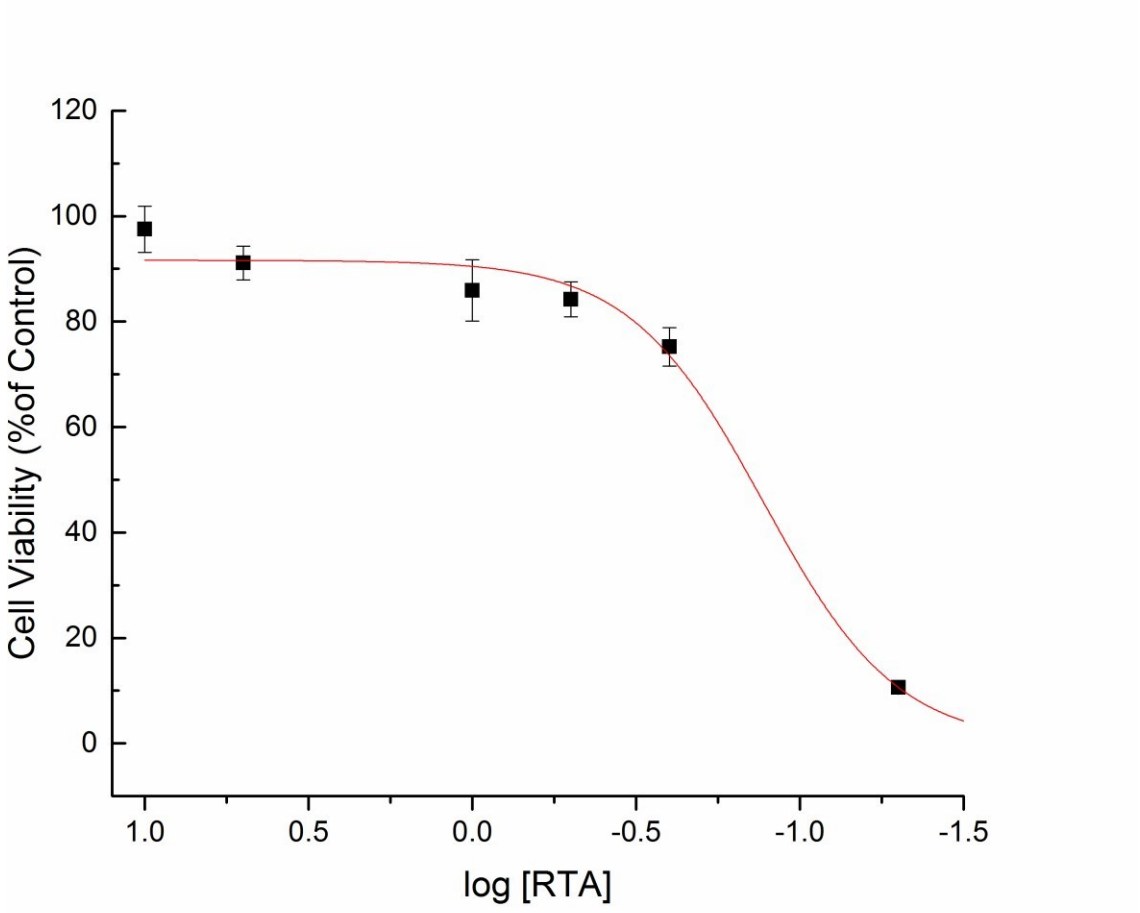

Figure S4.9. Normalized response curve for cell viability of RSL-3 induced Pfa-1 cells treated with 3-CN-Phenoxazine **4.5**.

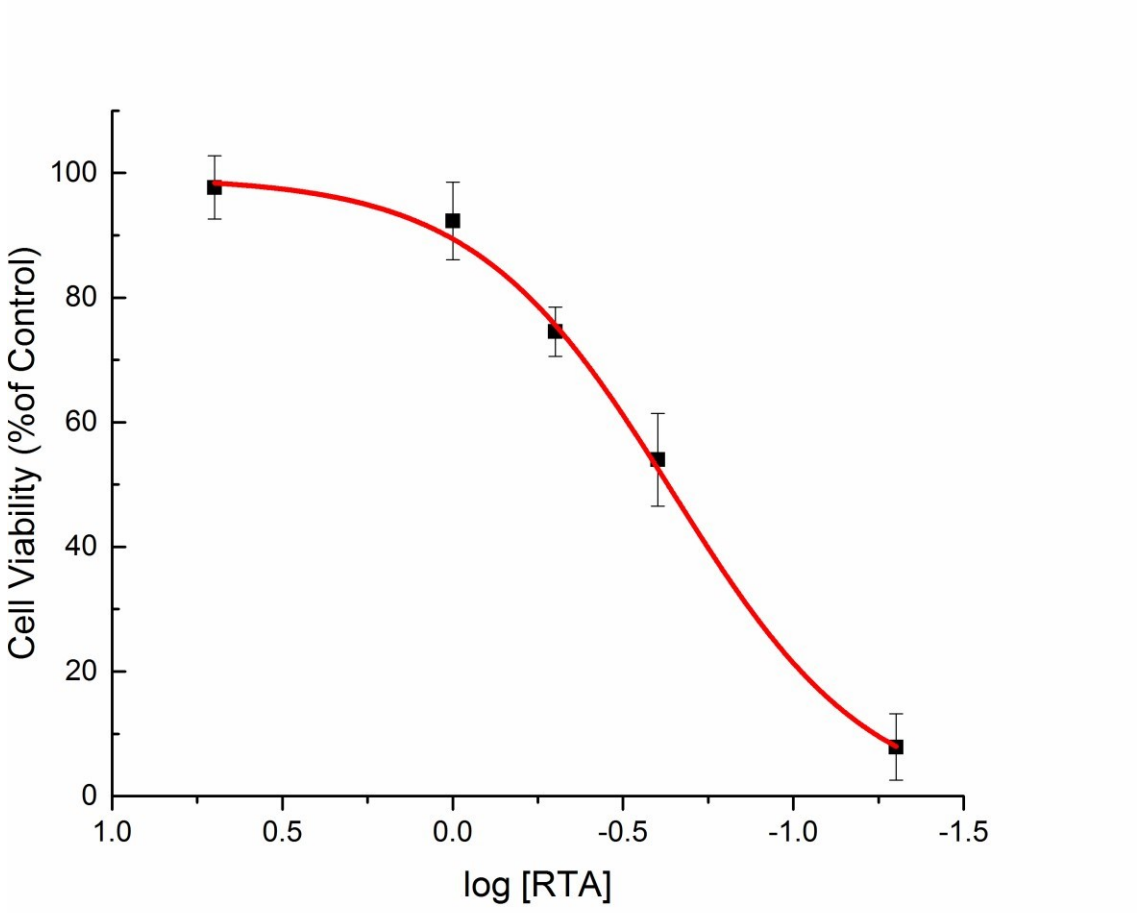

Figure S4.10. Normalized response curve for cell viability of RSL-3 induced Pfa-1 cells treated with 3-NO_2-Phenoxazine **4.4**.

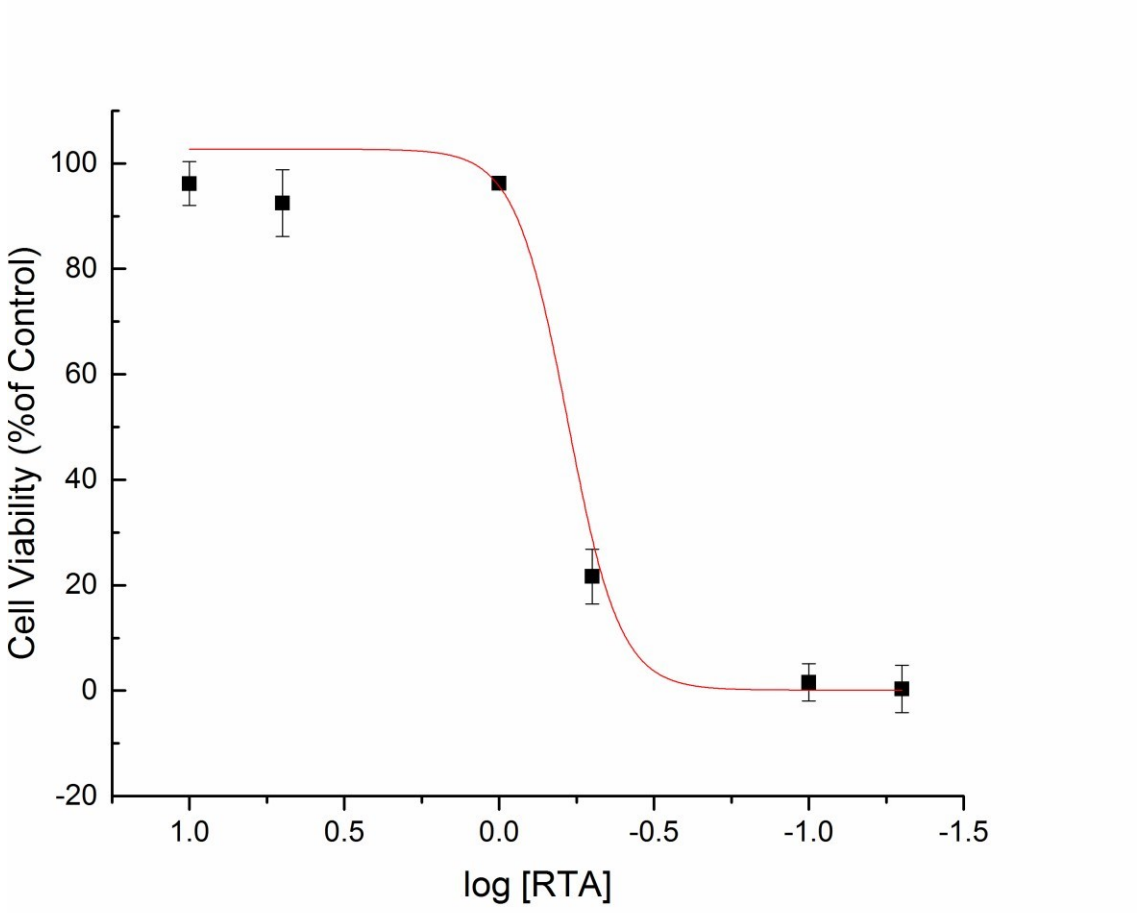

Figure S4.11. Normalized response curve for cell viability of RSL-3 induced Pfa-1 cells treated with 3-CN-7-NO_2-Phenoxazine **4.3**.

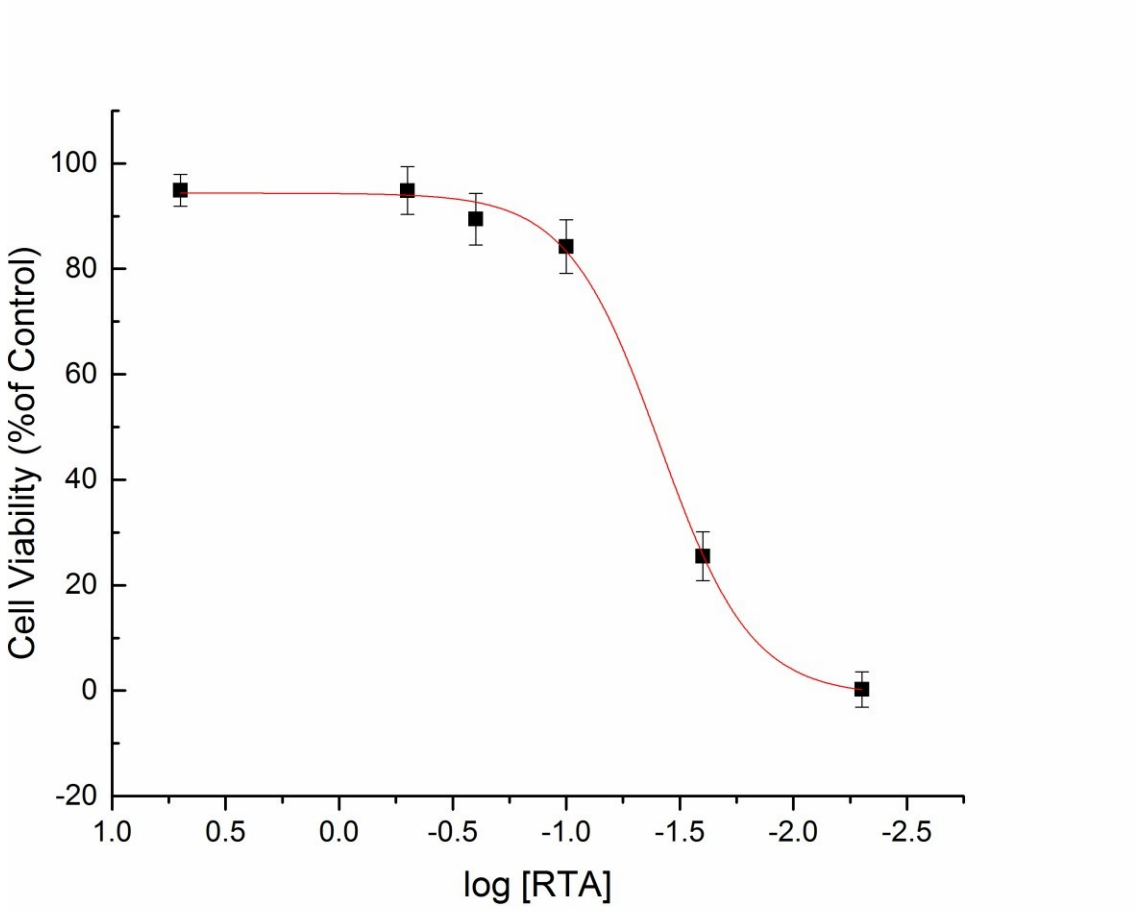

Figure S4.12. Normalized response curve for cell viability of RSL-3 induced Pfa-1 cells treated with 3-MeO-7-NO_2-Phenoxazine **4.8**.

211

4.7.3 Structures of Peripheral RTAs in Figure 4.1 and Figure 4.4

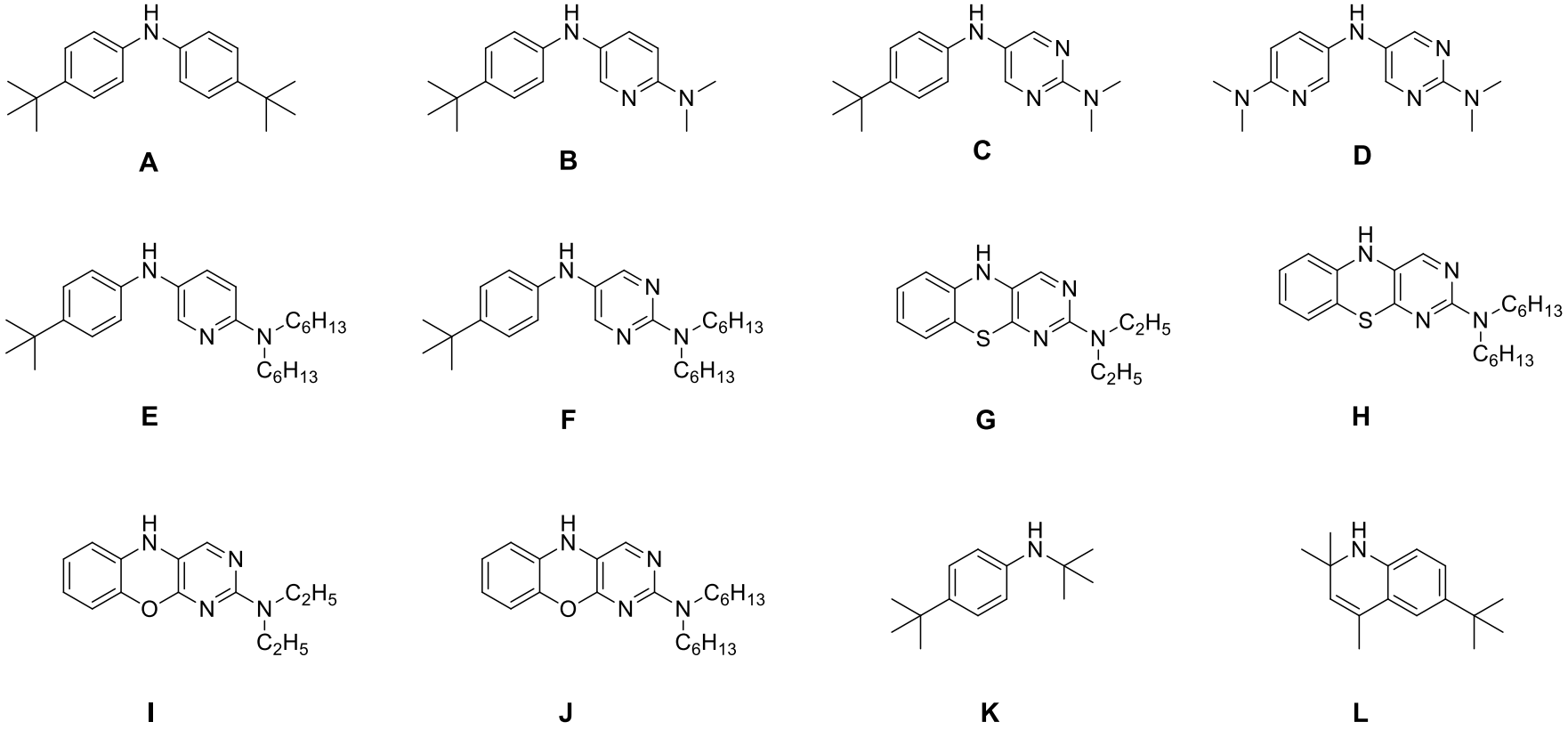

Chart S4.1. Structures of peripheral RTAs in Figures 4.1 and 4.5**.**

Appendix 1: NMR Spectra for Chapter 2

4-tert-Butyl-2-chloronitrobenzene (2.19) (impure/crude)

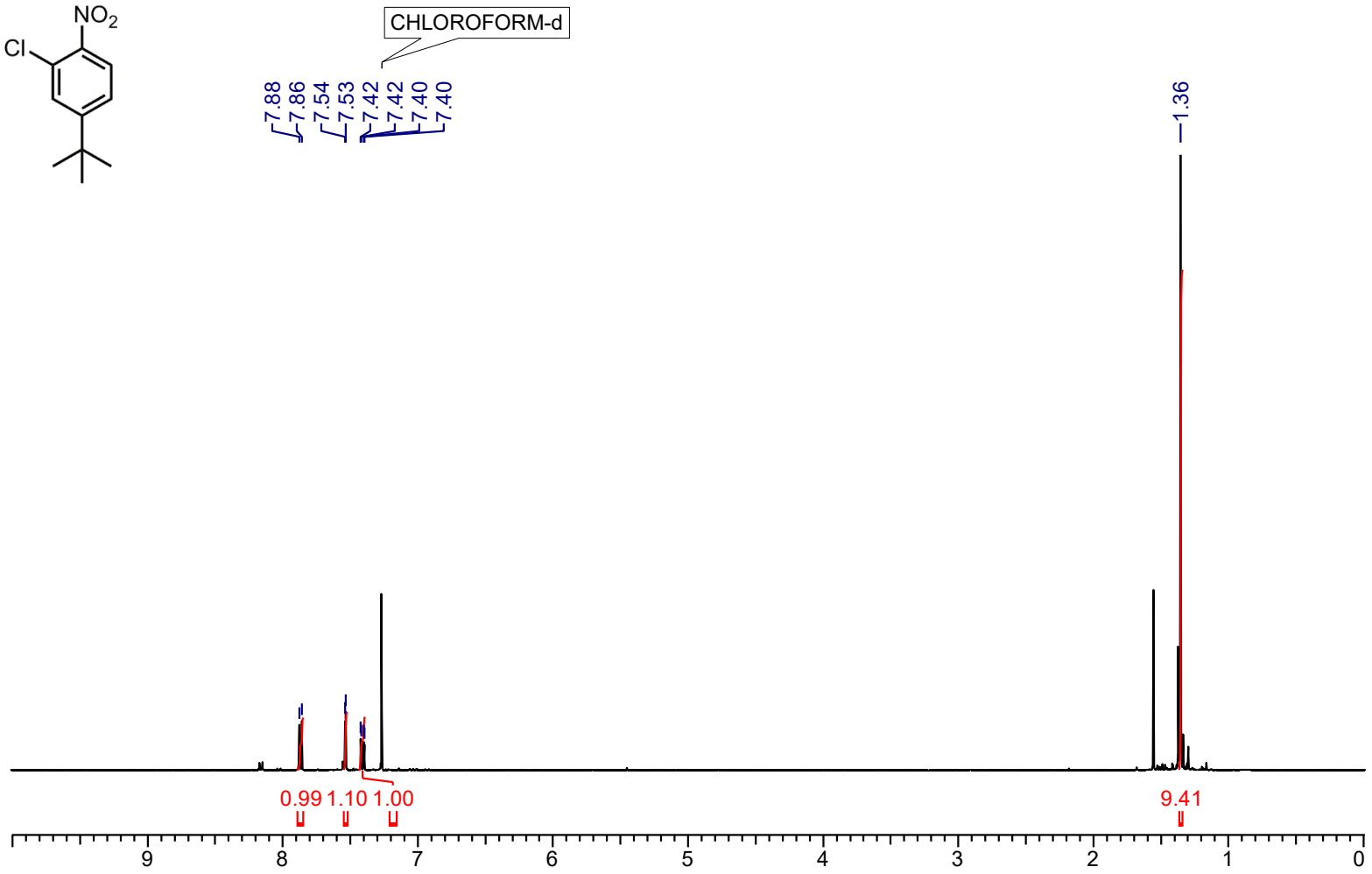

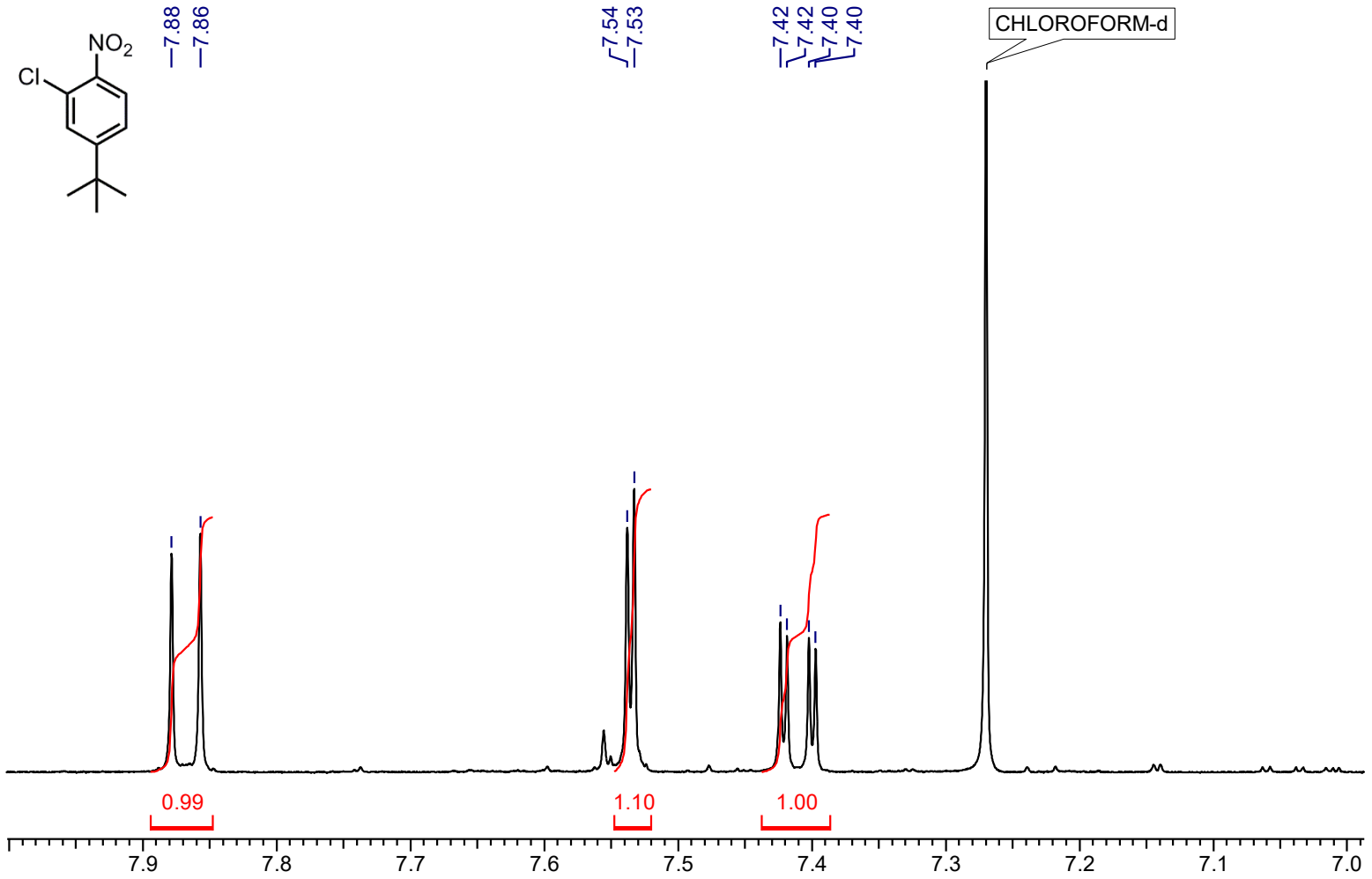
NO2
Cl
7.88
7.86
7.54
7.53
7.42
7.42
7.40
7.40
CHLOROFORM-d
0.99
1.10
1.00
7.9
7.8
7.7
7.6
7.5
7.4
7.3
7.2
7.1
7.0

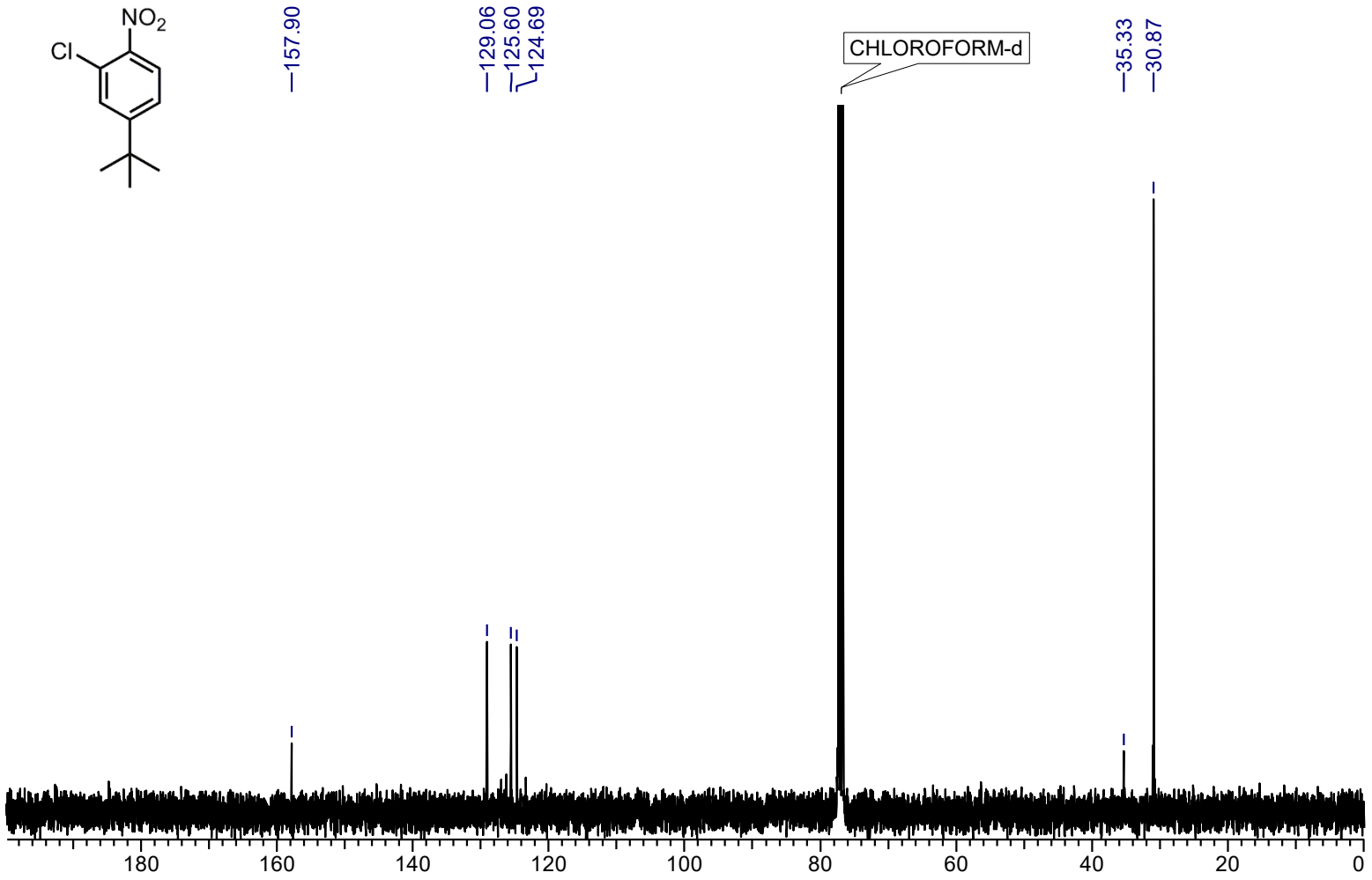
NO2
Cl
157.90
129.06
125.60
124.69
CHLOROFORM-d
35.33
30.87
180
160
140
120
100
80
60
40
20
0

4-tert-Butyl-1-iodo-2-(2-nitrophenoxy)benzene (2.20)

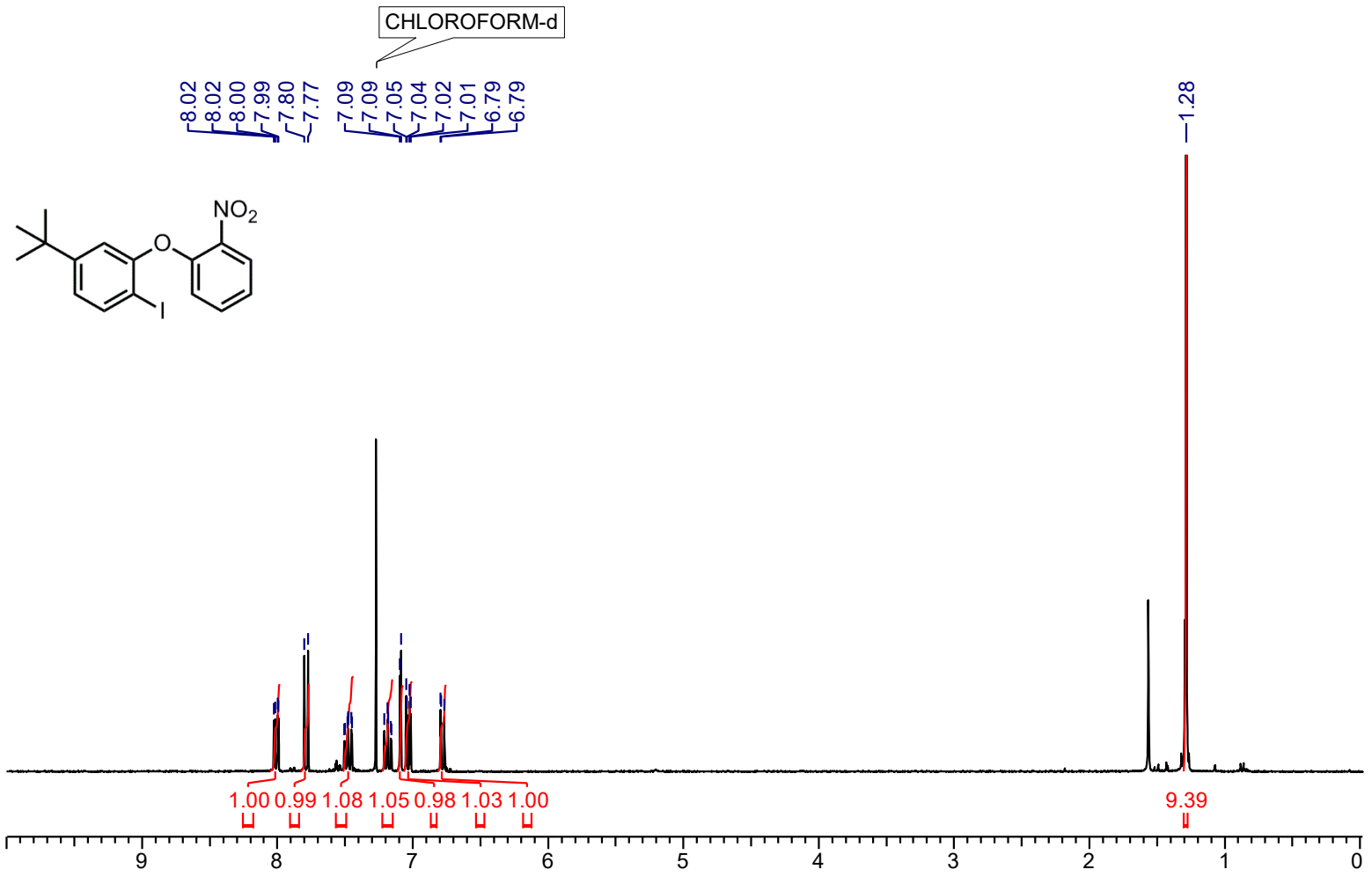

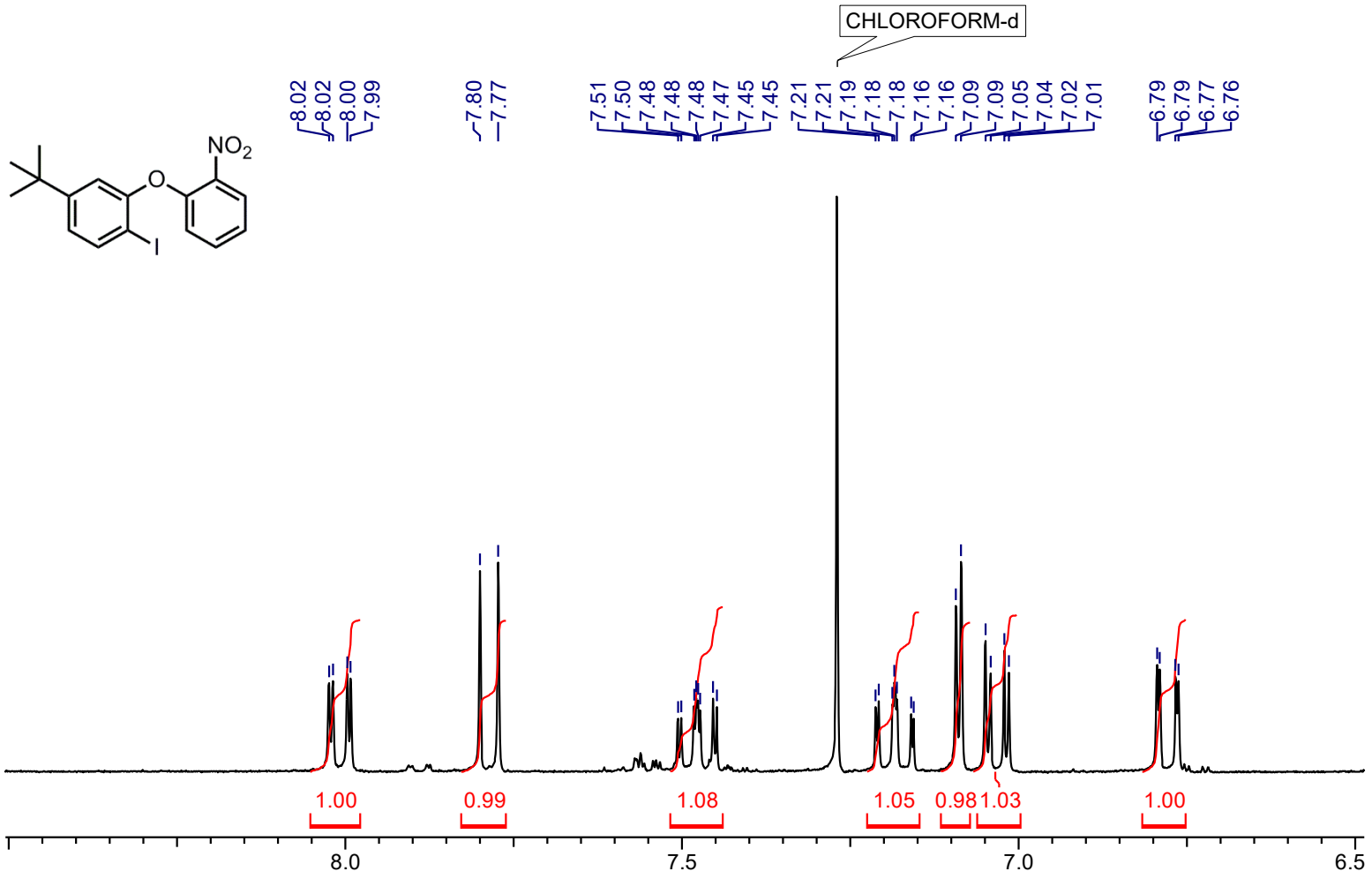
CHLOROFORM-d
8.02
8.02
8.00
7.99
7.80
7.77
7.51
7.50
7.48
7.48
7.48
7.47
7.45
7.45
7.21
7.21
7.19
7.18
7.18
7.16
7.16
7.09
7.09
7.05
7.04
7.02
7.01
6.79
6.79
6.77
6.76
NO2
O
I
1.00
0.99
1.08
1.05
0.98
1.03
1.00
8.0
7.5
7.0
6.5

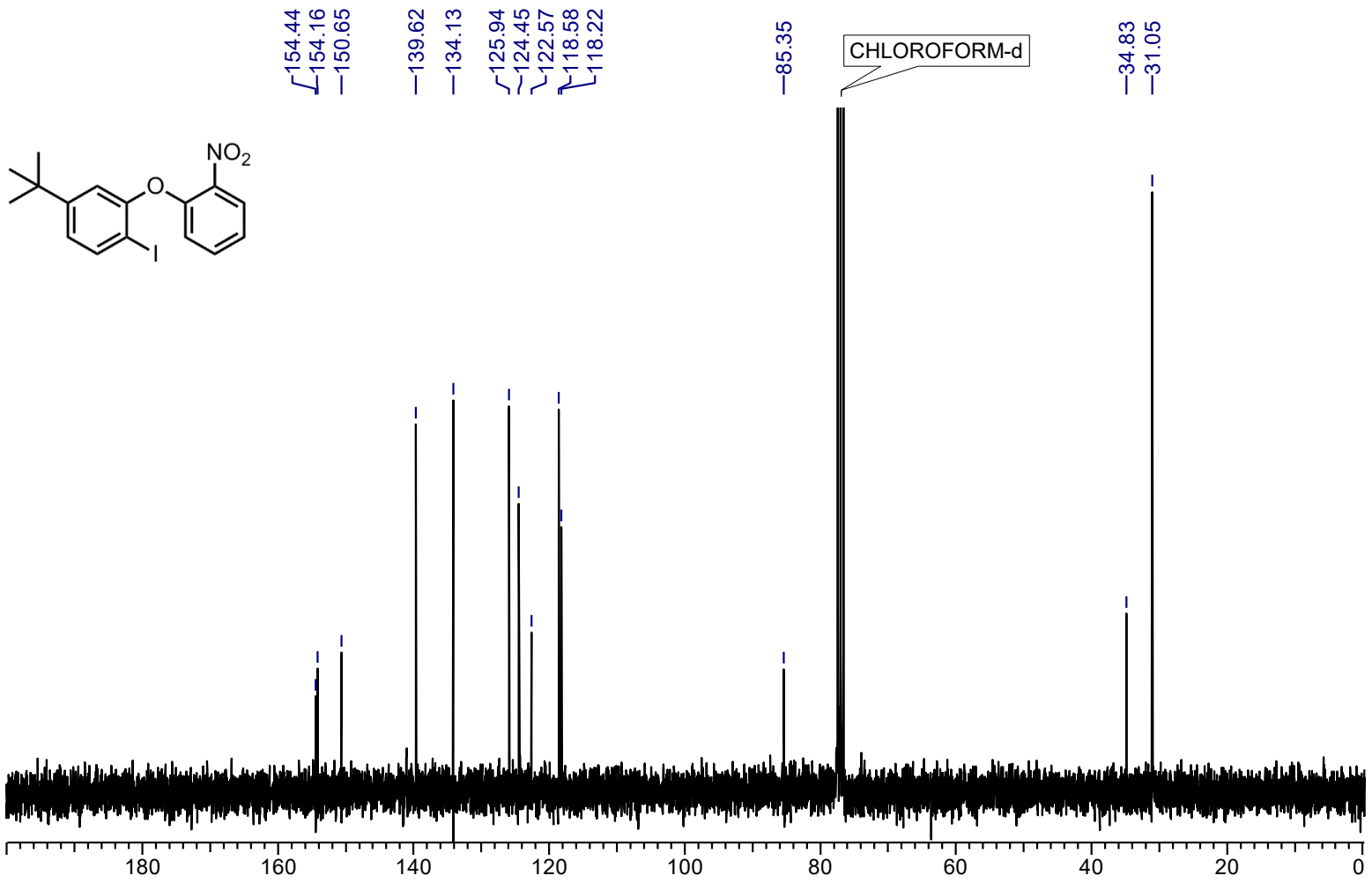
154.44
154.16
150.65
139.62
134.13
125.94
124.45
122.57
118.58
118.22
85.35
CHLOROFORM-d
34.83
31.05
NO2
O
I
180
160
140
120
100
80
60
40
20
0

4-(tert-Butyl)-2-(5-(tert-butyl)-2-iodophenoxy)-1-nitrobenzene (2.23)

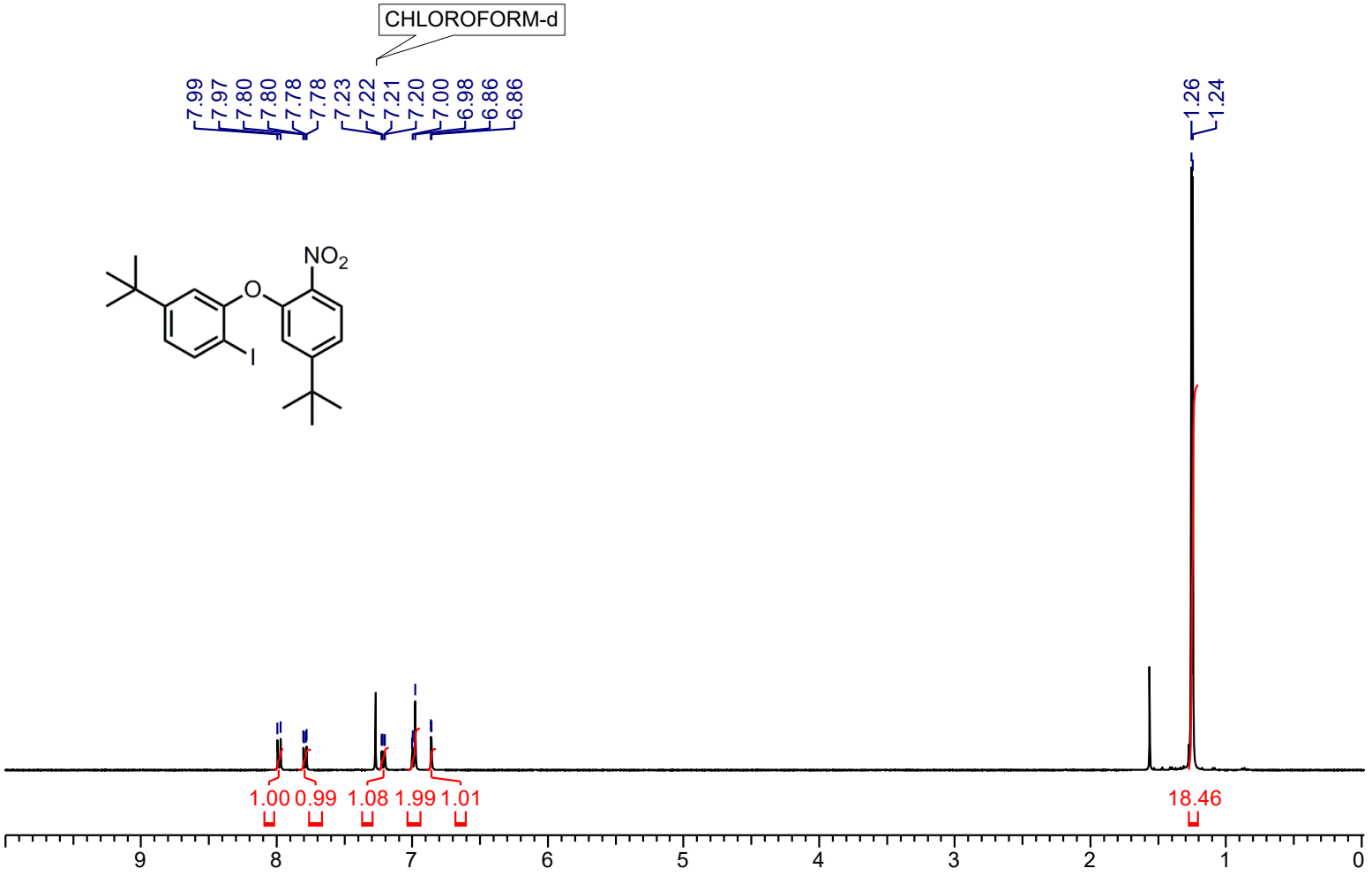

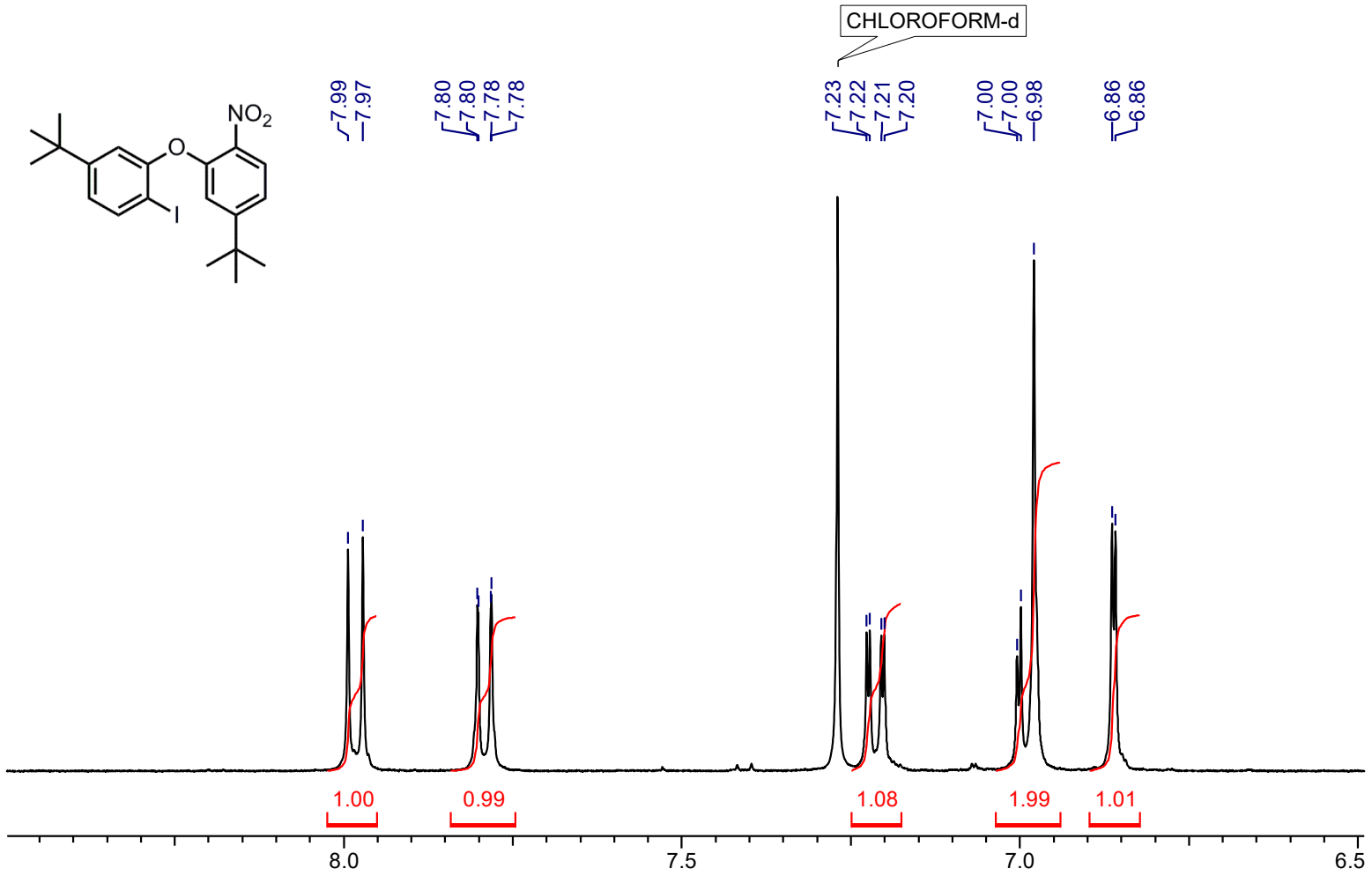
CHLOROFORM-d
7.99
7.97
7.80
7.80
7.78
7.78
7.23
7.22
7.21
7.20
7.00
7.00
6.98
6.86
6.86
NO2
O
I
1.00
0.99
1.08
1.99
1.01
8.0
7.5
7.0
6.5

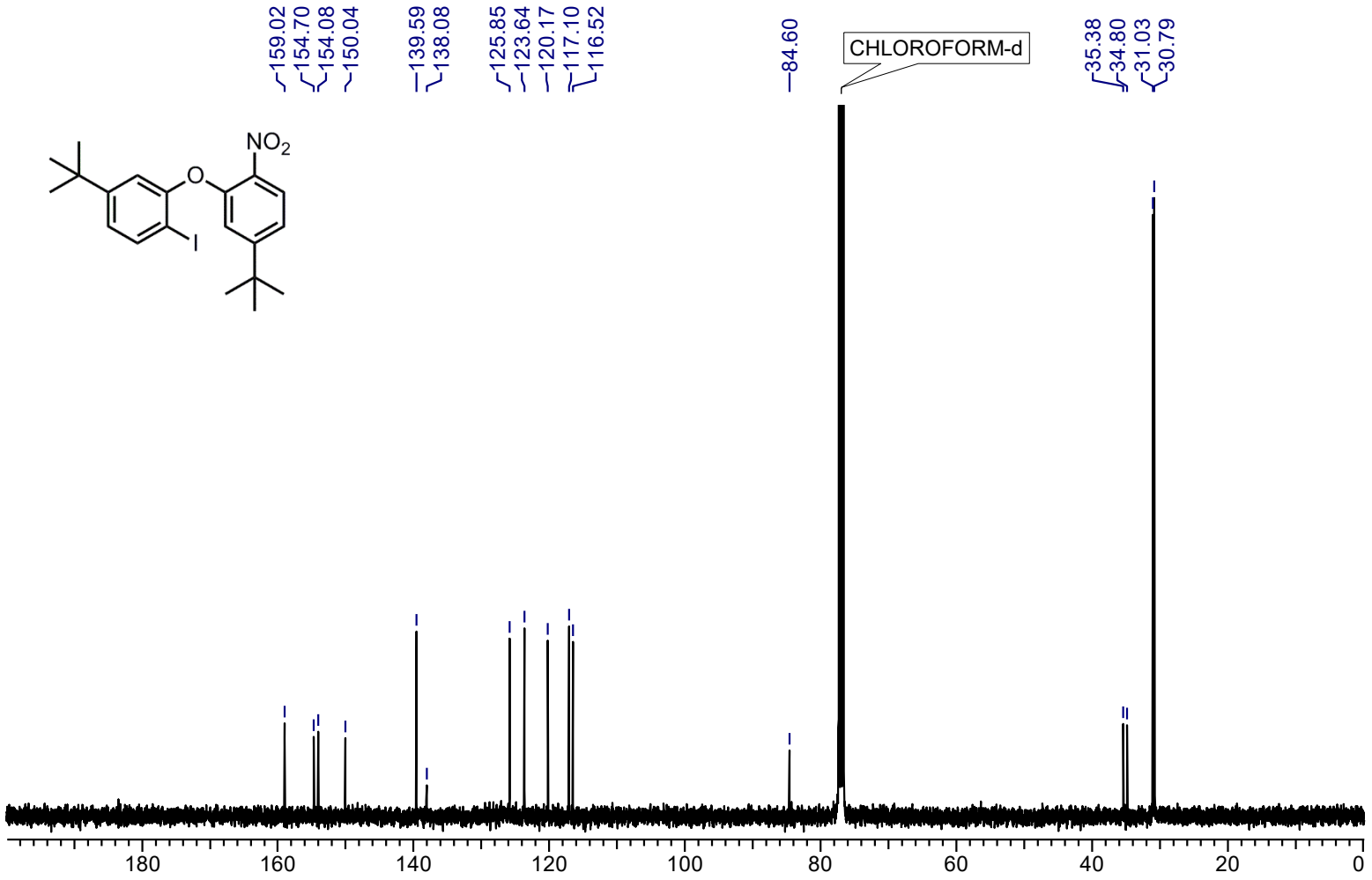
159.02
154.70
154.08
150.04
139.59
138.08
125.85
123.64
120.17
117.10
116.52
84.60
CHLOROFORM-d
35.38
34.80
31.03
30.79
NO2
O
I
180
160
140
120
100
80
60
40
20
0

1-(2-Bromophenoxy)-2-nitro-4-(trifluoromethyl)benzene (2.21)

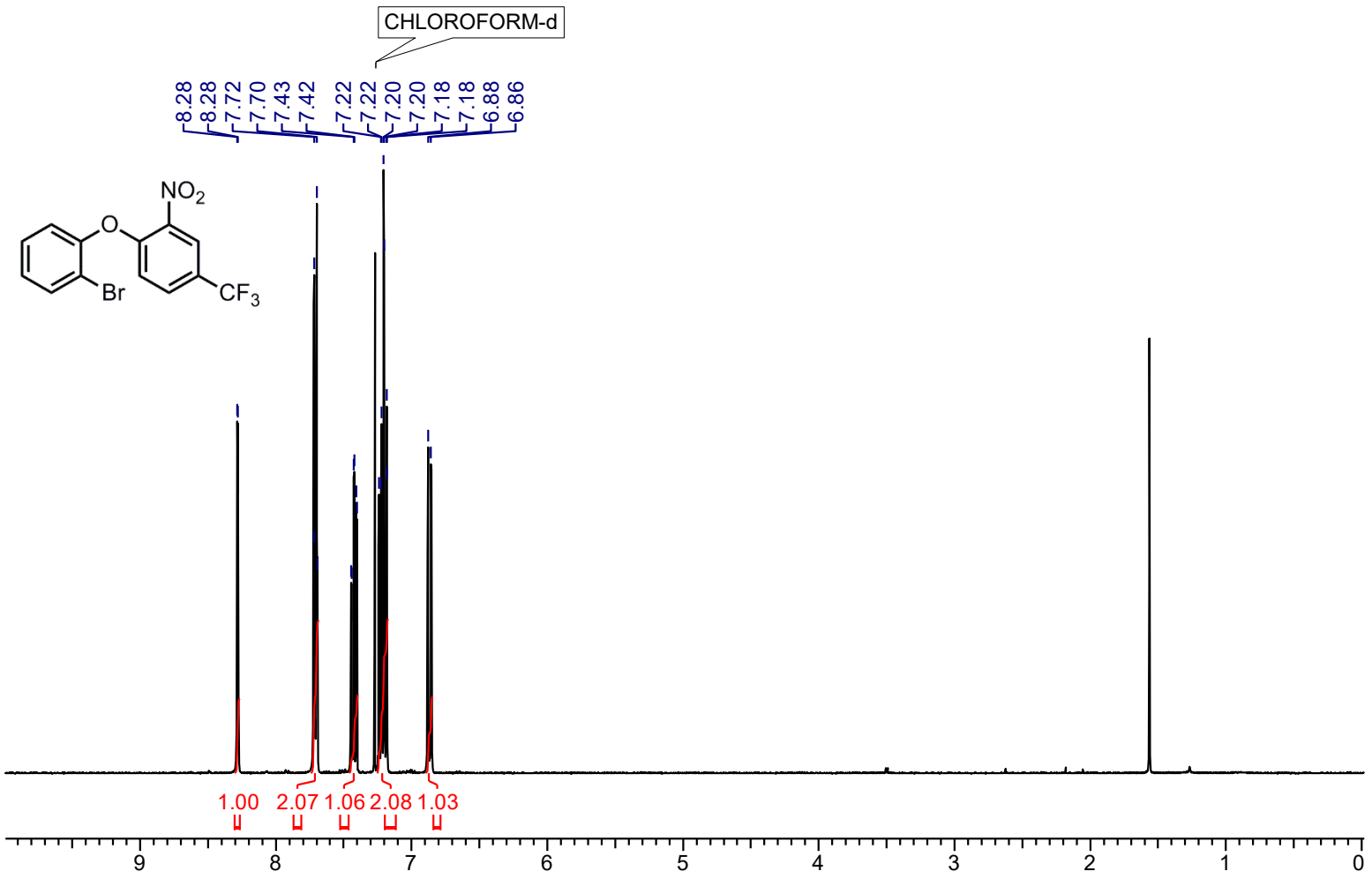

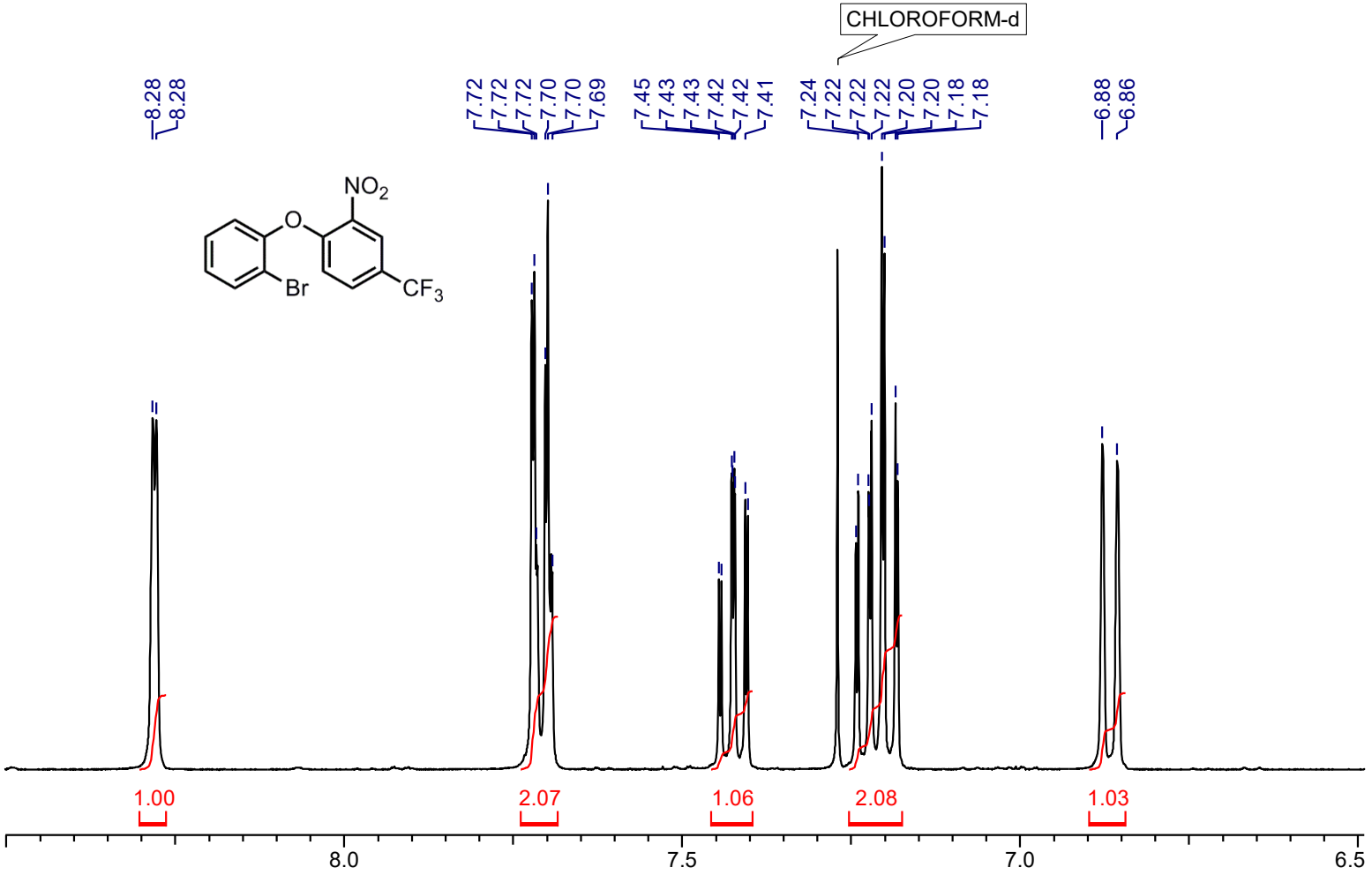
CHLOROFORM-d
8.28
8.28
7.72
7.72
7.72
7.70
7.70
7.69
7.45
7.43
7.43
7.42
7.42
7.41
7.24
7.22
7.22
7.22
7.20
7.20
7.18
7.18
6.88
6.86
NO2
O
Br
CF3
1.00
2.07
1.06
2.08
1.03
8.0
7.5
7.0
6.5

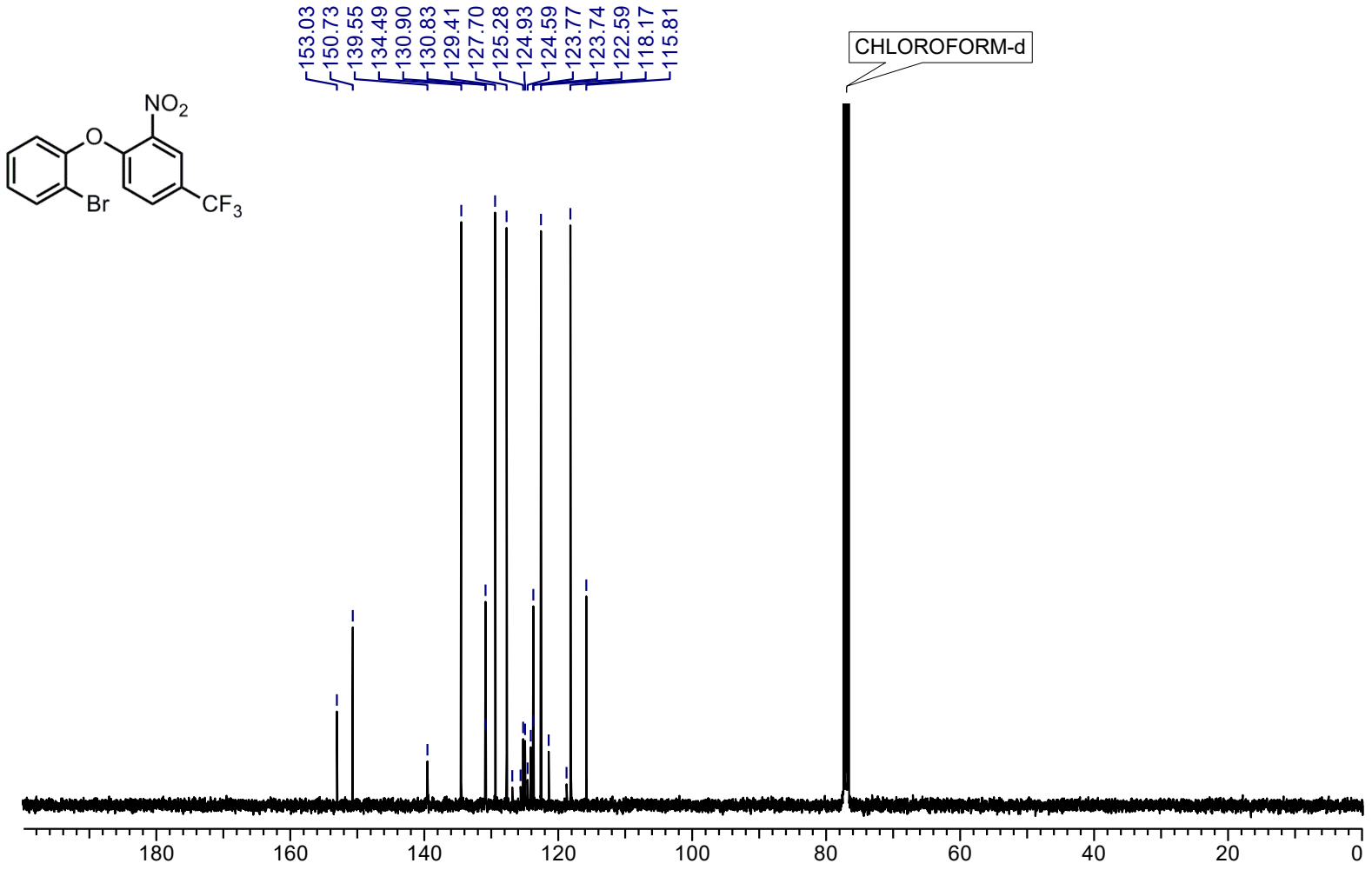
153.03
150.73
139.55
134.49
130.90
130.83
129.41
127.70
125.28
124.93
124.59
123.77
123.74
122.59
118.17
115.81
CHLOROFORM-d
NO2
O
Br
CF3
180
160
140
120
100
80
60
40
20
0

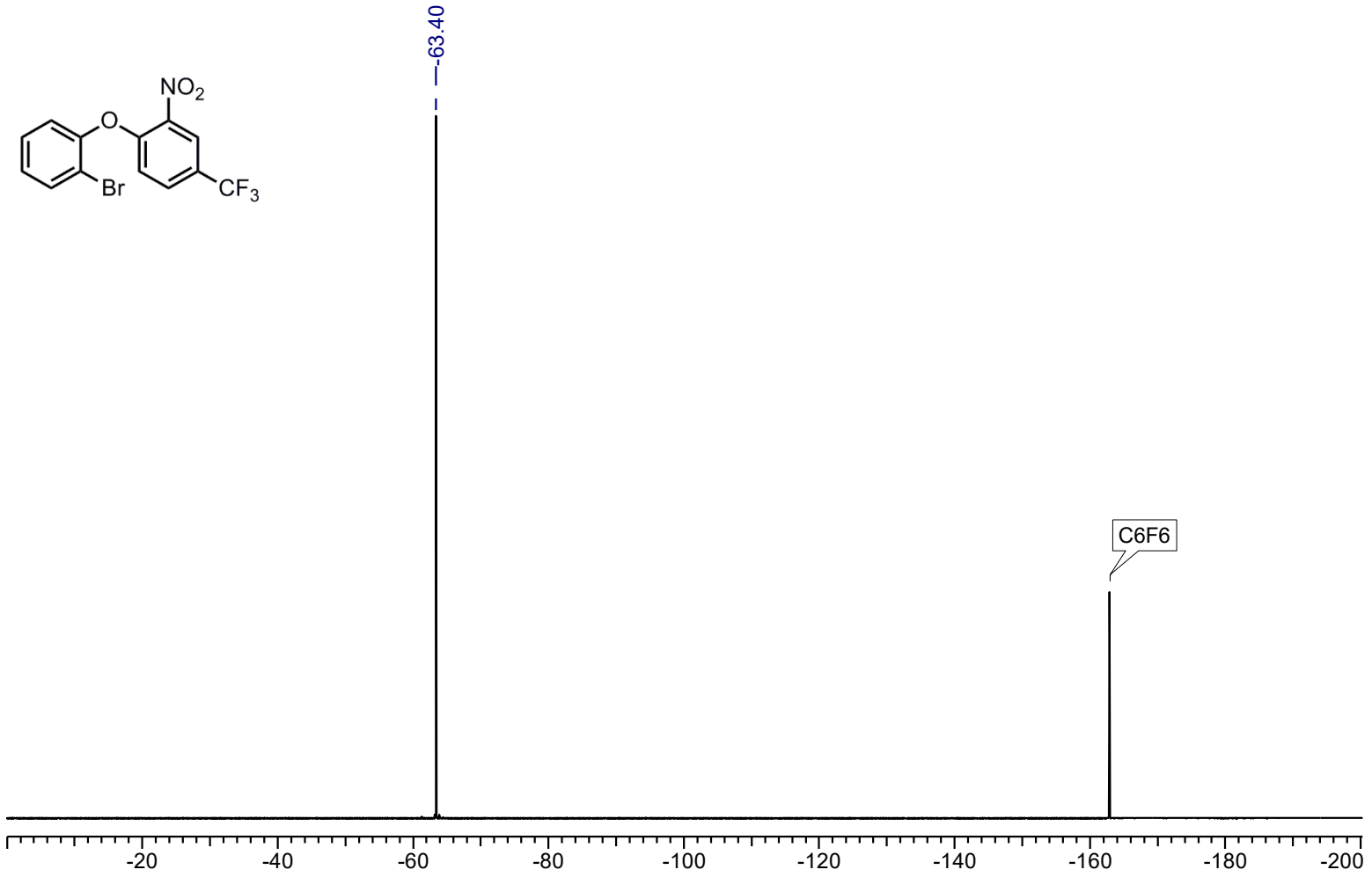
NO2
O
Br
CF3
-63.40
C6F6
-20
-40
-60
-80
-100
-120
-140
-160
-180
-200

1-Iodo-2-(2-nitrophenoxy)-4-(trifluoromethyl)benzene (2.22) (impure/crude)

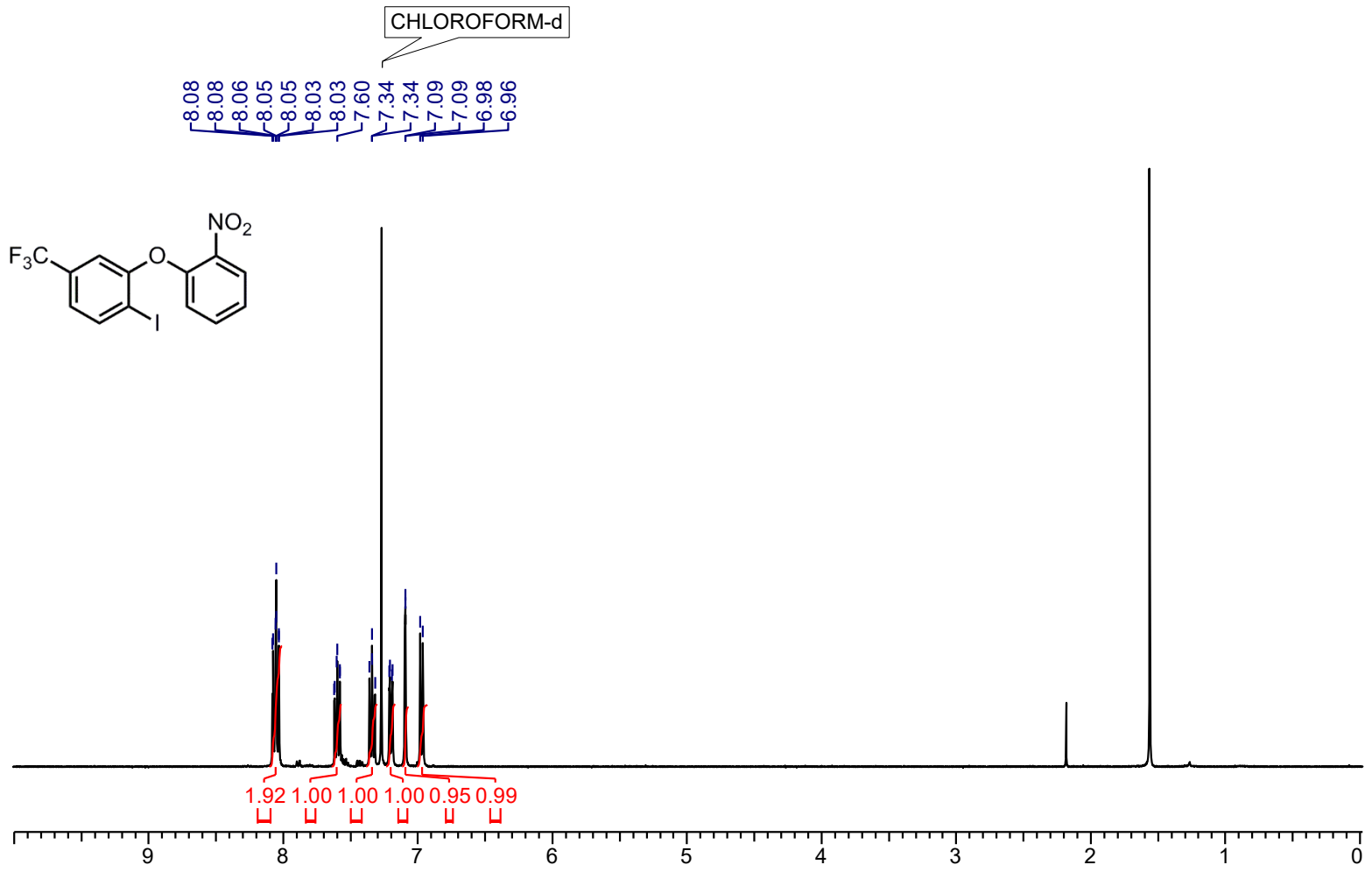

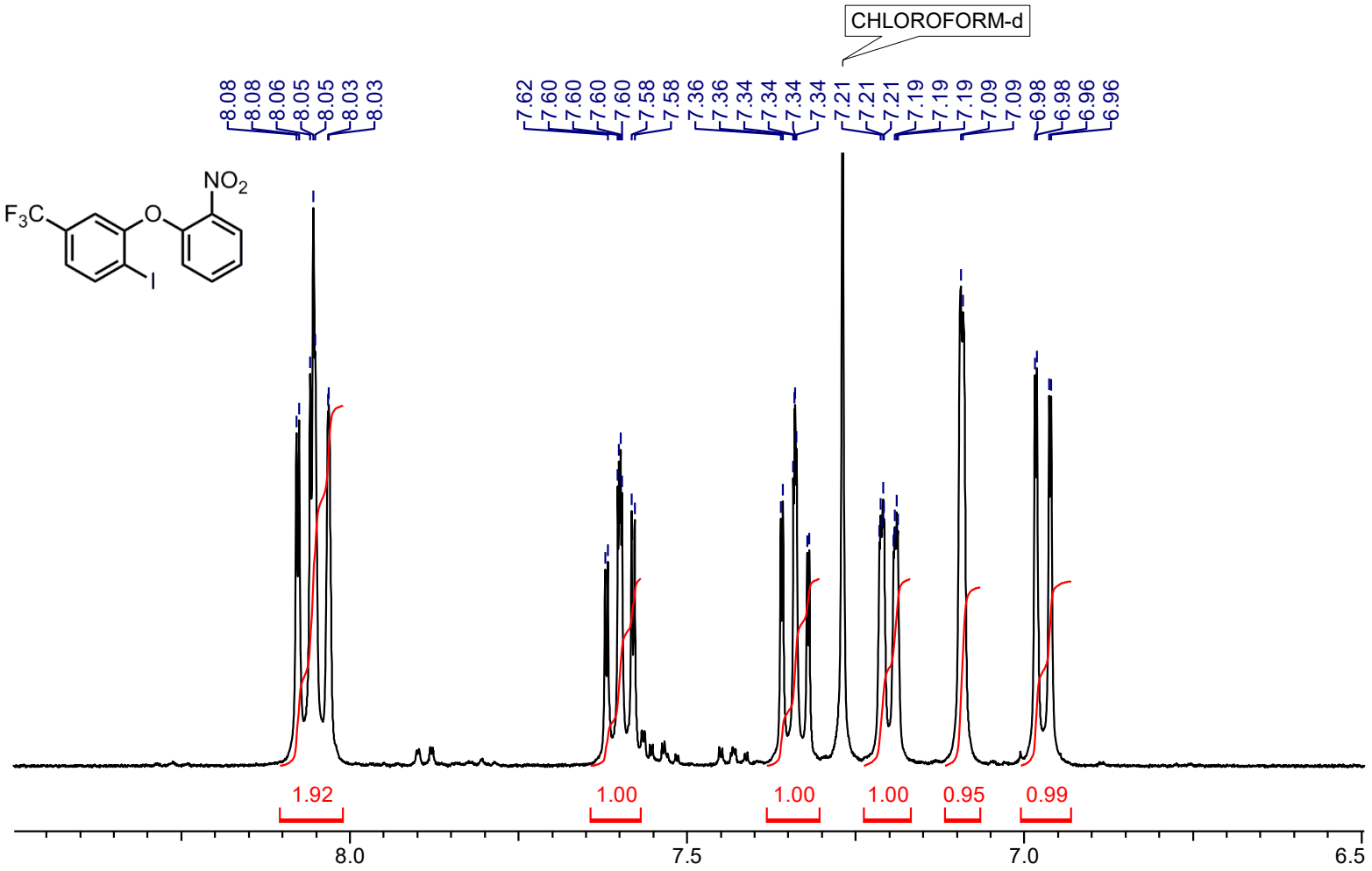
CHLOROFORM-d
8.08
8.08
8.06
8.05
8.05
8.03
8.03
7.62
7.60
7.60
7.60
7.60
7.58
7.58
7.36
7.36
7.34
7.34
7.34
7.34
7.21
7.21
7.21
7.19
7.19
7.19
7.09
7.09
6.98
6.98
6.96
6.96
NO2
F3C
O
I
1.92
1.00
1.00
1.00
0.95
0.99
8.0
7.5
7.0
6.5

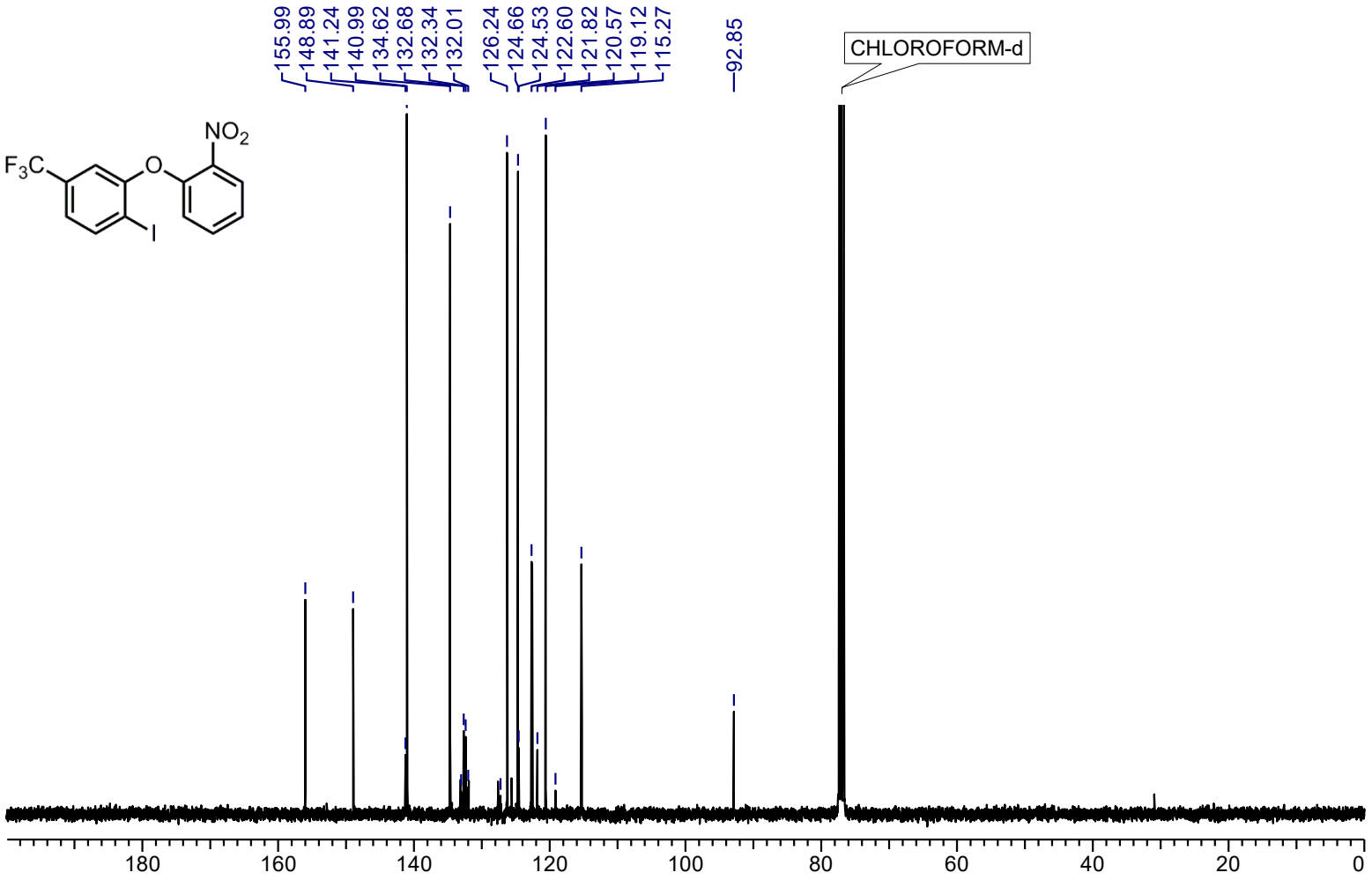
155.99
148.89
141.24
140.99
134.62
132.68
132.34
132.01
126.24
124.66
124.53
122.60
121.82
120.57
119.12
115.27
92.85
CHLOROFORM-d
NO2
F3C
O
I
180
160
140
120
100
80
60
40
20
0

N-(2-(5-(tert-Butyl)-2-iodophenoxy)phenyl)acetamide (2.24)

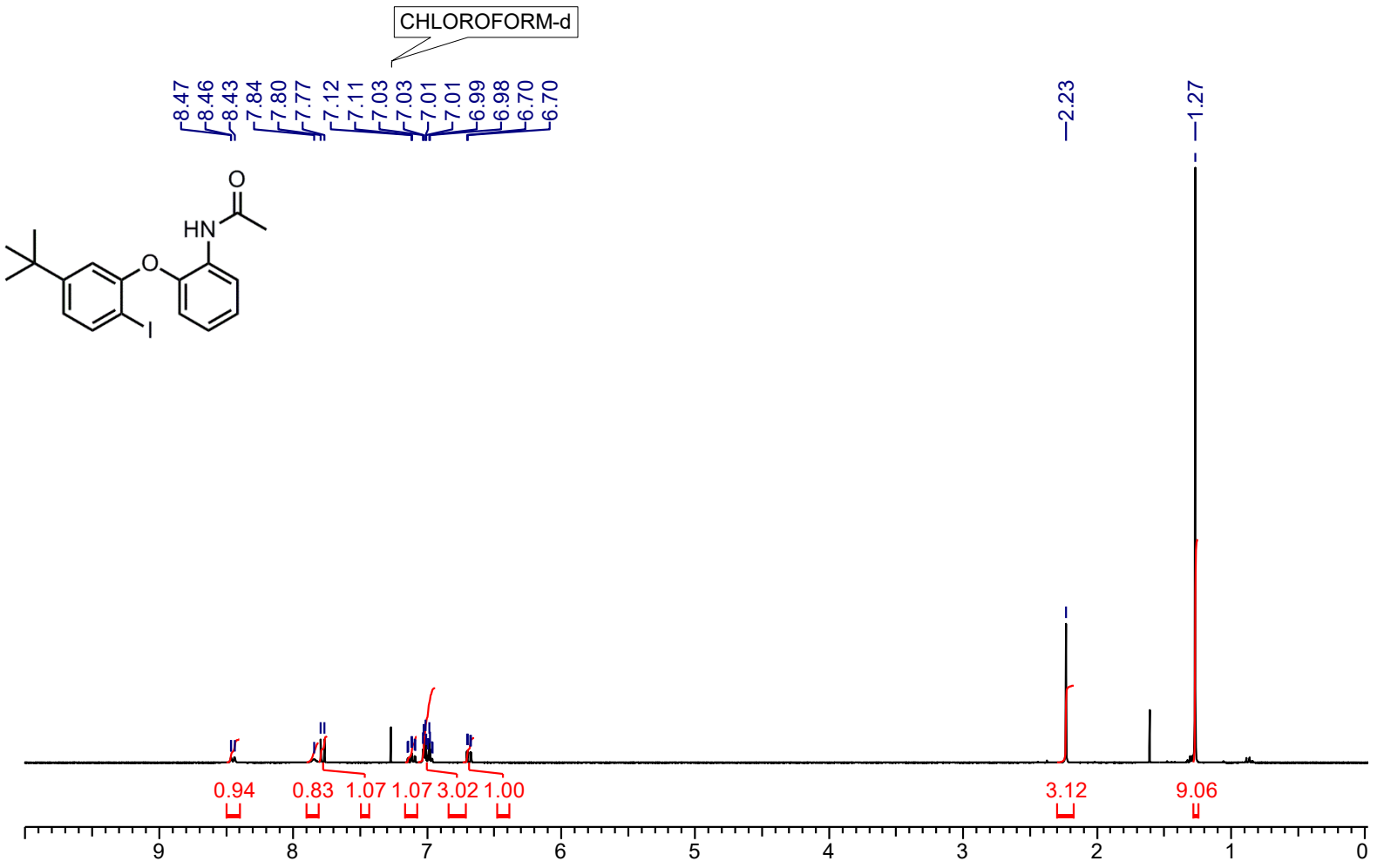

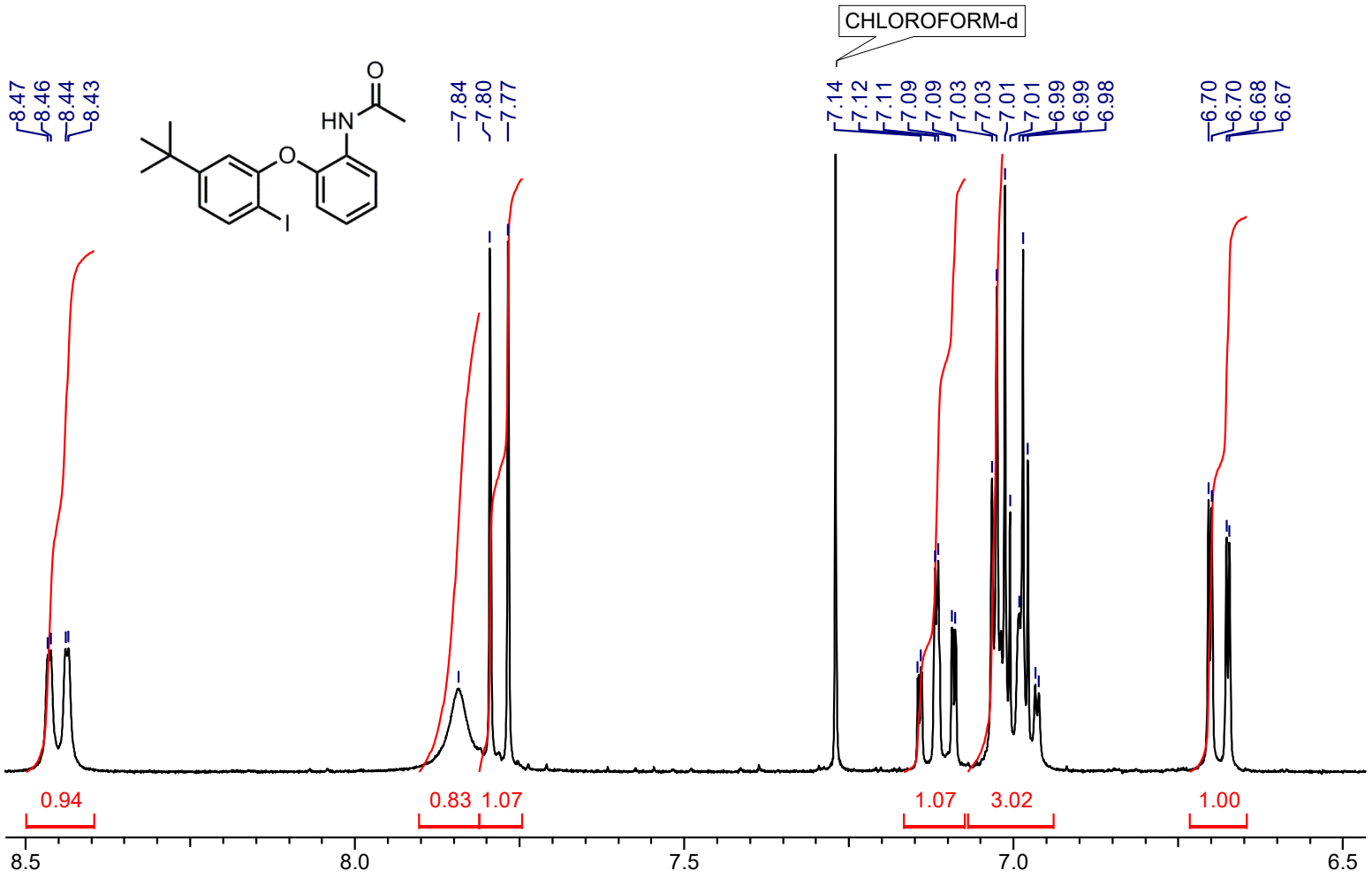
CHLOROFORM-d
8.47
8.46
8.44
8.43
7.84
7.80
7.77
7.14
7.12
7.11
7.09
7.09
7.03
7.03
7.01
7.01
6.99
6.99
6.98
6.70
6.70
6.68
6.67
HN
O
O
I
0.94
0.83
1.07
1.07
3.02
1.00
8.5
8.0
7.5
7.0
6.5

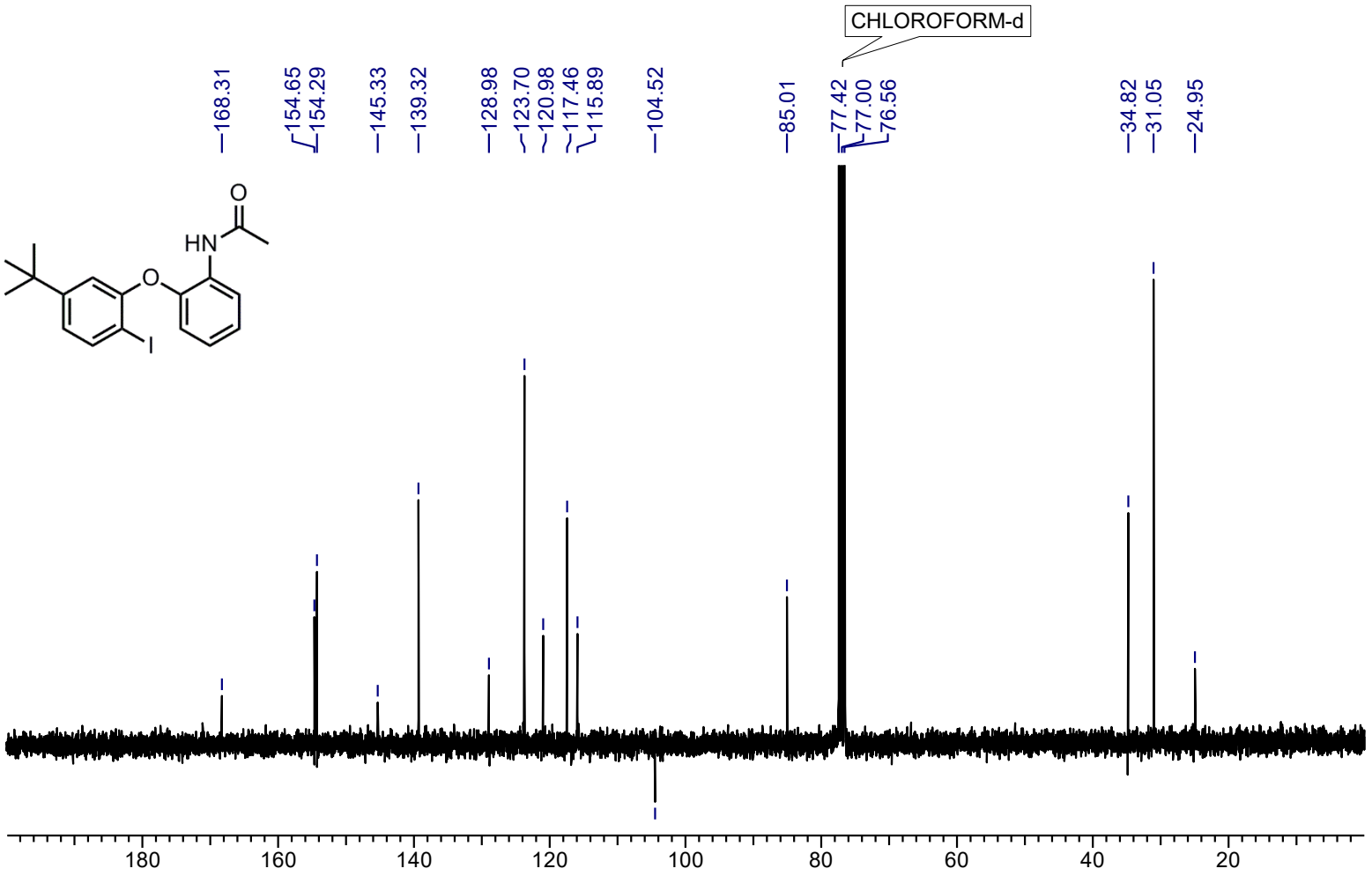
CHLOROFORM-d
168.31
154.65
154.29
145.33
139.32
128.98
123.70
120.98
117.46
115.89
104.52
85.01
77.42
77.00
76.56
34.82
31.05
24.95
O
HN
O
I
180
160
140
120
100
80
60
40
20

N-(4-(tert-Butyl)-2-(5-(tert-butyl)-2-iodophenoxy)phenyl)acetamide (2.27)

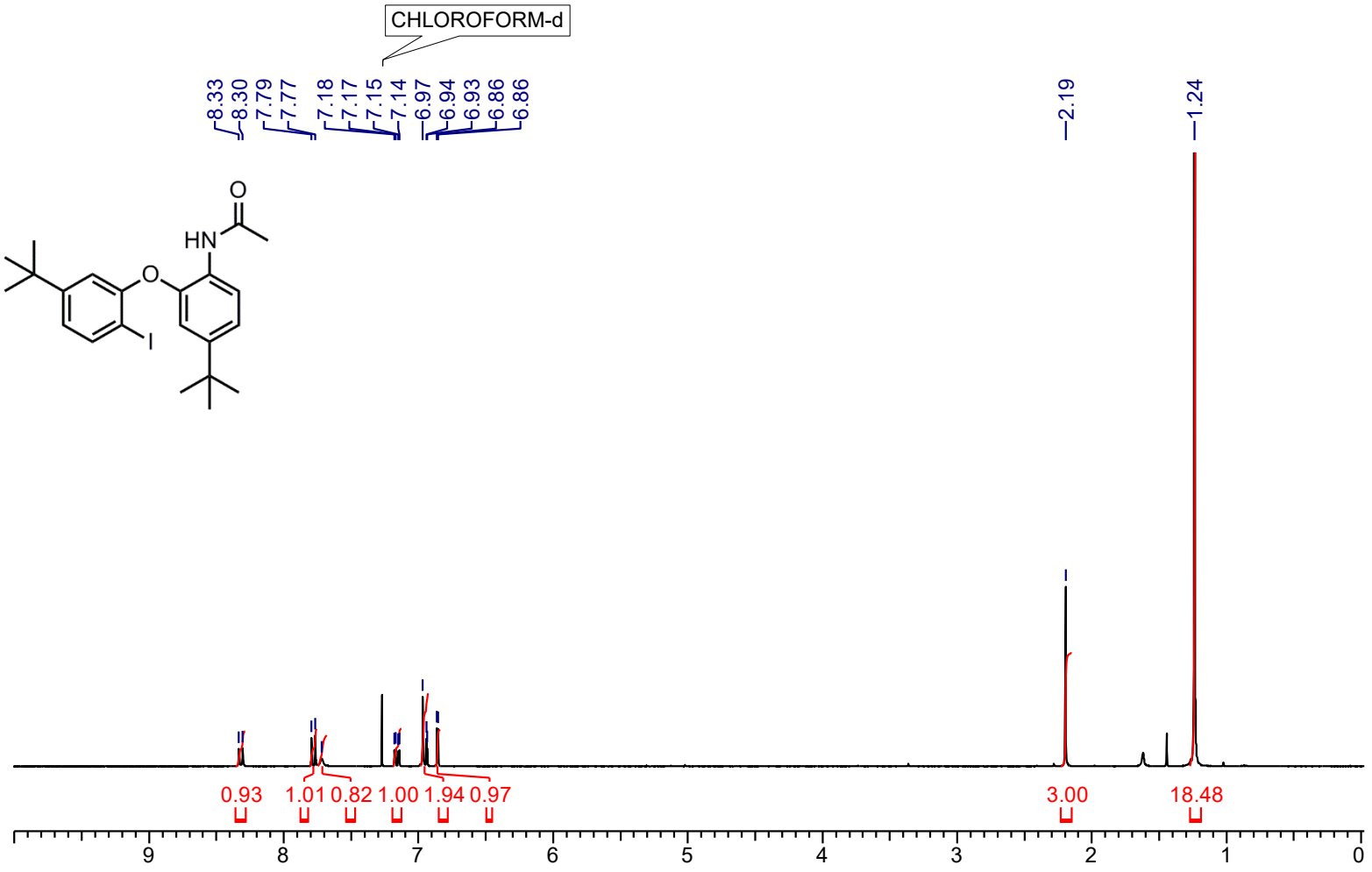

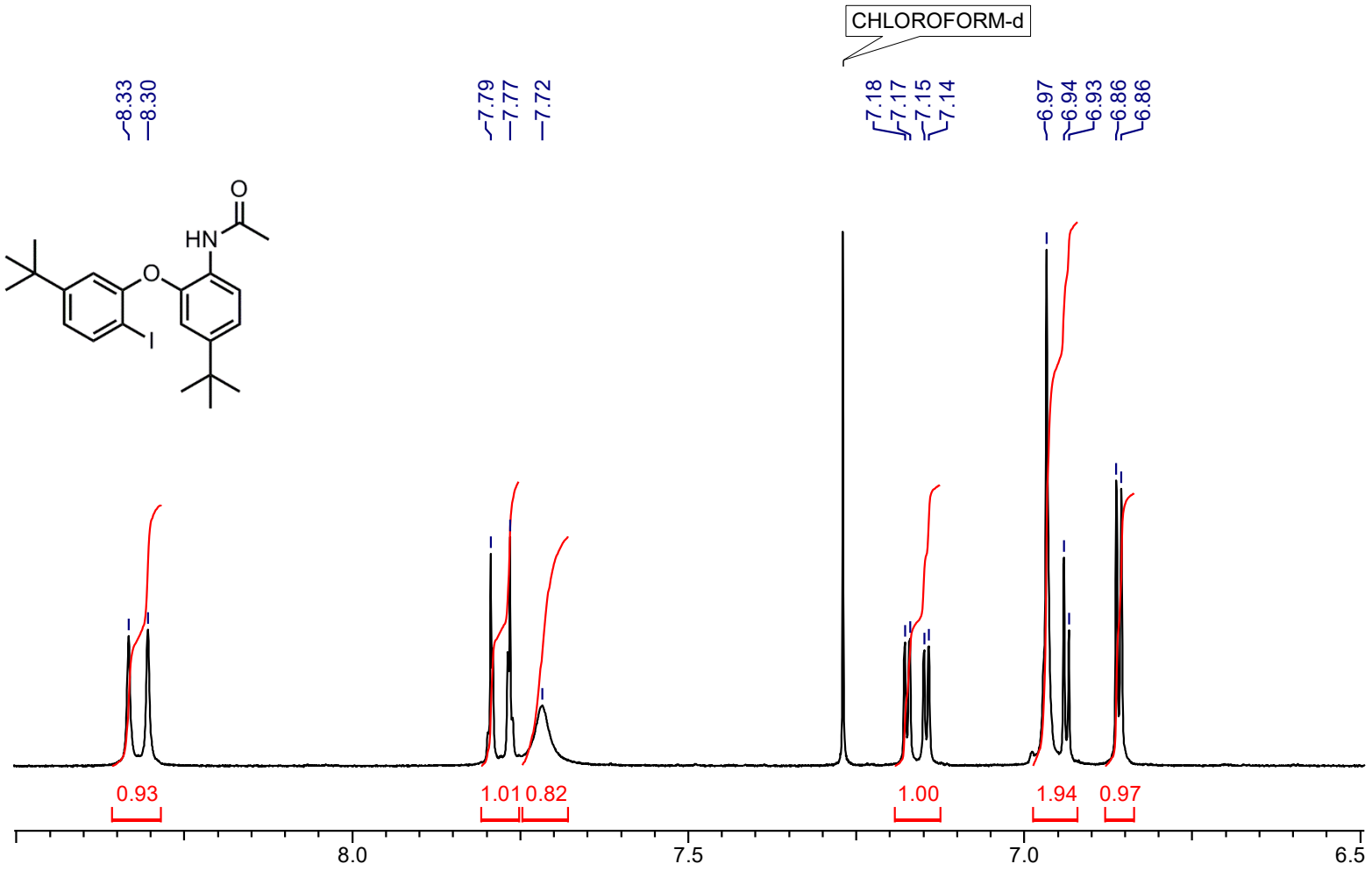
CHLOROFORM-d
8.33
8.30
7.79
7.77
7.72
7.18
7.17
7.15
7.14
6.97
6.94
6.93
6.86
6.86
HN
O
O
I
0.93
1.01
0.82
1.00
1.94
0.97
8.0
7.5
7.0
6.5

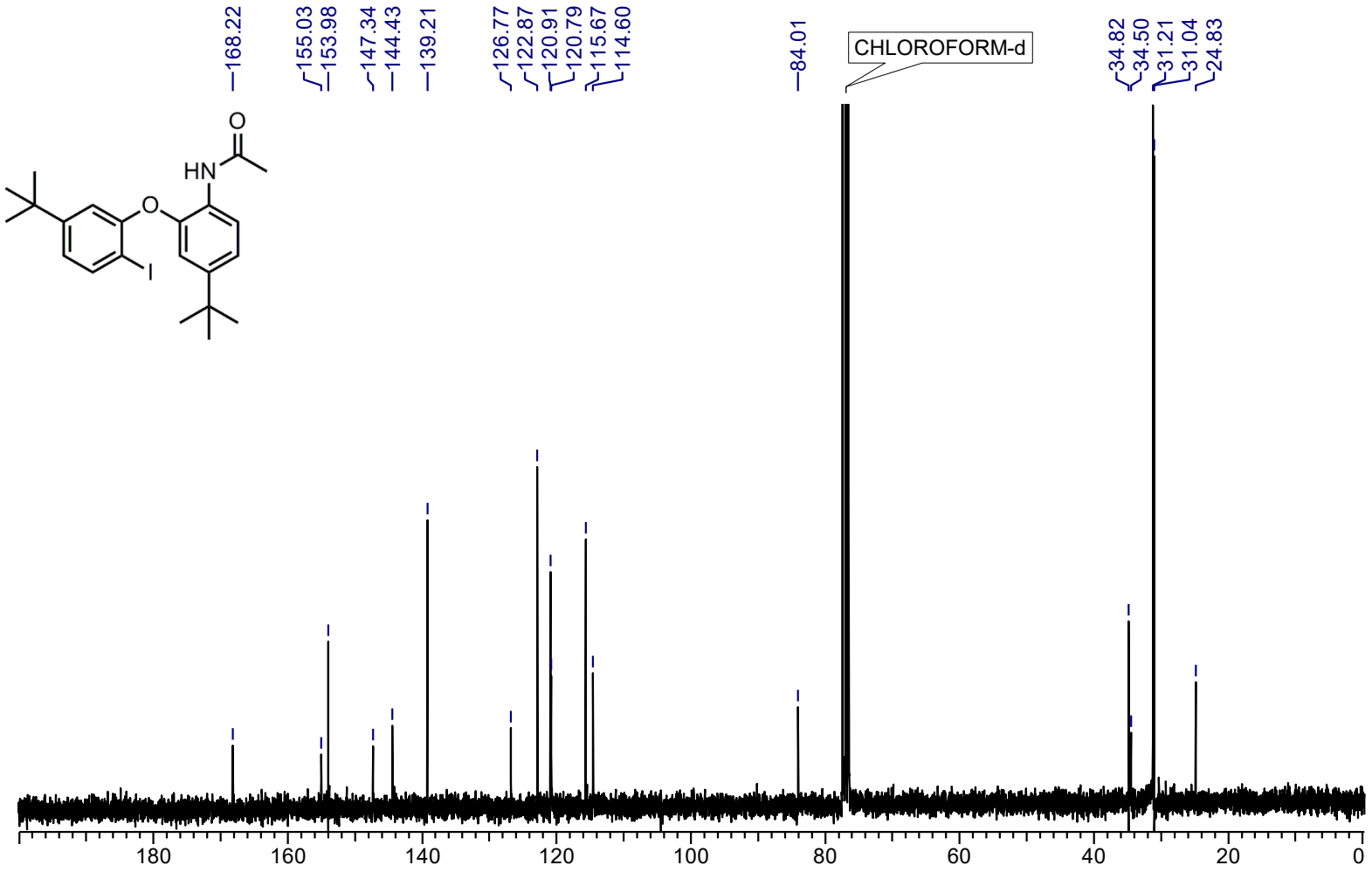
168.22
155.03
153.98
147.34
144.43
139.21
126.77
122.87
120.91
120.79
115.67
114.60
84.01
CHLOROFORM-d
34.82
34.50
31.21
31.04
24.83
HN
O
O
I
180
160
140
120
100
80
60
40
20
0

N-(2-(2-Bromophenoxy)-5-((trifluoromethyl)phenyl)acetamide (2.25)

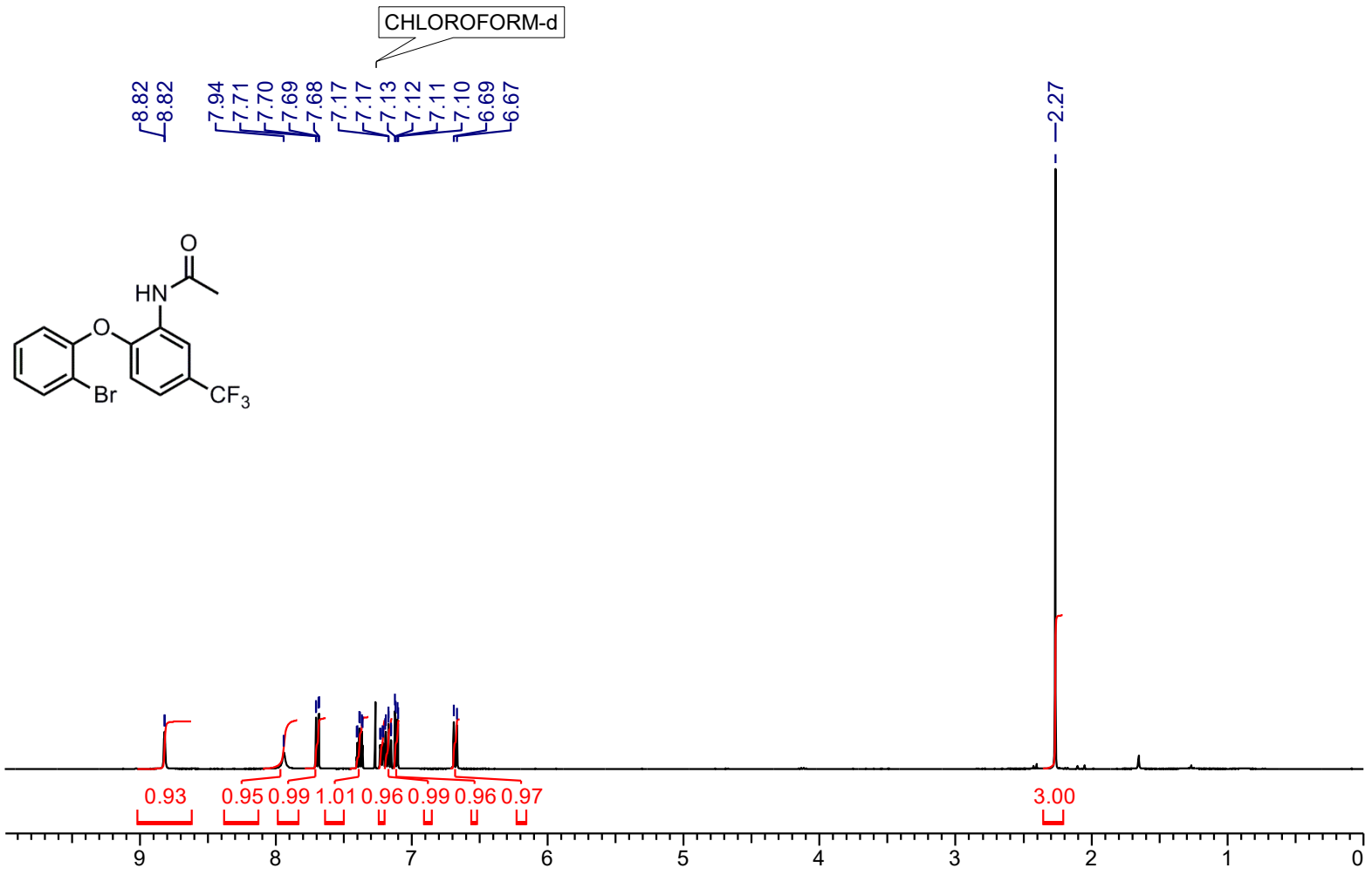

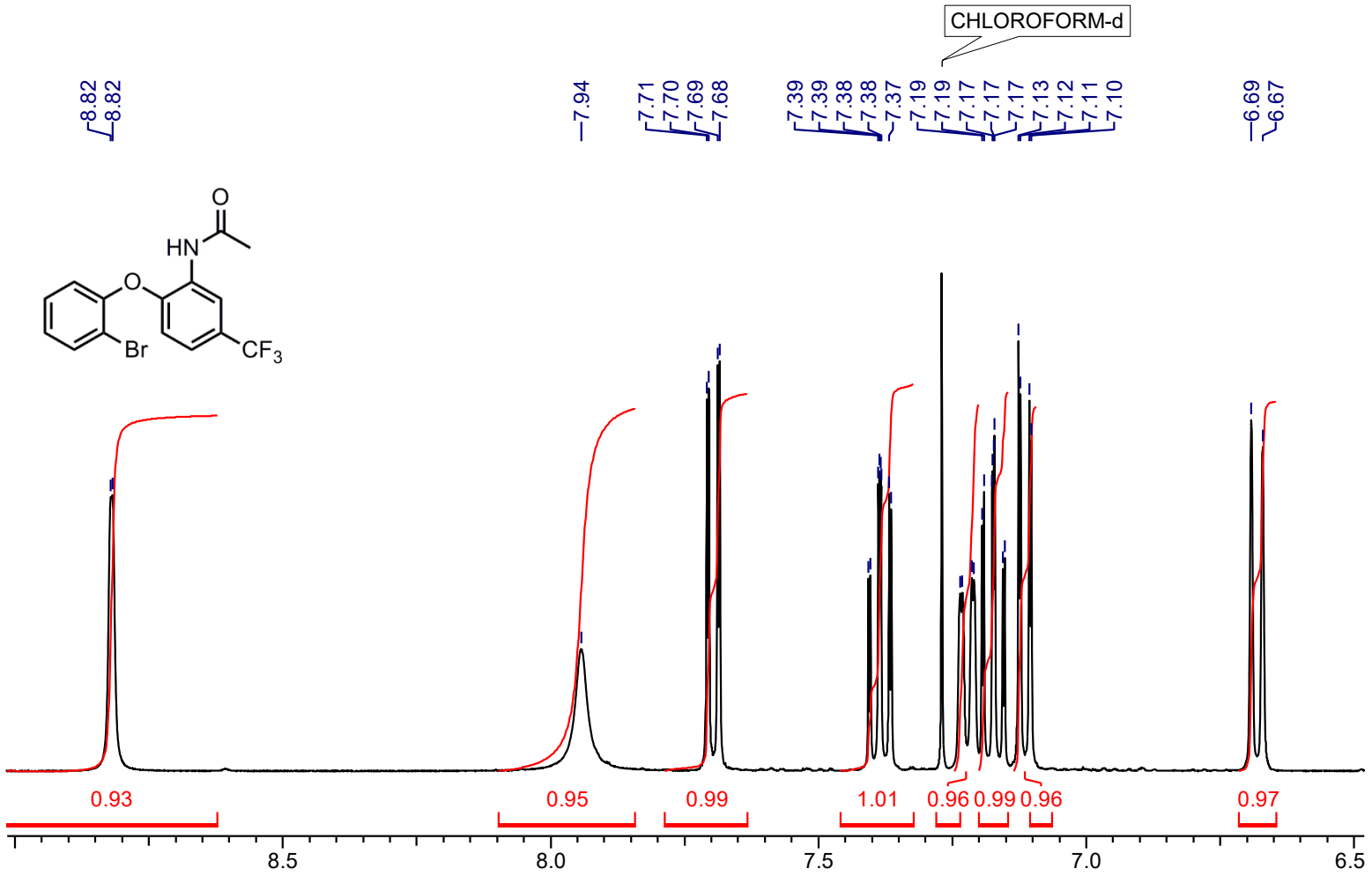
CHLOROFORM-d
8.82
8.82
7.94
7.71
7.70
7.69
7.68
7.39
7.39
7.38
7.38
7.37
7.19
7.19
7.17
7.17
7.17
7.13
7.12
7.11
7.10
6.69
6.67
HN
O
O
Br
CF3
0.93
0.95
0.99
1.01
0.96
0.99
0.96
0.97
8.5
8.0
7.5
7.0
6.5

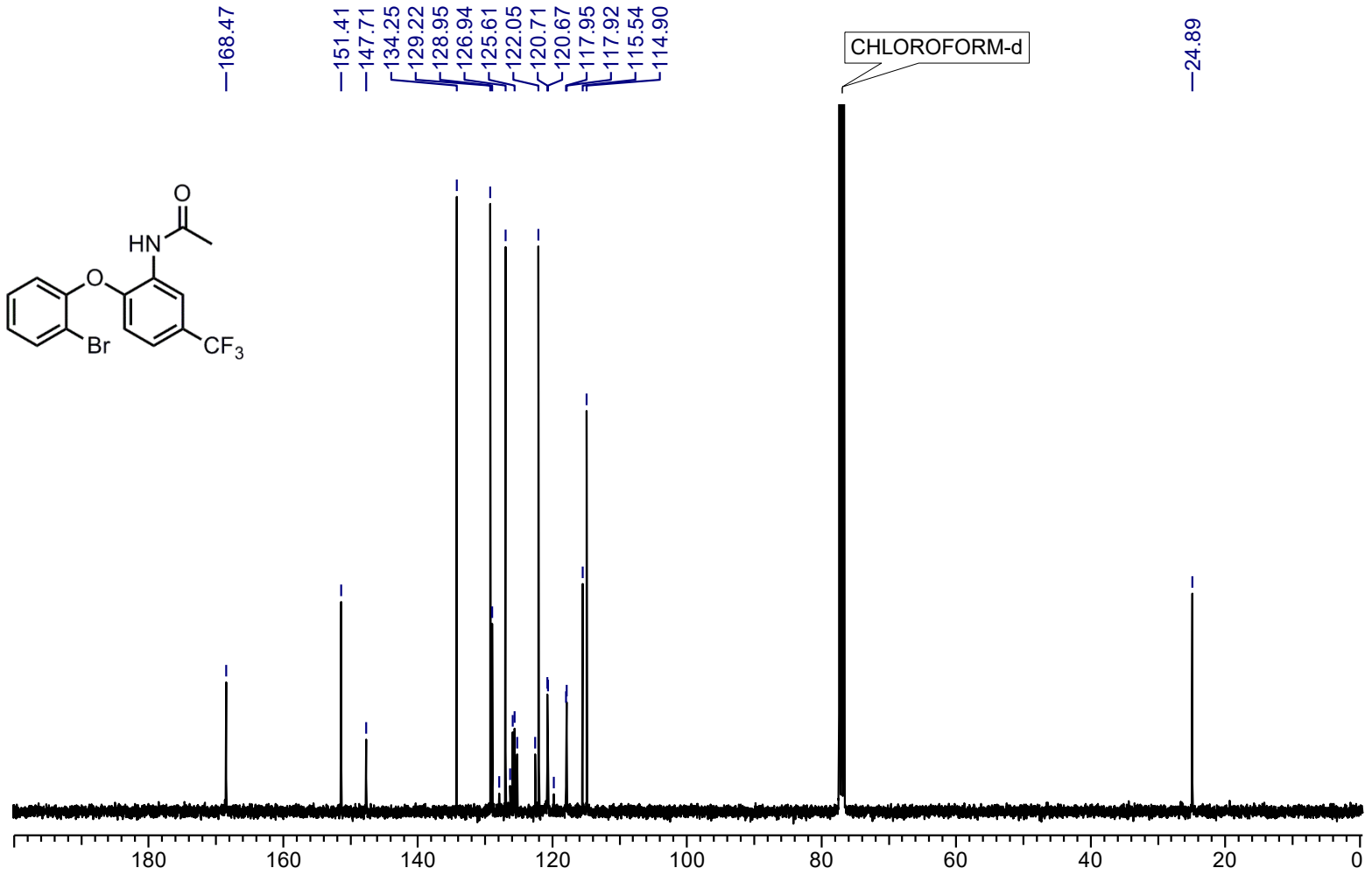
168.47
151.41
147.71
134.25
129.22
128.95
126.94
125.61
122.05
120.71
120.67
117.95
117.92
115.54
114.90
CHLOROFORM-d
24.89
O
HN
O
Br
CF3
180
160
140
120
100
80
60
40
20
0

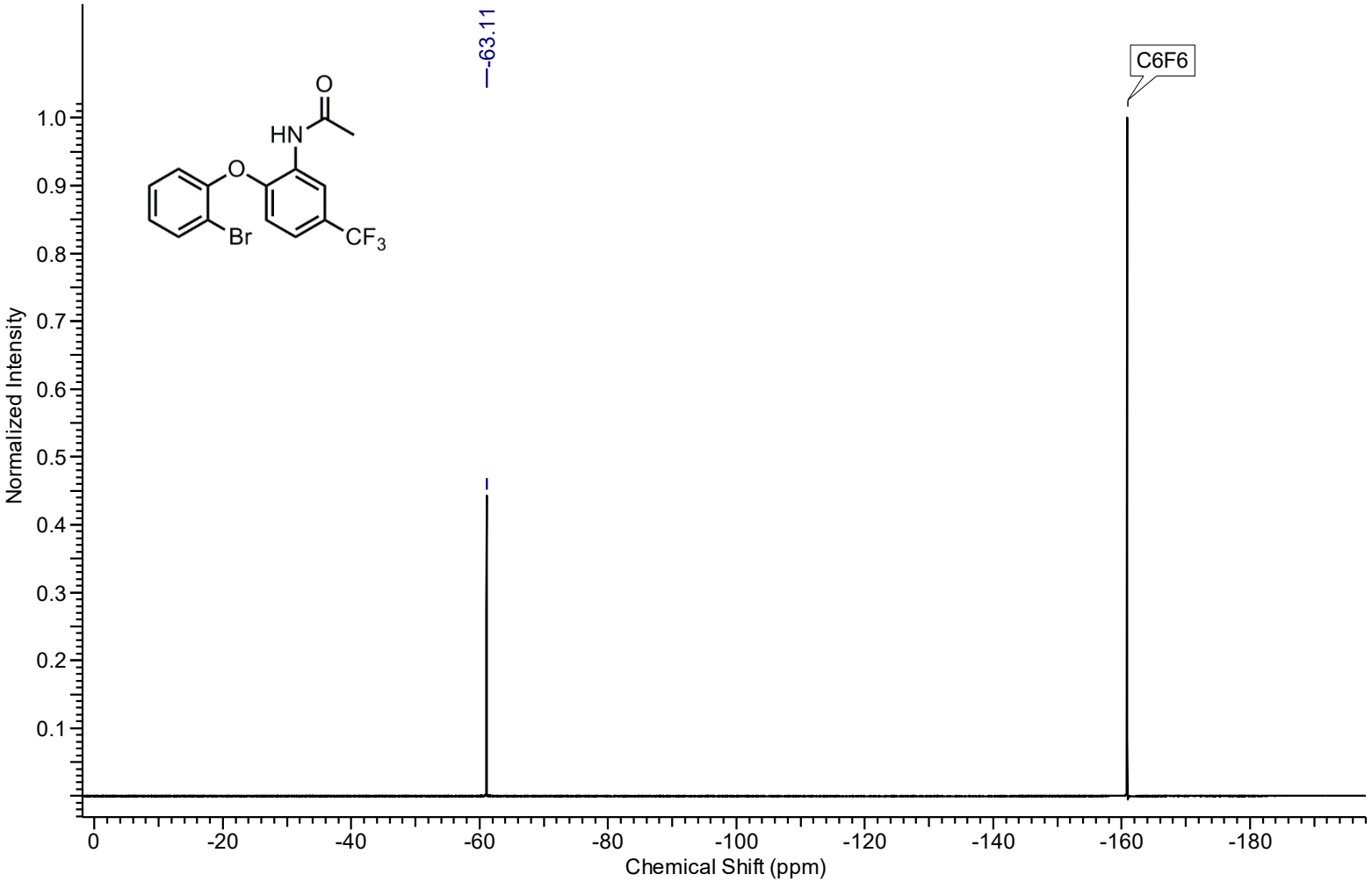
-63.11
C6F6
O
HN
O
Br
CF3
Normalized Intensity
1.0
0.9
0.8
0.7
0.6
0.5
0.4
0.3
0.2
0.1
0
-20
-40
-60
-80
-100
-120
-140
-160
-180
Chemical Shift (ppm)

N-(2-(2-Iodo-5-(trifluoromethyl)phenoxy)phenyl)acetamide (2.26)

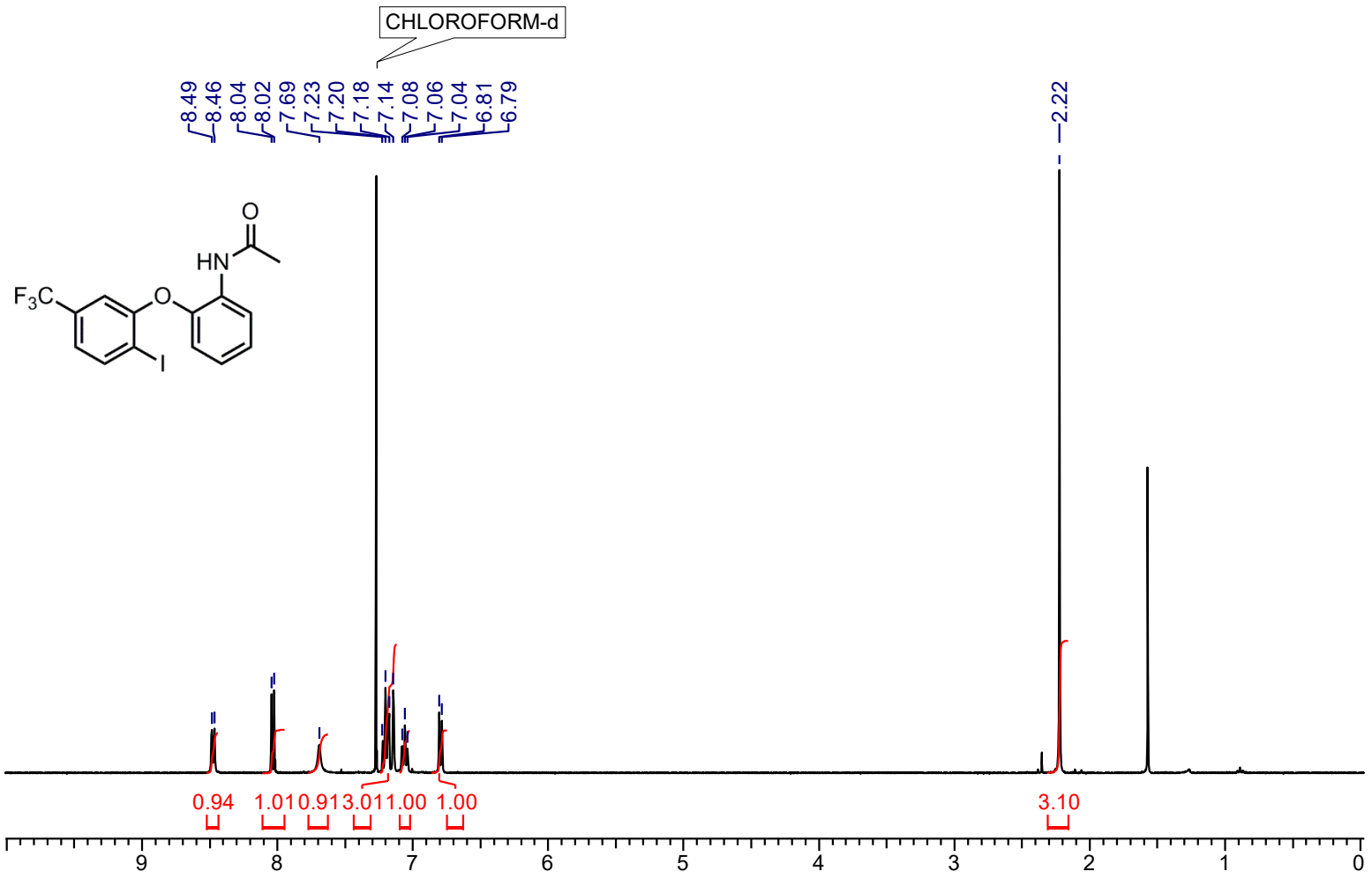

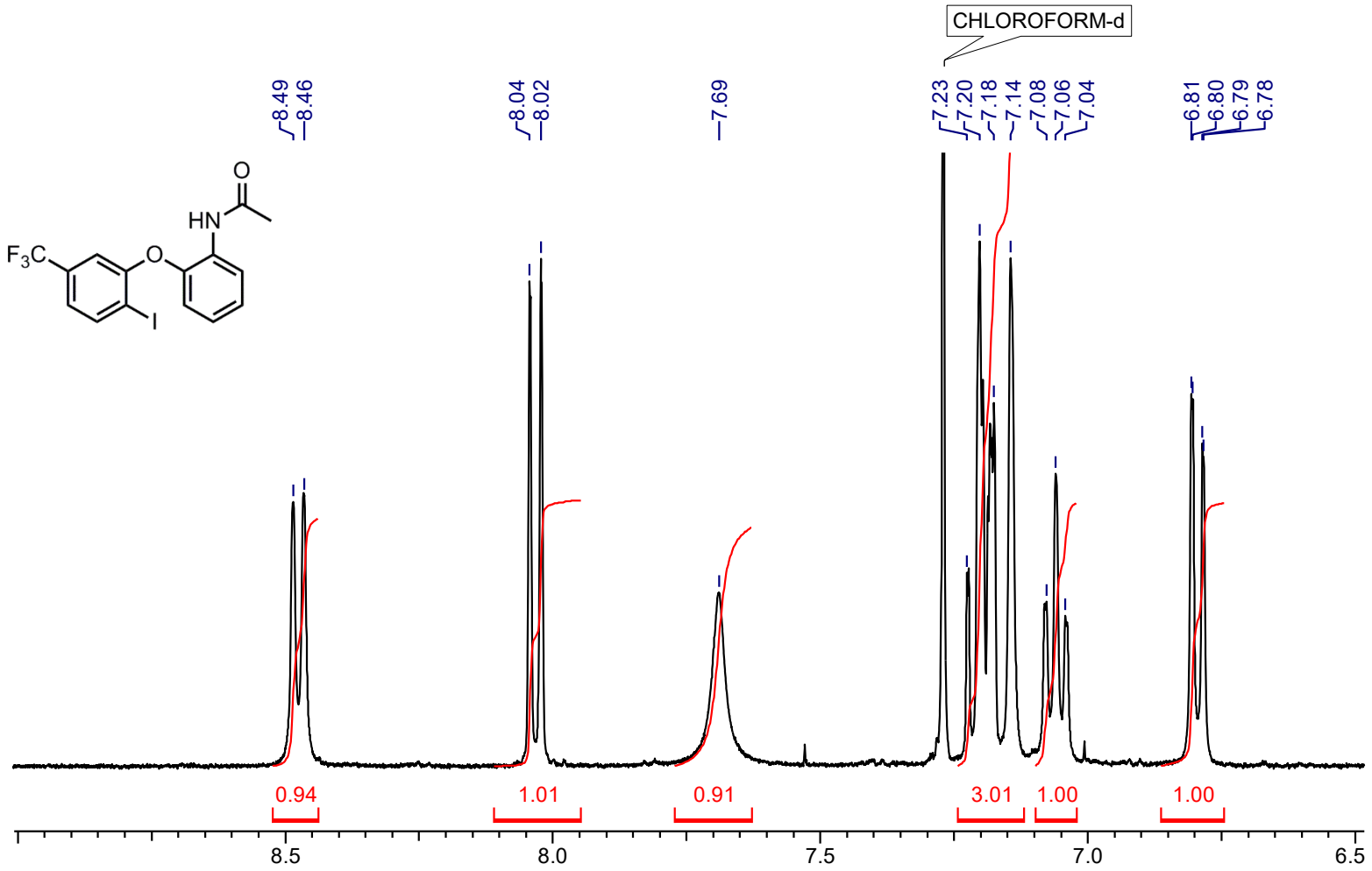
CHLOROFORM-d
8.49
8.46
8.04
8.02
7.69
7.23
7.20
7.18
7.14
7.08
7.06
7.04
6.81
6.80
6.79
6.78
O
HN
F3C
O
I
0.94
1.01
0.91
3.01
1.00
1.00
8.5
8.0
7.5
7.0
6.5

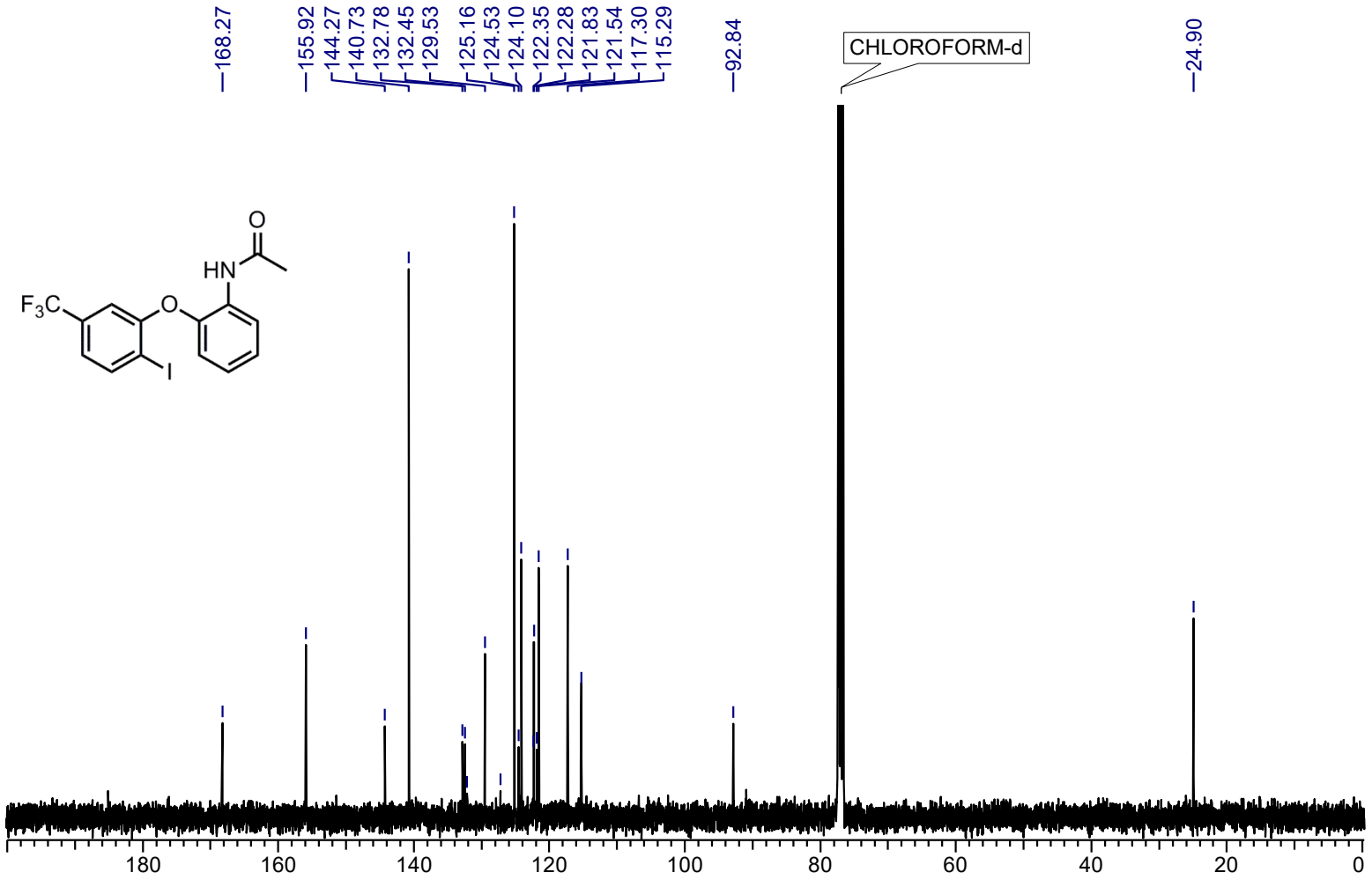
168.27
155.92
144.27
140.73
132.78
132.45
129.53
125.16
124.53
124.10
122.35
122.28
121.83
121.54
117.30
115.29
92.84
CHLOROFORM-d
24.90
O
HN
F3C
O
I
180
160
140
120
100
80
60
40
20
0

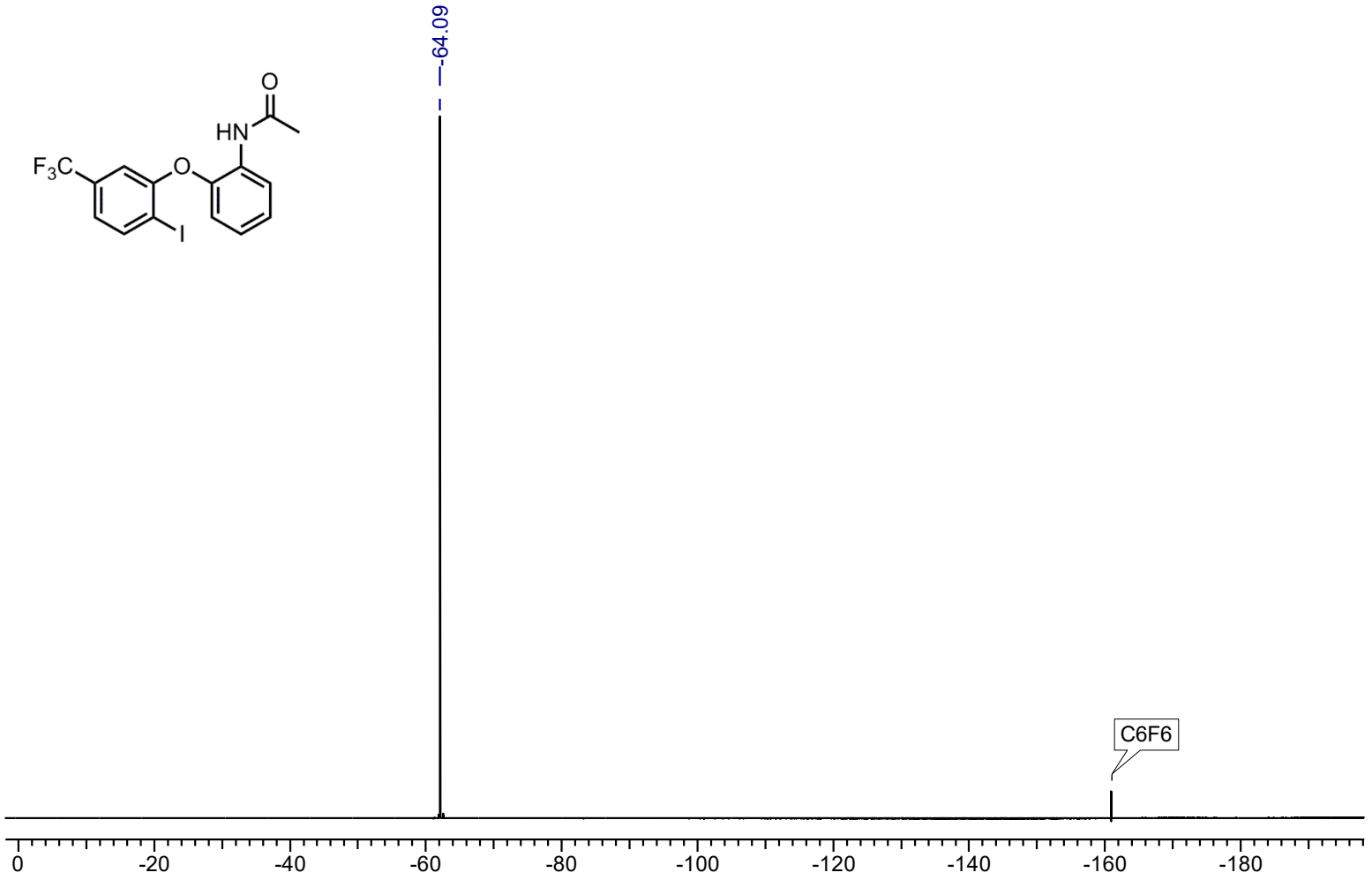
-64.09
O
HN
F3C
O
I
C6F6
0
-20
-40
-60
-80
-100
-120
-140
-160
-180

10-acetyl-3-tert-butylphenoxazine (2.29)

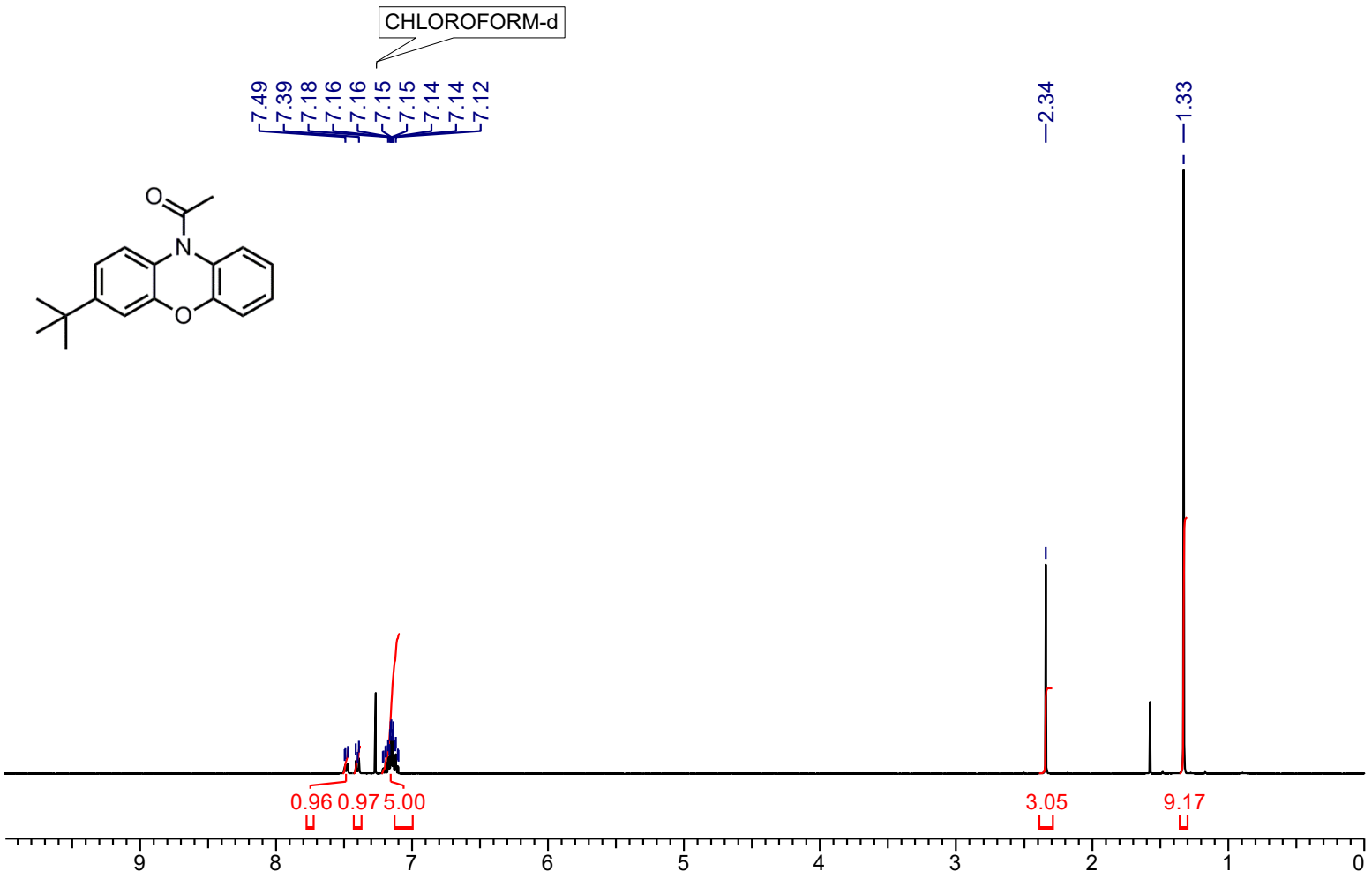

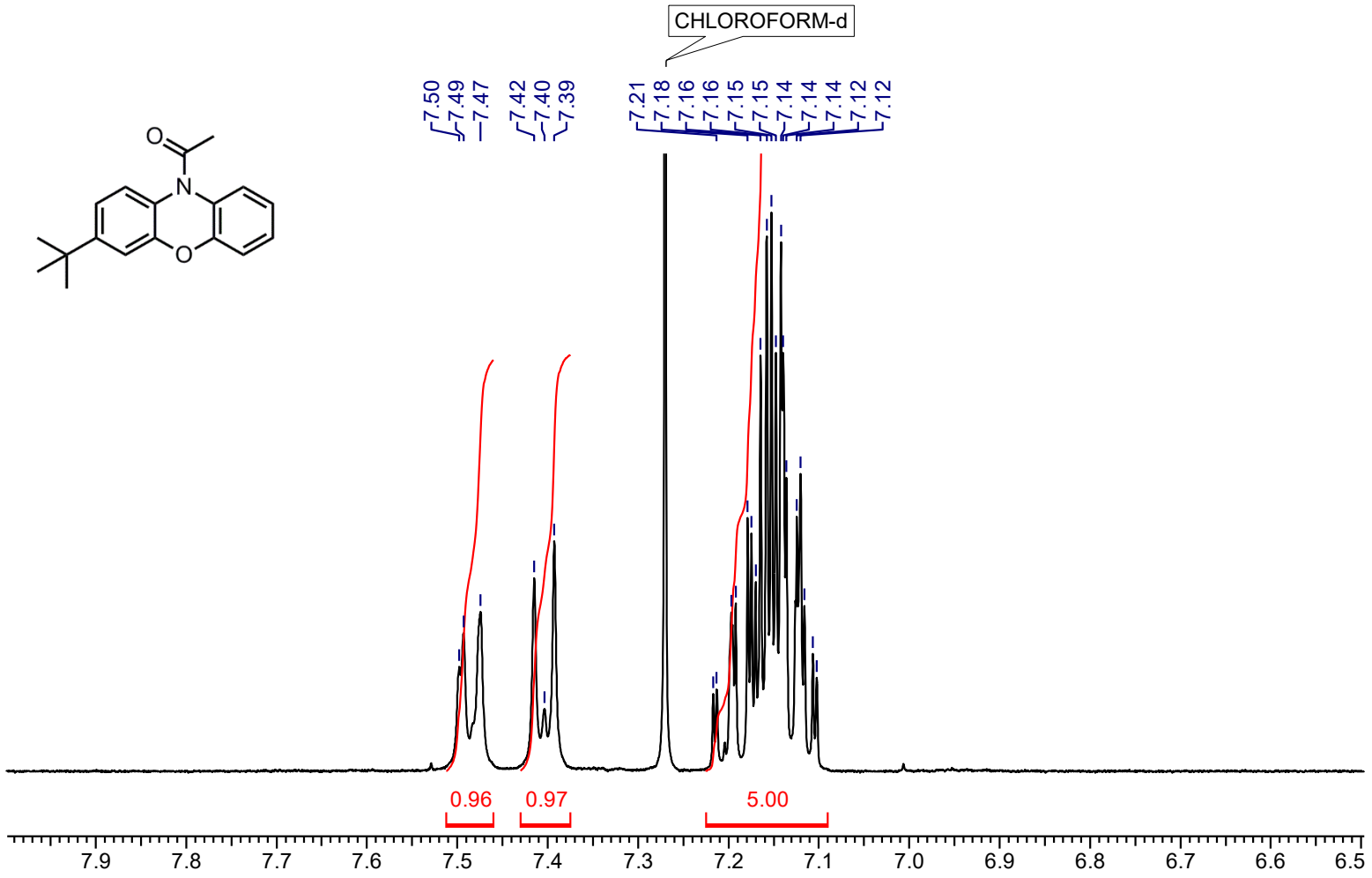
CHLOROFORM-d
7.50
7.49
7.47
7.42
7.40
7.39
7.21
7.18
7.16
7.16
7.15
7.15
7.14
7.14
7.14
7.12
7.12
O
N
O
0.96
0.97
5.00
7.9
7.8
7.7
7.6
7.5
7.4
7.3
7.2
7.1
7.0
6.9
6.8
6.7
6.6
6.5

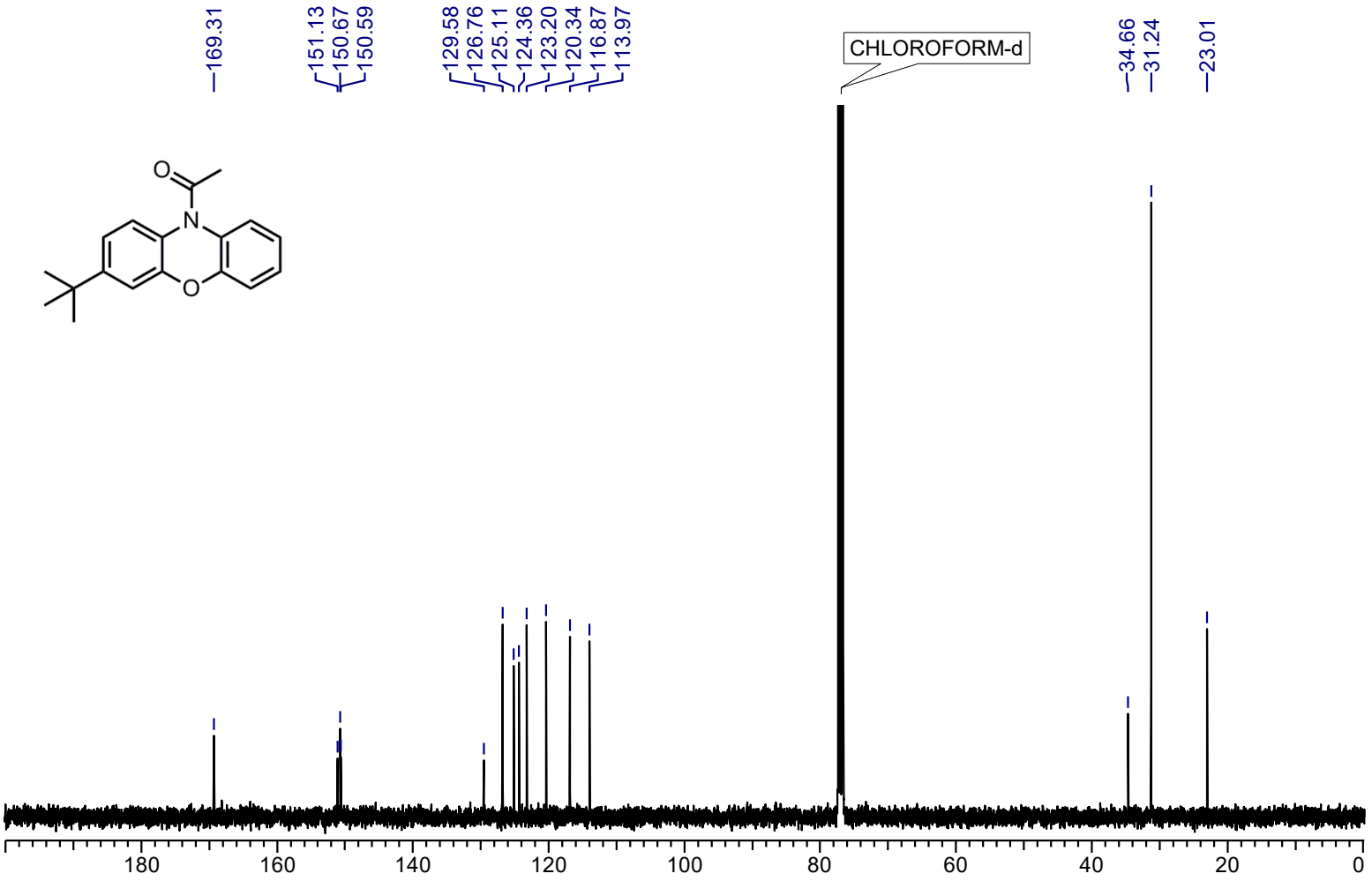
169.31
151.13
150.67
150.59
129.58
126.76
125.11
124.36
123.20
120.34
116.87
113.97
CHLOROFORM-d
34.66
31.24
23.01
O
N
O
180
160
140
120
100
80
60
40
20
0

O-Acetyl-3-hydroxy-10-acetylphenoxazine (2.31)

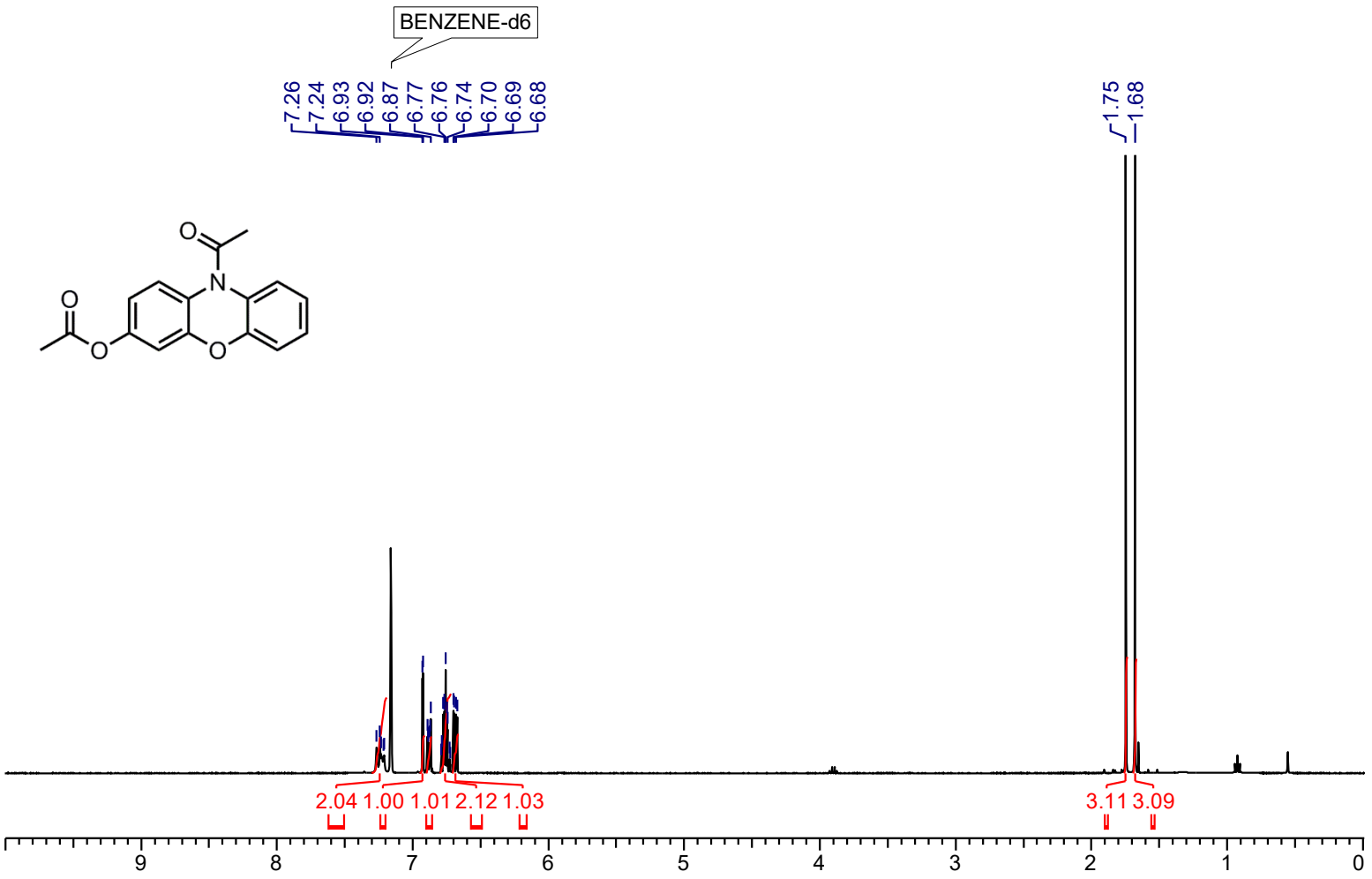

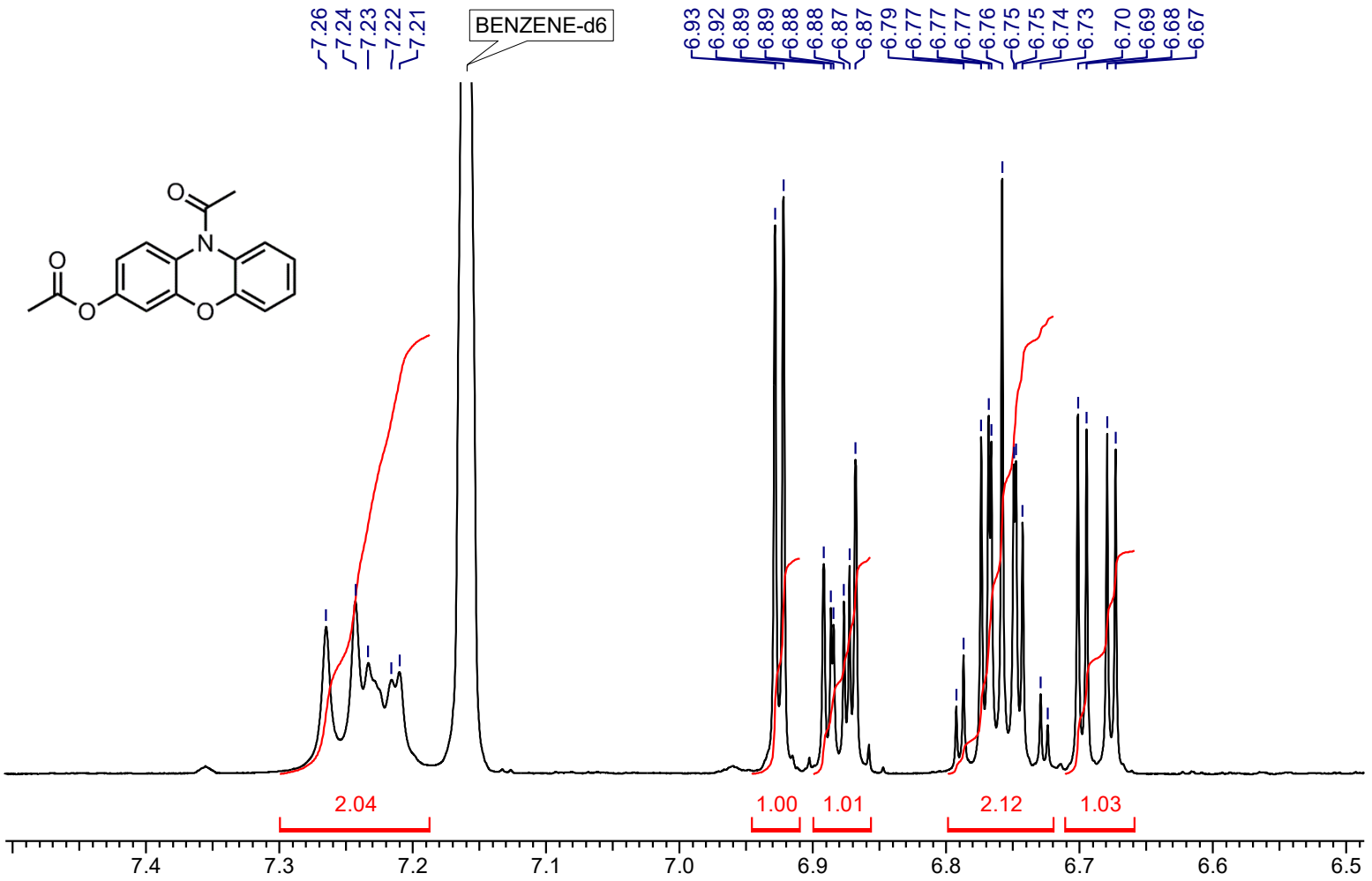
7.26
7.24
7.23
7.22
7.21
BENZENE-d6
6.93
6.92
6.89
6.89
6.88
6.88
6.87
6.87
6.79
6.77
6.77
6.77
6.76
6.75
6.75
6.74
6.73
6.70
6.69
6.68
6.67
O
N
O
O
O
2.04
1.00
1.01
2.12
1.03
7.4
7.3
7.2
7.1
7.0
6.9
6.8
6.7
6.6
6.5

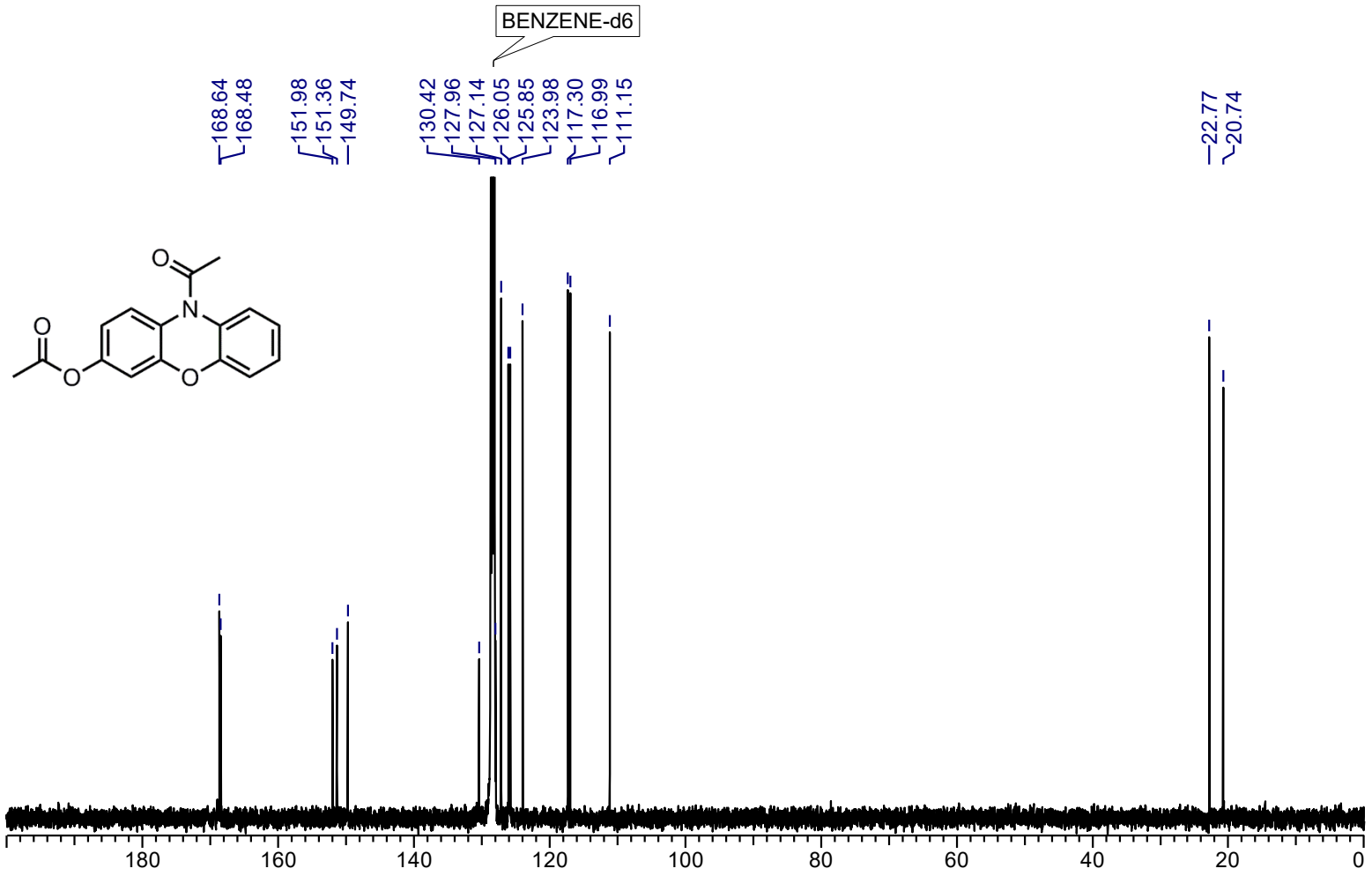
BENZENE-d6
168.64
168.48
151.98
151.36
149.74
130.42
127.96
127.14
126.05
125.85
123.98
117.30
116.99
111.15
22.77
20.74
O
N
O
O
O
180
160
140
120
100
80
60
40
20
0

3-Methoxy-10-acetylphenoxazine (2.32)

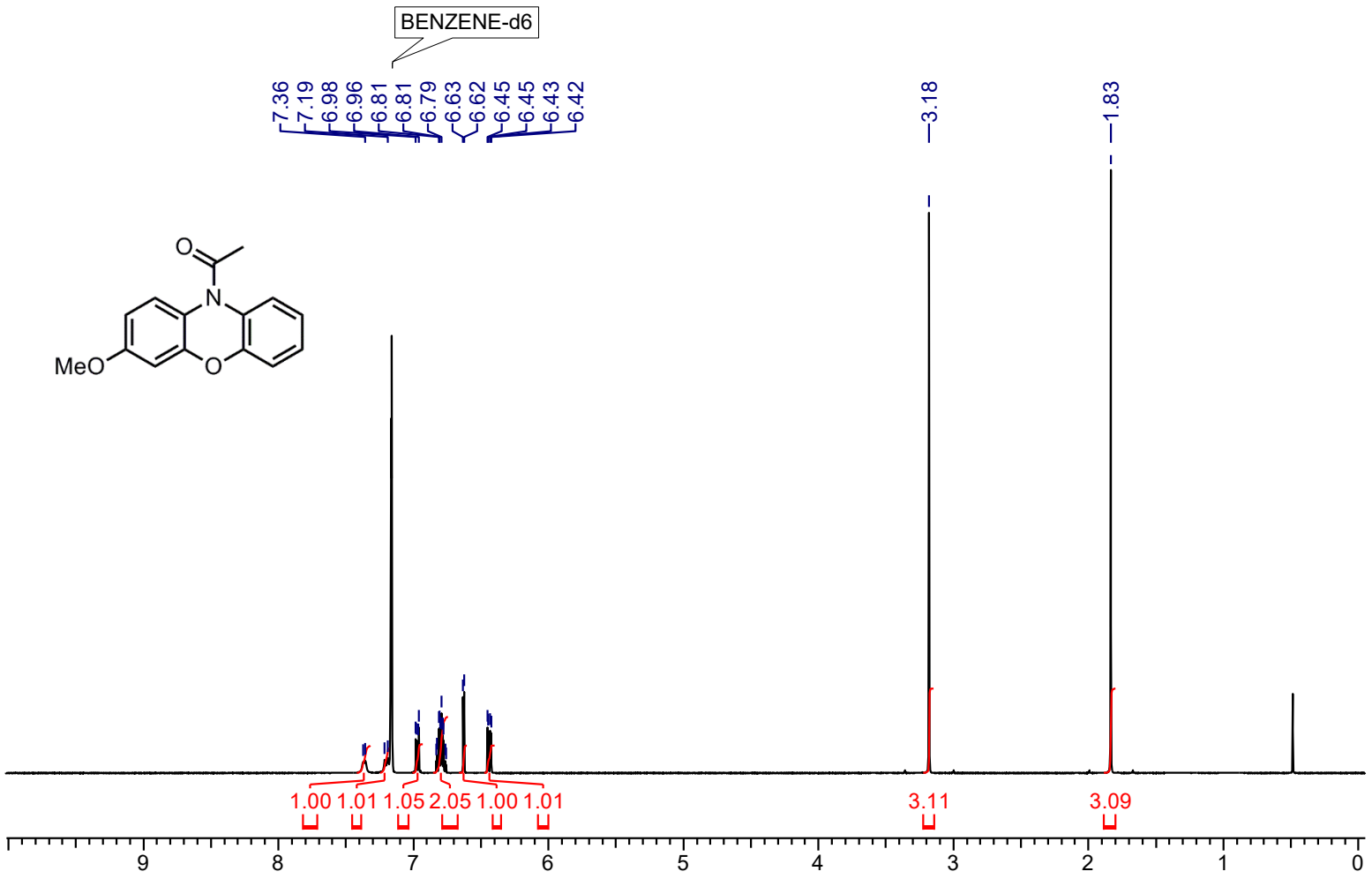

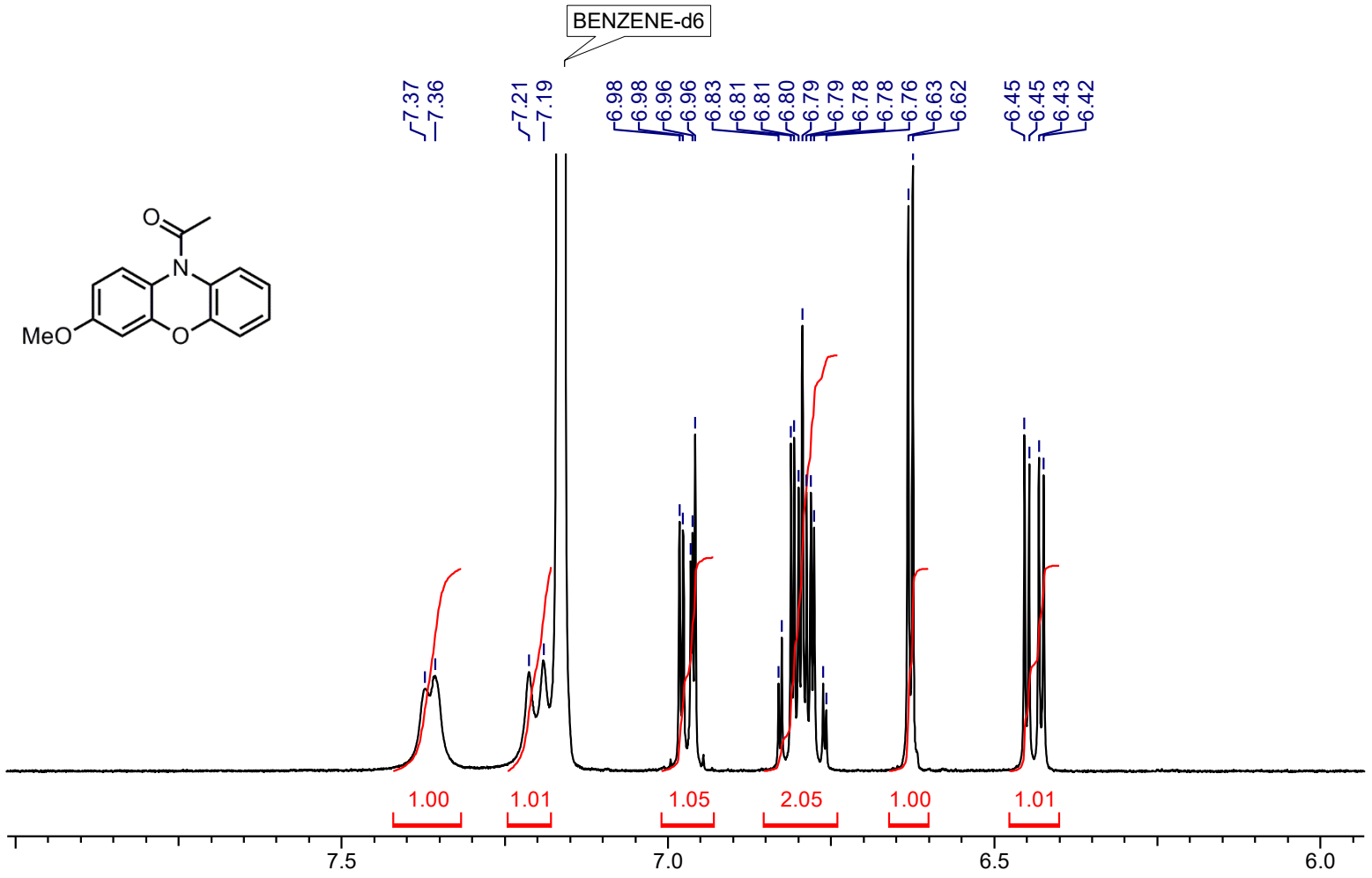
BENZENE-d6
7.37
7.36
7.21
7.19
6.98
6.98
6.96
6.96
6.83
6.81
6.81
6.80
6.79
6.79
6.78
6.78
6.76
6.63
6.62
6.45
6.45
6.43
6.42
O
N
MeO
O
1.00
1.01
1.05
2.05
1.00
1.01
7.5
7.0
6.5
6.0

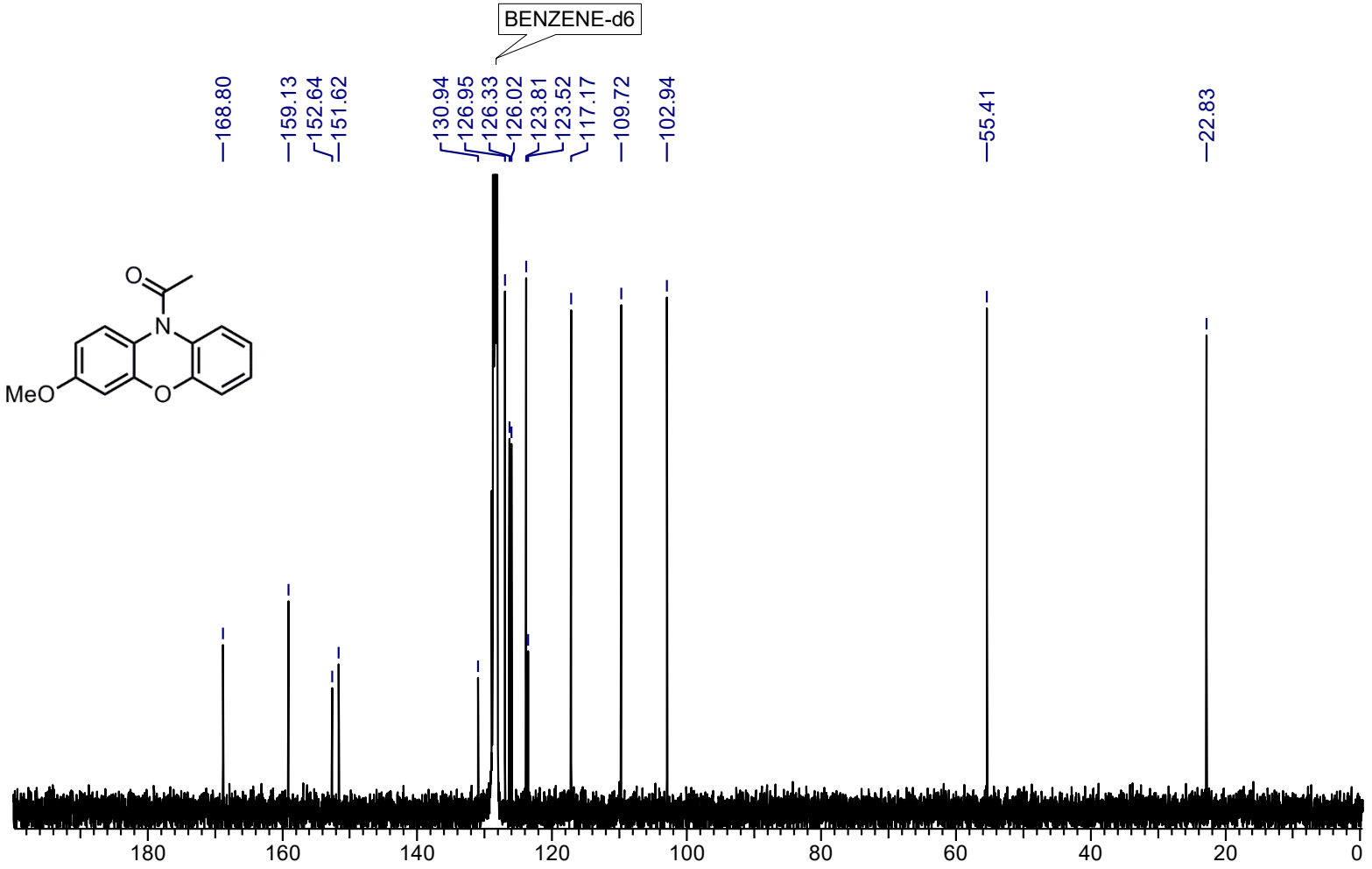
BENZENE-d6
168.80
159.13
152.64
151.62
130.94
126.95
126.33
126.02
123.81
123.52
117.17
109.72
102.94
55.41
22.83
O
N
O
MeO
180
160
140
120
100
80
60
40
20
0

3,7-Dimethoxy-10-acetylphenoxazine (2.33)

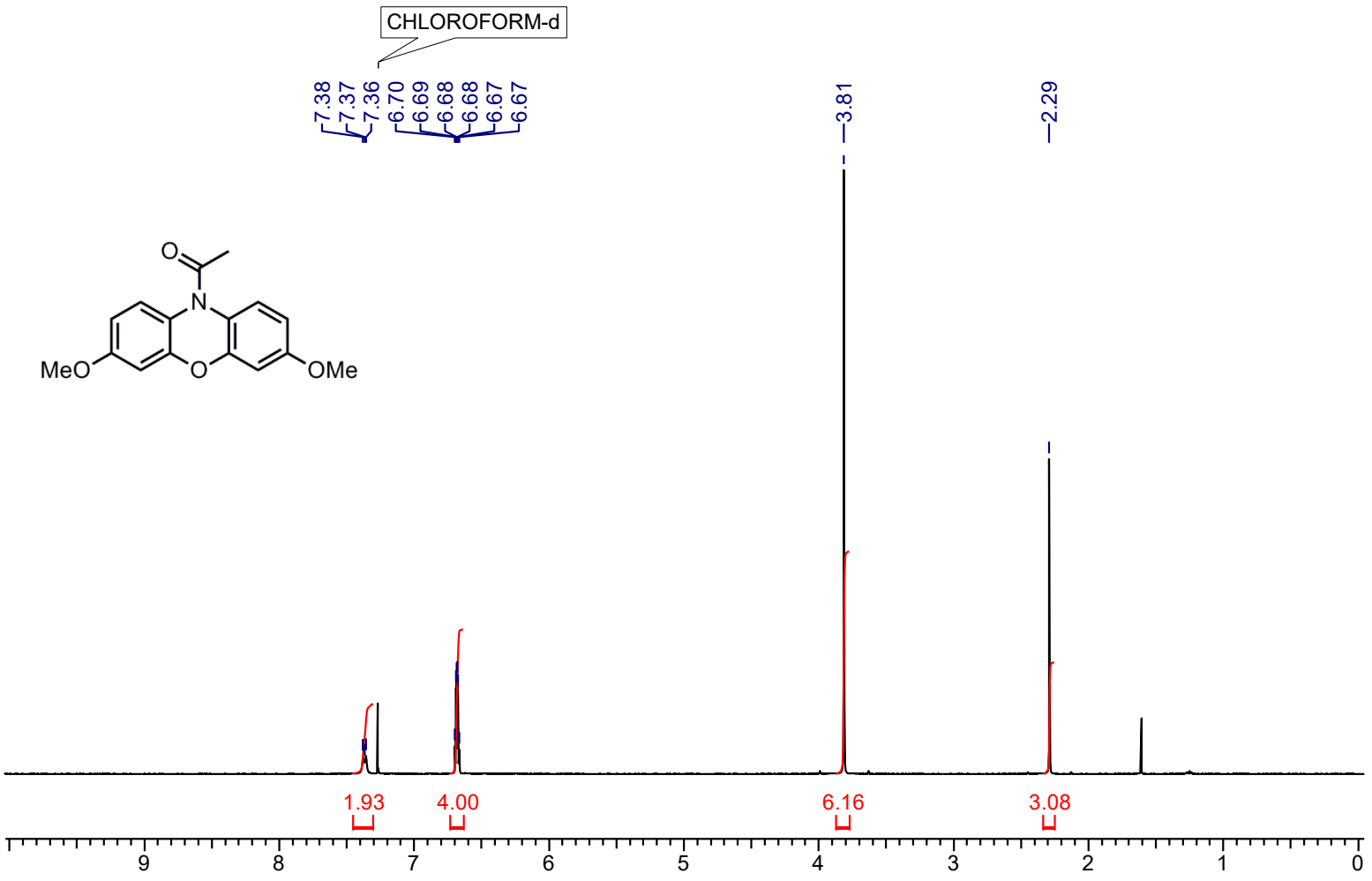

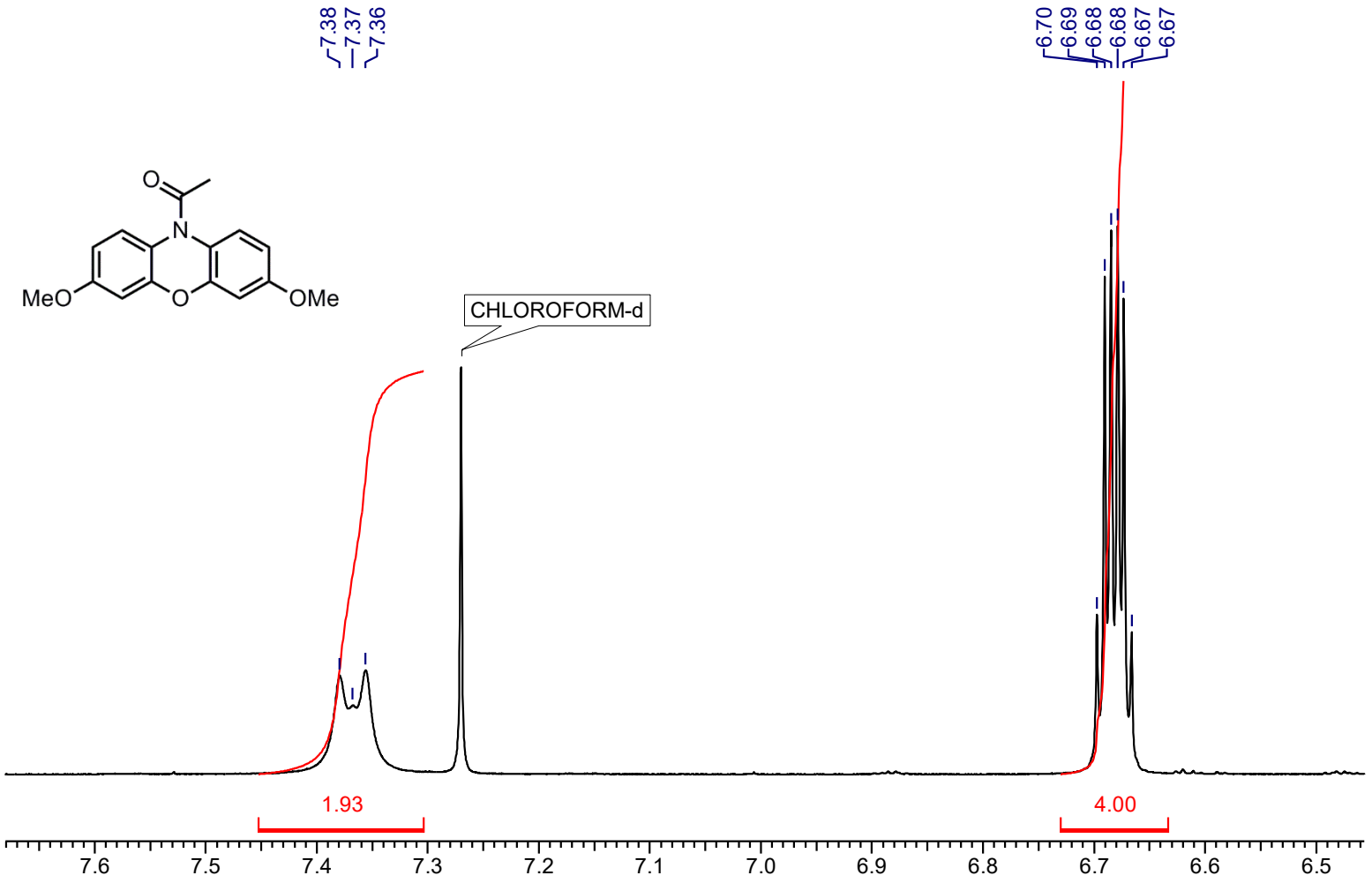
7.38
7.37
7.36
6.70
6.69
6.68
6.68
6.67
6.67
O
N
MeO
O
OMe
CHLOROFORM-d
1.93
4.00
7.6
7.5
7.4
7.3
7.2
7.1
7.0
6.9
6.8
6.7
6.6
6.5

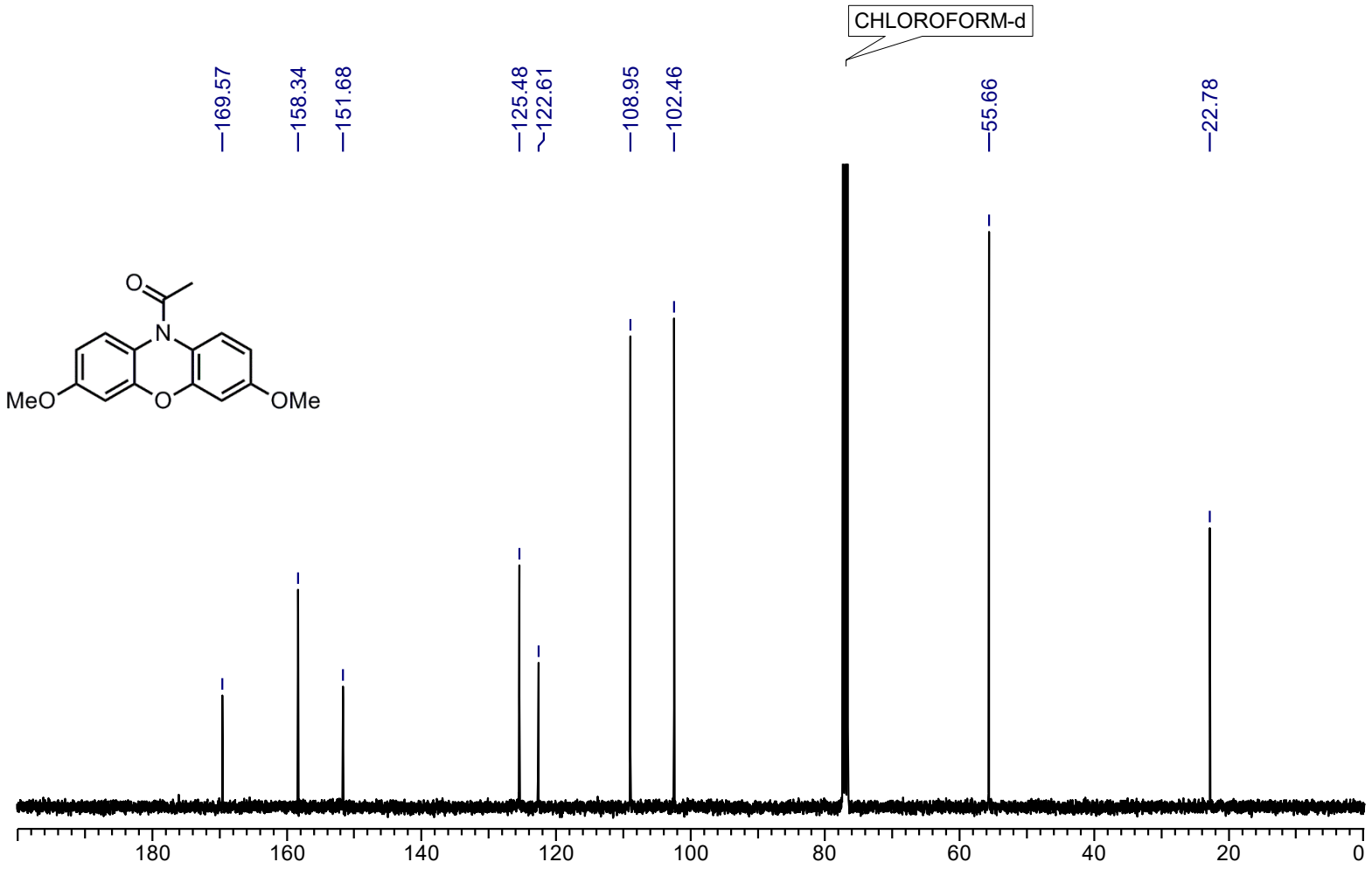
CHLOROFORM-d
169.57
158.34
151.68
125.48
122.61
108.95
102.46
55.66
22.78
O
N
MeO
O
OMe
180
160
140
120
100
80
60
40
20
0

3-Nitro-10-acetylphenoxazine (2.34)

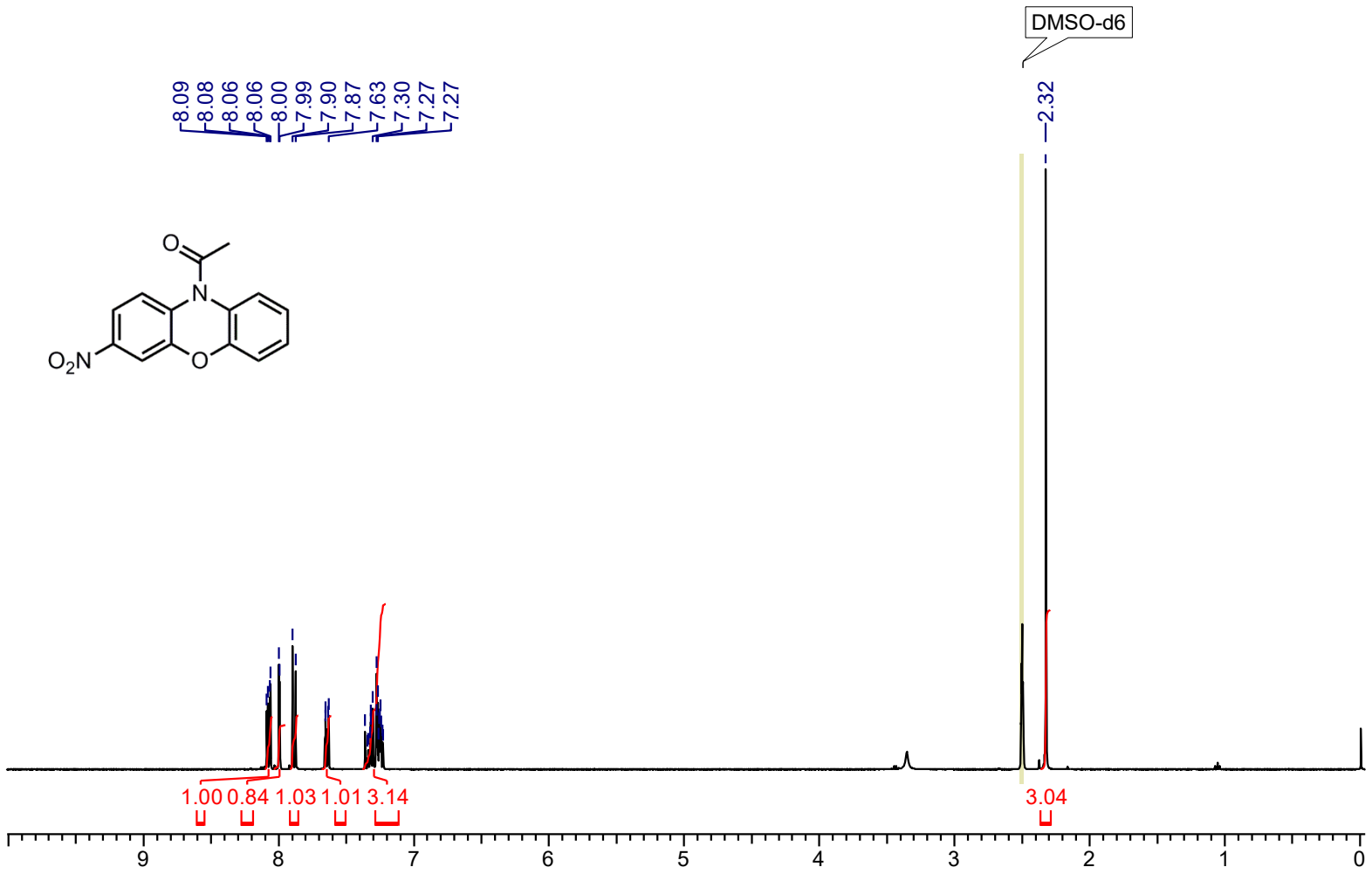

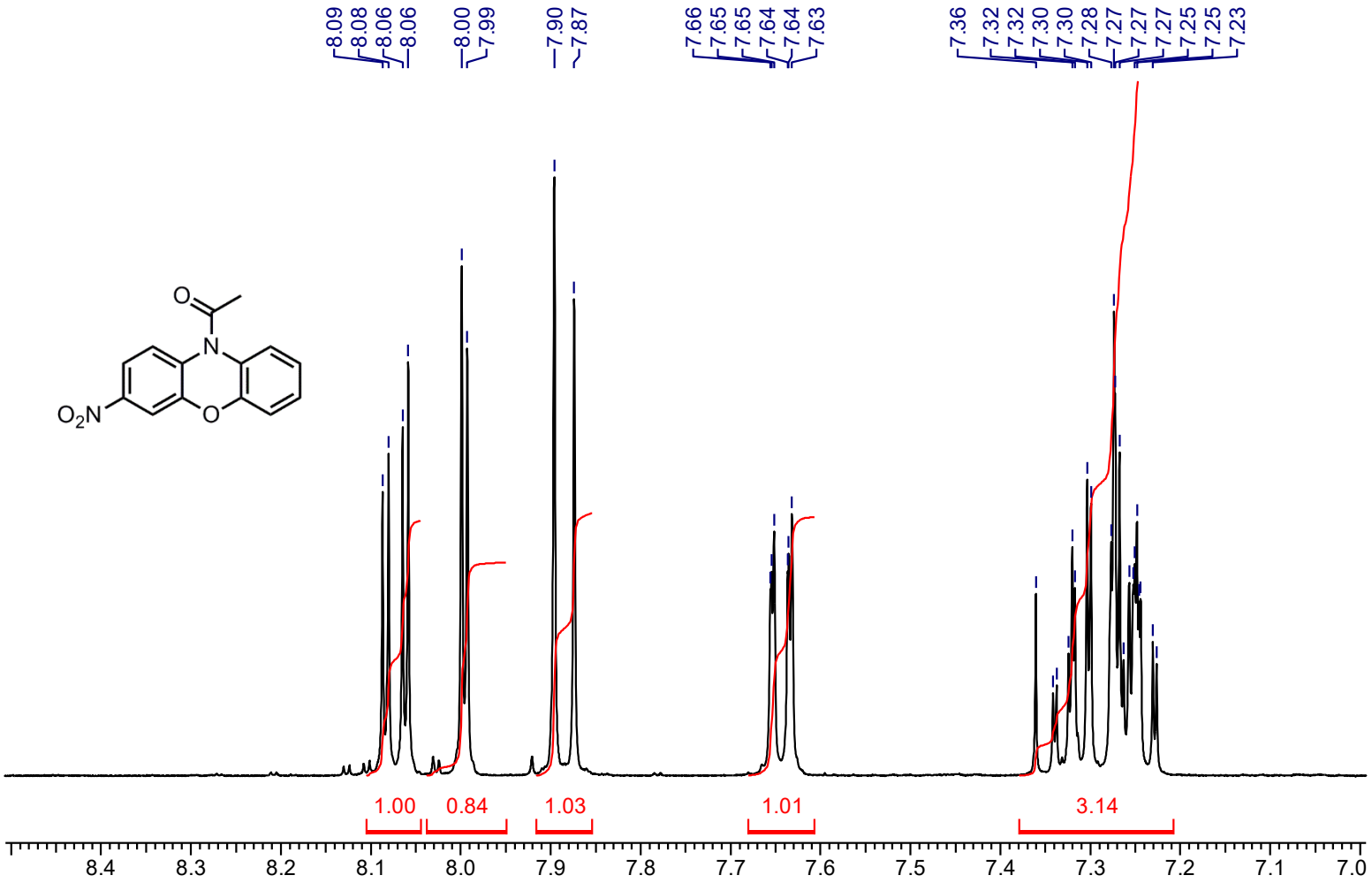
8.09
8.08
8.06
8.06
8.00
7.99
7.90
7.87
7.66
7.65
7.65
7.64
7.64
7.63
7.36
7.32
7.32
7.30
7.30
7.28
7.27
7.27
7.27
7.25
7.25
7.23
O
N
O
O2N
1.00
0.84
1.03
1.01
3.14
8.4
8.3
8.2
8.1
8.0
7.9
7.8
7.7
7.6
7.5
7.4
7.3
7.2
7.1
7.0

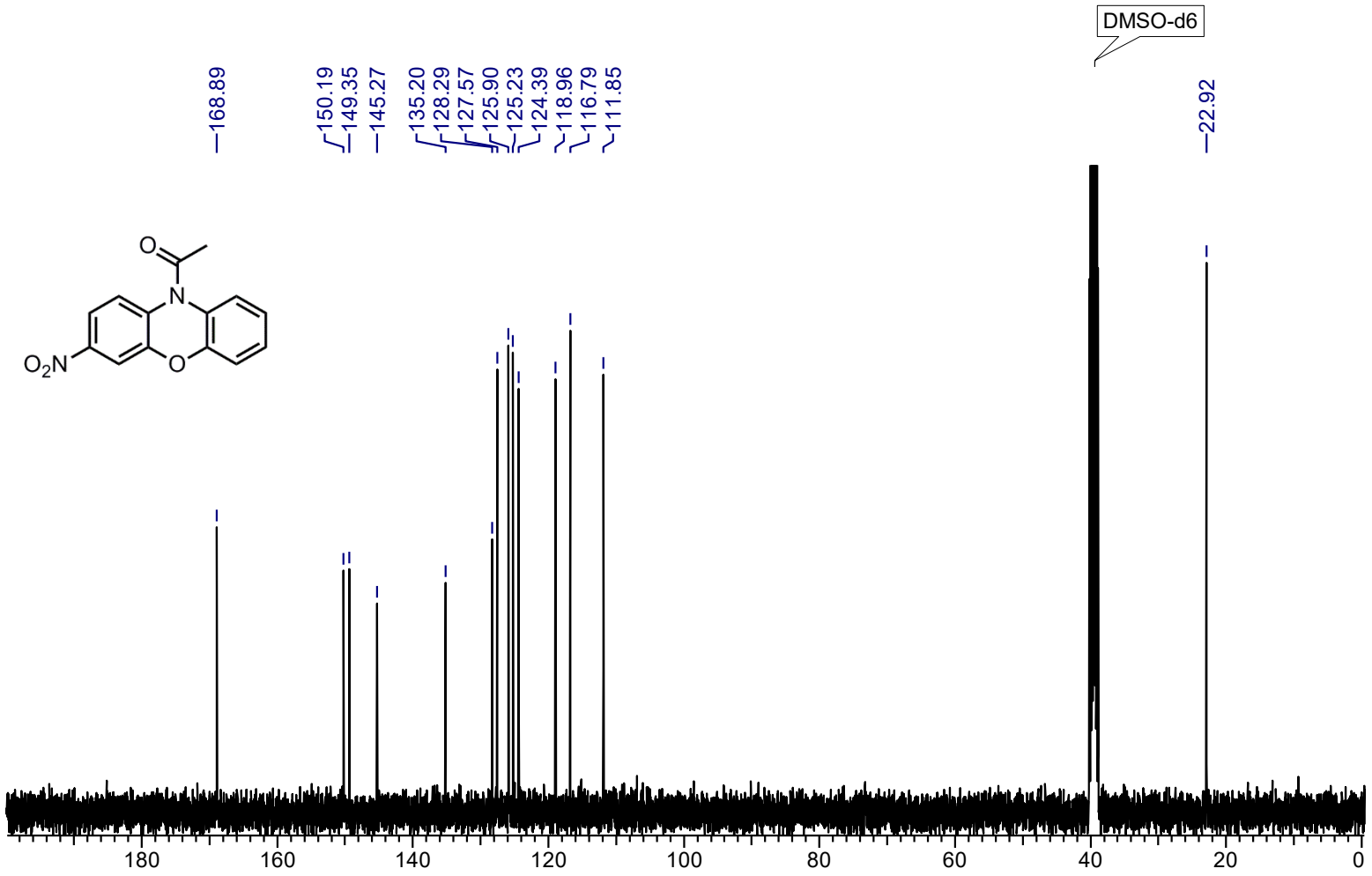
DMSO-d6
168.89
150.19
149.35
145.27
135.20
128.29
127.57
125.90
125.23
124.39
118.96
116.79
111.85
22.92
O
N
O2N
O
180
160
140
120
100
80
60
40
20
0

2-(2,4-Dinitrophenyl)amino-5-methoxyphenol (2.35)

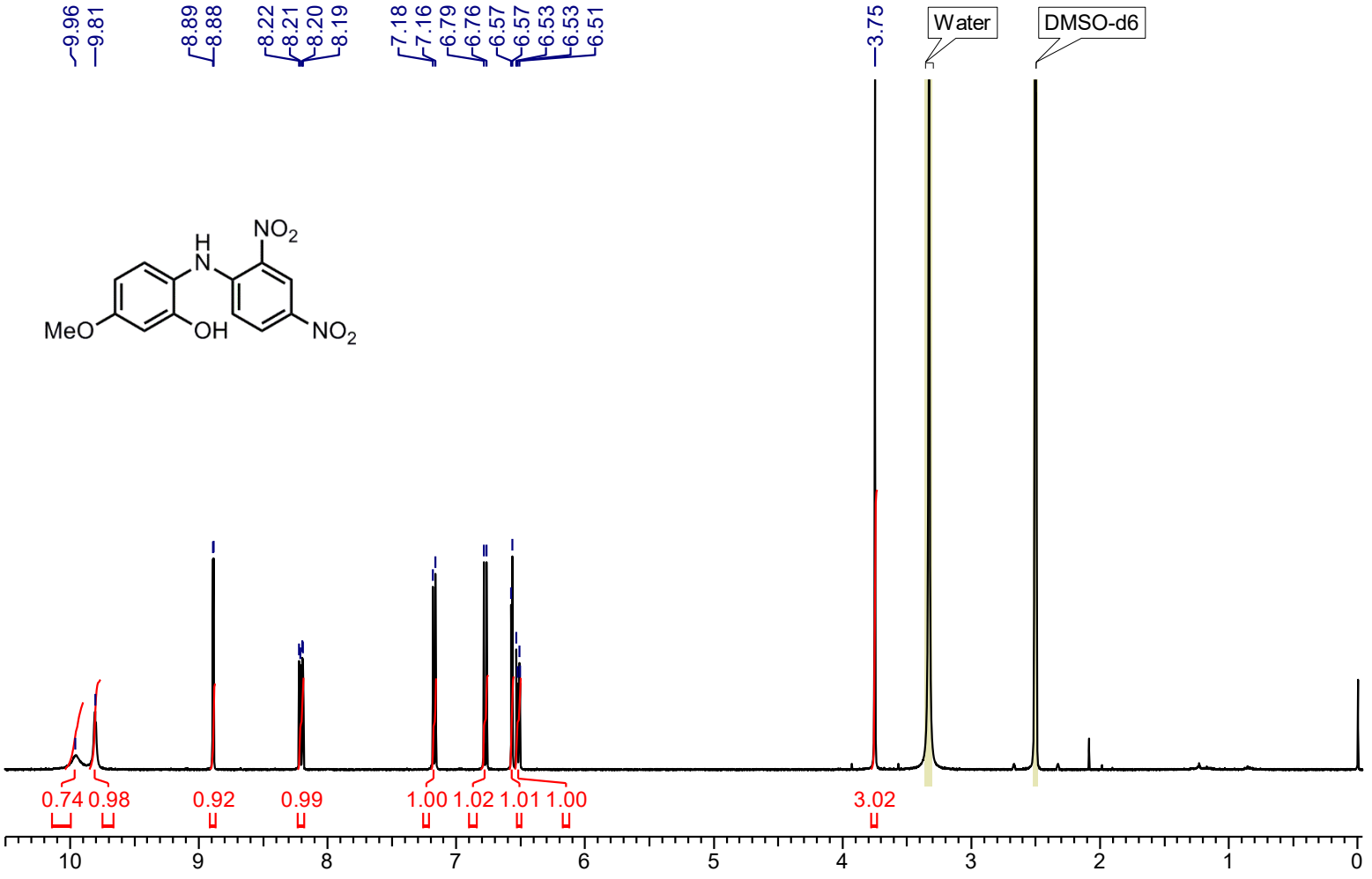

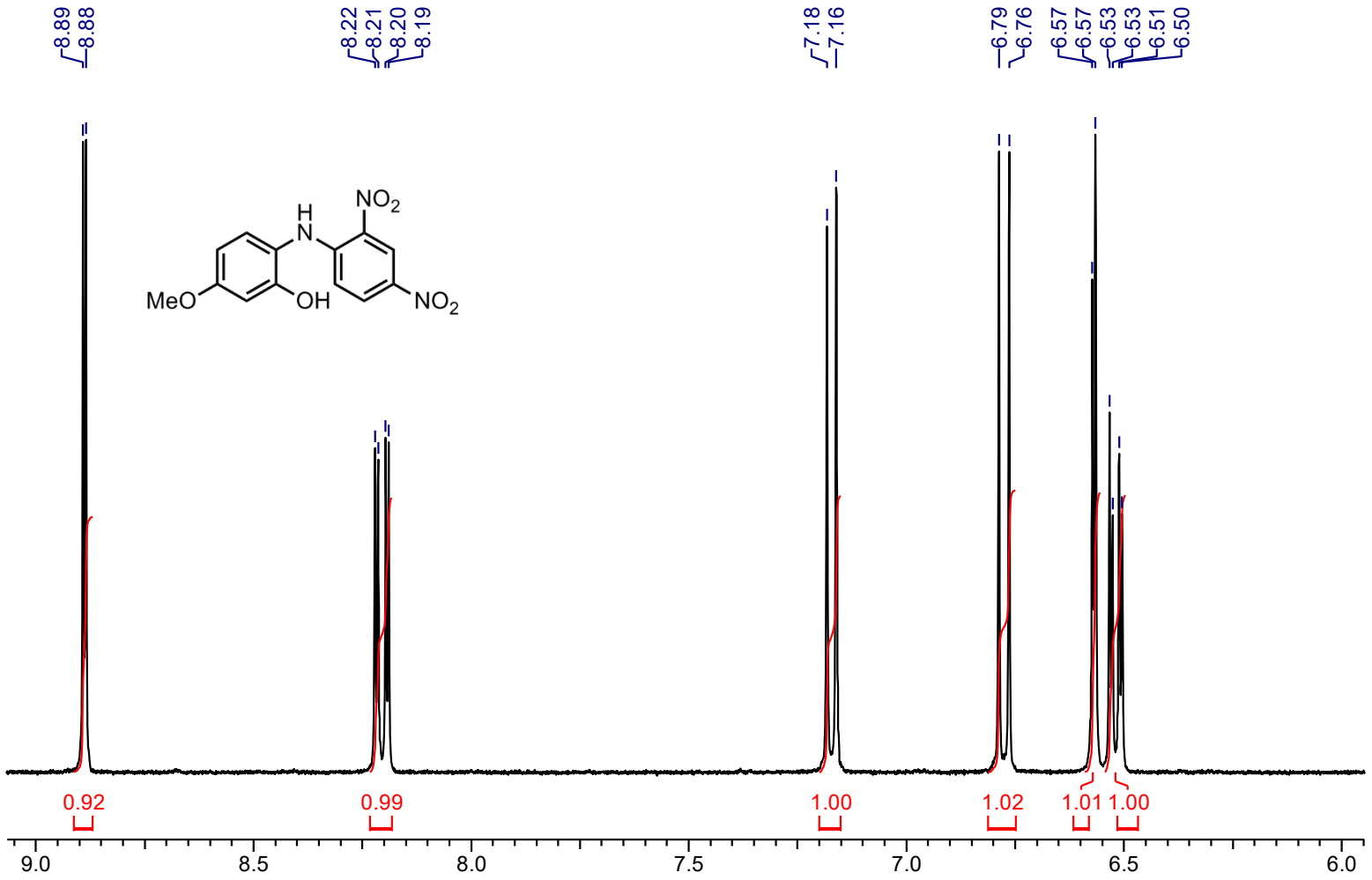
8.89
8.88
8.22
8.21
8.20
8.19
7.18
7.16
6.79
6.76
6.57
6.57
6.53
6.53
6.51
6.50
NO2
H
N
MeO
OH
NO2
0.92
0.99
1.00
1.02
1.01
1.00
9.0
8.5
8.0
7.5
7.0
6.5
6.0

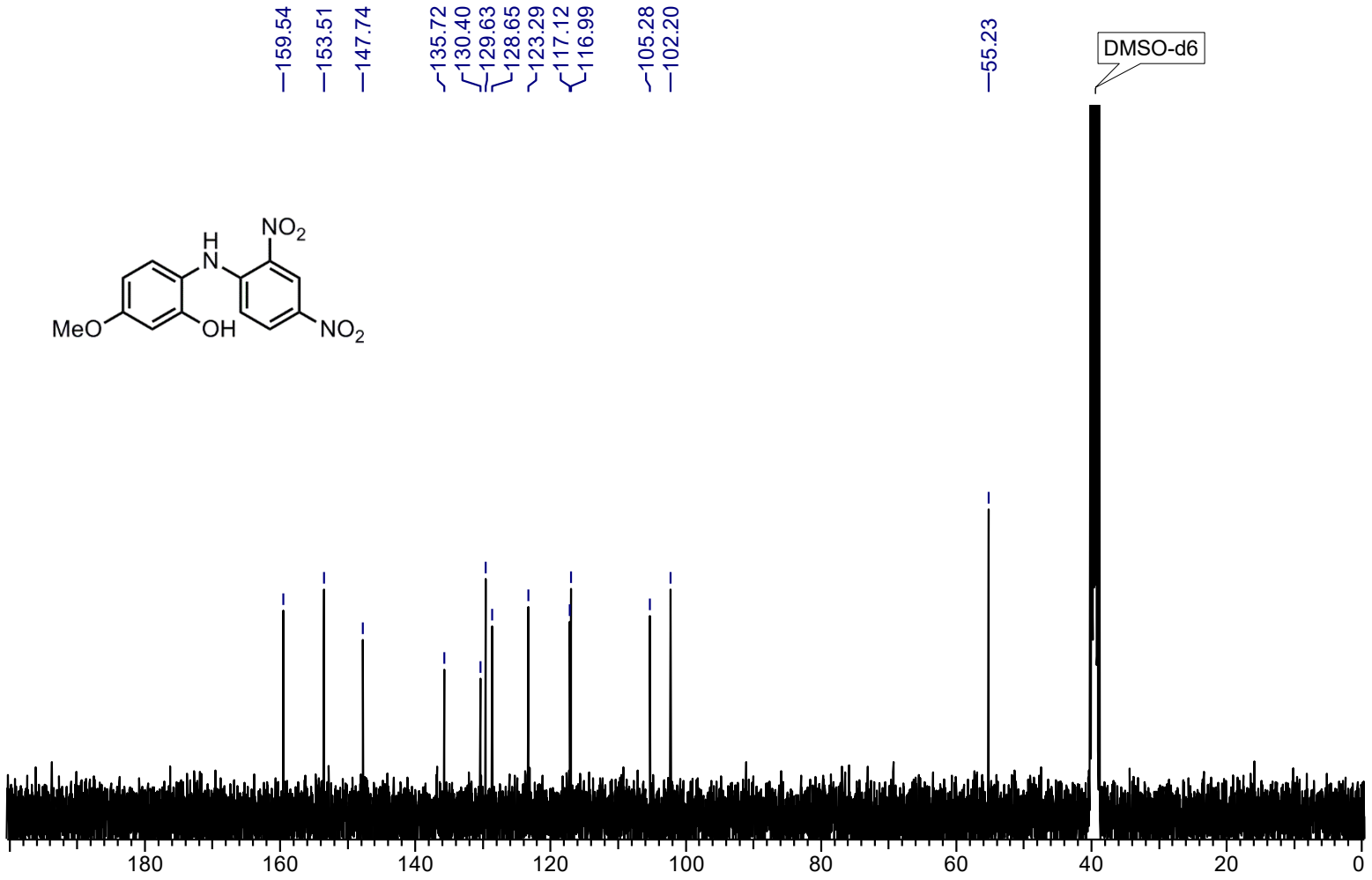
159.54
153.51
147.74
135.72
130.40
129.63
128.65
123.29
117.12
116.99
105.28
102.20
55.23
DMSO-d6
NO2
H
N
MeO
OH
NO2
180
160
140
120
100
80
60
40
20
0

3-Methoxy-7-nitrophenoxazine (2.13)

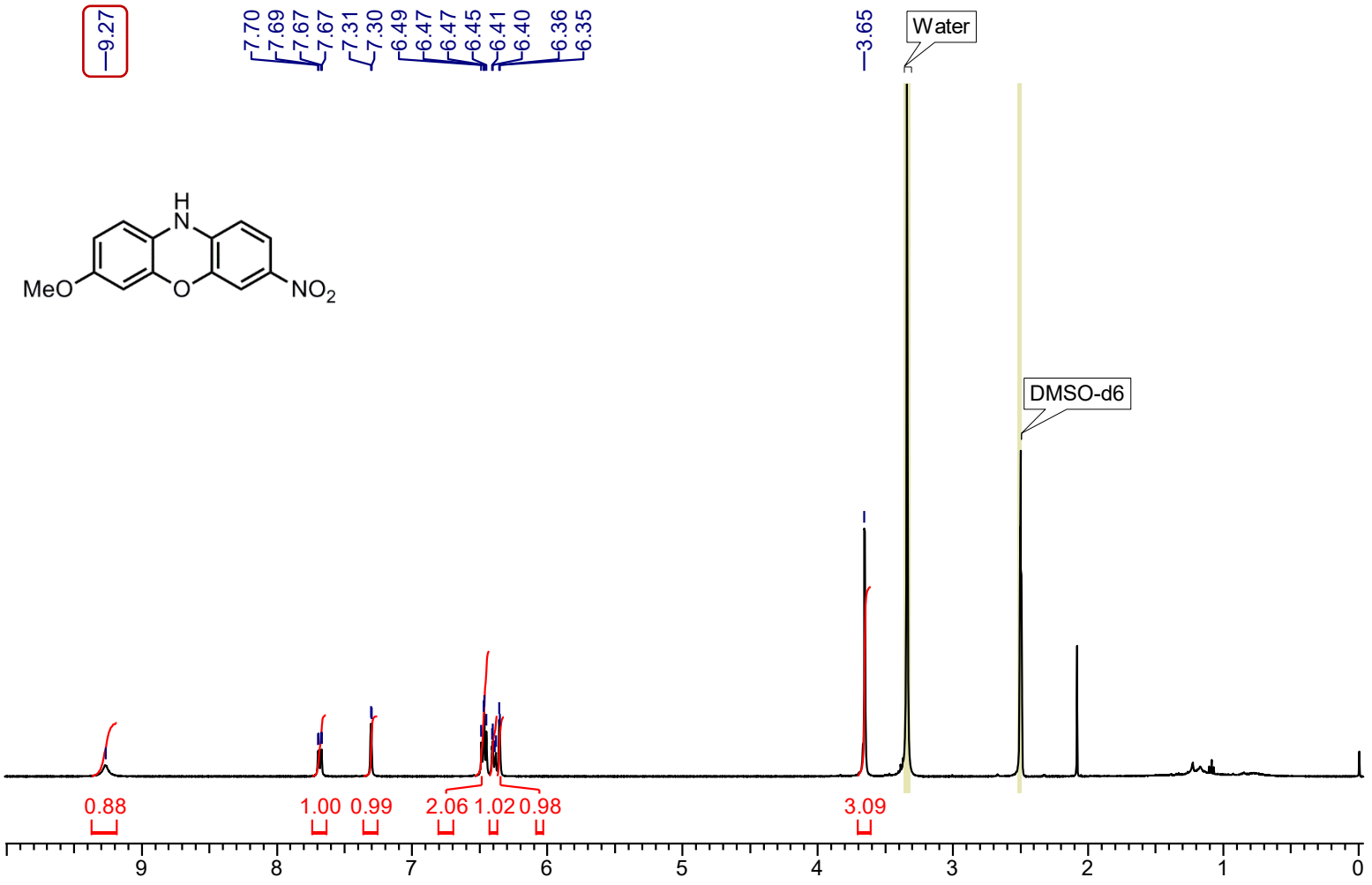

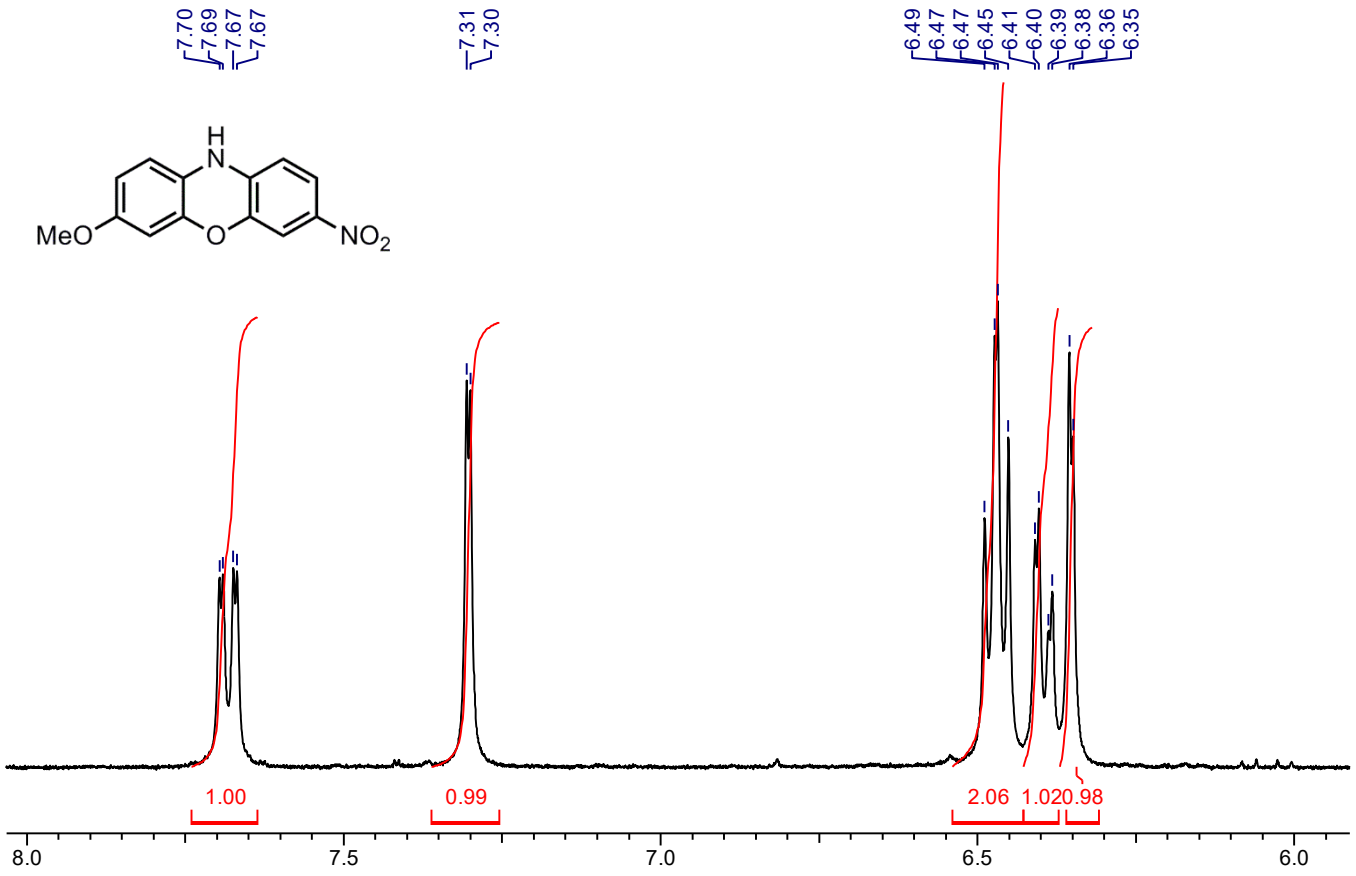
7.70
7.69
7.67
7.67
7.31
7.30
6.49
6.47
6.47
6.45
6.41
6.40
6.39
6.38
6.36
6.35
H
N
MeO
O
NO2
1.00
0.99
2.06
1.02
0.98
8.0
7.5
7.0
6.5
6.0

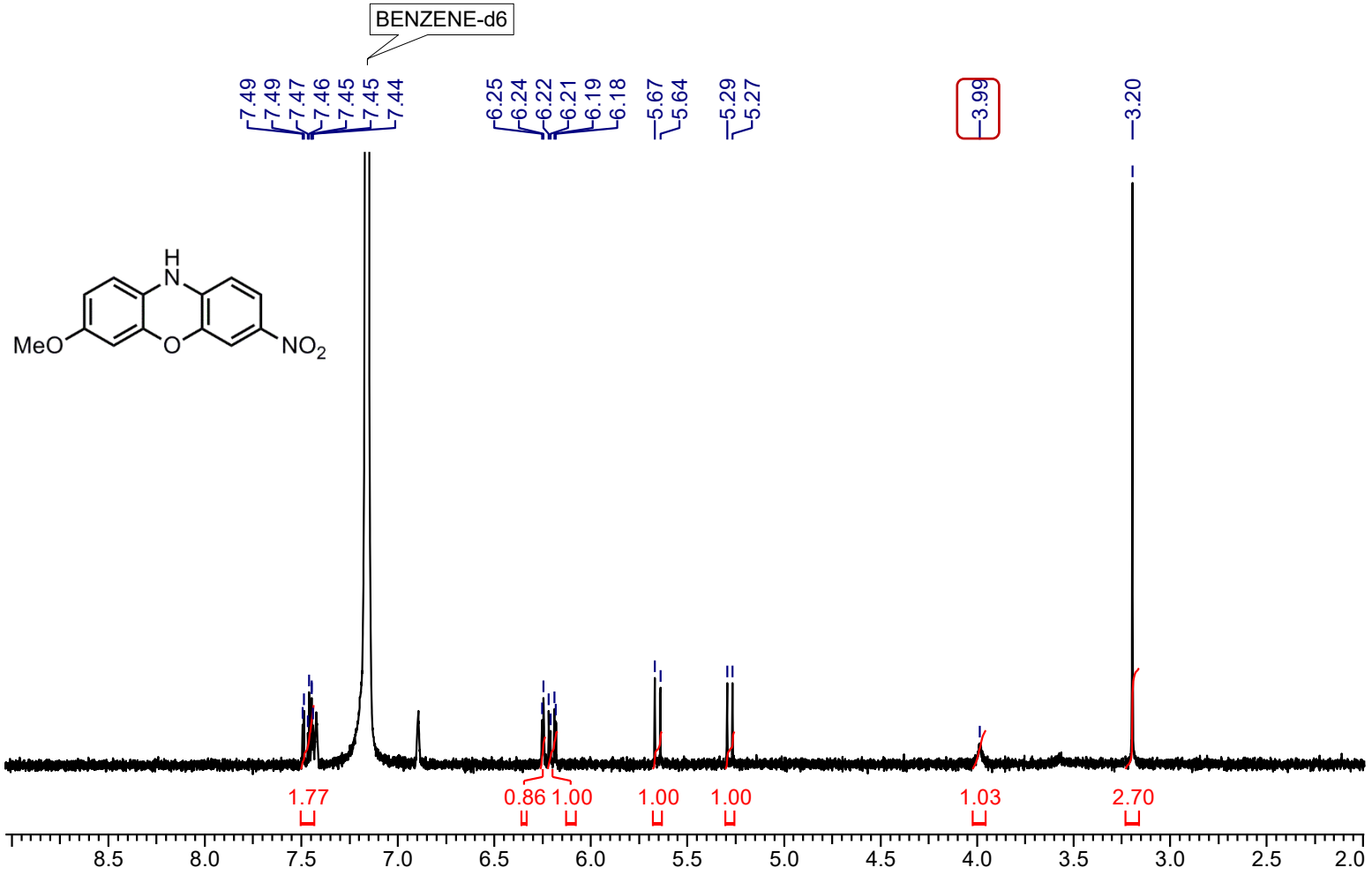
BENZENE-d6
7.49
7.49
7.47
7.46
7.45
7.45
7.44
6.25
6.24
6.22
6.21
6.19
6.18
5.67
5.64
5.29
5.27
3.99
3.20
H
N
O
MeO
NO2
1.77
0.86
1.00
1.00
1.00
1.03
2.70
8.5
8.0
7.5
7.0
6.5
6.0
5.5
5.0
4.5
4.0
3.5
3.0
2.5
2.0

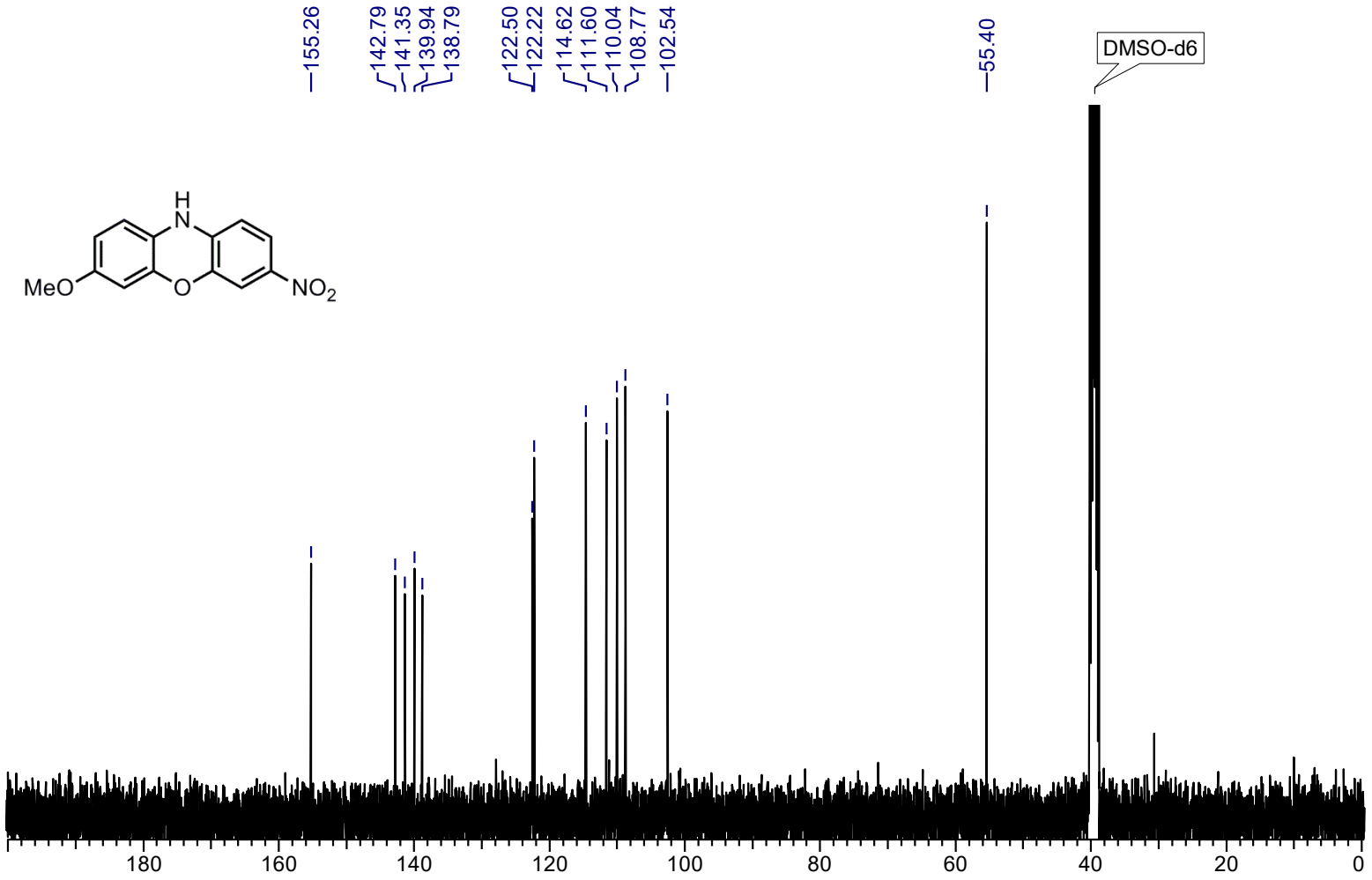
155.26
142.79
141.35
139.94
138.79
122.50
122.22
114.62
111.60
110.04
108.77
102.54
55.40
DMSO-d6
H
N
O
MeO
NO2
180
160
140
120
100
80
60
40
20
0

N,N-Diethyl-3-sulfonamidephenoxazine (2.11)

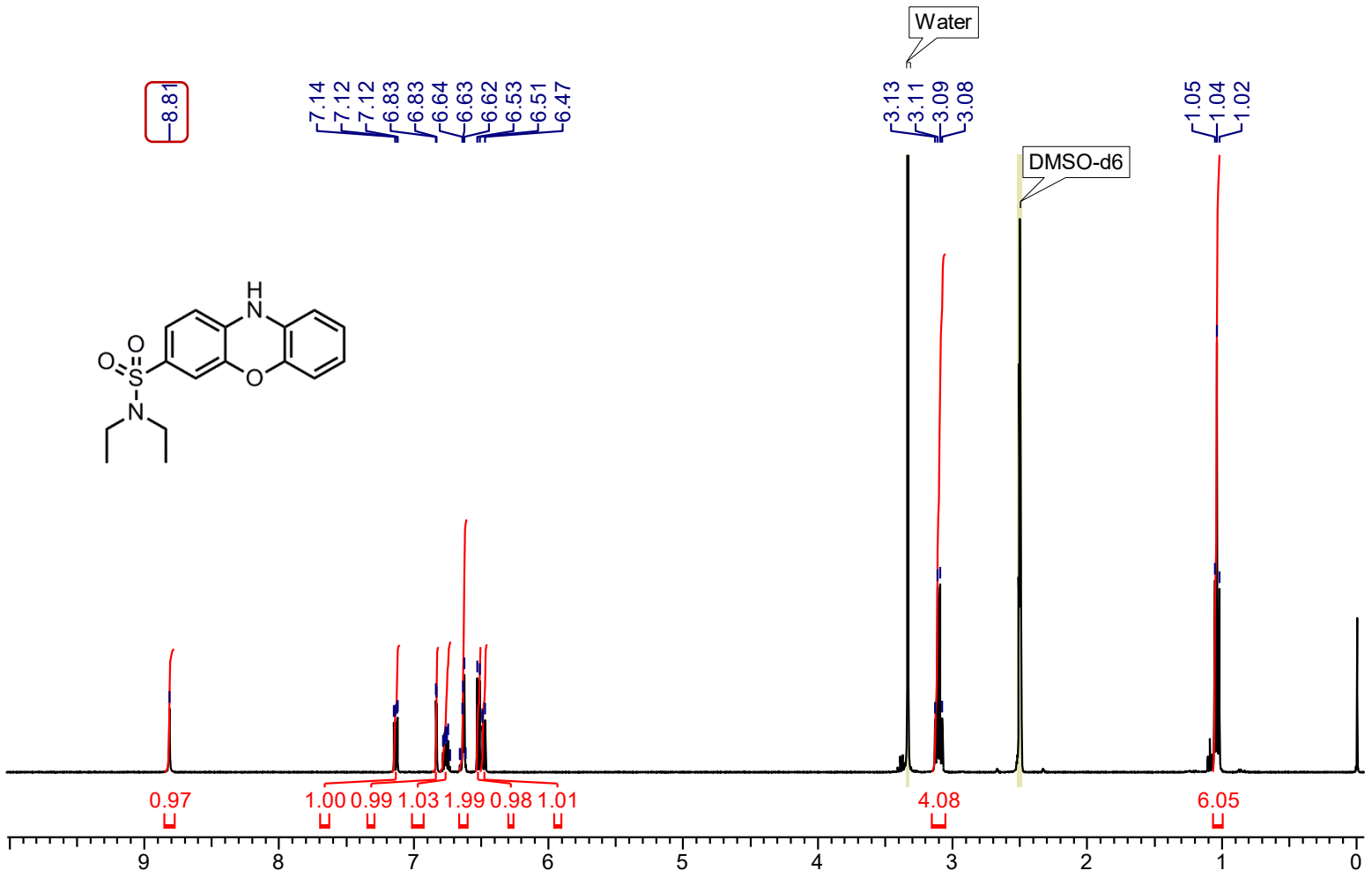

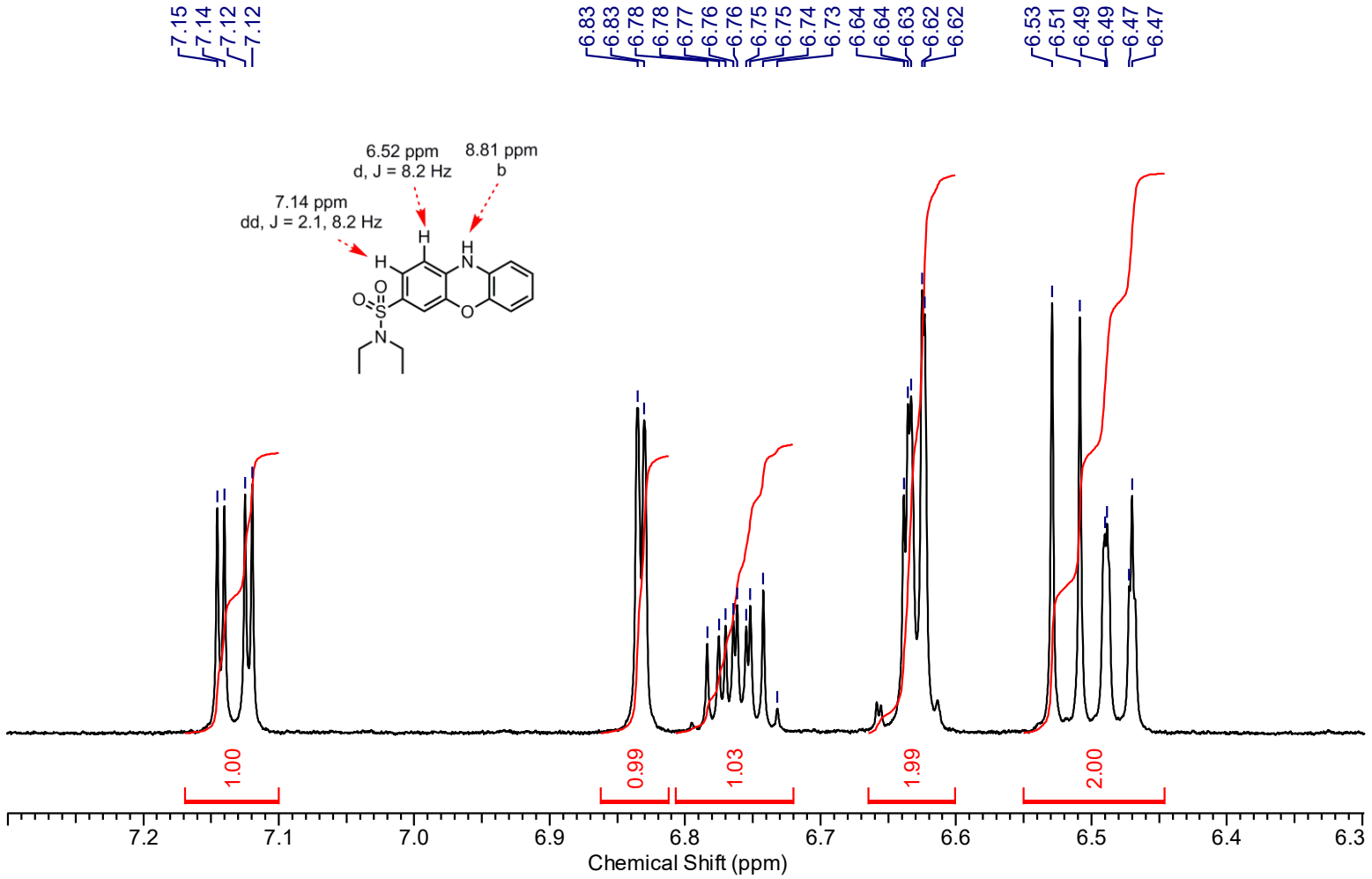
7.15
7.14
7.12
7.12
6.83
6.83
6.78
6.78
6.77
6.76
6.76
6.75
6.75
6.74
6.73
6.64
6.64
6.63
6.62
6.62
6.53
6.51
6.49
6.49
6.47
6.47
6.52 ppm
d, J = 8.2 Hz
8.81 ppm
b
7.14 ppm
dd, J = 2.1, 8.2 Hz
1.00
0.99
1.03
1.99
2.00
7.2
7.1
7.0
6.9
6.8
6.7
6.6
6.5
6.4
6.3
Chemical Shift (ppm)

NOESY

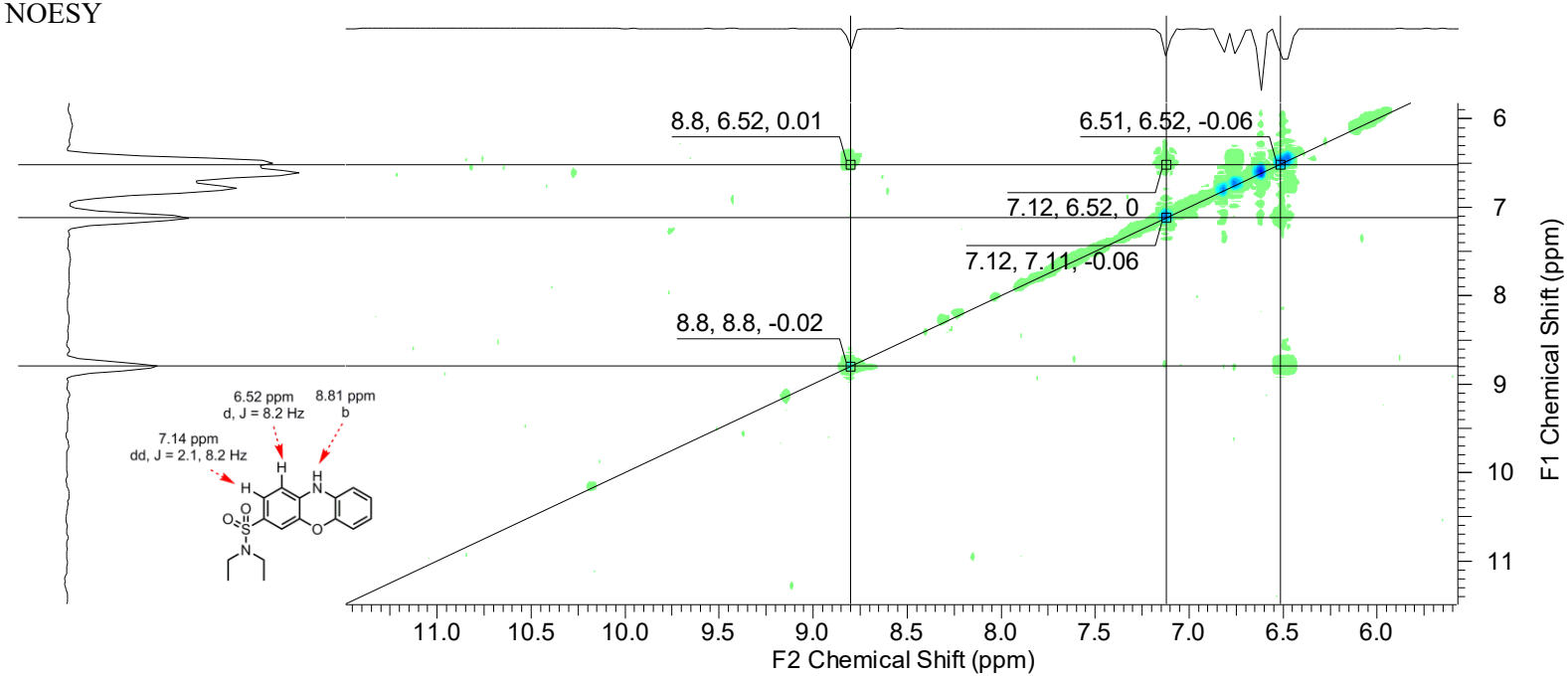
8.8, 6.52, 0.01
6.51, 6.52, -0.06
7.12, 6.52, 0
7.12, 7.11, -0.06
8.8, 8.8, -0.02
6.52 ppm
d, J = 8.2 Hz
8.81 ppm
b
7.14 ppm
dd, J = 2.1, 8.2 Hz
11.0
10.5
10.0
9.5
9.0
8.5
8.0
7.5
7.0
6.5
6.0
F2 Chemical Shift (ppm)
6
7
8
9
10
11
F1 Chemical Shift (ppm)

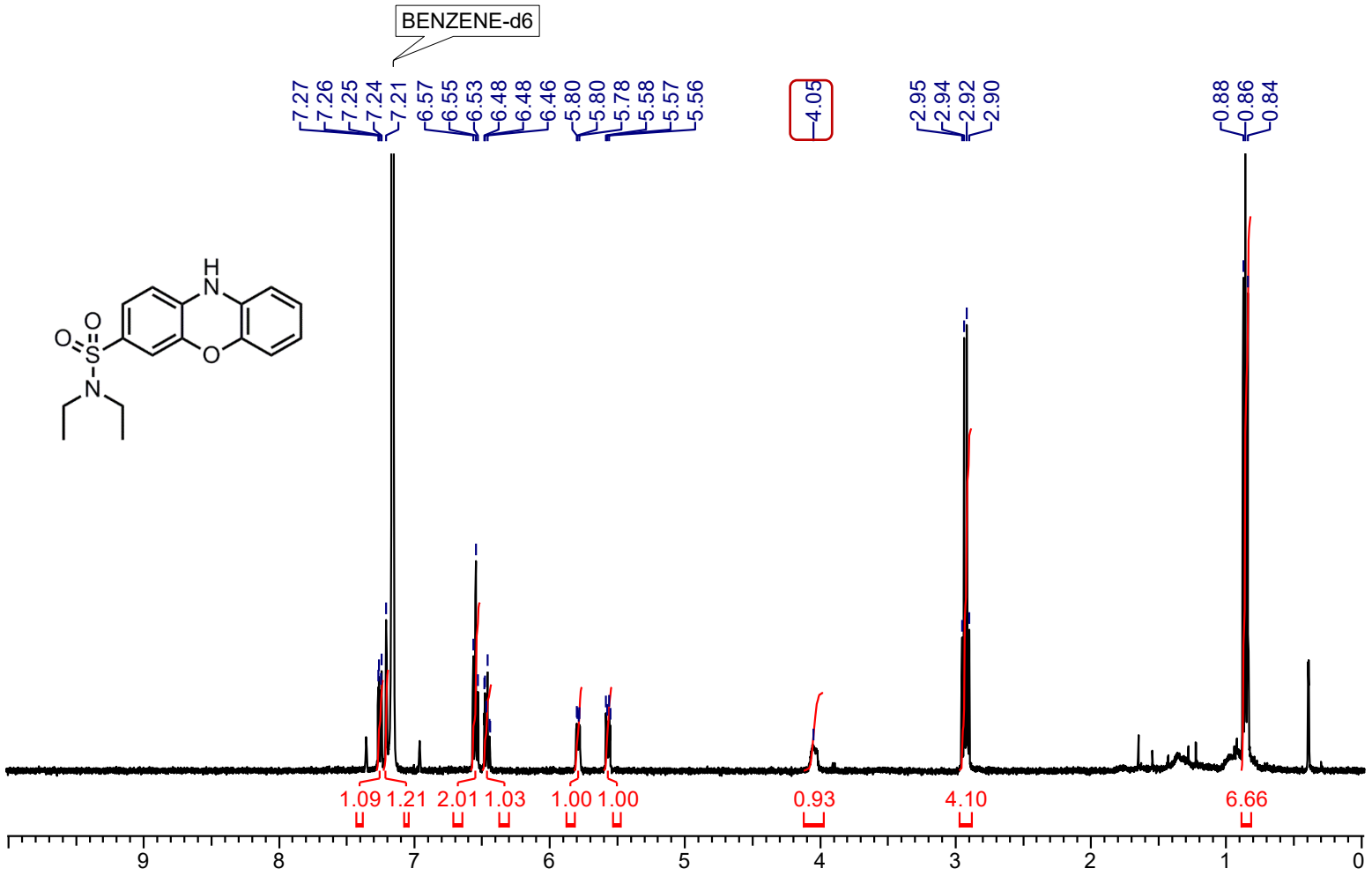
BENZENE-d6
7.27
7.26
7.25
7.24
7.21
6.57
6.55
6.53
6.48
6.48
6.46
5.80
5.80
5.78
5.58
5.57
5.56
4.05
2.95
2.94
2.92
2.90
0.88
0.86
0.84
H
N
O
O
S
O
N
O
1.09
1.21
2.01
1.03
1.00
1.00
0.93
4.10
6.66
9
8
7
6
5
4
3
2
1
0

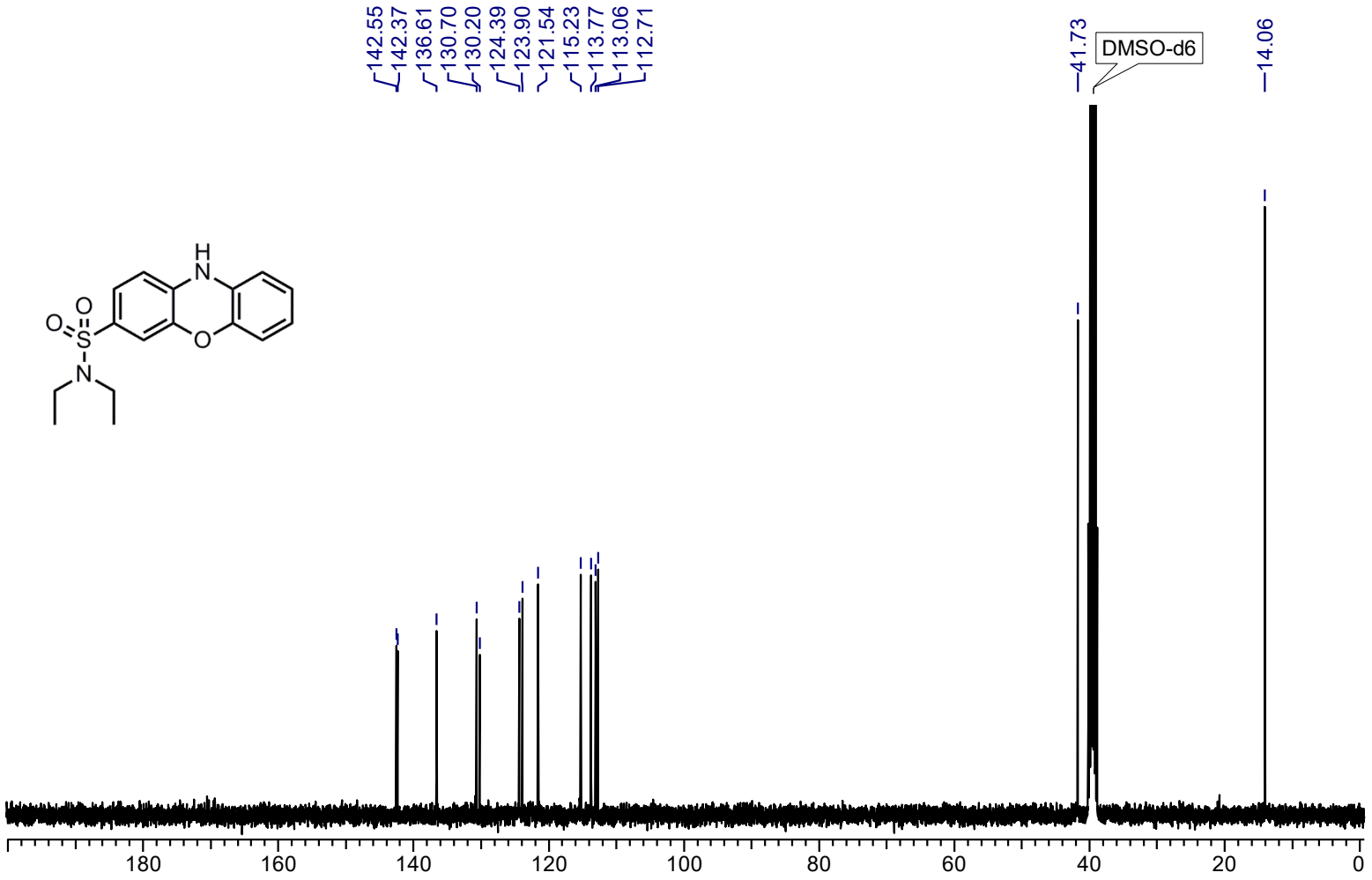
142.55
142.37
136.61
130.70
130.20
124.39
123.90
121.54
115.23
113.77
113.06
112.71
41.73
DMSO-d6
14.06
H
N
O
O
S
O
N
180
160
140
120
100
80
60
40
20
0

2,4,6,8-Tetra-tert-butylphenoxazine (2.9)

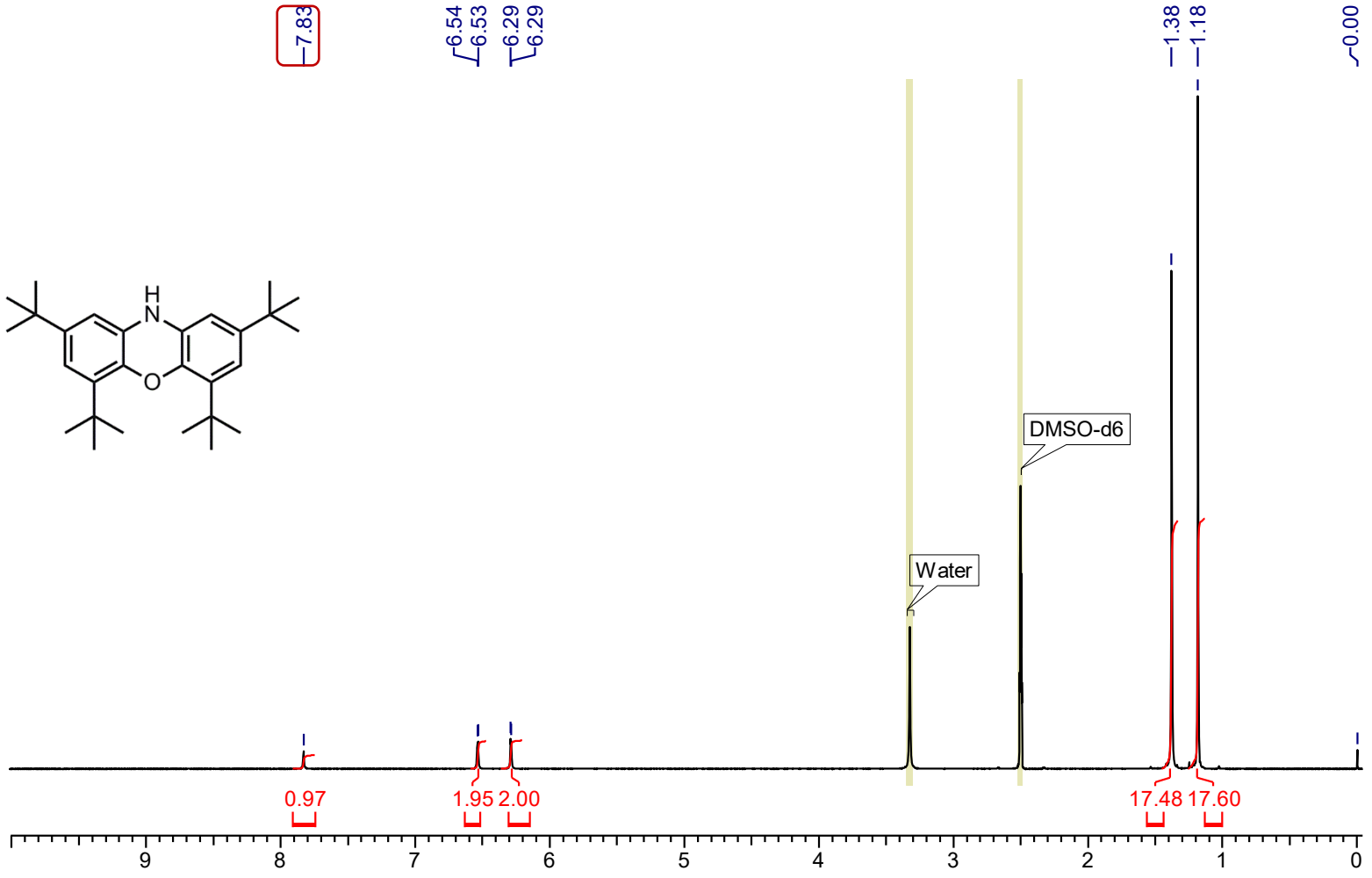

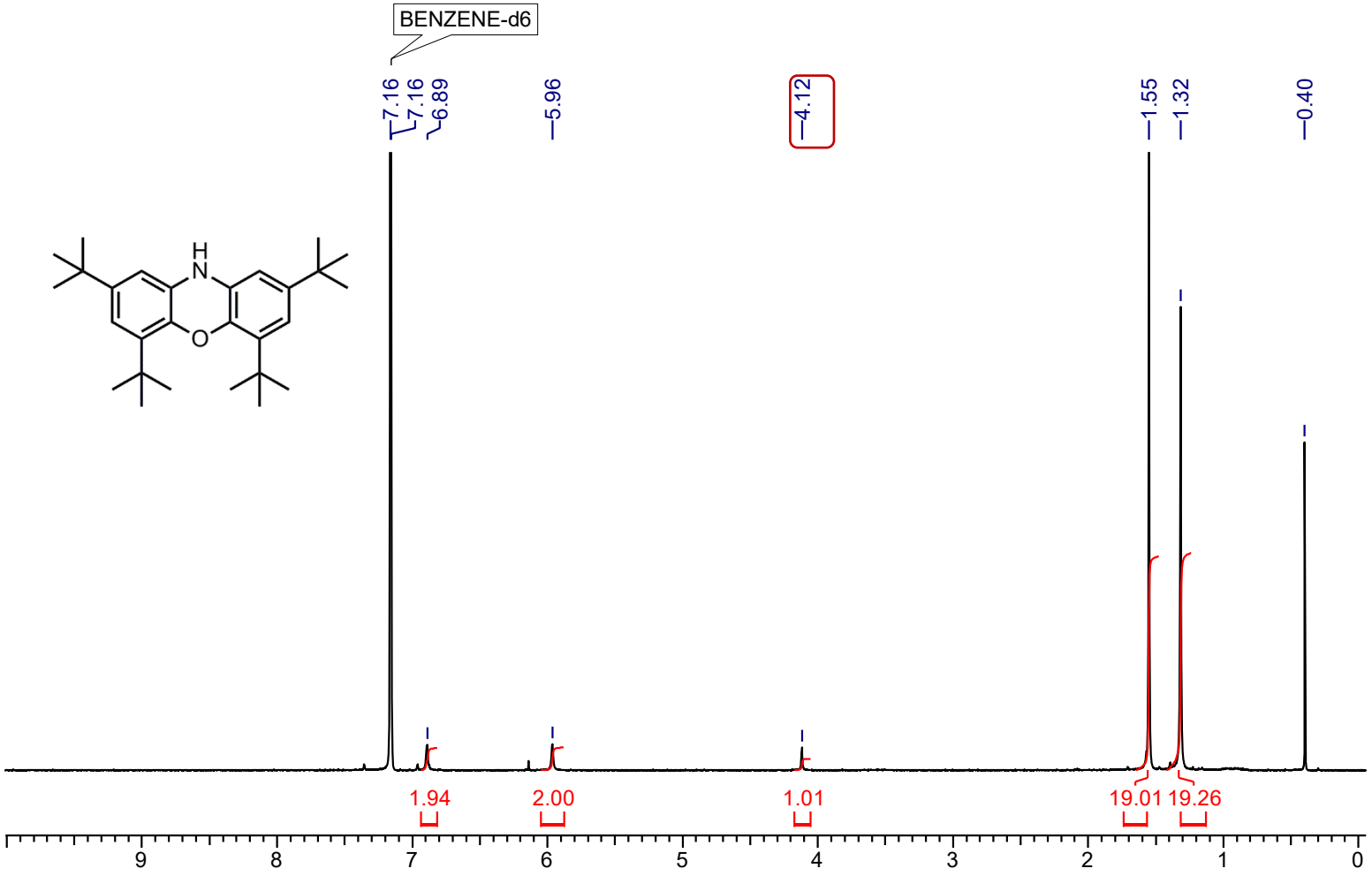
BENZENE-d6
7.16
7.16
6.89
5.96
4.12
1.55
1.32
0.40
H
N
O
1.94
2.00
1.01
19.01
19.26
9
8
7
6
5
4
3
2
1
0

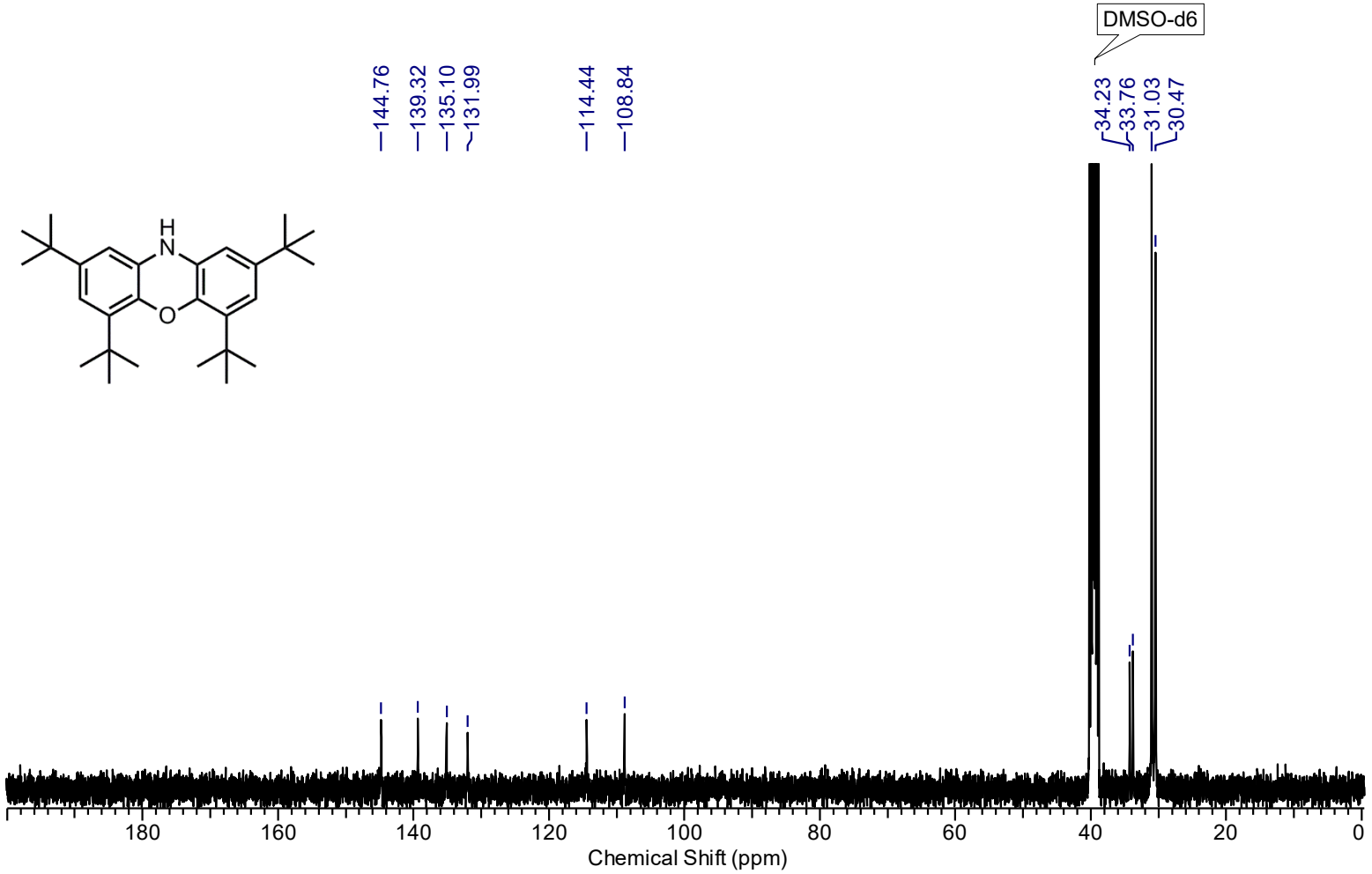
DMSO-d6
144.76
139.32
135.10
131.99
114.44
108.84
34.23
33.76
31.03
30.47
H
N
O
180
160
140
120
100
80
60
40
20
0
Chemical Shift (ppm)

2,8-di-tert-butylphenoxazine (2.10)

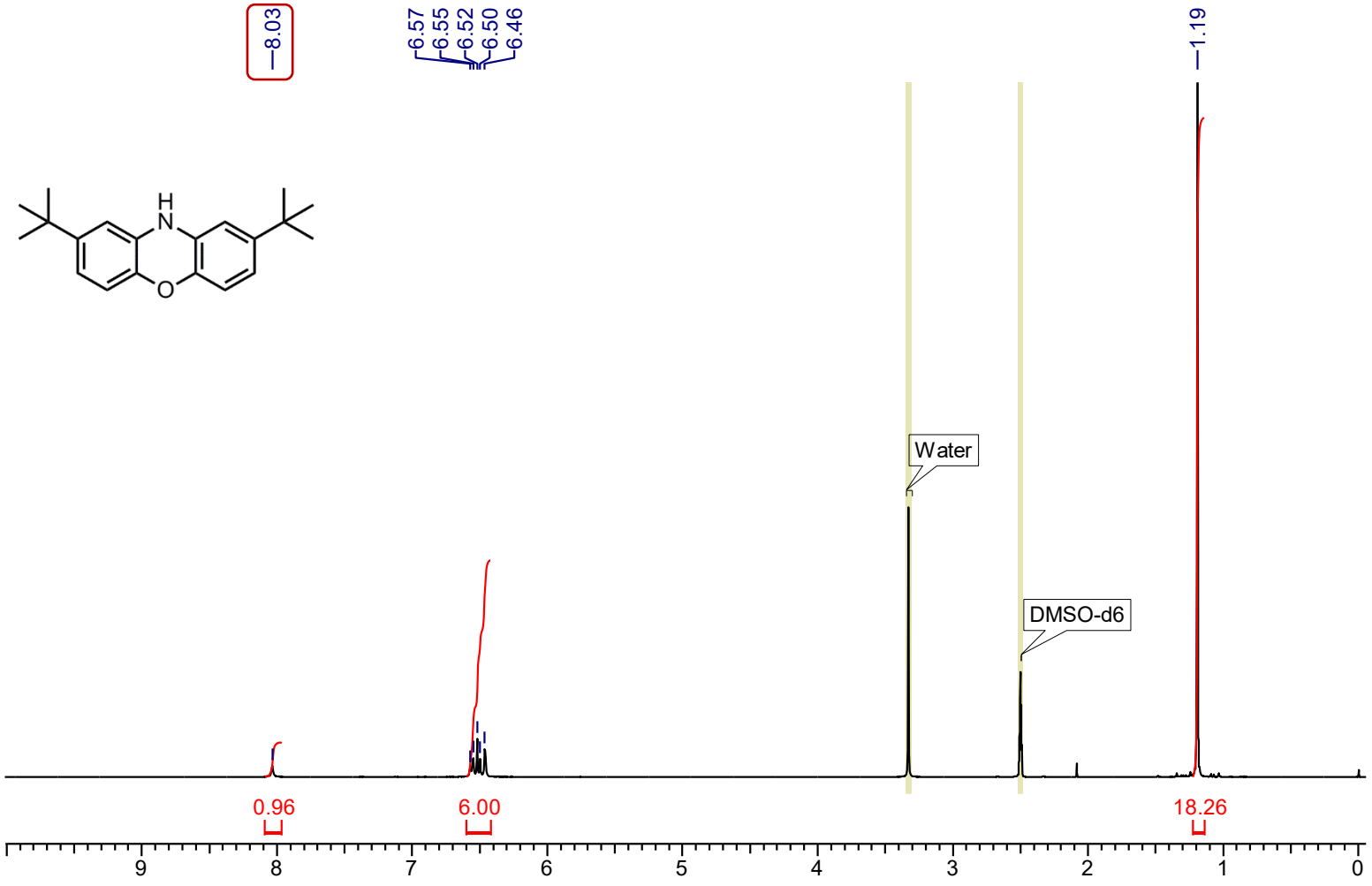

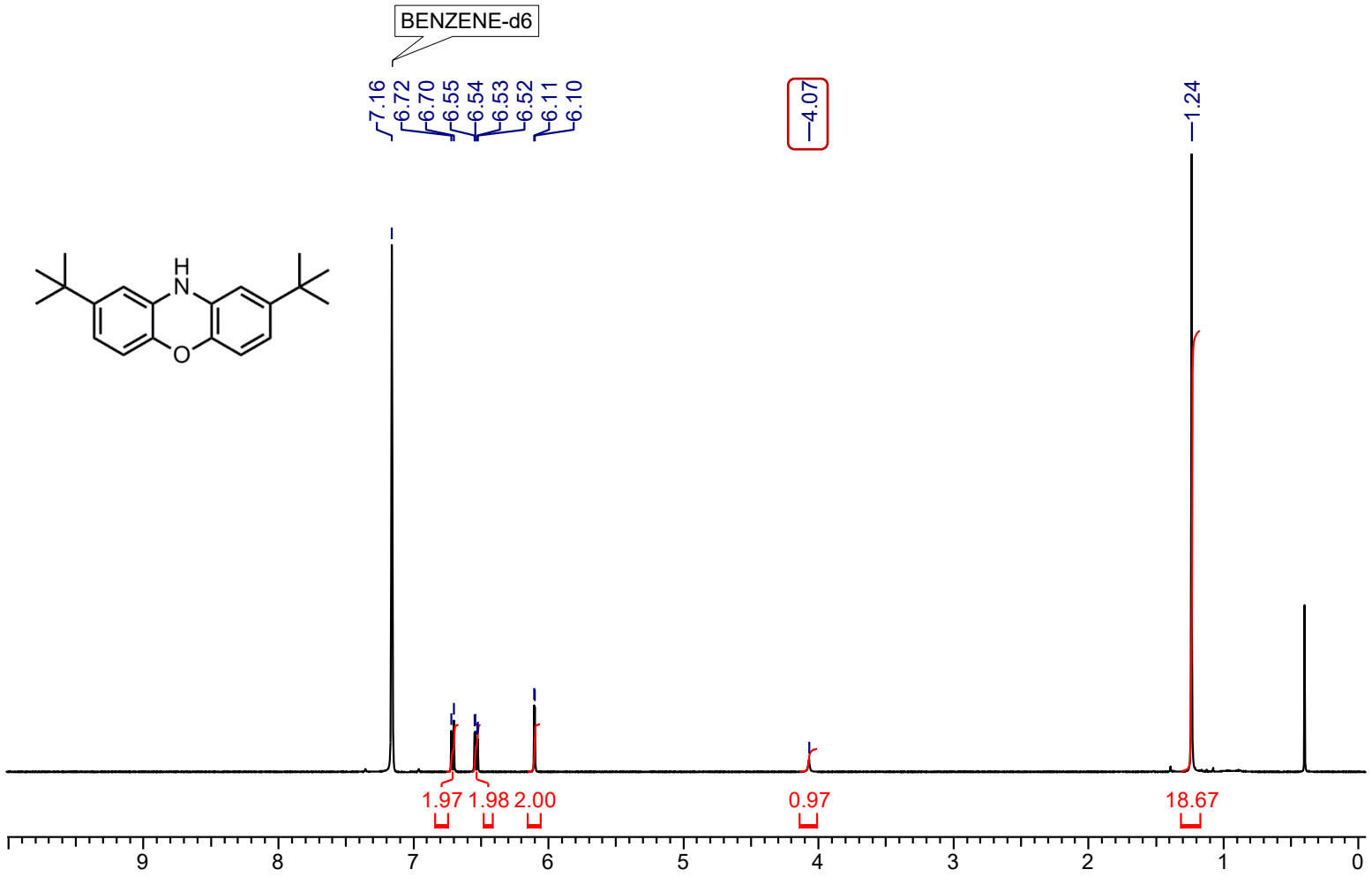
BENZENE-d6
7.16
6.72
6.70
6.55
6.54
6.53
6.52
6.11
6.10
4.07
1.24
H
N
O
1.97
1.98
2.00
0.97
18.67
9
8
7
6
5
4
3
2
1
0

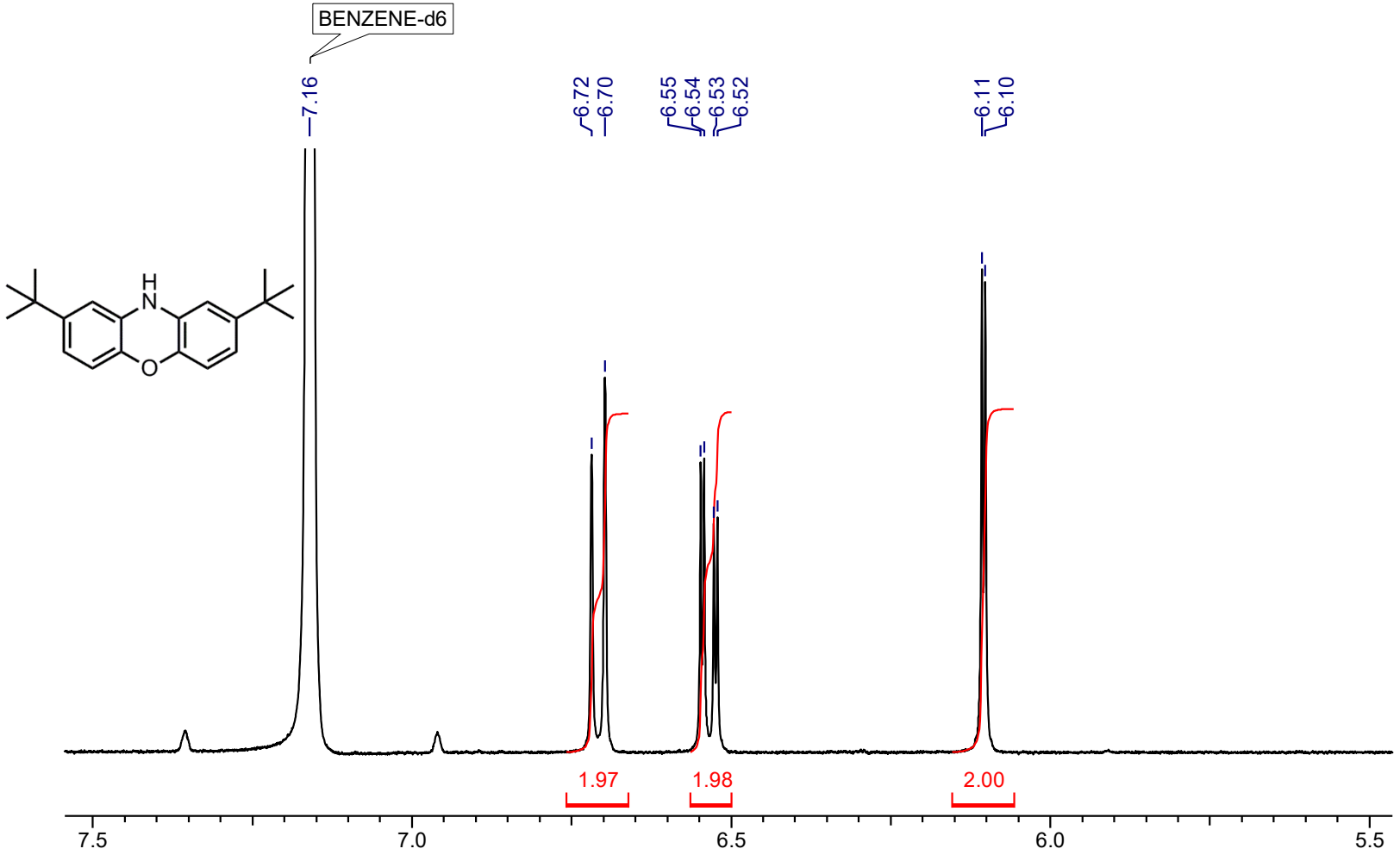
BENZENE-d6
7.16
6.72
6.70
6.55
6.54
6.53
6.52
6.11
6.10
H
N
O
1.97
1.98
2.00
7.5
7.0
6.5
6.0
5.5

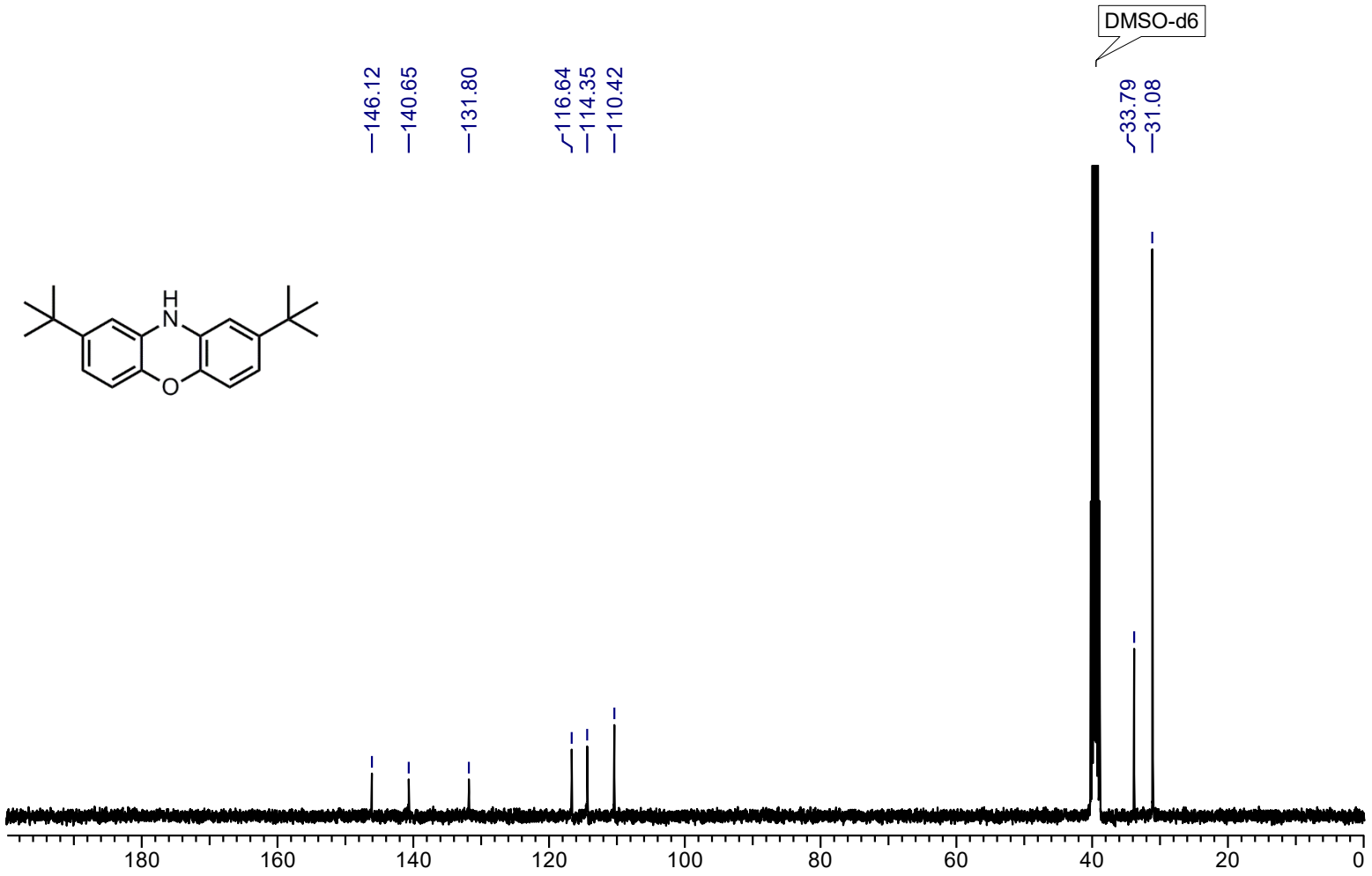
DMSO-d6
146.12
140.65
131.80
116.64
114.35
110.42
33.79
31.08
H
N
O
180
160
140
120
100
80
60
40
20
0

3-Nitro-7-cyanophenoxazine (2.15)

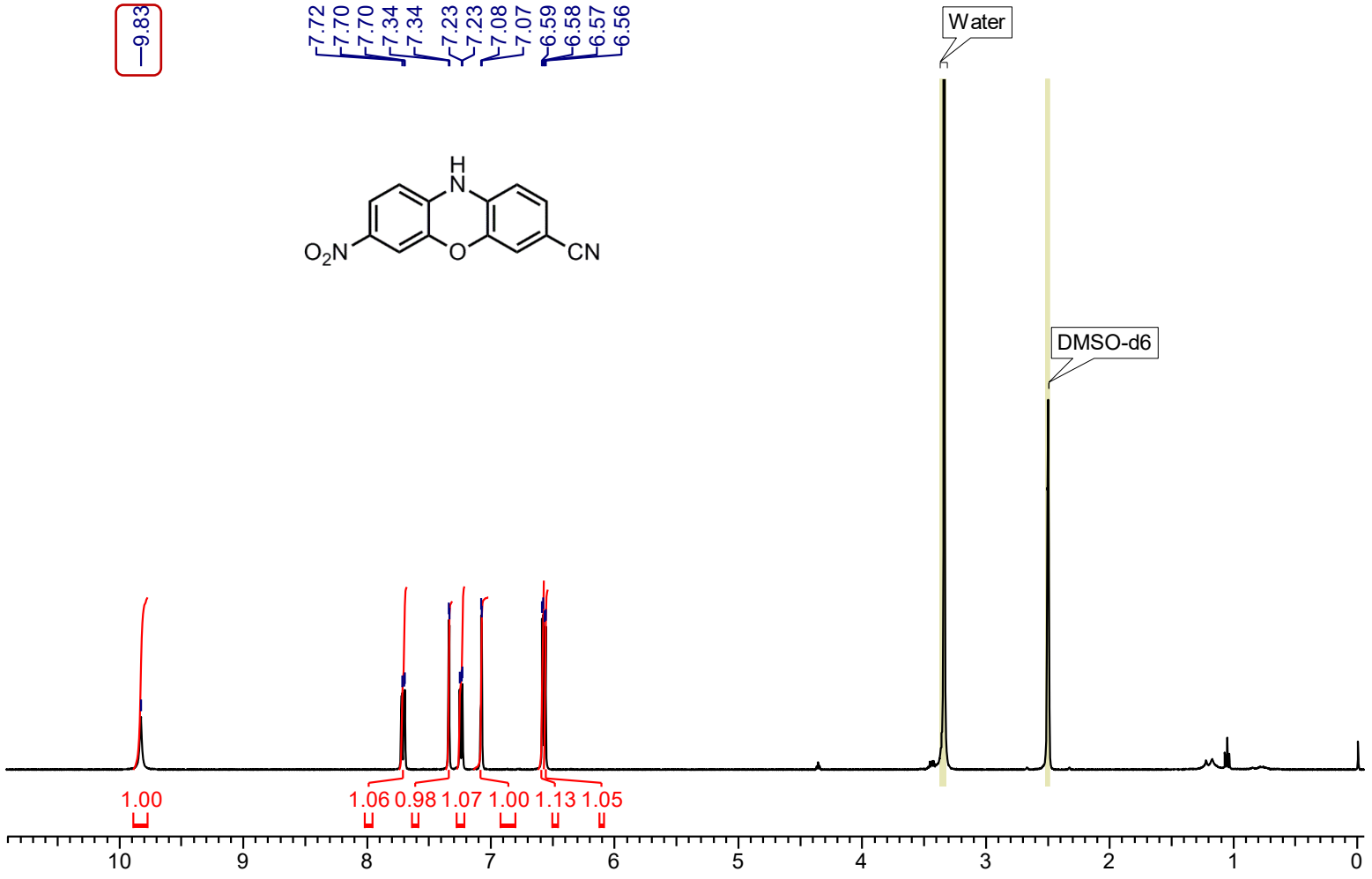

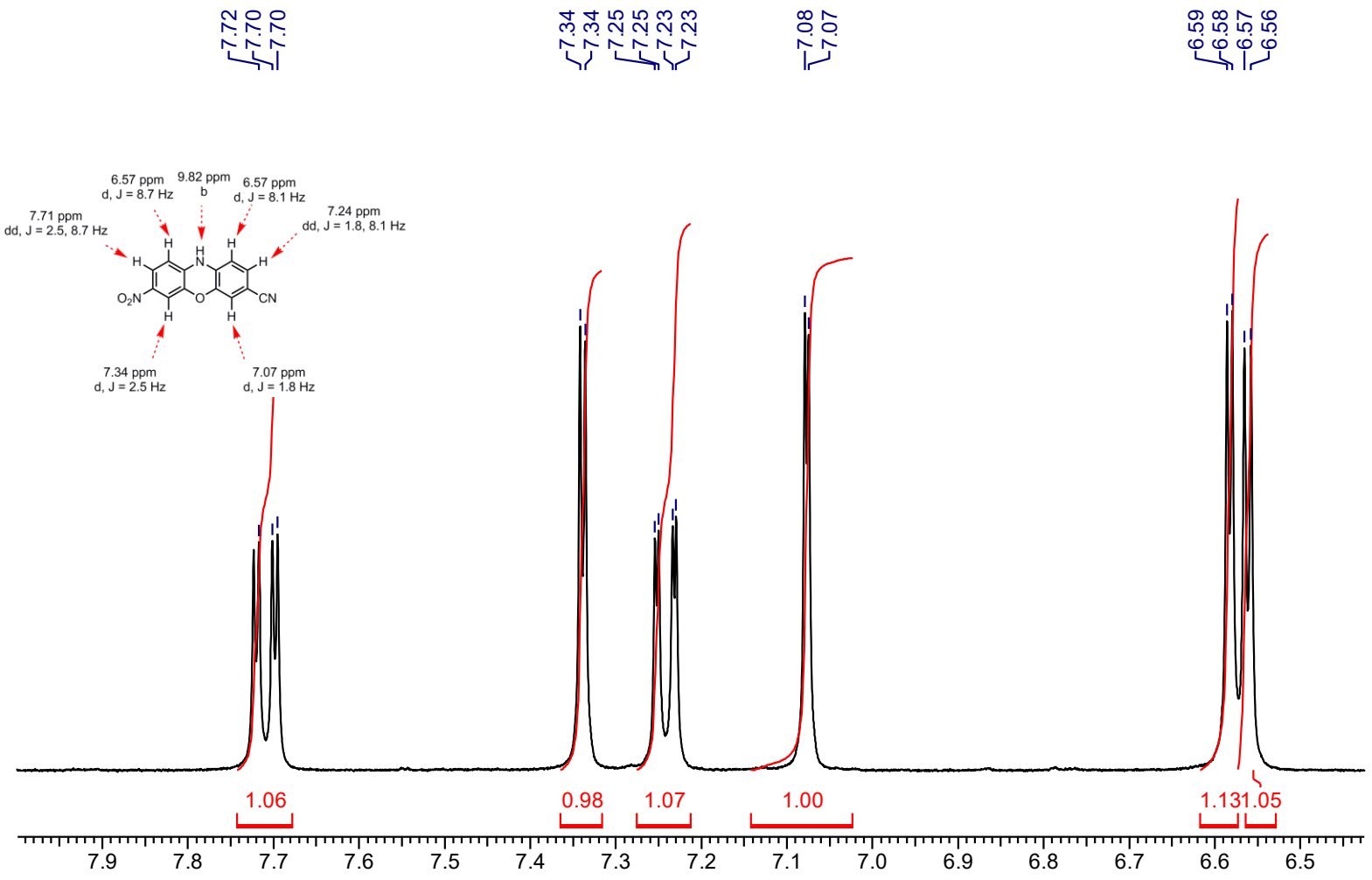
7.72
7.70
7.70
7.34
7.34
7.25
7.25
7.23
7.23
7.08
7.07
6.59
6.58
6.57
6.56
6.57 ppm
d, J = 8.7 Hz
9.82 ppm
b
6.57 ppm
d, J = 8.1 Hz
7.71 ppm
dd, J = 2.5, 8.7 Hz
7.24 ppm
dd, J = 1.8, 8.1 Hz
7.34 ppm
d, J = 2.5 Hz
7.07 ppm
d, J = 1.8 Hz
1.06
0.98
1.07
1.00
1.13
1.05
7.9
7.8
7.7
7.6
7.5
7.4
7.3
7.2
7.1
7.0
6.9
6.8
6.7
6.6
6.5

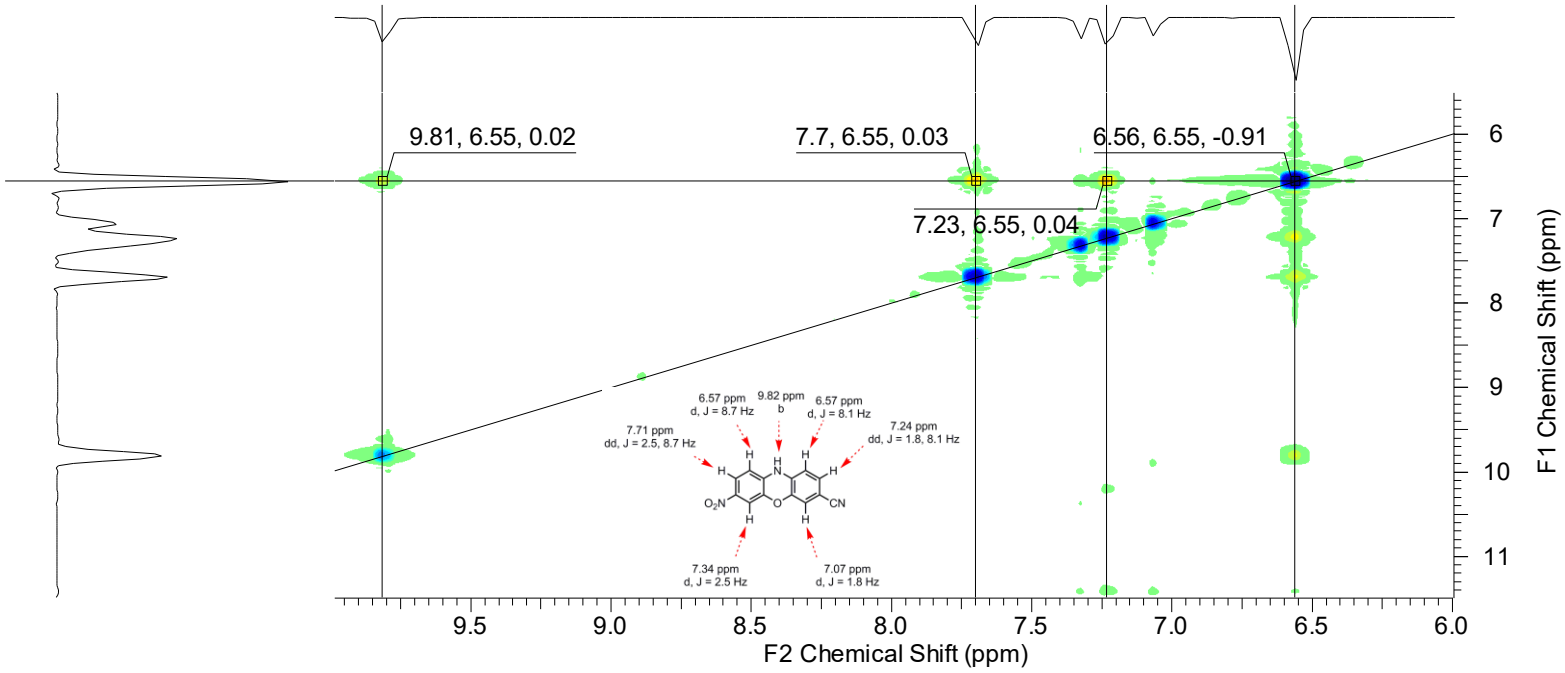
9.81, 6.55, 0.02
7.7, 6.55, 0.03
6.56, 6.55, -0.91
7.23, 6.55, 0.04
6.57 ppm
d, J = 8.7 Hz
9.82 ppm
b
6.57 ppm
d, J = 8.1 Hz
7.71 ppm
dd, J = 2.5, 8.7 Hz
7.24 ppm
dd, J = 1.8, 8.1 Hz
7.34 ppm
d, J = 2.5 Hz
7.07 ppm
d, J = 1.8 Hz
9.5
9.0
8.5
8.0
7.5
7.0
6.5
6.0
F2 Chemical Shift (ppm)
6
7
8
9
10
11
F1 Chemical Shift (ppm)

NOESY

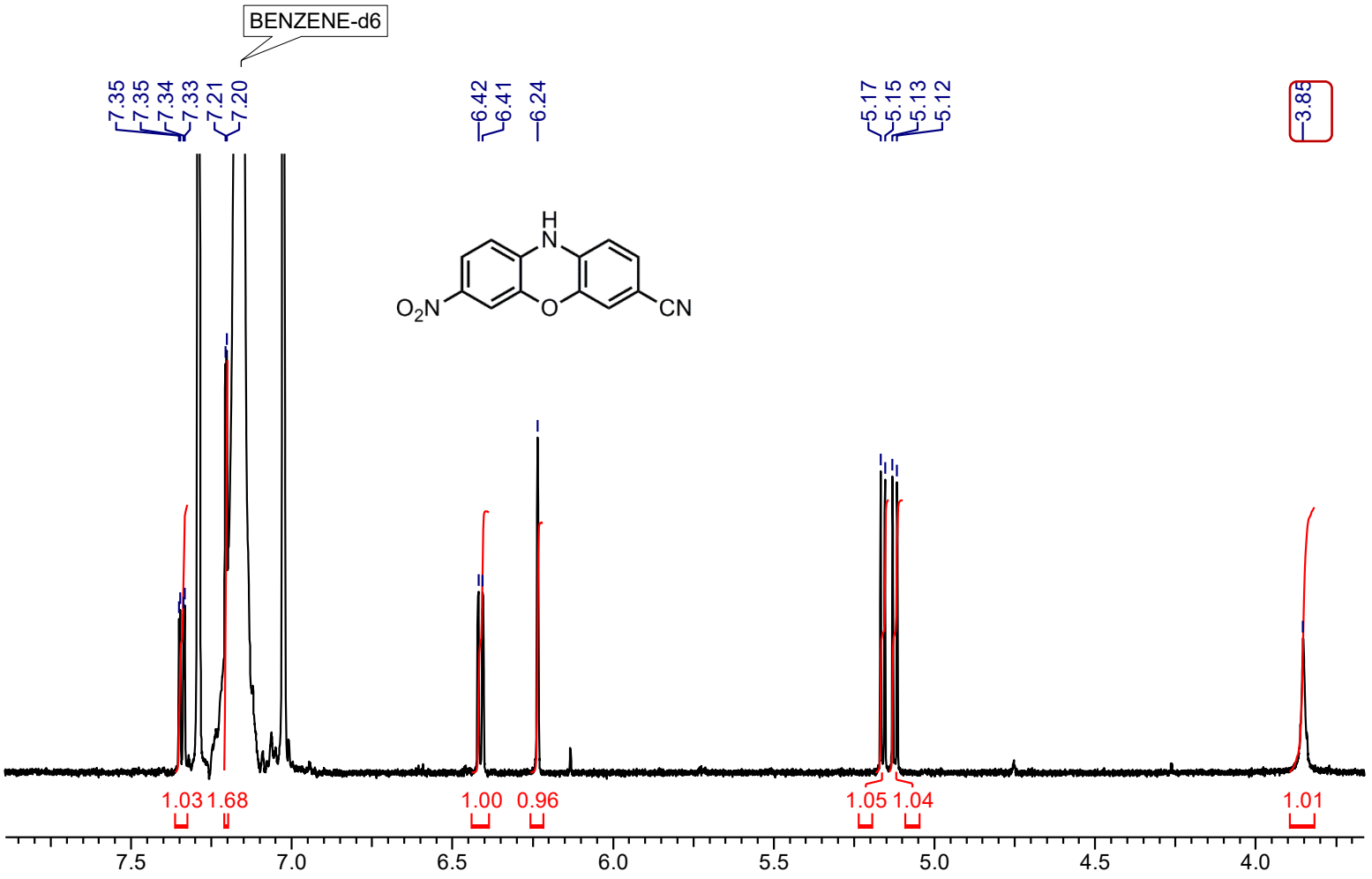
BENZENE-d6
7.35
7.35
7.34
7.33
7.21
7.20
6.42
6.41
6.24
5.17
5.15
5.13
5.12
3.85
H
N
O
O_2N
CN
1.03
1.68
1.00
0.96
1.05
1.04
1.01
7.5
7.0
6.5
6.0
5.5
5.0
4.5
4.0

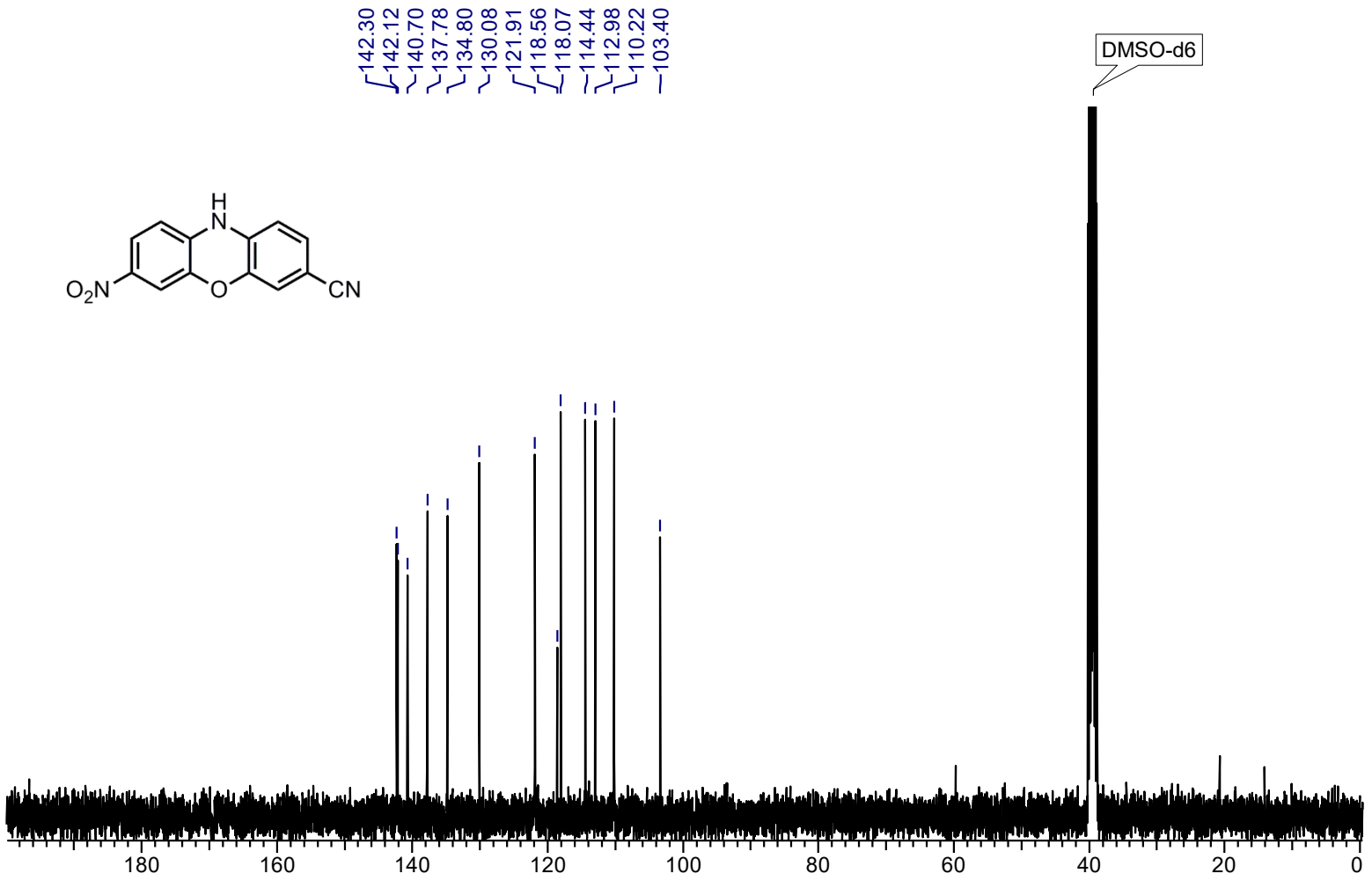
142.30
142.12
140.70
137.78
134.80
130.08
121.91
118.56
118.07
114.44
112.98
110.22
103.40
DMSO-d6
H
N
O
O_2N
CN
180
160
140
120
100
80
60
40
20
0

2-tert-Butylphenoxazine (2.6)

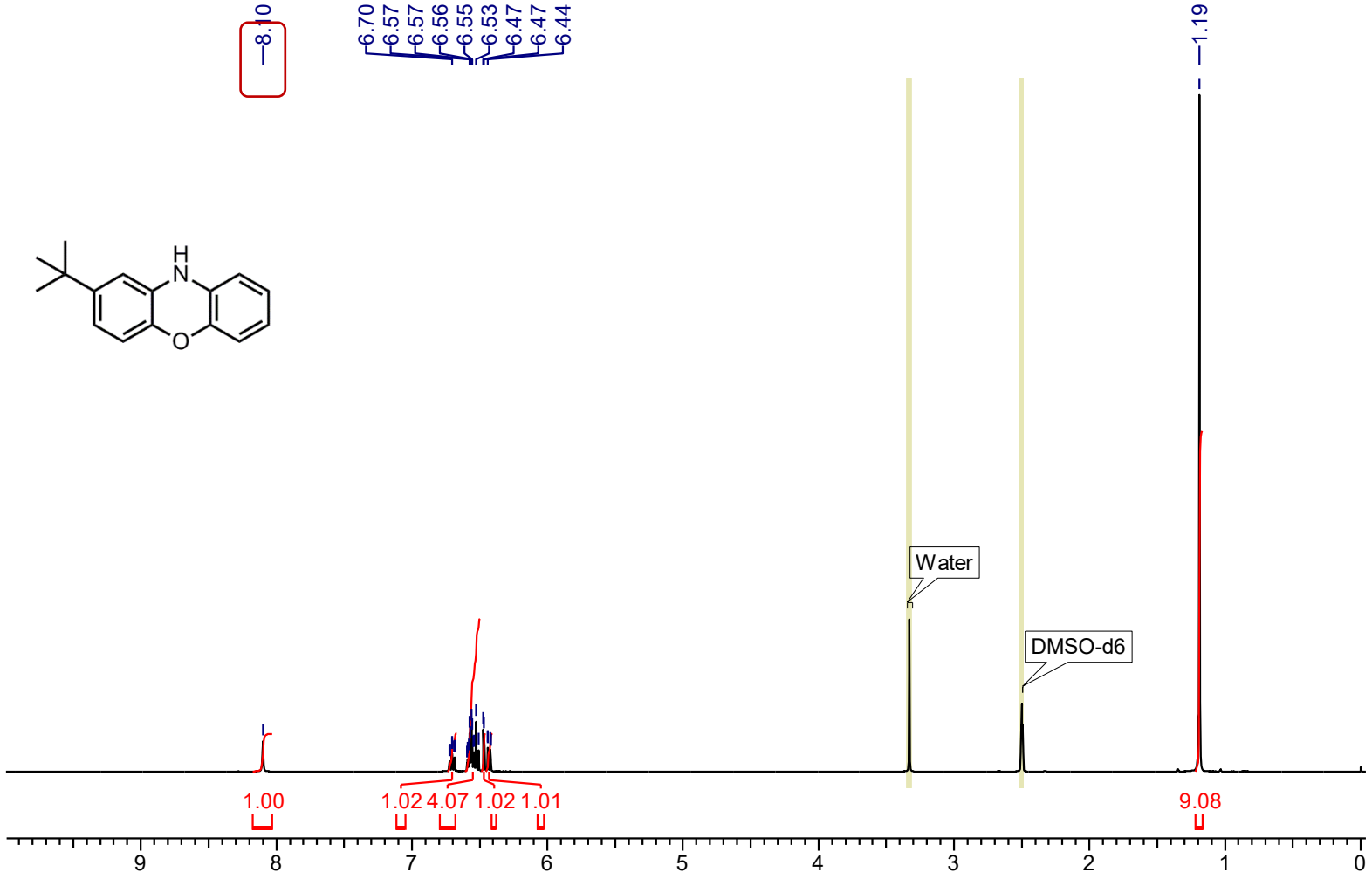

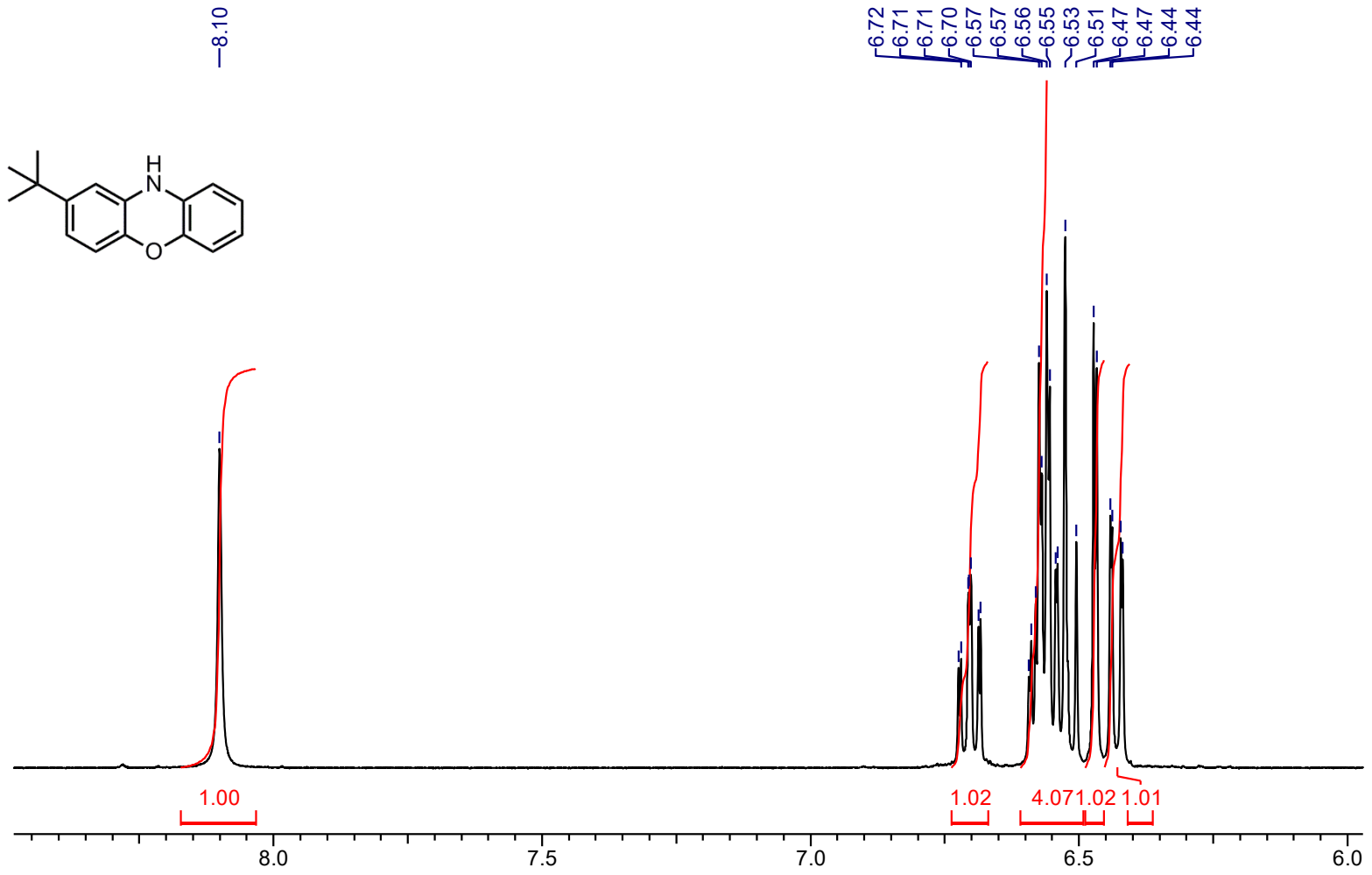
8.10
6.72
6.71
6.71
6.70
6.57
6.57
6.56
6.55
6.53
6.51
6.47
6.47
6.44
6.44
H
N
O
1.00
1.02
4.07
1.02
1.01
8.0
7.5
7.0
6.5
6.0

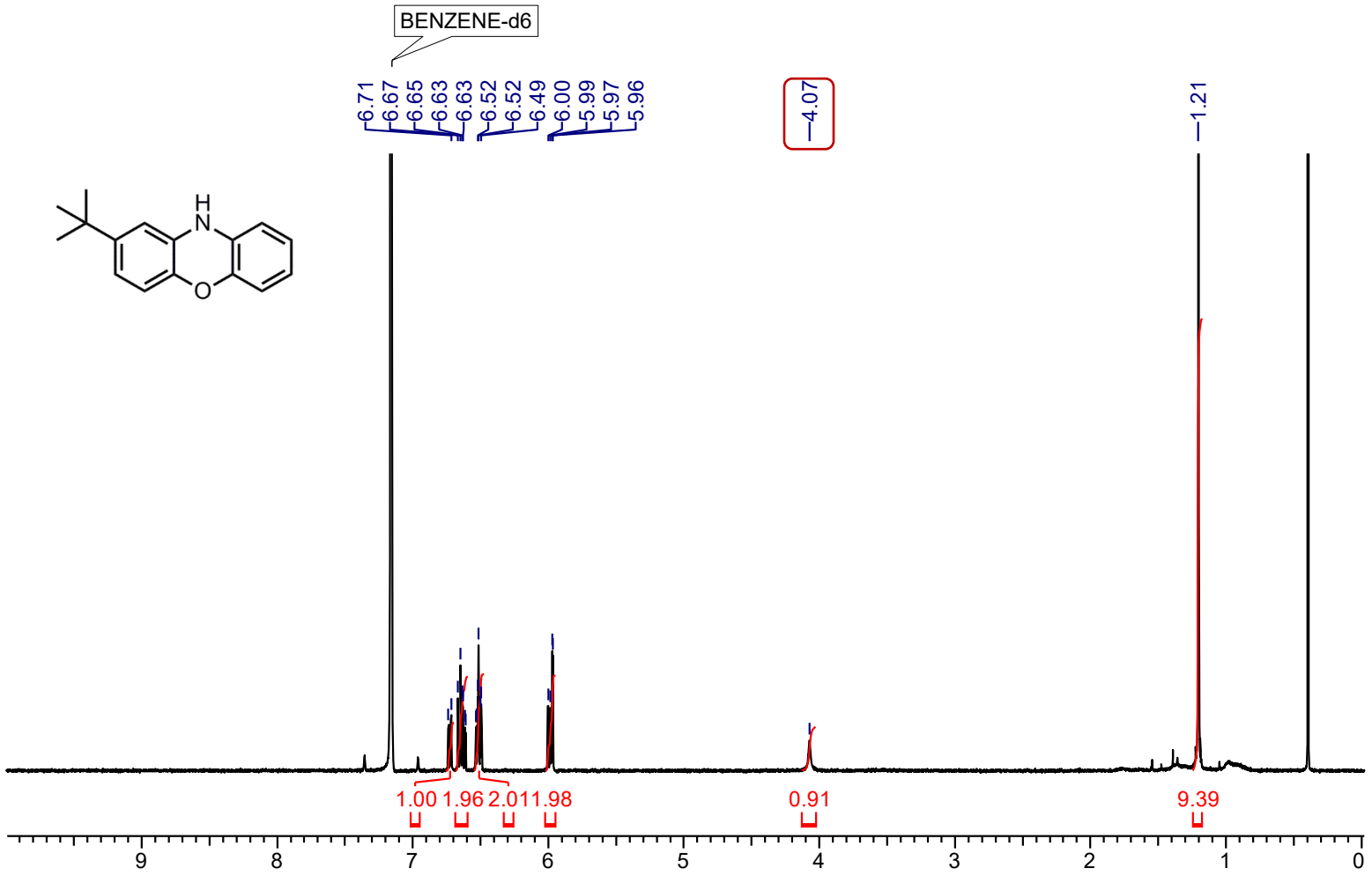
BENZENE-d6
6.71
6.67
6.65
6.63
6.63
6.52
6.52
6.49
6.00
5.99
5.97
5.96
4.07
1.21
H
N
O
1.00
1.96
2.01
1.98
0.91
9.39
9
8
7
6
5
4
3
2
1
0

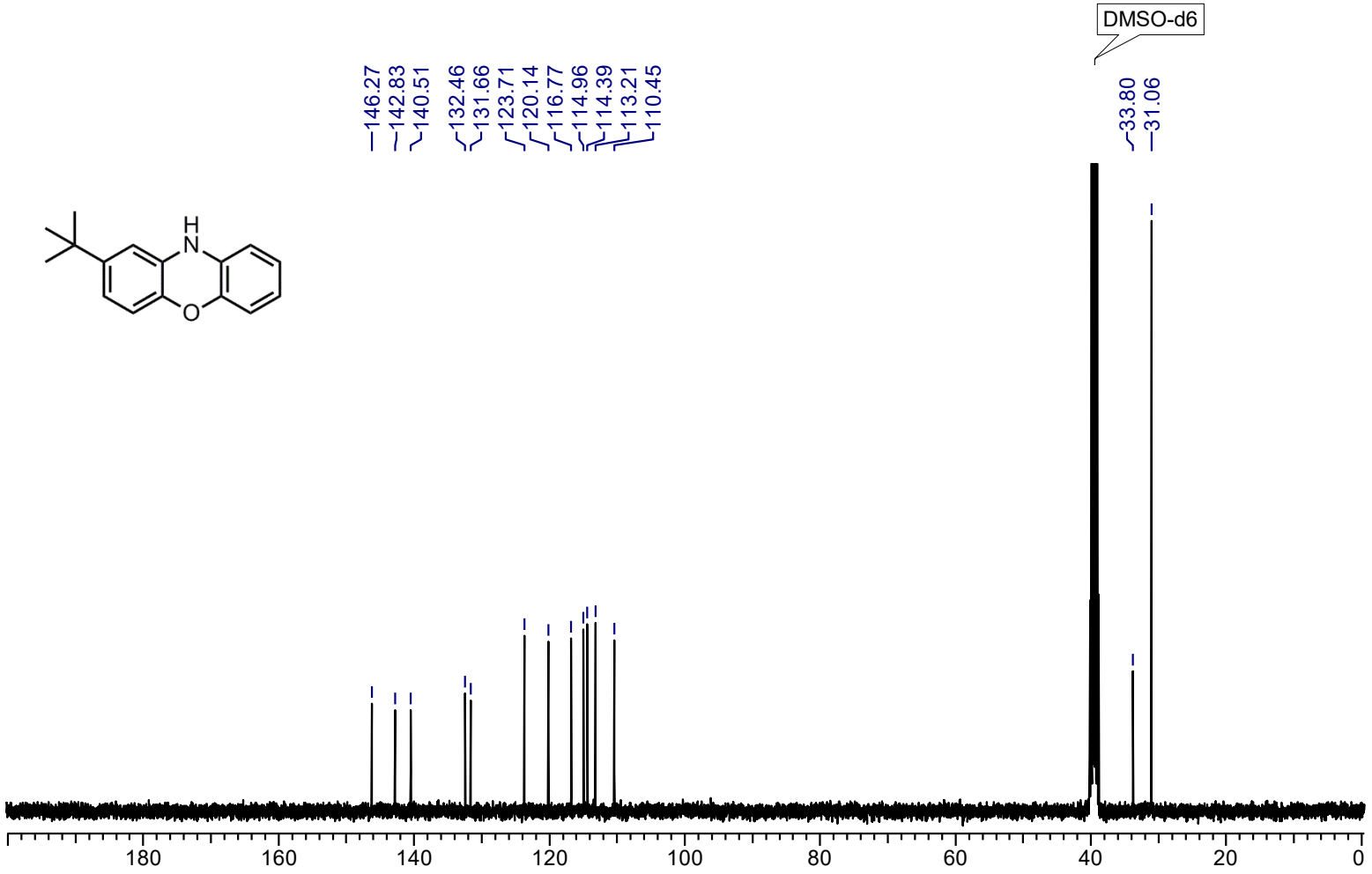
DMSO-d6
146.27
142.83
140.51
132.46
131.66
123.71
120.14
116.77
114.96
114.39
113.21
110.45
33.80
31.06
H
N
O
180
160
140
120
100
80
60
40
20
0

3-tert-Butylphenoxazine (2.7)

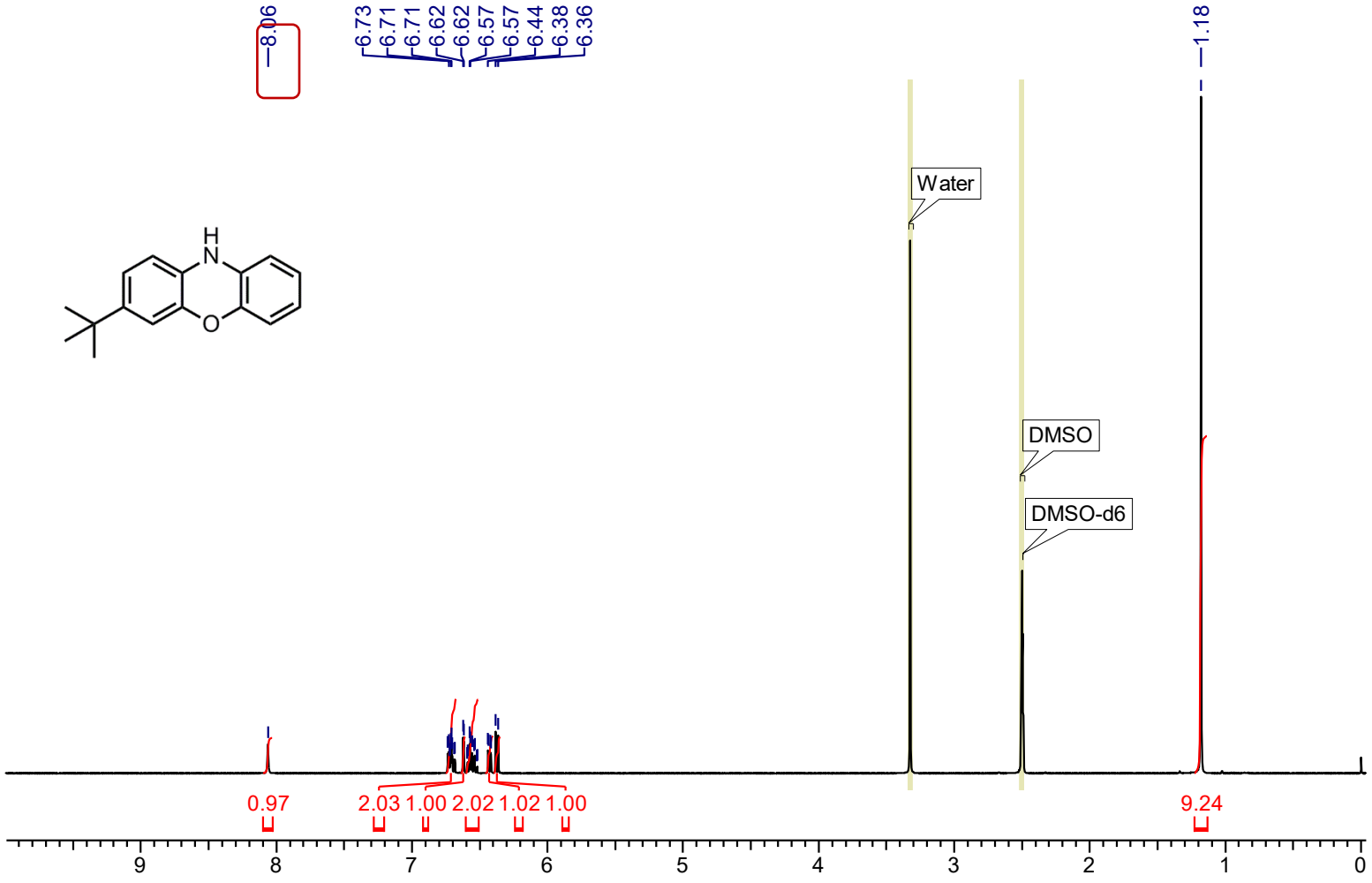

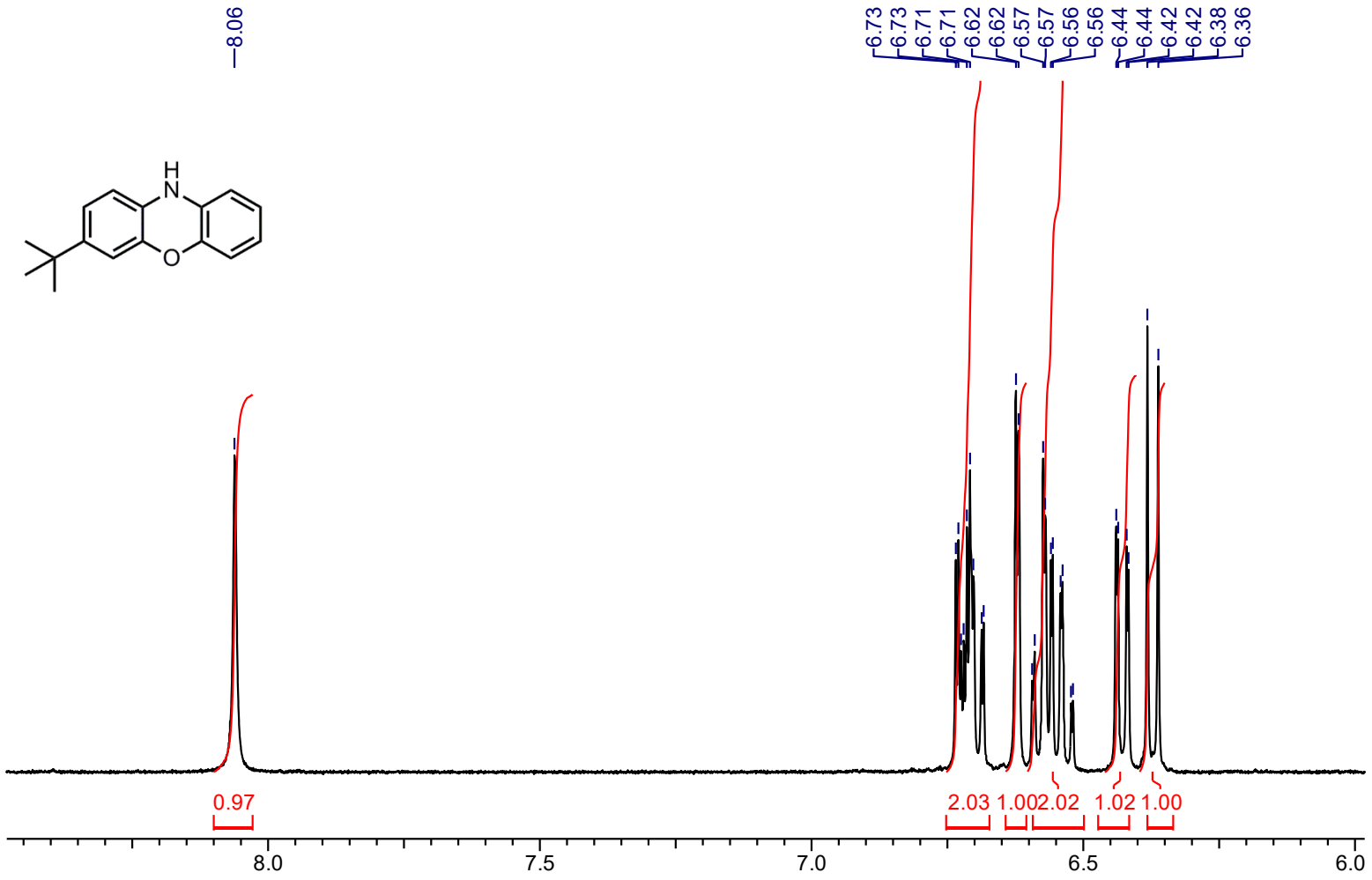
8.06
6.73
6.73
6.71
6.71
6.62
6.62
6.57
6.57
6.56
6.56
6.44
6.44
6.42
6.42
6.38
6.36
H
N
O
0.97
2.03
1.00
2.02
1.02
1.00
8.0
7.5
7.0
6.5
6.0

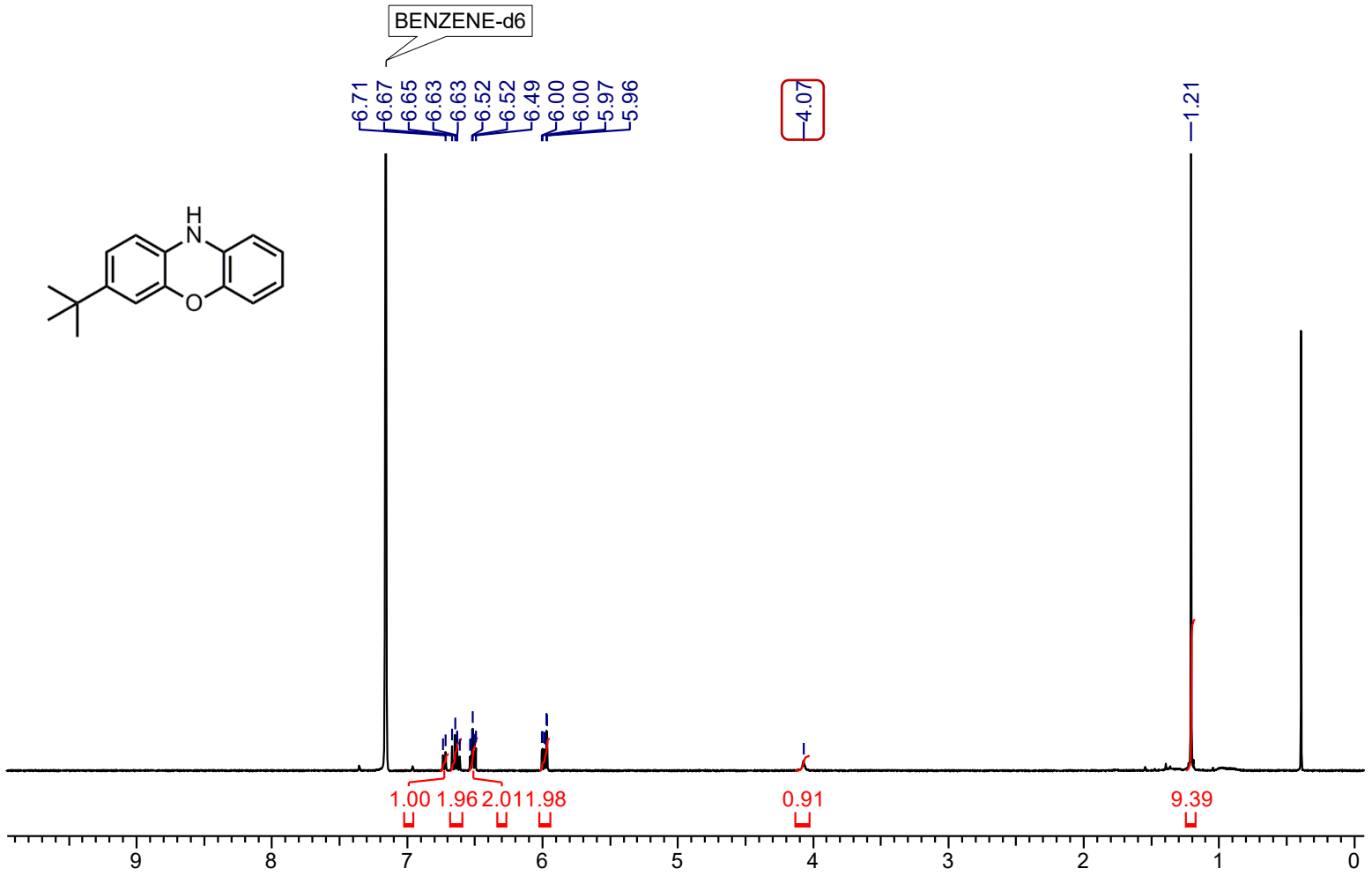
BENZENE-d6
6.71
6.67
6.65
6.63
6.63
6.52
6.52
6.49
6.00
6.00
5.97
5.96
4.07
1.21
H
N
O
1.00
1.96
2.01
1.98
0.91
9.39
9
8
7
6
5
4
3
2
1
0

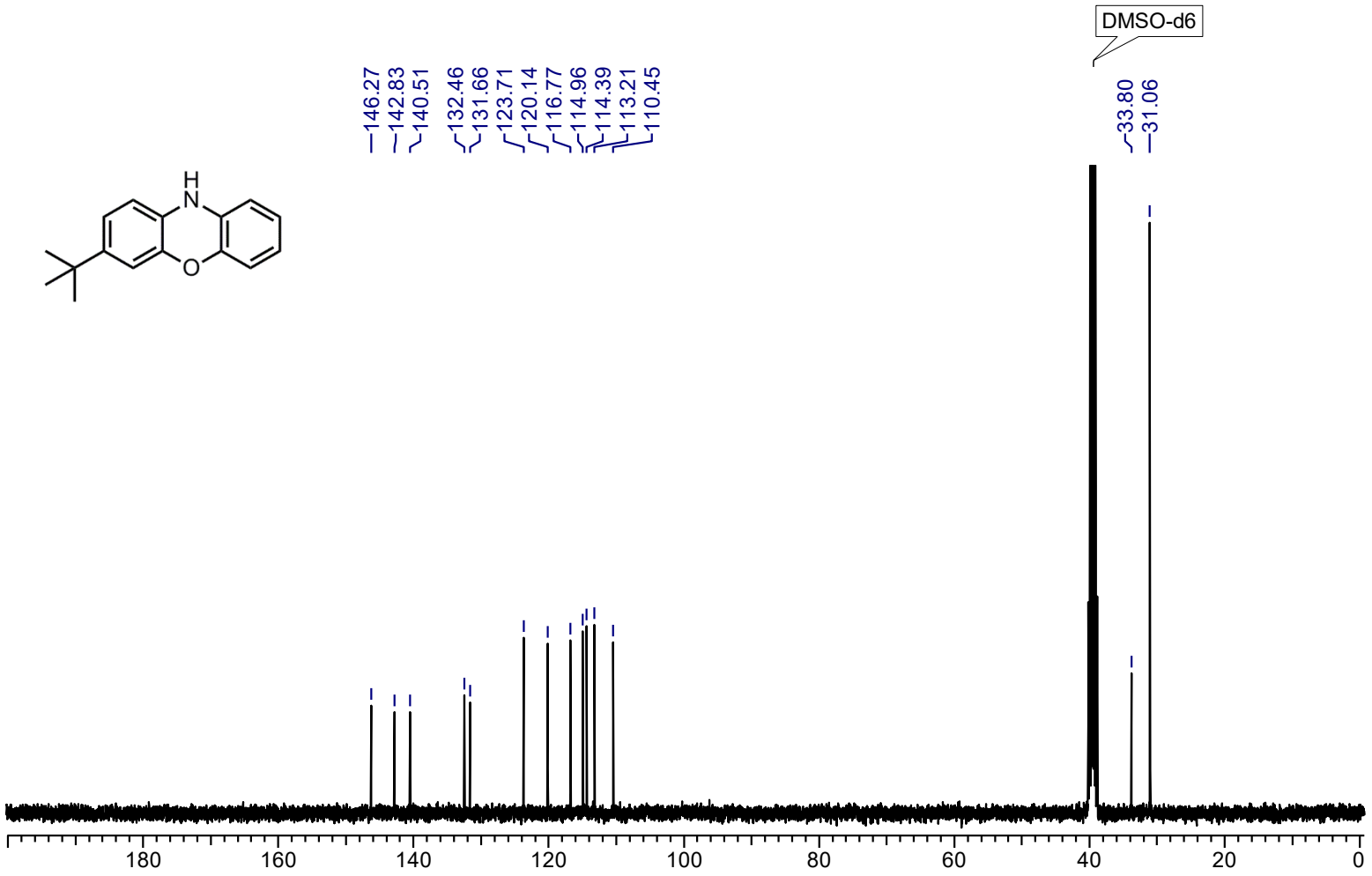
DMSO-d6
146.27
142.83
140.51
132.46
131.66
123.71
120.14
116.77
114.96
114.39
113.21
110.45
33.80
31.06
H
N
O
180
160
140
120
100
80
60
40
20
0

3,7-Di-tert-butylphenoxazine (2.8)

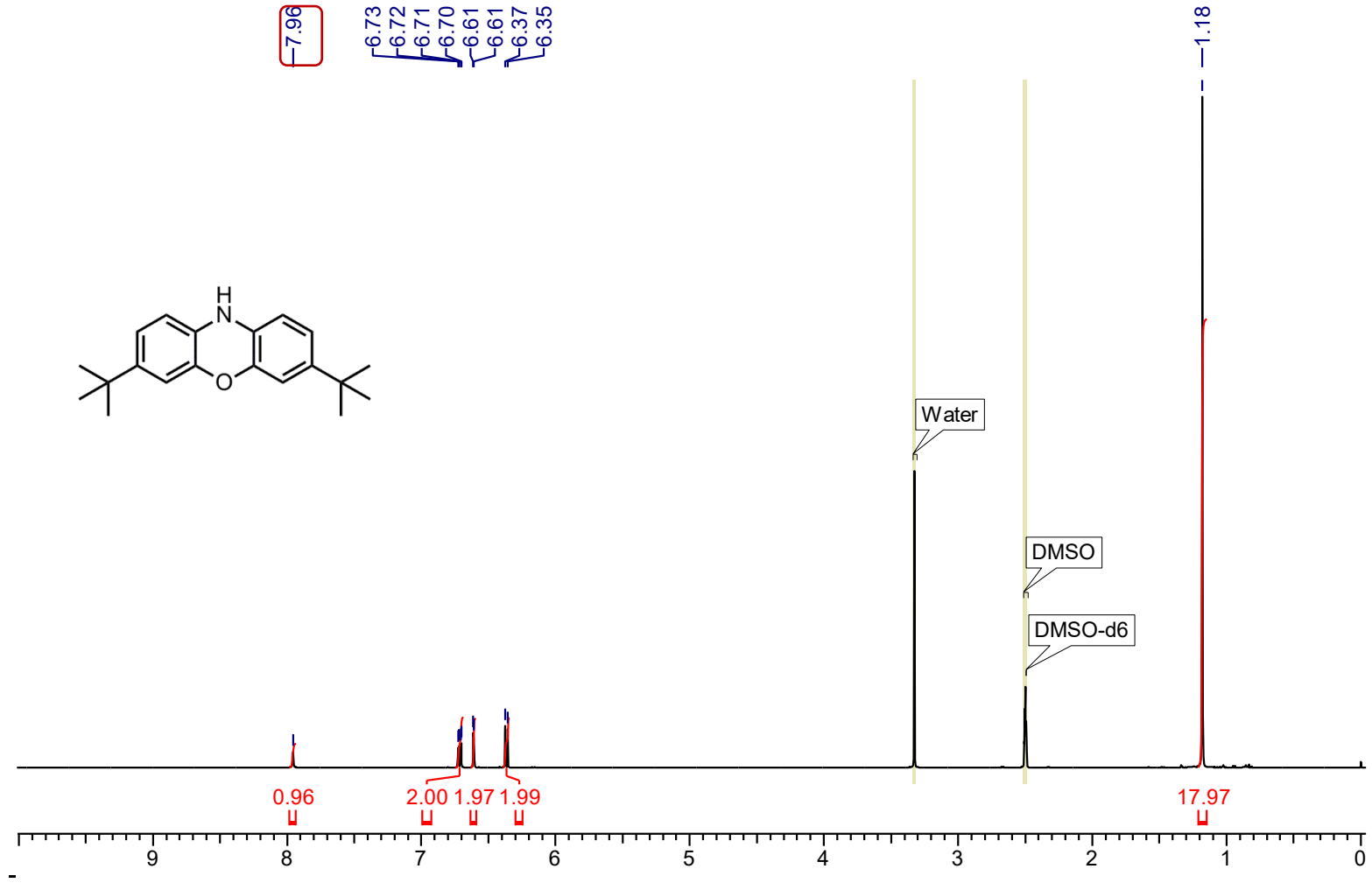

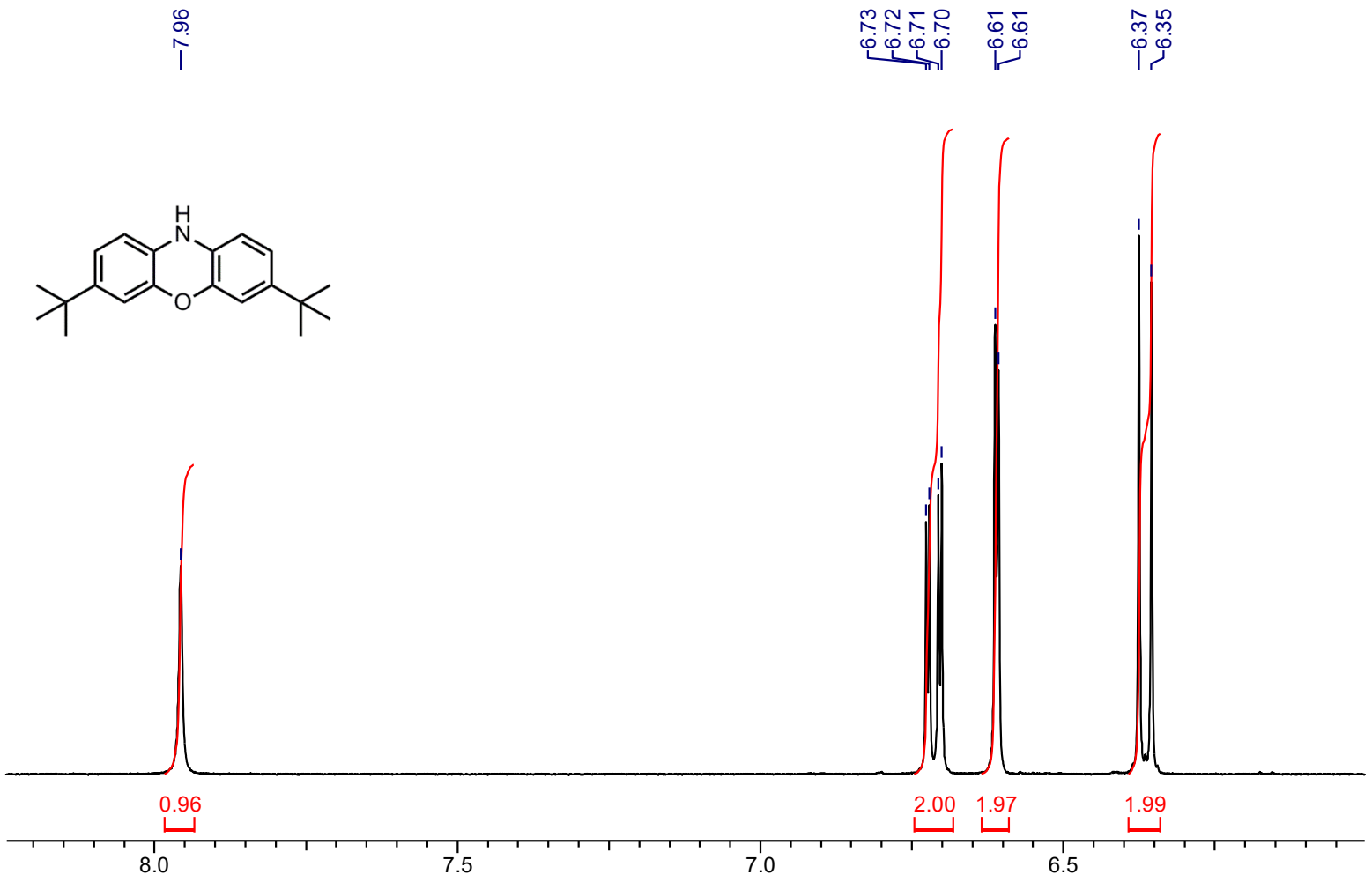
7.96
6.73
6.72
6.71
6.70
6.61
6.61
6.37
6.35
H
N
O
0.96
2.00
1.97
1.99
8.0
7.5
7.0
6.5

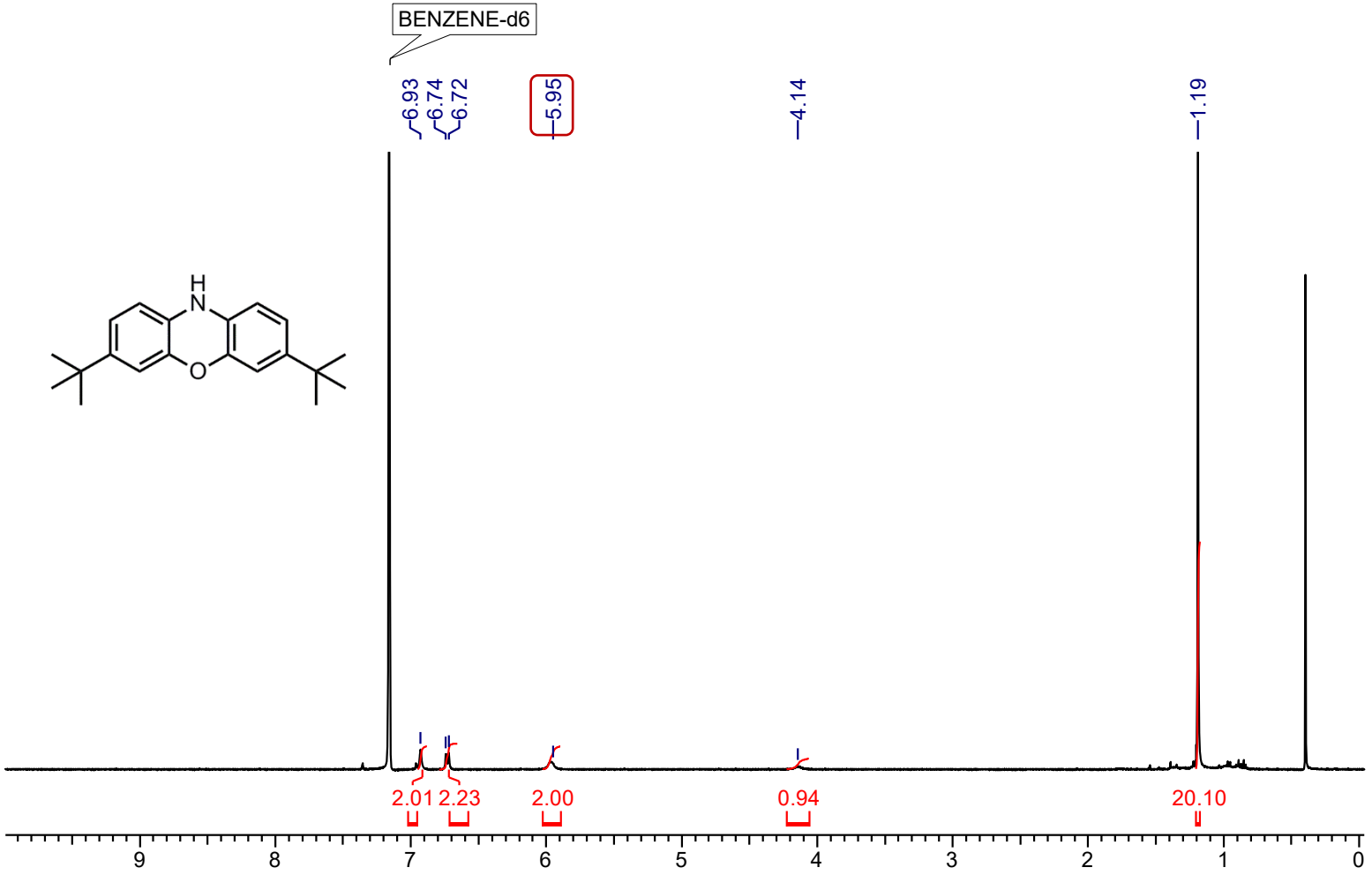
BENZENE-d6
6.93
6.74
6.72
5.95
4.14
1.19
H
N
O
2.01
2.23
2.00
0.94
20.10
9
8
7
6
5
4
3
2
1
0

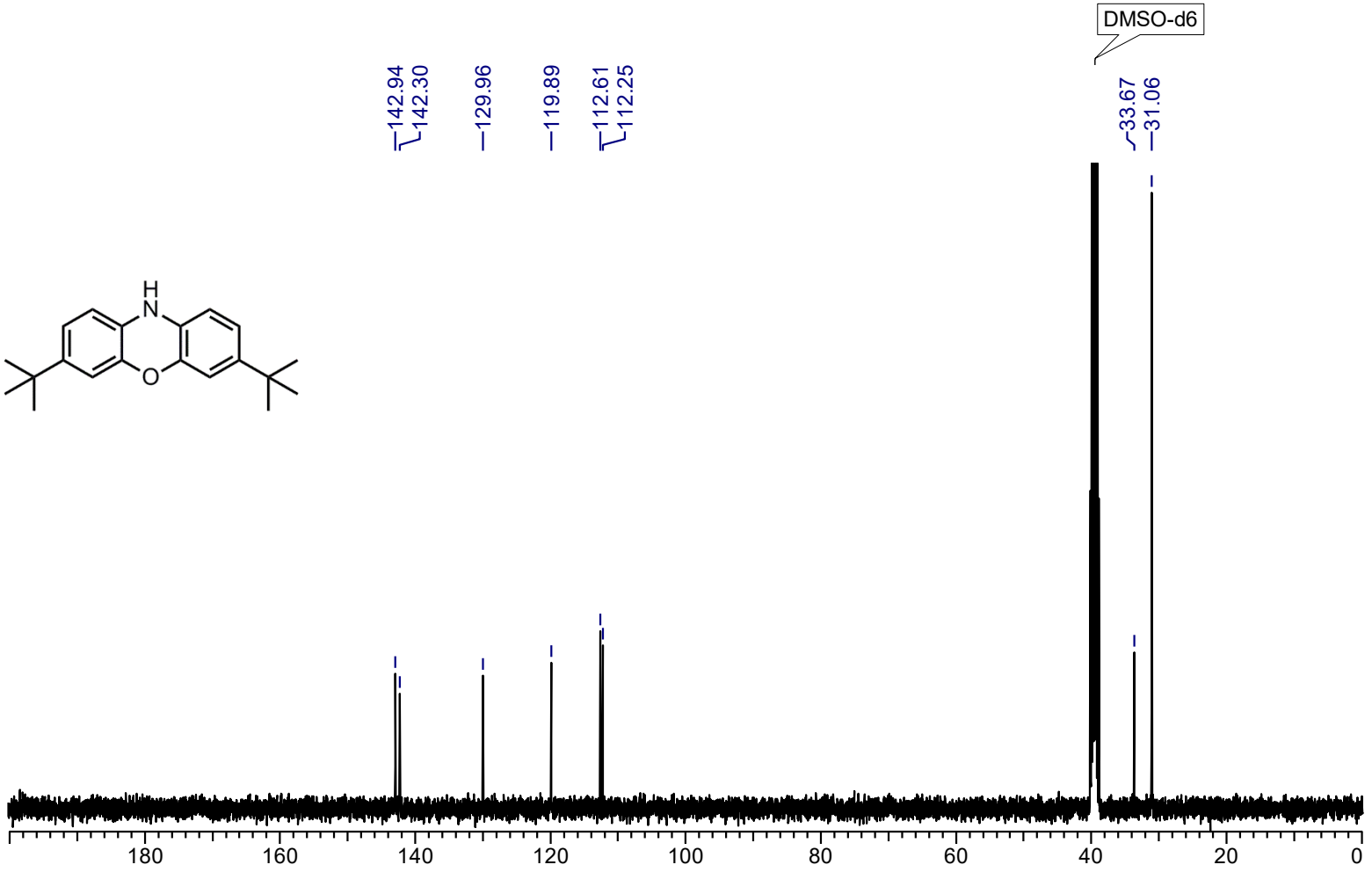
DMSO-d6
142.94
142.30
129.96
119.89
112.61
112.25
33.67
31.06
H
N
O
180
160
140
120
100
80
60
40
20
0

2-Trifluoromethylphenoxazine (2.4)

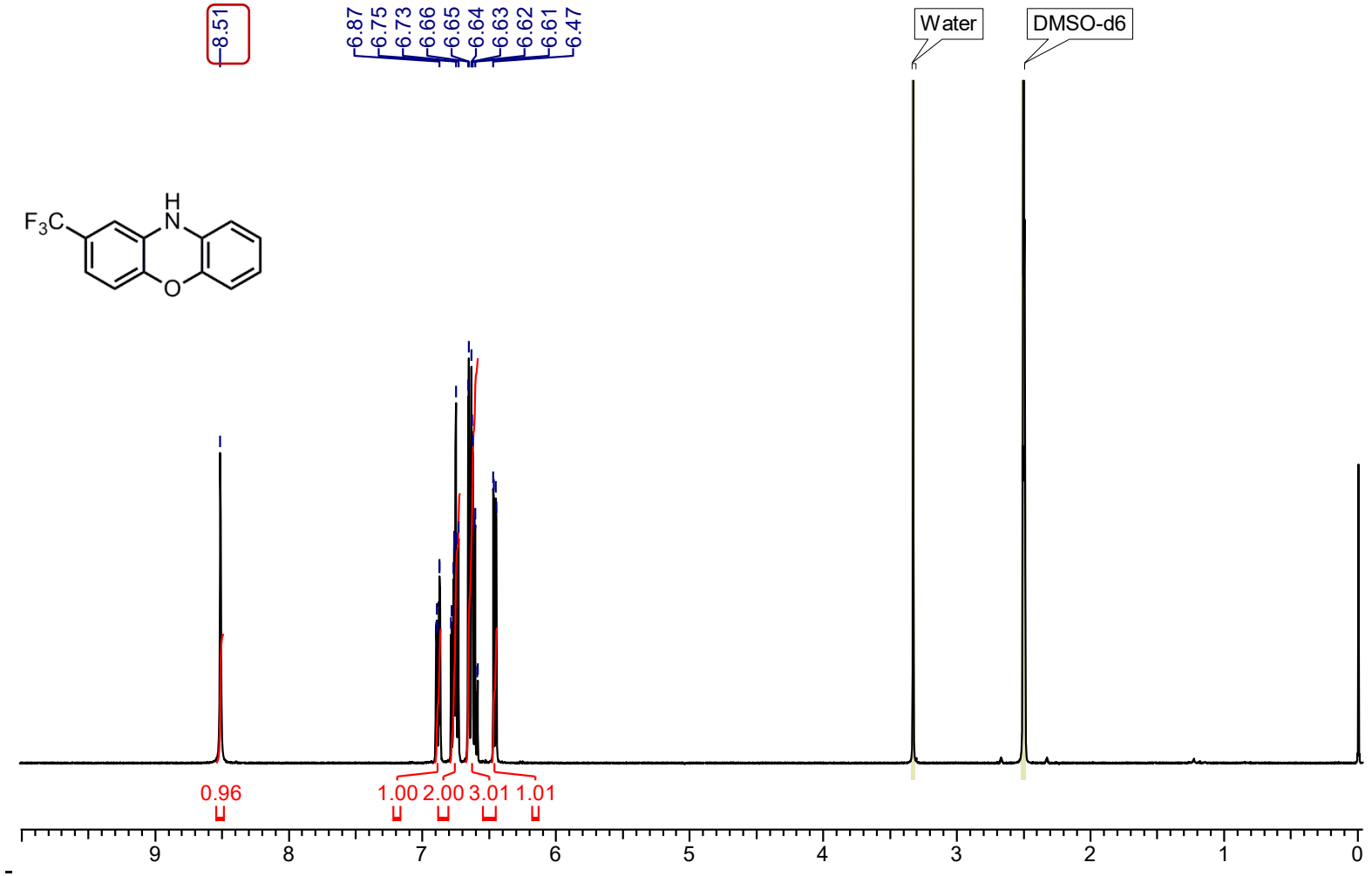

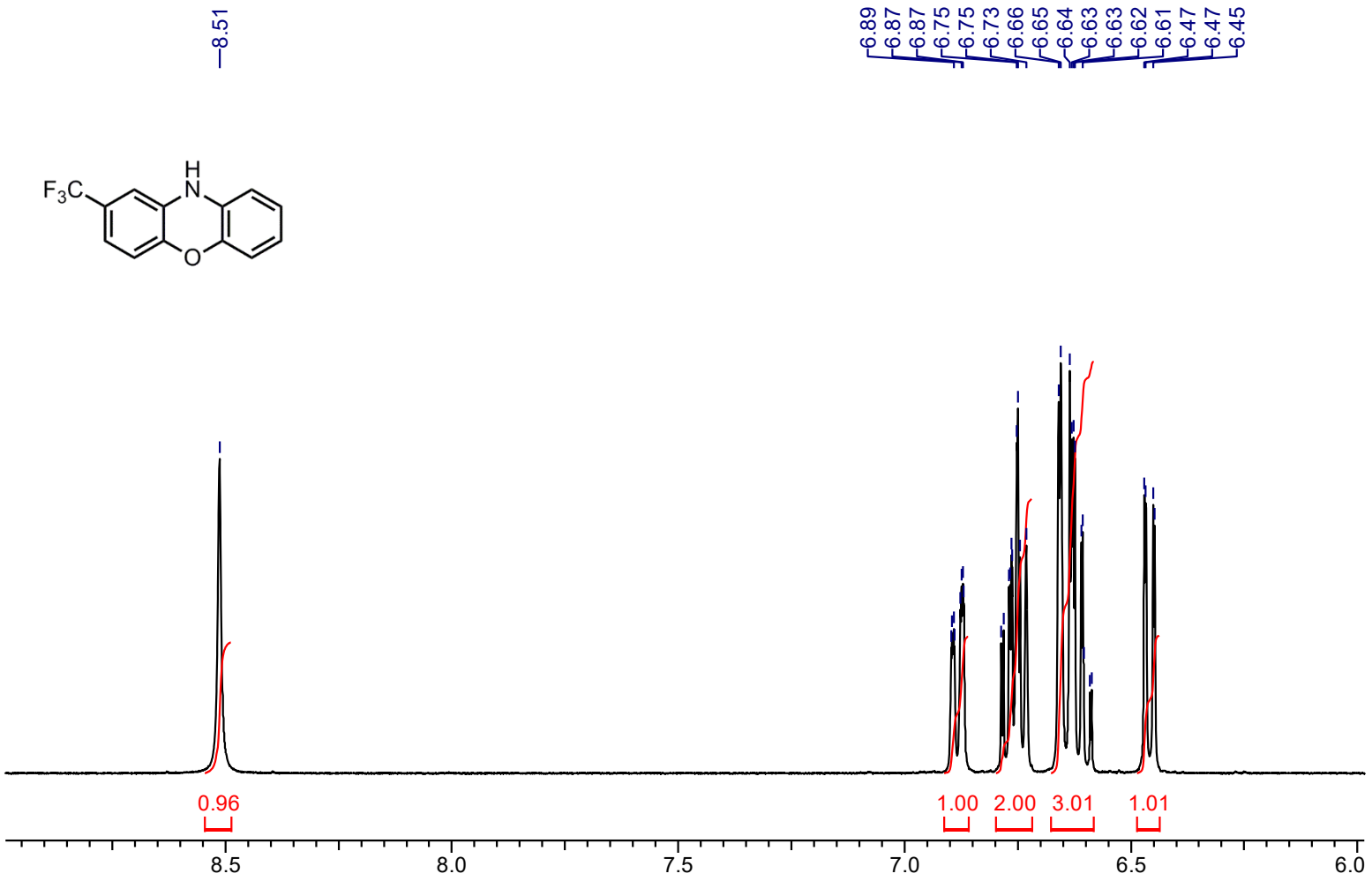
8.51
6.89
6.87
6.87
6.75
6.75
6.73
6.66
6.65
6.64
6.63
6.63
6.62
6.61
6.47
6.47
6.45
F3C
H
N
O
0.96
1.00
2.00
3.01
1.01
8.5
8.0
7.5
7.0
6.5
6.0

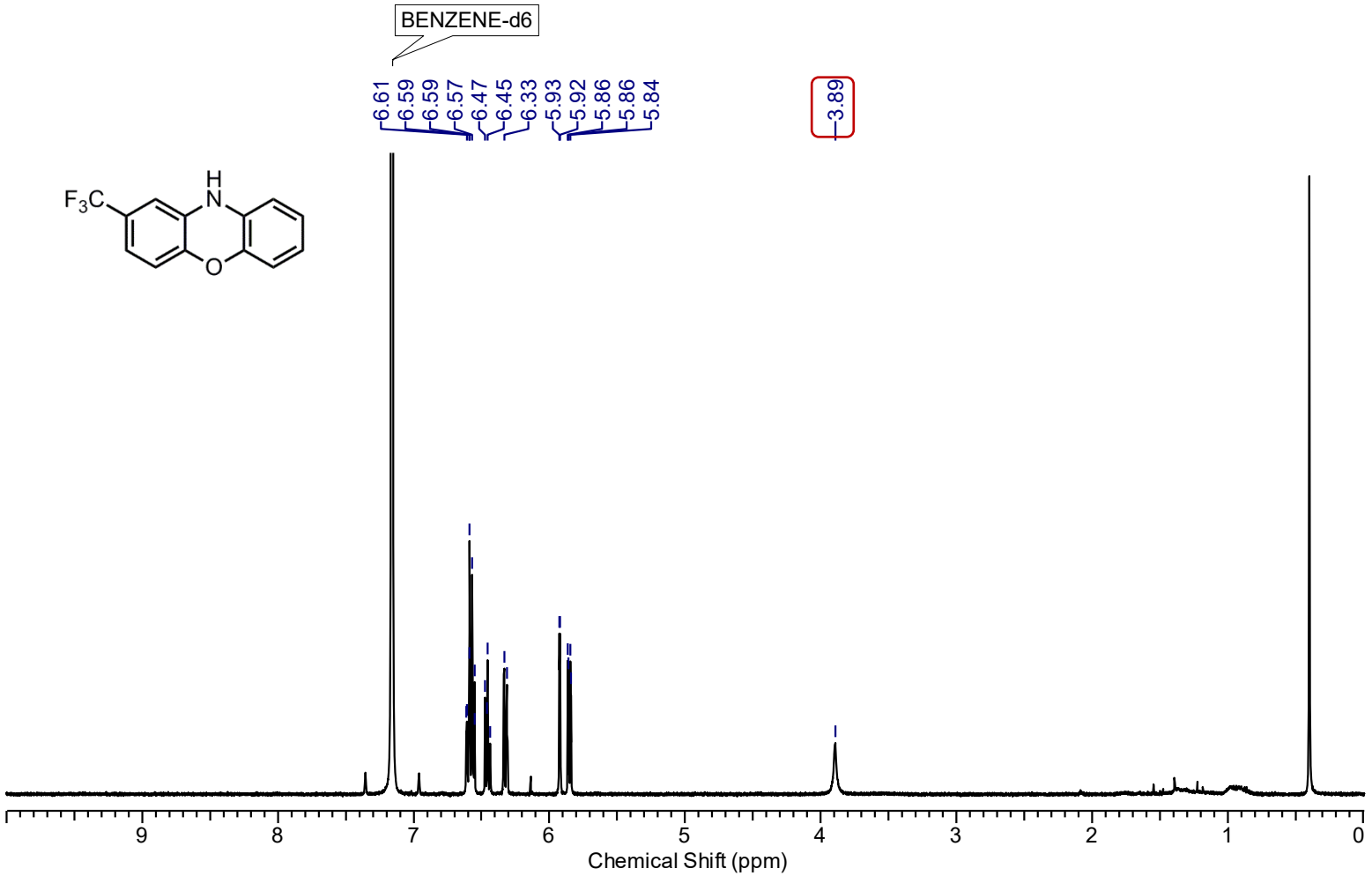
BENZENE-d6
6.61
6.59
6.59
6.57
6.47
6.45
6.33
5.93
5.92
5.86
5.86
5.84
3.89
F3C
H
N
O
9
8
7
6
5
4
3
2
1
0
Chemical Shift (ppm)

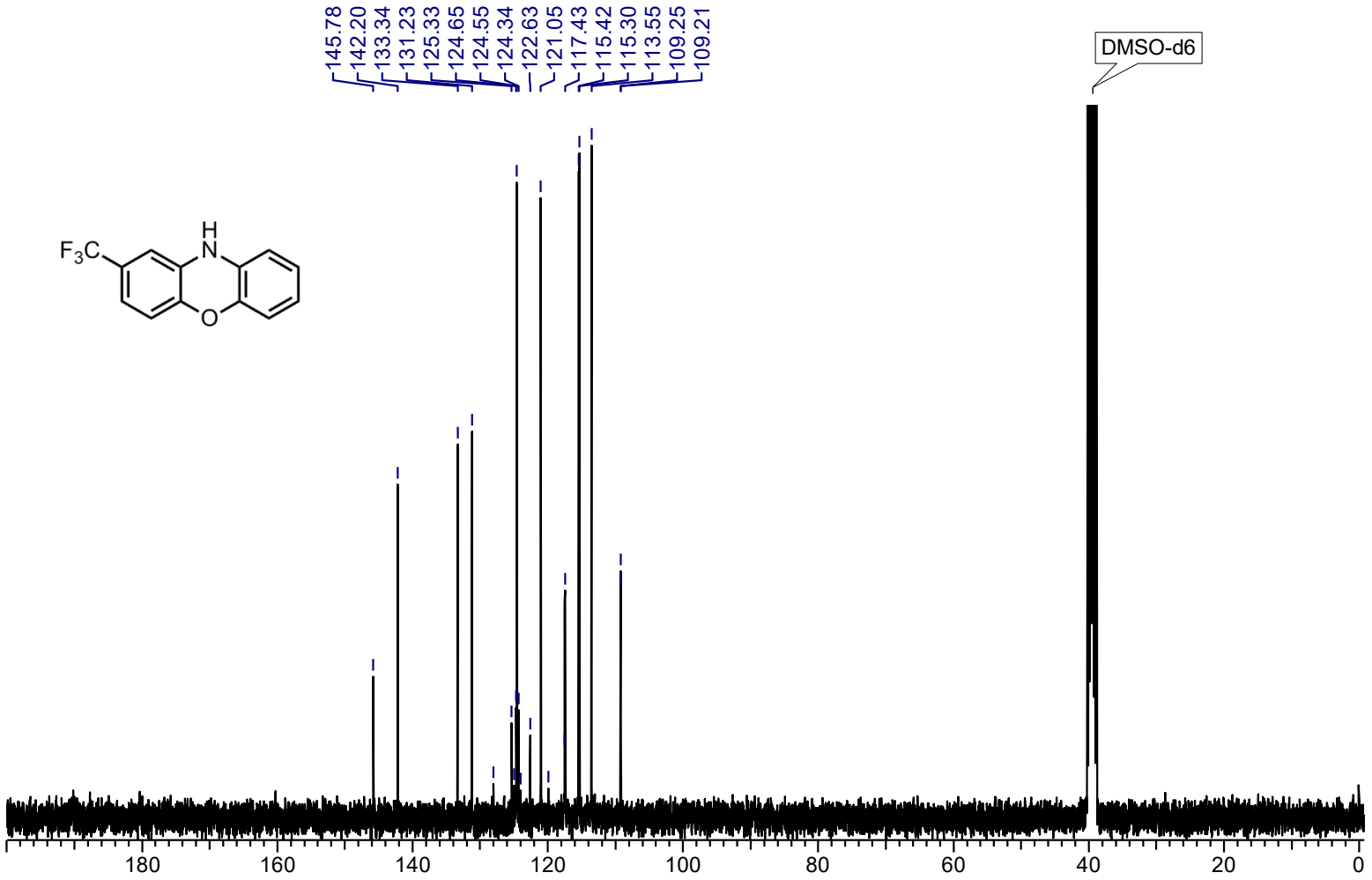
145.78
142.20
133.34
131.23
125.33
124.65
124.55
124.34
122.63
121.05
117.43
115.42
115.30
113.55
109.25
109.21
DMSO-d6
F3C
H
N
O
180
160
140
120
100
80
60
40
20
0

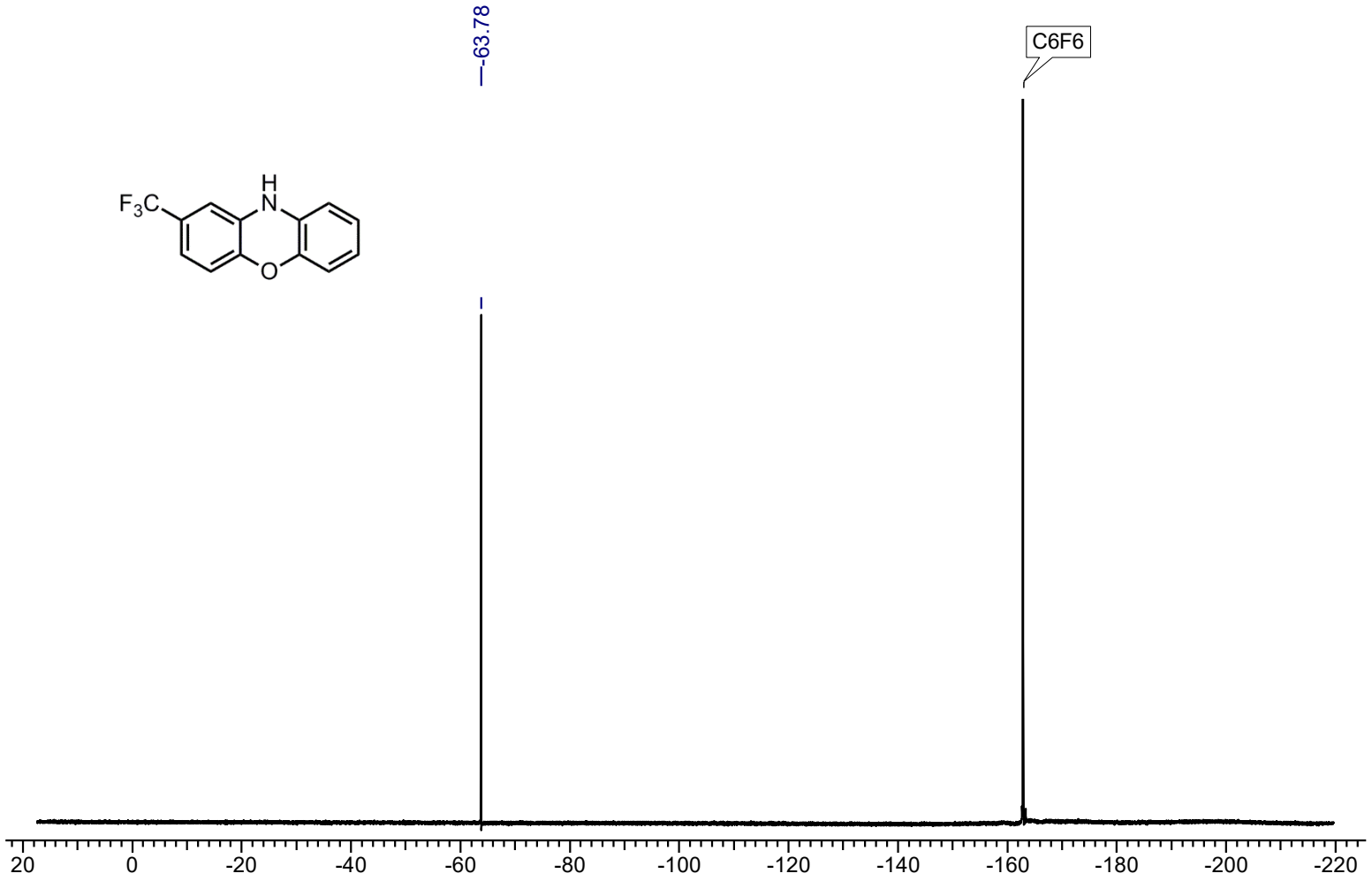
-63.78
C6F6
F3C
H
N
O
20
0
-20
-40
-60
-80
-100
-120
-140
-160
-180
-200
-220

3-Trifluoromethylphenoxazine (2.5)

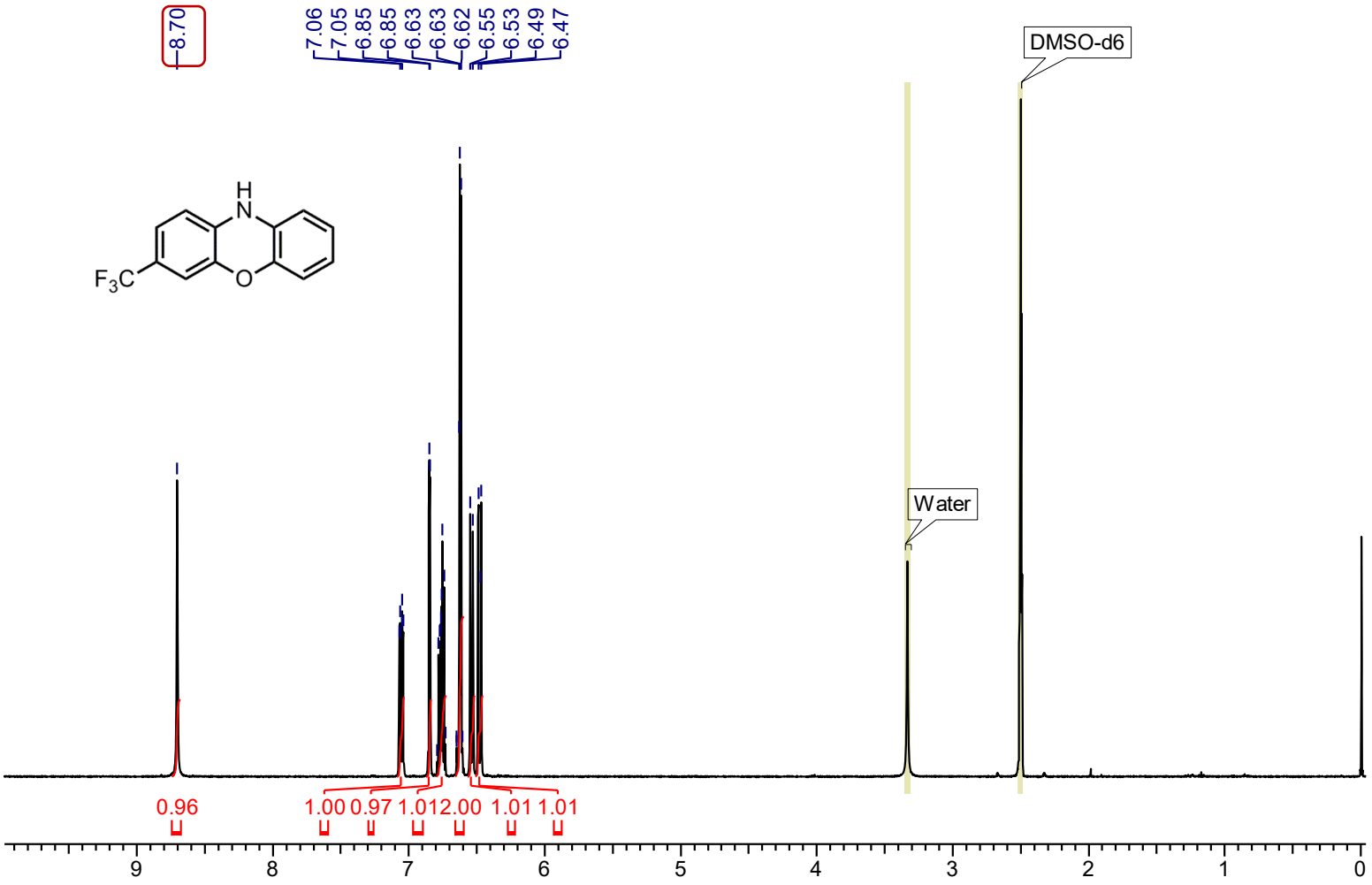

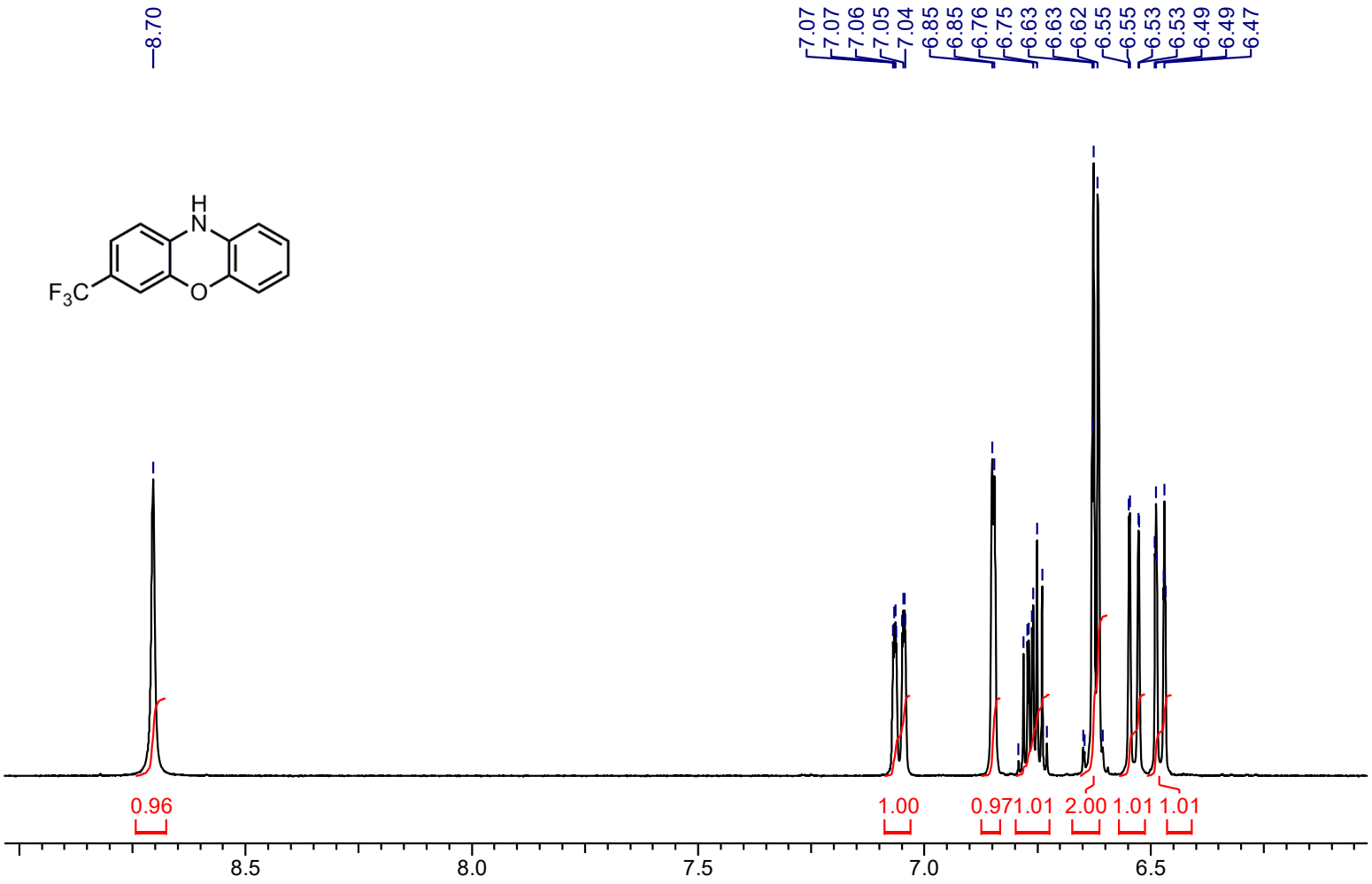
8.70
7.07
7.07
7.06
7.05
7.04
6.85
6.85
6.76
6.75
6.63
6.63
6.62
6.55
6.55
6.53
6.53
6.49
6.49
6.47
H
N
O
F3C
0.96
1.00
0.97
1.01
2.00
1.01
1.01
8.5
8.0
7.5
7.0
6.5

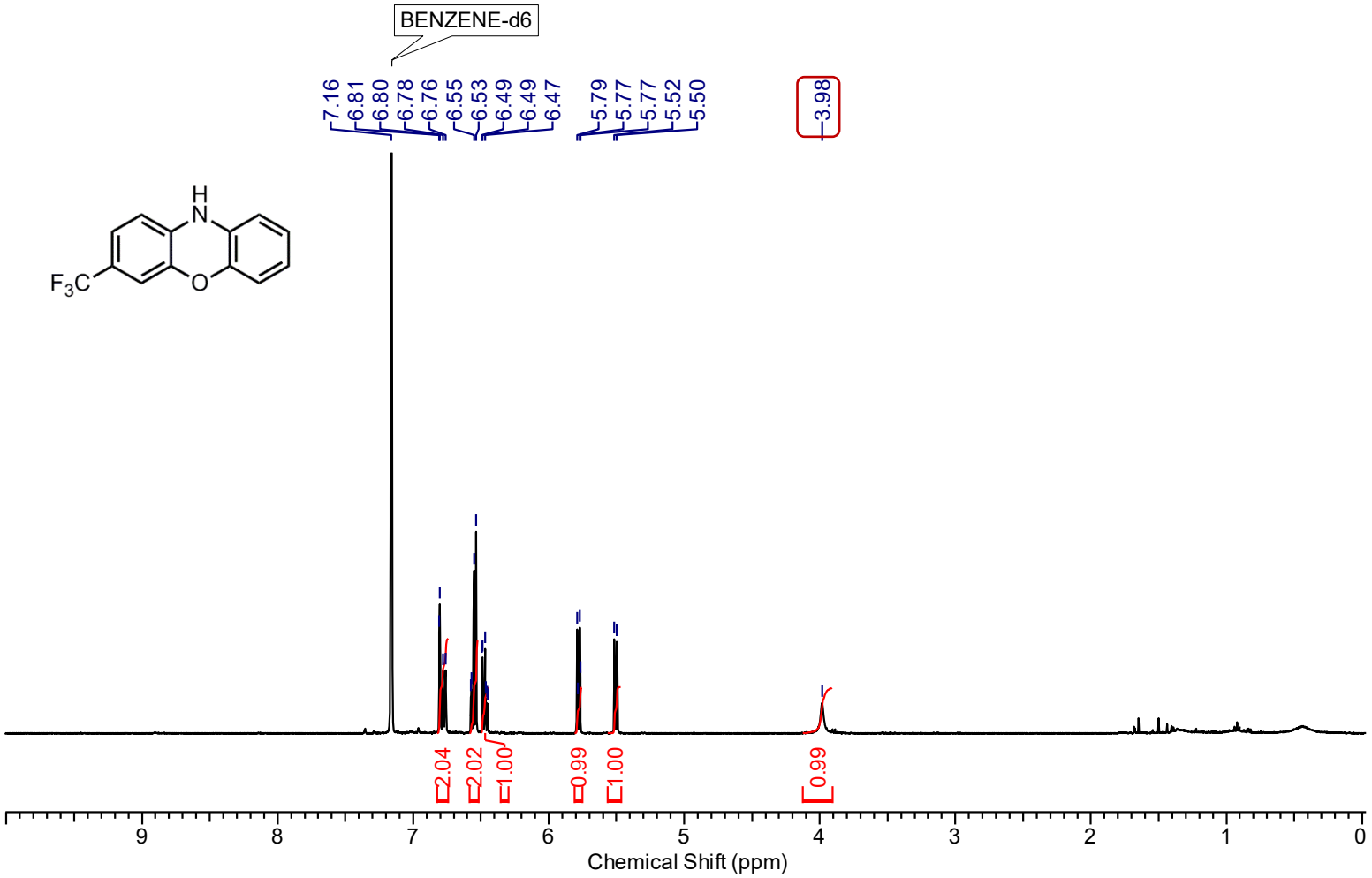
BENZENE-d6
7.16
6.81
6.80
6.78
6.76
6.55
6.53
6.49
6.49
6.47
5.79
5.77
5.77
5.52
5.50
3.98
H
N
F3C
O
2.04
2.02
1.00
0.99
1.00
0.99
9
8
7
6
5
4
3
2
1
0
Chemical Shift (ppm)

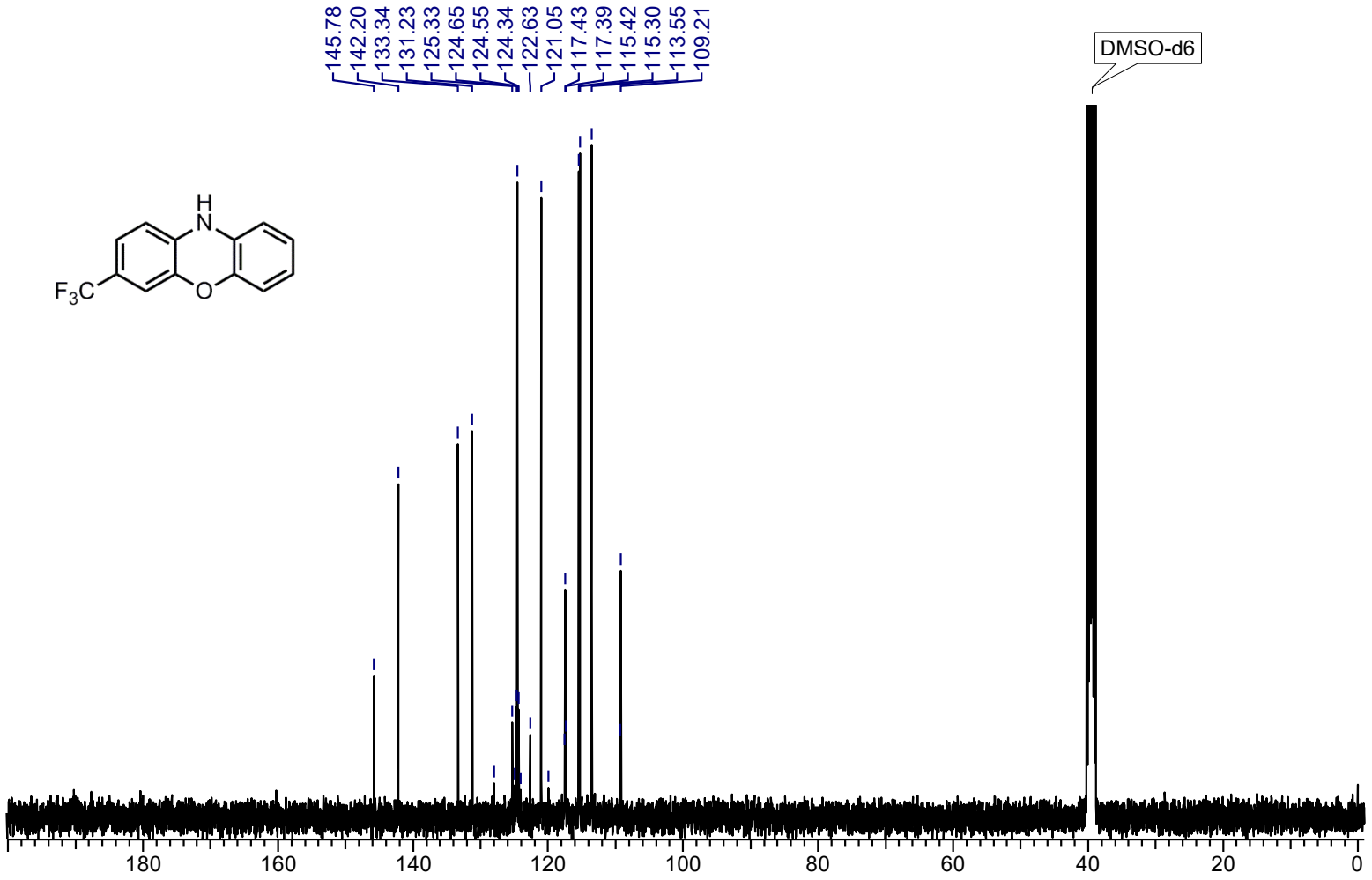
145.78
142.20
133.34
131.23
125.33
124.65
124.55
124.34
122.63
121.05
117.43
117.39
115.42
115.30
113.55
109.21
DMSO-d6
H
N
O
F3C
180
160
140
120
100
80
60
40
20
0

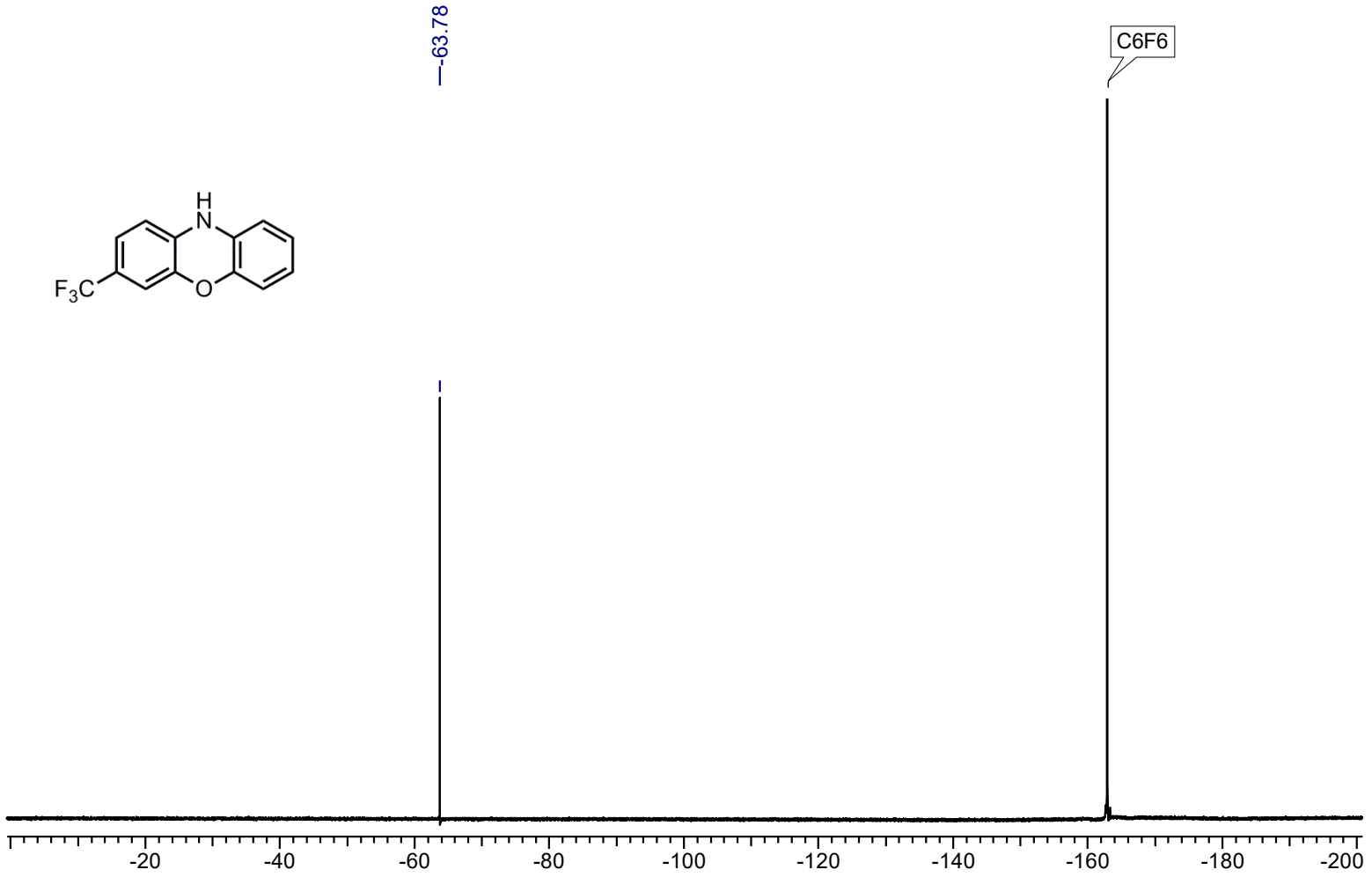
-63.78
C6F6
H
N
O
F3C
-20
-40
-60
-80
-100
-120
-140
-160
-180
-200

3-Methoxyphenoxazine (2.16)

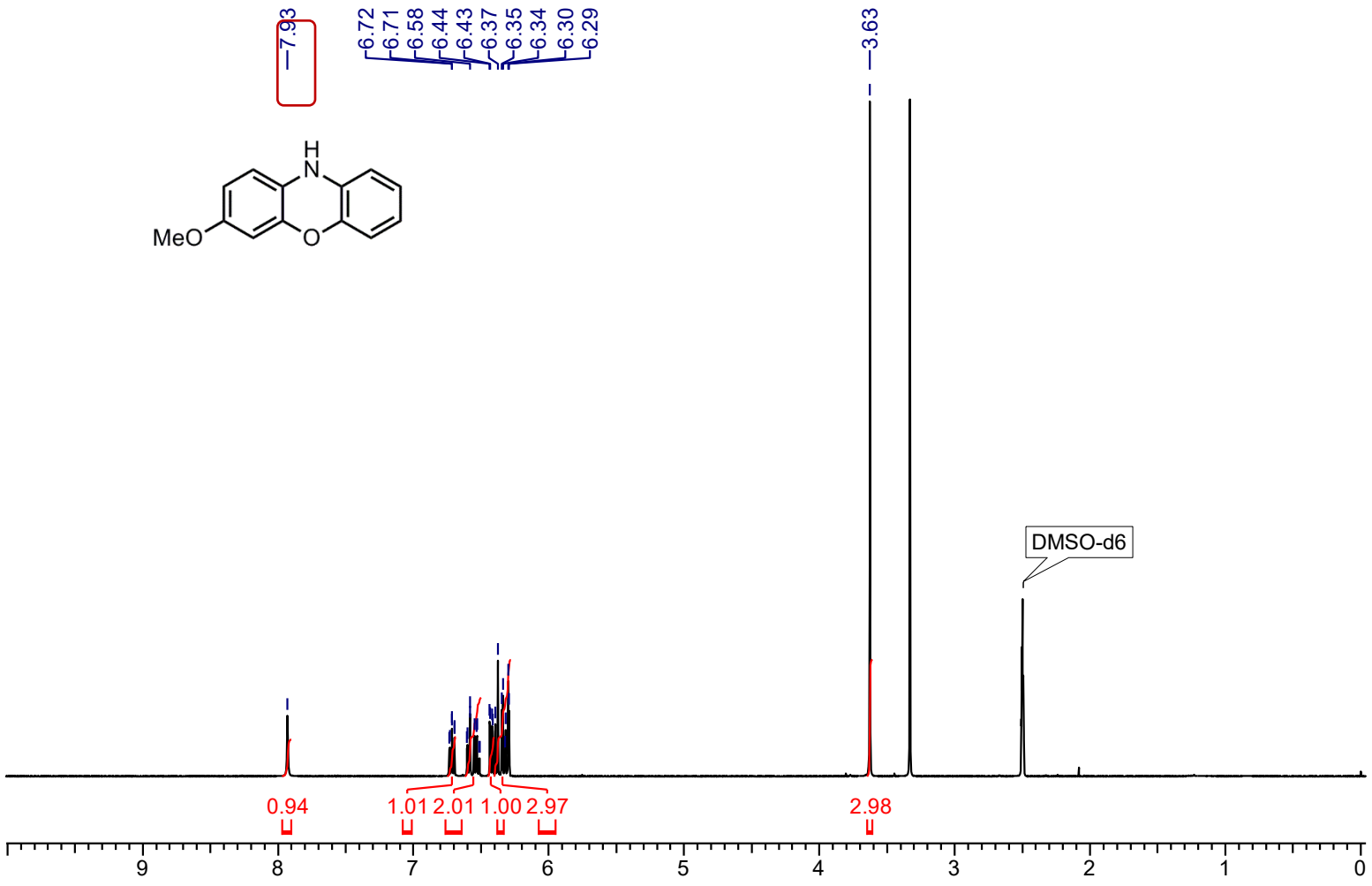

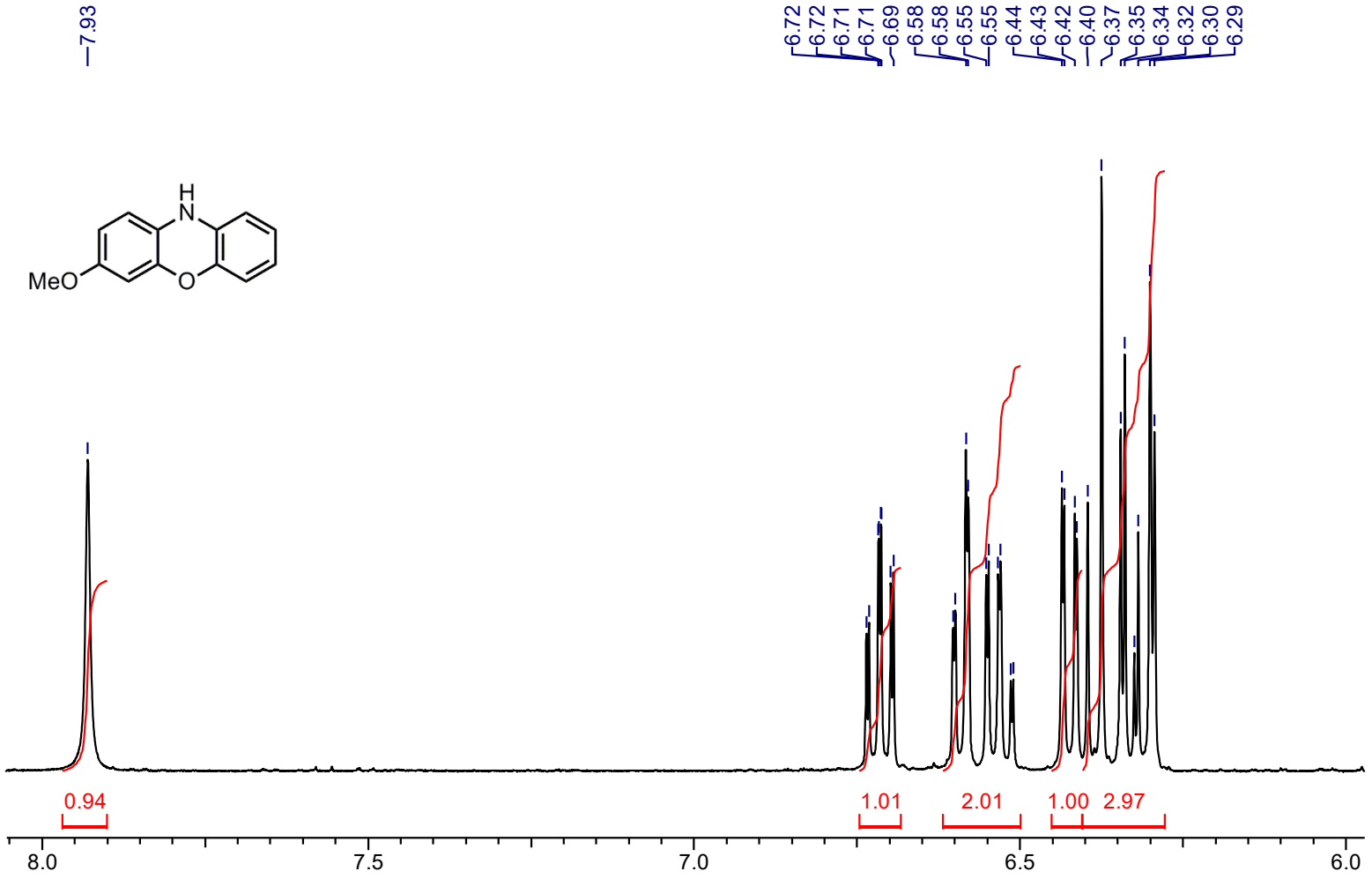
7.93
6.72
6.72
6.71
6.71
6.69
6.58
6.58
6.55
6.55
6.44
6.43
6.42
6.40
6.37
6.35
6.34
6.32
6.30
6.29
H
N
MeO
O
0.94
1.01
2.01
1.00
2.97
8.0
7.5
7.0
6.5
6.0

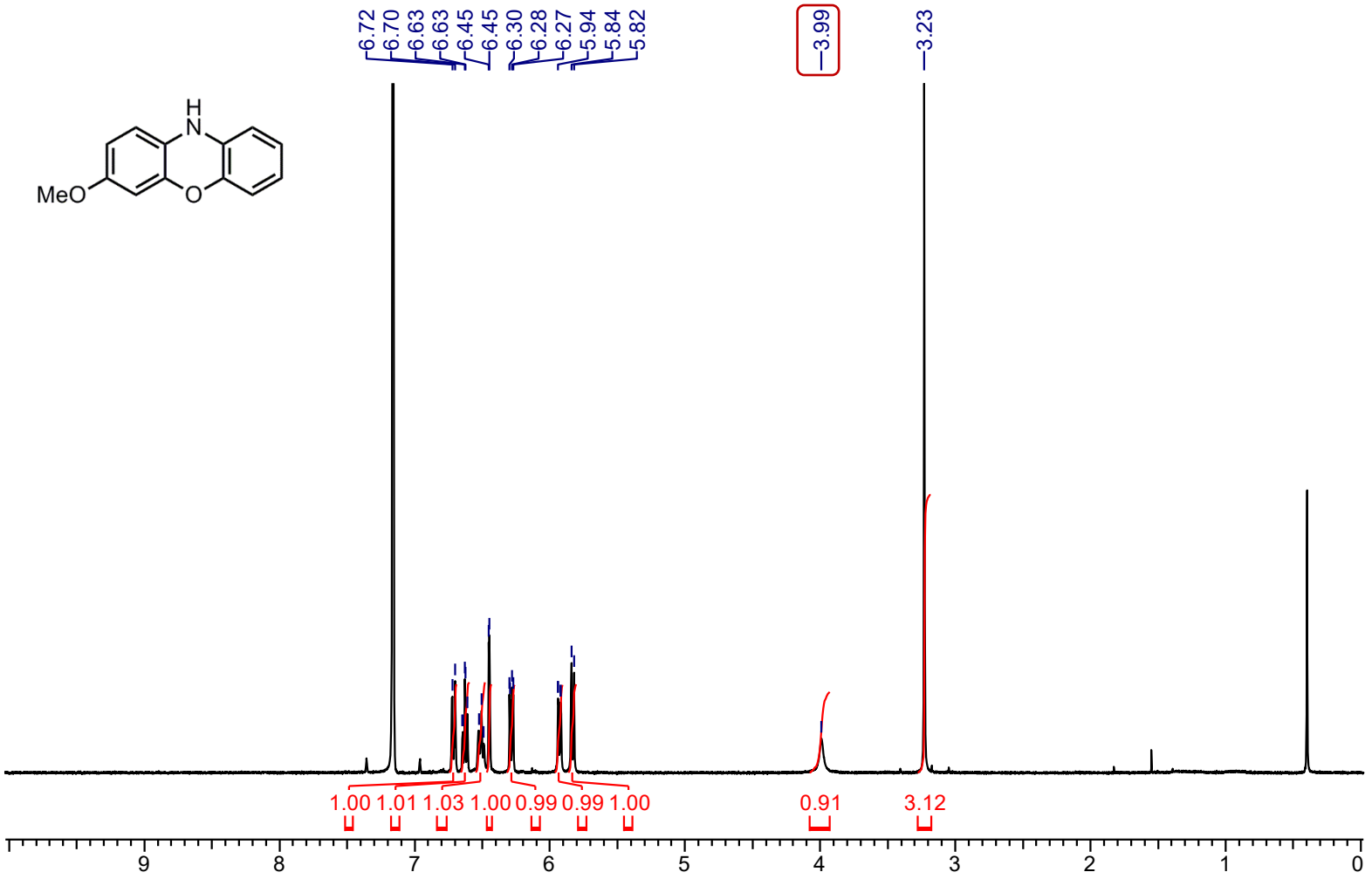
6.72
6.70
6.63
6.63
6.45
6.45
6.30
6.28
6.27
5.94
5.84
5.82
3.99
3.23
H
N
MeO
O
1.00 1.01 1.03 1.00 0.99 0.99 1.00
0.91
3.12
9
8
7
6
5
4
3
2
1
0

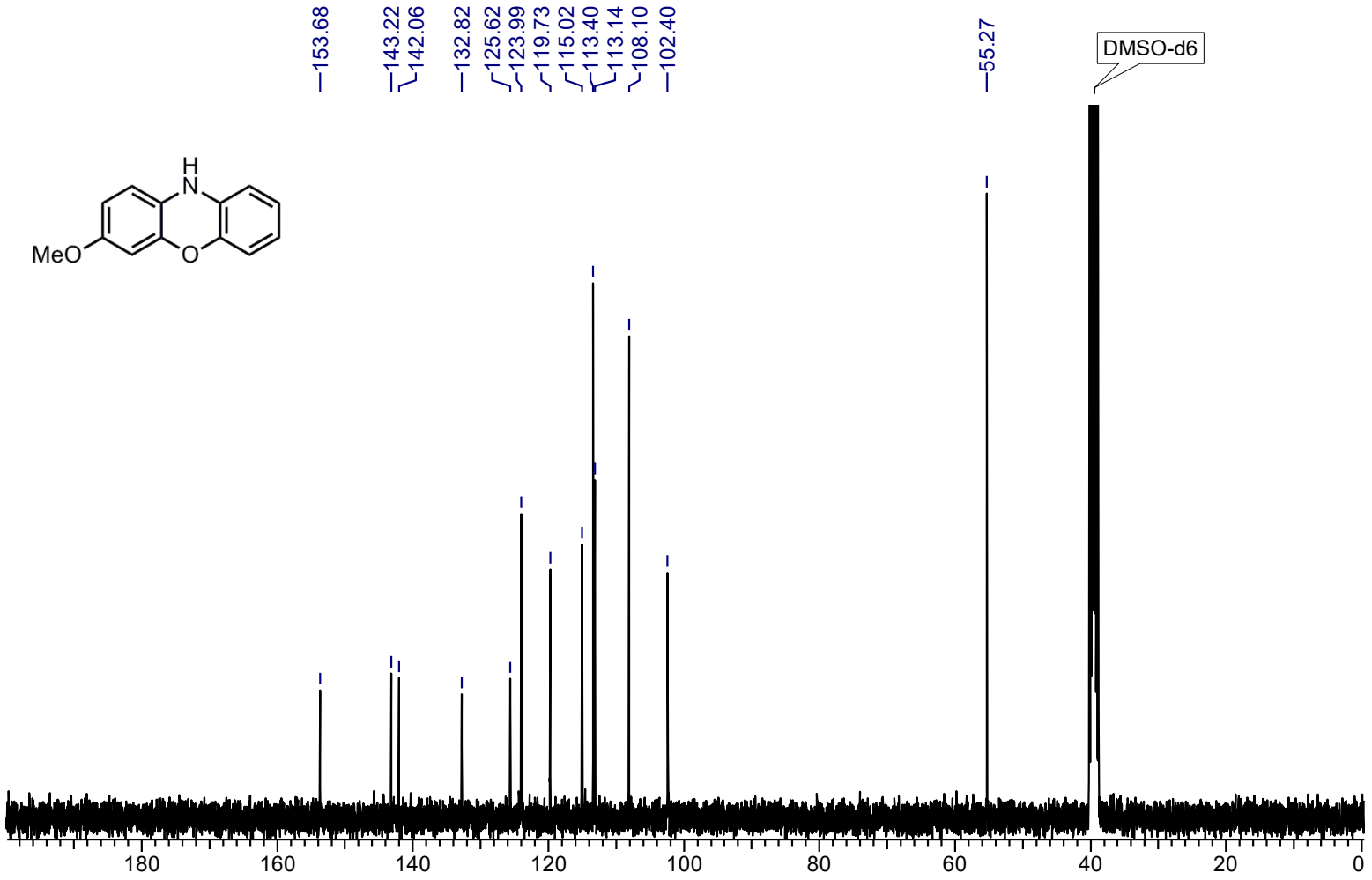
153.68
143.22
142.06
132.82
125.62
123.99
119.73
115.02
113.40
113.14
108.10
102.40
55.27
DMSO-d6
H
N
MeO
O
180
160
140
120
100
80
60
40
20
0

3,7-Dimethoxyphenoxazine (2.17)

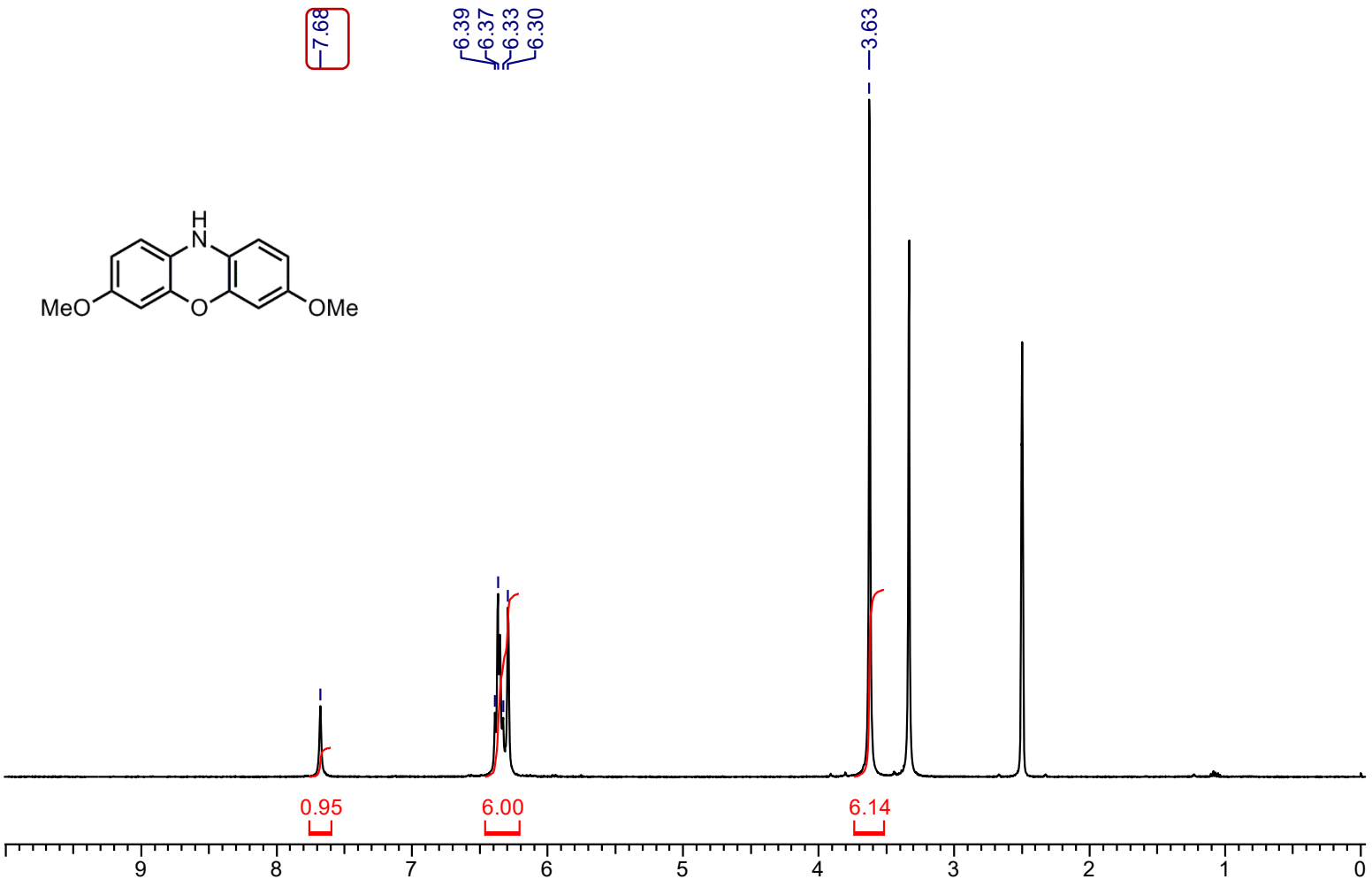

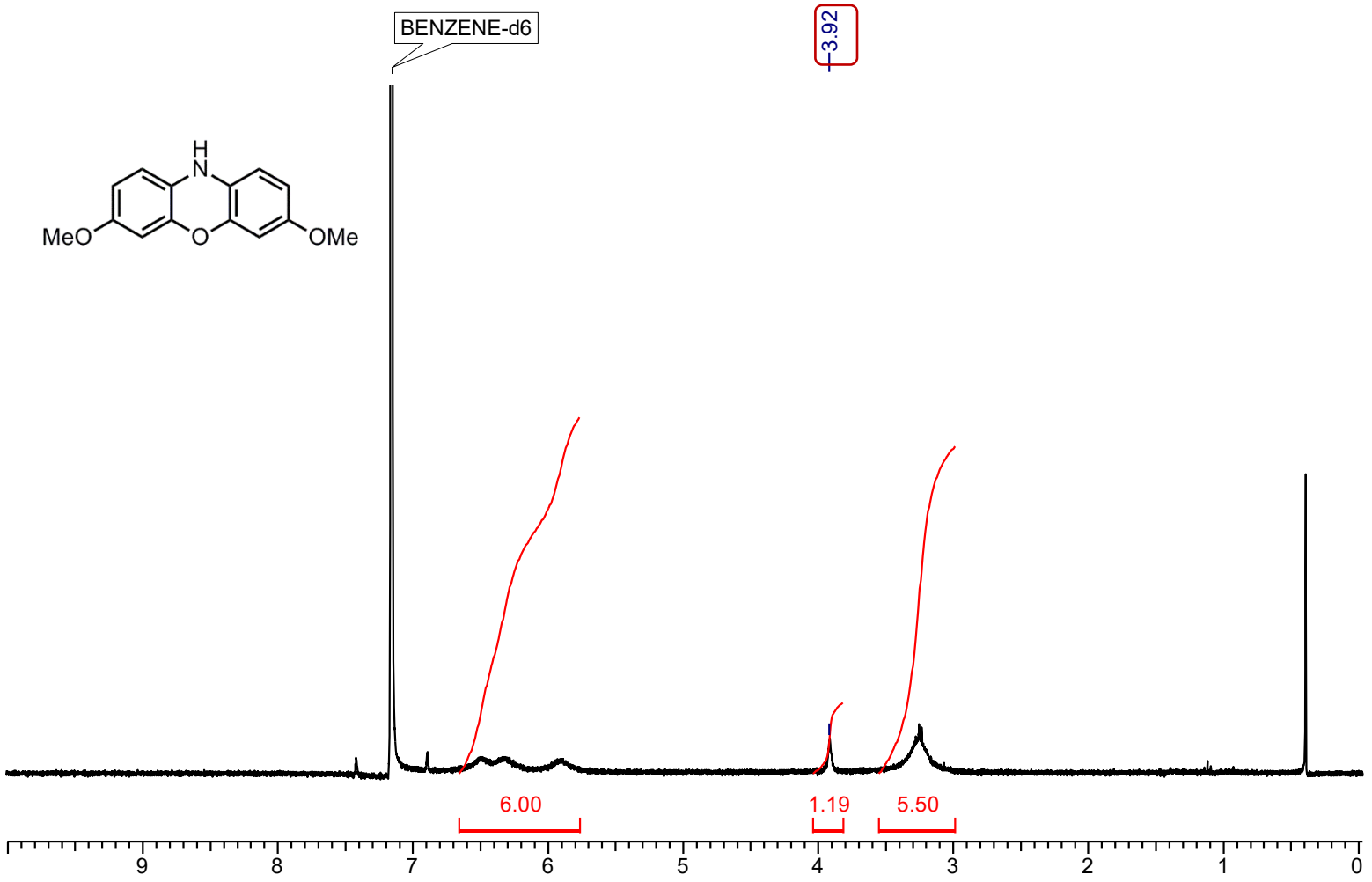
BENZENE-d6
3.92
H
N
MeO
O
OMe
6.00
1.19
5.50
9
8
7
6
5
4
3
2
1
0

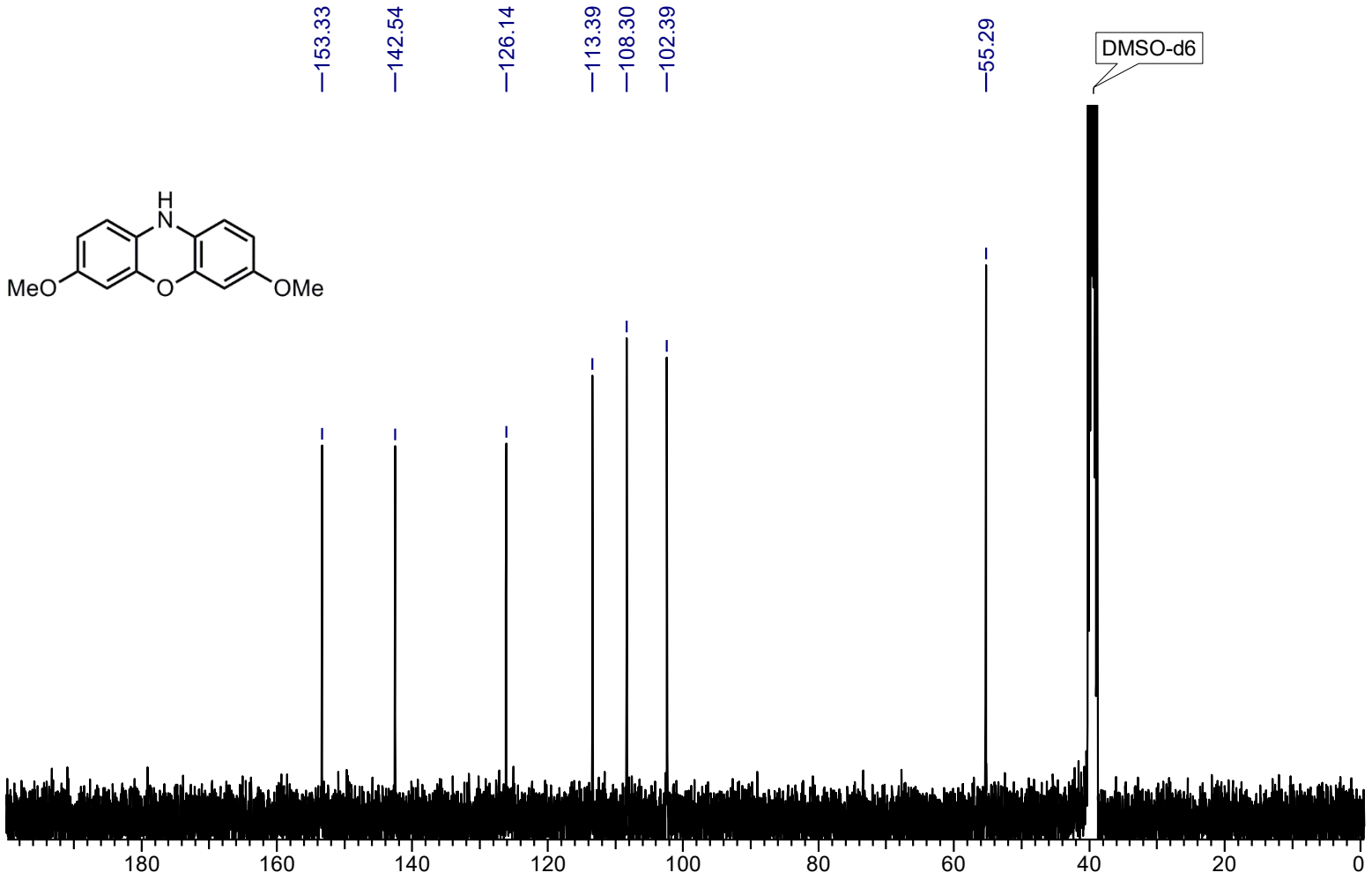
153.33
142.54
126.14
113.39
108.30
102.39
55.29
DMSO-d6
H
N
O
MeO
OMe
180
160
140
120
100
80
60
40
20
0

3-Nitrophenoxazine (2.14)

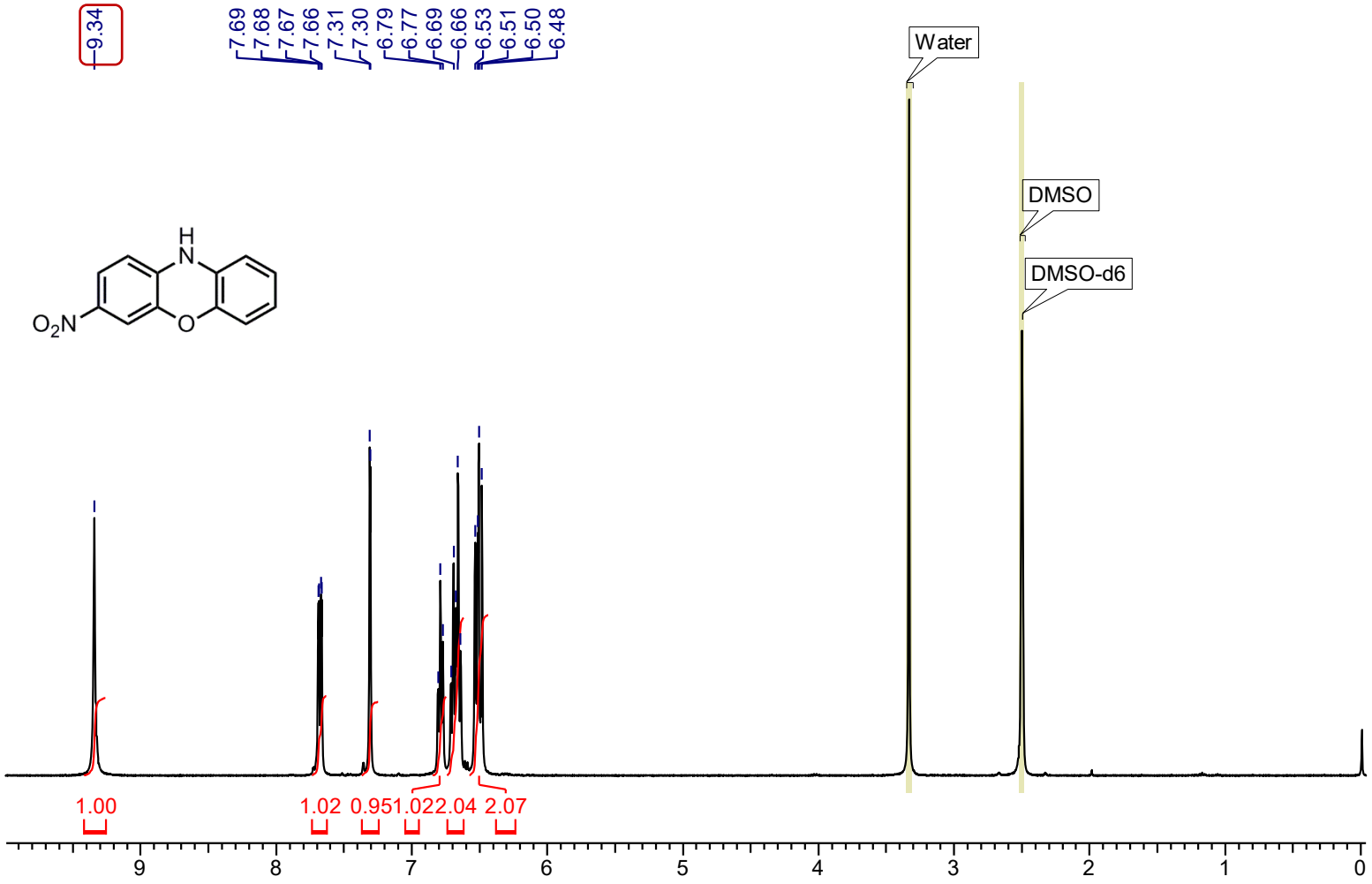

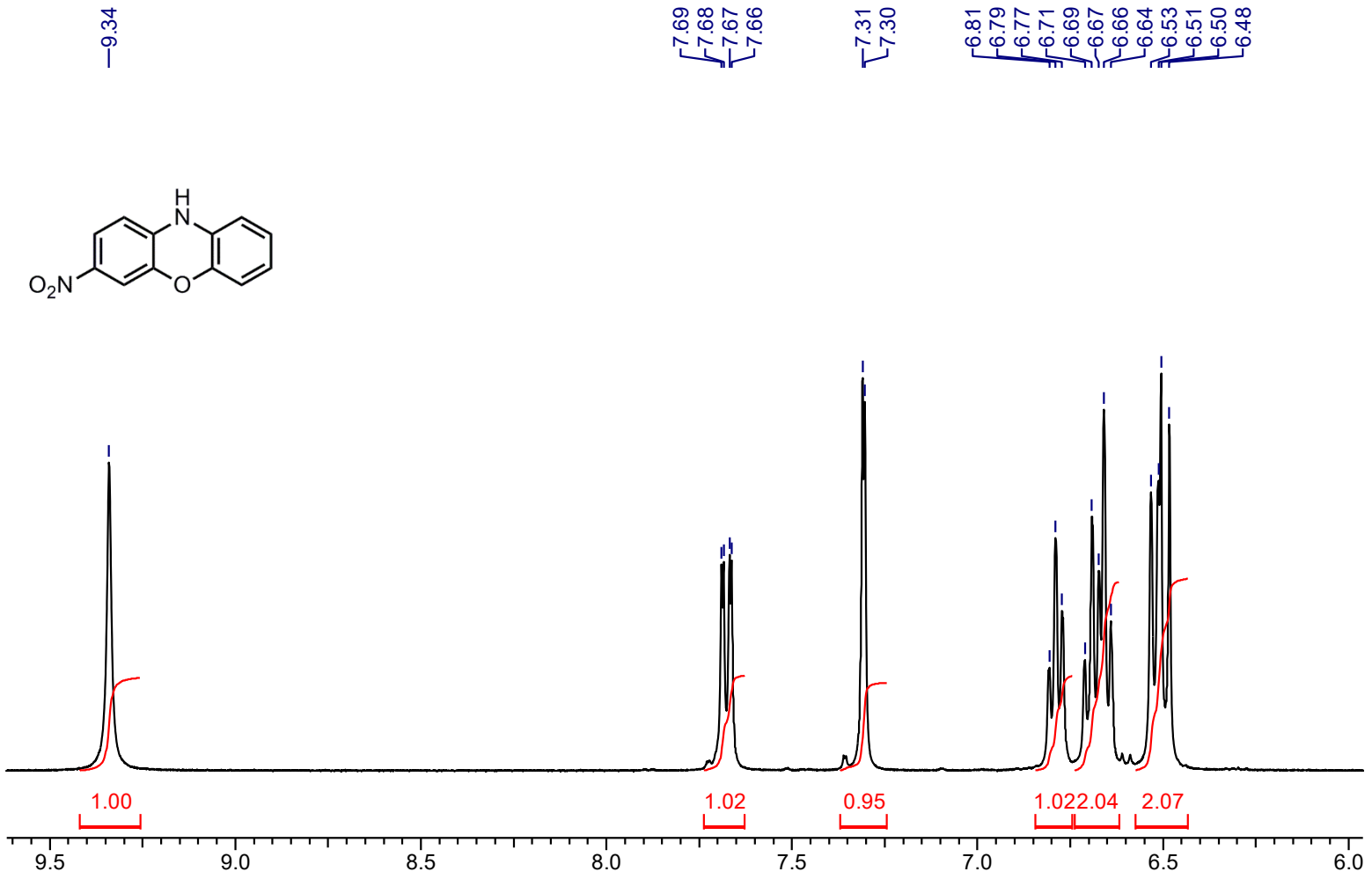
9.34
7.69
7.68
7.67
7.66
7.31
7.30
6.81
6.79
6.77
6.71
6.69
6.67
6.66
6.64
6.53
6.51
6.50
6.48
H
N
O2N
O
1.00
1.02
0.95
1.02
2.04
2.07
9.5
9.0
8.5
8.0
7.5
7.0
6.5
6.0

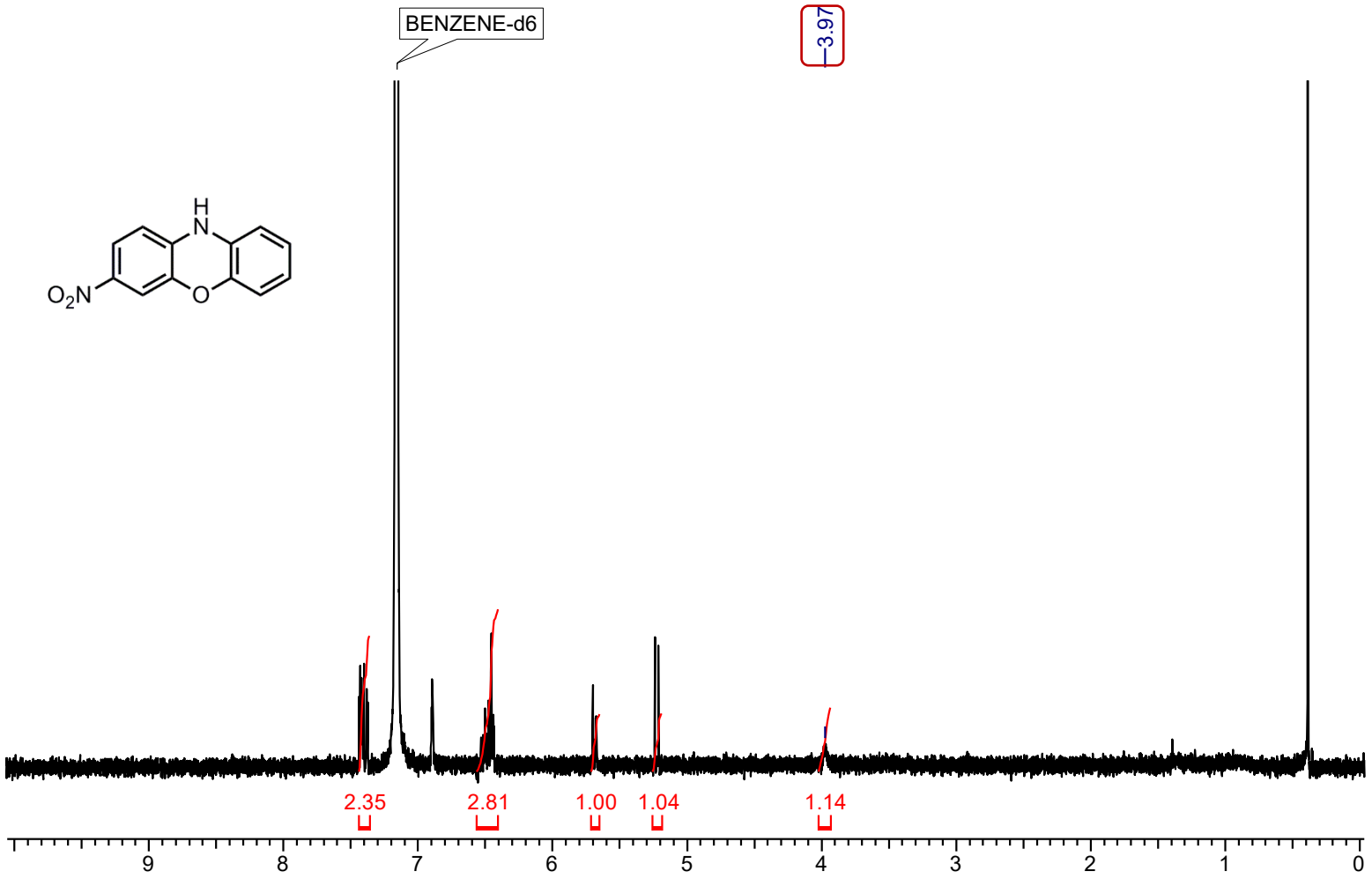
BENZENE-d6
3.97
H
N
O2N
O
2.35
2.81
1.00
1.04
1.14
9
8
7
6
5
4
3
2
1
0

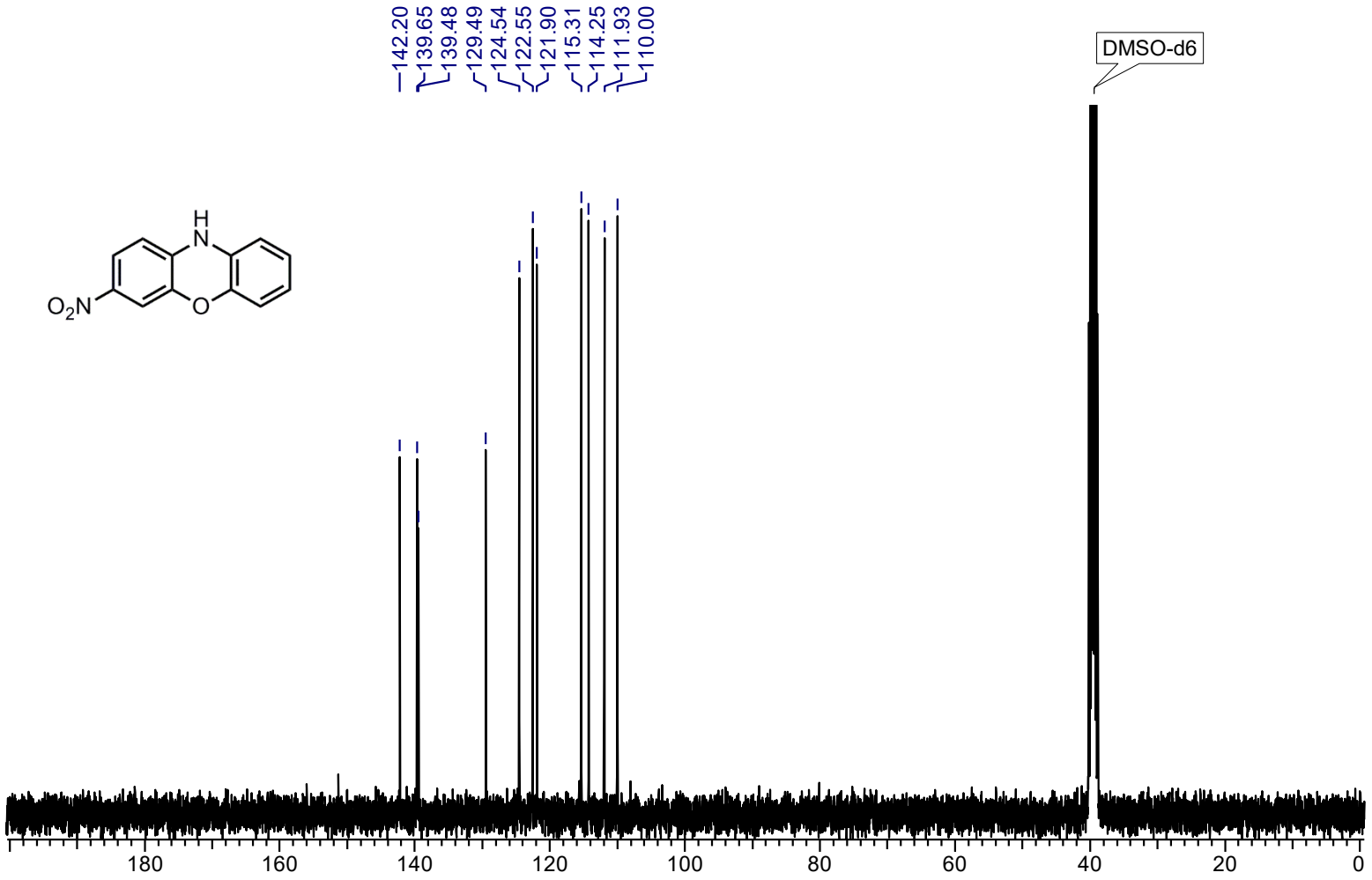
142.20
139.65
139.48
129.49
124.54
122.55
121.90
115.31
114.25
111.93
110.00
DMSO-d6
H
N
O
O_2N
180
160
140
120
100
80
60
40
20
0

3-Cyanophenoxazine (2.12)

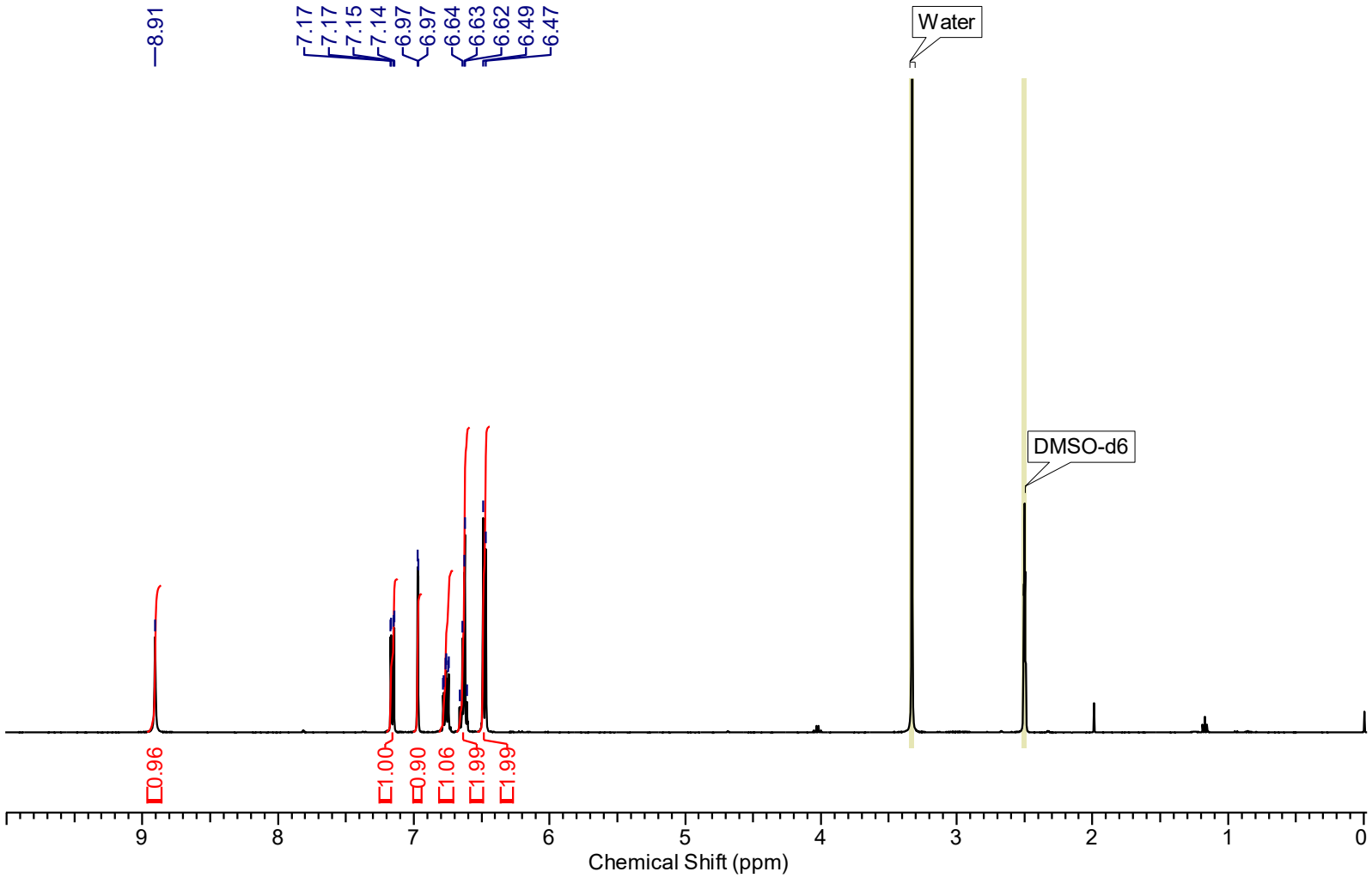

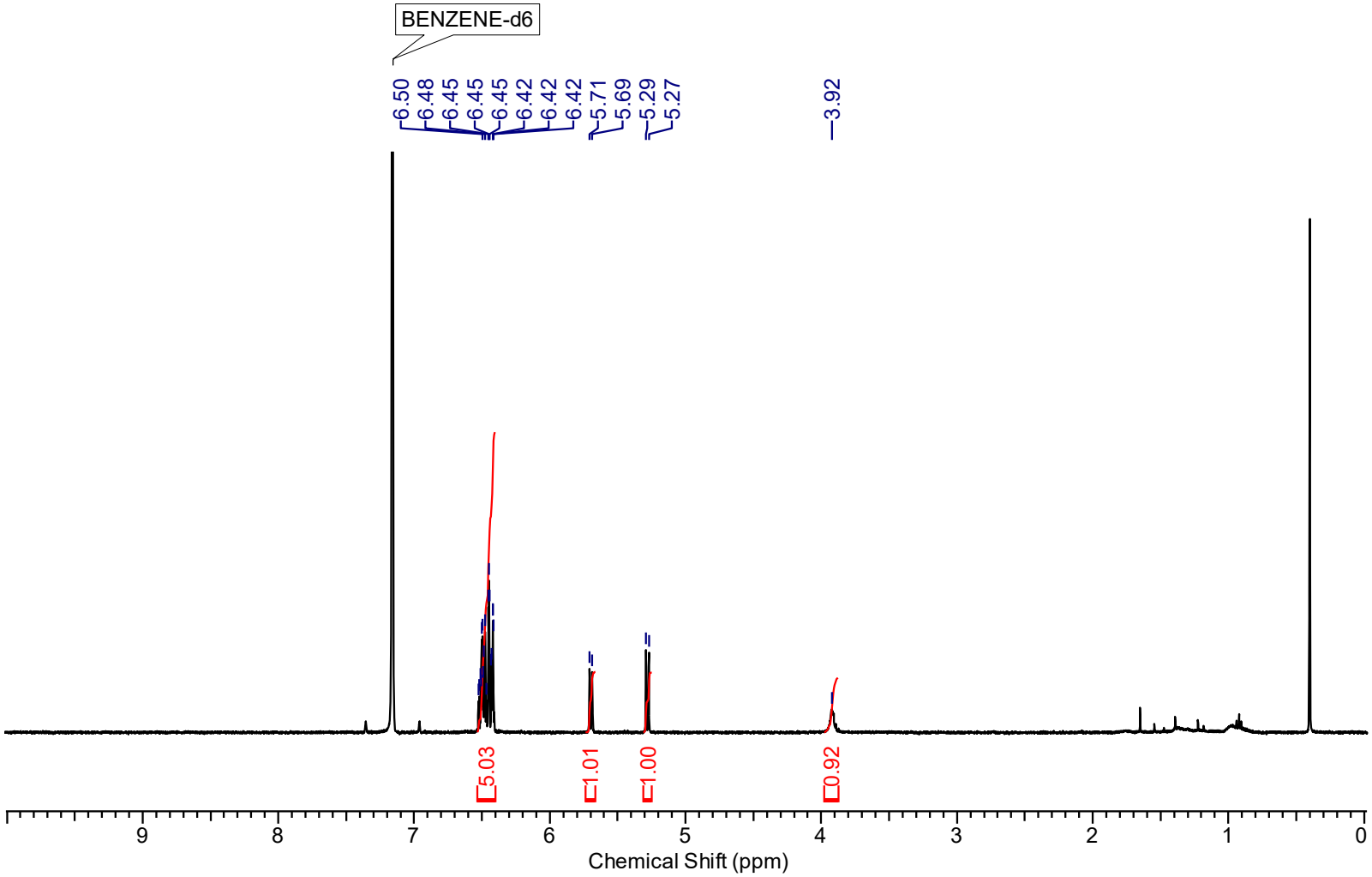
BENZENE-d6
6.50
6.48
6.45
6.45
6.45
6.42
6.42
6.42
5.71
5.69
5.29
5.27
3.92
5.03
1.01
1.00
0.92
9
8
7
6
5
4
3
2
1
0
Chemical Shift (ppm)